

PRODUCTION OF AMORPHOUS SILICA FROM RICE HUSK IN FLUIDISED
BED SYSTEM

(PENGHASILAN SILIKA AMORFUS DARIPADA SEKAM PADI DENGAN
SISTEM LAPISAN TERBENDALIR)

MOHD ROZAINEE BIN TAIB

RESEARCH VOT NO:

74526

Faculty of Chemical Engineering and
Natural Resources Engineering
Universiti Teknologi Malaysia

APRIL 2007

PRODUCTION OF AMORPHOUS SILICA FROM RICE HUSK IN FLUIDISED
BED SYSTEM
(PENGHASILAN SILIKA AMORFUS DARIPADA SEKAM PADI DENGAN
SISTEM LAPISAN TERBENDALIR)

MOHD ROZAINEE BIN TAIB

RESEARCH VOT NO:

74526

Faculty of Chemical Engineering and
Natural Resources Engineering
Universiti Teknologi Malaysia

APRIL 2007

ACKNOWLEDGEMENTS

The project team wishes to acknowledge the IPRA (Intensification Research on Priority Areas) Grant through Vot No. 74526 for sponsoring this research. Also, we would like to express our gratitude to Research Management Centre (RMC), UTM and the Faculty of Chemical Engineering & Natural Resources Engineering (FKKSA), UTM for providing all the necessary facilities and support for carrying out this research project.

ABSTRACT**PRODUCTION OF AMORPHOUS SILICA FROM RICE HUSK IN FLUIDISED
BED SYSTEM**

(Keywords: amorphous silica, rice husk, fluidised bed)

The objective of this research is to design and develop a pilot scale fluidized bed combustion system for the production of amorphous silica from rice husk. The scopes of the research include investigation of the basic combustion characteristics of rice husk, the optimum fluidisation, mixing and combustion parameters and also the optimum fluidised bed combustor design, to improve carbon burnout in siliceous ash product and to develop a pilot plant. Under this research, amorphous silica with very low residual carbon content (approximately 1.0wt% residual carbon) was successfully being produced. The optimum freeboard height to prevent sand contamination and to achieve complete carbon burnout in the rice husk ash was found to be at least 5000mm through computational fluid dynamics (CFD) modeling study. With the experimental and modeling results obtained, the pilot scale fluidized bed combustion system of Ø500mm x 6000mm has been successfully designed, fabricated, installed and commissioned for the production of amorphous silica from rice husk. However, due to time and budget constraints of this research, detailed combustion study has not been fully investigated for the production of amorphous products.

Key researchers:

Assoc. Prof. Dr. Mohd. Rozainee Bin Taib

Dr. Ngo Saik Peng

E-mail : rozainee@fkkksa.utm.my

Tel. No. : 07-553 5778

Vot No. : 74526

ABSTRAK**PENGHASILAN SILIKA AMORFUS DARIPADA SEKAM PADI DENGAN
SISTEM LAPISAN TERBENDALIR**

(Keywords: silica amorfus, sekam padi, sistem lapisan terbendalir)

Matlamat penyelidikan ini adalah untuk merekabentuk and menghasilkan sistem lapisan terbendalir untuk memperoleh silika amorfus daripada sekam padi. Skop penyelidikan ini melibatkan pengkajian sifat asas pembakaran sekam padi, oktima terbendaliran, parameter percampuran dan pembakaran serta rekabentuk oktima untuk pembakar lapisan terbendalir untuk mengatasi masalah pencemaran pasir dan memajukan pembakaran karbon dalam abu serta menghasilkan satu loji pandu sistem lapisan terbendalir. Di bawah projek penyelidikan ini, silika amorfus dengan kandungan sisa karbon serendah 1% berjaya dihasilkan. Permodelan komputer (CFD) telah menentukan ketinggian pembakar yang oktima iaitu sekurang-kurangnya 5000mm dapat menghasilkan silika amorfus yang bebas daripada pencemaran pasir dan sisa karbon. Berdasarkan kepada keputusan yang diperolehi daripada ujikaji dan permodelan komputer, satu loji pandu sistem lapisan terbendalir dengan saiz $\varnothing 500\text{mm} \times 6000\text{mm}$ telah berjaya di rekabentuk, dipasang dan diuji untuk menghasilkan silika amorfus daripada sekam padi. Walau bagaimanapun, disebabkan ketegangan masa dan belanjawan penyelidikan ini, pengkajian secara mendalam sistem pembakaran loji pandu untuk penghasilan produk amorfus tidak dapat dijalankan dengan sepenuhnya.

Penyelidik utama:

Assoc. Prof. Dr. Mohd. Rozainee Bin Taib

Dr. Ngo Saik Peng

E-mail : rozainee@fkkksa.utm.my

Tel. No. : 07-553 5778

Vot No. : 74526

TABLE OF CONTENTS

CHAPTER	TITLE	PAGE
	TITLE PAGE	i
	ACKNOWLEDGEMENT	ii
	ABSTRACT	iii
	ABSTRAK	iv
	TABLE OF CONTENTS	v
	LIST OF TABLES	xi
	LIST OF FIGURES	xxi
	LIST OF PLATES	xxxii
	LIST OF SYMBOLS	xxxiv
	LIST OF APPENDICES	xxxx
1	INTRODUCTION	1
1.1	Introduction	1
1.2	Benefits of Research	2
1.2.1	Amorphous Silica	2
1.2.2	Rice Husk as Silica Source	4
1.2.3	Market Review for Amorphous Silica from Rice Husk Ash	8
1.2.4	Evaluation of Available Technologies for Production of Amorphous Silica from Rice Husk	11

1.2.5	Fluidised Bed as Selected Technology	16
1.2.6	Types of Fluidised Bed	19
1.3	Objectives of Research	21
1.4	Scopes of Research	22
1.5	Expected Results	23
1.6	Layout of the Thesis	24
2	LITERATURE REVIEW	28
2.1	Research History on Thermal Treatment of Rice Husk in Fluidised Bed	28
2.2	Effects of Fluidisation Parameters on the Mixing Characteristics of Rice Husk in Fluidised Bed	30
2.2.1	Fluidising Velocity	31
2.2.2	Sand Size	33
2.2.3	Static Bed Height	35
2.3	Effects of Operating Parameters on the Combustion Efficiency of Rice Husk in Fluidised Bed	39
2.3.1	Time	39
2.3.2	Temperature	41
2.3.3	Presence of Impurities in Rice Husk	55
2.3.4	Air Supply	60
2.3.5	Moisture Content of Rice Husk	64
2.4	Effects of Fluidised Bed Design on the Combustion Efficiency of Rice Husk in Fluidised Bed	65
2.4.1	Freeboard Height	65
2.4.2	Feeding Design and Position of Feed Entry	67

3	METHODOLOGY	71
3.1	Introduction	71
3.2	Research Materials	71
3.3	Experimental Techniques	79
3.3.1	Thermal Treatment in Muffle Furnace	79
3.3.2	Fluidisation Study in 80-mm Inner Diameter Fluidised Bed Column	80
3.3.3	Combustion Study in 80-mm Inner Diameter Fluidised Bed Combustor	84
3.3.4	Combustion Study in 210-mm Inner Diameter Fluidised Bed Combustor	87
3.4	Analytical Techniques	94
3.4.1	Determination Silica Structure and Presence of Contaminants in Rice Husk Ash through X-Ray Diffraction (XRD) Analysis	94
3.4.2	Determination of Residual Carbon Content in Rice Husk Ash through Loss on Ignition (LOI) Test	94
3.4.3	Determination of Particle Size Distribution of Rice Husk Ash through Sieve Analysis	95
3.4.4	Determination of Oxygen Level in Combustion Gas	96
3.5	Modelling Technique through Computational Fluid Dynamics (CFD) Code of FLUENT	96
3.5.1	Governing Equations	97
3.5.2	Numerical Solutions	110

4	RESULTS AND DISCUSSIONS ON COMBUSTION OF RICE HUSK IN FLUIDISED BED TO PRODUCE AMORPHOUS SILICA	118
4.1	Basic Combustion Characteristics of Rice Husk	118
4.2	Effect of Temperature and Residence Time on the Formation of Silica Crystals in Rice Husk Ash	123
4.3	Effects of Fluidisation Parameters on the Mixing of Rice Husk in Fluidised Bed	134
4.3.1	Sand Size	136
4.3.2	Fluidising Velocity (U_{mf} Number)	139
4.3.3	Static Bed Height	141
4.4	Effect of Fluidisation Parameters on the Mixing of Rice Husk in Fluidised Bed during Combustion Process	143
4.4.1	Sand Size	143
4.4.2	Fluidising Velocity	154
4.5	Effect of Mixing Parameters on the Combustion Efficiency of Rice Husk in Fluidised Bed	157
4.5.1	Fluidising Velocity	157
4.5.2	Static Bed Height	168
4.6	Effect of Temperature on the Combustion Efficiency of Rice Husk in Fluidised Bed	182
4.6.1	Bed Temperature	182
4.6.2	Freeboard Temperature	185
4.6.3	Heat Loss	197
4.7	Effect of Washing of Rice Husk on Its Combustion Efficiency in Fluidised Bed	206
4.7.1	Determination of Pretreatment Method for Rice Husk	206

4.7.2	Effect of Alkali Metals Removal in Rice Husk on Its Combustion Efficiency in Fluidised Bed	209
4.7.2.1	Primary Stage Combustion	209
4.7.2.2	Secondary Stage Combustion	213
4.8	Effect of Air Supply on the Combustion Efficiency of Rice Husk in Fluidised Bed	224
4.8.1	Primary Air Factor	224
4.8.2	Primary-to-Secondary Air Ratio	231
4.8.3	Pneumatic Air Feeding Velocity	236
4.9	Effect of Moisture Content in Rice Husk on Its Combustion Efficiency in Fluidised Bed	245
4.10	Effect of Feeding Design on the Combustion Efficiency of Rice Husk in Fluidised Bed	250
4.10.1	Vortex Feeding	250
4.10.2	Vortex Feeding with Higher Fluidising Velocity	267
4.11	Summary of Findings	277
5	RESULTS AND DISCUSSIONS ON IMPROVEMENT IN DESIGN AND OPERATION OF THE FLUIDISED BED THROUGH CFD MODELLING	282
5.1	Increase in Fluidised Bed Freeboard Height	282
5.2	Improvement of Feeding Conditions	289
5.2.1	Feeding Velocity	289
5.2.2	Vortex Feeding	297
5.3	Summary of Findings	315

6	DESIGN, FABRICATION, INSTALLATION AND COMMISSIONING OF PILOT PLANT	318
6.1	Introduction	318
6.2	Pilot-Scale Fluidised Combustor Set-Up	320
6.2.1	Fluidised Bed Combustor	321
6.2.2	Cyclone	321
6.2.3	Fluidising and Pneumatic Air feeding System	323
6.2.4	Combustor Start-Up	324
6.2.5	Rice Husk feeding System	324
6.2.6	Temperature Measurement	325
6.2.7	Flue Gas Sampling and Analysis	327
	6.2.7.1 Measuring Principle	328
	6.2.7.2 Technical Specification and Measuring Ranges	329
6.3	Results and Discussion	330
6.3.1	Bed Pre-Heating and Starting of Combustor	330
6.3.2	Effect of Fluidising Velocity on Rice Husk Combustion	333
6.4	Conclusions	335
7	CONCLUSIONS AND RECOMMENDATIONS	336
7.1	Conclusions	336
7.2	Recommendations for Future Study	346
	REFERENCES	348
	APPENDICES	362

LIST OF TABLES

TABLE	TITLE	PAGE
Table 1-1:	Market prices for amorphous rice husk ash for use in cement industry	10
Table 1-2:	Existing methods and technologies for preparation of amorphous silica from rice husk	12
Table 1-3:	Performance of existing thermal treatment technologies in producing low carbon content rice husk ash	18
Table 2-1:	Properties of sewage sludge and rice husk (wt% dry basis)	32
Table 2-2:	Sand size and corresponding fluidisation velocity reported in literature for combustion of rice husk in fluidised bed	33
Table 2-3:	Minimum fluidising velocity of sand of various size ranges	35
Table 2-4:	Static bed height used for the combustion of rice husk as reported in existing literatures	36
Table 2-5:	Temperature limits reported in various literatures for the onset of crystallisation of silica in rice husk ash	46
Table 2-6:	Chemical properties of wheat straw and rice husk	58
Table 2-7:	Optimum air factor reported in literature (as reviewed by Natarajan et al., 1998a) for combustion of rice husk in fluidised bed	61
Table 2-8:	Different rice husk feeding arrangements reported in literature	68

Table 3-1:	Chemical properties of rice husk	72
Table 3-2:	List and identifications of combustion parameters investigated in the 210-mm inner diameter fluidised bed combustor	93
Table 3-3:	Diffraction peaks of crystalline silica	94
Table 3-4:	Properties of particles used in modelling the effect of feeding method on rice husk combustion in the 210-mm inner diameter fluidised bed combustor	117
Table 4-1:	Real-time tracking of combustion of a batch (4 g) of water-washed rice husk particles in the muffle furnace (650 – 750°C)	122
Table 4-2:	Effect of temperature and residence time on the formation of black char particles during thermal treatment of raw rice husk in the muffle furnace	126
Table 4-3:	Effect of temperature and residence time on the formation of black char particles during thermal treatment of water-washed rice husk* in the muffle furnace	127
Table 4-4:	Effect of temperature and residence time on the formation of black char particles during thermal treatment of water-washed rice husk* (submerged particles) in the muffle furnace	128
Table 4-5:	Effect of temperature and residence time on the formation of black char particles during thermal treatment of water-washed rice husk* (floating particles) in the muffle furnace	129
Table 4-6:	Diffractograms of rice husk ash samples from thermal treatment of raw rice husk in the muffle furnace at different temperatures and residence times	131
Table 4-7:	Diffractograms of rice husk ash samples from thermal treatment of water-washed rice husk* in the muffle furnace at different temperatures and residence times	132

Table 4-8:	Diffractograms of rice husk ash samples from thermal treatment of water-washed rice husk in the muffle furnace at 900°C for different residence times	133
Table 4-9:	Fluidisation properties of rice husk, rice husk char, rice husk ash and silica sand samples	135
Table 4-10:	Screening of commercial silica sand* size for experimental study of rice husk combustion in fluidised bed combustor systems	137
Table 4-11:	Mixing behaviours of rice husk in the 80-mm inner diameter fluidised bed column at different fluidising velocities (sand size = 250 – 595 μm , static bed height = 0.5 D_c , mass fraction of rice husk in sand bed = 10 wt%)	140
Table 4-12:	Mixing behaviours of rice husk in the 80-mm inner diameter fluidised bed column at different static bed heights (sand size = 250 – 595 μm , fluidising velocity = 4 U_{mf} , mass fraction of rice husk in sand bed = 10 wt%)	142
Table 4-13:	Fly ash samples from the combustion of rice husk in the 80-mm inner diameter fluidised bed combustor with a bed of 595 – 841 μm sand (fluidising velocity = 3 – 5 U_{mf} , static bed height = 0.5 D_c , primary air factor \approx 1.0)	144
Table 4-14:	Ash samples from the combustion of rice husk in the 80-mm inner diameter fluidised bed combustor with a bed of 250 – 595 μm sand (fluidising velocity = 3 – 5 U_{mf} , static bed height = 0.5 D_c , primary air factor \approx 1.0)	149
Table 4-15:	Ash samples from the combustion of rice husk in the 80-mm inner diameter fluidised bed combustor at different fluidising velocities (sand size = 250 –	

	595 μm , static bed height = $0.5 D_c$, primary air factor ≈ 1.0)	155
Table 4-16:	Diffraction patterns of fly ash samples from the combustion of rice husk in the 210-mm inner diameter fluidised bed at different fluidising velocities (sand size = 250 – 595 μm , static bed height = $0.5 D_c$, primary air factor ≈ 1.0)	161
Table 4-17:	Products and diffraction patterns of fly ash sample after sand de-contamination stage	162
Table 4-18:	Ash samples from the combustion of rice husk in the 210-mm inner diameter fluidised bed combustor at different fluidising velocities (sand size = 250 – 595 μm , static bed height = $0.5 D_c$, primary air factor ≈ 1.0)	165
Table 4-19:	Diffraction patterns of fly ash samples from the combustion of rice husk in the 210-mm inner diameter fluidised bed at different static bed heights (sand size = 250 – 595 μm , fluidising velocity $\approx 3 U_{mf}$, primary air factor ≈ 1.0)	178
Table 4-20:	Fly ash samples from the combustion of rice husk in the 210-mm inner diameter fluidised bed at different static bed heights (sand size = 250 – 595 μm , fluidising velocity $\approx 3 U_{mf}$, primary air factor ≈ 1.0)	181
Table 4-21:	Diffraction patterns of fly and bottom ashes from the combustion of rice husk in the 80-mm inner diameter fluidised bed at different bed temperatures (sand size = 250 – 595 μm , static bed height = $0.5 D_c$, fluidising velocity $\approx 4 U_{mf}$, primary air factor ≈ 1.0)	183
Table 4-22:	Diffraction patterns of ash samples from the combustion of rice husk in the 210-mm inner diameter fluidised bed combustor at different	

	freeboard temperatures (sand size = 250 – 595 μm , static bed height = 0.5 D_c , fluidising velocity = 4 – 5 U_{mf} , primary air factor \approx 1.0, oxygen level in cyclone \geq 6 vol%)	192
Table 4-23:	Ash samples from the combustion of rice husk in the 210-mm inner diameter fluidised bed at different freeboard temperatures (sand size = 250 – 595 μm , static bed height = 0.5 D_c , fluidising velocity = 4 – 5 U_{mf} , primary air factor \approx 1.0, oxygen level in cyclone \geq 6 vol%)	196
Table 4-24:	Diffractiongrams of fly ash samples from the combustion of rice husk in the non-insulated and insulated 210-mm inner diameter fluidised bed combustors (sand size = 250 – 595 μm , static bed height = 0.5 D_c , fluidising velocity \approx 3 U_{mf} , primary air factor \approx 1.5)	203
Table 4-25:	Ash samples from thermal treatment of raw, water-washed and acid-leached rice husk	208
Table 4-26:	Effect of alkali metals removal from rice husk on the bed temperatures during combustion of rice husk in the 210-mm inner diameter fluidised bed (primary stage combustion) (sand size = 250 – 595 μm , static bed height = 0.5 D_c , fluidising velocity \approx 3 U_{mf} , primary air factor \approx 1.2)	210
Table 4-27:	Physical appearances of the raw and water-washed rice husk samples	210
Table 4-28:	Diffractiongrams of ash samples from the combustion of raw and water-washed rice husk in the 210-mm inner diameter fluidised bed combustor (effect of alkali metals removal on combustion efficiency in the primary stage) (sand size = 250 – 595 μm , static bed height = 0.5 D_c , fluidising velocity \approx 3 U_{mf} , primary air factor \approx 1.2)	211

Table 4-29:	Ash samples from the combustion of raw and water-washed rice husk in the 210-mm inner diameter fluidised bed combustor (effect of alkali metals removal on combustion efficiency in the primary stage) (sand size = 250 – 595 μm , static bed height = 0.5 D_c , fluidising velocity $\approx 3 U_{mf}$, primary air factor ≈ 1.2)	212
Table 4-30:	Silica structures of ash samples from the combustion of raw and water-washed rice husk in the 210-mm inner diameter fluidised bed (effect of alkali metals removal on combustion efficiency in the secondary stage) (sand size = 250 – 595 μm , static bed height = 0.5 D_c , fluidising velocity $\approx 3 U_{mf}$, primary air factor ≈ 1.2 , oxygen level in cyclone = 6 – 12 vol%)	217
Table 4-31:	Ash samples from the combustion of raw and water-washed rice husk in the 210-mm inner diameter fluidised bed (effect of alkali metals removal on combustion efficiency in the secondary stage) (sand size = 250 – 595 μm , static bed height = 0.5 D_c , fluidising velocity $\approx 3 U_{mf}$, primary air factor ≈ 1.2 , oxygen level in cyclone = 6 – 12 vol%)	219
Table 4-32:	Comparisons of ash samples before and after loss on ignition tests (ash from combustion of raw rice husk in the 210-mm inner diameter fluidised bed at different freeboard temperatures; sand size = 250 – 595 μm , static bed height = 0.5 D_c , fluidising velocity $\approx 3 U_{mf}$, primary air factor ≈ 1.2 , oxygen level in cyclone = 6 – 12 vol%)	223
Table 4-33:	Diffractograms of fly and bottom ashes from the combustion of rice husk in the 210-mm inner diameter fluidised bed at different primary air	

	factors (sand size = 250 – 595 μm , static bed height = 0.5 D_c , fluidising velocity = 5 – 6 U_{mf})	227
Table 4-34:	Ash samples from the combustion of rice husk in the 210-mm inner diameter fluidised bed at different primary air factors (sand size = 250 – 595 μm , static bed height = 0.5 D_c , fluidising velocity = 5 – 6 U_{mf})	230
Table 4-35:	Ash samples from the combustion of rice husk in the 210-mm inner diameter fluidised bed at different primary-to-secondary air ratios (sand size = 250 – 595 μm , static bed height = 0.5 D_c , fluidising velocity = 5.7 U_{mf} , primary air factor = 0.65)	233
Table 4-36:	Ash samples from the combustion of rice husk in the 210-mm inner diameter fluidised bed combustor at different primary-to-secondary air ratios (sand size = 250 – 595 μm , static bed height = 0.5 D_c , fluidising velocity = 5.7 U_{mf} , primary air factor = 0.65)	235
Table 4-37:	Diffractiongrams of fly ash samples from the combustion of rice husk in the 210-mm inner diameter fluidised bed at different pneumatic air feeding velocities (sand size = 250 – 595 μm , static bed height = 0.5 D_c , fluidising velocity \approx 3 U_{mf} , primary air factor \approx 1.5)	240
Table 4-38:	Fly ash samples from the combustion of rice husk in the 210-mm inner diameter fluidised bed at different pneumatic air feeding velocities (sand size = 250 – 595 μm , static bed height = 0.5 D_c , fluidising velocity \approx 3 U_{mf} , primary air factor \approx 1.5)	244
Table 4-39:	Rice husk samples used for the combustion of water-washed rice husk at different moisture	

	contents in the 210-mm inner diameter fluidised bed combustor	245
Table 4-40:	Diffractograms of ash samples from the combustion of water-washed rice husk at different moisture contents in the 210-mm inner diameter fluidised bed combustor (sand size = 250 – 595 μm , static bed height = 0.5 D_c , fluidising velocity $\approx 3 U_{mf}$, primary air factor ≈ 1.2)	247
Table 4-41:	Ash samples from the combustion of water-washed rice husk at different moisture contents in the 210-mm inner diameter fluidised bed combustor (sand size = 250 – 595 μm , static bed height = 0.5 D_c , fluidising velocity $\approx 3 U_{mf}$, primary air factor ≈ 1.2)	249
Table 4-42:	Heat capacities of materials used in the experimental study	256
Table 4-43:	Comparisons of silica structures of ash samples from the combustion of rice husk in the 210-mm inner diameter fluidised bed with different feeding methods (sand size = 250 – 595 μm , static bed height = 0.5 D_c , fluidising velocity $\approx 3 U_{mf}$, primary air factor ≈ 1.2)	258
Table 4-44:	Ash samples from the combustion of rice husk in the 210-mm inner diameter fluidised bed with different feeding methods (sand size = 250 – 595 μm , static bed height = 0.5 D_c , fluidising velocity $\approx 3 U_{mf}$, primary air factor ≈ 1.2)	261
Table 4-45:	Comparisons of physical appearances of different particles from the combustion of rice husk in fluidised bed combustor	262
Table 4-46:	Expected trajectories of particles in the computational fluid dynamics (CFD) model of rice husk combustion in the 210-mm inner diameter	

	fluidised bed combustor with different feeding methods	266
Table 4-47:	Diffractiongrams of ash samples from the combustion of rice husk in the 210-mm inner diameter fluidised bed with inclined, tangential feeding port at different fluidising velocities (sand size = 250 – 595 μm , static bed height = 0.5 D_c , primary air factor ≈ 1.2)	270
Table 4-48:	Ash samples from the combustion of rice husk in the 210-mm inner diameter fluidised bed with inclined, tangential feeding port at different fluidising velocities (sand size = 250 – 595 μm , static bed height = 0.5 D_c , primary air factor ≈ 1.2)	272
Table 5-1:	Trajectories and mass loss history of burning rice husk particles with different sizes in the fluidised bed combustor model ($\varnothing 500\text{mm} \times 5250\text{mm}$)	286
Table 5-2:	Histograms for residence time distribution from computational fluid dynamics (CFD) modelling of burning rice husk particles in the 210-mm inner diameter fluidised bed combustor	291
Table 5-3:	Trajectories and residence times of burning rice husk particles in the 210-mm inner diameter fluidised bed combustor from CFD modelling	292
Table 5-4:	Computational fluid dynamics (CFD) modelling results on the trajectories and residence times of particles during the combustion of rice husk in the 210-mm inner diameter fluidised bed combustor with inclined feeding port (Model FM-A)	300
Table 5-5:	Computational fluid dynamics (CFD) modelling results on the trajectories and residence times of particles during the combustion of rice husk in the 210-mm inner diameter fluidised bed combustor with inclined, tangential feeding port (Model FM-B)	301

Table 5-6:	Trajectories and residence times of fly ash particles in Model FM-A (inclined feeding method)	304
Table 5-7:	Trajectories and residence times of fly ash particles in Model FM-B (inclined, tangential feeding method)	305
Table 5-8:	Trajectories of fly ash particles in Model FM-B (inclined, tangential feeding) when the tangential feeding velocity was reduced by half (from 1.1 m/s to 0.55 m/s)	306
Table 5-9:	Mass loss history of burning rice husk particles in Model FM-A (inclined feeding method)	308
Table 5-10:	Mass loss history of burning rice husk particles in Model FM-B (inclined, tangential feeding method)	309
Table 5-11:	Trajectories and residence times of bottom ash particles in Model FM-A (inclined feeding method)	311
Table 5-12:	Trajectories and residence times of bottom ash particles in Model FM-B (inclined, tangential feeding method)	312
Table 6-1:	General specification of SWG 300 ⁻¹ gas analyzer	329
Table 6-2:	Measuring ranges and accuracy as given by the manufacturer	330

LIST OF FIGURES

FIGURE	TITLE	PAGE
Figure 1-1:	Power generation potential from rice husk mills	8
Figure 2-1:	Diffraction pattern of fresh rice husk (taken from Liou, 2004)	42
Figure 2-2:	Diffraction pattern of crystallised rice husk ash showing characteristic crystal peak of cristobalite at 2θ angle of 21.93° (rice husk sample fired at 1000°C at different time intervals) (Ibrahim and Helmy, 1981)	43
Figure 2-3:	Effect of secondary airflow on the temperature distribution in the firebrick-insulated fluidised bed combustor during the combustion of rice husk (Chen et al., 1998)	63
Figure 2-4:	Chart for transport disengaging height (TDH) estimation of fine particle (Geldart A) beds (Zenz and Weil, 1958)	67
Figure 3-1:	Adiabatic flame temperatures from combustion of rice husk sample at different air factors computed using the FLAME programme code	73
Figure 3-2:	Particle size distribution of silica sand samples used in the experimental study	74
Figure 3-3:	Bed particles used in the combustion of rice husk in fluidised bed	75
Figure 3-4:	Boat-like shape of whole rice husk	75
Figure 3-5:	Diffraction pattern of fresh rice husk sample	76

Figure 3-6:	Diffractiongram of amorphous rice husk ash (from thermal treatment of rice husk in muffle furnace at 600°C and 1 hour)	77
Figure 3-7:	Diffractiongram of crystallised rice husk ash (exposure to temperature of 725°C for 10 hours in a muffle furnace)	77
Figure 3-8:	Diffractiongram of fresh silica sand	78
Figure 3-9:	Diffractiongram of used silica sand (from fluidised bed after combustion of rice husk)	78
Figure 3-10:	Experimental setup of the 80-mm inner diameter Perspex fluidised bed for investigation of fluidisation and mixing behaviours of rice husk	81
Figure 3-11:	Behavioural changes of bed with gas velocity in a conventional fluidised bed (Howard, 1989)	82
Figure 3-12:	Pressure drop versus gas velocity plot for increasing and decreasing gas flow	83
Figure 3-13:	Determination of terminal velocity from the plot of pressure drop versus fluidisation velocity (Hao et al., 1995)	83
Figure 3-14:	Positions of thermocouples (T1 – T6), feeding port and viewing port at the 210-mm inner diameter fluidised bed combustor	90
Figure 3-15:	Overall schematic diagram of the 210-mm inner diameter fluidised bed combustor system	91
Figure 3-16:	Algorithm for the solution of a non-adiabatic two-mixture-fraction case in pre-PDF and FLUENT	109
Figure 3-17:	Size distribution of elutriated sand particles during the combustion of rice husk in the 210-mm inner diameter fluidised bed (bed sand size 250 – 595 µm)	111
Figure 3-18:	Three-dimensional computational grid of the fluidised bed combustor model	111

Figure 3-19:	Three-dimensional computational grid of the 210-mm inner diameter fluidised bed combustor	113
Figure 3-20:	Three-dimensional computational grid of the 210-mm inner diameter fluidised bed combustor with inclined feeding port (Model FM-A)	115
Figure 3-21:	Three-dimensional computational grid of the 210-mm inner diameter fluidised bed combustor with inclined, tangential feeding port (Model FM-B)	115
Figure 4-1:	Experimental values of velocities range for the fluidising state of rice husk, rice husk char, rice husk ash and sand samples	136
Figure 4-2:	Real-time temperature profiles during combustion of rice husk in the 210-mm inner diameter fluidised bed at $3.3 U_{mf}$	158
Figure 4-3:	Real-time temperature profiles during combustion of rice husk in the 210-mm inner diameter fluidised bed at $2.5 U_{mf}$ and $1.5 U_{mf}$	159
Figure 4-4:	Residual carbon contents in fly ash samples from the combustion of rice husk in the 210-mm inner diameter fluidised bed at different fluidising velocities (sand size = 250 – 595 μm , static bed height = $0.5 D_c$, primary air factor ≈ 1.0)	163
Figure 4-5:	Estimated bubble size just before eruption at the bed surface and bubble rise velocity at different static bed heights in the 210-mm inner diameter fluidised bed combustor (sand size = 250 – 595 μm , fluidising velocity = $3 U_{mf}$)	169
Figure 4-6:	Real-time temperature profiles during the combustion of rice husk in the 210-mm inner diameter fluidised bed combustor with sand static bed height of $0.25 D_c$ (sand size = 250 – 595 μm , fluidising velocity $\approx 3 U_{mf}$, primary air factor ≈ 1.0)	171

- Figure 4-7: Real-time temperature profiles during the combustion of rice husk in the 210-mm inner diameter fluidised bed combustor with sand static bed height of $0.5 D_c$ (sand size = $250 - 595 \mu\text{m}$, fluidising velocity $\approx 3 U_{mf}$, primary air factor ≈ 1.0) 173
- Figure 4-8: Real-time temperature profiles during the combustion of rice husk in the 210-mm inner diameter fluidised bed combustor with sand static bed heights of $0.625 D_c$ and $0.75 D_c$ (sand size = $250 - 595 \mu\text{m}$, fluidising velocity $\approx 3 U_{mf}$, primary air factor ≈ 1.0) 175
- Figure 4-9: Temperature profiles during the combustion of rice husk in the 210-mm inner diameter fluidised bed combustor at different static bed heights (sand size = $250 - 595 \mu\text{m}$, fluidising velocity $\approx 3 U_{mf}$, primary air factor ≈ 1.0) 175
- Figure 4-10: Effect of static bed height on the bed temperature and residual carbon content in fly ash during combustion of rice husk in the 210-mm inner diameter fluidised bed combustor (sand size = $250 - 595 \mu\text{m}$, fluidising velocity $\approx 3 U_{mf}$, primary air factor ≈ 1.0) 179
- Figure 4-11: Residual carbon contents in ash samples from the combustion of rice husk in the 80-mm inner diameter fluidised bed at different bed temperatures (sand size = $250 - 595 \mu\text{m}$, fluidising velocity $\approx 4 U_{mf}$, primary air factor ≈ 1.0) 185
- Figure 4-12: Exact locations of thermocouples and secondary burners at the 210-mm inner diameter fluidised bed combustor column 186
- Figure 4-13: Statistical analysis on the bed temperatures (T1) during combustion of rice husk in the 210-mm inner diameter fluidised bed at different freeboard

- temperatures (sand size = 250 – 595 μm , static bed height = 0.5 D_c , fluidising velocity = 4 – 5 U_{mf} , primary air factor \approx 1.0, oxygen level in cyclone \geq 6 vol%) 187
- Figure 4-14: Statistical analysis on the freeboard temperatures (T3 – T6) during combustion of rice husk in the 210-mm inner diameter fluidised bed – Lower freeboard temperature range (400 – 600°C) (sand size = 250 – 595 μm , static bed height = 0.5 D_c , fluidising velocity = 4 – 5 U_{mf} , primary air factor \approx 1.0, oxygen level in cyclone \geq 6 vol%) 189
- Figure 4-15: Statistical analysis on the freeboard temperatures (T3 – T6) during combustion of rice husk in the 210-mm inner diameter fluidised bed – Higher freeboard temperature range (600 – 700°C) (sand size = 250 – 595 μm , static bed height = 0.5 D_c , fluidising velocity = 4 – 5 U_{mf} , primary air factor \approx 1.0, oxygen level in cyclone \geq 6 vol%) 190
- Figure 4-16: Comparisons of residual carbon contents in ash samples from the combustion of rice husk in the 210-mm inner diameter fluidised bed at different freeboard temperatures (sand size = 250 – 595 μm , static bed height = 0.5 D_c , fluidising velocity = 4 – 5 U_{mf} , primary air factor \approx 1.0, oxygen level in cyclone \geq 6 vol%) 194
- Figure 4-17: Real-time temperature profiles during combustion of rice husk in the non-insulated 210-mm inner diameter fluidised bed combustor system (Case Study HL1) (sand size = 250 – 595 μm , static bed height = 0.5 D_c , fluidising velocity \approx 3 U_{mf} , primary air factor \approx 1.5) 198
- Figure 4-18: Real-time temperature profiles during combustion of rice husk in an insulated 210-mm inner diameter

- fluidised bed combustor system (Case Study HL2)
(sand size = 250 – 595 μm , static bed height = 0.5 D_c , fluidising velocity $\approx 3 U_{mf}$, primary air factor ≈ 1.5) 200
- Figure 4-19: Average combustor temperatures during combustion of rice husk in the non-insulated and insulated 210-mm inner diameter fluidised bed combustors (sand size = 250 – 595 μm , static bed height = 0.5 D_c , fluidising velocity $\approx 3 U_{mf}$, primary air factor ≈ 1.5) 202
- Figure 4-20: Fly ash samples from the combustion of rice husk in the non-insulated and insulated 210-mm inner diameter fluidised bed combustors (sand size = 250 – 595 μm , static bed height = 0.5 D_c , fluidising velocity $\approx 3 U_{mf}$, primary air factor ≈ 1.5) 204
- Figure 4-21: Real-time temperature profile during combustion of raw rice husk in the 210-mm inner diameter fluidised bed combustor (sand size = 250 – 595 μm , static bed height = 0.5 D_c , fluidising velocity $\approx 3 U_{mf}$, primary air factor ≈ 1.2 , oxygen level in cyclone = 6 – 12 vol%) 214
- Figure 4-22: Real-time temperature profile during combustion of water-washed rice husk in the 210-mm inner diameter fluidised bed combustor (sand size = 250 – 595 μm , static bed height = 0.5 D_c , fluidising velocity $\approx 3 U_{mf}$, primary air factor ≈ 1.2 , freeboard temperatures (T4 – T6) = 700 – 900°C, oxygen level in cyclone = 6 – 12 vol%) 215
- Figure 4-23: Comparisons of average bed temperatures during combustion of rice husk in the 210-mm inner diameter fluidised bed at different primary air

- factors (sand size = 250 – 595 μm , static bed height = 0.5 D_c , fluidising velocity = 5 – 6 U_{mf}) 226
- Figure 4-24: Residual carbon contents of ash samples from the combustion of rice husk in the 210-mm inner diameter fluidised bed at different primary air factors (sand size = 250 – 595 μm , static bed height = 0.5 D_c , fluidising velocity = 5 – 6 U_{mf}) 228
- Figure 4-25: Average combustor temperatures during combustion of rice husk in the 210-mm inner diameter fluidised bed at different primary-to-secondary air ratios (sand size = 250 – 595 μm , static bed height = 0.5 D_c , fluidising velocity = 5.7 U_{mf} , primary air factor = 0.65) 231
- Figure 4-26: Temperature profiles during the combustion of rice husk in a non-insulated combustor (Armesto et al., 2002) 232
- Figure 4-27: Temperature profile along the 210-mm inner diameter fluidised bed combustor during combustion of rice husk at different pneumatic air feeding velocities (sand size = 250 – 595 μm , static bed height = 0.5 D_c , fluidising velocity \approx 3 U_{mf} , primary air factor \approx 1.5) 237
- Figure 4-28: Average bed temperatures and residual carbon contents in ash samples from the combustion of rice husk in the 210-mm inner diameter fluidised bed at different pneumatic air feeding velocities (sand size = 250 – 595 μm , static bed height = 0.5 D_c , fluidising velocity \approx 3 U_{mf} , primary air factor \approx 1.5) 242
- Figure 4-29: Total air velocity at the freeboard region of the fluidised bed combustor at different pneumatic air feeding velocities 242

- Figure 4-30: Comparisons of bed temperatures during combustion of water-washed rice husk at different moisture contents in the 210-mm inner diameter fluidised bed combustor (sand size = 250 – 595 μm , static bed height = 0.5 D_c , fluidising velocity $\approx 3 U_{mf}$, primary air factor ≈ 1.2) 246
- Figure 4-31: Comparisons of residual carbon contents of ash samples from the combustion of water-washed rice husk at different moisture contents in the 210-mm inner diameter fluidised bed combustor (sand size = 250 – 595 μm , static bed height = 0.5 D_c , fluidising velocity $\approx 3 U_{mf}$, primary air factor ≈ 1.2) 248
- Figure 4-32: Real-time temperature profiles during combustion of rice husk in the 210-mm inner diameter fluidised bed combustor with inclined feeding port (Case Study FM1) (sand size = 250 – 595 μm , static bed height = 0.5 D_c , fluidising velocity $\approx 3 U_{mf}$, primary air factor ≈ 1.2) 252
- Figure 4-33: Real-time temperature profiles during combustion of rice husk in the 210-mm inner diameter fluidised bed combustor with inclined, tangential feeding port (Case Study FM2) (sand size = 250 – 595 μm , static bed height = 0.5 D_c , fluidising velocity $\approx 3 U_{mf}$, primary air factor ≈ 1.2) 253
- Figure 4-34: Average combustor temperatures during combustion of rice husk in the 210-mm inner diameter fluidised bed combustor utilising different feeding methods (sand size = 250 – 595 μm , static bed height = 0.5 D_c , fluidising velocity $\approx 3 U_{mf}$, primary air factor ≈ 1.2) 254
- Figure 4-35: Histogram of particle size distribution for fly ash from the combustion of rice husk in the 210-mm inner diameter fluidised bed combustor with

- different feeding methods (sand size = 250 – 595 μm , static bed height = 0.5 D_c , fluidising velocity $\approx 3 U_{mf}$, primary air factor ≈ 1.2) 264
- Figure 4-36: Histogram of particle size distribution for bottom ash from the combustion of rice husk in the 210-mm inner diameter fluidised bed combustor with different feeding methods (sand size = 250 – 595 μm , static bed height = 0.5 D_c , fluidising velocity $\approx 3 U_{mf}$, primary air factor ≈ 1.2) 265
- Figure 4-37: Average temperatures in the combustor during combustion of rice husk in the 210-mm inner diameter fluidised bed combustor with inclined, tangential feeding port at different fluidising velocities (sand size = 250 – 595 μm , static bed height = 0.5 D_c , primary air factor ≈ 1.2) 268
- Figure 4-38: Comparisons of residual carbon contents in ash samples from the combustion of rice husk in the 210-mm inner diameter fluidised bed combustor with inclined tangential feeding port at different fluidising velocities (sand size = 250 – 595 μm , static bed height = 0.5 D_c , primary air factor ≈ 1.2) 273
- Figure 4-39: Particle size distribution of fly ash samples from the combustion of rice husk in the 210-mm inner diameter fluidised bed combustor with inclined, tangential feeding at different fluidising velocities (sand size = 250 – 595 μm , static bed height = 0.5 D_c , primary air factor ≈ 1.2) 275
- Figure 4-40: Particle size distribution of bottom ash samples from the combustion of rice husk in the 210-mm inner diameter fluidised bed combustor with inclined, tangential feeding at different fluidising velocities (sand size = 250 – 595 μm , static bed height = 0.5 D_c , primary air factor ≈ 1.2) 276

Figure 5-1:	Trajectory of the 25 μm sand particle in the fluidised bed combustor model ($\text{\O}500\text{mm} \times 5250\text{mm}$)	283
Figure 5-2:	Trajectory of the 50 μm sand particle in the fluidised bed combustor model ($\text{\O}500\text{mm} \times 5250\text{mm}$)	283
Figure 5-3:	Trajectory of the 75 μm sand particle in the fluidised bed combustor model ($\text{\O}500\text{mm} \times 5250\text{mm}$)	284
Figure 5-4:	Trajectory of the 100 μm sand particle in the fluidised bed combustor model ($\text{\O}500\text{mm} \times 5250\text{mm}$)	284
Figure 5-5:	Trajectory of the 125 μm sand particle in the fluidised bed combustor model ($\text{\O}500\text{mm} \times 5250\text{mm}$)	285
Figure 5-6:	Residence time of burning rice husk particles with different sizes in the fluidised bed model ($\text{\O}500\text{mm} \times 5250\text{mm}$)	288
Figure 5-7:	Statistical analysis on the residence time distribution from computational fluid dynamics (CFD) modelling of burning rice husk particles in the 210-mm inner diameter fluidised bed combustor at different pneumatic air feeding velocities	290
Figure 5-8:	Recirculating zone near the feeding port of the combustor in Model IV (pneumatic air feeding velocity = 1.36 m/s)	293
Figure 5-9:	Absence of recirculating zones inside the fluidised bed combustor in Models I, II and III (pneumatic air feeding velocities of 0.42 – 0.85 m/s)	294
Figure 5-10:	Char fraction of a burning rice husk particle in Model III (pneumatic air feeding velocity = 0.85 m/s)	296

Figure 5-11:	Char fraction of a burning rice husk particle in Model IV (pneumatic air feeding velocity = 1.36 m/s)	296
Figure 5-12:	Gas flow profile as indicated by trajectory of tracer particle in the 210-mm inner diameter fluidised bed with inclined feeding port (Model FM-A)	297
Figure 5-13:	Gas flow profile inside in fluidised bed combustor with inclined feeding port (Model FM-A)	298
Figure 5-14:	Gas flow profile as indicated by trajectory of tracer particle in the 210-mm inner diameter fluidised bed with inclined, tangential feeding port (Model FM-B)	298
Figure 5-15:	Comparisons of residence time of fly ash of different sizes in Model FM-A (inclined feeding) and Model FM-B (inclined, tangential feeding)	307
Figure 6-1:	Schematic diagram of fluidised bed combustor	322
Figure 6-2:	a) Blower set-up b) Pipe fittings for fluidizing air inlet into combustor	323
Figure 6-3:	Feeding system of pilot-scale fluidised bed combustor	325
Figure 6-4:	Schematic diagram of thermocouple position in a pilot-scale fluidised bed combustor	326
Figure 6-5:	Flue gas analyzer, MRU	327
Figure 6-6:	Oxygen measurement principle	328
Figure 6-7:	Temperature profile during bed pre-heating	331
Figure 6-8:	Real time temperature profile of rice husk combustion at a) 4,5 and 6 U_{mf} b) 7 U_{mf} fluidizing velocity	334

LIST OF PLATES

PLATE	TITLE	PAGE
Plate 3-1:	The 80-mm inner diameter fluidised bed combustor system	86
Plate 3-2:	The 210-mm inner diameter fluidised bed combustor system (shown without insulation material)	92
Plate 4-1:	Ash product from burning raw rice husk inside the muffle furnace (650 – 750°C) after 10 minutes of combustion time	119
Plate 4-2:	Higher flaming times for a group of rice husk particles spread widely apart in the muffle furnace (650 – 750°C)	120
Plate 4-3:	Formation of dead zone at nearly two-third of the sand bed (595 – 841 μm) at fluidising velocity of $3 U_{mf}$	145
Plate 4-4:	Burning of rice husk was restricted to the top of the sand bed (595 – 841 μm) at fluidising velocity of $3 U_{mf}$	145
Plate 4-5:	Rapid accumulation of char and ash in the sand bed (595 – 841 μm) at fluidising velocity of $3 U_{mf}$	146
Plate 4-6:	Suspension burning of rice husk at fluidising velocity of $4 U_{mf}$ (sand size 595 – 841 μm)	147
Plate 4-7:	Suspension burning of rice husk at fluidising velocity of $5 U_{mf}$ (sand size 595 – 841 μm)	147

Plate 4-8:	Good mixing during the combustion of rice husk (sand size 250 – 595 μm) at fluidising velocity of $3 U_{mf}$	150
Plate 4-9:	Penetration of rice husk, char and ash into the sand bed during combustion (sand size 250 – 595 μm) at fluidising velocity of $3 U_{mf}$	150
Plate 4-10:	Some degree of suspension burning during the combustion of rice husk (sand size 250 – 595 μm) at fluidising velocity of $4 U_{mf}$	152
Plate 4-11:	Vigorous bed bubbling with good mixing of char and rice husk in the sand bed during the combustion of rice husk (sand size 250 – 595 μm) at fluidising velocity of $5 U_{mf}$	152
Plate 4-12:	Residual bottom ash retained in the bed after the combustion of rice husk (sand size 250 – 595 μm) at fluidising velocity of $5 U_{mf}$	153
Plate 4-13:	The inclined feeding port at the 210-mm inner diameter fluidised bed combustor	251
Plate 4-14:	The inclined, tangential feeding port at the 210-mm inner diameter fluidised bed combustor	251

LIST OF SYMBOLS

A	-	Area, (m ²)
Ar	-	Archimedes number $\left(= \frac{\rho_f (\rho_p - \rho_f) g d_m^3}{\mu_f^2} \right)$, (dimensionless)
$C_{1\epsilon}, C_{2\epsilon}$	-	Empirical constants, ($C_{1\epsilon} = 1.42, C_{2\epsilon} = 1.68$)
C_d, C_g	-	Constants in PDF equations, ($C_d = 2.0, C_g = 2.86$), (dimensionless)
C_D	-	Drag coefficient, (dimensionless)
C_p	-	Heat capacity, [J/(kg • K)]
d_b	-	Bubble size, (m)
d_{bm}	-	Limiting size of bubble expected in a very deep bed, (m)
d_{bo}	-	Initial bubble size, (m)
D_c	-	Column diameter or fluidised bed inner diameter, (m)
d_m	-	Mean particle diameter, (m)
d_p	-	Particle diameter, (m)
d_{pi}	-	Arithmetic mean diameter of screen apertures, (m)
d_{vs}	-	Volume-surface mean diameter $\left(= \frac{1}{\sum_{i=1}^n (X_i / d_{pi})} \right)$, (m)
f	-	Mixture fraction, (dimensionless)
\bar{f}	-	Time-averaged value of f , (dimensionless)
f'^2	-	Mixture fraction variance, (dimensionless)
f_c	-	Fractional conversion $\left(= \frac{m'}{m_{initial} - m_{final}} \right)$, (dimensionless)

F_D	-	Drag force, (N)
g	-	Gravitational acceleration, (= 9.81 m/s ²)
G_k	-	Generation of turbulent kinetic energy, (m ² /s ²)
h_c	-	Natural or forced convection coefficient, [W/(m ² • K)]
h_r	-	Radiation heat transfer coefficient, [W/(m ² • K)]
H^*	-	Instantaneous enthalpy, (kJ/kg)
$\Delta\hat{H}_c$	-	Heat of combustion of the fuel at reference temperature of 25°C, (J)
\hat{H}_i	-	Specific enthalpy of the i th component at 25°C, [J/(kg • K)]
H_v	-	Heat of vaporization of water, (J/mol)
k	-	Thermal conductivity, [W/(m • K)]
l	-	Latent heat of vaporisation, (J/kg)
L_e	-	Eddy length scale, (m)
l_{or}	-	Spacing between adjacent holes on a perforated plate, (m)
m	-	Mass, (kg)
\dot{m}	-	Instantaneous mass, (kg)
m_i	-	Local mass fraction, (dimensionless)
n	-	Number of mole, (kg-mol)
n_i	-	Mole of the i th component in the feed or product, (kg-mol)
N_{or}	-	Number of orifices on a perforated plate, (dimensionless)
p	-	Partial fraction, (dimensionless)
P	-	Pressure, (N/m ²)
$p(f)$	-	Probability Density Function i.e. fraction of time that the fluctuating variable f takes on a value between f and $f + \Delta f$, (s), (dimensionless)
p_1	-	PDF of f_{fuel} , (dimensionless)
p_2	-	PDF of p_{sec} , (dimensionless)
Q_c	-	Rate of heat absorbed by inlet air, (MJ/min)
Q_{loss}	-	Rate of heat loss through convection and radiation, (MJ/min)
Q_p	-	Rate of heat evolved from the combustion process, assuming complete reaction (MJ/min)
Q_s	-	Heat required for sustaining the combustion process, (MJ)

Q_v	-	Rate of heat consumed to vaporise the moisture content in the feed material, (MJ/min)
r	-	Radius, (m)
R	-	Effects of rapid strain and streamline curvature, (kg/s ⁴)
Re	-	Reynolds number $\left(= \frac{\rho_f U d_p}{\mu_f} \right)$, (dimensionless)
S_m	-	Transfer of mass from reacting particles into gas phase, [kg/(m ³ • s)]
T	-	Temperature, (K)
T_{ad}	-	Adiabatic flame temperature, (K)
t_{cross}	-	Particle eddy crossing time, (s)
T_L	-	Fluid Lagrangian integral time $\left(T_L \approx 0.15 \frac{\kappa}{\varepsilon} \right)$, (s)
u	-	Velocity component or velocity component in x -direction, (m/s)
u'	-	Fluctuating component of u , (m/s)
\bar{u}	-	Instantaneous velocity component, (m/s)
u_i, u_j	-	Time-averaged velocity component
U, U_o	-	Fluidising gas velocity, (m/s)
U_b	-	Bubble rise velocity, (m/s)
U_{mf}	-	Minimum fluidising velocity, (m/s)
$U_{mf,m}$	-	Minimum fluidising velocity of a mixture of bed particles, (m/s)
U_{ms}	-	Minimum spouting velocity, (m/s)
v	-	Velocity component in y -direction, (m/s)
V_m	-	Bubble ejection velocity, (m/s)
w	-	Velocity component in z -direction, (m/s)
x_i	-	Mass fraction of the i -th size range in the particles screen analysis, (dimensionless)
z	-	Height of bed of particles, (m)

Greek Letters

α_ε	-	Inverse effective Prandtl number for turbulent dissipation rate, (dimensionless)
α_κ	-	Inverse effective Prandtl number for turbulent kinetic energy, (dimensionless)
α_s	-	Swirl constant, (dimensionless)
δ	-	Empirical constant, (dimensionless)
ε	-	Turbulent dissipation rate, (m^2/s^3)
ξ	-	Emissivity of the combustor surface, (dimensionless)
ϕ_i	-	Instantaneous species concentration, density or temperature, (kmol/m^3 , kg/m^3 or K)
ϕ_s	-	Particle sphericity, (dimensionless)
\varnothing	-	Inner diameter of fluidised bed column, (m)
ζ	-	Normally distributed random number, (dimensionless)
Ω	-	Swirl angular velocity, (rad/s)
ρ	-	Density, (kg/m^3)
σ_t	-	Constant in PDF equations (= 0.7), (dimensionless)
τ	-	Particle relaxation time (s)
τ_e	-	Characteristic lifetime of the eddy, (s)
τ_i	-	Fraction of time that f spends in the Δf band, (s)
θ	-	Bragg angle in x-ray diffraction analysis, ($^\circ$)
κ	-	Turbulent kinetic energy, (m^2/s^2)
μ	-	Dynamic fluid viscosity, ($\text{kg}/\text{m}\cdot\text{s}$)

Subscripts

a	-	Air
$feed$	-	Feed
$final$	-	Final
$fuel$	-	Fuel
i	-	i-direction or chemical species i

<i>initial</i>	-	Initial
<i>j</i>	-	j-direction or chemical species j
<i>m</i>	-	Mixture
<i>s</i>	-	Sand
<i>sec</i>	-	Secondary fuel
<i>t</i>	-	Turbulent conditions
<i>w</i>	-	Water

Abbreviation

ASEAN	Association of South-East Asian Nations
ASTM	American Society for Testing Materials
BET	- Brunauer, Emmett and Teller
CFD	- Computational Fluid Dynamics
DRW	- Discrete Random Walk
EC	- European Commission
FKKKSA	Fakulti Kejuruteraan Kimia dan Kejuruteraan Sumber Asli
FSDP	- Full-Scale Demonstration Project
HHV	- Higher Heating Value
IARC	- International Agency for Research on Cancer
ID	- Internal Diameter
LCD	- Liquid Crystal Display
LHV	- Lower Heating Value, (MJ/kg)
LOI	- Loss on Ignition
LPG	- Liquefied Petroleum Gas
LPM	- Litre per Minute
MSW	- Municipal Solid Waste
NIOSH	National Institute for Occupational Safety and Health
NO _x	- Nitrogen Oxides
PDF	- Probability Density Function
PMET	- Pittsburg Mineral & Environmental Tech. Inc.
RHA	- Rice Husk Ash
RM	- Ringgit Malaysia
RMS	- Root Mean Square

SEM	-	Scanning Electron Microscopy
TDH	-	Transport Disengaging Height, (m)
USD	-	United States Dollar (USD 1 = RM 3.80)
UTM	-	Universiti Teknologi Malaysia
XRD	-	X-Ray Diffraction

LIST OF APPENDICES

APPENDIX	TITLE	PAGE
Appendix A:	Estimation of Bubble Eruption Velocity	362
Appendix B:	Determination of Particle Sphericity (ϕ_s)	363
Appendix C:	Properties of Rice Husk for its Definition as the Burning Fuel Particle in CFD Modelling (Input Data to Preprocessor PrePDF)	365
Appendix D:	Properties of Rice Husk for its Definition as the Burning Fuel Particle in CFD Modelling (Input Data to Preprocessor PrePDF)	366
Appendix E:	Chart for Determining Sphericity (ϕ_s) of Particles and Theoretical Equations for Estimating Minimum Fluidising Velocity (U_{mf}) and Terminal Velocity (U_t)	368
Appendix F:	Real-Time Temperature Profiles during Combustion of Rice Husk in the 210-mm Inner Diameter Fluidised Bed at Different Freeboard Temperatures	370
Appendix G:	Mass Balance to Determine the Amount of Stoichiometric Air for Combustion of Rice Husk	371
Appendix H:	Real-Time Temperature Profiles during Combustion of Raw and water-Washed Rice Husk in the 210-mm Inner Diameter Fluidised Bed	372

CHAPTER 1

INTRODUCTION

1.1 Introduction

The purpose of this research was to produce amorphous silica from rice husk through thermal treatment using the fluidised bed technology. Rice husk ash contains among the highest amount of biogenic silica still in its amorphous form (in the excess of 95 wt% silica, SiO_2) (Kaupp, 1984; Kapur, 1985; James and Rao, 1986) compared to other biomass materials, such as ash from sugarcane bagasse (57 – 73% SiO_2) (Jenkins et al., 1996; Natarajan et al., 1998b; Stephens et al., 2003). In addition, the percentage of ash in rice husk is many times higher (at 13 – 25 wt%, dry basis) (Jenkins et al., 1998; Natarajan et al., 1998b; Armesto et al., 2002) compared to that of sugarcane bagasse (at only 1.9 – 6.8 wt%, dry basis) (Jenkins et al., 1998; Natarajan et al., 1998b; Das et al., 2004). Further, it was reported that such a high percentage of silica is very unusual within nature and that no other plant waste even approaches the amount of silica found in rice husk (Beagle, 1974). The recovery of amorphous silica from rice husk is deemed the most economical source of silica due to the presence of abundant source of rice husk around the country, with annual generation rate of approximately 0.5 million tonnes (in the year 2003, Department of Statistics Malaysia). Rice husk has a high calorific value, which at approximately 13 MJ/kg is sufficient to promote sustainable combustion process, thus reducing the cost of fuel required for the conversion process. This is in contrast with the conventional preparation methods which are either energy-intensive (vapour-phase reaction and thermal decomposition technique) or involves high raw

material costs (alkaline extraction method), all of which result in high production costs.

1.2 Benefits of Research

1.2.1 Amorphous Silica

Silica or silicon dioxide (SiO_2) exists in two forms, amorphous and crystalline. Processing of silica of specific quality results in several types of specialty silicas, such as colloidal silica, fumed silica, fused silica, high-purity ground silica, silica gel and precipitated silica (McDonald, 1991). The global demand for specialty silicas is growing at an annual rate of 3% with revenue generation of more than RM 9.5 billion (USD 2.5 billion) (MineSet Partners LLC, 2004). Currently, the Asia Pacific region is the leading consumer in specialty silica with demand exceeding RM 3 billion (USD 800 million) in 2003 (MineSet Partners LLC, 2004).

Among these specialty silicas, silica in its amorphous form has wider industrial applications (as high-purity ground silica and fumed silica) since crystalline silica is carcinogenic to humans and is categorised as an IARC (International Agency for Research on Cancer) Group 1 agent, whereby its exposure could lead to the risk of silicosis. Amorphous silica is used mainly in specialty coatings, plastics, rubber, electronics, abrasives, refractories and optics (McDonald, 1991). It is also a much sought after raw material for the synthesis of various fine chemicals (sodium silicate, zeolite catalysts, aerogel, very pure silicon, silicon nitride, silicon carbide and magnesium silicide). Since 1997, the world consumption of amorphous silica is estimated to be in the excess of 1 million tonnes per annum valued at approximately RM 4,500 per tonne (Chemlink Pty Ltd., 1997). The price of amorphous silica is highly dependent on its grade (particle size and level of impurities) and could range from RM 440 (USD 120; coarse, impure form) to RM 21,000 (USD 5,500; ultra-fine, highly pure form) (McDonald, 1991). By processing into higher end products such as sodium silicate, its economic value is

further elevated. For example, the production of one tonne of sodium silicate requires approximately 135 kg of amorphous silica as raw material. Thus, one tonne of amorphous silica will produce an equivalent of 7.4 tonnes of sodium silicate, which in turn commands a price of RM 2,100 per tonne (USD 550 per tonne; Chemical Market Reporter, 1999). Sodium silicate is then used for the synthesis of nano-chemicals such as aerogel, with selling price of up to RM 19,000 per tonne (USD 500 per 100 g; The Star, 2003).

Conventional methods for preparation of amorphous silica requires the use of high temperature (in the excess of 1500°C) and pressure for extracting silicon in pure form from natural deposits of quartzite rock or quartz sand, such as through the thermal decomposition technique and vapour-phase reaction (Tanner et al., 2000; Wu et al., 2000; Sadasivan et al., 1998, Bogush et al., 1988 and Dielt et al., 1981). Quartz sand is used as the raw material as it is the second most common mineral on earth, therefore making it the most common form of crystalline silica. Another preparation method is the sol-gel process but it involves high raw materials cost (Tomozawa et al., 2001). Such preparation methods results in extremely high production costs, which is subsequently reflected in its high market price.

Rice husk is found to contain amorphous silica in the range of 20 – 25 wt% (Hamad, 1981 – 1982; Hanna et al., 1984; Patel et al., 1987; Nakata et al., 1989; Real et al., 1996; Liou, 2004), which upon thermal degradation yields an ash product with an excess of 95 wt% silica. In addition, rice husk is a form of waste from the rice milling industries and is produced in abundance around the country. The amorphous nature of silica in rice husk makes it extractable at a lower temperature range (Kalapathy et al., 2002) and hence, thermal treatment of rice husk to produce amorphous silica is viewed as a more economical process having the potential to replace the conventional high temperature processes. This is because thermal treatment of rice husk actually produces energy instead of consuming energy. The energy produced could be recovered in the form of heat or electricity.

1.2.2 Rice Husk as Silica Source

The presence of silica in rice husk has been discovered as far back as 1938 (Martin, 1938; Chandrasekhar et al., 2003) while its recovery potential had been realised since 1984 (Kaupp, 1984). It is considered a good source of silica having the potential for large-scale production due to the following reasons:-

a) High Silica Content with Amorphous Characteristic

Rice husk contains silica in the range of 20 – 25 wt% (Real et al., 1996; Patel et al., 1987, Conradt et al., 1992 and Chouhan et al., 2000). The silica (SiO_2) in rice husk exists in the hydrated amorphous form like silica gel. Thermal degradation and pyrolysis of rice husk, followed by combustion of the char, result in a highly porous and amorphous silica particulate mass with a varying percentage of unburnt carbon (Kapur, 1985). Combusted at moderate temperature, the white ash obtained from rice husk contains approximately 92 – 97 wt% amorphous silica (Mishra et al., 1985 and Chakraverty et al., 1988) and some amount of metallic impurities that can be further removed by a simple acid-leaching treatment. Other studies consistently reported that rice husk ash contains very high silica content such as Armesto et al. (2002) (87.7 wt% as SiO_2), Liou (2004) (>90 wt% silica), Kapur (1985) (>95 wt% silica) and Houston (1972) (87 – 97 wt% silica).

b) Abundant and Cheap Source of Silica

Rice is cultivated in more than 75 countries (Natarajan et al., 1998a) and over 97% of rice husk are generated in developing countries (Armesto et al., 2002). Rice husk accounted for 14 – 35 wt% of the paddy harvested, depending on the variety, with an average of 20 wt% (Jenkins, 1989 and Mahin, 1986). Thus, worldwide annual husk output is estimated at 80 million tonnes (Kapur, 1985).

Closer to home, the annual paddy output in Malaysia, up to 2003, was 2.26 million tonnes (Department of Statistics Malaysia) and considering rice husk accounted for 22% of this value, the amount of rice husk generated was approximately 0.5 million tonnes per annum. Rice husk is considered as a form of waste from rice milling processes and are often left to rot slowly in the field or burnt in the open. Although a

small portion of the rice husk is used as a component in animal beddings, the fact that it is a cheap and abundant source of silica remains largely unrealised. To some extent, rice husk has been utilised as fuel for cooking and parboiling of paddy rice in some developing country, but it is neither fully nor efficiently utilised. Such under-utilisation clearly shows the wastage and loss of resources which in reality could generate revenue through the recovery of silica via methods such as combustion.

Kaupp (1984) noted that the ash content of approximately 20 wt% in rice husk (which comprise of over 95 wt% silica) would make rice husk utilisation systems become very economically attractive. According to Kapur (1985), when rice husk is burnt under controlled conditions, the resulting ash is easily the cheapest bulk source of highly reactive silica with a BET (Brunauer, Emmett and Teller method) surface area which can be as high as 80 m²/g or more. Further, since the ash is obtained as a fine powder, it does not require further grinding (James and Rao, 1986) and thus, making it the most economical source of nanoscale silica (Liou, 2004).

c) Quality of Silica Comparable with Other Expensive Sources of Silica

As reviewed by Real et al. (1996), a number of published literatures (such as Mishra et al., 1985; Chakraverty et al., 1988; and James and Rao, 1986) had concluded that rice husk are an excellent source of high-grade amorphous silica. The silica obtained from rice husk ash is a good material for synthesis of very pure silicon (Amick et al., 1980; Amick, 1982 and Hunt et al., 1984), silicon nitride (Real et al., 1996; Yalçın and Sevinç, 2001), silicon carbide (Krishnarao and Subrahmayam, 1995; Gorthy and Pudukottah, 1999) and magnesium silicide (Ghosh et al., 1991). In addition, this silica has been claimed (Amick, 1982; Chakraverty et al., 1985; and Hunt et al., 1984) to be an excellent source of very pure silicon, useful for manufacturing solar cells for photovoltaic power generation and semiconductors. In the manufacture of silicon carbide from rice husk silica, the processing temperature could be lowered to 1500°C due to the high surface area and intimate contact available from carbon and silica in rice husk. This is considered to be less energy-intensive compared to conventional methods using coal and quartz sand in electric furnaces (Hanna et al., 1984), whereby the processing temperatures are in the order of 2500°C. With silica content in the excess of 95 wt%, rice husk ash can also be used as a substitute for silica in cement manufacture. Preliminary study conducted by Ajiwe et al. (2000)

showed that the produced cement had similar standard compared to commercial cement.

d) Disposal Problem

The current practices to dispose of the large quantities of rice husk through open burning or rotting in field are not environmental-friendly. Open burning results in air pollution with the formation of smoke and particulate matters in the form of char and ash. Rotting in field, on the other hand, results in formation of methane (CH₄), which is a potent greenhouse gas. Combustion of biomass such as rice husk can actually reduce the greenhouse effect by converting emissions that would have been methane into the less potent greenhouse gas carbon dioxide. Since CH₄ is some 25 times more potent as a greenhouse gas than carbon dioxide (CO₂), and since the two gases have similar atmospheric residence times, trading off CH₄ emissions for CO₂ emissions from combustion leads to a large net reduction of the greenhouse effect associated with the disposal of rice husk. Rotting in the field leads to a slow decay of the material, with eventual emissions of approximately equal amount of CH₄ and CO₂ from the carbon that is released during the decay (Morris et al., 1991).

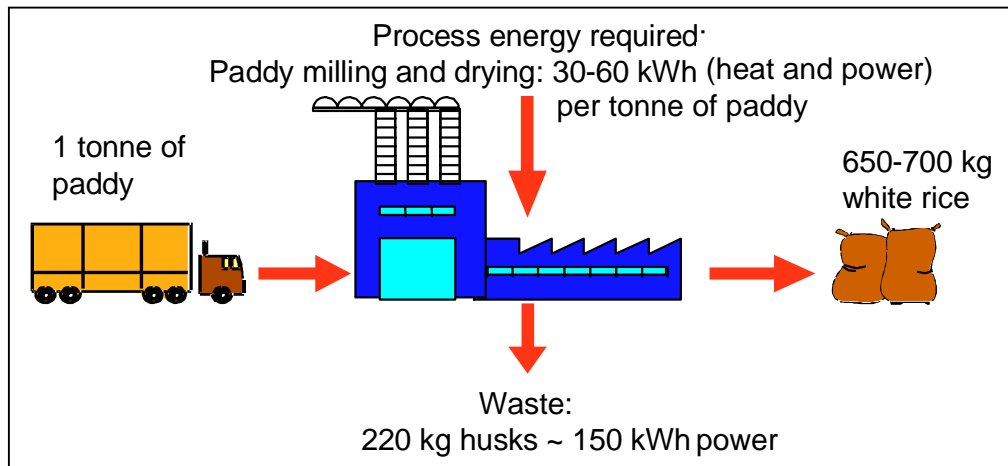
e) High Energy Content

Rice husk has an average lower heating value (LHV) of 13 – 16 MJ/kg (Jenkins, 1989; Mahin, 1986 and Kapur, 1985). Comparisons by Natarajan et al. (1998a) indicated that the LHV of rice husk is about one-third that of furnace oil, one-half that of good quality coal and comparable with sawdust, lignite and peat. It was also reported that the world annual energy potential of rice husk is 1.2×10^9 GJ, with a corresponding heating value of 15 MJ/kg. Thus, rice husk is a good renewable energy source. Apart from solving its disposal problems, combustion offers the potential for energy recovery from this waste.

In Malaysia, with a reported annual generation rate of rice husk at 0.424 million tonnes in the year 2000, the potential energy generation from rice mills is 263 GWh per annum. This translates to a potential capacity of 30 MW (National Energy Balance Malaysia Year 2000 Report). The pressure to search for renewable energy sources is mounting due to the depletion of fossil fuels and the rapid increase in

energy demand, from 25,558 toe (tonne of oil equivalent or equivalent to 42 GJ of lower heating value) in 1998 to 31,515 toe in 2001 (National Energy Balance Malaysia Reports for Year 1998 and 2001). In the Eighth Malaysia Plan (2001 – 2005), the Government replaces the Four-Fuel Diversification Policy with the new Five-Fuel Diversification Policy, which adds renewable energy as a potential source alongside existing four fuels utilised for power generation (oil, gas, coal and hydro). The renewable energy focus is on biomass and the target contribution towards the total electricity generation mix is 5% by 2005 and 10% by 2010. Utilising only 5% of renewable energy could save the country RM5 billion over five years (NSTP, 29th June 2002).

The use of rice husk as renewable energy has already been practised in Malaysia, whereby Bernas and a private rice miller operate a few small (< 1 MW) rice husk cogeneration plants to produce electricity and steam for paddy drying. As shown in Figure 1-1, milling of 1 tonne of paddy produces about 220 kg of rice husk or equivalent to approximately 150 kWh of potential power. In the year 1997, a Full-Scale Demonstration Project (FSDP) under COGEN 3 using rice husk as fuel had been implemented in Ban Heng Bee Rice Mill (1952) Sdn. Bhd. with the commissioning of its 450 kW rice husk-fired cogeneration plant. COGEN 3 is the third phase of the EC-ASEAN cooperation programme initiated by the European Commission (EC) and the Association of South-East Asian Nations (ASEAN). It is financed by the European Commission. COGEN 3 accelerates the implementation of proven, clean and efficient cogeneration projects using biomass, coal or gas as fuel. The projects are implemented through partnerships between ASEAN industrial companies and European equipment suppliers.



Source: EC-ASEAN COGEN Programme

Figure 1-1: Power generation potential from rice husk mills

1.2.3 Market Review for Amorphous Silica from Rice Husk Ash

Currently, the two major commercial applications for amorphous silica from rice husk ash (RHA) are as pozzolan in the cement industry and for manufacture of sodium silicate in the fine chemicals industry. It can also be used in the steel industry as insulator during the steel casting process. However, since it will transform into crystalline form at the end of the steel making process due to prolonged heating at high temperatures (i.e. 1500°C for 4 hours), it is more economically-feasible to use crystalline rice husk ash for such purpose since the price of amorphous ash is higher compared to crystalline ash. The market for crystalline ash (up to 1.0 wt% crystals, carbon content 2.5 – 5.0 wt%) in the steel industry is well-established, with an average price of RM 570 per tonne (USD 150 per tonne) (Bronzeoak, 2003).

a) Cement Industry

Amorphous RHA has been widely researched as mineral cement replacement material (MCRM). The two main research areas for the utilisation of RHA in the cement industry are in the manufacture of low cost building blocks and in the production of high quality cement. Traditionally, silica fume, which is a byproduct

of metallurgical industry, is used for exactly the same purpose but its supply is becoming limited and expensive for developing economies. The current price of silica fume is reported to be RM 4,560 per tonne (USD 1,200 per tonne) in India (Torftech News, 24th November 2003).

Research such as that conducted at FEUP (Faculdade de Engenharia, Universidade do Porto or Faculty of Engineering of University of Porto) in Portugal had shown that RHA concrete performed better than silica fume concrete. Further, studies by Nehdi et al. (2003) showed that depending on the addition rate, RHA increased the compressive strength of concrete by up to 40% at 56 days and was thus deemed superior compared to silica fume. They also concluded that the performance of RHA in reducing the rapid chloride penetrability of concrete was comparable to silica fume and was slightly more efficient than silica fume in resisting surface scaling due to deicing salts. Preliminary studies conducted by Ajiwe et al. (2000) also showed that RHA-formulated cement (RHA substitution of 24.5 wt%, based on the analysis by Bogue (1989) that the theoretical percentage fraction of silica in tricalcium silicate or Portland cement was 26.3 wt%) had similar standard in terms of its compressive strength and setting time compared to commercial cement.

The market of RHA for cement industry is not as well-developed as steel, but there is a great potential due to the pozzolanic properties of RHA that are comparable to cement. The potential is also driven by the absence of any health issues associated with the use of crystalline ash (as in the steel industry) due to the use of amorphous ash. In the United States of America, RHA has already been used commercially by Pittsburg Mineral & Environmental Tech. Inc. (PMET) which is part of Alchemix Corporation, Arizona, as a substitute for silica fume in the production of specialist concrete. PMET specifies that the RHA for use as substitute for silica fume should contain less than 1% of crystalline silica (>99% amorphous), carbon content less than 6% and mean particle size of 7 – 9 μm (passing 45 μm sieve). The current market prices for RHA sold to the cement industry were shown in Table 1-1. The price could reach as high as RM 2,280 per tonne (USD 600 per tonne) for high quality amorphous RHA with more than 85% silica content.

Table 1-1: Market prices for amorphous rice husk ash for use in cement industry

No.	Source/Reference	Price (per tonne)		Remarks
		RM	USD	
1	Torftech Application Description (August 2002)	1,140	300	-
2	The Hindu Newspaper (19 th January 2003)	1,900 – 2,280	500 – 600	Price for super pozzolana (RHA containing high silica content in the excess of 85%)

b) Fine Chemicals Industry

The emerging use of amorphous RHA is for the manufacture of water glass (sodium silicate or Na_2SiO_3), which in turn is an intermediate raw material for synthesis of a wide array of fine chemicals. The current market price for water glass is RM 2,100 per tonne (USD 550 per tonne, Chemical Market Reporter, 18th January 1999).

The conventional process of manufacturing sodium silicate is through the fusion of silica sand with high-purity soda ash in furnaces at high temperatures (1300 – 1500°C), forming water glass (a solid) which is then crushed and dissolved in water and digested under pressure with steam. According to Stephens et al. (2003), the production of water glass through this route formed the foundation of all commercial processes for making sodium or other soluble silicate solutions today. Both the high-temperature fusion and high-temperature and pressure digestion processes are very energy-intensive, thus very expensive. In addition, the silicates produced generally contain metal contaminants found in the earth in amounts ranging from 400 to 10,000 ppm.

The potential for obtaining this expensive sodium silicate solution through the relatively less costly process of caustic digestion of RHA had been reported by Stephens et al. (2003). In their patent (U.S. Patent No. 6,638,354) describing the synthesis of precipitated silicas and silica gels (with and without deposited carbon), the sodium silicate solution required for the synthesis was obtained from digestion of amorphous RHA in a caustic solution of sodium hydroxide. Maintaining the amorphous structure in the RHA is important for its use in the synthesis of chemicals as the silica maintains a porous skeletal structure which provides better chemical reactivity and solubility, especially during operations such as caustic

digestion of the ash (Stephens et al., 2003). Nonetheless, some crystalline silica in the ash could be accommodated by manipulating the variables during the caustic digestion process, such as the temperature and pressure. The unique advantage of synthesising sodium silicate from RHA is that the inherent carbon molecules present as residual carbon in the RHA act like 'activated carbon' to absorb or react with colour forming agents to produce a clear, homogeneous solution (Rieber et al., 2003). This eliminates the necessity for addition of carbon black, as with other processes, to absorb the polyvalent metals, organic metals and other impurities that is originally present in rice husk. The residual carbon content in the RHA was preferably in the range of 2 – 8 wt% although excess carbon (up to 40 wt%) is not harmful to the digestion process, whereas the minimum amount is 1 wt% (Rieber et al., 2003). Another added bonus of this synthesis method is that the activated carbonaceous material and concentrated manganese converted from the oxide or silicate of the biogenic silica (RHA contains 0.1 – 0.2% MnO) in the residue from the filtration stage are side products which have commercial applications.

1.2.4 Evaluation on Available Technologies for Production of Amorphous Silica from Rice Husk

Screening for the available methods or technologies showed that amorphous silica could be produced from rice husk through alkaline extraction or heat treatment in various thermal treatment technologies (inclined step-grate furnace, cyclonic furnace, muffle furnace, fixed bed, rotary kiln and tubular reactor), as shown in Table 1-2.

Table 1-2: Existing methods and technologies for preparation of amorphous silica from rice husk

Method / Technology	Descriptions	Reference(s)
Alkaline extraction	Sodium hydroxide (NaOH) was added to rice husk ash and the mixture boiled in a covered Erlenmeyer flask for 1 hour with constant stirring. The solution was then filtered through ashless filter paper and the residue (carbon) was removed. The filtrate formed was sodium silicate, which was cooled to room temperature and titrated very slowly with acid (hydrochloric acid, HCl or sulphuric acid, H ₂ SO ₄) with constant stirring until pH 7. The solution was aged for 18 hours at room temperature to form gel (silica).	Kamath and Proctor (1998), Kalapathy et al. (2000) and Kalapathy et al. (2002)
Inclined (stepped or perforated) grate furnace	Rice husk was fed at the top of the grate while the air flowed from the bottom.	Beagle (1974)
Cyclonic furnace	Rice husk was burnt at a temperature of less than 700°C to produce amorphous silica with a residual carbon content ranging from 12 – 14 wt%.	Pitt (1976)
Muffle / electric furnace	Silica from rice husk ash was prepared by heating rice husk in a laboratory muffle furnace and a fixed bed combustor at temperatures ranging from 500 – 1150°C.	Hamad and Khattab (1981)
	Raw and acid-leached (at 75°C for 1 hour) rice husk were combusted in a vertical electric furnace at temperatures of 500 – 750°C. Amorphous silica which was complete white in colour could be obtained from the acid-leached rice husk at a husk bed temperature of up to 720°C.	Chakraverty and Kaleemullah (1991)
	Heating of rice husk in a thermal gravimetric column at 600 – 800°C for 3 hours under helium flow, followed by combustion of the residual carbon under a pure oxygen flow.	Real et al. (1996)
	Rice husk was burned in a muffle furnace at 600°C for 4 hours in static air and in a stainless steel tubular reactor placed in a muffle furnace at 600°C in various flowing atmospheres (i.e argon and oxygen, air or oxygen).	Yalçın and Sevinç (2001)
	Active silica with high specific surface area could be produced after heat-treating at 700°C for 6 hours in air in an electric oven.	Della et al. (2002)
Rotary kiln	Rice husk was carbonised in a first rotary kiln heated to 300 – 400°C, then charged into a second rotary kiln heated at 600°C.	Sugita (1994)
Tubular reactor	Rice husk was heated in tubular reactor made of quartz at temperatures between 27 – 727°C.	Liou (2004)

The alkaline extraction method is capable of producing high purity silica but involves a significant amount of time (1 – 2 days) and a high number of steps with the use of various chemicals, thus resulting in expensive production cost. In addition, the starting material for the alkaline extraction method is carbonaceous rice husk ash containing for example, 61 wt% silica and 36 wt% carbon (Kamath and Proctor, 1998), whereby the rice husk need to be subjected first to a carbonisation step to remove the organic constituents of cellulose, hemicellulose and lignin. On the other hand, the major concerns associated with the use of heat treatment are the risk of silica crystallisation in the rice husk ash due to exposure to high temperature, low carbon conversion efficiency and long reaction time. Conventional furnace systems used to burn rice husk have poor performance especially in terms of the resulting ash quality and combustion behaviour. Rice husk is one of the more difficult fuels to burn due to its peculiar silica-wood composite morphological structure, high mineral content, large bulk volume and a pronounced tendency to cake and agglomerate easily (Kapur, 1985). In addition, it does not combust easily or cleanly, is flame retarding and is either self-extinguishing or smoky at low temperatures (Beagle, 1978; and Kaupp and Goss, 1981 – 1982).

Three thermal treatment technologies which had been widely used to produce amorphous silica from rice husk are muffle furnace, rotary kiln and stepped grate furnace. The fluidised bed technology had been used for combustion of rice husk as early as 1980 (Peel and Santos, 1980) but not for the purpose of producing amorphous silica. However, the fluidised bed technology is capable of achieving high carbon conversion efficiency at moderate operating temperatures (below the crystallisation point of silica in rice husk ash) at rapid reaction times, which are the characteristics necessary in overcoming the the major concerns in heat treatment of rice husk as discussed previously. As such, evaluations were conducted on these four technologies and the results were as follows:-

a) Muffle Furnace

The major disadvantages of this method for thermal treatment of rice husk are its high energy consumption (electrical power), batch-like process, absence of mixing amongst the reactants, low production rate, long reaction time and risk of explosion. To maintain

the temperature in the range of 600 – 700°C for the conversion process to take place, substantial heat need to be supplied through electrical heating. There is no mixing between the reactants (rice husk and oxygen) to increase the rates of mass and heat transfer, and therefore the rice husk feed has to be spread as a very thin layer inside the furnace to ensure sufficient oxygen transfer on a micro-level. This in turn limits the amount of rice husk that could be processed at any one time. For example, a batch of 800 g of rice husk required a total time of 10 hours to obtain white ash with high reactivity (amorphous) (Sugita, 1994). It was a two-stage method, namely carbonisation (maintaining furnace temperature at 280°C for 1.5 hours and 350°C for another 1.5 hours) and incineration or combustion (maintaining furnace temperature at 400 – 800°C for 2 hours) before discharging the ash 5 hours later. The production rate of ash, therefore, is approximately 16 g/hr (assuming ash content of 20% in rice husk).

The absence of mixing also resulted in the formation of ash with intact skeleton-like shape, which tends to entrap any unburnt carbon and makes it difficult to be oxidised. Since the process is taking place in a closed system, the absence of free-flowing oxygen also resulted in incomplete oxidation of carbon in the husk. To prevent the risk of crystallisation, the furnace need to be operated at a lower temperature range (such as 400 – 600°C), which in turn required a long residence time (3 – 6 hours) in order to achieve high carbon conversion efficiency. Rice husk contains a high amount of volatiles (in the excess of 60 wt%, wet basis) and the sudden release of these volatiles upon exposure to high temperature in a closed system such as that of the muffle furnace might pose the risk of explosion.

b) Rotary Kiln

The use of rotary kiln for producing amorphous silica from rice husk is an innovation on the muffle furnace concept in order to provide some degree of mixing to the rice husk and to overcome the batch-like process. The system, which comprises two rotary kilns in tandem, was patented by Sugita (1994) in 1994 and offers a continuous method for producing amorphous rice husk ash. The upstream rotary kiln is heated by a burner, electrical heater or other heat source to 300 – 400°C to carbonise the rice husk. The

carbonised rice husk is then fed into the downstream rotary kiln to be burnt into ash at about 600°C. However, its major disadvantages, some of which are similar to the muffle furnace, are as follows:-

- i) Requires temperature of at least 850°C (typically 1000°C) to achieve self-sustainable combustion;
- ii) Combustion at temperatures less than 700°C (to prevent crystallisation of ash) need to be sustained by auxiliary fuel;
- iii) High possibility of run-away reaction during char-combustion stage;
- iv) Long reaction time;
- v) High energy consumption;
- vi) Inferior mixing and possibility of hot-spots formation.

c) Inclined Grate Furnace

The inclined step-grate type furnace is used almost universally for burning of rice husk. One disadvantage of this technology is the non-uniformity in fuel-to-air ratio due to the non-uniform loading of husk into the furnace (Natarajan et al., 1998a). This leads to a significant amount of unburnt carbon in the ash and a considerable loss in efficiency. However, the most prominent disadvantage is that it produces rice husk ash of a poor quality with 10 – 30 wt% carbon content (Hamad, 1981 – 1982), and in the worst cases, the ash is a mixture of char containing up to 50 wt% combustible matter and hard-burnt crystalline ash. Also, the presence of localised hot-spots in the combustion chamber resulted in the formation of inert fused lumps. Thus, the erratic ash quality represents a major obstacle to the profitable utilisation of silica in rice husk ash.

d) Fluidised Bed

The fluidised bed technology is capable of overcoming all the disadvantages associated with the use of muffle furnace, rotary kiln and inclined grate furnace for the production of amorphous silica. It offers a continuous and self-sustaining process without the need for auxiliary fuel, except during the brief start-up period. In fact, the combustion of rice husk in fluidised bed offers an added bonus of heat recovery. The reaction time is also very rapid (in the order of minutes), thus increasing the production rate significantly. The

turbulent bubbling action in the sand bed provides a high degree of mixing between the reactants and more importantly aids in breaking down the rigid skeleton-like structure of the ash. The high level of turbulence in the bed also eliminated the formation of hot-spots and leads to uniform temperature distribution within the bed region.

1.2.5 Fluidised Bed as Selected Technology

Based on the technology evaluations in the previous section, the fluidised bed technology is selected for the production of amorphous silica from rice husk. The key factors are as follows:-

a) Uniform Temperature Distribution

The bubbling action in the fluidised bed provides a high degree of turbulence and mixing in the bed region, which results in high heat transfer rates within the bed. Therefore, the heat evolved during the combustion process is distributed uniformly within the bed, with temperature variations within the bed region typically not exceeding 5 – 8°C (Niessen, 1995). The formation of hot-spots is thus eliminated. The presence of hot-spots in the combustion zone poses the risk crystallising the silica in the rice husk ash. In addition, the high rates of heat transfer also leads to high combustion efficiency. As such, the combustion temperatures can be kept low, typically in the range of 600 – 800°C while enabling autogenous combustion to take place compared to other types of combustors (for example the inclined grate system).

b) Lower Operating Temperature Range

The lower range of operating temperatures in the fluidised bed is also very important for the following reasons:-

- i) **To prevent the crystallisation of rice husk ash** – Operating at temperatures in the excess of 700°C might expose the silica in the ash to the risk of crystallisation.
- ii) **The formation of nitrogen oxides (NO_x) can be minimised** – The rate of formation of thermal NO_x is highly temperature sensitive, becoming rapid only at

flame temperatures (in the range of 1650 – 2000°C). Combustion at temperatures well below 1300°C forms much smaller concentrations of thermal NO_x.

- iii) **To prevent slagging and fouling problems** – The presence of alkali metals in rice husk ash, in particular potassium and sodium compounds (K₂O and Na₂O) cause the ash to remain sticky at much lower temperature than the melting point of ash. Sodium and potassium salts react with silica in the ash to form eutectic mixtures having low melting points. The melting point of these eutectic mixtures might be as low as 600 – 700°C at high concentration of sodium or potassium (Armesto et al., 2002). The low ash fusion temperature resulted in the adhesion of particles which can lead to excessive slagging and fouling problems.

c) Rapid Reaction Time

When the rice husk particles are introduced into the hot bubbling fluidised bed region, their drying and devolatilisation reactions (both endothermic) occur instantaneously. Most of the volatile constituents in rice husk are released while the remaining char particles are oxidised within the bed to provide heat source for the endothermic reactions. The intense abrasive action of the turbulent bubbling bed tends to remove any surface deposits (char or ash) from the rice husk particles, thus continuously exposing a ‘clean’ reaction surface to the surrounding hot gases. Due to the change in bulk density, the char particles are entrained into the freeboard region where they spend a few seconds undergoing further oxidation process. Besides, the char and ash particles are brittle and are easily broken down into smaller fragments by the abrasive action of the bubbling bed, making them more easily entrained to the freeboard region. As a result, the residence time of rice husk in the fluidised bed is only in the order of a few minutes compared to hours in other types of thermal treatment systems. Such rapid reaction time increases the throughput value of rice husk in the combustor and subsequently the production rate of ash.

d) High Carbon Conversion Efficiency

The residual carbon content in the rice husk ash after being thermally-treated in various types of combustors or furnaces was tabulated in Table 1-3. Based on these data, it was

observed that fluidised bed gives the highest carbon conversion efficiency, i.e. as high as 99%.

Table 1-3: Performance of existing thermal treatment technologies in producing low carbon content rice husk ash

Technology	Reference	Residual Carbon in Ash (wt%)
Heating in electric furnace	Patent No. 4,049,464 (Tutsek et al., 1977)	2 – 3
Cyclonic furnace	Patent No. 3,959,007 (Pitt, 1976 and 1994)	12 – 14
	Swasdisevi et al. (2000)	3 – 11
Tube furnace	Patent No. 6,444,186 (Vempati, 2002)	< 3
Fluidised bed	Bhattacharya et al. (1984)	2
	Preto et al. (1987)	1 – 4
	Bhattacharya and Wu (1989)	1 – 3

e) High Combustion Intensity

Rice husk has high ash content (16 wt% dry-ash-free), low bulk density (approximately 100 kg/m³), poor flow characteristics and low ash melting point that render it unsuitable to be burned in conventional combustion systems, such as inclined grate furnaces. Beagle (1974) reported that in general, traditional methods of rice husk combustion in inclined (stepped or perforated) grate furnaces are quite inefficient and convert about half the energy available in the husk. Moreover, the furnace area required is quite large. According to Bhattacharya et al. (1984), a combustion intensity of as high as 530 kg/h/m² could be achieved in a fluidised bed reactor, compared to a maximum combustion intensity of about 70 kg/h/m² achievable in grate type furnace (Singh et al., 1980). Thus, the combustion intensity in a fluidised bed is approximately 7.5 times higher than the maximum possible combustion intensity in a grate type furnace per unit grate area. In addition, the combustion intensity in a fluidised bed increased with bed height due to increase in bed volume, as reported by Bhattacharya et al. (1984).

f) Ash Composition and Its Removal

Rice husk ash also has a rigid skeleton-like structure due to its high silica content, resulting in a considerable amount of carbon being trapped in the skeleton and cannot be burned or gasified. Due to its high silica content, carbon in rice husk char is located in points which are interlaced with silica so that access to carbon is difficult (Mukunda et al., 1996). In order to obviate this problem, rice husk could be pulverised prior to thermal treatment but this in turn led to the increase in operation cost, health risk associated with the handling of powdered rice husk and operational hazard in the form of dust explosion. In a fluidised bed, the turbulence due to fluidisation in the bed can break the rigid ash skeleton to make the trapped carbon available for conversion. Simultaneous attrition of ash particles in the fluidised bed resulted in smaller ash particles compared to that obtained from a grate type furnace (Bhattacharya et al., 1984). The ash produced is fine with sizes less than 375 μm , which can be easily elutriated out of bed even by a low fluidisation velocity (Preto et al., 1987) of about 0.54 m/s. Therefore, the ash can easily be removed from the fluidised bed by entrainment in the gas stream, from which it can be separated by a particle separating system such as a cyclone.

Further, according to a study performed by Black and Veatch (2000) to determine the most suitable technology for thermal treatment of various biomass, fluidised bed was given a high rating for rice husk, followed by the stoker system or pulverised fuel suspension-fired system (medium rating). This review showed that the fluidised bed is the best candidate for burning rice husk.

1.2.6 Types of Fluidised Bed

There are four variants of fluidised bed, namely the bubbling fluidised bed, spouted bed, circulating fluidised bed and spinning fluidised bed. The spinning fluidised bed is a novel concept and is a relatively new variant of fluidised bed, which had only been used for combustion of sludges (Rozainee, 1998 and Wong et al., 2000). Study on

the combustion of biomass in particular rice husk has not been reported. The application of circulating fluidised bed for rice husk is limited to the purpose of power generation through gasification (Leung et al., 2001 and Yin et al., 2002) and had only been used more recently for the combustion of rice husk (Fang et al., 2004). The circulating fluidised bed is operated at high fluidising velocities whereby the fly ash and bed media (usually sand) is mixed and circulated in a closed-loop, which rendered the collection of the final ash product very difficult.

Meanwhile, the investigations of rice husk combustion in fluidised bed and spouted bed had been conducted since 1980 (Peel and Santos, 1980) and 1987 (Bhattacharya and Shah, 1987), respectively. Studies on the selection of the most suitable type of fluidised bed for combustion of rice husk had been conducted in UTM (Environmental Engineering Group) since the year 1999 using an 80-mm inner diameter fluidised bed. Results showed that the bubbling fluidised bed is more suitable for the combustion of rice husk due to the weaknesses in the spouted bed, which were as follows:-

- i) **Poor mixing behaviour.** The circulation pattern of rice husk and sand in the bed is lost due to the build-up of rice husk at the annulus (outer ring) region of the spouted bed. This led to the stratification of the bed as the rice husk could not penetrate the spout (central region) to be distributed uniformly in the sand bed. The high velocity at the spout of the spouted bed causes fast movement of sand but at the annulus region, the movement of the sand is only due to the gravitational force. On the other hand, the fluidising air is distributed evenly in the bubbling fluidised bed and thus, the whole bed has the necessary driving force to mix the bed and rice husk particles uniformly.
- ii) **Poor combustion behaviour due to the bad mixing behaviour.** Sustainable burning is very difficult to be achieved during combustion of rice husk in the spouted bed due to uneven distribution of heat in the bed and also the rapid build-up of unburnt rice husk at the annulus region. Studies on the combustion of palm wastes (Lim, 2002) showed that oxygen distribution in the spouted bed was

- uneven and burning only occurred at the spout and freeboard region, where the oxygen concentration was high. He further concluded that combustion was more complete in the bubbling fluidised bed due to the even distribution of oxygen in the entire bed.
- iii) **Narrower operating range.** The minimum spouting velocity (U_{ms}) is dependant on the static bed height of the spouted bed and correspondingly, each static bed height has a maximum spoutable bed height. Beyond the maximum spoutable bed height, the entire bed is characterised by a combination of slugging, spout blockage and fluidisation on the upper surface of the bed (San José et al., 1996). This phenomenon directly affects the throughput value (rate of rice husk feeding). In his studies on the combustion of palm wastes, Lim (2002) showed that the bubbling fluidised bed had a much higher turndown ratio (up to 2.3) compared to a spouted bed (turndown ratio of up to 1.4 only) as the bubbling fluidised bed could be operated at higher U_{mf} numbers.
- iv) **Lower combustion efficiency.** Studies on the combustion of palm wastes (Lim, 2002) showed that the bubbling fluidised bed has higher combustion efficiency (up to 80%) compared to the spouted bed (with combustion efficiency of up to 60% only).

Hence, in this research, the bubbling fluidised bed is selected as the thermal treatment of choice for producing amorphous silica from rice husk. Throughout this thesis, the term 'fluidised bed' is used to refer to bubbling fluidised bed, unless otherwise specified.

1.3 Objectives of Research

This research is aimed at recovering amorphous silica via combustion of rice husk in fluidised bed. The objectives of this research works are:-

- a) To design and develop a pilot scale fluidized bed combustion system.
- b) To determine the optimum mixing parameters for combustion of rice husk in fluidised bed;
- c) To determine the optimum combustion parameters for high combustion efficiency of rice husk in fluidised bed;
- d) To determine the optimum ash quality for production of amorphous silica from rice husk in fluidised bed; and
- e) To determine the optimum fluidised bed combustor design to overcome existing problems during combustion of rice husk in fluidised bed.

1.4 Scopes of Research

The scopes of work for this research are:-

a) To investigate the basic combustion characteristics of rice husk

The experiments will be carried out in a muffle furnace to determine the following parameters:-

- i) Time for complete combustion of rice husk to liberate carbon-free, siliceous ash
- ii) Time-temperature relationship for onset of silica crystallisation in rice husk ash

b) To investigate the optimum fluidisation parameters to achieve good mixing of rice husk in fluidised bed

The experiments will be carried out in an 80-mm inner diameter fluidised bed column made of transparent Perspex material to determine the following parameters:-

- i) Sand size
- ii) Fluidising velocity

- iii) Static bed height
- c) To investigate the optimum mixing parameters for good combustion efficiency of rice husk in fluidised bed**

The experiments will be carried out in an 80-mm inner diameter fluidised bed combustor to determine the following parameters:-

- i) Sand size
- ii) Fluidising velocity
- iii) Static bed height

The 80-mm inner diameter fluidised bed combustor is used because it is equipped with a glass section at the bottom of the combustor, which enables viewing of the mixing behaviours of rice husk in the bed during experiments.

- d) To investigate the optimum combustion parameters to achieve high combustion efficiency of rice husk in fluidised bed**

The experiments will be carried out in a 210-mm inner diameter fluidised bed combustor to determine the following parameters:-

- i) Temperature (bed temperature, freeboard temperature and effect of combustor heat loss)
- ii) Air supply (primary air factor, primary-to-secondary air ratio and pneumatic air feeding velocity)
- iii) Effect of rice husk washing
- iv) Effect of rice husk moisture content
- v) Feeding design

In scopes (c) and (d), the optimum combustion parameters will be determined based on the following qualities of the resulting rice husk ash:-

- i) Silica structure and contamination with carry-over sand via X-Ray Diffraction (XRD) analysis
- ii) Carbon content via loss on ignition test
- iii) Particle size distribution via sieve analysis

- e) **To investigate the optimum fluidised bed combustor design to overcome the problems of sand contamination and to improve carbon burnout in the siliceous ash product**

Computational Fluid Dynamics (CFD) modelling using the programme code of FLUENT will be carried out to determine the following parameters:-

- i) Freeboard height
- ii) Feeding conditions (feeding velocity and inclusion of vortex flow)

- f) **To design, fabricate, install and commission a pilot scale fluidized bed combustion system**

To apply the optimum set of operating parameters for production of amorphous siliceous ash obtained from experiments conducted in a 210 mm fluidised bed combustor and recommendations from Computational Fluid Dynamics (CFD) modelling to design, fabricate, install and commission a pilot-scale fluidised bed combustion system.

1.5 Expected Results

To meet the objectives of this research, the following results are expected to be obtained:-

- a) Minimum residence time required for complete combustion of rice husk particles to liberate carbon-free, siliceous ash.
- b) Upper limits of temperature-residence time combinations during combustion of rice husk to maintain amorphous structure in the resulting ash.
- c) Optimum sand size, fluidising velocity and static bed height to achieve good mixing behaviour in fluidised bed for combustion of rice husk.

- d) Optimum temperature, air supply, type of rice husk feed, moisture content of rice husk and feeding design to achieve high combustion efficiency of rice husk in fluidised bed.
- e) Optimum ash quality (silica structure, carbon content and particle size) that could be produced from combustion of rice husk in fluidised bed.
- f) Optimum fluidised bed freeboard height and feeding conditions (feeding velocity and presence of vortex flow) to prevent sand contamination and to improve carbon burnout in the ash.

1.6 Layout of the Report

This report describes the research work to develop a pilot fluidized bed combustion system for production of amorphous silica from rice husk. This work includes the investigation of the mixing and combustion characteristics of rice husk in two fluidised beds combustors (having inner diameters of 80mm and 210mm, respectively) to determine the optimum operating parameters to obtain amorphous, carbon-free siliceous ash. Computational fluid dynamics (CFD) modelling was also carried out to determine the optimum fluidised bed design to overcome the problems associated with the operation of both fluidised bed combustors used in this research. Design, fabricate, install and commission the pilot plant.

Chapter 2 provides the history of research on combustion of rice husk in fluidised bed. It also reviews the previous findings on the fluidisation and combustion parameters used for combustion of rice husk in fluidised bed, including the effect of fluidised bed design on the combustion efficiency of rice husk. From this literature review, hypotheses related to the research were developed to serve as a guide for the experimental and modelling works.

Chapter 3 presents the methodology in carrying out the research, which includes the descriptions of the experimental, analytical and modelling techniques. Procedures to calculate the combustion parameters such as combustion stoichiometry and combustion temperature were also included.

Chapter 4 discusses the results of the investigation of combustion of rice husk in the fluidised bed combustors to produce amorphous, carbon-free siliceous ash. The effects of sand size, fluidising velocity and static bed height on the mixing and combustion characteristics in the 80-mm inner diameter fluidised bed combustor were discussed. Then, the effects of temperature, presence of impurities in rice husk, air supply, moisture content in rice husk and feeding design on the combustion efficiency of rice husk in the 210-mm inner diameter fluidised bed combustor were presented. Based on these experimental results, the optimum sand size, fluidising velocity, static bed height, temperature, air supply, moisture content in rice husk and feeding design for production of amorphous, carbon-free silica from rice husk were selected.

Chapter 5 discusses the CFD modelling works for design improvement of the fluidised bed combustors to overcome the problems encountered during the experimental works. The modelling works included the determination of sufficient freeboard height of the fluidised bed combustor to overcome the problem of sand contamination in the ash product and incomplete oxidation of carbon in the ash. The possibility of improving the turbulence in the freeboard region of the fluidised bed combustor was also explored through the use vortex feeding and different feeding velocities.

Chapter 6 discusses the design, fabrication, installation and commissioning of the pilot-scale fluidized bed combustion system for production of amorphous silica from rice husk based on the conclusion and recommendations from the experimental works and Computational Fluid Dynamics (CFD) modelling.

Chapter 7 provides the conclusions and recommendations. It presents the conclusions derived from this research and the recommendations for future study of combustion of rice husk in fluidised bed to produce amorphous, carbon-free silica.

CHAPTER 2

LITERATURE REVIEW

2.1 Research History on Thermal Treatment of Rice Husk in Fluidised Bed

The fluidised bed technology has been used for the thermal treatment of rice husk since the year 1980 (Peel and Santos, 1980). Previous studies on the thermal treatment of rice husk in fluidised bed include investigations on the mixing and combustion characteristics (Peel and Santos, 1980; Chen et al., 1998; Hao et al., 1995; Madhiyanon et al., 2004), combustion efficiency and ash behaviour (Bhattacharya et al., 1984; Preto et al., 1987; Bhattacharya and Wu, 1989; Armesto et al., 2002; Permchart and Kouprianov, 2004), pyrolysis (Sharma and Rao, 1999; Islam and Ani, 2000; Williams and Nugranad, 2000) and gasification (van den Arsen et al., 1982; Hiler, 1982; Xu et al., 1985; Bingyan and Zongnan, 1987; Flanigan et al., 1987; Lin et al., 1998; Hartiniati et al., 1989; Boateng et al., 1992; Sanchez and Lora, 1994; Hao et al., 1995; Mansaray et al., 1999; Ashish Bhat et al., 2001).

Thus far, no study had been reported on the combustion of rice husk in fluidised bed with the main purpose of producing amorphous, carbon-free silica. Luan and Chou (1990) had studied the recovery of silica from rice husk through gasification of rice husk mixed with coal in a modified fluidised bed with presence of a pilot flame. They found that the bottom ash contained silica as high as 89 wt%, however, no indication was provided whether the ash remained in the amorphous form. Another study by Sumran and Kongkachuichay (2003) showed that amorphous silica with high purity (99.8 wt% SiO₂) could be obtained from rice husk

via the method by Pongsak (1992), which involved pyrolysing pretreated rice husk in a fluidised bed burner at 550°C for 15 minutes under flowing nitrogen and then burned under flowing oxygen at 600°C for 3 hours. The pretreatment of rice husk involved the boiling of rice husk in 1 M HCl for 3 hours followed by rinsing with distilled water and drying at 120°C for 4 hours. This method was largely different from the current research as the rice husk was prepared under strictly-monitored conditions, which required the use of nitrogen as well as oxygen instead of the readily available air from the atmosphere. Also, the preparation time was quite long, as rice husk only requires a brief period (2 – 3 minutes) to burn to completion in an air atmosphere when exposed to the temperature range which allows for high carbon oxidation rate to take place, such as 650 – 700°C (Sen and Ghosh, 1992). A temperature of at least 500°C is required for the complete oxidation of chars (Di Blasi et al., 1999). The low temperature used in the reported method (550 – 600°C) was only slightly higher than the minimum temperature required for the complete oxidation of char, thus the need for long residence time of the rice husk in the fluidised bed.

More recently, a combined concept of muffle furnace and fluidised bed had been used by Huang et al. (2001) to obtain silica white from rice husk. However, their study was found to be largely similar to other existing studies on production of silica from rice husk in the muffle furnace except for the innovative concept of incorporating a fluidised bed as an agitator to promote mixing amongst the rice husk. In addition, the ash obtained contained considerably high carbon content (the bottom ash contained 14.4 wt% of carbon even after being retained in the bed for 4 hours). The ash were then purified by leaching with hydrochloric acid to remove metallic compounds and subsequently roasted in a bed of ash in the combined fluidised bed-muffle furnace combustor. The final silica white products were amorphous but still contained residual carbon content of 2.0 wt%.

The latest development in the use of fluidised bed in part to recover amorphous silica from rice husk could be found in a patent application publication by De Souza et al. (2004). They described that amorphous silica could be recovered from vegetal matters including rice husk through a series of processing steps involving hydrolysis with acid, washing and drying, fragilisation and disaggregation

of the material structure, calcination, and finally milling. They stated that adequate ways to carry out the calcinations step (in the temperature range of 410 – 900°C) was through the use of a fluidised bed oven but other calcinations equipment could also be used, such as muffle furnace and rotary oven. This rendered the use of fluidised bed as optional and was not an integral part of the process to produce silica from vegetal matters such as rice husk.

2.2 Effects of Fluidisation Parameters on the Mixing Characteristics of Rice Husk in Fluidised Bed

The fluidisation or bubble formation characteristics affect the degree of mixing in the fluidised bed. The mixing behaviour, in turn affects the combustion efficiency, with good mixing behaviour promoting high combustion efficiency. This is because good mixing provides turbulence and higher residence time amongst the reactants and therefore, two of the three fundamental requirements for the combustion reaction (temperature, turbulence and residence time) could be fulfilled.

Depending on the combustor operating conditions, particle combustion may be controlled by chemical reaction or transport phenomena. At low temperatures, chemical reaction is a dominating factor but not at high temperatures, where chemical kinetics are fast. At high temperatures, intra- and extra-particle mass transfer resistance of the oxidising agent plays a major role in determining the combustion rate. Combustion at these high temperatures regime, therefore, is diffusion limited. In fluidised bed combustion, the combustion process was widely believed to be limited by the char oxidation stage (Kulasekaran et al., 1998) as the conversion of carbon to CO₂ generates three times the heat released in comparison to its conversion to CO. It had been reported by Dutta and Wen (1977) that for coal chars, combustion is diffusion limited for temperature above 650°C. Chars from biomass materials such as rice husk belong to the most reactive of technical carbon materials due to their porous and highly-disordered carbon structure (Henrich et al., 1999). Therefore, it is expected that the temperature regime for diffusion-limited combustion of biomass chars such as rice husk char is lower. The speculation that

combustion of rice husk chars is diffusion limited beyond the temperature of 650°C is further supported by the thermogravimetric analysis (TGA) on rice husk. As reported by Mansaray and Ghaly (1998b) in their study on the thermal degradation of rice husk in an air atmosphere, it was observed through the mass loss profile that the char oxidation stage took place at the temperature range of 300 – 500°C. This showed that below the temperature of 500°C, the combustion of rice husk chars was expected to be kinetically-controlled.

At conditions whereby the combustion is diffusion-limited, the importance of turbulence and residence time is significantly enhanced. Higher degree of turbulence increases the contact between reactants (rice husk and air) and the heat source (high temperature), thereby increasing the rates of heat and mass transfer to the reactants at the micro-level. In addition, the turbulence in the bubbling sand bed is also responsible for the breakage of the rigid char skeleton that formed after the devolatilisation of the rice husk, thereby making the entrapped carbon more readily available for further oxidation process.

With the use of a same distributor design, the bubble formation characteristics and thus the mixing in the fluidised bed is governed by the fluidisation parameters such as fluidising velocity, sand size and static bed height.

2.2.1 Fluidising Velocity

The choice of sand size to be used for the operation of the fluidised bed combustor affects the amount of air input required in order to maintain a certain fluidising condition. It was reported by Rozainee (1998) that a fluidisation number (U/U_{mf}) of 3 was necessary to produce the turbulent regime crucial in attaining good mixing behaviour in a fluidised bed. In his study of sludge combustion in a shallow fluidised bed, it was found that sludge incineration was stable at a fluidisation number (U/U_{mf}) of 3, and that at fluidisation number of 5, the combustion efficiency was similar to that of fluidisation number of 3. Similar results were reported by Ho et al. (1988), who found that the rate of sludge incineration at fluidisation numbers

of 3 and above was essentially constant. The properties of sludge and rice husk do not differ considerably much from each other, as shown in Table 2-1. Both materials are constituted mainly of volatile matters and it was expected that the same phenomenon in which the combustion efficiency remained essentially constant at fluidising numbers beyond 3 will be observed during combustion of rice husk in fluidised bed. Further, Chen et al. (1998) reported that fluidising numbers ranging from $3 - 7 U_{mf}$ were required to obtain good combustion behaviour of rice husk in the fluidised bed.

Table 2-1: Properties of sewage sludge and rice husk (wt% dry basis)

Constituents	Sewage Sludge*	Rice Husk [#]
Volatile matters	66	71.3
Fixed carbon	9	12.4
Ash	25	16.3
Carbon (C)	42.3	37.8
Hydrogen (H)	5.9	5.0
Oxygen (O)	22.3	40.3
Nitrogen (N)	2.9	0.6
Sulfur (S)	1.6	ND
HHV (MJ/kg dry basis)	17.7	14.8

Note:

- * - Taken from Rozainee (1998)
- # - From analysis (Ngo, 2002)
- HHV - Higher Heating Value
- ND - Not Detectable

Hence, it was hypothesised that a fluidising velocity of $3 - 7 U_{mf}$ was necessary to obtain good mixing behaviour of rice husk in the fluidised bed.

2.2.2 Sand Size

According to Bhattacharya et al. (1984), the operating velocity of air for combustion of rice husk in a fluidised bed was optimum at 0.185 – 0.37 m/s at room temperature and pressure for sand particle sizes between 351 – 420 μm . After some trial runs with different sand sizes, they concluded that this sand size was deemed the most suitable for the combustion of rice husk in fluidised bed as there was considerable sand entrainment with sand size much smaller than 351 μm . On the other hand, sand particles that are too large would not mix well with rice husk, resulting in poor combustion behaviour. This was found to be consistent with other studies which reported the use of sand with sizes less than 830 μm , mostly in the range of 300 – 500 μm (Table 2-2).

Table 2-2: Sand size and corresponding fluidisation velocity reported in literature for combustion of rice husk in fluidised bed

No.	Reference	Sand Size (μm)	Fluidising Velocity (m/s)
1	Peel and Santos (1980)	< 830	1.0 – 1.5
2	Bhattacharya et al. (1984)	351 – 420	0.19 – 0.37
3	Preto et al. (1987)	500	0.4 – 2.2
4	Bhattacharya and Wu (1989)	300 - 500	NA
5	Armesto et al. (2002)	500 – 1000	1.0 – 1.2

Note:

NA – Not available

Rice husk has very low bulk density (approximately 100 kg/m^3) and has a low terminal velocity (reported to be 1.1 m/s by Sen and Ghosh, 1992). During rice husk combustion, the bed consists of a mixture of rice husk, char and ash in addition to the inert bed material (sand). There is a delicate balance to maintain good mixing by introducing fluidising air much higher than the minimum fluidisation velocity (namely 3 – 5 U_{mf}) whilst ensuring that the rice husk would not be elutriated prior to being burnt to completion. Using sand in the range of 710 – 850 μm (Table 2-3) is deemed to be the upper limit for sand size as maintaining a fluidising velocity at 3 U_{mf} (the minimum fluidisation number required to promote good mixing in the bed)

will result in a superficial velocity of approximately 1.0 m/s, which is sufficient to elutriate the rice husk particles. This is consistent with the findings by various researchers (Sen and Ghosh, 1992; Bingyan and Zhongnan, 1987; Xu et al., 1985; Natarajan et al., 1998a), who recommended a superficial fluidising velocity of 0.6 – 1.0 m/s to achieve good fluidisation of sand, rice husk and its char and ash mixture.

On the other hand, if the sand size is too small, the sand particles might be trapped in the voids of the ash skeleton, resulting in significant sand contamination of the ash product. In addition, since a large volume of the sand is required for the operation of the fluidised bed (for topping up and replacing used sand), it is necessary that the sand source is commercially available. It was found that the sand sizes of 595 – 841 μm (screen 20/30) and 250 – 595 μm (screen 30/60) are commercially available by Johor Silica Industries Sdn. Bhd. in Kota Tinggi, Johor. Preliminary sieve analysis showed that the mean particle size of these sand sizes are 672 μm and 342 μm , respectively. Fluidisation experiments showed that the U_{mf} for the 595 – 841 μm and 250 – 595 μm sand samples were 0.30 m/s and 0.09 m/s, respectively (Table 2-3). Maintaining the fluidising number as high as 5 U_{mf} for the sand size of 250 – 595 μm will only result in a superficial velocity of 0.45 m/s, less than half the terminal velocity of rice husk. Meanwhile, for the sand size of 595 – 841 μm , operating at 5 U_{mf} will result in a fluidising velocity of 1.50 m/s, which might be sufficient to elutriate the sand particles.

Further, Rao and Bheemarasetti (2001) reported that the minimum fluidising velocities for binary mixtures of particles with different densities and sizes (such as rice husk and sand), differ according to mass fraction of the mixture materials. For example, increasing the mass fraction of rice husk in a bed of sand particles from 2 wt% to 15 wt% could lead to an increase in the minimum fluidising velocities of the mixture ($U_{mf,m}$) by up to 2.6 times. This phenomenon could lead to a poorer mixing behaviour of the mixture material as the U_{mf} number was computed based on the U_{mf} of the bed material. However, the drastic increase in the value of $U_{mf,m}$ was only observed at higher mass fractions, such as when increasing the rice husk mass fraction in the bed from 10 wt% to 15 wt%. The increase in $U_{mf,m}$ was found to be less than 60% when the mixture fraction of rice husk was kept at below 10 wt%.

Table 2-3 : Minimum fluidising velocity of sand of various size ranges

Size range (μm)	U_{mf} (m/s)
850 – 1000	0.44
710 – 850	0.33
600 – 710	0.28
500 – 600	0.19
*595 – 841	0.30
*250 – 595	0.09

Note:

All values of U_{mf} taken from Rozainee (1998) through determination from the pressure drop plot except for the value denoted *, which was obtained from experiment

Hence, it was hypothesised that when operating at fluidising velocities of 3 – 5 U_{mf} , sand in the size range of 250 – 850 μm could give good mixing of rice husk in the fluidised bed while preventing excessive elutriation of the low-density rice husk particles. It was also necessary to limit the amount of rice husk present in the bed to less than 10 wt% of the weight of the entire bed materials to prevent significant difference between the minimum fluidising velocity of the bed material (U_{mf}) and the minimum fluidising velocity of the mixture materials ($U_{mf,m}$).

2.2.3 Static Bed Height

The static bed height in the fluidised bed is usually expressed in terms of the ratio of the static height of bed materials (z) to the column diameter (D_c). A bed height of 1 D_c means that H is equals to D_c . Existing literatures reported using a sand bed height ranging from 0.15 – 1.25 D_c for the combustion of rice husk (Table 2-4).

Table 2-4: Static bed height used for the combustion of rice husk as reported in existing literatures

No.	Reference	Bed Height (D_c)
1	Peel and Santos (1980)	0.15 – 0.75
2	Bhattacharya et al. (1984)	0.67
3	Armesto et al. (2002)	1.25

The combustion intensity is influenced by the bed height, the intensity being higher for higher bed height due to the increase in bed volume (Bhattacharya et al., 1984 and Natarajan et al., 1998a). In addition, since the bed acts as a thermal ‘fly-wheel’, namely temporarily storing and then transferring the heat evolved during the combustion process to the feed materials, it is preferable to use a higher bed height to increase the thermal capacity of the bed. However, several drawbacks are associated with the use of higher bed height, such as the higher pressure drop incurred (which translates to higher investment cost for compressed air source) and the higher fuel cost for start-up of the bed. In his studies of palm waste burning in a fluidised bed, Lim (2002) concluded that a sand bed height of $0.5 D_c$ (in an 80-mm inner diameter fluidised bed combustor) was optimum due to the following reasons:-

- i) Easier start-up of bed via pre-heating with premixed LPG-air combustion compared to higher beds (i.e. $0.75 - 1 D_c$). The entire bed at $0.5 D_c$ could be pre-heated up to a temperature of 900°C in less than 8 minutes (Lim, 2002) whereas for the $0.75 D_c$ and $1 D_c$ bed heights, the bed could only reach a temperature of up to 750°C even after being pre-heated for more than 10 minutes and 20 minutes, respectively.
- ii) Easier control of bed temperature. Thicker beds result in bigger bubbles as they rise to the bed surface. Eruption of such big bubbles makes it very difficult for the LPG flame to remain inside the bed.
- iii) Better mixing behaviour in the absence of slugging or channelling as observed in beds with height of $0.75 D_c$ and $1 D_c$ (Lim, 2002).

Hence, it was hypothesised that a sand static bed height of $0.5 D_c$ in the existing experimental rigs (with inner diameters of 80-mm and 210-mm) could give good mixing behaviour during the combustion of rice husk in the fluidised bed.

a) Prediction of Bubble Behaviours at Different Static Bed Heights

Mixing of particles in a fluidised bed is largely governed by the behaviours of gas bubbles rising through the bed, with the bubble size playing a significant role. In order to achieve maximum gas-to-particle interaction, namely high heat and mass transfer rates imperative in combustion process, small and slowly rising bubbles are preferable. According to Kunii and Levenspiel (1991), the sizes of bubbles in a fluidised bed is largely dependant on the particle size, with bubbles reaching a small limiting size in fine particle systems and a larger size in larger particle systems. They noted that for Geldart B and D particles, the bubble size, d_b at any height z in the bed can be estimated through a correlation developed by Mori and Wen (1975):-

$$\frac{d_{bm} - d_b}{d_{bm} - d_{bo}} = e^{-\frac{0.3z}{D_c}} \quad (2-1)$$

where

$$\begin{aligned} d_{bo} &= \text{initial bubble size, m} \\ &= \frac{1.30}{g^{0.2}} \left[\frac{U_o - U_{mf}}{N_{or}} \right]^{0.4} ; d_{bo} \leq l_{or} \text{ and } N_{or} = \frac{1}{l_{or}^2} \text{ for square array of holes} \\ d_{bm} &= \text{limiting size of bubble expected in a very deep bed, m} \\ &= 0.65 \left[\frac{\pi}{4} D_c^2 (U_o - U_{mf}) \right]^{0.4} \\ D_c &= \text{bed inner diameter, m} \end{aligned}$$

This correlation is valid for the following conditions:-

- i) $D_c \leq 1.3 \text{ m}$
- ii) $0.005 \leq U_{mf} \leq 0.20 \text{ m/s}$
- iii) $60 \leq d_p \leq 450 \text{ } \mu\text{m}$
- iv) $U_o - U_{mf} \leq 0.48 \text{ m/s}$

Equation 2-1 could be used to determine the bubble sizes along the height of the fluidised bed at different fluidising air velocities. More specifically, the size of the bubbles just before they erupt at the surface of the bed at different bed heights being investigated experimentally could be compared. Bigger bubble eruptions resulted in more vigorous splashing of sand particles into the freeboard region as well as a more turbulent bed. Although a more turbulent bed is able to give better mixing, the vigorous upward splashing of sand particles might hinder the rice husk particles from penetrating the bed in order to absorb the heat they require for devolatilisation and subsequently the oxidation of carbon.

Further, it was reported by Rozainee (1998) that the initial velocity of ejected particles is independent of the size and density of the particles, being largely dependant on the size and rise velocity of the bubble (Caram et al., 1984). It was further reported that if the ejected particles were from bubble wakes, the particle ejection velocity could be as high as 2.5 times the bubble rise velocity ($V_m = 2.5 U_b$) (Pemberton and Davidson, 1986). The velocity of bubble swarms can be estimated by the following equation by Davidson and Harrison (1963):-

$$U_b = U - U_{mf} + 0.71 \sqrt{gd_b} \quad (2-2)$$

where

- U_b = bubble velocity
- U = fluidising velocity
- U_{mf} = minimum fluidising velocity
- d_b = bubble diameter

2.3 Effects of Operating Parameters on the Combustion Efficiency of Rice Husk in Fluidised Bed

The operating parameters that affect the combustion efficiency of rice husk in the fluidised bed are time (residence time of rice husk in the combustor), temperature, level of impurities in rice husk, air supply and moisture content of rice husk. The factor of time is related to the period required for the rice husk to burn to completion to liberate carbon-free ash while simultaneously maintaining the amorphous structure of silica in the ash. Meanwhile, the factors of temperature and levels of impurities in rice husk are related to the crystallisation of silica in the ash, carbon burnout rate and ash melting point. On the other hand, both parameters of time and temperature are interrelated to the factors of air supply and moisture content in rice husk, and as such affect the carbon burnout rate.

2.3.1 Time

a) Time for Complete Combustion of Rice Husk in a Fluidised Bed

According to Mukunda et al. (1996), the char conversion times for raw rice husk are an order of magnitude larger than flaming times. However, they further found that the combustion times varied according to the amount of rice husk used (Sridhar et al., 1996). They found that single particle combustion for raw rice husk in a muffle furnace at 700°C has flaming times of about 3 – 4 seconds and char burning times of 40 – 65 seconds, while a group of particles (75 husks) put together randomly elevated the flaming times and char conversion times to 6 – 8 seconds and 152 seconds, respectively. This could be attributed to the difference in the rates of heat and mass transfer when a group of particles was used. With the absence of mixing, there was a certain lag time in heat transfer to the particles located in the inner layer of the rice husk pile, thus resulting in devolatilisation times (or flaming times) which were twice higher compared to the case of a single particle. Similarly, the lag time in mass (oxygen) transfer to these particles resulted in char conversion times which were up to four times higher.

Apart from the factor of oxygen supply, the combustion time is also highly dependent on the combustion temperatures. Based on the thermogravimetric analysis (TGA) of rice husk in an air atmosphere, the devolatilisation of rice husk took place in the temperature range of 230 – 330°C while the char oxidation stage took place in the temperature range of 300 – 500°C (Mansaray and Ghaly, 1998b). As such, the combustion reaction of rice husk is expected to be diffusion-limited at the temperature of 700°C in the study by Sridhar et al. (1996). The controlling factor during diffusion-limited reactions is turbulence. In the fluidised bed, the presence of bubble swarms in the bed provides the oxygen supply to the rice husk, while the rise of these bubble swarms and their subsequent eruption at the bed surface creates turbulence in the bed. Hence, it is expected that when operated at the diffusion-controlled regime (i.e. temperatures above 500°C), the time required for rice husk to burn to completion in the fluidised bed is less than that observed by Sridhar et al. (1996) for the case of single particle combustion. With the presence of high heat and mass transfer rates due to turbulence in the fluidised bed, it is further hypothesised that the combustion times of rice husk in the fluidised bed is independent of the amount of rice husk used, as opposed to that observed by Sridhar et al. (1996).

b) Time for Formation of Silica Crystals in Rice Husk Ash during Combustion in Fluidised Bed

According to Della et al. (2002), burning out temperature and time are the most important factors to define whether the silica remains amorphous in rice husk ash or become crystalline. This finding agreed well with that of Shinohara and Kohyama (2004), who found that the percentage of crystalline silica in rice husk ash increased when subjected to heating at higher temperature or higher residence time. It was further reported by Gorthy and Pudukottah (1999) that crystallisation is a gradual process which requires a certain period of time to complete. The formation of cristobalite in rice husk ash could be explained as follows:-

- i) Si–O bonds are liberated from the long polymeric chains (Si–O–C / Si–O–Si) at elevated temperatures (below crystallisation point of silica);
- ii) Subsequent cooling of the Si–O bonds have little or no tendency to crystallise;

- iii) When the pyrolysis temperatures are increased, more and more Si–O and C–O / C–C are released, which gradually transform to crystalline silica (cristobalite) and crystalline carbon (graphite).

The temperatures for the onset of silica crystallisation in rice husk ash were reported in various literatures to be in the range of 700 – 900°C (Hanafi et al., 1980; Hamad and Khattab, 1981; Kaupp, 1984; Kapur, 1985 ; Patel et al., 1987; Chakraverty et al., 1988 ; Nakata et al.; 1989; Schiefelbein, 1989; Conradt et al., 1992; Gorthy and Pudukottah, 1999; Chouhan et al., 2000 ; Huang et al., 2001 ; Della et al., 2002 ; Sumran and Kongkachuichay, 2003). However, there are no reported studies on the combined effect of temperature and exposure time on the onset of silica crystallisation in rice husk ash. Previous studies on the temperature limits were mostly carried out for a long period of time (1 – 15 hours) in the muffle furnace where mixing was practically non-existent. In the fluidised bed, rice husk is exposed very briefly to the combustion temperature (less than two minutes) due to its rapid reaction time. In addition, the high degree of turbulence in the bubbling bed region prevents the formation of hot-spots and aids in breaking down the rigid char skeleton to release the entrapped carbon for further conversion. Hence, it was hypothesised that the fluidised bed could be operated at temperatures of 700°C or higher without the risk of crystallising the silica due to the brief exposure time of the ash to high temperatures. The brief exposure time even at such high temperatures might not be sufficient for the re-alignment of the oxygen and silicon atoms into three-dimensional repeating patterns to form crystals.

2.3.2 Temperature

To achieve both objectives of obtaining amorphous and carbon-free rice husk ash in a simultaneous manner, there is the challenge to maintain the temperature in the fluidised bed low enough to preserve the amorphous structure of silica but sufficiently high enough to achieve effective and complete conversion of carbon. Thus, the key to achieve such objectives lies in the efforts to reach a compromise in the operating temperature. For such purpose, the understanding of the temperature

for onset of crystallisation of silica in the ash as well as the temperature required for complete conversion of carbon in rice husk are crucial.

a) Temperature Limit for Onset of Silica Crystallisation in Rice Husk Ash

Silica in rice husk is amorphous in nature, as indicated by a broad peak centred around 2θ angle of 22° in **Error! Reference source not found.**, which confirmed the amorphous nature of the silica. According to the phase diagram of silicon dioxide (SiO_2) when it is at a relatively pure state, amorphous silica must be heated in excess of about 1427°C (2600°F) before there is a transition to cristobalite and tridymite forms of silica (Pitt, 1976 and 1994). At atmospheric pressure, tridymite and cristobalite are crystallised at $867 - 1470^\circ\text{C}$ and $1470 - 1727^\circ\text{C}$, respectively (Shinohara and Kohyama, 2004). However, due to the impure form of silica found in rice husk, the transition from amorphous to crystalline cristobalite and tridymite forms occurs at a much lower temperature. The presence of impurities significantly reduced the transition temperature.

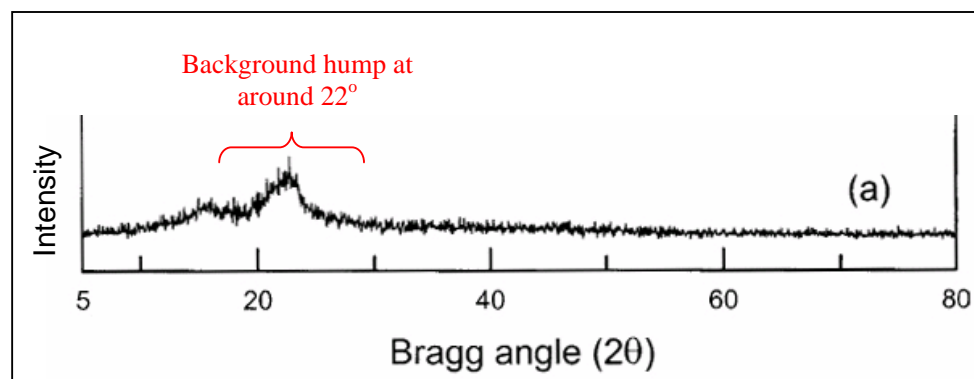


Figure 2-1: Diffractogram of fresh rice husk (taken from Liou, 2004)

The crystallisation of silica in rice husk ash does not result in the formation of quartz crystals, as confirmed by Kapur (1985). In his study on rice husk combustion in a tube-in-basket burner, the resulting ash is amorphous up to 600°C , except for an unexplained trace of quartz material. This trace amount of quartz had been proven by Jauberthie et al. (2000) to originate from contamination by wind-blown sand on the rice husk prior to being heat-treated. The crystallisation of silica in rice husk ash is characterised first by the formation of the cristobalite crystals and then the tridymite crystals (Hanafi et al., 1980; Hamad and Khattab, 1981; Ibrahim and

Helmy, 1981; Kapur, 1985; Shinohara and Kohyama, 2004). The presence of the cristobalite crystals is indicated by prominently sharp peaks at 21.93° (primary peak), 36.11° (secondary peak) and 31.46° (tertiary peak) (National Institute of Occupational Safety and Health, 1998). The formation of tridymite, meanwhile, only starts at the temperature of approximately 1000°C and become more prominent at temperatures beyond 1200°C . Its presence is indicated by sharp peaks at 21.62° (primary peak), 20.50° (secondary peak) and 23.28° (tertiary peak) on the diffractogram. Example of a crystallised sample of rice husk ash was as shown in Figure 2-2. Upon heating from the temperature at the onset of crystallisation (approximately 700°C) up to 1200°C , the formation of crystals in rice husk ash is dominated by cristobalite, whereas the heating at higher temperatures results in higher concentration of tridymite than cristobalite (Shinohara and Kohyama, 2004). This is because at higher temperatures, the cristobalite tends to convert to tridymite (Houston, 1972).

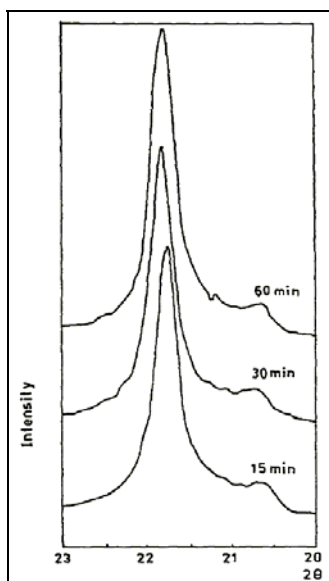


Figure 2-2: Diffractogram of crystallised rice husk ash showing characteristic crystal peak of cristobalite at 2θ angle of 21.93° (rice husk sample fired at 1000°C at different time intervals) (Ibrahim and Helmy, 1981)

Studies on the temperature limits for the crystallisation of silica in rice husk ash had been carried out since the year 1974 (Bartha and Huppertz, 1974). Since then, many similar studies had been carried out, as shown in Table 2-5. The reported

temperature limits ranged from 700 – 900°C but thus far there is no conclusive findings with regard to the exact temperature limit that initiate the formation of silica crystals in rice husk ash. This could be attributed to the differences in thermal treatment methods, combustion environments (reducing or oxidising), heating periods and types of rice husk used in these studies. For example, studies performed in a closed system such as muffle furnace or a continuous system such as fixed bed might affect the combustion environment, in particular the oxygen supply. Through their experiments of rice husk combustion in a fixed bed unit, Hamad and Khattab (1981) showed that amorphous silica was obtained at lower air rates but at higher air rates, crystallisation of the ash occurred. The type of thermal treatment method also affects the degree of mixing or turbulence, which in turn governs the temperature distribution in the combustion zone. Even with the use of the same thermal treatment method (muffle furnace), the heating period was found to affect the formation of crystals in rice husk ash, whereby a heating period of 12 – 15 hours resulted in cristobalite formation at 800°C in the study by Kapur (1985) compared to 900°C in the study by Nakata et al. (1989), who used a shorter heating period of 1.5 hours. The levels of impurities in rice husk differ according to the rice husk variety and sources, and removal of these impurities was found to affect the crystallisation temperature. For example, ash from water-washed rice husk in the study by Gorthy and Pudukottah (1999) was found to be amorphous even after heating to temperatures of up to 900°C for one hour. Heating raw rice husk for a similar heating period resulted in the formation of crystals at 725°C in the study by Bartha and Huppertz (1974).

As such, the crystallisation of silica in rice husk ash is dependent on the complex and interlinked factors of temperature, turbulence, combustion environment, heating period and levels of impurities in rice husk. In the fluidised bed, the degree of turbulence is high due to the vigorous bed bubbling action and this leads to uniform temperature distribution in the combustor. In addition, rice husk is exposed to a very brief heating period due to the rapid processing rate. Hence, it was hypothesised that during the combustion of rice husk in the fluidised bed, the crystallisation temperatures of the silica in the ash might differ from that reported in existing literatures. The closest reference could be found in the study by Huang et al. (2001),

who found that silica in the ash remained amorphous up to the temperature of 800°C when combusted in an electrically-heated fluidised bed.

Table 2-5: Temperature limits reported in various literatures for the onset of crystallisation of silica in rice husk ash

Temperature Limit (°C)	Reference	Remarks
700	Chakraverty et al. (1988)	Ash obtained from combustion of untreated and various HCl-treated rice husk samples at 700°C for 1.5 hours all showed amorphous form. Subjecting acid treatment to the husk did not affect the silica structure.
	Patel et al. (1987)	The temperature of carbonisation of rice husk should be preferably below 700°C to avoid any transformation of amorphous to crystalline form.
	Kaupp (1984) and Schiefelbein (1989)	Studies showed that physical structural transformation of silica from its original amorphous state to a crystalline state occurred should the oxidation of rice husks be carried out at a temperature beyond 700°C. Residual carbons will be encapsulated inside the crystallised silica, making the combined carbon unavailable for further oxidation reactions even at higher temperatures.
	Conradt et al. (1992)	The rice husk ash was no longer amorphous at temperatures $\geq 700^\circ\text{C}$. It transformed to cristobalite and tridymite by annealing at temperatures $\geq 700^\circ\text{C}$.
	Della et al. (2002)	Rice husk ash obtained from burning during the process of rice manufacture was heated in an electric oven at 400 – 700°C for 1 – 6 hours. Amorphous silica powder could be produced after heat-treating at 700°C for 6 hours.
	Sumran and Kongkachuichay (2003)	Silica from rice husk was prepared via three methods, namely one-step combustion, fluidised bed combustion and alkaline extraction. Amorphous silica was obtained at temperature of 600°C (one step combustion) and 700°C (fluidised bed combustion).
800	Hamad and Khattab (1981)	Rice husk was thermally decomposed in a muffle furnace at 500 – 1150°C for 1 hour. Rice husk silica still existed in the amorphous state below 600°C while crystallisation of cristobalite took place at 800°C.
	Kapur (1985)	Rice husk was burnt in air in an electric muffle furnace at 350 – 1400°C for 12 – 15 hours. Silica in ash remained in amorphous state up to 600°C. The phase transformation of silica began between 600 – 800°C with the first appearance of cristobalite phase at 800°C.
	Huang et al. (2001)	Rice husk is combusted in a fluidised bed with an electric furnace surrounding the bed. Amorphous silica is obtained when the bed temperatures were maintained between 700 – 800°C.
900	Hanafi et al. (1980)	Rice husk ash was fired at various temperatures from 500 – 1400°C for 3 hours in an atmosphere of air. No crystallisation modification was detected (via X-Ray Diffraction analysis) for heating of rice husk at 800 – 900°C. However, at 900°C nucleation process for the formation of the low-form cristobalite phase was pronounced.
	Nakata et al. (1989)	Pyrolysed rice husk was combusted in an electric furnace at the temperature range of 400 – 1500°C with flowing air and a holding time of one hour. Rice husk combusted below 800°C was amorphous silica while above 900°C, the silica in the ash was cristobalite accompanied with a small amount of ash.
	Gorthy and Pudukottah (1999)	Black rice husk ash was subjected to heating in a tubular furnace at 400 – 1100°C for 1 hour in high purity argon atmosphere. No apparent crystalline phase formation or reaction occurred up to around 900°C.
	Chouhan et al. (2000)	X-ray diffraction showed that highly amorphous silica was released by ashing at 700°C and an increase in ashing temperature up to 900°C led to increase in crystalline nature of silica.

b) High-Temperature Requirement for Complete Carbon Burnout in Rice Husk

During any combustion process, the temperature is preferably high, in the region of 800 – 1000°C in order to achieve fast and complete burnout of materials. However, in the case of rice husk, this is limited by the crystallisation temperature of the silica in order to preserve the resulting ash in its amorphous state. James and Rao (1986) had concluded that on isothermal heating, a minimum temperature of 402°C was required for the complete destruction of the organic matters in rice husk to liberate silica. Further, according to Di Blasi et al. (1999), a temperature of at least 500°C was required for the complete oxidation of biomass chars. This was confirmed by Chakraverty et al. (1988), which reported that the temperature for rice husk combustion should be preferably more than 500°C to produce white ash within a reasonable time. In their studies on the combustion of rice husk in a muffle furnace, reaction times ranging from 16 – 24 hours were required to produce carbon-free white ash at temperatures ranging from 300 – 500°C. When subjected to a temperature of 700°C, the reaction time was significantly reduced to 1.5 hours as compared to the reaction time of 5 hours when heating at 500°C. This showed that the burning of the residual carbon in the ash requires a temperature of at least 500°C, preferably in the region of 700°C. Further, the temperature requirement of 700°C to achieve complete carbon burnout in the rice husk had been proven by Chouhan et al. (2000). In their studies on the ashing of rice husk in an electric muffle furnace at temperatures ranging from 700 – 900°C for one hour, scanning electron microscopy (SEM) micrographs for rice husk silica ashed at temperatures of 500°C and 600°C still contained significant quantity of carbonaceous matter whereas ashing at 700°C led to carbon-free silica.

Hence, it was hypothesised that in order to obtain carbon-free ash from rice husk, the fluidised bed should be operated at a temperature of at least 700°C.

c) Calculations of Combustion Temperature

The adiabatic flame temperature is the resultant temperature of the combustion products when the combustion of a fuel is complete and all the heat evolved is used to heat the

combustion products. The energy balance for combustion of fuel from the first law of thermodynamics is as follows:-

$$\Delta H = n_f \Delta \hat{H}_c + \sum_{output} n_i \hat{H}_i(T_{ad}) - \sum_{input} n_i \hat{H}_i(T_{feed}) = 0$$

Rearrangement of this equation results in:-

$$\sum_{output} n_i \hat{H}_i(T_{ad}) = -n_f \Delta \hat{H}_c + \sum_{input} n_i \hat{H}_i(T_{feed}) \quad (2-3)$$

where

$\Delta \hat{H}_c$ = heat of combustion of the fuel at reference temperature of 25°C

n_i = mole of the i^{th} component in the feed or product

\hat{H}_i = specific enthalpy of the i^{th} component at 25°C

T_{ad} = adiabatic flame temperature (°C)

In Equation 2-3, $\Delta \hat{H}_c$ is evaluated at 25°C where water is produced in its liquid state, thereby giving $\Delta \hat{H}_c$ as the higher heating value (HHV) of the fuel. However, water is produced in its gaseous state during the combustion process. Therefore, the latent heat stored in the water vapour has to be taken into consideration in the heat balance calculation. During the combustion process, the net heat produced is the lower heating value (LHV) of the fuel, which could be calculated from the higher heating value as follows:-

$$LHV = HHV - n \Delta H_v(H_2O, 25^\circ C) \quad (2-4)$$

where n is the moles of water produced when a unit mass of fuel is combusted. The heat of vaporisation of water is

$$\Delta H_v(H_2O, 25^\circ C) = 44.013 \text{ kJ/mol} \quad (2-5)$$

Simplification of the adiabatic flame temperature calculation can be made by replacing the term $n_f \Delta \hat{H}_c$ in Equation 2-3 with $-n_f LHV$ ($\Delta \hat{H}_c$ is negative while LHV is positive) where n_f is the moles of fuel being combusted. The heat capacities of the product gases in J/(mol • °C) are:-

$$\begin{aligned} (C_p)_{CO_2} &= 36.11 + 4.233 \times 10^{-2} T - 2.887 \times 10^{-5} T^2 + 7.464 \times 10^{-9} T^3 \\ (C_p)_{H_2O} &= 33.46 + 0.688 \times 10^{-2} T + 0.7604 \times 10^{-5} T^2 - 3.593 \times 10^{-9} T^3 \\ (C_p)_{O_2} &= 29.10 + 1.158 \times 10^{-2} T - 0.6076 \times 10^{-5} T^2 + 1.311 \times 10^{-9} T^3 \\ (C_p)_{N_2} &= 29.00 + 0.2199 \times 10^{-2} T + 0.5723 \times 10^{-5} T^2 - 2.871 \times 10^{-9} T^3 \end{aligned}$$

With the use of waste materials, the heat capacity of the inlet fuel is difficult to evaluate. However, assuming feeding at the reference temperature, the heat capacity for the inlet fuel is not necessary. The resulting heat balance equation is in a quartic form requiring a trial-and-error solution procedure to solve for T_{ad} . A simpler alternative to determine the adiabatic flame temperature is through the use of the FLAME computer code developed by the University of Leeds. The model in FLAME calculates the compositions and temperatures of combustion at equilibrium.

The combustion temperature could be determined from the adiabatic flame temperature after adjustment for heat loss to the surroundings. The degree of heat loss to the surroundings varies according to the combustor conditions (insulated or non-insulated) as well as the surrounding environment.

a. Heat Loss in a Non-Insulated Fluidised Bed Combustor

In a non-insulated combustor, the heat loss is primarily governed by loss through convection and radiation, with the latter being more significant at high combustion temperatures. The heat to sustain the combustion process in a non-insulated combustor could be computed as follows:-

$$Q_s = Q_p - Q_{loss} - Q_v - Q_c \quad (2-6)$$

where

- Q_s = Heat required for sustaining the combustion process (MJ)
- Q_p = Rate of heat evolved from the combustion process, assuming complete reaction (MJ/min)
- Q_{loss} = Rate of heat loss through convection and radiation (MJ/min)
- Q_v = Rate of heat consumed to vaporise the moisture content in the feed material (MJ/min)
- Q_c = Rate of heat absorbed by inlet air (MJ/min)

In Equation 2-6, Q_s is the heat required to sustain the burning of the feed materials in the fluidised bed of a certain static height of bed media, and could be computed as follows:-

$$Q_s = \frac{m_s C_{ps} \Delta T}{10^6} \quad (2-7)$$

where

- m_s = Mass of sand bed (g)
- C_{ps} = Heat capacity of bed media = 0.799 J/(g • °C) (for sand)

ΔT = Temperature difference between the desired bed temperature and the temperature of initially-charged bed media

It should be noted that in order for Equation 2-7 to be applicable in Equation 2-6, the values derived from Equation 2-7 has to be divided by an assumed heating period for the sand (which is typically 30 minutes) so that the resulting unit is consistent with that of the value from Equation 2-6.

Assuming complete combustion to take place, Q_p could be computed as follows:-

$$Q_p = \frac{F \times HHV}{1000} \quad (2-8)$$

where

F = Total feeding rate of materials (g/min)

HHV = Higher heating value for feed material (MJ/kg)

The stability of the combustion process in the non-insulated combustor is governed by the amount of heat loss from the combustor, computed via the following equation:-

$$Q_{loss} = q_{conv} + q_{rad} = \frac{60}{10^6} (h_c + h_r) A (T_1 - T_2) \quad (2-9)$$

where

$$h_r = 5.676 \xi \frac{\left[\left(\frac{T_1}{100} \right)^4 - \left(\frac{T_2}{100} \right)^4 \right]}{(T_1 - T_2)} \quad (2-10)$$

and

h_c	=	Natural or forced convection coefficient
	=	20 W/(m ² • K) [still air = 2.8 – 23 W/(m ² • K)]
h_r	=	Radiation heat transfer coefficient [W/(m ² • K)]
A	=	Heat transfer area (m ²)
T_1	=	Temperature in the combustor (°C)
T_2	=	Temperature outside the combustor (°C)
ξ	=	Emissivity of the combustor surface (dimensionless)
	=	0.57 or 0.66 (at 232° and 949°C)

During the drying process, heat is absorbed by the moisture content in the feed material. The heat consumed to vaporise the moisture in the feed could be predicted via:-

$$Q_v = \frac{m_w C_{pw} \Delta T + m_w l}{10^6}$$

where

m_w	=	Mass of water (g)
C_{pw}	=	Heat capacity of water = 4.183 J/(g • °C)
ΔT	=	Temperature difference between the combustor temperature and the temperature of the initially-charged feed material
l	=	Latent heat of vaporisation for water = 2257 J/g

Heat is also absorbed by the air being fed into the combustor, which includes the fluidising air as well as any secondary air. The extent of heat absorbed, nevertheless, is insignificant compared to the amount of heat loss. The amount of heat required to bring up the temperature of the air at ambient to the combustor temperature is as follows:-

$$Q_c = n \frac{C_{pa}}{29} \left[\frac{(T_1 - T_2)}{10^6} \right] \quad (2-11)$$

where

C_{pa} = Heat capacity of air = 1.0341 J/(g • °C)

n = Total air feed (mol)

Based on Equation 2-6, the minimum feed rate to sustain combustion at a certain temperature (assuming complete reaction) could be determined. Thereafter, the percentage of heat loss could be estimated.

b. Heat Loss in an Insulated Fluidised Bed Combustor

Compared to the non-insulated combustor, the heat loss via radiation in an insulated combustor is very low and could be rendered negligible. In this case, the term Q_{loss} in Equation 2-6 could be replaced by the following term:-

$$Q_{loss} = \left(\frac{T_1 - T_2}{R_1 - R_2} \right) \frac{60}{10^6}$$

where

$$R_1 = \frac{r_2 - r_1}{k_A A_{Alm}}; \quad A_{Alm} = \frac{A_2 - A_1}{\ln\left(\frac{A_2}{A_1}\right)}$$

$$R_2 = \frac{r_3 - r_{21}}{k_B A_{Blm}}; \quad A_{Blm} = \frac{A_3 - A_2}{\ln\left(\frac{A_3}{A_2}\right)}$$

r_1 = Inner radius of the combustor column (m)

r_2 = Outer radius of the combustor column (m)

r_3 = Outer radius of the combustor column + thickness of insulator (m)

A_1	=	Area of inner combustor column (m^2)
A_2	=	Area of outer combustor column (m^2)
A_3	=	Area of insulation material on the combustor column (m^2)
k_A	=	Thermal conductivity of combustor column
	=	16.3 W/(m • K) (for stainless steel)
k_B	=	Thermal conductivity of insulator

d) Freeboard Temperature

As soon as the rice husk feed enters the hot fluidised bed combustor, drying and to a certain extent some devolatilisation took place instantaneously. In general, the combustion process of high-volatile materials such as rice husk in the fluidised bed proceeds at three distinct stages, namely:-

- i) *Primary stage:* Drying and the majority of devolatilisation take place due to the available heat provided by the hot sand bed for the endothermic reactions. Some char burning in the hot bubbling bed also takes place due to the high temperature to initiate oxidation of carbon. Studies by Chen et al. (1998) had shown that the combustion ratio of density phase zone (bed region) to dilute phase zone (freeboard region) for rice husk was 4:6.
- ii) *Secondary stage:* Burning of the evolved volatiles and some oxidation of unburnt residual carbon in the ash particles take place, as these particles is being entrained towards the cyclone. Chen et al. (1998) reported that the combustion of rice husk was concentrated in the dilute phase zone (freeboard), with the highest intensity in the middle region due to the high volatile content of rice husk (in the excess of 60 wt%). If sufficient freeboard height is available, the remaining 60% of the combustion reaction takes place in the freeboard area.
- iii) *Tertiary stage:* Burning of the residual volatile gas and carbon in the ash continues in the cyclone in the event that the freeboard height is insufficient to complete the secondary stage combustion.

Since the majority of the combustion reaction is expected to take place in the freeboard region, provision of high freeboard temperature is necessary especially when burning low-density materials such as rice husk. Such provision ensures that any incomplete burning of the evolved volatiles and char could proceed in the freeboard region. In addition, combustion of some portion of the low-density rice husk especially broken fragments and fines, which tend to be elutriated upon entry into the combustor, could still take place.

Hence, it is necessary to maintain a high freeboard temperature (such as 800 – 1000°C) in the fluidised bed combustor during combustion of rice husk to enable effective oxidation of carbon as the ash particles are being entrained towards the cyclone . This could be achieved, for example, through the use of auxiliary burners located at the freeboard region.

2.3.3 Presence of Impurities in Rice Husk

Studies by Jenkins et al. (1996) showed that the 11 most prevalent inorganic components in biomass fuels such as rice husk are Al, Ca, Cl, Fe, K, Mg, Na, Si, Ti, S and P. Biomass such as rice husk contains significant amounts of silica, potassium, sodium, sulphur and chlorine. These inorganic components in biomass fuels were further categorised by Miles and Miles (1995) into the following categories:- (1) refractory materials with little solubility (Si, Ti and Al); (2) alkaline and alkaline earth elements with varying degrees of solubility (K, Na, Ca and Mg); (3) non-metallic (anionic) materials typically occurring as biomass nutrients (Cl, S and P) and (4) iron (Fe).

In its pure form, silica has high melting point ($> 1650^{\circ}\text{C}$) and does not readily forming low melting point compounds. However, the presence of high level of volatile alkali metals (potassium and sodium) in the biomass sufficiently lower the fusion temperature of the ash (Miles and Miles, 1995), which subsequently led to the formation

of surface melt that entrapped any unburnt carbon for further oxidation (Krishnarao et al., 2001). In rice husk, the major inorganic constituent next to silicon (as silicon dioxide, at 20 – 25 wt%) is potassium, which upon thermal degradation forms potassium oxide (at 1 – 3 wt%) in the ash (Mansaray and Ghaly, 1997; Krishnarao et al., 2001; Shinohara and Kohyama, 2004). Potassium and sodium are common constituents of illite, which is the most prevalent form of clay in soils. According to Jenkins et al. (1996), the reaction between potassium and silicon (in the form of silica) leads to the rapid formation of heavily sintered and fused glassy deposits and slags at normal furnace operating temperature (800 – 900°C). In such reaction, chlorine acts as a facilitator in alkali vaporisation, whereby it reacts with alkali metals in the form of silicates to form relatively volatile and stable alkali chlorides. Chlorine also promotes the development of alkali sulfates through condensation of chlorides on surfaces with the presence of sulphur.

Tests by Jenkins et al. (1996) had shown that in general, large fractions of potassium, chlorine, sodium and sulphur in biomass could be removed by water washing. The removal of these impurities could eliminate the inherent problem of formation of low melting point compounds which interferes with the oxidation of carbon. The presence of potassium oxide at such relatively high concentrations interferes with the formation of silica crystals, carbon burnout and melting or agglomeration characteristics of rice husk ash.

a) Effect on the Formation of Crystals in Rice Husk Ash

Due to the impure form of silica found in rice husk, the transition from amorphous to crystalline cristobalite and tridymite forms occurs at much lower temperatures. The presence of impurities significantly reduced the transition temperature.

The formation of cristobalite was reported to be accelerated with the presence of potassium (Nakata et al. 1989). This probably explained the reason why the crystallisation of silica in rice husk starts with cristobalite and then tridymite as reported in various studies (Hanafi et al., 1980; Ibrahim and Helmy, 1981; Hamad and Khattab,

1981; Kapur, 1985; Shinohara and Kohyama, 2004), in contrast with the crystallisation of pure silica which starts with tridymite followed by cristobalite. However, higher concentration of potassium as well as the presence of impurities favoured the formation of tridymite at 1200°C (Ibrahim et al., 1980; Ibrahim and Helmy, 1981; Hanna et al., 1984, Shinohara and Kohyama, 2004). Further, Shinohara and Kohyama (2004) found that grinding of the ash samples tended to distribute the potassium and silica homogenously in the ash, which accelerated the crystallisation of tridymite. The crystallisation of silica in ground ash was dominated by tridymite compared to that of unground ash, which was dominated by cristobalite. Hanna et al. (1984) found that the addition of iron in the rice husk (impregnation with ferrous sulphate solution and soaking in ammonia solution) could act as an inhibitor for the formation of crystals from silica and carbon in the ash.

Since potassium is found to be responsible for lowering the crystallisation temperature of silica in rice husk ash, it is expected that its removal could alter the crystal transition temperatures to the range similar to that of pure silica. Potassium is an alkali earth metal that is highly soluble in water and therefore, washing the rice husk with water is expected to be able to remove this impurity. Further, it is hypothesised that using such pretreated rice husk for the combustion of rice husk in the fluidised bed could enable it to be operated at temperature range of 700 – 900°C without the risk of crystallising the resulting siliceous ash.

b) Effect on the Formation of Entrapped Carbon in Rice Husk Ash

Based on the thermogravimetric analysis (TGA) of rice husk in an air atmosphere, Mansaray and Ghaly (1998b) reported that the char oxidation stage took place at a temperature range of 300 – 500°C. Further, according to Di Blasi et al. (1999) in his study on the reactivities of biomass chars in air, the temperature for complete conversion of wheat straw chars was 517°C while the ignition temperature was as low as 146°C. However, a temperature of 385°C was necessary to achieve the maximum combustion rate. Rice husk has similar properties as wheat straw, as can be seen in Table 2-6. Therefore, the reactivity of rice husk char and wheat straw char is expected to be similar.

Table 2-6: Chemical properties of wheat straw and rice husk

Parameter	Wheat Straw*	Rice Husk [#]
Proximate Analysis (%)		
Moisture	8.0	10.1
Volatile Matter	71.7	64.1
Fixed Carbon	15.1	11.1
Ash	5.2	14.7
Ultimate Analysis (% dry-ash-free)		
Carbon (C)	47.7	45.2
Hydrogen (H)	6.0	6.0
Oxygen (O)	44.0	48.1
Nitrogen (N)	0.5	0.7
Calorific Value (MJ/kg)	19.25	17.7

Note:

* - Jones et al. (2000)

[#] - from analysis

According to Krishnarao et al. (2001), the major impurity of potassium (1 – 3 wt% as potassium oxide, K₂O) in rice husk accelerated the carbon fixation in its ash. The dissociation of potassium oxide at 347°C forms elemental potassium which melts at very low temperature (melting point for potassium is 64°C). The melting of potassium forms a surface melt mixture at the surface of the ash, thereby entrapping the carbon content and making the carbon unavailable for further conversion even at higher temperatures because the carbon is not in direct contact with air. Further, in their studies on the formation of black particles in rice husk ash, Krishnarao et al. (2001) found that the formation of entrapped carbon was more prominent when rice husk were subjected to sudden heating at high temperatures (600 – 700°C). During slow heating whereby the rice husk were slowly heated up to 600 – 700°C from room temperature, the carbon in the rice husk could be oxidised before it reached the dissociation temperature of K₂O. As discussed previously, the oxidation of carbon (char) in rice husk could take place as low as 146°C (Di Blasi et al., 1999) and became more pronounced at temperatures beyond 300°C (Mansaray and Ghaly, 1998b). Thus, during slow-heating, carbon oxidation in the rice husk was already taking place in the temperature band of 150 – 350°C. On the contrary, during sudden heating, the dissociation of K₂O followed by surface melting and

the formation of carbon due to the evolution of volatiles took place simultaneously. The tendency of the carbon to be entrapped in the surface melt was very high, hence resulting in overall higher residual carbon content in the ash compared to that obtained from slow-heating.

Heating the rice husk to the temperature beyond the dissociation temperature of potassium oxide (347°C) is deemed the prerequisite to recover the silica from rice husk as studies by James and Rao (1986) had proven that a minimum temperature of 402°C (during isothermal heating) was required for the complete destruction of organic matters in rice husk to liberate silica. Sen and Ghosh (1992) in their studies on the combustion of rice husk in fluidised bed showed a temperature of at least 700°C for 3 minutes was sufficient for the complete combustion of whole husk particles, with the time reduce to 1 minute for ground rice husk due to larger surface contact area with oxidants and heat. Further, they found that complete combustion could not be achieved beyond 900°C due to the phenomenon of carbon entrapment in the ash.

During combustion of rice husk in the fluidised bed, rice husk at ambient temperature will be fed directly into the hot bubbling bed region (600 – 700°C). Hence, sudden heating of the rice husk will take place and the formation of entrapped carbon in the ash is expected to occur. Hence, the removal of the detrimental impurity of potassium from rice husk prior to its combustion in the fluidised bed is hypothesised to eliminate the phenomenon of carbon entrapment in the ash. This subsequently leads to a higher rate of carbon oxidation and thus, producing ash with very low residual carbon content.

c) Effect on the Melting Point / Onset of Agglomeration of Rice Husk Ash

According to Kaupp and Goss (1981 – 1982), rice husk ash are eutectic mixtures with their melting point largely determined by the ratio of various mineral fractions. They further reported that any small change in the mineral contents of rice husk especially the potassium and sodium contents, may introduce a significant drop in the melting point. Pure silica has high melting point, such as quartz (1470°C) or cristobalite (1700°C) (Perry et al., 1997). Amorphous silica, as with other amorphous materials, do not have a definite

melting point and therefore its melting point ranges from 1460 – 1610°C (Lide, 2001). However, the melting point of silica in rice husk ash was found to be lower, as shown in the ash fusibility test (or pyrometric cone test) by Mansaray and Ghaly (1998a), which yielded the following results: initial deformation temperature = 1440°C, softening temperature = 1498°C, hemispherical temperature = 1580°C and fluid temperature = 1650°C. The presence of potassium and sodium compounds (K_2O and Na_2O) causes the ash to remain sticky at much lower temperature than the melting point of ash. Sodium and potassium salts react with silica in the ash to form eutectic mixtures having low melting points. The melting point of these eutectic mixtures might be as low as 600 – 700°C at high concentration of sodium or potassium (Armesto et al., 2002). Further, studies by Jenkins et al. (1996) showed that raw rice straw samples with potassium and sodium levels of 11.3 wt% and 1.9 wt% (in ash on a dry basis) respectively, demonstrated sintering and fusing effects at temperatures between 900°C and 1000°C. When these potassium and sodium compounds were removed, the sintering and fusing temperatures were elevated to 1100°C and 1600°C, respectively.

In the fluidised bed, surface melting of ash resulted in the formation of agglomerated bed particles which led to the defluidisation phenomenon (Seville et al., 1998). Mixing of bed particles is interrupted and therefore, defluidisation is detrimental to the operation of the fluidised bed. Since the washing step to remove alkali metals in rice husk such as potassium and sodium could increase the melting point of rice husk ash, it is hypothesised that such defluidisation phenomenon could be eliminated.

2.3.4 Air Supply

According to existing literatures reviewed by Natarajan et al. (1998a), the air factor (or equivalence ratio) for the combustion of rice husk in fluidised bed ranged from 1.1 – 4.4 (Table 2-7).

Table 2-7: Optimum air factor reported in literature (as reviewed by Natarajan et al., 1998a) for combustion of rice husk in fluidised bed

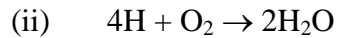
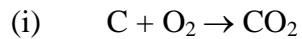
No.	Reference	Air Factor
1	Peel and Santos (1980)	1.15
2	Bhattacharya et al. (1984)	1.14
3	Preto et al. (1987)	1.30 – 1.95
4	Bhattacharya and Wu (1989)	1.1 – 4.4

The temperature in the fluidised bed is influenced by the air factor, as theoretically, combustion temperature is the highest at air factor of 1 (stoichiometric air). Beyond air factor above stoichiometric, part of the heat evolved from the combustion process is used to heat up the excess air, therefore resulting in a steady drop in temperature as the air factor is increased. Besides, feeding air at near-stoichiometric level is preferable to ensure sufficient oxygen for the oxidation of rice husk in the bed. Further, the silica structure of the resulting ash (amorphous or crystal) had been shown to be influenced by air factor. Hamad and Khattab (1981) found that the use of higher air rates during combustion in a fixed bed resulted in the crystallisation of rice husk ash. Although not in quantitative form (i. e. values of air factor were not reported specifically), these results gave an important perspective to the current research. This is because apart from maintaining good, stable combustion of rice husk in the fluidised bed, the air factor that will be selected should also ensure that crystallisation of the resulting ash do not take place. Therefore, air factors of below and above the stoichiometric level will be investigated during the experimental study. The air supply into the fluidised bed could be split into three portions, as primary air, secondary air and pneumatic air in the case whereby pneumatic air is used to convey rice husk into the fluidised bed.

a) Primary Air

The combustion process in the fluidised bed proceeds at two distinct zones, namely the density phase zone (bubbling bed) and the dilute phase zone (freeboard). The amount of primary air (fluidising air) used directly affects the bed temperature. Therefore, during combustion in the fluidised bed, the bed temperature is manipulated through the primary air factor. The primary air factor, in turn, could be manipulated through the amount of

rice husk feed. If the stoichiometric air amount for the rice husk feed is known, then the amount of rice husk feed could be calculated based on the value of primary air factor to be investigated. The amount of stoichiometric air for combustion of rice husk could be computed by assuming complete reaction as follows:-



The oxygen requirement is computed from the following formula:-

$$\text{Oxygen requirement} = \text{mol C} + \frac{1}{4} (\text{mol H}) - \frac{1}{2} (\text{mol O}) \quad (2-12)$$

The ultimate contents of the rice husk feed needs to be known in order for Equation 2-11 to be used. The computed amount of oxygen is then multiplied by the factor of 4.76 to obtain the amount of air required.

b) Secondary Air

According to Chen et al. (1998), the combustion intensity during the combustion process of rice husk in the fluidised bed was concentrated in the dilute phase zone and as such, the temperature at that zone was higher than that in the density phase zone. In their studies of rice husk combustion in a firebrick-insulated fluidised bed, the combustor temperatures were found to achieve peak values at the freeboard due to the burning of high amount of volatile gases. Further, it was noted that the combustion intensity in the middle region of the dilute phase zone was the strongest as the highest peak temperature was achieved in that region. They also noted that increasing the secondary airflow into the fluidised bed resulted in the increase in freeboard temperatures (Figure 2-3), as the increased amount of secondary air facilitated the volatile combustion of rice husk and char burnout, thereby enhancing the overall burnout percentage of rice husk. They further suggested that the reasonable primary to secondary air ratio for combustion of rice husk in a fluidised bed was 7:3.

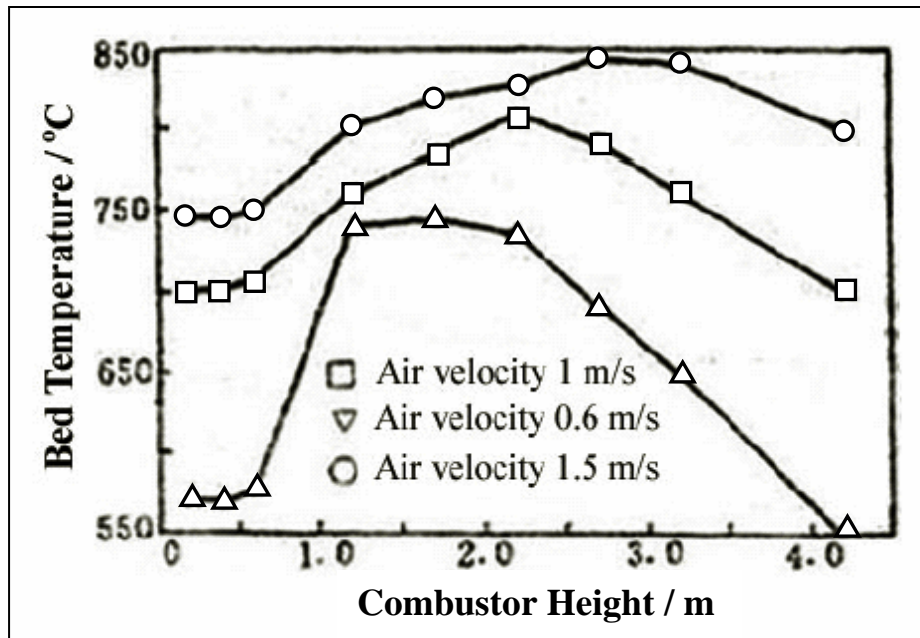


Figure 2-3: Effect of secondary airflow on the temperature distribution in the firebrick-insulated fluidised bed combustor during the combustion of rice husk (Chen et al., 1998)

c) Pneumatic Air

During the feeding of low bulk density materials such as rice husk into the fluidised bed, the use of pneumatic air is necessary in order to convey the particles into the combustor. Further, it is preferable to convey these rice husk particles as near as possible to the bed region so that they could be easily engulfed into the hot bubbling bed region and be burnt effectively thereon. The velocity of this pneumatic air should also be carefully manipulated so as to prevent backflow in the feeding chute as well as to prevent excessive elutriation due to the increased velocity in the freeboard region. The lower limit of the pneumatic air feeding velocity is governed by the operating fluidising velocity at the bed region, whereby a feeding velocity slightly higher than that of the upward flowing fluidising velocity is necessary to prevent backflow of materials in the feeding chute. On the other hand, the upper limit is governed by the elutriation rate of the rice husk particles, which in turn depends on the terminal velocity of the rice husk particles. Besides, the use of higher amount of pneumatic air results in the cooling effect near the feed entry region, which is undesirable.

With the location of the pneumatic air inlet being similar, the amount of pneumatic air entering the combustor does affect the hydrodynamics inside the combustor, in particular the trajectories of the rice husk particles and subsequently its residence time inside the combustor. To obtain higher carbon burnout of rice husk, it is desirable for the rice husk particles to penetrate deep into the hot bubbling sand bed as well as minimising the entrainment of unburnt or partly-burnt rice husk particles, thereby increasing their residence time.

2.3.5 Moisture Content in Rice Husk

Rice husk is relatively dry, with moisture content of approximately 10 wt% only (Mansaray and Ghaly, 1997). The amount of moisture present in rice husk prior to feeding into the fluidised bed combustor affects the feeding characteristics and bed temperature. Washing rice husk with water to remove the impurities of potassium and sodium results in wet rice husk. There is a possibility of feeding these wet rice husk particles directly into the fluidised bed, thus eliminating the need for drying process. However, wet husk tends to clump together, thus preventing their smooth drainage from the hopper to feeding device, for example a screw conveyor. Further, due to the clumping effect, they tend to drop to the bed in relatively large amount compared to their dry, loose form. One advantage of this is that the rice husk particles are encouraged to be burnt inside the bed. On the other hand, this might also disrupt the bubbling and subsequently the bed mixing behaviour. In addition, the wet rice husk absorbs the heat available from the bed and converts it into latent heat of vaporisation for the drying process. The bed temperature is lowered, thus posing the risk of quenching the combustion process. Lower bed temperature leads to the lower rate of carbon oxidation.

Nevertheless, the presence of more moisture might be beneficial as the water molecules dissociate at high temperatures to form free radicals of hydrogen (H^{\bullet}) and

hydroxyl ($\bullet\text{OH}$), which participate in the oxidation kinetics of carbon monoxide (Niessen, 1995). According to Henrich et al. (1999), complete char combustion requires a surplus of oxygen and carbon monoxide should not be present for thermodynamic reasons. Some processes even employed the injection of steam to take advantage of this phenomenon, such as the study by Boateng et al. (1992). As such, the presence of higher moisture content in the rice husk is expected to increase the conversion rate of carbon monoxide to carbon dioxide. This in turn enables the complete oxidation of char to take place, resulting in carbon-free ash.

2.4 Effects of Fluidised Bed Design on the Combustion Efficiency of Rice Husk in Fluidised Bed

Apart from operating parameters, the combustion efficiency is also affected by the design of the fluidised bed such as the freeboard height and feeding arrangement. The freeboard height is related to the elutriation rate of bed particles and carbon conversion efficiency, whereas the feeding arrangement is related to the carbon conversion efficiency and ash particle size.

2.4.1 Freeboard Height

According to Briens et al. (1988), the gas leaving the top of the bed in a column containing a bed of fluidised solids carries with it the entrained solid particles. The flux of the entrained solid decreases until a certain height above the bed surface, defined as the transport disengaging height (TDH), is reached. From that height onwards, the flux of the entrained solids remains essentially constant. Hence, fluidised bed columns are designed in such a way that the gas exits above the TDH. The TDH will also act as a

freeboard region in which secondary combustion process of evolved volatile matters will take place. In short, the TDH will serve dual functions of:-

- i) returning bed particles ejected into the freeboard region as a result of bubble eruption at the bed surface, and
- ii) acting as secondary combustion zone for further oxidation of elutriated rice husk particles, unburnt volatile gases or residual carbon in the fly ash.

The transport disengaging height could be estimated from the chart developed by Zenz and Weil (1958), as shown in Figure 2-4. For combustion of rice husk, the upper limit of fluidising velocity is approximately 1.1 m/s (Sen and Ghosh, 1992), which is the terminal velocity of rice husk. Assuming that the secondary air in the freeboard is half the amount of fluidising air used, the gas velocity in the freeboard is approximately 1.6 m/s. From the Figure 2-4, with fluidised bed inner diameter of 210-mm such as that used in the current experimental study, the required TDH is approximately 4 metres. However, the reasonable height to diameter ratio for fluidised bed combustors is 13 (Madhiyanon et al., 2004). This ratio is related to the stability of the equipment structure. In the case of the 210-mm diameter fluidised bed, this ratio is approximately 20. Therefore, in order to achieve a reasonable height to diameter ratio, it is necessary to increase the column inner diameter, for example to 500mm. Using this value of column diameter, the TDH is found then found to be approximately 5 metres.

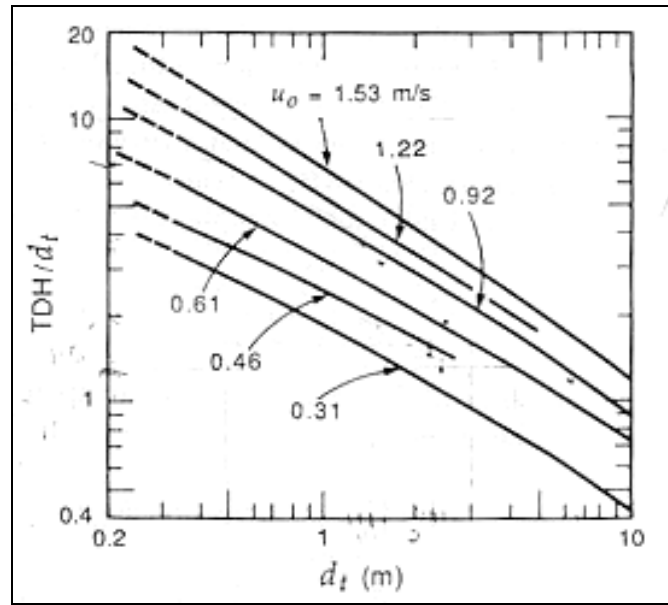


Figure 2-4: Chart for transport disengaging height (TDH) estimation of fine particle (Geldart A) beds (Zenz and Weil, 1958)

The height of the 210-mm fluidised bed combustor used in this experimental study is only 2 metres. Hence, the elutriation of sand is expected to occur and this could lead to the contamination of quartz crystals in the ash product.

2.4.2 Feeding Design and Position of Feed Entry

Rice husk has poor flow characteristics, rendering it difficult to be handled and fed into the fluidised bed. It has low bulk density (approximately 100 kg/m^3), abrasive and is interlocking in nature. Therefore, it is usually force-fed into the fluidised bed, either mechanically by a screw feeder or pneumatically by air (Natarajan et al., 1998a). Various feeding methods of rice husk into the fluidised bed combustors had been studied and reported in the literature (Table 2-8). These include feeding at the bottom of the bed (Armesto et al., 2002), feeding via a dual distributor type feeding mechanism which feeds rice husk to the bottom of the distributor (Mansaray et al., 1999), feeding just above the bed (Bhattacharya et al., 1984) and feeding at the freeboard region (Huang et al., 2001).

Feeding at the freeboard region might cause the rice husk entering the combustor to be elutriated before they drop to the bed to be burned. On the other hand, feeding directly into the bed might affect the hydrodynamics of the bed (mixing and fluidising characteristics). Therefore, it is imperative that an optimum feeding method at an optimum location be determined to prevent these undesirable conditions. However, studies on the effect of different feeding methods on the ash quality (primarily residual carbon content and silica structure) for the combustion of rice husk in fluidised beds are non-existent in literature.

Table 2-8: Different rice husk feeding arrangements reported in literature

No.	Reference	Reactor Shape and Size (mm)	Rice husk Feeding Arrangement	Fuel Flowrate (kg/hr)
1	Peel and Santos (1980)	Cylindrical (200)	Screw or pneumatic feeding	NA
2	Hiler (1982)	Cylindrical (300)	Screw and star feed wheel	NA
3	Van den Aarsen et al. (1982)	Cylindrical (300)	Screw feeding into bed	50
4	Bhattacharya et al. (1984)	Square (50 × 150)	Screw feeding	2 – 15
5	Xu et al. (1985)	Cylindrical (152)	Fuel augered into bed at 45 cm from distributor	9 – 22
6	Bingyan and Zhongnan (1987)	Cylindrical (150)	Ground and whole rice husk fed into bed at 0.5 m and 1.8 m above distributor, respectively	15 – 20
7	Flanigan et al. (1987)	Cylindrical (150)	Fuel augered into bed at 1.8 m from distributor plate	14 – 18
8	Preto et al. (1987)	Rectangular (380 × 406)	Underbed feeding by screw feeder	NA
9	Bhattacharya and Wu (1989)	Cylindrical (150)	Fed by screw feeder 70 cm above distributor plate	7 – 9
10	Hartiniati et al. (1989)	Cylindrical (400)	Fed just above distributor plate by screw feeder	75 – 105
11	Sanchez and Lora (1994)	Cylindrical (200)	Fed by screw conveyor 50 mm above distributor	NA
12	Mansaray et al. (1999)	Cylindrical (255)	Dual type feeding mechanism which fed rice husk to bottom of distributor, rice husk entered bed together with fluidising air	NA

Note:

Adopted from Natarajan et al. (1998a) (pg. 537) except item (12)

NA – Not available

During combustion of rice husk in a fluidised bed, the feeding method and position affect both the combustion behaviours and ash quality. Upon feeding into the fluidised bed, the retention of the rice husk particles in the bed region as well as their tendency to elutriate into the freeboard region towards the cyclone play an important role in governing the

combustion characteristics inside the combustor. These factors subsequently affect the quality of the resulting ash, in terms of the carbon burnout and the particle size.

a) Effect on Rice Husk Retention in the Sand Bed and Elutriation into the Freeboard Region

Rice husk particles have relatively low terminal velocity due to their low density nature, rendering them easy to be entrained into the fluidising air of a fluidised bed combustor and subsequently be elutriated out of the combustor. The terminal velocities of rice husk particles were reported to range from 0.76 m/s (Hao et al., 1995) to 1.1 m/s (Sen and Ghosh, 1992), which in comparison was much lower than that of the bed media, usually silica sand (for example, the terminal velocity of rice husk was 20 – 50% lower than that of the estimated terminal velocity of silica sand of size 250 – 595 μm , at 1.4 m/s, that was used in the current experimental study). Thus, during the combustion of rice husk in a fluidised bed combustor, the probability of the rice husk particles being elutriated prior to the completion of burning process is high, thereby lowering their overall residence time in the combustor. The probability of unburnt rice husk particles being elutriated out of the combustor, on the other hand, is related to the feeding conditions, namely the types of feeding method and the position of the feed entry. For rice husk, force-feeding into the combustor is necessary due to their interlocking nature, usually by screw feeder or via the use of pneumatic air to convey the particles into the combustor. Further, the position of feed entry is also of prime importance in order to encourage the rice husk particles to be retained in the bed region for a sufficient period of time for the burning process to take place due to the availability of heat source, oxidising agent (air) and high turbulence in that region. In addition, bubble eruption at the bed surface tends to ‘engulf’ these particles, thereby aids in increasing their residence time as well as breaking their rigid skeleton-like structure to release the entrapped carbon for ease of further conversion. Therefore, feeding of rice husk near the bed region is favourable as opposed to feeding at the freeboard region, where excessive elutriation of unburnt rice husk particles were known to occur. Ideally, feeding directly into the bed region shall be able to give the highest residence time of rice husk particles in the bed region. However, apart from the mechanical complexities associated with feeding into a bed of hot bubbling particles

(escape of bed particles through the feeding chute, backflow of feed particles and initiation of devolatilisation of feed materials in the feeding chute to high temperature at the bed region), this method also tends to disrupt the bed bubbling behaviour and thus the overall bed hydrodynamics, and therefore, is deemed to be of low practicality in actual combustion study. Hence, it is hypothesised that the use of pneumatic air feeding with the feed entry positioned as near as possible to the bed region is sufficient to encourage the rice husk particles to enter the bubbling bed region while being able to prevent excessive elutriation into the freeboard region.

b) Effect on Ash Quality (Particle Size and Carbon Burnout)

As discussed earlier, feeding of rice husk particles near the bed region enables these particles to penetrate deep into the hot, turbulent bubbling bed and thus the resulting ash tend to be finer in size with higher carbon burnout (lower residual carbon content). The circulation of the rice husk particles in the bed region as they proceeded to be burnt resulted in an overall higher residence time as opposed to particles that were elutriated into the freeboard region. Besides, the vigorous action from the turbulent bubbling bed enabled the rigid, skeleton-like structure of the rice husk particles to be broken into smaller fragments and allowing the entrapped carbon to be released for further conversion. Hence, it could be hypothesised that:-

- ii) If feeding is near the bed region, the resulting ash will be finer in size (broken into smaller fragments) as well as whiter in shade (lower residual carbon content); and
- iii) If feeding is initiated at the freeboard region of the combustor, burning only takes place at the freeboard region (devolatilisation and some degree of char oxidation), thus resulting in ash with skeleton-like structure and darker in shade (higher residual carbon content).

CHAPTER 3

METHODOLOGY

3.1 Introduction

In this chapter, the methodologies for carrying out the research works were presented. These include descriptions of the research materials, experimental, analytical and modelling techniques.

3.2 Research Materials

The materials required for this research were sand and rice husk. Silica sand used as the bed media for the fluidised bed was obtained from Johor Silica Industries Sdn. Bhd. in Kota Tinggi, Johor. Meanwhile, rice husk as the raw material for production of amorphous silica were obtained from a rice mill in Muar, Johor. The mill currently disposes the rice husk via open field burning.

a) Chemical Properties of Rice Husk

The chemical properties of the rice husk sample, as determined from proximate and ultimate analyses, were as shown in Table 3-1.

Table 3-1: Chemical properties of rice husk

Parameter	From analysis	Mansaray et al. (1997)
Proximate Analysis (wt% wet basis)		
Moisture	10.1	8.7 – 10.4
Volatile matter	64.1	57.2 – 63.5
Fixed carbon	11.1	9.2 – 13.1
Ash	14.7	16.5 – 22.2
Gross calorific value (MJ/kg)	13.3	14.7 – 18.3
Ultimate Analysis (wt% dry basis)		
Carbon (C)	37.8	37.6 – 44.5
Hydrogen (H)	5.0	4.7 – 5.5
Oxygen (O)	40.3	31.5 – 35.2
Nitrogen (N)	0.6	0.4 – 0.5
Ash	16.3	14.3 – 23.4
Sulphur (S)	ND	0.01 – 0.03

Note:

- i) ND – Not Detectable
- ii) Proximate analysis according to the American Society for Testing Materials (ASTM) methods D3173 (moisture), D3174 (ash), D3175 (volatile matters), D240-76 (gross calorific values)
- iii) Ultimate analysis according to UOP Method 86-86 (Determination of Carbon, Hydrogen and Nitrogen by Oxidative Analysis). Content of Oxygen (O) by differential method: $O = 100 - (C + H + N + S + \text{ash})$ in dry basis

Based on the chemical properties of rice husk, the adiabatic flame temperatures during combustion of rice husk at different air factors were computed using the FLAME program code and the results were shown in Figure 3-1.

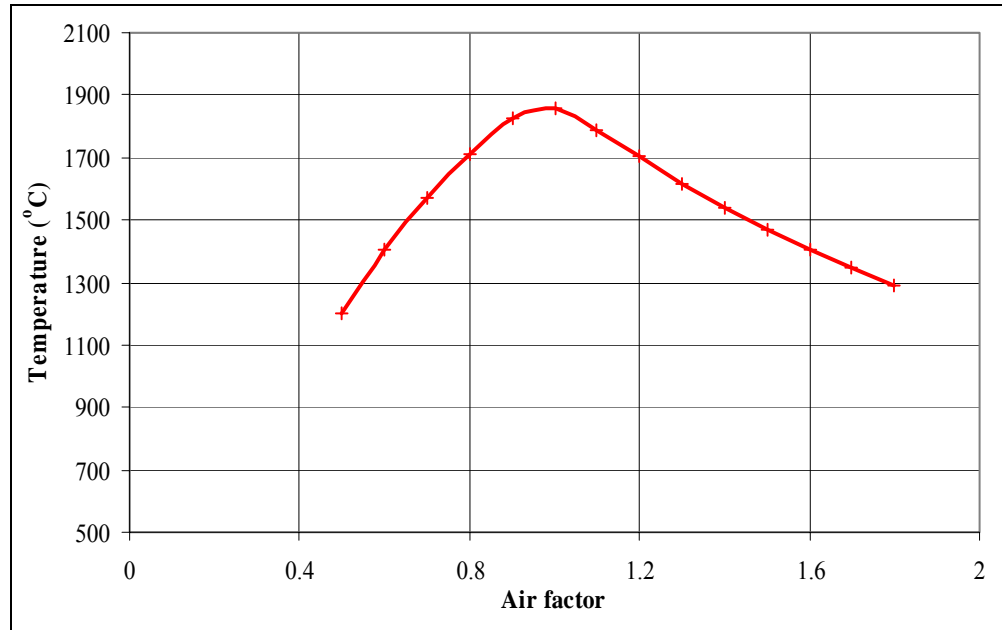


Figure 3-1: Adiabatic flame temperatures from combustion of rice husk sample at different air factors computed using the FLAME programme code

b) Size Distribution of Sand

Two sand samples with the size ranges of 250 – 595 μm and 595 – 841 μm , respectively were subjected to sieve analysis and their particle size distribution were as shown in Figure 3-2. The volume-surface mean diameters of these sand samples were computed to be 342 μm and 672 μm , respectively.

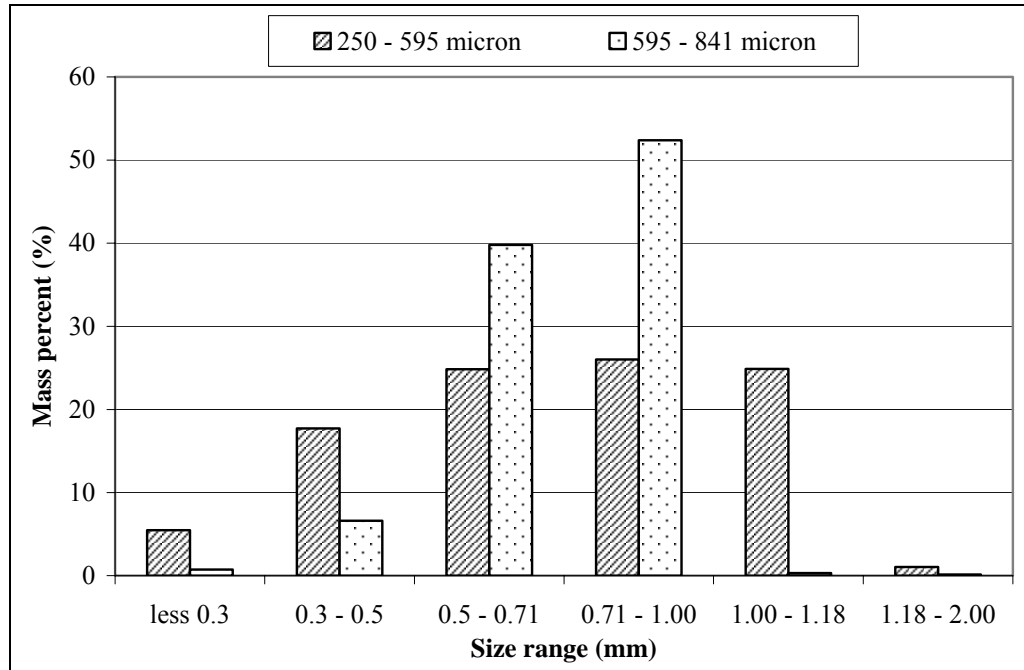


Figure 3-2: Particle size distribution of silica sand samples used in the experimental study

c) Fluidisation Properties of Rice Husk, Rice Husk Char, Rice Husk Ash and Silica Sand

The bed particles used in the research works were shown in Figure 3-3. It was observed that rice husk particles have a boat-like shape (Figure 3-4) consisting of two interlocking halves that makes it very difficult to fluidise (Huang et al., 2001). The whole husk particles have average length and width of 8 – 10 mm and 1.5 – 2.5 mm, respectively. Sen and Ghosh (1992) also reported that rice husk is difficult to fluidise due to its cylindrical shape, non-granular and flaky nature. Its length to width ratio is as high as 4 and its rough surface results in large inter-particle friction. However, when mixed with other solid particles to form a multisolid system, its fluidisation behaviour was improved (Xu et al., 1985; Sen and Ghosh, 1992; Bingyan and Zongnan, 1987). Hence, it is necessary to include other particles such as silica sand into the fluidised bed to form its bed media, thereby improving the overall fluidisation quality, and thus the mixing in the bed. During the combustion process, rice husk char and ash are also present in addition to rice husk and sand in the bed region. Therefore, apart from sand, the fluidisation properties of rice husk, its ash and char were also determined (as outlined in Section 3.3.2).



Silica sand (595 – 841 μm)



Silica sand (250 – 595 μm)

Figure 3-3: Bed particles used in the combustion of rice husk in fluidised bed



Figure 3-4: Boat-like shape of whole rice husk

d) Silica Structures in Rice Husk, Rice Husk Ash and Sand Samples

All particle samples used in this research were analysed for their silica structures using X-Ray Diffraction (XRD) analysis (as outlined in Section 3.4.1). Fresh rice husk contained amorphous silica (Figure 3-5), which upon thermal treatment remained in the amorphous form (Figure 3-6) if the treatment temperature was kept below its crystallisation temperature. Silica in rice husk ash formed cristobalite crystals beyond its crystallisation temperature, which were detected as a peak at 2θ angle of 21.93° in the diffractogram (Figure 3-7). Meanwhile, silica in the fresh sand sample were present as quartz crystals (Figure 3-8), which remained unaltered after their usage as bed material in the fluidised bed (Figure 3-9).

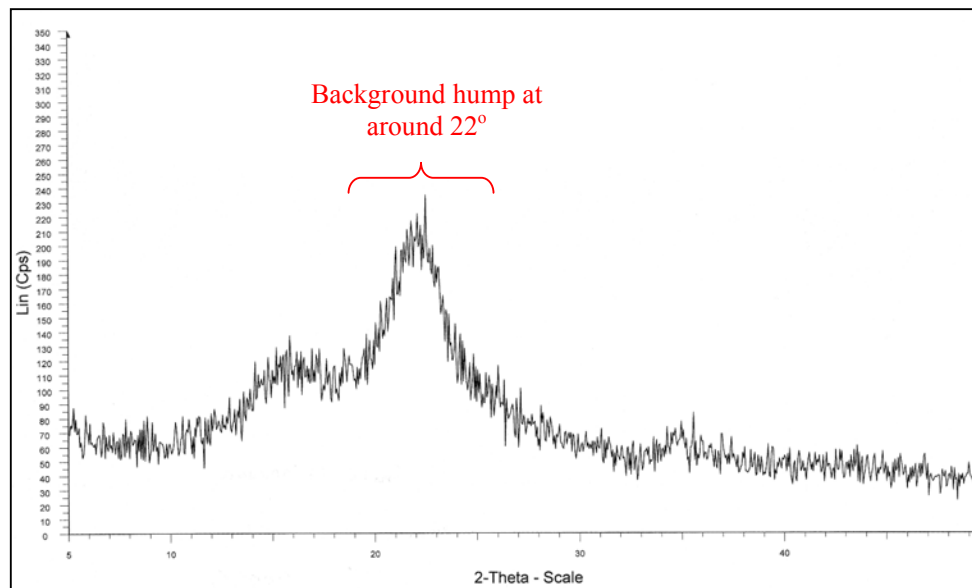


Figure 3-5: Diffractogram of fresh rice husk sample

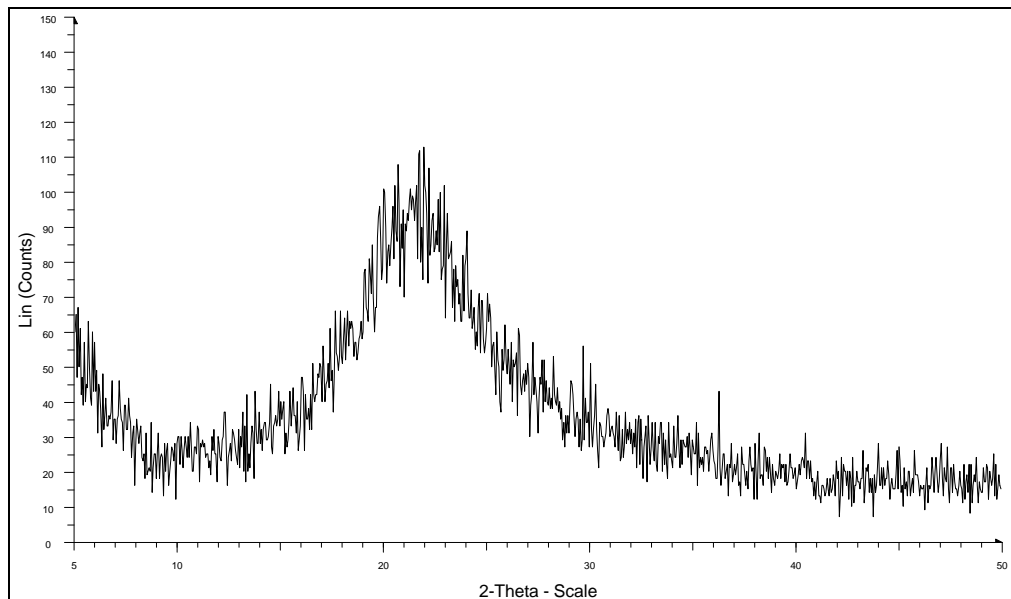


Figure 3-6: Diffractogram of amorphous rice husk ash (from thermal treatment of rice husk in muffle furnace at 600°C and 1 hour)

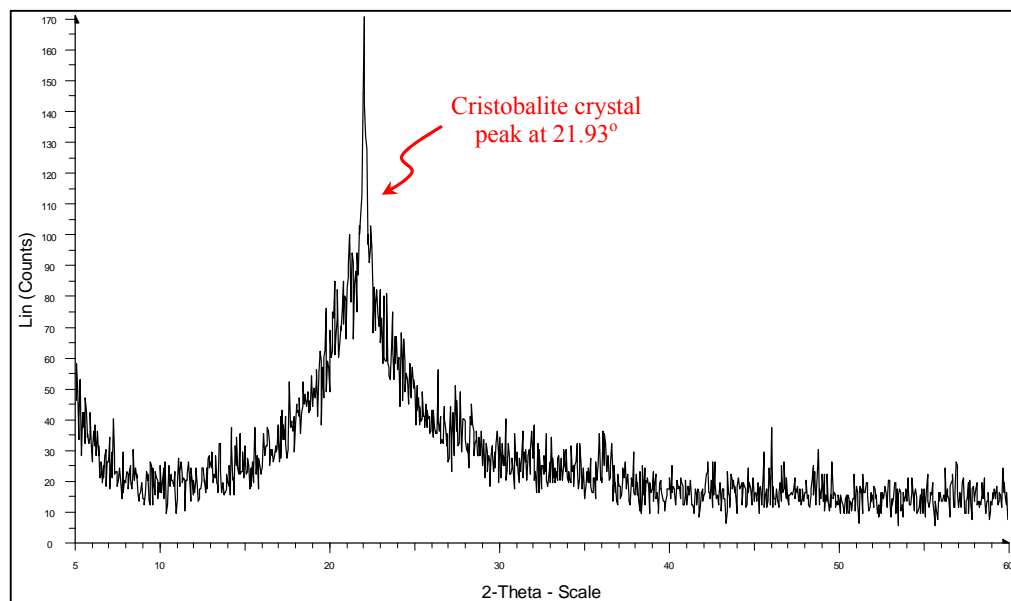


Figure 3-7: Diffractogram of crystallised rice husk ash (exposure to temperature of 725°C for 10 hours in a muffle furnace)

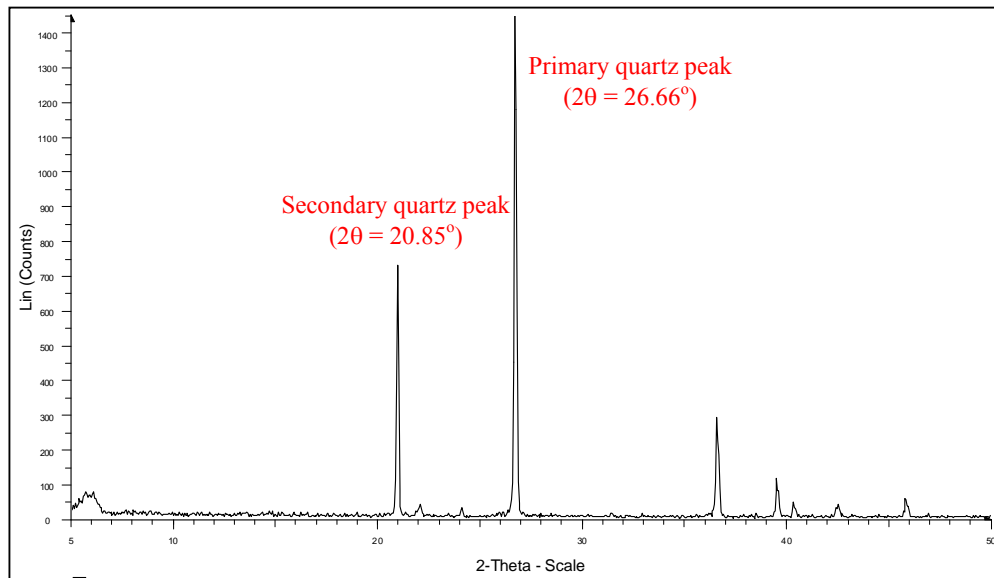


Figure 3-8: Diffractogram of fresh silica sand

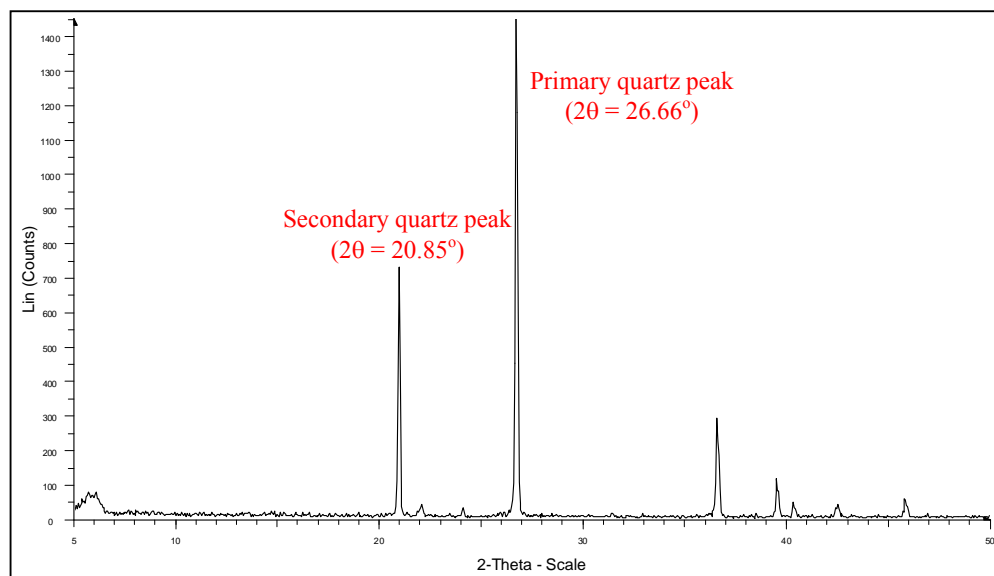


Figure 3-9: Diffractogram of used silica sand (from fluidised bed after combustion of rice husk)

3.3 Experimental Techniques

3.3.1 Thermal Treatment in Muffle Furnace

A muffle furnace (BOLE Model HF2) was used to investigate the following:-

i. Basic Combustion Characteristics and Combustion Times of Rice Husk

A stainless steel plate was placed inside the muffle furnace and the furnace was heated up to temperatures in the range of 650 – 750°C. Maintaining the furnace at these temperatures, a batch of ten whole husk particles (raw rice husk) were then spread out widely apart onto the steel plate and the time count started. This experimental setting represented the model of single particle combustion. The times for the flaming and char combustion processes to complete were recorded. The experiment was performed ten times to obtain the average flaming and char combustion times. The same experiment was repeated by using larger amount of rice husk (approximately 4 g) spread out widely apart on the steel plate. This setting represented the model of group particle combustion. Subsequently, all these procedures were repeated using water-washed rice husk.

ii. Time-Temperature Relationship for the Onset of Silica Crystallisation in Rice Husk Ash

Both the raw and water-washed rice husk samples were subjected to thermal treatment in the muffle furnace set at temperatures of 700°C, 750°C, 800°C and 850°C. During the study, these temperatures were controlled to the accuracy of $\pm 10^\circ\text{C}$. For each experiment, the muffle furnace was heated up to the desired temperature, after which approximately 2 g of rice husk sample were placed immediately onto a stainless steel plate inside the muffle furnace and the time count started. The residence time of each type of rice husk sample inside the muffle furnace at each temperature being investigated ranged from 1 – 3 minutes, controlled to the accuracy of ± 5 seconds. Each experiment was repeated several times to collect sufficient samples (approximately 10 g) for analyses of their silica structures and residual carbon contents.

3.3.2 Fluidisation Study in 80-mm (Inner Diameter) Fluidised Bed Column

The fluidisation properties of rice husk, rice husk char, rice husk ash and silica sand samples were investigated in an 80-mm inner diameter fluidised bed to determine their minimum fluidisation velocities and terminal velocities. The fluidised bed column was made of Perspex and the distributor was a perforated plate (1mm diameter hole, 3% orifice area). A manometer was used to measure the pressure drop while a rotameter was used to measure the volumetric flow rate of air supply from the high-pressure blower. The fluidising air was first dried in an air filter to prevent the air humidity from interfering with the fluidisation process. Then, the effects of fluidisation parameters on the mixing behaviour of rice husk in the fluidised bed were investigated. The schematic diagram of the experimental setup was shown in Figure 3-10.

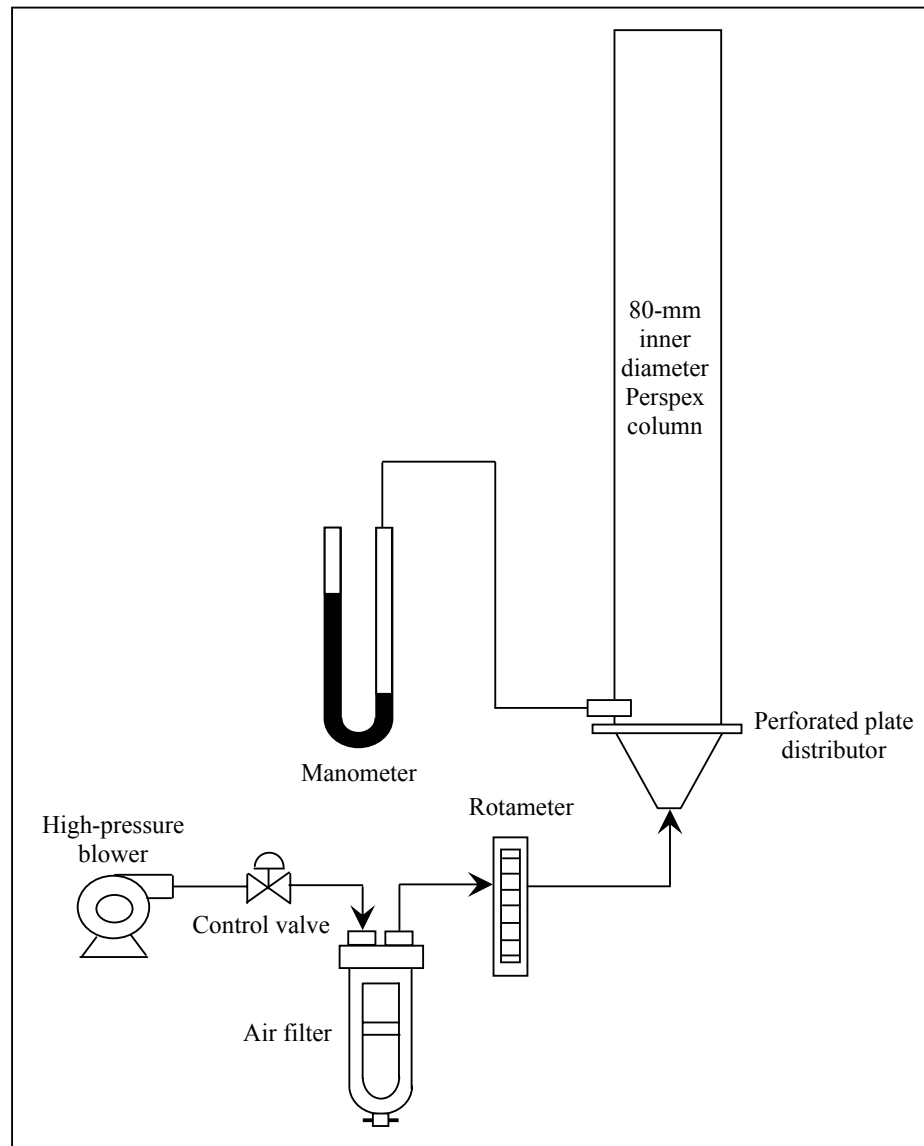


Figure 3-10: Experimental setup of the 80-mm inner diameter Perspex fluidised bed for investigation of fluidisation and mixing behaviours of rice husk

a) Determination of Fluidisation Properties of Rice Husk, Rice Husk Char, Rice Husk Ash and Silica Sand Samples

i) *Minimum Fluidising Velocity*

An amount of rice husk was charged into the fluidised bed column to give a static bed height of $1 D_c$ (80mm). The fluidising air velocity was increased in small intervals and the corresponding pressure drop recorded. When the bed pressure drop was observed to reach a constant value indicating that the whole bed had been

fluidised, the air velocity was decreased in small intervals and the corresponding pressure drop also recorded. The pressure drop values obtained were plotted against the fluidising air velocities. The minimum fluidising velocity, U_{mf} , was given by the intersection of the extrapolations from the region of fixed bed and fluidised bed (horizontal line) on the plot (Figure 3-11). The value of U_{mf} was taken from the plot of decreasing flow as the value obtained from the increasing flow was affected by the hysteresis loops (Figure 3-12). The formation of these hysteresis loops were due to the packing of bed material when it was at its initial fixed state, which resulted in its sudden transition to the fluidising state at increasing air velocities. The same procedures were then repeated for the rice husk char, rice husk ash and silica sand samples.

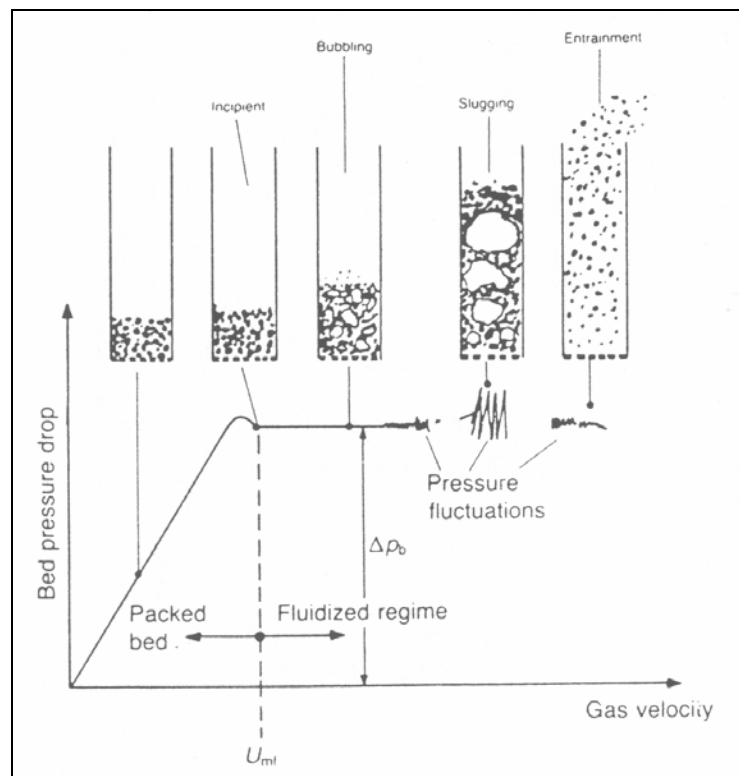


Figure 3-11: Behavioural changes of bed with gas velocity in a conventional fluidised bed (Howard, 1989)

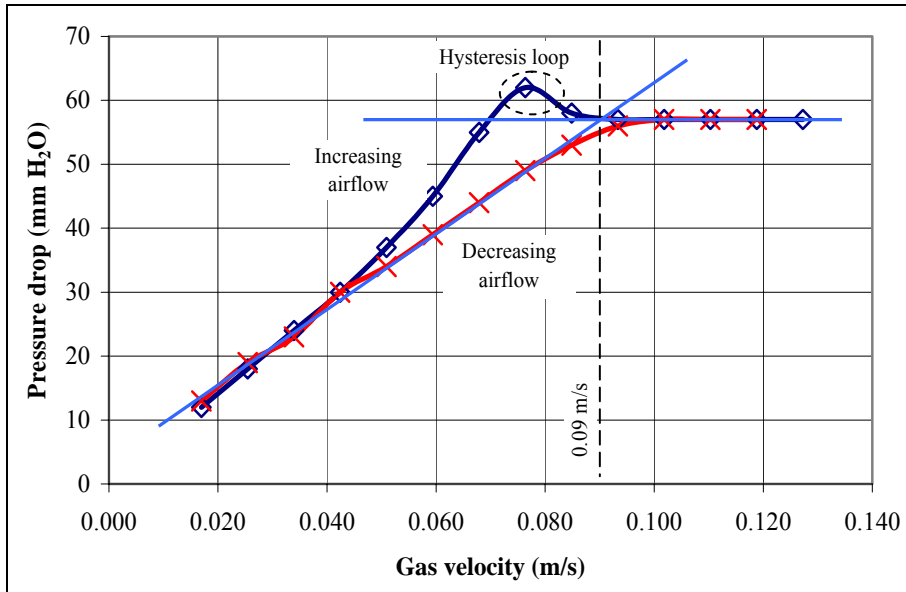


Figure 3-12: Pressure drop versus gas velocity plot for increasing and decreasing gas flow

ii. Terminal Velocity

During the experiment to determine the minimum fluidising velocity with increasing air flow, the fluidising velocity was increased further until the bed material was observed to be blown out from the fluidised bed column. The loss of bed material resulted in the decrease in bed pressure (Figure 3-13), and therefore the interpolation of the first point of pressure decrease to the x-axis gave the terminal velocity of the bed material.

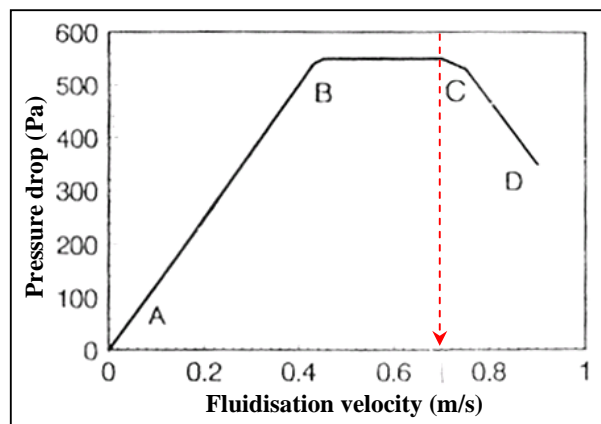


Figure 3-13: Determination of terminal velocity from the plot of pressure drop versus fluidisation velocity (Hao et al., 1995)

b) Investigation on the Effect of Fluidisation Parameters on Mixing of Rice Husk in Fluidised Bed

i) Sand Size

Approximately 300g of sand sample with size of 250 – 595 μm , which gave a static bed height of $0.5 D_c$ (40mm), was charged into the fluidised bed column. Air was introduced into the column to give a constant fluidising velocity of $4 U_{mf}$. Then, 33g of rice husk (giving approximately 9 wt% of rice husk in the sand-rice husk mixture) was charged into the column and their mixing behaviour was observed. The same procedures were then repeated with sand sample of size 595 – 841 μm .

ii) Fluidising Velocity

Sand sample with the selected size from (i) was charged into the fluidised bed column up to a static bed height of $0.5 D_c$. Air was introduced into the column to give a fluidising velocity of $2 U_{mf}$. Then, 30g of rice husk was charged into the column and their mixing behaviour was observed. The same procedures were repeated by varying the fluidising velocity to 3-, 4-, 5-, 6-, 7- and 8 U_{mf} .

iii) Static Bed Height

Sand sample with the selected size from (i) was charged into the fluidised bed column up to a static bed height of $0.25 D_c$ (20mm). Air was introduced into the column to give a constant fluidising velocity of $4 U_{mf}$. Then, rice husk (mass fraction of 10 wt% of total bed mass) was charged into the column and their mixing behaviour was observed. The same procedures were repeated by varying the static bed heights to $0.5 D_c$ (40mm), $0.75 D_c$ (60mm) and $1.0 D_c$ (80mm).

3.3.3 Combustion Study in 80-mm (Inner Diameter) Fluidised Bed Combustor System

The 80-mm inner diameter fluidised bed combustor system (Plate 3-1) consisted of the following components:-

i) Fluidised Bed Combustor Column

The combustor consists of a cylindrical column made of carbon steel with an internal diameter (ID) of 80mm and height of 1000mm. The lower section of the combustor (225mm) is substituted with a glass column of similar diameter to enable the observation of bed mixing and combustion characteristics. The bottom of the combustor consists of a cone of angle 60° . The distributor is a perforated plate with orifice diameter of 1mm and a total opening area of 3%.

ii) Cyclone

The cyclone is of the standard design (medium efficiency and medium pressure drop) with a body internal diameter of 80mm. The cyclone has dual functions of removing the fly ash from the flue gas, thus acting as a particulate control device while simultaneously acting as the tertiary combustion chamber to burn off any unreacted gaseous components.

iii) Screw Feeding System

The screw feeder conveys the feed from the hopper into the combustor via an opening at the sidewall of the column. The location of the sidewall is 300mm above the distributor plate.

iv) Compressed Air Supply

Compressed air is supplied by a compressor and is passed through air filters to remove any moisture. The air flow is metered using a rotameter before entering the combustor via the apex of the cone.

v) LPG Supply

LPG is metered via a rotameter prior to being premixed with air. The premixed LPG-air mixture enters through the apex of the cone to the fluidised bed combustor.

vi) **Temperature Measuring System**

A type-K thermocouple was placed 20mm above the distributor plate to measure the bed temperature. It is connected to the data logger for temperature monitoring.

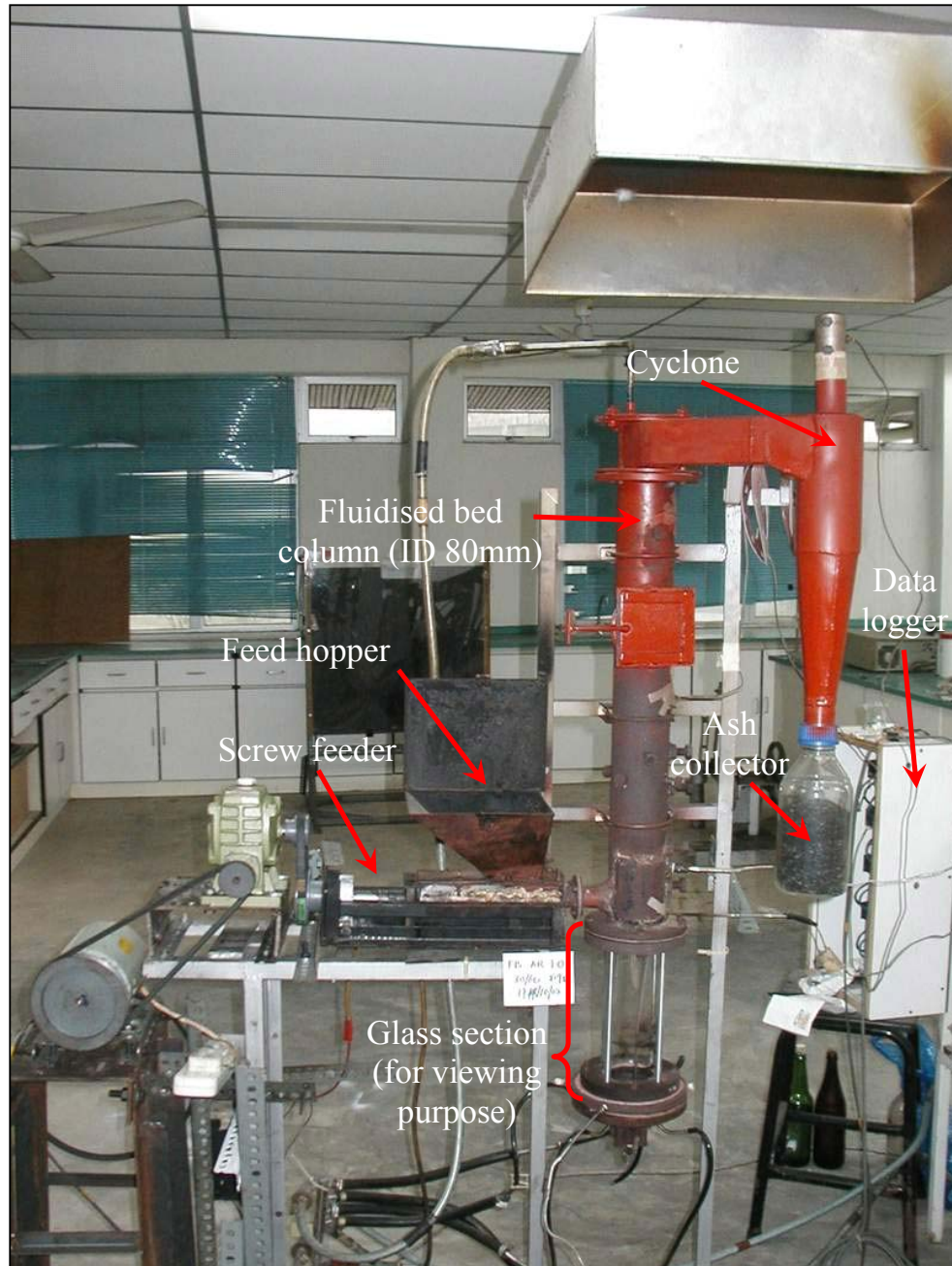


Plate 3-1: The 80-mm inner diameter fluidised bed combustor system

3.3.4 Combustion Study in 210-mm (Inner Diameter) Fluidised Bed Combustor System

The 210-mm inner diameter fluidised bed combustor system consisted of the following components:-

i) Fluidised Bed Combustor Column

The combustor consists of a cylindrical column made of stainless steel with an internal diameter (ID) of 210mm and height of 2000mm. The combustor is equipped with a viewing port located at a height of 365mm from the distributor plate and inclined at an angle of 45°. The bottom of the combustor consists of a cone of angle 60°. The distributor is a perforated plate with orifice diameter of 2mm and a total opening area of 1.5%.

ii) Cyclone

The cyclone is of the standard design (medium efficiency and medium pressure drop) with a body internal diameter of 160mm. The cyclone has dual functions of removing the fly ash from the flue gas, thus acting as a particulate control device while simultaneously acting as the tertiary combustion chamber to burn off any unreacted gaseous components.

iii) Compressed Air Supply

Compressed air is supplied by a high-pressure blower with a capacity of 1200 m³/hr and 4m H₂O pressure drop. The air is passed through air filters to remove any moisture. The air flow is metered using a rotameter (0 – 1000 LPM) as primary air into combustor through the apex of the cone and another rotameter (0 – 150 LPM) as pneumatic/secondary air, which enters the combustor via the feeding port.

iv) LPG Supply

LPG is metered via a rotameter (0 – 50 LPM) prior to being premixed with air. The premixed LPG-air enters through the apex of the cone to the fluidised bed combustor.

v) **Rice Husk Feeding System**

The feeding system consists of a screw feeder which conveys the rice husk from the primary hopper into the secondary hopper. From thereon, the pneumatic air conveyed the rice husk from the secondary hopper into the combustor via the feeding port, which is located 365mm above the distributor plate. The feeding port is inclined at an angle of 45°.

vi) **Temperature Measuring System (Thermocouples and Data Logger)**

Six (6) type-K thermocouples are placed at different heights of the combustor (Figure 3-14) to measure the combustor temperature at different heights. The thermocouples are connected to a temperature logging system to display and record the real-time temperatures at a desktop computer.

The overall schematic diagram of the 210-mm inner diameter fluidised bed combustor system was as shown in Figure 3-15. Meanwhile, Plate 3-2 showed the setup of the combustor system in the absence of insulation material.

For each experiment of rice husk combustion, the bed was preheated to the desired temperature range prior to the commencement of feeding. The bed starting-up procedure for each experiment was outlined as follows:-

- 1) A quantity of bed material (silica sand) giving the desired static bed height is poured into the fluidised bed combustor column.
- 2) Fluidising (primary) air giving the desired fluidising velocity (U_{mf} number) at the corresponding bed temperature (ranging from 650 – 800°C) is passed through the bed via the distributor plate.
- 3) If necessary, the freeboard temperatures (indicated by thermocouples T3 – T6) of the fluidised bed combustor is increased by means of secondary burner(s) to the range of 700 – 950°C.
- 4) The bed is preheated through premixed combustion of Liquefied Petroleum Gas (LPG) and air. First, an igniter (e.g. kerosene-soaked tissue ball) is dropped into the bed. Then, the premixed LPG-air mixture is passed through the bed with its flowrate adjusted so as to enable the flame to remain in the bed. Burning of the premixed gas mixture in the bed region will emit a loud

'popping' noise due to the eruption of bubbles in the bed during combustion. It will take approximately 30 – 45 minutes to preheat the bed to the temperature range of 600 – 650°C.

- 5) When the bed temperature (T1 and T2) reached the range of 600 – 650°C, rice husk feeding is initiated. The amount of rice husk feed is manipulated based on the amount of primary air in order to give the desired primary air ratio.
- 6) Depending on the specific parameters to be investigated, the temperature in the bed is maintained in the range of 650 – 800°C (by adjusting the burning rate of primary LPG) while the freeboard in the range of 600 – 950°C (by adjusting the burning rate of secondary burners) during the feeding period.
- 7) The feeding period is carried out for at least 30 minutes in order for the combustion process to be stable, which could be determined from the temperature profile which has reached its equilibrium level.
- 8) Fly ash is collected from the cyclone during the feeding period whereas bottom ash is collected by purging the ash that is accumulated in the bed region at the end of the combustion test.
- 9) For each test, a sample of at least 250 g for each ash type is collected for analytical analyses. Data on real-time temperature profile recorded by the data-logger is also compiled and analysed.

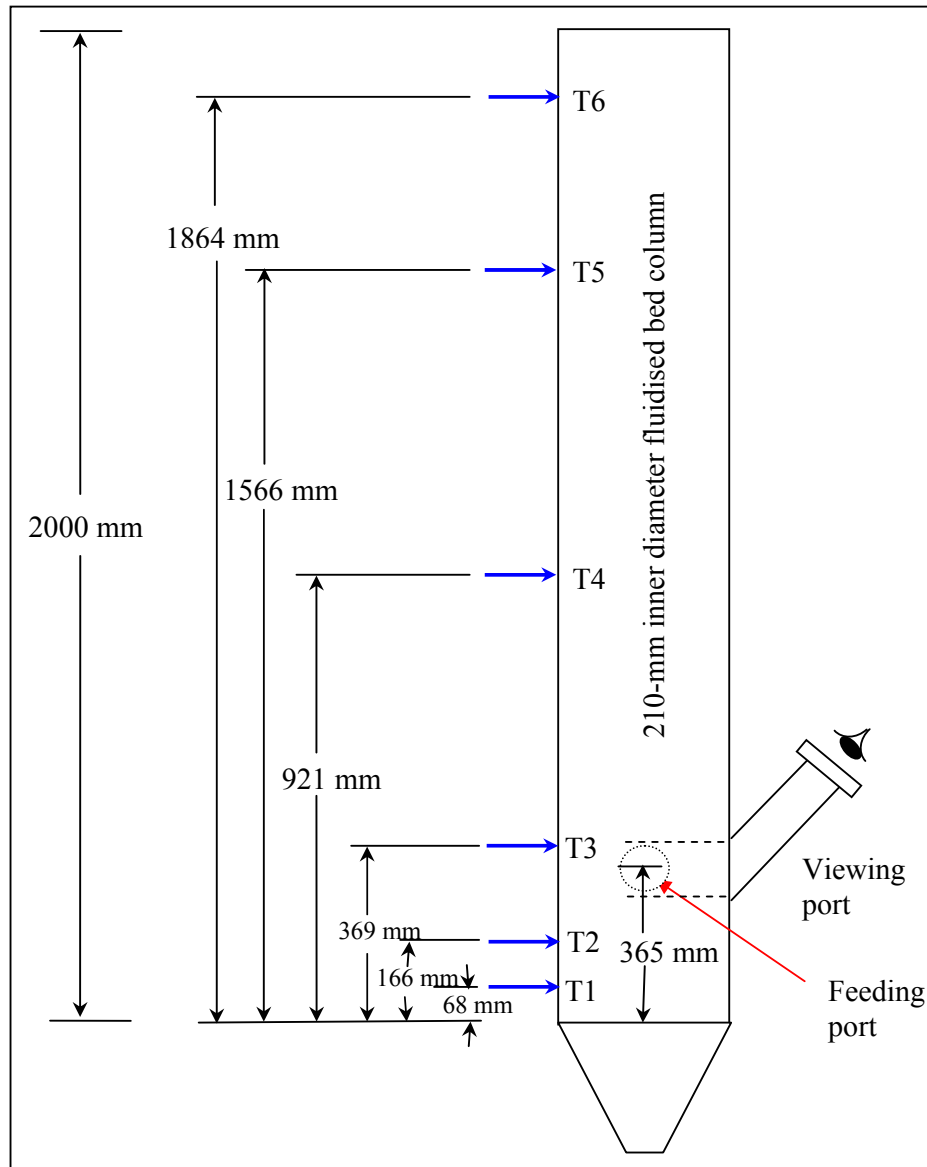


Figure 3-14: Positions of thermocouples (T1 – T6), feeding port and viewing port at the 210-mm inner diameter fluidised bed combustor

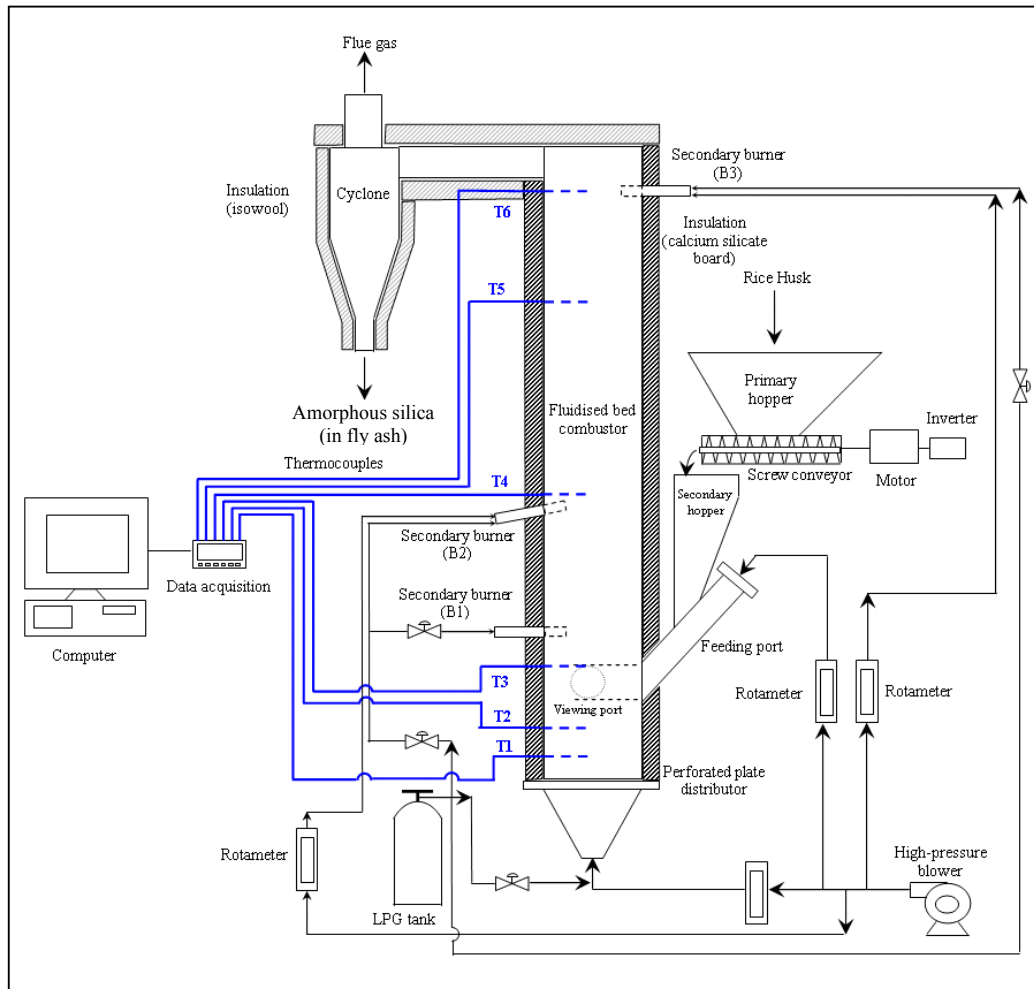


Figure 3-15: Overall schematic diagram of the 210-mm inner diameter fluidised bed combustor system

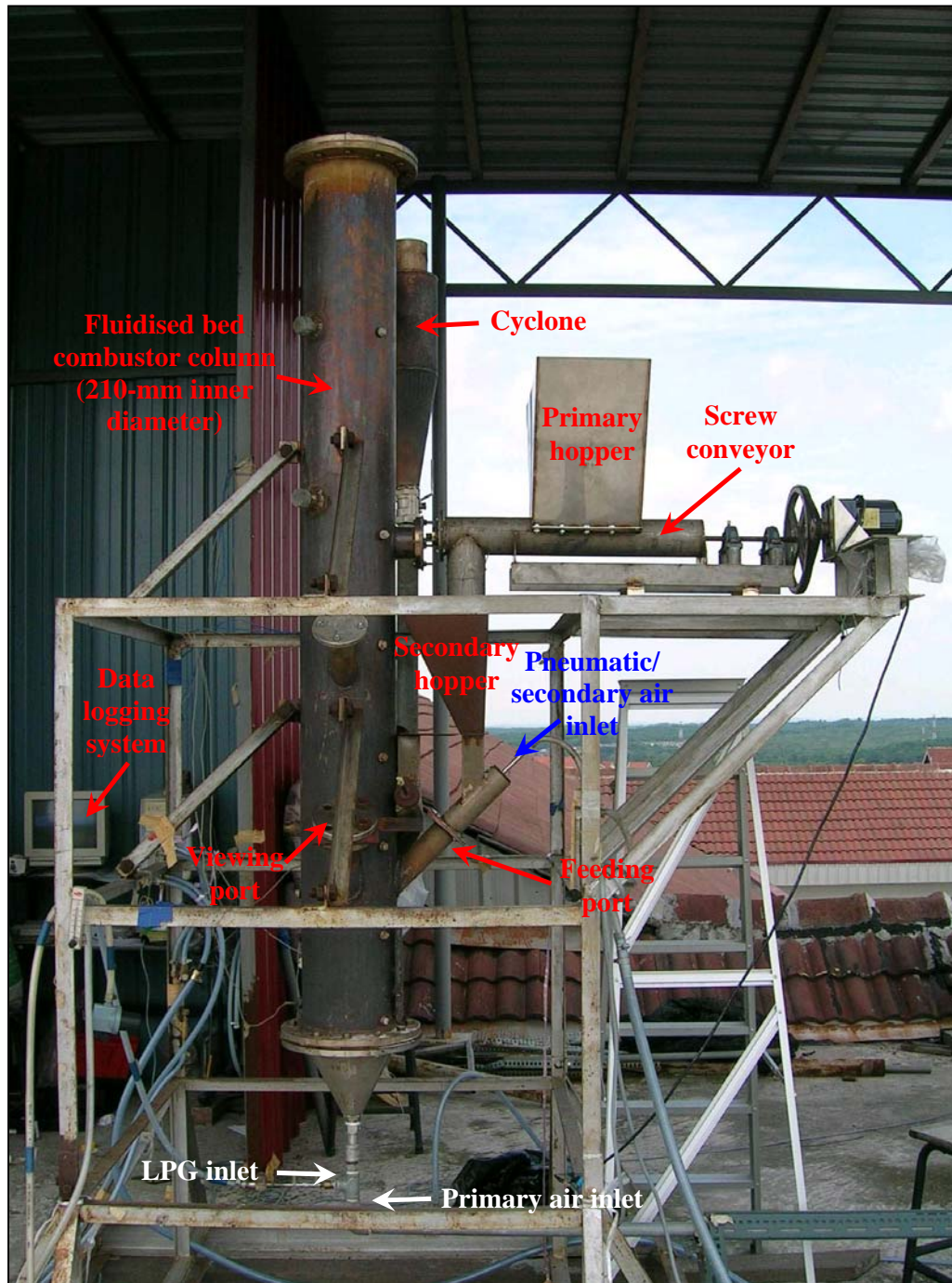


Plate3-2: The 210-mm inner diameter fluidised bed combustor system (shown without insulation material)

The combustion parameters investigated in the 210-mm inner diameter fluidised bed combustor were listed in Table 3-2 along with their respective experimental identifications.

Table 3-2: List and identifications of combustion parameters investigated in the 210-mm inner diameter fluidised bed combustor

No.	Combustion Parameter	Case Study	Values of Variables Investigated	Remarks
1	Fluidising velocity (FV)	FV1	8.1 U_{mf}	1 U_{mf} = 0.09 m/s for sand size of 250 – 595 μ m
		FV2	5.4 U_{mf}	
		FV3	4.5 U_{mf}	
		FV4	3.3 U_{mf}	
		FV5	2.5 U_{mf}	
		FV6	1.5 U_{mf}	
2	Static bed height (BH)	BH1	0.25 D_c	D_c = inner diameter fluidised bed combustor, 1 D_c = 210mm
		BH2	0.375 D_c	
		BH3	0.5 D_c	
		BH4	0.625 D_c	
		BH5	0.75 D_c	
3	Freeboard temperature (FT)	FT1	400 – 600°C	Freeboard temperatures as indicated by thermocouples T4 – T6 located at heights of 921 – 2000mm from distributor plate
		FT2	550 – 600°C	
		FT3	600 – 650°C	
		FT4	600 – 700°C	
4	Heat loss (HL)	HL1	Non-insulated	Combustor insulated with calcium silicate boards, cyclone with rockwool
		HL2	Insulated	
5	Alkali metals compounds in rice husk (PRH)	PRH1	Raw rice husk (presence of alkali metals compounds)	Burning of raw rice husk carried out at different freeboard temperatures i.e. 700 – 900°C (PRH1-a), 500 – 700°C (PRH1-b) and 400 – 550°C (PRH1-c)
		PRH2	Water-washed rice husk (negligible amount of alkali metals compounds)	
6	Primary air factor (PAF)	PAF1	0.65	Stoichiometric air factor = 1.0
		PAF2	0.81	
		PAF3	1.01	
		PAF4	1.41	
7	Primary-to-secondary air ratio (PSR)	PSR1	6:4	Secondary air source = pneumatic air source (for feeding of rice husk)
		PSR2	7:1	
8	Pneumatic air feeding velocity (PV)	PV1	0.42 m/s	Velocity of pneumatic air inside feeding port with 50mm inner diameter
		PV2	0.63 m/s	
		PV3	0.85 m/s	
		PV4	1.36 m/s	
9	Moisture content in rice husk (MC)	MC1	10.0 wt%	Moisture content in water-washed rice husk after different stages of air-drying
		MC2	26.0 wt%	
		MC3	31.0 wt%	
		MC4	57.5 wt%	
10	Feeding method (FM)	FM1	Inclined feeding	Inclination of feeding port = 45°
		FM2	Inclined tangential feeding	
11	Fluidising velocity at inclined, tangential feeding (FMV)	FMV1	3.2 U_{mf}	1 U_{mf} = 0.09 m/s for sand size of 250 – 595 μ m
		FMV2	3.9 v	
		FMV3	4.6 U_{mf}	

3.4 Analytical Techniques

3.4.1 Determination of Silica Structure and Presence of Contaminants in Rice Husk Ash through X-Ray Diffraction (XRD) Analysis

The rice husk ash samples (obtained from combustion experiments) were subjected to X-Ray Diffraction (XRD) analysis using an X-Ray Diffractometer to determine their silica structure. Prior to analysis, the ash samples were ground to a powder form by simple pounding using a mortar and pestle due to its brittle nature. The ground samples were analysed by Cu K α radiation with a scanning rate of 0.05° per second. The X-Ray Diffractometer (Model Bruker D8 Advance) is available for use at the Ibnu Sina Institute for Fundamental Science Studies, UTM Skudai. An X-Ray Diffractometer is a mechanical device for obtaining x-ray intensities as a function of the angle between the incident and the diffracted beams. The resulting phase diagram (called a diffractogram) showed the different phases present in the sample via various peak positions (Table 3-3). The phase concentration is indicated by the peak height, with higher peak representing higher concentration. The amorphous structure is indicated by a background hump at peak position of approximately 22° on the diffractogram.

Table 3-3: Diffraction peaks of crystalline silica

Type of Silica Crystals	2 θ scale		
	Primary	Secondary	Tertiary
Quartz	26.66	20.85	50.16
Cristobalite	21.93	36.11	31.46
Tridymite	21.62	20.50	23.28

Source: National Institute for Occupational Safety and Health, NIOSH (1998)

3.4.2 Determination of Residual Carbon Content in Rice Husk Ash through Loss on Ignition (LOI) Test

The residual carbon content in the rice husk ash samples were determined via loss on ignition (LOI) analysis. The dried ash sample was each subjected to a

temperature of 900°C in a muffle furnace for two hours or until no further weight loss was observed. The residual carbon content in the ash is given by the mass loss between the initial and final ash sample.

Ash samples containing mostly carbon (i.e. mostly black) were subjected to proximate analysis to determine the total amount of combustible matters (volatile matters and fixed carbon). The proximate analyses are conducted according to the American Society for Testing Materials (ASTM) methods, as follows:-

- 1) Moisture - ASTM D3173
- 2) Ash - ASTM D3174
- 3) Volatile matters - ASTM D3175

The amount of fixed carbon is obtained through the differential method: fixed carbon (dry wt%) = 100% - [volatile matter (dry wt%) + ash (dry wt%)]

The oven and muffle furnace required for conducting the analyses were available for use at Pollution Control Laboratory, 2nd Level, Block N12, FKKKSA, UTM.

3.4.3 Determination of Size Distribution of Particles through Sieve Analysis

The size distributions of particles used in this study (sand, rice husk and rice husk ash) were determined by means of sieve analysis. Sieving tests were carried out in a sieve shaker manufactured by Pascall Engineering Co. Ltd. A sufficient amount of particles was sieved for approximately 30 minutes. The particles were sieved into five size ranges: 0.30 – 0.50 mm, 0.50 – 0.71 mm, 0.71 – 1.00 mm, 1.00 – 1.18 mm and 1.18 – 2.00 mm. Particles of smaller size (i.e. rice husk ash) were sieved into smaller ranges: 20 – 53 µm, 53 – 63 µm, 63 – 71 µm, 71 – 90 µm, 90 – 106 µm and 106 – 125 µm.

3.4.4 Determination of Oxygen Level in Combustion Gas

The concentration of oxygen in the combustion gas of the fluidised bed combustor was determined via in-situ measurement with a gas analyser (TELEGAN TEMPEST 100). The equipment operates by drawing in a small sample of combustion gas to be detected by an oxygen gas sensor. The analysis of the gas is based on an electrochemical cell equipped with a selective diffusion membrane. The measured oxygen concentration is displayed on the Liquid Crystal Display (LCD) of the gas analyser.

3.5 Modelling Technique through Computational Fluid Dynamics (CFD) Code of FLUENT

Computational fluid dynamics (CFD) is the numerical solution of the equations of continuity and momentum, along with other additional equations for energy and material species in order to solve the problems of non-isothermal flow, mixing and chemical reaction. The basic steps are: (1) subdivision of the flow domain into discrete cells or elements; (2) discretisation of governing equations where exact partial differential equations to be solved are replaced by approximate algebraic equations written in terms of the nodal values of the dependent variables and (3) solution of algebraic equations. The results are displayed in graphical forms which improved the ability to examine results of very large quantities of solution data. Its ability to replicate actual trends observed experimentally had been proven in various research and industrial studies. As such, its applications in all new design and development techniques are becoming more widespread due to its huge cost- and time-saving approach without compromising the reliability of the results.

In this research, the CFD code of FLUENT was used to investigate the optimum freeboard height and feeding design of the fluidised bed to prevent the problem of sand elutriation and to improve the carbon burnout of fly ash in the freeboard region. The FLUENT models could provide information on the hydrodynamics and combustion behaviours inside the fluidised bed. FLUENT is a

powerful general-purpose computer programme for modelling fluid flow, heat transfer and chemical reaction. The basic approach utilised is that of solving the conservation equations for mass, momentum, energy and chemical species using a control volume-based finite difference method.

Researchers such as Nasserzadeh et al. (1993) and Rozainee (1998) had proven the validity of the results obtained through modelling in FLUENT. In their study of the flows and combustion profiles in a municipal solid waste (MSW) incinerator, Nasserzadeh et al. (1993) found that the programme was capable in predicting all the major features of the incinerator flow and temperature fields. On the other hand, Rozainee (1998) showed that modelling results had correctly indicated the trends in gaseous combustion and particle trajectories in a vertical rotating fluidised bed. Hence, the results obtained in this modelling works could be utilised with a very high level of confidence.

3.5.1 Governing Equations

The governing equations used during the modelling study in FLUENT consisted of mathematical models of the gas phase, particle movement and reactive chemistry.

a) Mathematical Model of the Gas Phase

Prediction of the flow field in the computational grid is through solution of the equations for the conservation of mass and momentum in their time averaged form.

Conservation of mass (incompressible flow):-

$$\frac{\partial}{\partial x_i}(\rho u_i) = 0 \quad (3-1)$$

The velocity at any one point in turbulent flows is taken as the sum of the mean (ensemble-averaged) and fluctuating components:-

$$u_i = \overline{u_i} + u_i' \quad (3-2)$$

Substituting expression of this form into the instantaneous momentum equations yields the ensemble-averaged momentum equation:-

$$\frac{\partial}{\partial x_j} (\rho u_i u_j) = \frac{\partial}{\partial x_j} \left\{ \mu \left[\left(\frac{\partial u_i}{\partial x_j} + \frac{\partial u_j}{\partial x_i} \right) - \frac{2}{3} \frac{\partial u_l}{\partial x_l} \delta_{ij} \right] \right\} - \frac{\partial P}{\partial x_i} + \frac{\partial}{\partial x_j} (-\rho \overline{u_i u_j'}) \quad (3-3)$$

A turbulence model is required since the process of Reynolds decomposition and time averaging results in unknown correlations of the fluctuating velocity components. Using the $\kappa - \varepsilon$ model, the second order tensor of “Reynold stresses” or $(-\rho \overline{u_i u_j'})$ (incorporating the effect of turbulence) is modelled using the Boussinesq hypothesis. The Reynold stresses are related to the mean velocity gradients via:-

$$(-\rho \overline{u_i u_j'}) = \frac{2}{3} \left(\rho \kappa + \mu_t \frac{\partial u_i}{\partial x_i} \right) \delta_{ij} - \mu_t \left(\frac{\partial u_i}{\partial x_j} + \frac{\partial u_j}{\partial x_i} \right) \quad (3-4)$$

For swirling flows inside a cyclone and freeboard region of the fluidised bed, the RNG (renormalization group) $\kappa - \varepsilon$ model was used. Belonging to the $\kappa - \varepsilon$ family of models, the model equations in their RNG form are similar to those for the standard $\kappa - \varepsilon$ model. The standard $\kappa - \varepsilon$ model is widely applied in engineering practice (Tobiš, 2000). However, several researchers (Srinivasan and Moagia, 1980; Sturgess and Syed, 1985; Sloan et al., 1986; and Xia et al., 1998) noted that its performance is less satisfactory for swirling flows as it poorly predicts the size and strength of recirculating zones. It tends to produce an excessive solid-body component type of rotation for swirling flows. The RNG $\kappa - \varepsilon$ model, on the other hand, takes better account of the effect of extra strain rates, as indicated by Hanjalic (1994). In general, turbulence in swirling flows is affected by rotation or swirl in the

mean flow. The RNG model in FLUENT provides an option to account for the effects of swirl or rotation by modifying the turbulent viscosity appropriately. A differential form of the relation for effective viscosity was employed, yielding an accurate description on how the effective turbulent transport varies with the effective Reynolds number.

The turbulent viscosity, μ_t was computed from the functional form:-

$$\mu_t = \mu_{t0} f\left(\alpha_s, \Omega_c, \frac{\kappa}{\varepsilon}\right) \quad (3-5)$$

where

$$\begin{aligned} \mu_{t0} &= 0.0845 \rho \frac{\kappa^2}{\varepsilon} \\ \Omega_c &= \text{characteristic swirl number (evaluated within FLUENT)} \\ \alpha_s &= \text{swirl constant} \\ &\quad (0.05 \text{ for mildly swirling flow; } 0.07 \text{ for swirl-dominated flow}) \end{aligned}$$

The values of turbulent kinetic energy, κ and its rate of dissipation, ε were determined by numerical integration of the system of differential Equation 3-6 and Equation 3-7:-

$$\frac{\partial}{\partial x_i}(\rho u_i \kappa) = \frac{\partial}{\partial x_i} \left(\alpha_\kappa \mu_t \frac{\partial \kappa}{\partial x_i} \right) + G_\kappa - \rho \varepsilon \quad (3-6)$$

$$\frac{\partial}{\partial x_i}(\rho u_i \varepsilon) = \frac{\partial}{\partial x_i} \left(\alpha_\varepsilon \mu_t \frac{\partial \varepsilon}{\partial x_i} \right) + C_{1\varepsilon} G_\kappa \frac{\varepsilon}{\kappa} - C_{2\varepsilon} \rho \frac{\varepsilon^2}{\kappa} - R \quad (3-7)$$

The term G_κ represents the generation of turbulent kinetic energy due to the mean velocity gradients, given by:-

$$G_{\kappa} = -\overline{\rho u_i' u_j'} \frac{\partial u_j}{\partial x_i} \quad (3-8)$$

or, consistent with the Boussinesq hypothesis,

$$G_{\kappa} = \mu_t \left(\frac{\partial u_i}{\partial x_j} + \frac{\partial u_j}{\partial x_i} \right) \frac{\partial u_j}{\partial x_i} \quad (3-9)$$

The effects of rapid strain and streamline curvature is given by the last term in Equation 3-7, where

$$R = \frac{0.0845 \rho \eta^3 \left(1 - \frac{\eta}{4.38} \right) \varepsilon^2}{1 + 0.012 \eta^3} \kappa \quad (3-10)$$

and

$$\eta = S \frac{\kappa}{\varepsilon}$$

$$S = \text{modulus of the mean rate-of-strain tensor } \left(\sqrt{2 S_{ij} S_{ij}} \right)$$

$$S_{ij} = \text{mean strain rate, } \left[\frac{1}{2} \left(\frac{\partial u_i}{\partial x_j} + \frac{\partial u_j}{\partial x_i} \right) \right]$$

For high Reynolds number, the values of the inverse Prandtl numbers for κ and ε (α_{κ} and α_{ε}) are approximately 1.393. The coefficients $C_{1\varepsilon}$ and $C_{2\varepsilon}$ are empirical constants having the following values:-

$$C_{1\varepsilon} = 1.42 \text{ and } C_{2\varepsilon} = 1.68$$

b) Equation of Motion for a Particle

FLUENT predicts the trajectory of a discrete phase particle by integrating the force balance on the particle, which is written in a Lagrangian reference frame. This force balance equates the particle inertia with the forces acting on the particle, and can be written (for the x direction in Cartesian coordinates) as

$$\frac{du_p}{dt} = F_D(u - u_p) + \frac{g_x(\rho_p - \rho)}{\rho_p} \quad (3-11)$$

where $F_D(u - u_p)$ is the drag force per unit particle mass and

$$F_D = \frac{18\mu}{\rho_p D_p^2} \frac{C_D Re}{24} \quad (3-12)$$

Here, u is the fluid phase velocity, u_p is the particle velocity, μ is the molecular viscosity of the fluid, ρ is the fluid density, ρ_p is the density of the particle, and d_p is the particle diameter. Re is the relative Reynolds number, which is defined as

$$Re = \frac{\rho d_p |u_p - u|}{\mu} \quad (3-13)$$

The drag coefficient, C_D can be taken from either

$$C_D = a_1 + \frac{a_2}{Re} + \frac{a_3}{Re^2} \quad (3-14)$$

where a 's are constants that apply for smooth spherical particles over several ranges of Re given by Morsi and Alexander (1972) or

$$C_D = \frac{24}{Re} \left(1 + b_1 Re^{b_2}\right) \frac{b_3 Re}{b_4 + Re} \quad (3-15)$$

where

$$b_1 = 2.3288 - 6.4581\phi + 2.4486\phi^2$$

$$b_2 = 0.0964 + 0.5565\phi$$

$$b_3 = 4.905 - 13.8944\phi + 18.4222\phi^2 - 10.2599\phi^3$$

$$b_4 = 1.4681 + 12.2584\phi - 20.7322\phi^2 + 15.8855\phi^3$$

which is taken from Haider and Levenspiel (1989) for nonspherical particles. The shape factor, ϕ_s , is defined as

$$\phi_s = \frac{s}{S} \quad (3-16)$$

where s is the surface area of a sphere having the same volume as the particle, and S is the actual surface area of the particle.

The trajectory equations were solved by stepwise integration over discrete time steps. Integration in time of Equation 3-11 yielded the velocity of the particle at each point along the trajectory, with the trajectory itself predicted by

$$\frac{dx}{dt} = u_p \quad (3-17)$$

$$\frac{dy}{dt} = v_p \quad (3-18)$$

$$\frac{dz}{dt} = w_p \quad (3-19)$$

The particle phase was assumed to be sufficiently dilute, thus rendering negligible effects on the continuous phase. Meanwhile, fluctuations in the mean phase fluid velocity are taken account through the use of the stochastic tracking approach.

i) The Stochastic Tracking Approach

FLUENT predicts the trajectories of particles using the mean phase fluid velocity, \bar{u} or the instantaneous value of the fluctuating gas velocity, $u = \bar{u} + u'$ in the trajectory calculation in Equation 3-11 to predict the dispersion of the particles due to turbulence. The stochastic or random walk model was used in order to determine the instantaneous gas velocity. In the stochastic tracking approach, the turbulent dispersion of particles was predicted by integrating the trajectory equations for individual particles along the particle path during integration using the instantaneous

fluid velocity. The random effects of turbulence on the particle dispersion may be accounted for through the use of the Discrete Random Walk (DRW) model, in which the fluctuating velocity components are discrete piecewise constant functions of time. Their random value is kept constant over a time interval given by the characteristic lifetime of the eddies.

The time spent in turbulent motion along the particle path, ds is described by the concept of integral time scale, T :-

$$T = \int_0^{\infty} \frac{u'_p(t)u'_p[t+s]}{u_p'^2} ds \quad (3-20)$$

Larger value of the integral time corresponds to more turbulent motion in the flow, as it is proportional to the particle dispersion rate. For small tracer particles having zero drift velocity and moving with the fluid, the integral time becomes the fluid Lagrangian integral time, T_L as is approximated by

$$T_L \approx 0.15 \frac{\kappa}{\varepsilon} \quad (3-21)$$

for the $\kappa - \varepsilon$ model and its variants.

The interaction of a particle with a succession of discrete stylised fluid phase turbulent eddies is simulated in the DRW or “eddy lifetime” model. Characterisation of each eddy is by a Gaussian distributed random velocity fluctuation (u' , v' and w') and a time scale, τ_e . The values of u' , v' and w' that prevail during the lifetime of the turbulent eddy are sampled through assumption that they obey a Gaussian probability distribution, such that:-

$$u' = \zeta \sqrt{u'^2} \quad (3-22)$$

where ζ is a normally distributed random number, and the remainder of the right-hand side is the local root mean square (RMS) value of the velocity fluctuations. In the $\kappa - \varepsilon$ model and its variants, by assuming isotropy, the values of the RMS fluctuating components can be obtained as

$$\sqrt{u'^2} = \sqrt{v'^2} = \sqrt{w'^2} = \sqrt{\frac{2\kappa}{3}} \quad (3-23)$$

since the kinetic energy of turbulence is known at each point of the flow.

The characteristic lifetime of the eddy is defined as:-

$$\tau_e = 2T_L \quad (3-24)$$

The particle eddy crossing time is defined as

$$t_{cross} = -\tau \ln \left[1 - \left(\frac{L_e}{\tau |u - u_p|} \right) \right] \quad (3-25)$$

where τ is the particle relaxation time, L_e is the eddy length scale and $|u - u_p|$ is the magnitude of the relative velocity. Interaction of the particle with the fluid phase eddy was assumed to take place over the smaller of the eddy lifetime and the eddy crossing time. A new value of the instantaneous velocity is obtained by applying a new value of ζ into Equation 3-24 when the time mentioned previously is reached.

The values of u, v, w (namely $\left(\sqrt{u'^2} = \sqrt{v'^2} = \sqrt{w'^2} \right)$) are updated whenever migration into the neighbouring cells occurs. Combination of the old and new time constraints resulted in a time interval during which the gas flow velocity remains constant. This subsequently permits the direct integration of the equations of motion to obtain a local closed form solution.

c) Mathematical Model for Reactive Chemistry

Modelling of rice husk particle combustion in the fluidised bed involved the use of the mixture fraction or probability density modelling approach.

**i) Mixture Fraction / Probability Density Function (PDF) Modelling
Approach for Particle Combustion**

The mixture fraction / PDF modelling approach involves the solution of transport equations for one or two conserved scalars (the mixture fractions). Through this approach, instead of solving the transport equations for individual species, the individual component concentrations for a certain species of interest are derived from the predicted mixture fraction. Therefore, the usually unknown reaction mechanisms need not be explicitly user-defined but is treated using certain system chemistry calculations (e.g. the flame sheet approximation, equilibrium assumption and non-equilibrium chemistry). Physical properties of chemical species and equilibrium data are retrieved from the chemical database while the interaction of turbulence and chemistry is accounted for with a probability density function or PDF.

The PDF modelling approach is specifically developed for reaction processes in which turbulence mixing is the limiting rate for reaction progress. By allowing intermediate species formation, dissociation effects and the coupling between turbulence and chemistry to be accounted for in a rigorous way, this method is computationally efficient by making the solution of a large number of species transport equations unnecessary. The basis of the mixture fraction approach is that under a certain set of simplifying assumptions, the instantaneous thermochemical state of the fluid is related to a conserved scalar quantity known as the mixture fraction, f . Being a conserved scalar quantity, the value of f at each point in the flow domain is computed in FLUENT through the solution of the conservation equation for mean (time-averaged) value of f in the turbulent flow field, \bar{f} :-

$$\frac{\partial}{\partial x_i} (\rho u_i \bar{f}) = \frac{\partial}{\partial x_i} \left(\frac{\mu_t}{\sigma_t} \frac{\partial \bar{f}}{\partial x_i} \right) + S_m \quad (3-26)$$

where S_m represents the transfer of mass from reacting particles into the gas phase.

In addition to solving the conservation equation for the mean mixture fraction, a conservation equation for the mixture fraction variance, $\overline{f'^2}$ is also solved:-

$$\frac{\partial}{\partial x_i} (\rho u_i \overline{f'^2}) = \frac{\partial}{\partial x_i} \left(\frac{\mu_t}{\sigma_t} \frac{\partial \overline{f'^2}}{\partial x_i} \right) + C_g \mu_t \left(\frac{\partial \overline{f}}{\partial x_i} \right)^2 - C_d \rho \frac{\varepsilon}{\kappa} \overline{f'^2} \quad (3-27)$$

where the constants σ_t , C_g and C_d take the values of 0.7, 2.86 and 2.0, respectively. The mixture fraction variance is used in the closure model describing the turbulence-chemistry interactions.

Calculation of a single conserved scalar field, f enables the derivation of other important scalars (individual species mole fractions, density and temperature) without the need to solve their respective transport equations. Provided the description of the reacting system chemistry, the mixture fraction value at each point in the flow field can be used to compute the instantaneous values of these scalars. If a secondary stream is included in a non-adiabatic system, the instantaneous values will depend on the instantaneous fuel mixture fraction, f_{fuel} , the secondary partial fraction, p_{sec} and the enthalpy, H^* :-

$$\phi_i = \phi_i(f_{fuel}, p_{sec}, H^*) \quad (3-28)$$

where ϕ_i represents the instantaneous species concentration, density or temperature, while H^* is given by:-

$$H^* = \sum_i m_i H_i = \sum_i m_i \left[\int_{T_{ref_i}}^T c_{p,i} dT + h_i^o(T_{ref_i}) \right] \quad (3-29)$$

The non-adiabatic model is required in particle-laden flows (particle combustion systems) since such flows include heat transfer to the dispersed phase.

The functional relationship between ϕ_i (species, density and temperature) and mixture fraction depend on the description of the system chemistry. For modelling of rice husk particle combustion in which the formation of intermediate species takes place, the equilibrium assumption chemistry model is appropriate. This is in

view of its ability to predict the formation of intermediate species and does not require the knowledge of detailed chemical kinetic rate data. With this model, no specific reaction mechanism and specific reaction rates are required. Only important chemical species that will be present in the system need to be defined. Prediction of the mole fraction of each species will then be carried out by FLUENT based on chemical equilibrium.

However, FLUENT prediction of the turbulent reacting flow is concerned with the prediction of the time-averaged values of the scalars in Equation 3-28. The next step, hence, is to relate these instantaneous values to their respective time-averaged values based on the turbulence-chemistry interaction model, which in this case applies the PDF approach as its closure model since the mixture fraction / PDF modelling approach is used.

The probability density function, written as $p(f)$, describes the fraction of time that the fluctuating variable f takes on a value between f and $f + \Delta f$. Expressed mathematically, it takes on the following form:-

$$p(f) \Delta f = \lim_{T \rightarrow \infty} \frac{1}{T} \sum_i \tau_i \quad (3-30)$$

where τ_i is the fraction of time that f spends in the Δf band.

The probability density function, $p(f)$ which describes the temporal fluctuations of f in the turbulent flow, is used to compute time-averaged values of variables that depend on f . Time-averaged values of species mole fractions and temperature can be computed, in a non-adiabatic system with a secondary stream, as:-

$$\overline{\phi_i} = \int_0^1 \int_0^1 \phi_i(f_{fuel}, p_{sec}, \overline{H^*}) p_1(f_{fuel}) p_2(p_{sec}) df_{fuel} dp_{sec} \quad (3-31)$$

where p_1 is the PDF of f_{fuel} , p_2 is the PDF of p_{sec} , and $\overline{H^*}$ is the time-averaged enthalpy solved from:-

$$\frac{\partial}{\partial x_i} (\rho u_i \overline{H^*}) = \frac{\partial}{\partial x_i} \left(\frac{k_i}{c_p} \frac{\partial \overline{H^*}}{\partial x_i} \right) + \tau_{ik} \frac{\partial u_i}{\partial x_k} + S_h \quad (3-32)$$

where S_h accounts for source terms due to radiation, heat transfer to wall boundaries, and heat exchange with the second phase.

In a similar form, the true time-averaged fluid density is computed as:-

$$\frac{1}{\rho} = \int_0^1 \int_0^1 \frac{p_1(f_{fuel}) p_2(p_{sec})}{\rho(f_{fuel}, p_{sec}, \overline{H^*})} df_{fuel} dp_{sec} \quad (3-33)$$

In Equation 3-33, $\rho(f_{fuel}, p_{sec}, \overline{H^*})$ is the instantaneous density obtained using the instantaneous species mole fractions and temperature in the gas law equation. Using Equations 3-31 and Equation 3-33, the shape of the function $p_1(f_{fuel})$ and $p_2(p_{sec})$ need to be specified in order to determine the local time-averaged state of the fluid at all points in the flow field. In FLUENT, the shape of the PDF, $p(f)$, is described by either the double delta function or the β -function. Since the β -function is thought to represent most closely experimentally observed PDF's than the easily computed but less accurate double delta function, it is therefore used in this modelling study. The β -function PDF shape is given by the following function of \overline{f} and $\overline{f'^2}$:-

$$p(f) = \frac{f^{\alpha-1} (1-f)^{\beta-1}}{\int f^{\alpha-1} (1-f)^{\beta-1} df} \quad (3-34)$$

where

$$\alpha = \overline{f} \left[\frac{\overline{f(1-f)}}{\overline{f'^2}} - 1 \right] \quad \text{and} \quad \beta = (1-\overline{f}) \left[\frac{\overline{f(1-f)}}{\overline{f'^2}} - 1 \right]$$

ii) **Modelling and Solution Procedures**

For the two-mixture-fraction (secondary stream) case, the preprocessor prePDF calculates the instantaneous values for the temperature, density and species mole fractions (Equation 3-28) and stores them in the look-up tables. For the non-adiabatic case with two mixture fractions, the 3D look-up table contains the physical properties as functions of the fuel mixture fraction, the secondary partial fraction and the instantaneous enthalpy. The PDF functions p_1 and p_2 of the fuel mixture fraction and the secondary partial fraction, respectively, are calculated inside FLUENT from the values of the fractions and their variances. The PDF integrations for calculating the mean values for the properties are also performed inside FLUENT (using Equation 3-31 together with Equation 3-33). The instantaneous values required in the integrations are obtained from the look-up tables. The algorithm for solving a non-adiabatic two-mixture-fraction case was depicted in Figure 3-16.

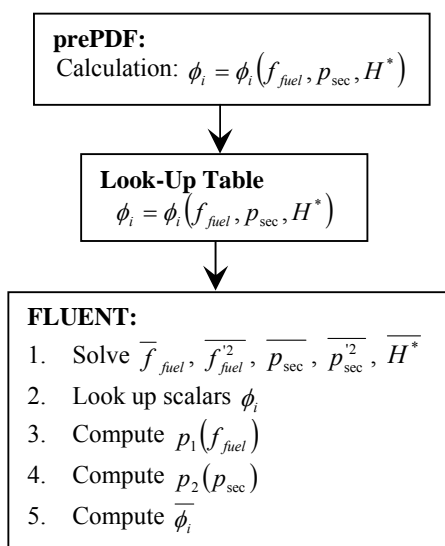


Figure 3-16: Algorithm for the solution of a non-adiabatic two-mixture-fraction case in pre-PDF and FLUENT

For two-mixture-fraction problems, the 3D look-up table allows FLUENT to determine the instantaneous values for the scalar properties from instantaneous values of f_{fuel} , p_{sec} and H^* . The three-dimensional table is the visual representation of Equation 3-28. These instantaneous values are used to perform the integration of Equation 3-31.

3.5.2 Numerical Solutions

a) **Modelling the Effect of Freeboard Height**

The increase in freeboard height of the fluidised bed combustor was investigated for its effect on sand elutriation behaviour and carbon conversion efficiency in the freeboard region.

i) ***Modelling the Elutriation Behaviour of Sand Particles***

The size distribution of elutriated sand particles, which were present as contaminants in the fly ash during combustion of rice husk in the 210-mm inner diameter fluidised bed (combustor height of 2000mm), were shown in Figure 3-17. It was observed that the elutriated sand were mostly in the size range of 53 – 106 μm , constituting 95 wt% of the total amount of elutriated sand. Their surface mean diameter (D_{vs}) was computed to be 69 μm . Therefore, sand particles (sphericity of 0.92) with sizes of 25 μm , 50 μm , 75 μm , 100 μm and 125 μm were used to investigate their elutriation behaviour in the fluidised bed combustor model ($\varnothing 500\text{mm} \times 5250\text{mm}$). The fluidised bed model was constructed using the pre-processor of GAMBIT and consisted of an structured grid of 367,806 cells employing the Cooper meshing scheme. It consisted of hexahedral cells as shown in figure 3-18. It was assumed that the sand particles were thrown to the freeboard region through bubble eruption at the bed surface at the height of 250mm (equivalent to 0.5 D_c), and as such, each particle was applied an ejection velocity in the y-direction (Appendix A) with the fluidising velocity at 3 U_{mf} (or 0.3 m/s for sand of size 250 – 595 μm). The superficial gas velocity at the freeboard was set at 0.5 m/s consistent with actual experimental data. The trajectories of these particles in the fluidised bed were then tracked and recorded. The default convergence criteria were that iterations were performed until the scaled residuals decrease to a value of 10^{-3} for all equations.

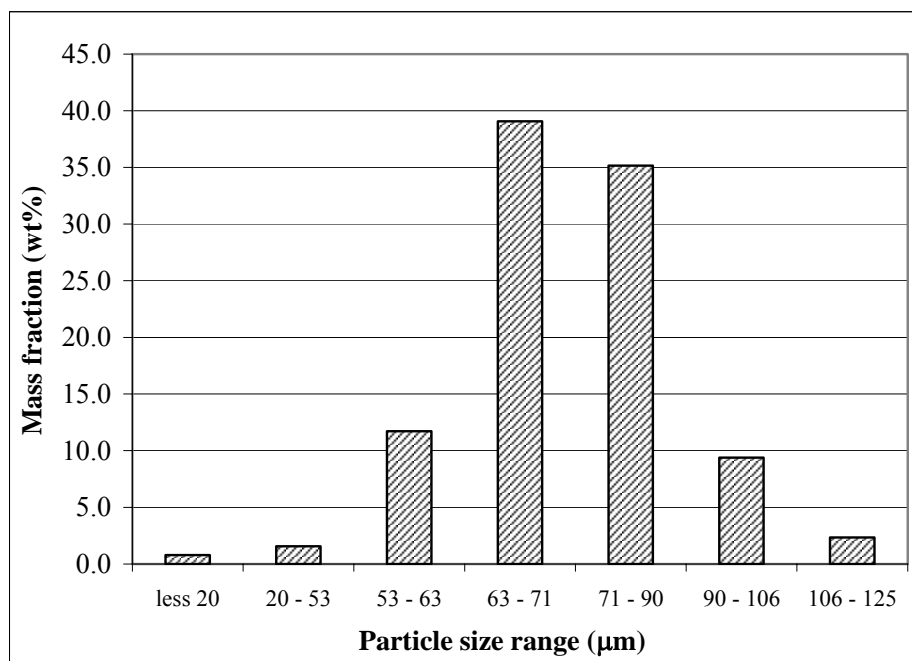


Figure 3-17: Size distribution of elutriated sand particles during the combustion of rice husk in the 210-mm inner diameter fluidised bed (bed sand size 250 – 595 μm)

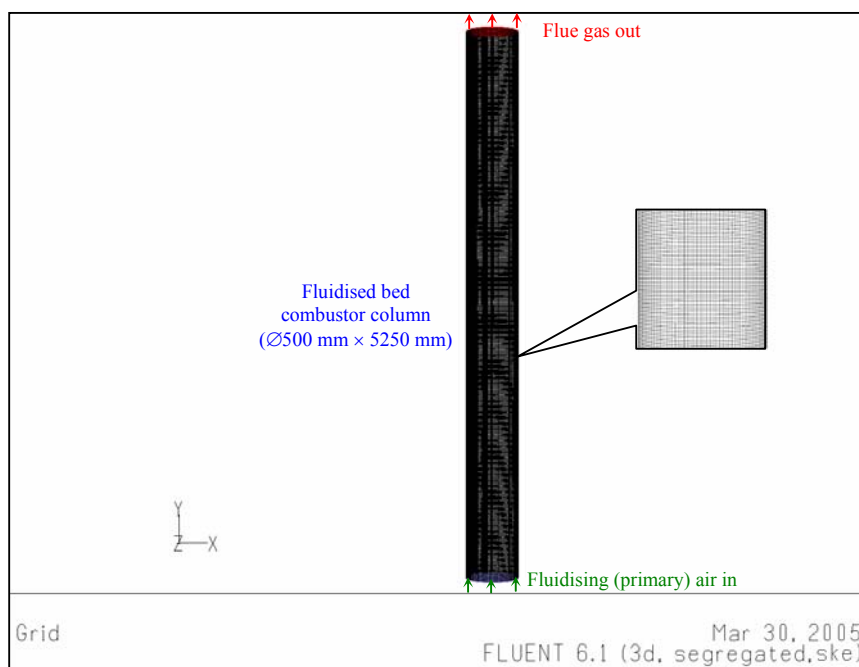


Figure 3-18: Three-dimensional computational grid of the fluidised bed combustor model

ii) *Modelling the Combustion Efficiency of Rice Husk in the Freeboard Region*

The same fluidised bed combustor model ($\text{Ø}500\text{mm} \times 5250\text{mm}$) was used to investigate the combustion efficiency of rice husk in the freeboard region. The model was based on the worst-case scenario whereby the rice husk particles were assumed to be entrained to the freeboard region through application of a sufficiently high freeboard gas velocity (at 1.0 m/s). Further, they were released from the bed surface from the eruption of bubbles at the bed surface and attained an ejection velocity in the y-direction (Appendix A). The rice husk particles were expressed in terms of their equivalent diameters and have a sphericity of 0.19. Procedures to determine the sphericity of rice husk were included in Appendix B. Five (5) sizes of rice husk were used (1.6 mm for whole husk, 1-mm fragment, 750- μm fragment, 500- μm fragment and 300- μm fragment). The chemical properties of rice husk used to define rice husk as the fuel particle in the combustor were included in Appendix C. These data were used to generate the 3D look-up tables (which stored the instantaneous values of temperature, density and species mole fractions) using the pre-processor pre-PDF. The bed was assumed to be operated at a fluidising velocity of $5 U_{mf}$ and it was further assumed that the heat required to initiate the combustion of rice husk particles was provided by the fluidising air entering at 700°C . The trajectories and mass loss profiles of these particles were determined from the model. The default convergence criteria were that iterations were performed until the scaled residuals decrease to a value of 10^{-3} for all equations except for energy, whereby the value of 10^{-6} applies.

b) *Modelling the Effect of Feeding Conditions*

The effect of feeding conditions on the combustion efficiency of rice husk in the fluidised bed were investigated for two parameters, namely the pneumatic air feeding velocity and the use of vortex feeding.

i) *Modelling the Effect of Pneumatic Air Feeding Velocity*

The FLUENT computer code (version 6.1) together with the desired operating conditions as boundary conditions (from experimental study), were used to model the effect of pneumatic air feeding velocity on the combustion of rice husk in the

fluidised bed. The model was constructed using the pre-processor of GAMBIT and consisted of an unstructured grid of 137,622 cells employing the TGrid meshing scheme, consisting primarily of tetrahedral cells, with hybrid (hexahedral, pyramidal and wedge) cells being placed at appropriate locations (Figure 3-19).

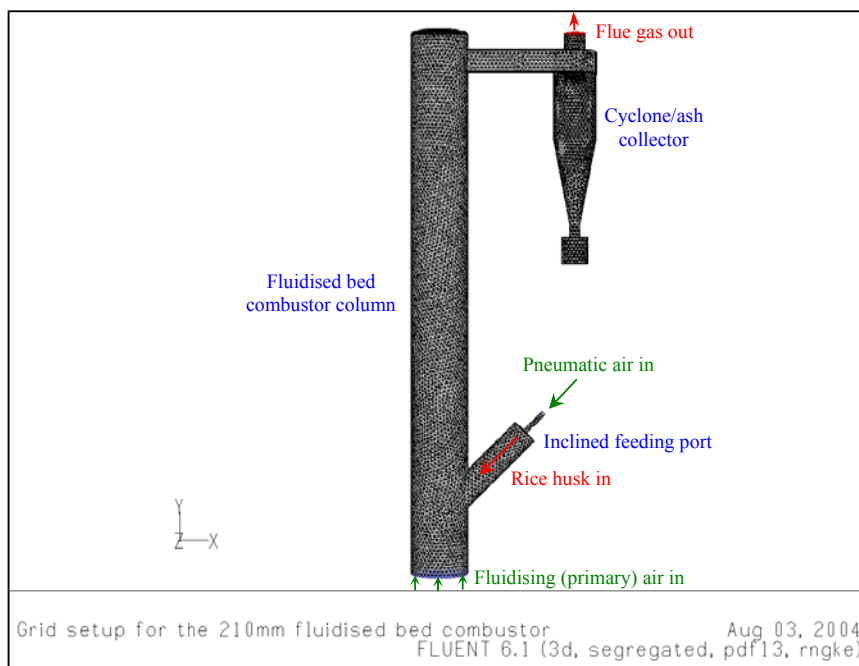


Figure 3-19: Three-dimensional computational grid of the 210-mm inner diameter fluidised bed combustor

To simulate the combustion of rice husk particles inside the bubbling bed, five (5) streams of rice husk particles were injected concentrically at the surface of the bed with the effect of bubble eruption at the bed surface taken into account by applying ejection velocities in the y-direction (Appendix A) consistent with a particular set of operating conditions to these particles. Due to the limitation of the current CFD code (which did not allow for simultaneous modelling of burning particle (Lagrangian approach) and bubbling bed (Eulerian approach)), it was assumed that the heat required to initiate the combustion of rice husk particles was provided by the fluidising air entering at the combustion temperatures (i.e. average bed temperatures recorded experimentally for each case study). The rice husk particles used in this modelling study were assumed to be whole husk particles having a mean diameter of 1.6 mm (volume-surface mean diameter from particle screen analysis) and a

sphericity of 0.19 (disk-like shape, determined from fluidisation study data). In all cases, the trajectories of all 5 streams of burning particles were tracked stochastically for 20 iterations each, giving a total of 100 streams of particles. The residence times from these 100 particle streams was subsequently used to plot histograms for the residence time distribution of the burning particles inside the fluidised bed. The default convergence criteria were that iterations were performed until the scaled residuals decrease to a value of 10^{-3} for all equations except for energy, whereby the value of 10^{-6} applies.

ii) Modelling the Effect of Vortex Feeding

The FLUENT computer code (version 6.1) together with the desired operating conditions as boundary conditions (from experimental study), were used to model the effect of different feeding methods on the combustion of rice husk in the fluidised bed. Two models were set up using the pre-processor of GAMBIT to simulate both rice husk combustion experiments of feeding via the inclined feeding port (Model FM-A) and inclined, tangential feeding port (Model FM-B). Model FM-A consisted of an unstructured grid of 137,622 cells employing the TGrid meshing scheme, consisting primarily of tetrahedral cells, with hybrid (hexahedral, pyramidal and wedge) cells being placed at appropriate locations (Figure 3-20).

Model FM-B, on the other hand, consisted of 168,771 tetrahedral cells also employing the TGrid meshing scheme, but with cells in the region of tangential feed inlet ($300 \text{ mm} < y < 650 \text{ mm}$) being refined due to the highly-turbulent, swirl-dominated flow for better capture of the velocity gradients in this region (Figure 3-21).

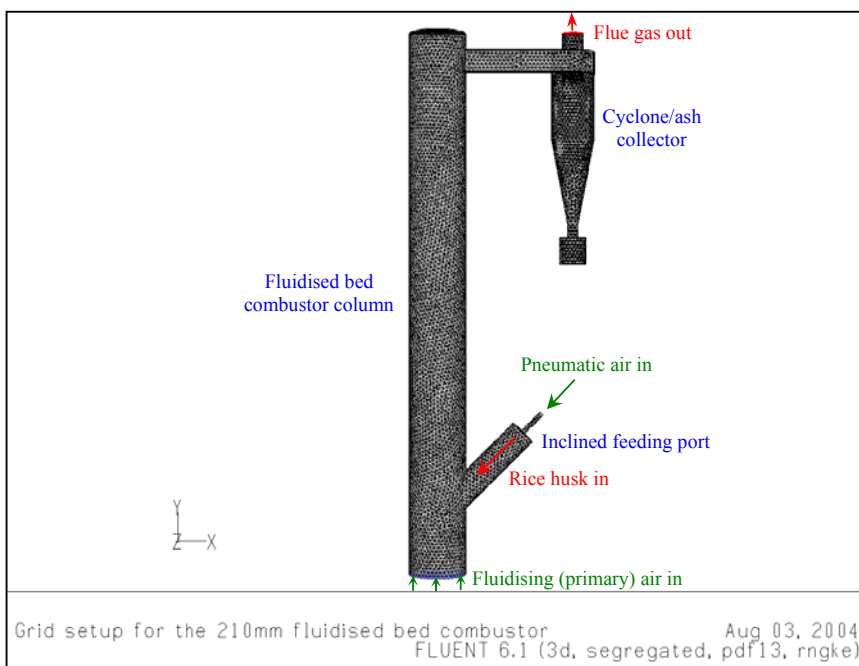


Figure 3-20: Three-dimensional computational grid of the 210-mm inner diameter fluidised bed combustor with inclined feeding port (Model FM-A)

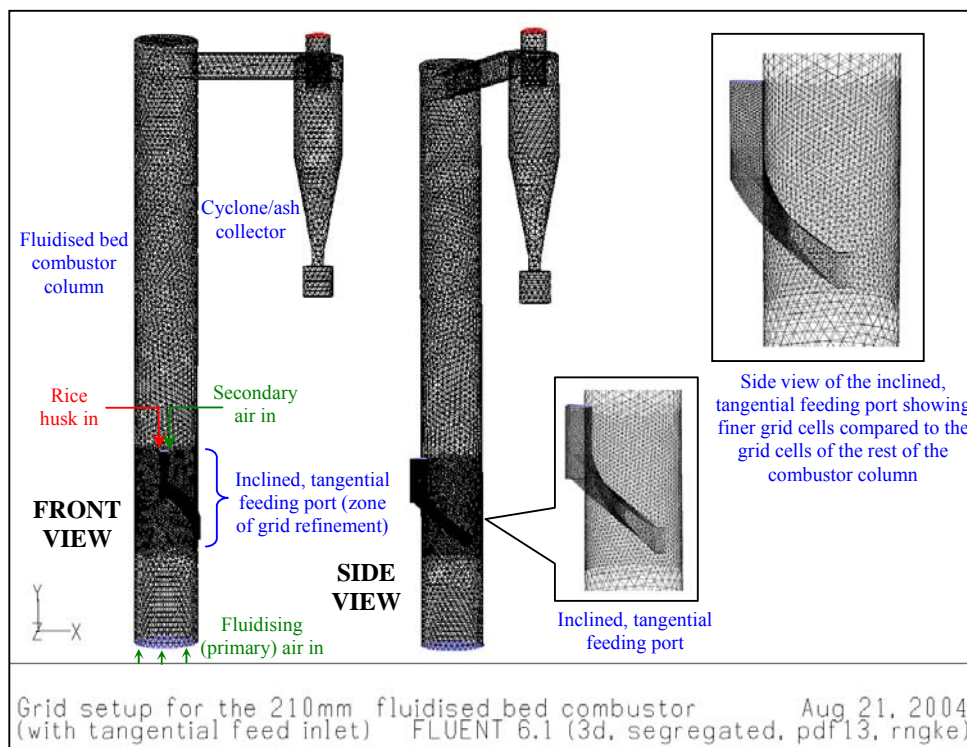


Figure 3-21: Three-dimensional computational grid of the 210-mm inner diameter fluidised bed combustor with inclined, tangential feeding port (Model FM-B)

A 5- μm tracer particle with particle density of 1000 kg/m^3 (consistent with that used by Nasserzadeh et al. (1994) in their CFD modelling of gas residence time in large municipal incinerators) was used to determine the gas flow profile inside both CFD models. To simulate the combustion of rice husk particles inside the bubbling bed, 10 streams of rice husk particles with different sizes (expressed in terms of equivalent diameters) were injected at the inlet port of both models, and assumed to enter the combustor together with the pneumatic air at ambient temperature (30°C). Due to the limitation of the current CFD code (which did not allow for simultaneous modelling of burning particle (Lagrangian approach) and bubbling bed (Eulerian approach)), it was assumed that the heat required to initiate the combustion of rice husk particles was provided by the fluidising air entering at the combustion temperatures (average bed temperatures recorded experimentally for each case study). The rice husk particles used in this modelling study were assumed to have a sphericity of 0.19 (disk-like shape, determined from data from fluidisation study) and will burn according to the shrinking core model (particle swell coefficient of 1.0). Therefore, the particle density of the burnt rice husk will reduce as the particle burnt to completion to form ash ($\rho \propto \text{mass}$). However, this was not the case in actual as the resulting ash was known to have a higher particle density (approximately 2000 kg/m^3) due to the evolution of silica. Hence, to determine the fate of the resulting ash particles (either being retained in the combustor or being elutriated into the cyclone), another 10 streams of silica (inert) with variable diameters were injected at the surface of the bed. These particles represented the rice husk particles that has burnt out completely inside the bed (sphericity also at 0.19) and the effect of bubble eruption at the bed surface were taken into due consideration by applying ejection velocities in the y-direction (Appendix A) consistent with the actual operating conditions for each model (Model FM-A or Model FM-B). In total 21 streams of particles (1 stream of inert gas tracer, 10 streams of reacting rice husk particles and 10 streams of inert silica particles) were tracked inside each fluidised bed combustor model, the details of which were shown in Table 3-4. The default convergence criteria were that iterations were performed until the scaled residuals decrease to a value of 10^{-3} for all equations except for energy, whereby the value of 10^{-6} applies.

Table 3-4: Properties of particles used in modelling the effect of feeding method on rice husk combustion in the 210-mm inner diameter fluidised bed combustor

No.	Type of Particle	Reactivity	Point of Injection	Diameter (micron)	Particle density (kg/m ³)
1	Gas tracer	Inert	Bed surface, with bubble eruption velocity	5	1000
2	Rice husk	Reacting	Feed inlet port	25	650*
3				50	
4				75	
5				100	
6				200	
7				300	
8				500	
9				750	
10				1000	
11				1600 [†]	
12				Silica (final ash)	
13	25				
14	50				
15	75				
16	150				
17	300				
18	500				
19	750				
20	1000				
21	1600				

Note:

The choice of particle diameters used in the modelling study was based on the results of screen analysis performed on the ash samples (fly and bottom ashes) obtained from corresponding actual experimental studies

* From actual experimental measurement

[†] Average particle diameter of rice husk expressed in terms of volume surface mean diameter (D_{vs}) from screen analysis

CHAPTER 4

RESULTS AND DISCUSSIONS ON COMBUSTION OF RICE HUSK IN FLUIDISED BED TO PRODUCE AMORPHOUS SILICA

4.1 Basic Combustion Characteristics of Rice Husk

Both raw and water-washed rice husk samples were used in this study to compare their combustion times. The raw rice husk sample was used on a 'as received' basis without any pretreatment. For the water-washed rice husk sample, the rice husk were soaked overnight (approximately 24 hours) in tap water at ambient temperature (30°C), drained, dried in an oven (at 105°C) and finally left to sit in the ambient atmosphere until the equilibrium moisture content was reached (in order to closely simulate the original moisture content in the raw rice husk, at approximately 10 wt%). Washing with water removed the highly soluble alkali metals compounds such as potassium oxide and sodium oxide present as impurities in rice husk.

a) Raw Rice Husk

i) *Single Particle Combustion*

When the rice husk sample (ten whole husk particles spread out widely apart) was placed onto the steel plate inside the muffle furnace at the desired temperatures of investigation (650 – 750°C), it was observed that the rice husk particles immediately flashed or devolatilised, resulting in flaming combustion (long trailing orange flame) for 3 – 4 seconds. The resulting char particles took another 16 – 27 seconds to burn out completely into ash in the form of glowing combustion with short, slight bluish flame surrounding the char particles. As such, the entire combustion process

(devolatilisation and char burning) of the single particle model of rice husk took 20 – 30 seconds to complete. However, the final ash product from the combustion of these raw rice husk particles was not completely white. Completely white ash product could never be obtained from burning raw rice husk particles due to the surface melting phenomenon, irrespective of how long the particles were retained inside the muffle furnace (Plate 4.1-1). Sudden exposure of the raw rice husk particles to high temperatures (650 – 750°C) caused the alkali metal compounds of potassium oxide and sodium oxide to melt, thus forming a surface melt mixture on the char and/or ash particles. Any unburnt carbon molecules were therefore ‘trapped’ in this melt mixture and were unavailable for further oxidation (Krishnarao et al., 2001). In this experiment, the final ash product from burning a batch of ten whole raw rice husk particles was found to contain an average of 70% white ash particles, 15% grey ash particles and 15% black char particles. Hence, the combustion times determined from this experiment were based on the best estimates whereby no further change in terms of the colour of the ash product was first observed.

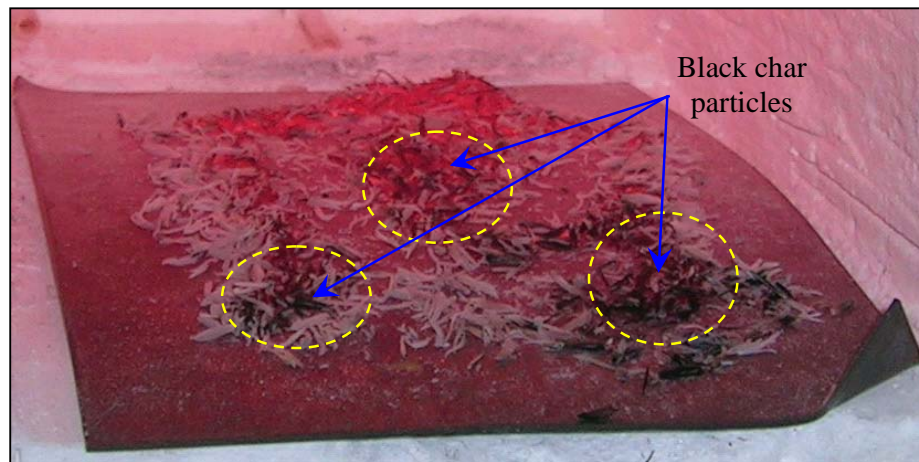


Plate 4.1-1: Ash product from burning raw rice husk inside the muffle furnace (650 – 750°C) after 10 minutes of combustion time

Results on combustion times from this experiment was consistent with that reported by Mukunda et al. (1996), which noted that the char conversion times were an order of magnitude larger than flaming times. They found that single particle combustion for raw rice husk in a muffle furnace at 700°C has flaming times of about 3 – 4

seconds and char burning times of 40 – 65 seconds. Nevertheless, the higher char burning times reported by them were due probably to the inevitable presence of black char particles associated with burning raw rice husk, which presented an ambiguity in the determination of the time for complete char combustion.

ii) Group Particle Combustion

For a group of rice husk particles, the flaming times were observed to be higher, at 4 – 7 seconds (Plate 4.1-2). This could be attributed to the lag time in heat transfer to each rice husk particle in order to initiate the devolatilisation process, as the overlapping amongst these particles formed the ‘barriers’ to the heat transfer path. Similarly, the overlapping of particles also formed ‘barriers’ to the mass (oxygen) transfer path, leading to a lag time in the transfer of oxygen to each rice husk particle in order for char oxidation to take place. The char burning times were thus elevated to 35 – 45 seconds. In total, the combustion times for a group of rice husk particles ranged from 39 to 52 seconds.



Plate 4.1-2: Higher flaming times for a group of rice husk particles spread widely apart in the muffle furnace (650 – 750°C)

Sridhar et al. (1996) reported that a group of particles (75 husks) put together randomly had flaming times and char conversion times of 6 – 8 seconds and 152 seconds, respectively. Again, the discrepancy between the char combustion time observed in this experiment with that of Sridhar et al. (1996) could be attributed to

the ambiguity in determining the time for complete combustion of char particles associated with burning raw rice husk particles. Another contributing factor could be due to the distribution of the group of rice husk particles in the muffle furnace, whereby placing the particles in a heap or spread widely apart could affect the rate of oxygen transfer and thus the char combustion times.

b) Water-Washed Rice Husk




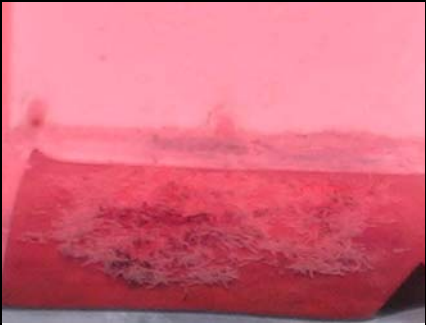
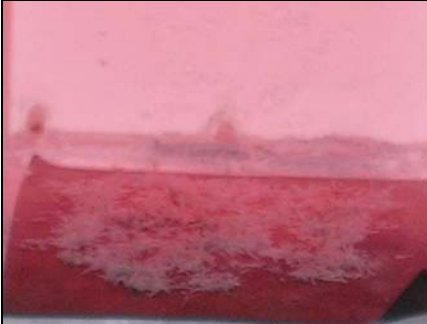
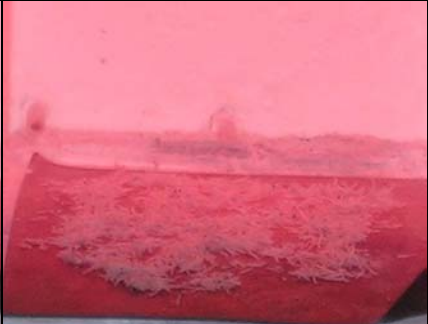
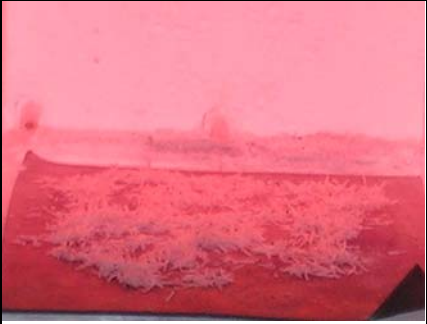
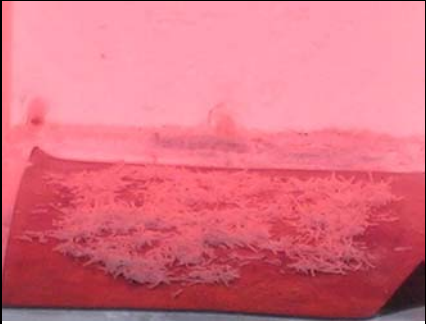
i) Single Particle Combustion

There was no significant difference on the combustion times of water-washed rice husk compared to raw rice husk (flaming times of 3 – 4 seconds, char combustion times of 16 – 27 seconds), except for the final ash product. The final ash product from burning water-washed rice husk was completely white. This enabled the distinct determination of the char combustion times, whereby the first formation of completely white ash signified the complete combustion of chars.

ii) Group Particle Combustion

Similar to the case of single particle combustion, there was no significant difference in the combustion times of burning a group of water-washed rice husk compared to burning a group of raw rice husk (flaming times of 4 – 7 seconds, char combustion times of 35 – 45 seconds). Also, the final ash product from burning water-washed rice husk was completely white, as shown in the real-time tracking of the combustion 4 g of rice husk particles in the muffle furnace (Table 4.1-1).

Table 4.1-1: Real-time tracking of combustion of a batch (4 g) of water-washed rice husk particles in the muffle furnace (650 – 750°C)

			
t = 1 s	t = 11 s	t = 21 s	t = 33 s
			
t = 47 s	t = 64 s	t = 83 s	t = 101 s

c) **Comparison of Rice Husk Combustion in a Muffle Furnace and a Fluidised Bed Combustor**

Rice husk combustion tests were conducted in the 80-mm inner diameter fluidised bed to compare the combustion times of rice husk in the fluidised bed with that in the muffle furnace. Water-washed rice husk was used as this enabled the distinct visual distinguishment of completion of char burning process while the 80-mm inner diameter fluidised bed was used as it was equipped with a glass section at the bed region for viewing purposes. Once the bed was pre-heated by combustion of LPG-air mixture to 650 – 700°C, a batch of 4 g of rice husk particles were dropped into the bed and the time count started. The average flaming times of the rice husk particles were recorded to be 3 – 4 seconds whereas the average char burning times were 25 – 30 seconds. These findings showed that combustion of rice husk in the fluidised bed proceeded according to the single particle combustion model. This could be attributed to the bubbling action in the bed region, which aided in distributing the rice husk particles uniformly amongst the hot bed particles as the rice husk dropped into the bed region. The hot bed particles in turn provided the heat source to enable immediate devolatilisation process of rice husk to take place while bubble swarms within the bed provided intimate contact of oxygen with the rice husk particles, leading to effective char combustion. As such, on a micro-level, the rice husk particles were burning as individual single particles with no or very minimal overlapping of particles as found in other combustors, such as the muffle furnace or fixed bed reactors. This advantage of the fluidised bed is very crucial, especially to preserve the amorphous structure of silica in the ash by minimising the exposure time to high temperature as well as enabling a higher throughput value for the combustor.

4.2 Effect of Temperature and Residence Time on the Formation of Silica Crystals in Rice Husk Ash

The resulting samples from the investigation of time-temperature relationship on the onset of silica crystallisation in rice husk ash were analysed for the formation of black char particles and silica structure.

a) Formation of Black Char Particles

The ash samples obtained from the experiments were compared in Table 4.1-2 (raw rice husk) and Table 4.1-3 (water-washed rice husk). Observations between Table 4.1-2 and Table 4.1-3 showed that the ash from combustion of raw, untreated rice husk were generally darker in shade compared to the ash from combustion of water-washed rice husk, due primarily to the presence of significant amount of char skeletons in the former. Once formed, as in the case of raw rice husk, it was increasingly more difficult to remove high content of residual carbon in the ash, even at higher residence time or temperature. This confirmed the reported literature findings that impurities in the rice husk, mainly the low melting-point alkali metals, did play a significant role in the burnout of rice husk. This is because the alkali metals compounds such as potassium oxide and sodium oxide tends to dissociate at low temperatures (such as 350°C for potassium oxide) and the resulting alkali metals melt at even lower temperatures (such as 64°C for potassium and 98°C for sodium). The melting of these alkali metals form a surface melt mixture at the surface of the rice husk ash, thereby entrapping the carbon content and making the carbon unavailable for further conversion even at higher temperatures. In addition, potassium and sodium compounds (K_2O and Na_2O) cause the ash to remain sticky at much lower temperature than the melting point of ash (initial deformation temperature of 1440°C and fluid temperature of 1650°C, according to Mansaray and Ghaly, 1998a). Sodium and potassium salts react with silica in the ash to form eutectic mixtures having low melting points. The melting point of these eutectic mixtures might be as low as 600 – 700°C at high concentration of sodium or potassium (Armesto et al., 2002).

Further, as the major impurity in rice husk ash is potassium (2 – 3 wt% as potassium oxide, K_2O as reported by Shinohara and Kohyama (2004)), its presence is expected to be accelerating the carbon fixation in rice husk ash (Krishnarao et al., 2001). This is because the carbon entrapped in the potassium rich melt could not be oxidised as it is not in direct contact with air. Also, according to Krishnarao et al. (2001), the dissociation of potassium oxide at 347°C subsequently forms elemental potassium which causes surface melting as well as accelerates the crystallisation of amorphous silica to form cristobalite. Potassium and sodium are highly soluble in water and therefore, a simple washing step with water effectively removed the potassium and

sodium responsible for causing the surface melting phenomenon. Consequently, the resulting ash from the combustion of water-washed rice husk contained significantly less char skeletons, with overall much lighter shade compared to the ash from raw rice husk. The presence of some char skeletons in the ash from the combustion of water-washed rice husk in Table 4.1-3 was speculated to be due to the ineffective removal of potassium from some portions of the rice husk, especially those consisting of complete two-halves which tend to float in water. Rice husk particles consisting of complete two-halves tend to repel water due to its wax-like outer layer. It is the inner layer which tends to absorb water and makes the particle sink. This was further confirmed by conducting the combustion tests on water-washed rice husk separated into completely floating and sinking particles. The particles that completely sank in the water comprised primarily of one-halves of rice husk that enable the water absorption on the inner layer as well as broken fragments of rice husk.

The resulting ash from the combustion tests on the separate samples of water-washed rice husk were shown in Table 4.1-4 (completely sinking particles) and Table 4.1-5 (floating particles). The removal of potassium and sodium from rice husk in the completely sinking particles was very effective, as reflected in the resulting ash samples which showed the absence of char skeletons at all the range of temperatures and residence times investigated (Table 4.1-4). On the other hand, ineffective removal of potassium and sodium from the floating rice husk particles (during water-washing step) resulted in the formation of some char skeletons in the ash samples, prominently for all samples with residence of 1 minute. This could be attributed to the presence of surface melt on these particles, which form a 'barrier' to prevent direct contact between the carbon molecules and oxygen. These subsequently led to a lower rate of carbon oxidation, thereby resulting in ash samples containing considerable amount of char skeletons after being thermally-treated for 1 minute. Increasing the residence times (to 2 – 3 minutes) did remove these char skeletons, however, the resulting ash samples were not as white as those from the completely sinking rice husk particles, due to the presence of some amber-coloured ash skeleton (expected to be due to presence traces of potassium that prevented complete carbon burnout to take place).

Table 4.1-2: Effect of temperature and residence time on the formation of black char particles during thermal treatment of raw rice husk in the muffle furnace








































Temp. (°C)	Residence time (min)		
	1	2	3
700			
750			
800			
850			

Table 4.1-3: Effect of temperature and residence time on the formation of black char particles during thermal treatment of water-washed rice husk* in the muffle furnace

Temp. (°C)	Residence time (min)		
	1	2	3
700			
750			
800			
850			

Note:* Soaked in tap water for 24 hours, mixture of sinking and floating particles

Table 4.1-4: Effect of temperature and residence time on the formation of black char particles during thermal treatment of water-washed rice husk* (submerged particles) in the muffle furnace

Temp. (°C)	Residence time (min)		
	1	2	3
700			
750			
800			
850			
900			

Note: *Soaked in tap water for 24 hours, totally submerged particles

Table 4.1-5: Effect of temperature and residence time on the formation of black char particles during thermal treatment of water-washed rice husk* (floating particles) in the muffle furnace

Temp. (°C)	Residence time (min)		
	1	2	3
700			
750			
800			
850			

Note: *Soaked in tap water for 24 hours, floating particles

b) Silica Structure

The diffractograms of all the ash samples from Table 4.1-2 and Table 4.1-3 were shown in Table 4.1-6 and Table 4.1-7, respectively. It was observed that all these ash samples were still in their amorphous form, as indicated by a background hump at peak position of approximately 22° on each diffractogram. Exposure of the rice husk to temperatures in the range of $700^\circ\text{C} - 850^\circ\text{C}$ (which were the reported temperatures for crystallisation of silica in rice husk ash) for a brief period of time (less than 3 minutes) were found to be insufficient for the formation of crystals (cristobalite) to take place. According to Gorthy and Pudukottah (1999), the formation of cristobalite occurred gradually, requiring a certain period of time to complete. As proven in this study, the period of up to 3 minutes was still insufficient for the complete transformation of amorphous silica to cristobalite to take place. This finding was very significant to the operation of the fluidised bed combustor, as the combustor temperature could be confidently maintained in the range of $700 - 850^\circ\text{C}$ in order to achieve very high carbon burnout without the risk of damaging the product (whereby crystallisation of the siliceous ash occurs) due to the short residence time of rice husk in the combustor (less than 2 minutes). Hence, it is very crucial to note that the crystallisation of silica in the rice husk ash depend largely on the residence time as it is to the temperature, and due emphasis shall be given on the effect of the former in considering the optimum temperature range for operation of a fluidised bed combustor to obtain amorphous, carbon-free siliceous rice husk ash. This finding also accentuated the advantage of the fluidised bed combustor for the purpose of production of amorphous silica from rice husk, as the high temperature range ($700 - 850^\circ\text{C}$) in other types of combustors (i.e. fixed bed, grate-type etc.) might cause the silica in the ash to crystallise due to the relatively longer residence time of ash in these combustors compared to the fluidised bed.

In order to test the time-dependant temperature limit for the onset of silica crystallisation in rice husk ash, the water-washed rice husk (completely sinking particles) were subjected to a temperature of $900 \pm 10^\circ\text{C}$ in the muffle furnace. Results from the XRD analysis showed that the residence time of up to 3 minutes was still insufficient for the crystallisation of silica to take place, as observed in Table 4.1-8 which showed that all the samples still retained their amorphous form.

Table 4.1-6: Diffractograms of rice husk ash samples from thermal treatment of raw rice husk in the muffle furnace at different temperatures and residence times

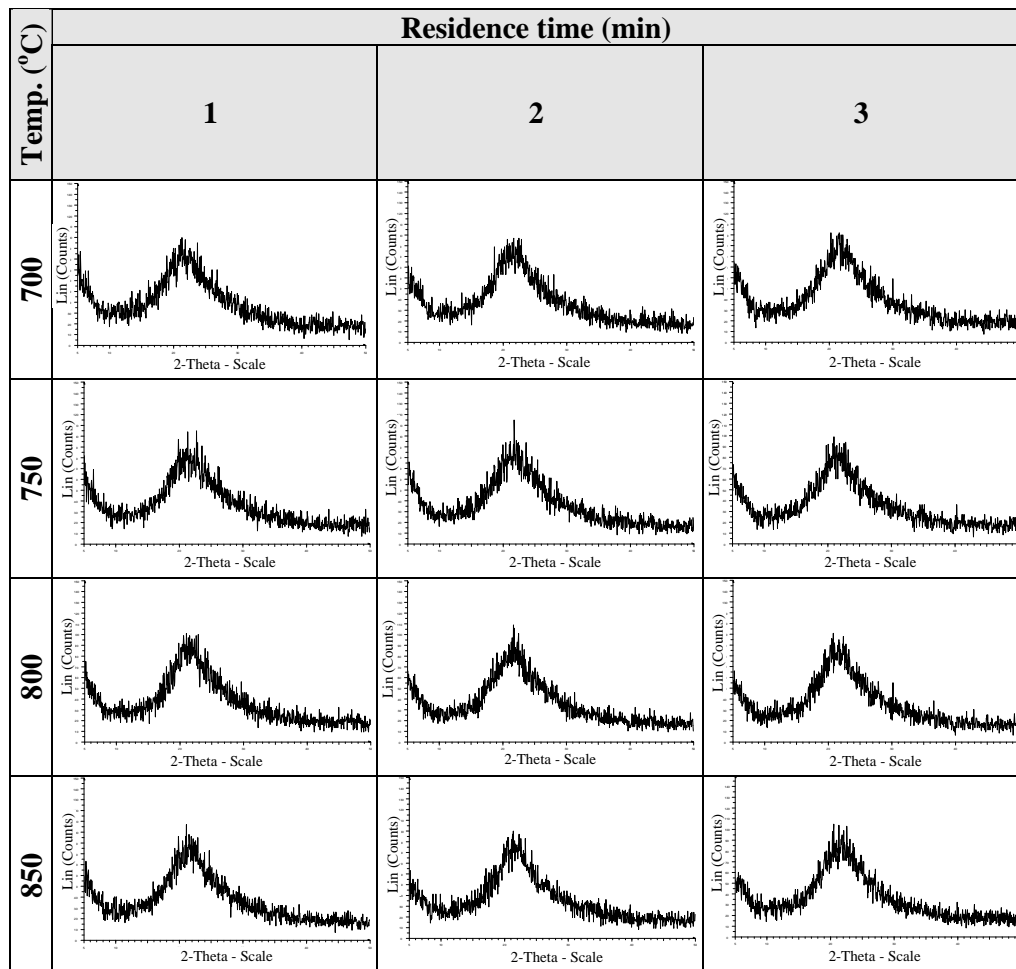
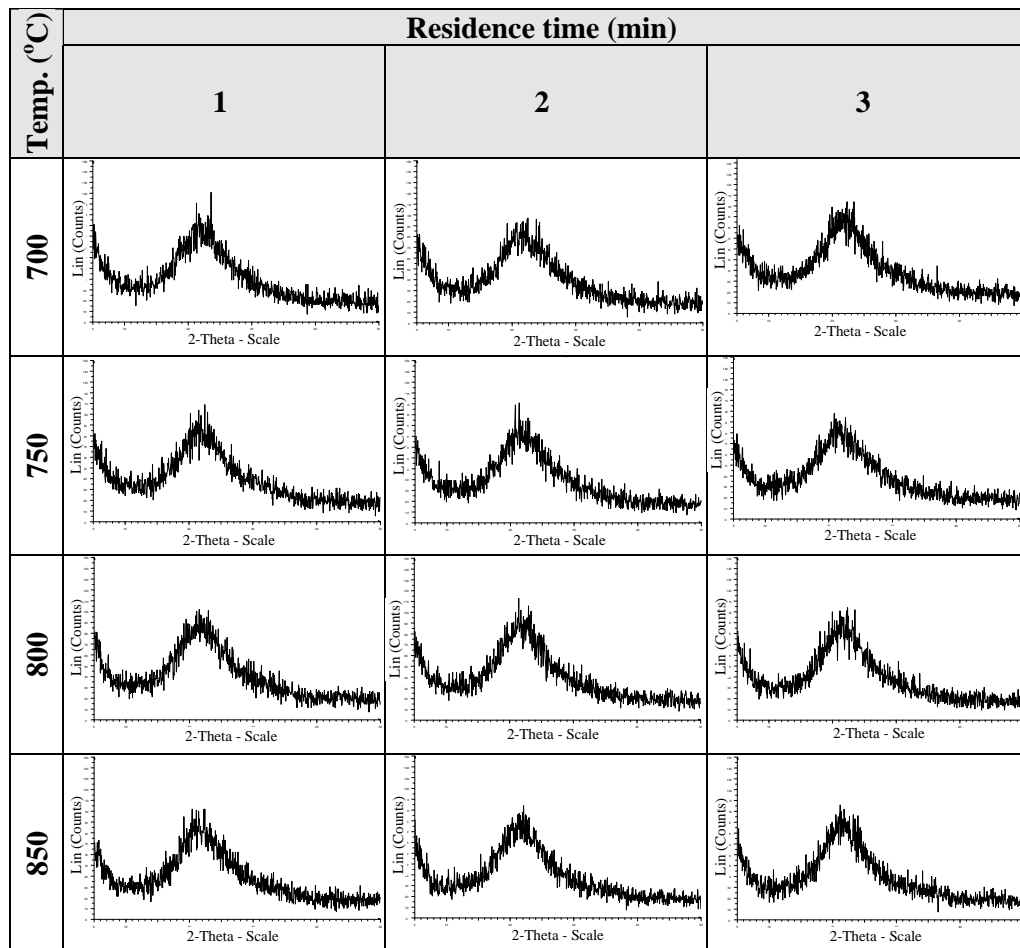


Table 4.1-7: Diffractograms of rice husk ash samples from thermal treatment of water-washed rice husk* in a muffle furnace at different temperatures and residence times



Note: *Soaked in tap water for 24 hours

Table 4.1-8: Diffractograms of rice husk ash samples from thermal treatment of water-washed rice husk in a muffle furnace at 900°C for different residence times

Residence Time (min)	XRD of sample after exposure to very high temperature (900°C)	Remarks
1		Amorphous
2		Amorphous
3		Amorphous

From the current study, it could be concluded that:-

- i) The presence of low-melting point alkali metals compounds (potassium oxide and sodium oxide) in rice husk resulted in the formation of surface melt on the rice husk particles during the combustion process and consequently the formation of char skeletons (black particles) in the ash.
- ii) The removal of the highly-soluble potassium and sodium in the rice husk particles through washing with water at ambient temperature (30°C) was

effective in eliminating the formation of char skeletons in the ash, thereby producing white ash with low residual carbon content (high burnout of carbon).

- iii) Exposure of rice husk particles to the temperature of up to 850°C (raw rice husk) or 900°C (water-washed rice husk) for up to 3 minutes was insufficient to cause crystallisation of silica in the resulting ash.
- iv) It was hypothesised that the fluidised bed combustor could be operated confidently up to the temperature range of 850 – 900°C during the combustion of rice husk while preserving the amorphous structure of the resulting siliceous ash. This was due to the short residence time in the combustor (less than 2 minutes).

4.3 Effects of Fluidisation Parameters on the Mixing of Rice Husk in Fluidised Bed

The fluidisation properties of particles present during the combustion of rice husk in the fluidised bed was tabulated in Table 4.1-9. The experimental values obtained were compared with those obtained from existing literatures wherever available.

The velocities at which a material is in its fluidising state lie within the range of its minimum fluidising velocity (U_{mf}) and its terminal velocity (U_t). The velocities range obtained from experiment for the fluidising state of rice husk, its char and ash as well as sand samples was compared in Figure 4.1-1.

Table 4.1-9: Fluidisation properties of rice husk, rice husk char, rice husk ash and silica sand samples

Properties		Rice Husk (Whole Husk)	Rice Husk Char (Devolatilised Whole Husk)	Rice Husk Ash	Sand (250 – 595 μm)	Sand (595 – 841 μm)
Density (kg/m^3)	Bulk (ρ_b)	100	54 – 60	i) 120 – 140 (2 – 10 wt% carbon) ii) 220 – 260 (< 1 wt% carbon)	1460	1480
	Particle (ρ_p)	650	560	i) 1590 (2 – 10 wt% carbon) ii) 2000 (< 1 wt% carbon)	2430	2440
Mean particle diameter (mm)		1.6 [†]	Similar to rice husk	0.108	0.342	0.672
Bed voidage, ε		0.85	0.90	0.93 – 0.94	0.40	0.39
Sphericity, ϕ_s	Theoretical calculation	0.19	0.11	0.23 – 0.25	0.92	0.96
	Chart (Brown, 1950) [§]	NA	NA	NA	0.90	0.93
Minimum fluidising velocity, U_{mf} (m/s)	Literature	i) 0.50* ii) 0.46 [#] iii) 0.60 ^β	0.45 [#]	i) 0.30 [#] ii) 0.16 ^ψ	NA	NA
	Theoretical calculation (Wen and Yu, 1966) [§]	0.35	0.32	0.008	0.09	0.30
	Experimental (pressure drop plot)	0.64	0.56	0.060	0.09	0.30
Terminal velocity, U_t (m/s) @ ambient (30°C)	Literature	i) 0.76* ii) 1.1 [#]	1.15 [#]	i) 0.8 ^ψ ii) 0.7 [#]	NA	NA
	Estimated from theoretical calculation (Haider and Levenspiel, 1989) [§]	1.0	0.75	0.17	1.4	4.8
	Experimental (pressure drop plot)	0.9	0.8	0.10 – 0.25	1.2	5.3

Note:

NA – Not applicable

[†] - Surface mean diameter calculated from the mesh analysis of rice husk (Mansaray and Ghaly, 1997) and as reported in Chen et al. (1998)

* - Hao et al. (1995)

[#] - Sen and Ghosh (1992)

^ψ - Xu et al. (1985)

^β - Fang et al. (2004)

[§] - Chart and theoretical equations included in Appendix D

Rice husk burns according to the shrinking core model and therefore its char has mean particle diameter similar to rice husk

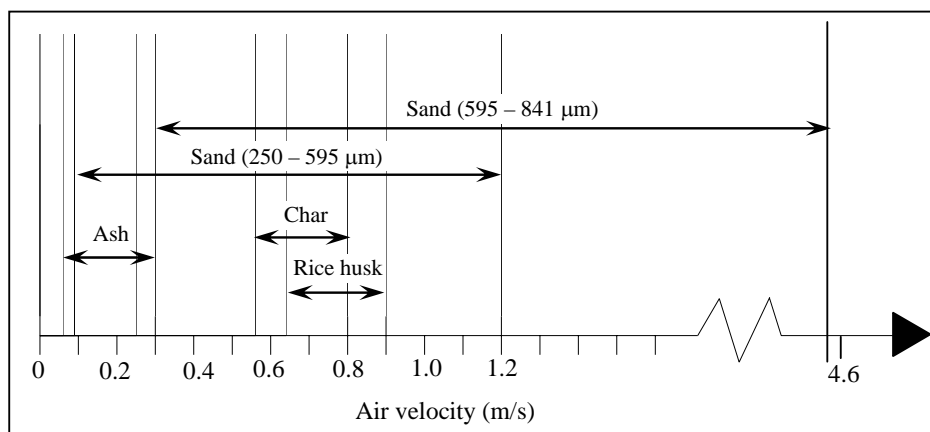


Figure 4.1-1: Experimental values of velocities range for the fluidising state of rice husk, rice husk char, rice husk ash and sand samples

4.3.1 Sand Size

Experiments were narrowed down to using sand of sizes which, when operating at fluidising numbers of $3 - 5 U_{mf}$, will give fluidising velocity below the terminal velocity of rice husk (at $0.8 - 1.1$ m/s, Table 4.1-9) to prevent excessive carry-over of rice husk into the freeboard region. Further, the lower limit of the fluidising velocity is governed by the terminal velocity of the resulting ash (as low as 0.1 m/s, Table 4.1-9), whereby fluidising velocities higher than this value is preferable to enable elutriation of the resulting ash towards the cyclone thus facilitating the removal of ash from the bed region.

In addition, commercial silica sand was used due to the necessity of repeating the same experiments in larger-scale fluidised bed combustor, which required a substantial amount of sand thus rendering efforts to sieve the sand to the desired range highly infeasible. The available size ranges of commercial silica sand and the preliminary screening of sand size for experimental study were shown in Table 4.1-10. Based on the screening results, two size ranges of sand were selected for experimental study on the mixing behaviours of rice husk in the fluidised bed. They were: (i) screen 20/30 with a size range of $595 - 841$ μm and (ii) screen 30/60 with a size range of $250 - 595$ μm .

Table 4.1-10: Screening of commercial silica sand* size for experimental study of rice husk combustion in fluidised bed combustor systems

Screen Designation	Size Range (μm)	Particle Mean Diameter [†] from Screen Analysis (mm)	Minimum Fluidising Velocity (U_{mf}) from Experimental Pressure Drop Plot (m/s)	Operating Gas Velocity at $3 - 5 U_{mf}$ (m/s)	Implications of Operating Gas Velocity on Ash / Rice Husk Elutriation	Accepted / Rejected for Experimental Study
40/60	250 – 420	0.23	0.05	0.15 – 0.25	Too low for elutriation of resulting ash, might cause excessive accumulation of ash in the bed region	Rejected
30/60	250 – 595	0.34	0.09	0.27 – 0.45	Sufficient for elutriation of resulting ash but still insufficient for elutriation of whole rice husk; within the range of superficial fluidising velocities of 0.185 – 0.37 m/s as recommended by Bhattacharya et al. (1984)	Accepted
20/30	595 – 841	0.67	0.30	0.90 – 1.50	Sufficient for elutriation of resulting ash and some rice husk in particular broken fragments or fines; within the range of superficial fluidising velocities of 0.6 – 1.0 m/s as recommended by Xu et al. (1985), Bingyan and Zhongnan (1987), Sen and Ghosh (1992) and Natarajan et al. (1998a)	Accepted
10/20	841 – 2000	1.05	0.55	1.65 – 2.75	Too high, might cause excessive elutriation whole rice husk and resulting ash	Rejected

* From Johor Silica Industries, Kota Tinggi, Johor

† Volume-surface mean diameter, d_{vs} for use in fluidisation studies (Botterill et al., 1982)

For the sand size of 595 – 841 μm , operating at the fluidising velocity of 4 U_{mf} resulted in an air velocity of 1.2 m/s. This velocity was higher than the terminal velocity of whole husk particles, and as such, most of the rice husk in particular broken fragments tended to be elutriated into the freeboard region. This reduced the amount of rice husk reaching the bed region, thus preventing them from being mixed within the bubbling bed region. It was also observed that bigger air bubbles were formed within the sand bed due to the bigger particle size. As these bubbles erupted at the bed surface, the sand particles were observed to be splashed more turbulently into the freeboard region compared to the bed comprising 250 – 595 μm sand particles. The upward splashing motion further prevented the rice husk particles from penetrating the bed region.

With the sand size of 250 – 595 μm , it was observed that a considerable amount of rice husk was being mixed within the bed. Only a small amount of rice husk, mostly fine fragments, was elutriated into the freeboard region. Operating at 4 U_{mf} for this sand size resulted in a fluidising velocity of 0.4 m/s. This velocity was less than half the terminal velocity of whole rice husk particles (Table 4.1-9), thus enabling them to reach the bed region. Upon reaching the bed, the bubbling action of the sand bed tended to engulf and distribute them uniformly within the bed. The granular nature of sand particles eliminated the interlocking nature of rice husk and enabled them to fluidise uniformly within the bed region. This probably explained why the rice husk could be fluidised even though the air velocity was below its minimum fluidising velocity. Rao and Bheemarasetti (2001) had shown that the minimum fluidising velocity for a binary mixture of particles ($U_{mf,m}$) with different densities and sizes was different from their individual minimum fluidising velocity (U_{mf}), with $U_{mf,m}$ being largely dependent upon the mass fraction of particles in the mixture. They found that as the mass fraction of rice husk was increased in a bed of sand particles (250 – 355 μm and 355 – 600 μm , particle density of 2500 kg/m^3), the values of $U_{mf,m}$ were elevated to values approaching the U_{mf} of rice husk. Nevertheless, $U_{mf,m}$ was found to be slightly higher than the U_{mf} of the sand particles (less than 60% difference) when the mass fraction of rice husk in the mixture was kept below 10 wt%. During the combustion process, the mass fraction of rice husk in the bed region was expected to be kept low as they are continuously being burnt

off to form chars and ash. Hence, it was expected that the $U_{mf,m}$ of these mixture materials could be well-represented by the U_{mf} of the majority of sand particles and as such, the fluidising number of the bed material shall be referred with relation to the U_{mf} of sand particles during the subsequent mixing and combustion studies.

4.3.2 Fluidising Velocity

The mixing behaviour of rice husk in the bed region at different fluidising velocities were summarised in Table 4.1-11. It was observed that the minimum air velocity to break the interlocking layer of rice husk at the bed surface was $3 U_{mf}$. Beyond $3 U_{mf}$ up to $6 U_{mf}$, the degree of rice husk mixing within the bed region increased. However, this was accompanied by the elutriation of more broken fragments of rice husk, thus reducing the amount of rice husk that reached the bed region. The terminal velocity of fragmented rice husk particles was reached when operating at the fluidising velocity of $7 U_{mf}$, thereby resulting in significant elutriation rate of rice husk fragments. At $8 U_{mf}$, most of the rice husk could not reach the highly turbulent, bubbling bed region upon feeding but was suspended instead at the freeboard region with broken fragments being blown out of the column.

Table 4.1-11: Mixing behaviours of rice husk in the 80-mm inner diameter fluidised bed column at different fluidising velocities (sand size = 250 – 595 μm , static bed height = 0.5 D_c , mass fraction of rice husk in sand bed = 10 wt%)

Fluidising Number (U_{mf})	Air Velocity (m/s)	Mixing Behaviour
2	0.18	Rice husk tended to form a thin, interlocking layer at the bed surface. Bed bubbling was disrupted and rice husk could not be mixed within the bed.
3	0.27	Bubbling in the bed become more energetic with stable and steady formation of gas bubbles. Most of the rice husk could reach the bed and be mixed within.
4	0.36	Bubbling in the bed become more vigorous. The amount of rice husk reaching the bed was slightly lower as the fine fragments tended to be blown towards the freeboard region. Mixing of rice husk in the bed region was better with higher circulation rate of rice husk from the top to the bottom of the bed.
5	0.45	Bed become more turbulent and but more broken fragments of rice husk was blown towards the freeboard region. The whole husk particles reaching the bed were mixed uniformly within the bed at higher circulation rate.
6	0.54	The bed was bubbling very vigorously and tended to splash the sand particles up to the freeboard region. More broken fragments of rice husk were elutriated along with some whole husk particles. The sand splashing made it difficult for the rice husk particles to penetrate the bed. However, once these rice husk particles reached the bed, they were mixed uniformly within the bed at a more rapid rate.
7	0.63	Bubbling of bed particles become very turbulent and the elutriation rate of rice husk particles (broken fragments) become more significant as their terminal velocities had been reached. The small amount of rice husk reaching the bed region was distributed evenly amongst the bed particles in a very rapid manner.
8	0.72	Most of the rice husk particles were suspended in the freeboard region upon feeding. Elutriation of some fine sand particles from the bed was also observed. The bed was bubbling very turbulently with splashing of sand particles higher up to the freeboard. Only a very small amount of rice husk was mixed within the bed.

4.3.3 Static Bed Height

The mixing behaviours of rice husk in the bed region at different static bed heights were summarised in Table 4.1-12. It was observed that thin bed, such as that at $0.25 D_c$, resulted in poor mixing of rice husk within the bed region as the gas bubbles that were responsible to provide agitation force within the bed was not allowed to be formed completely. As the bed depth was increased, these bubbles coalesced as they moved upwards to form bigger gas bubbles. At $0.5 D_c$, the gas bubbles that formed were not too big to cause vigorous eruption at the bed surface while still able to provide enough agitation force to distribute the rice husk particles within the bed region. As the bed depths were increased beyond $0.5 D_c$, the eruption of big bubbles at the surface of these beds tended to splash the sand particles upwards, thus making it difficult for rice husk to penetrate the bed. As such, the amount of rice husk being mixed within the bed was reduced.

Table 4.1-12: Mixing behaviours of rice husk in the 80-mm inner diameter fluidised bed column at different static bed heights (sand size = 250 – 595 μm , fluidising velocity = $4 U_{mf}$, mass fraction of rice husk in sand bed = 10 wt%)

Static Bed Height (D_c)	Bed Depth (mm)	Mixing Behaviour
0.25	20	Bed was too thin for complete formation of gas bubbles. The incomplete bubbles that formed could not provide enough mixing force to agitate the bed materials. Rice husk tended to form small clumps within the bed due to the insufficient turbulence to break the interlock amongst the rice husk particles.
0.5	40	Small gas bubbles formed and erupted continuously upon reaching the bed surface. The agitation due to the movement of these gas bubbles provided the mixing force to distribute the rice husk particles uniformly within the bed. The eruption of gas bubbles at the bed surface was not very vigorous, thus enabling rice husk to be easily engulfed into the bed region upon reaching the bed.
0.75	60	The higher bed depth allowed for the formation of bigger gas bubbles as they coalesced along their path to the surface of the bed. The bed became more turbulent due to the higher agitation force from the movement of these bigger gas bubbles, allowing better mixing rate of rice husk. However, this was accompanied by higher turbulence at the bed surface as these bigger bubbles erupted. This reduced the chances of rice husk particles to reach the bed thus resulting in an overall lower amount of rice husk being mixed within the bed.
1.0	80	The bed became very turbulent with the presence of even bigger bubbles. The agitation force was high to distribute any rice husk particles that managed to reach the bed region. The chances of rice husk particles to reach the bed region was reduced significantly due to the turbulent upward splashing of sand particles into the freeboard region arising from the eruption of the big bubbles.

4.4 Effects of Fluidisation Parameters on the Mixing of Rice Husk in Fluidised Bed during Combustion Process

4.4.1 Sand Size

Experiments were conducted using two size ranges of sand, namely as follows:-




- i) Screen 20/30 with a size range of 595 – 841 μm
- ii) Screen 30/60 with a size range of 250 – 595 μm

For each sand size studied, the static bed height was fixed at $0.5 D_c$ or equivalent to 40mm while the fluidising velocities were varied from $3 U_{mf}$ to $5 U_{mf}$ (at combustion temperatures). In each case, rice husk was fed at stoichiometric level (primary air factor of 1.0) upon bed pre-heating with LPG to a temperature of 700°C .

a) Sand Size of 595 – 841 μm

The bed temperature throughout the combustion of rice husk using this sand size was in the range of $750 - 850^\circ\text{C}$. The resulting fly ash samples were compared in Table 4.1-13.

Table 4.1-13: Fly ash samples from the combustion of rice husk in the 80-mm inner diameter fluidised bed combustor with a bed of 595 – 841 μm sand (fluidising velocity = $3 - 5 U_{mf}$, static bed height = $0.5 D_c$, primary air factor ≈ 1.0)

Fluidising Velocity* (U_{mf} Number)	Fly Ash	Remarks
$3 U_{mf}$		Constituted mainly of black chars interspersed with small amount of white ash
$4 U_{mf}$		Consisted of black chars only
$5 U_{mf}$		Consisted of black chars which retained their rigid skeleton-like shape

Note: * At corresponding bed temperature

At the fluidising velocity of $3 U_{mf}$, mixing in the bed was not good, with the formation of dead zone at nearly two-third of the sand bed, as shown in Plate 4.1-3. Burning of rice husk was restricted to the top of the sand bed without penetration of the resulting ash or char into the sand bed (Plate 4.1-4). As such, the accumulation of char and ash just above the sand bed was rapid (Plate 4.1-5).

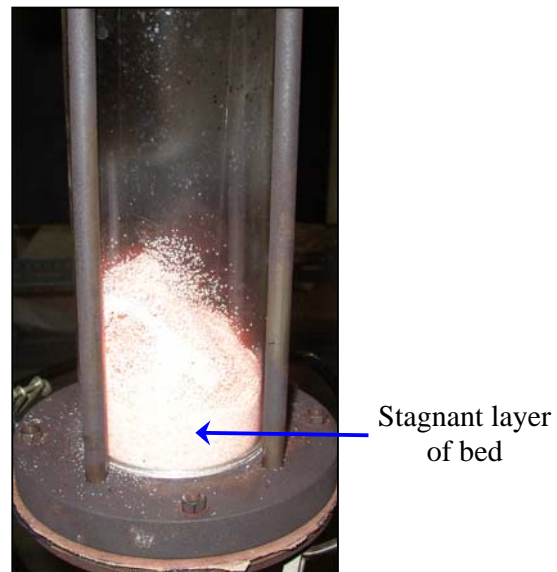


Plate 4.1-3: Formation of dead zone at nearly two-third of the sand bed (595 – 841 μm) at fluidising velocity of $3 U_{mf}$

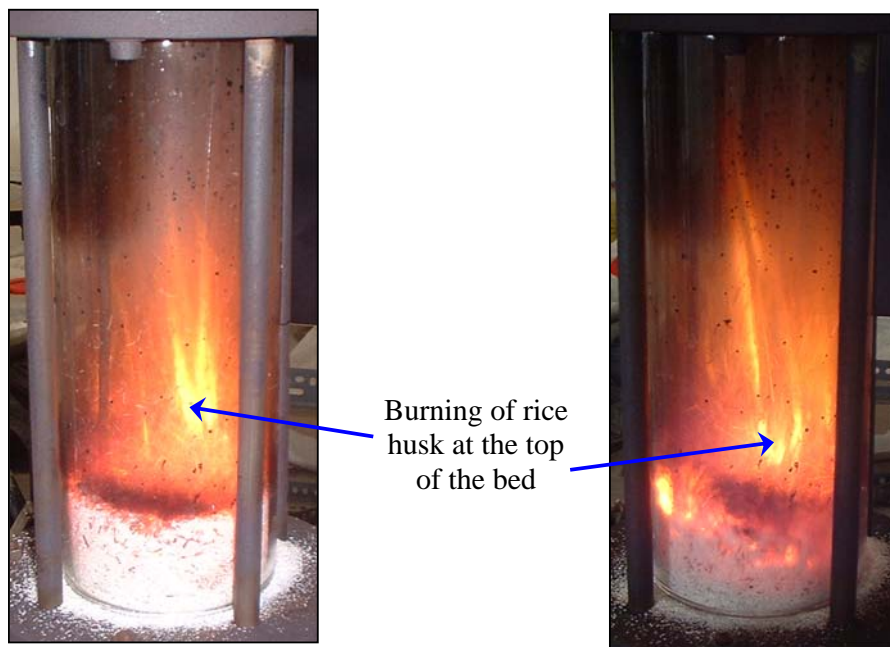
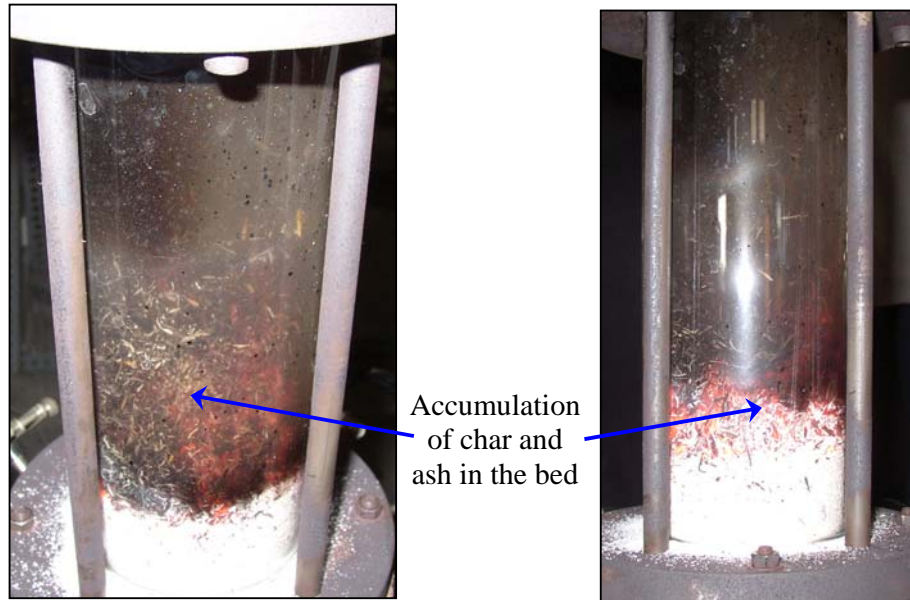


Plate 4.1-4: Burning of rice husk was restricted to the top of the sand bed (595 – 841 μm) at fluidising velocity of $3 U_{mf}$



**Plate 4.1-5: Rapid accumulation of char and ash in the sand bed (595 – 841 μm)
at fluidising velocity of $3 U_{mf}$**

When the fluidising velocity was increased to $4 U_{mf}$, some degree of bed mixing with slight penetration of rice husk and char into the sand bed was observed. Burning of rice husk was mostly in the suspension form (Plate 4.1-6) since the fluidising velocity of $4 U_{mf}$ with this sand size, at 1.2 m/s, was above the terminal velocity of the rice husk (in the range of 0.8 – 1.1 m/s as shown Table 4.1-9). As such, most of the rice husk tended to elutriate towards the cyclone upon entering the fluidised bed, and the exposure of high temperature in the freeboard region resulted in mainly the devolatilisation of the rice husk. Consequently, the fly ash was primarily black char (Table 4.1-13) with very high carbon content (31.0 wt%). Increasing the fluidising velocity further to $5 U_{mf}$ (equivalent to 1.5 m/s) resulted in more severe elutriation of rice husk with the majority of combustion taking place as suspension burning in the freeboard region. The bubbling of the sand bed, however, was more vigorous compared to that of $4 U_{mf}$. The resulting fly ash was also constituted mainly of black chars which still retained their rigid skeleton-like shape, indicating that most of the rice husk just devolatilised in the freeboard region without entering the sand bed.

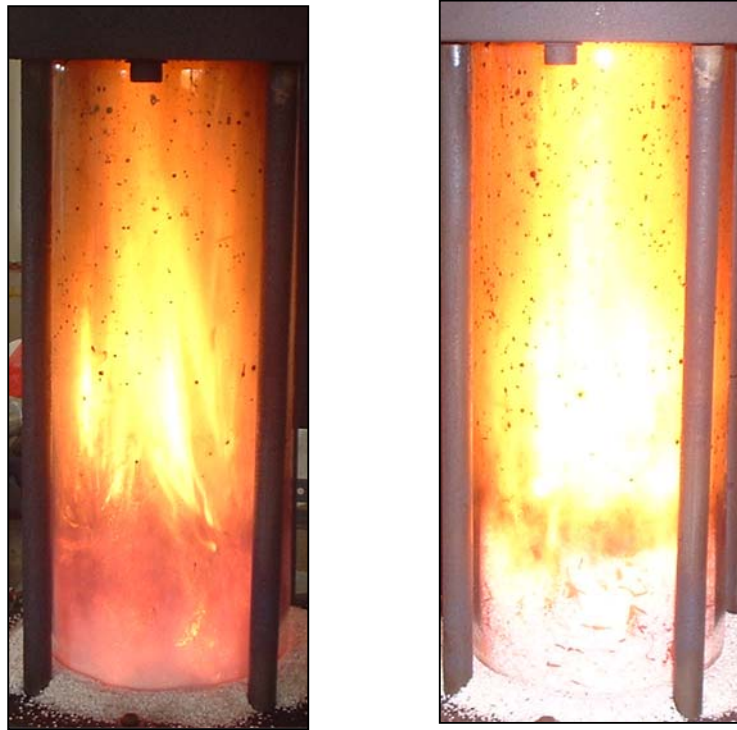


Plate 4.1-6: Suspension burning of rice husk at fluidising velocity of $4 U_{mf}$ (sand size 595 – 841 μm)









Plate 4.1-7: Suspension burning of rice husk at fluidising velocity of $5 U_{mf}$ (sand size 595 – 841 μm)

These findings were as expected because the sand particles of size 595 – 841 μm fell into Category D according to the Geldart Classification of particles (Geldart, 1973) with their diameter in the excess of 600 μm . Their behaviour is erratic and unpredictable, giving large exploding bubbles or severe channelling, as well as spouting when the gas distribution is uneven. Mixing of particles in this category in the freely bubbling condition is inferior to those of categories A and B. At low fluidising velocities, such as at $3 U_{mf}$, bubbling at the bed was not uniform leading to the formation of dead zones. To achieve better bubbling and mixing behaviours at the bed region, operating at higher fluidising velocities such as that $4 - 5 U_{mf}$ were necessary. However, these high fluidising velocities (at 1.2 – 1.5 m/s) were above the terminal velocity of rice husk, thereby resulting in severe elutriation of rice husk and burning was mainly in the suspension form.

b) Sand Size of 250 – 595 μm

The bed temperature throughout the combustion of rice husk using this sand size was in the range of 650 – 720°C. The ash samples (fly and bottom) were compared in Table 4.1-14.

Table 4.1-14: Ash samples from the combustion of rice husk in the 80-mm inner diameter fluidised bed combustor with a bed of 250 – 595 μm sand (fluidising velocity = 3 – 5 U_{mf} , static bed height = 0.5 D_c , primary air factor ≈ 1.0)

Fluidising Velocity* (U_{mf} Number)	Ash Sample		Remarks
	Fly Ash (FA)	Bottom Ash (BA)	
3 U_{mf}			FA: Consisted of black chars and considerable amount of white ash BA: Consisted mostly of white ash with small amount of black chars
4 U_{mf}			FA: Blacker in shade compared to that obtained at 3 U_{mf} , absence of white ash BA: Blacker in shade but finer in size compared to that obtained at
5 U_{mf}			FA: Blacker in shade compared to that obtained at 4 U_{mf} , absence of white ash BA: Blacker in shade but finer in size compared to that obtained at

Note: * At corresponding bed temperature

At the fluidising velocity of 3 U_{mf} , mixing between the sand particles and rice husk was good during the combustion process, as shown in Plate 4.1-8. It was observed that there was a high rate of penetration of char and ash into the sand bed (Plate 4.1-9). Thus, combustion of these rice husk particles in the bed region resulted in considerable amount of white ash in both the fly and bottom ashes, as shown in Table 4.1-14.

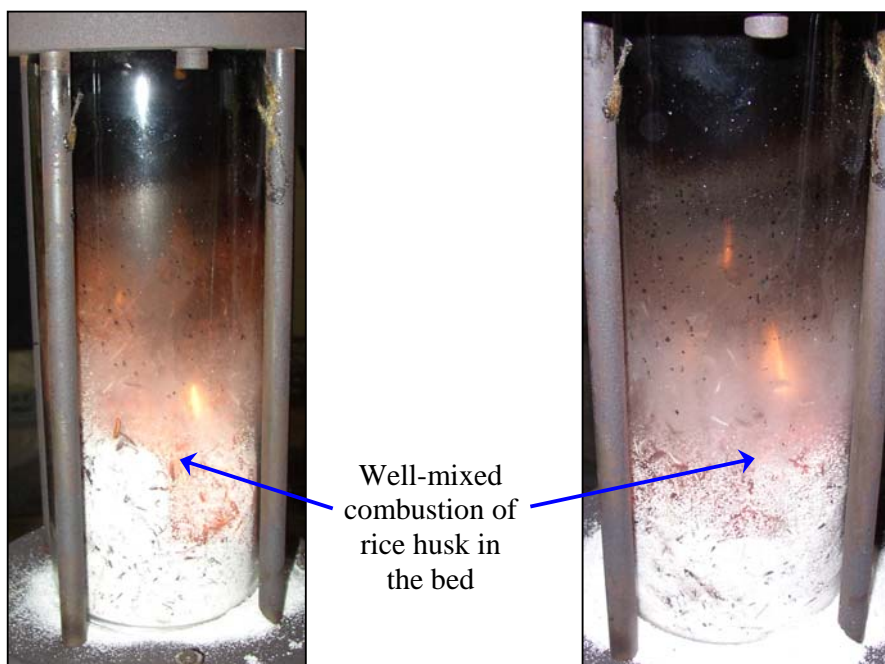


Plate 4.1-8: Good mixing during the combustion of rice husk (sand size 250 – 595 μm) at fluidising velocity of $3 U_{mf}$

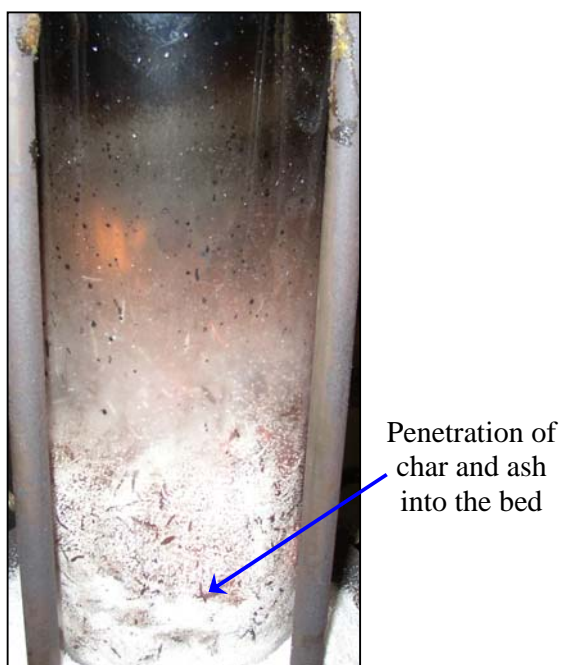


Plate 4.1-9: Penetration of rice husk, char and ash into the sand bed during combustion (sand size 250 – 595 μm) at fluidising velocity of $3 U_{mf}$

Increasing the fluidising velocity further to $4 U_{mf}$ still gave good mixing behaviour in the sand bed, with considerable amount of rice husk and char penetration into the bed region. Due to the higher fluidising velocity (at 0.36 m/s compared to 0.27 m/s at $3 U_{mf}$), there was some degree of suspension burning of rice husk just above the bed surface (Plate 4.1-10), which resulted in fly ash that was blacker than that obtained at $3 U_{mf}$. Nevertheless, rice husk combustion at the bed region was still good due to the good mixing behaviour, giving bottom ash that consisted of considerable amount of white ash.

Further increase in the fluidising velocity to $5 U_{mf}$ led to a more turbulent bed with vigorous splashing of particles to the bed surface due to the eruption of more and bigger gas bubbles. The vigorous splashing tended to throw the char particles to the freeboard region whereby they were further oxidised. Such vigorous splashing also made it more difficult for the fresh rice husk feed to penetrate the bed region, thus giving fly ash of even poorer quality than that obtained at $4 U_{mf}$. At $5 U_{mf}$, the corresponding velocity was 0.45 m/s, which was much lower than the terminal velocities of rice husk (0.8 – 1.1 m/s as shown in Table 4.1-9) or char (1.15 m/s according to Sen and Ghosh, 1992). As such, these particles tended to be returned to the turbulent bed region upon upward splashing due to bubble eruption until the ash portion were liberated through further combustion. This was evident from the particle size of the bottom ash which was much finer than that obtained from experiments at $3 U_{mf}$ or $4 U_{mf}$ (Table 4.1-14). Thereafter, the low terminal velocities of ash particles (0.10 – 0.25, as shown in Table 4.1-9) enabled them to be blown towards the cyclone as fly ash. Ash particles with whiter shade were found to be more dense (particle density as high as 2000 kg/m^3 compared to 1590 kg/m^3 for fly ash, as shown in Table 4.1-9 and 560 kg/m^3 for black char) due to the presence of higher amount of silica and were retained in the bed as residual bottom ash even after purging out of most of the bottom ash (Plate 4.1-12).

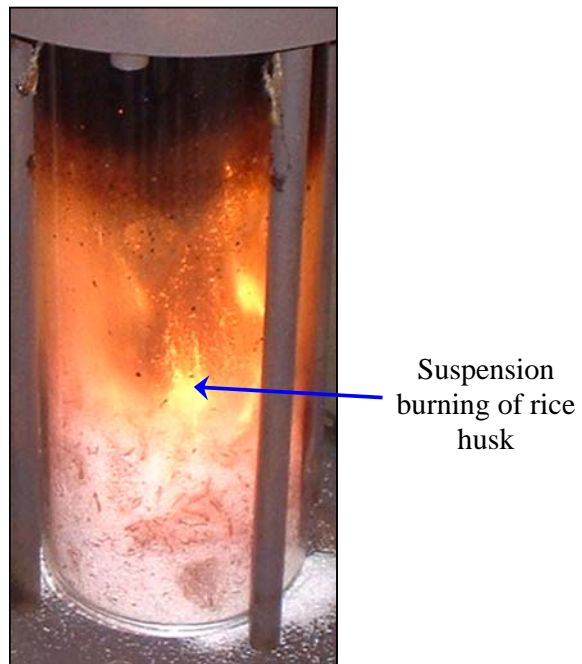


Plate 4.1-10: Some degree of suspension burning during the combustion of rice husk (sand size 250 – 595 μm) at fluidising velocity of $4 U_{mf}$

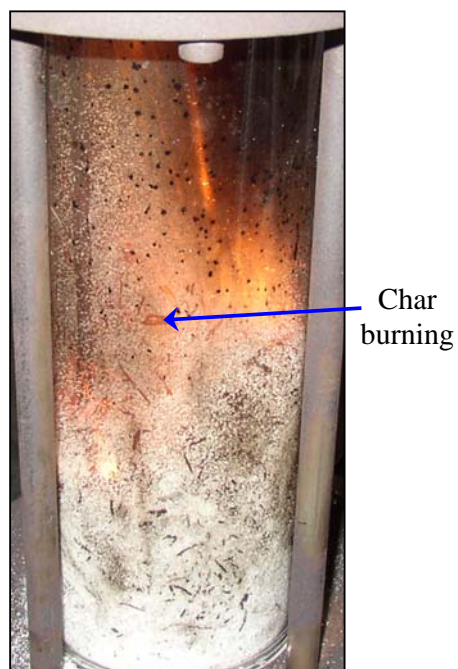


Plate 4.1-11: Vigorous bed bubbling with good mixing of char and rice husk in the sand bed during the combustion of rice husk (sand size 250 – 595 μm) at fluidising velocity of $5 U_{mf}$

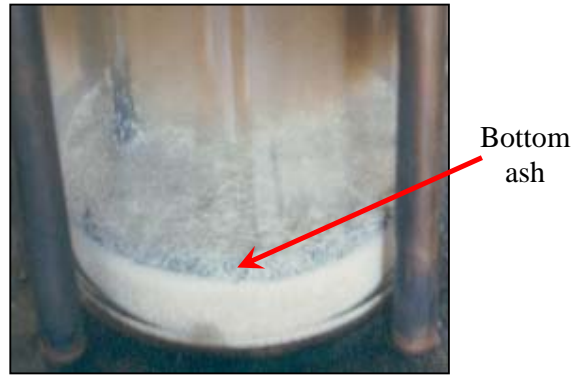


Plate 4.1-12: Residual bottom ash retained in the bed after the combustion of rice husk (sand size 250 – 595 μm) at fluidising velocity of 5 U_{mf}

Sand of size 250 – 595 μm used in the current experimental study fell into Category B according to the Geldart Classification of particles. These particles exhibit good fluidising behaviour with vigorous bubbling action and bubble enlargement upon reaching the bed surface. Hence, the observed mixing behaviour of rice husk in the fluidised bed using a sand size of 250 – 595 μm was consistent with the fluidising behaviour of Geldart B particles. Such good mixing behaviour subsequently led to good combustion behaviour and an overall better ash quality compared to that obtained when using sand of size 595 – 841 μm .

c) Findings

Based on the experimental results, the sand size of 250 – 595 μm was chosen for further experimental study due to the following reasons:-

- i) Better bed mixing. The char and ash tended to penetrate deep into the bed;
- ii) Better temperature control during feeding due to good mixing behaviour without rapid shoot-up of temperature to as high as 850°C (as encountered with the sand size 595 – 841 μm); and
- iii) Ease of ash separation from the bed as most ash particles tended to fly out into the cyclone and the quality was better with the presence of considerable amount of white ash.

These results were consistent with that reported by Bhattacharya et al. (1984), which concluded that sand particle with sizes of 351 – 420 μm was deemed most suitable

for combustion of rice husk in fluidised beds. Larger particles were not able to mix well with rice husk, resulting in poor combustion behaviour whereas smaller particles resulted in considerable sand entrainment.

4.4.2 Fluidising Velocity

Experiments were conducted at fluidising velocities ranging from $1 - 8 U_{mf}$ using the sand of size $250 - 595 \mu\text{m}$. For each experiment, the static bed height was fixed at $0.5 D_c$ or equivalent to 40mm while rice husk was fed at stoichiometric level (primary air factor of 1.0) upon bed pre-heating with LPG to a temperature of 700°C . The bed temperature was maintained at approximately 700°C throughout the experiment by manipulating the rate of LPG combustion.

At the minimum fluidising velocity ($1 U_{mf}$), mixing of rice husk in the bed region during the combustion process was poor. Rice husk did not penetrate the bed region upon feeding, therefore preventing the transfer of heat from the bed to the rice husk in order to initiate the combustion process. As the experiment progressed, more and more unburnt rice husk accumulated at the surface of the bed, which in turn disrupted the bed bubbling behaviour. The temperature in the bed decreased rapidly until eventually, the combustion process was quenched. The bottom product was found to be a mixture of mostly unburnt rice husk and skeleton-like chars.

When the fluidising velocity was increased to $2 U_{mf}$, the mixing of rice husk in the bed improved but was still insufficient to distribute the rice husk uniformly in the bed region. The rice husk also tended to form a layer at the bed surface, thus disrupting the overall bed mixing behaviour. The bed mixing behaviour and ash samples from experiments at fluidising velocities of $2 - 8 U_{mf}$ were compared in Table 4.1-15.

Table 4.1-15: Ash samples from the combustion of rice husk in the 80-mm inner diameter fluidised bed combustor at different fluidising velocities (sand size = 250 – 595 μm , static bed height = 0.5 D_c , primary air factor ≈ 1.0)













Fluidising velocity* (U_{mf} Number)	Ash Sample		Bed Mixing Behaviour
	Fly Ash	Bottom Ash	
$2 U_{mf}$			Very little mixing in the bed region. Rice husk formed a layer at the bed surface thus disrupting the overall bed mixing behaviour. Burning of rice husk was restricted to this top rice husk layer. Bottom ash retained the skeleton-like shape while broken fragments were elutriated as fly ash but in very little amount.
$3 U_{mf}$			Good mixing of rice husk in the bed region without formation of rice husk layer at the bed surface. Retention of rice husk in the hot bubbling bed enabled some of the rice husk to be burnt to completion to form white ash, which was subsequently elutriated together with broken fragments of char as fly ash. Bottom ash also contained more white ash.
$4 U_{mf}$			Better mixing in the bed region. Higher turbulence in the bed region tended to break the char skeletons into smaller fragments. However, the higher fluidising velocity resulted in lower residence time of these char fragments in the bed, giving higher amount of fly ash which was also darker in shade. The bottom ash contained less white ash skeletons and more fine greyish ash.
$5 U_{mf}$			More turbulent mixing in the bed region. Fly ash was higher in amount, finer in size and darker in shade. The bottom ash contained no skeleton-like shapes and attained a dark-greyish shade.
$6 U_{mf}$			Very turbulent mixing in the bed. Rice husk could still penetrate and got burnt in the bed region. Due to the higher degree of turbulence in the bed, the carbon burnout of the rice husk was higher, giving fly ash that was dark-greyish in shade and finer in size. The bottom ash was a mixture of white and grey ash fragments.

Table 4-15 (continued...): Ash samples from the combustion of rice husk in the 80-mm inner diameter fluidised bed combustor at different fluidising velocities (sand size = 250 – 595 μm , static bed height = 0.5 D_c , primary air factor \approx 1.0)

Fluidising velocity* (U_{mf} Number)	Ash Sample		Bed Mixing Behaviour
	Fly Ash	Bottom Ash	
7 U_{mf}			Highly turbulent mixing in the bed region. Rice husk encountered difficulty to penetrate the bed due to the high fluidising velocity and upward splashing of sand from the eruption of bubbles at the bed surface. The fly ash was a mixture of char skeletons (from rice husk devolatilising in the freeboard region) and small char fragments (from the bed). Very little white ash in the resulting bottom ash.
8 U_{mf}		-	Vigorous bed bubbling action and high fluidising velocity prevented rice husk from penetrating the bed. Rice husk mostly devolatilised in freeboard region resulting in fly ash in the form of char skeletons and negligible amount of bottom ash.

Note: * At corresponding bed temperature of 700°C

It was observed that a fluidising velocity of at least 3 U_{mf} was necessary in order to achieve good mixing behaviour of rice husk in the bed region. Increasing the fluidising velocity increased the degree of turbulence in the bed due to the more vigorous bed bubbling action. This in turn led to the higher rates of heat and mass transfer in the bed region, giving bottom ash particles which were whiter (burnt more completely) and finer in size, as could be seen from the bottom ash samples obtained at 3 – 6 U_{mf} . However, this increase in fluidising velocity also tended to decrease the residence time of ash in the bed region, making them more easily elutriated as fly ash. In addition, due to the high superficial velocity in the freeboard region, the residence time of fly ash in this region was also decreased. Thus, the fly ash samples contained more unburnt carbon (fly ash samples from 3 – 5 U_{mf}) as the fluidising velocity was increased. At higher fluidising velocities, the high turbulence at the bed region coupled with the high gas velocity made it difficult for rice husk particles to enter the bed. As such, they tended to be devolatilised in the freeboard region, giving fly ash particles which were mostly black chars and very little bottom ash. At the fluidising velocity of 8 U_{mf} , the fly ash consisted of black chars with

negligible amount of bottom ash. Further, it was observed that higher amount of sand particles (quartz crystals) were elutriated together with the fly ash into the cyclone as the fluidising velocities were increased. This showed that the height of the 80-mm fluidised bed column, at only 1000mm, was insufficient to disengage any sand particles which were ejected to the freeboard region due to the eruption of bubbles at the bed surface. Thus, it was necessary to conduct further experiments in a taller fluidised bed, such as the 210-mm inner diameter fluidised bed with a height of 2000mm.

4.5 Effects of Mixing Parameters on the Combustion Efficiency of Rice Husk in Fluidised Bed

4.5.1 Fluidising Velocity

The fluidising velocities were varied from $1.5 - 8 U_{mf}$ (at corresponding bed temperatures) to investigate their effects on the combustion efficiency of rice husk. In all experiments, the static bed height was held constant at $0.5 D_c$ (250 – 595 μm sand), the primary air factors at 1.0 and feeding was commenced once the bed had been pre-heated to the temperature range of 600 – 650°C.

a) Temperature Profiles and Combustion Characteristics

At $8 U_{mf}$, the bed was bubbling vigorously and most of the sand particles were thrown upwards to the freeboard region. This made it difficult for the rice husk to penetrate the bed. The high gas velocity also tended to blow the rice husk particles into the freeboard region, resulting in most of them being burnt in suspension form. The absence of rice husk combustion in the bed region led to the rapid decrease in bed temperature as the experiment progressed.

Lowering the fluidising velocities to the range of $4 - 5 U_{mf}$ reduced the entrainment rate of rice husk particles into the freeboard region. The amount of rice husk penetrating and being mixed within the bed was increased, leading to the increase in

bed temperature. However, some degree of suspension burning was still observed at the freeboard region due to the high fluidising velocities, which tended to entrain smaller fragments of rice husk, its char and or ash.

During combustion of rice husk at the fluidising velocity of $3.3 U_{mf}$, it was observed that mixing of rice husk within the bed region was good. There was a steady stream of slowly-rising bubbles erupting at the bed surface, and this enabled the rice husk to penetrate deep into the sand bed and got burnt thereafter. The char particles were observed to be broken into smaller fragments due to the turbulence in the sand bed, thereby making the carbon in the char easily available for conversion. The bed temperature (T1) was maintained steadily at approximately 650°C throughout the experiment (Figure 4.1-2). Slightly after the commencement of feeding (approximately 6 minutes), the supply of primary LPG was cut-off and the combustion of rice husk in the bed was found to be autogenous. This showed that mixing of rice husk in the bed region was good, and their combustion in the bed region released sufficient heat to sustain the bed temperature. As can be seen from Figure 4.1-2, the temperatures in the combustor during the combustion of rice husk were stable and hovered in the range of $650 - 700^{\circ}\text{C}$.

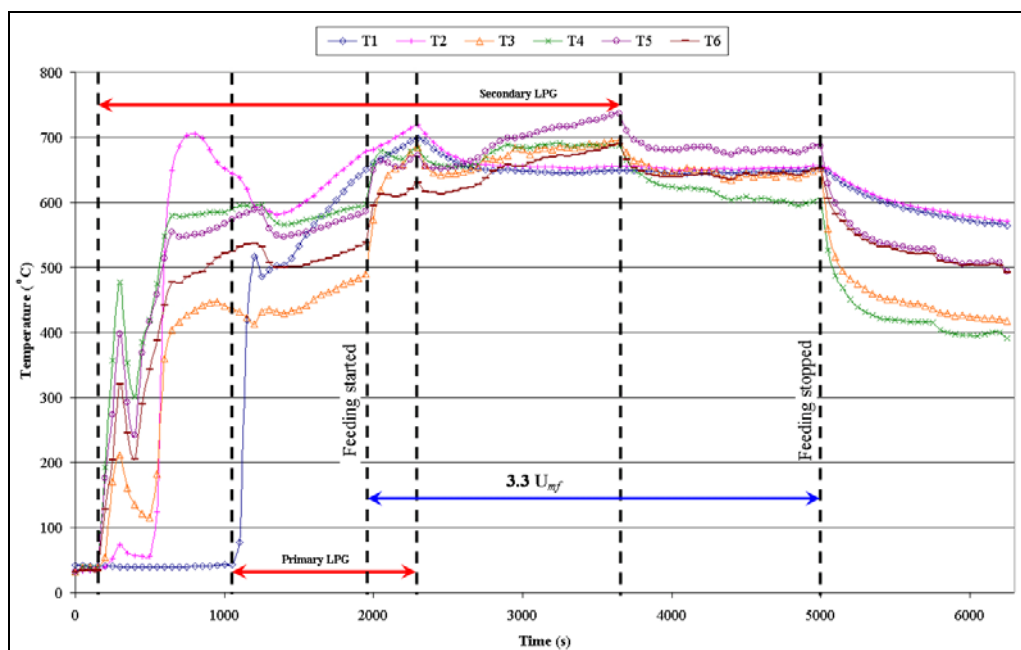


Figure 4.1-2: Real-time temperature profiles during combustion of rice husk in the 210-mm inner diameter fluidised bed at $3.3 U_{mf}$

When the fluidising velocity was reduced to $2.5 U_{mf}$, it was observed that bubble eruption at the bed surface was not as vigorous compared to the case of $3.3 U_{mf}$. Although the rice husk particles were observed to penetrate the sand bed to a certain degree, some of them tended to accumulate at the bed surface, forming a thin burning layer of rice husk. This was reflected in the temperature profile (Figure 4.1-3), whereby the temperature at this burning layer was at the region of 700°C (as registered by T2, located 166 mm above the distributor plate, the sand bed height was 105 mm) compared to only $650 - 675^{\circ}\text{C}$ when burning at $3.3 U_{mf}$ (Figure 4.1-2). This phenomenon also subsequently resulted in the bed temperature to drop as the experiment progressed.

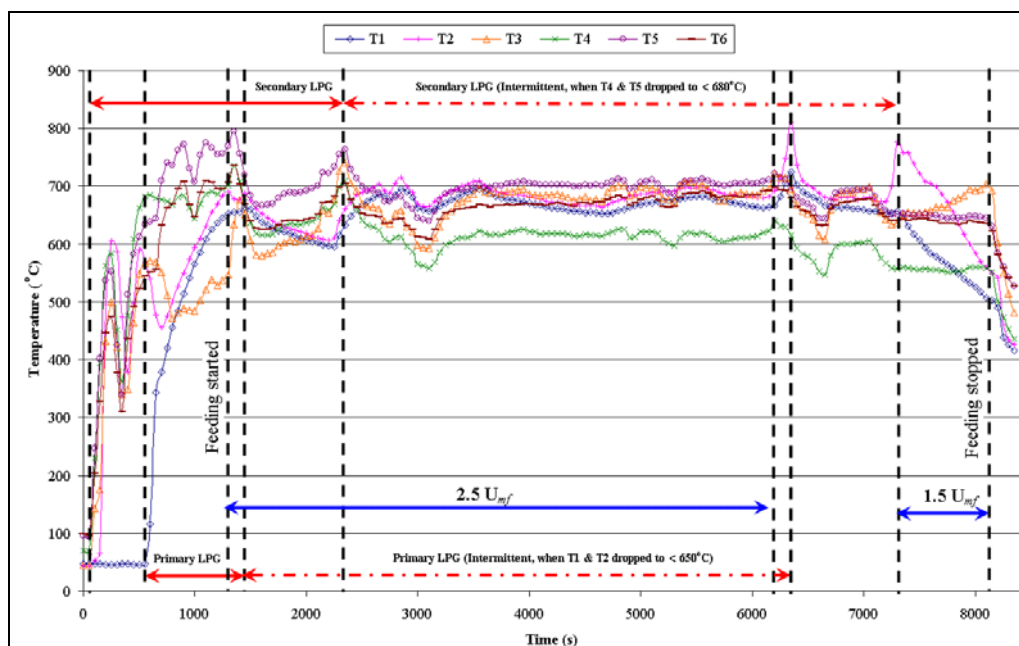


Figure 4.1-3: Real-time temperature profiles during combustion of rice husk in the 210-mm inner diameter fluidised bed at $2.5 U_{mf}$ and $1.5 U_{mf}$

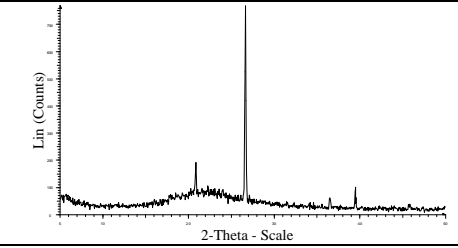
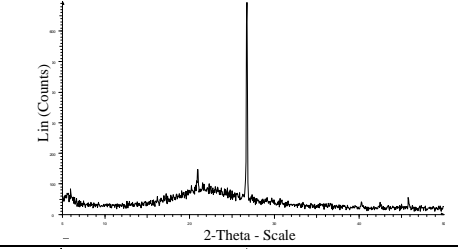
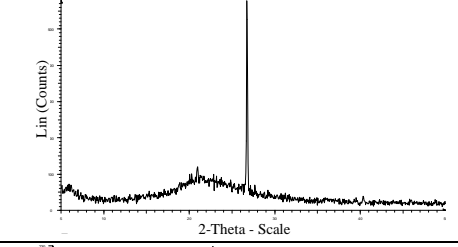
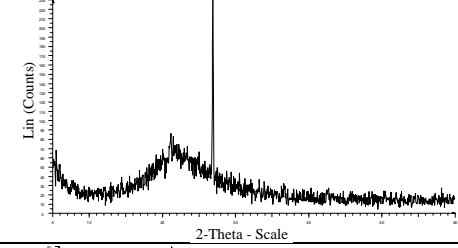
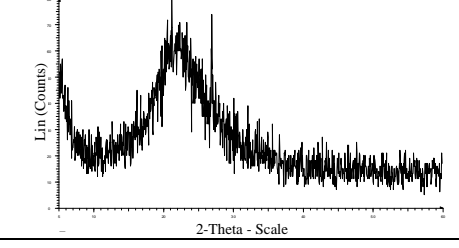
When the fluidising velocity was reduced to $1.5 U_{mf}$, mixing of particles in the bed was totally diminished. The rice husk formed a stagnant layer above the bed and burning was only restricted to this layer. This layer was increasing with time as the experiment progressed. Consequently, the bed temperature (T1) dropped drastically, prompting the experiment to be stopped. The bottom ash purged from the combustor contained mostly chars with trace amounts of white ash.

b) Ash Quality***i) Silica Structure***

The diffractograms of fly ash samples from the experiments were compared in Table 4.1-16. It was observed that the silica in all these ash samples still retained their amorphous structures due to the absence of any cristobalite or tridymite peaks. However, it was found that the higher the fluidising velocity, the higher the amount of sand particles that were blown out from the bed towards the cyclone, which ended up contaminating the fly ash. The concentration of the sand particles in the ash was reflected in the height of the quartz peaks in the diffractogram. At a fluidising velocity of $8.1 U_{mf}$, the intensity of the primary quartz peak at 2θ angle of 26.66° was as high as 770 counts per second (cps). These primary quartz peaks were observed in the resulting diffractograms from all fluidising velocities investigated except at the fluidising velocity of $1.5 U_{mf}$. The lowest concentration of quartz was found in the fly ash obtained at the fluidising velocity of $2.5 U_{mf}$ (at 74 cps for primary quartz peak, Table 4.1-16).

Preliminary studies showed that the phenomenon of sand contamination in the fly ash samples could be solved by first grinding the ash samples into a powder form, followed by fluidisation in a cold-model fluidised bed at fluidising velocities of 0.10 – 0.25 m/s. This velocity range was above the terminal velocity of powdered rice husk ash, but below the terminal velocity of sand impurities. As a result, only powdered rice husk ash will be elutriated and subsequently be collected at the cyclone. The top product entrained into the cyclone as well as the bottom product retained in the bed, were then subjected to XRD analysis. The resulting products and their respective diffractograms were as show in Table 4.1-17. The terminal velocities of sand (250 – 595 μm) was up to 10 times higher than that of rice husk ash (fly ash), as shown in Table 4.1-9. Thus, when subjected to fluidising velocities higher than 0.1 m/s but lower than 1.2 m/s, the ash particles could be separated from the sand particles. This method represented a form of de-contamination stage that could be applied to remove the traces of sand particles that was present in the fly ash samples.

Table 4.1-16: Diffractograms of fly ash samples from the combustion of rice husk in the 210-mm inner diameter fluidised bed at different fluidising velocities (sand size = 250 – 595 μm , static bed height = 0.5 D_c , primary air factor ≈ 1.0)

Sample	U_{mf} Number	Fly Ash Sample	Qualitative Comparison of the Extent of Sand Entrainment
FV1	8.1		Presence of high concentration of sand particles (quartz primary peak at intensity of 770 cps, secondary peak at 200 cps)
FV2	5.4		Presence of less sand particles compared to Case FV1 (quartz primary peak at 700 cps and secondary peak at 150 cps)
FV3	4.5		Presence of less sand particles compared to Case FV2 (quartz primary peak at 570 cps and secondary peak at 120 cps)
FV4	3.3		Presence of less sand particles compared to Case FV3 (quartz primary peak at intensity of 230 cps)
FV5	2.5		Presence of traces of sand particles (quartz primary peak at intensity of 74 counts per second, cps)

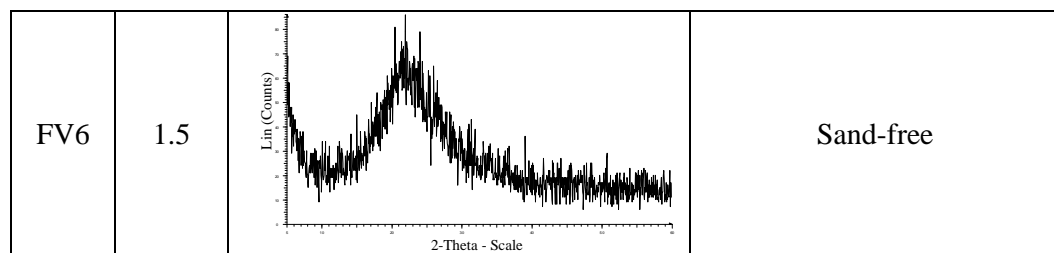

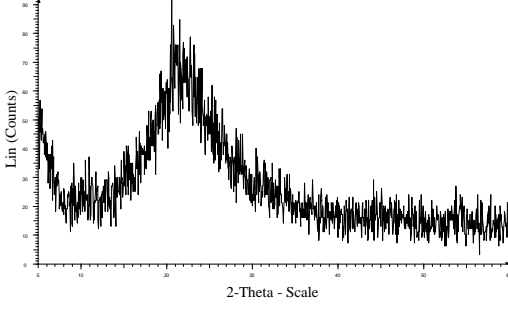

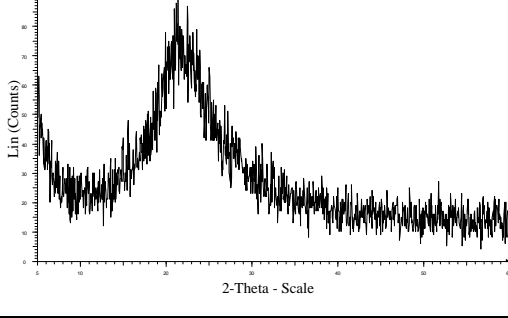

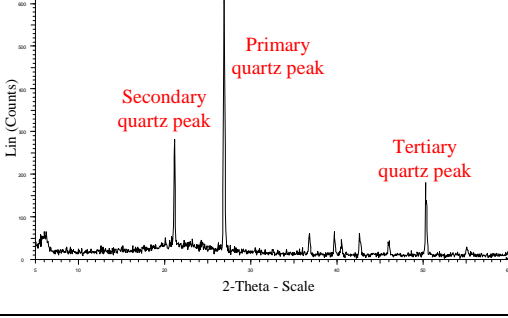


Table 4.1-17: Products and diffractograms of fly ash sample after sand de-contamination stage

Product	Fly Ash Sample	Diffractogram	Remarks
Top product (1 st purge)			Amorphous and sand-free
Top product (2 nd purge)			Amorphous and sand-free
Bottom product			Presence of mostly sand particles and white ash

Note:

Fly ash samples were from experimental study (Case FV3: fluidising velocity = $4.5 U_{mf}$)

The particle density of rice husk ash lies in the range of $1800 - 2100 \text{ kg/m}^3$ (Yalçın and Sevinç, 2001; Nehdi et al., 2003; Feng et al., 2004). The drastic increase of the particle density (rice husk particle density is 650 kg/m^3) is due to the presence of silica, which is usually in the excess of 90% (Houston, 1972; Kapur, 1985; Mishra et al., 1985; Chakraverty et al., 1988; Huang et al., 2001; Liou, 2004). Unburnt chars have lower particle density ($400 - 560 \text{ kg/m}^3$) (Zevenhoven and Järvinen, 2002; Watari et al., 2003; Bishnoi et al. 2004 as well as from experimental determination).

Due to the lower particle density of chars, they are easily being elutriated thus resulting in blacker shades of the top products from the decontamination stage. The bottom product was much whiter in shade as most of the high-density siliceous ash particles were being retained.

ii) Residual Carbon Content

The residual carbon contents in the fly ash samples were compared in Figure 4.1-4. It was observed that the lowest residual carbon content was obtained at the fluidising velocity of approximately $3 U_{mf}$.

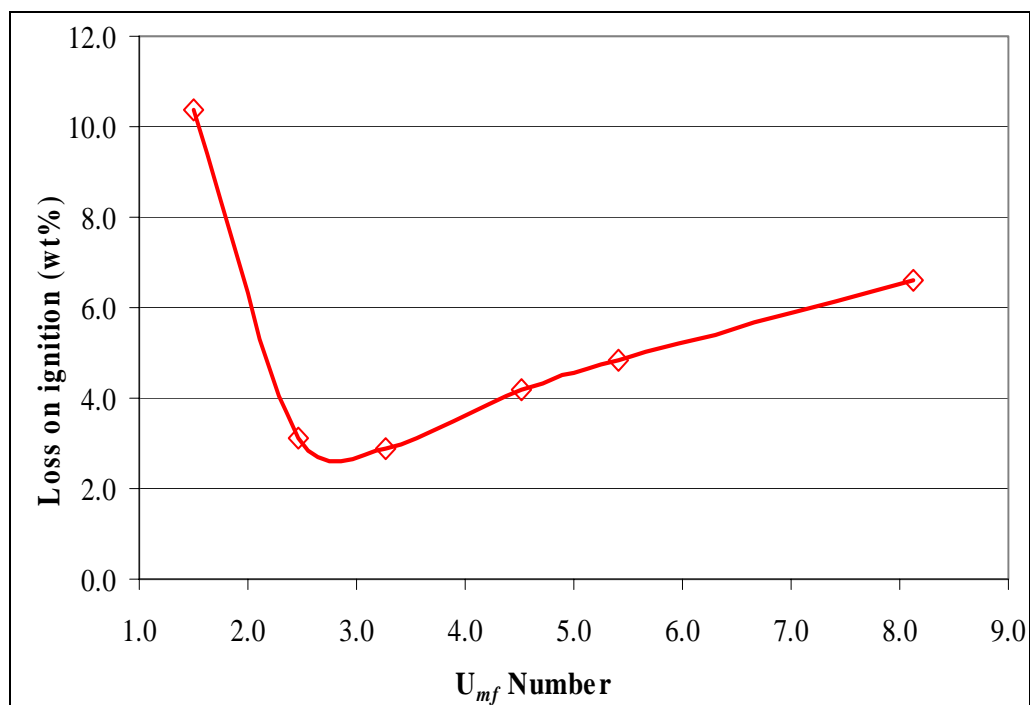


Figure 4.1-4: Residual carbon contents in fly ash samples from the combustion of rice husk in the 210-mm inner diameter fluidised bed at different fluidising velocities (sand size = 250 – 595 μm , static bed height = $0.5 D_c$, primary air factor ≈ 1.0)

The fly ash samples from the experiments were compared in Table 4.1-18. Fly ash from the combustion of rice husk at $8.1 U_{mf}$ (Case FV1) contained mostly char skeletons and partially burnt rice husk. It contained residual carbon content as high as 6.6 wt% (Figure 4.1-4). This was because the high fluidising velocity at the bed did not allow the rice husk to penetrate the bubbling bed. Upon feeding, the rice

husk tended to be blown to the freeboard region towards the cyclone. The burning of the rice husk occurred mainly at the freeboard region and thus, the residence time of the husk in the fluidised bed was not sufficient to enable complete combustion to take place. Basically, the burning process that took place at the freeboard region in Case FV1 was the pyrolysis of the rice husk particles due to the heat at this region (temperatures in the range of 600 – 650°C), which resulted in the formation of char particles that still retained their skeleton-like shapes. The low residence time in the combustor also resulted in the presence of partially-burnt rice husk in the collected fly ash. The turbulence in the sand bed due to the vigorous bubbling action was supposed to break down the skeleton-like structure in order to release the entrapped carbon in the char particles for further reaction.

As the fluidising velocity was reduced to $5.4 U_{mf}$ (Case FV2), the fly ash sample contained more white ash compared to Case FV1. The ash sample still contained partially-burnt rice husk due to insufficient residence time in the combustor. The residual carbon content was reduced by approximately 26% (to 4.9 wt%) compared to fly ash sample from Case FV1. However, the particle size of the ash was similar to that from Case FV1. This showed that most of the rice husk still did not penetrate the bubbling sand bed upon feeding. The ash sample contained less residual carbon content compared to that of Case FV1 as the fluidising velocity (0.49 m/s at corresponding bed temperature) was approximately 33% lower than the fluidising velocity in Case FV1 (at 0.73 m/s at corresponding bed temperature). Thus, the residence time of the fly ash in the freeboard region of the combustor at fluidising velocity of $5.4 U_{mf}$ was generally much higher than that of $8.1 U_{mf}$. Although the residence time was higher, the fact that the carbon in the fly ash was still entrapped in the skeleton-like structure and not readily available for conversion still resulted in fly ash with high residual carbon content. This further accentuated one of the inherent advantages of fluidised bed combustors, as the turbulence in the bubbling sand bed is crucial for breaking up the feed materials into smaller fragments in order to increase the rates of heat and mass transfer (oxygen as in fluidising air) to the feed materials.

Table 4.1-18: Ash samples from the combustion of rice husk in the 210-mm inner diameter fluidised bed combustor at different fluidising velocities (sand size = 250 – 595 μm , static bed height = 0.5 D_c , primary air factor ≈ 1.0)







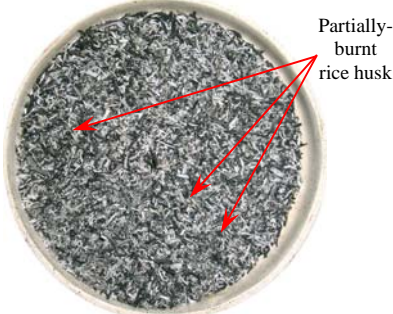
Sample	U_{mf} Number	Fly Ash Sample	Qualitative Comparison of Particle Size
FV1	8.1		Presence of char skeletons and partially-burnt rice husk, contained mostly black chars with some white ash (still retaining the shape of rice husk skeleton)
FV2	5.4		Similar to sample FV1, but with more white ash
FV3	4.5		No char skeleton, finer in size compared to sample FV2 but contained mostly black chars and some partially-burnt rice husk
FV4	3.3		Finer than sample FV2, absence of char skeletons as char particles had been broken into smaller fragments, some of the white ash retained the shape of rice husk

Table 4-18 (continued...): Ash samples from the combustion of rice husk in the 210-mm inner diameter fluidised bed combustor at different fluidising velocities (sand size = 250 – 595 μm , static bed height = 0.5 D_c , primary air factor ≈ 1.0)

Sample	U_{mf} Number	Fly Ash Sample	Qualitative Comparison of Particle Size
FV5	2.5		Retained the original shape of rice husk, presence of mostly white ash with small amount of intact char skeletons
FV6	1.5		Retained the original shape of rice husk, presence of large amount of intact char skeletons
			Bottom ash contained mostly char skeletons and partially burnt rice husk

Decreasing the fluidising velocity to 4.5 U_{mf} resulted in fly ash with finer size compared to Case FV2. This showed the rice husk did penetrate the bubbling sand bed to a certain degree, as the turbulence in the bed broke down the ash into smaller fragments. However, the residual carbon content was just 13.4% lower than that of Case FV2. The resulting fluidising velocity at the corresponding bed temperature was 0.41 m/s, which was just 16.6% lower than the fluidising velocity at Case FV2. Therefore, it was expected that the residence time of the fly ash in the freeboard region of the combustor remained more or less similar to that of Case FV2. Based on

the U_{mf} of rice husk ash at 0.06 m/s (Table 4.1-9), the fluidising velocity of 0.41 m/s was computed to be $6.8 U_{mf}$ for the ash, which explained the low residence time of the ash in the freeboard region. Lowering the fluidising velocity to less than $4.5 U_{mf}$, therefore, was expected to increase the residence time of the rice husk or ash in the sand bed and freeboard region of the combustor.

At a fluidising velocity of $3.3 U_{mf}$, the resulting fly ash was finer in size compared to that of Case FV3. This showed that the rice husk particles did indeed penetrate the bubbling sand bed, thus enabling them to be broken down into smaller fragments by the bubbling actions in the sand bed. In addition, the lower fluidising velocity at the freeboard region resulted in a higher residence time of the ash particles compared to that of Case FV3. Thus, the resulting fly ash attained a greyish shade and contained only 2.9 wt% residual carbon. Further, as the fluidising velocity was lowered to $2.5 U_{mf}$, most of the fly ash retained the original skeleton-like shape and also contained whole char skeletons. The residual carbon content was higher than Case FV4, at 3.1 wt%. Lowering the fluidising velocity to slightly higher than the minimum fluidising velocity (namely at $1.5 U_{mf}$) resulted in fly ash that contained mostly black char skeletons and trace amounts of white ash skeletons. The bottom ash was of slightly better quality than the fly ash, as it contained more white ash skeletons due to its relatively higher residence time in the bed compared to the fly ash. The residual carbon content in the fly ash was very high, at 10.4 wt% whereas the bottom ash contained only 3.5 wt% residual carbon.

c) Findings

High fluidising velocities in the range of $4.5 - 8 U_{mf}$ were undesirable for the combustion of rice husk as these high fluidising velocities prevented the low-density rice husk particles from penetrating the sand bed. Consequently, the degree of rice husk burning in the bed was minimal as most of the rice husk particles were just pyrolysed in the freeboard region upon feeding. The resulting ash were mostly char skeletons which still retained the rigid structure, thereby entrapping the carbon inside these skeletons and making them not readily available for conversion. Thus, the residual carbons in the resulting ashes were high, ranging from 4.2 – 6.6 wt%. Secondly, the high fluidising velocities also resulted in higher entrainment rate of sand particles into the cyclone, thereby contaminating the fly ash with quartz

crystals. Lowering the fluidising velocity to approximately $3 U_{mf}$ was deemed the optimum as most of the rice husk particles penetrated and got burnt in the sand bed. Mixing of rice husk with the sand particles were observed to be good with steady eruption of bubbles at the bed surface, which aided in engulfing the rice husk particles into the sand bed. The turbulence in the bubbling bed further aided in breaking the rigid char skeletons into smaller fragments, therefore releasing the trapped carbon for further oxidation. The resulting ash were finer in size and contained the lowest amount of residual carbon (at 2.9 wt%). The degree of sand contamination in the fly ash was also low, which was easily solved by subjecting the ground ash to a fluidised bed separator. Using a fluidising velocity of less than $3 U_{mf}$ resulted in inferior mixing behaviour as the formation of bubbles was less vigorous. The rice husk tended to form a thin layer above the sand bed (at $2.5 U_{mf}$), which disrupted the overall mixing and combustion behaviours. In the worst condition (at $1.5 U_{mf}$), the rice husk formed a thick stagnant layer and burning was restricted to this layer only. All the ash samples obtained in this study still retained their amorphous structure but were contaminated with sand particles in the form of quartz crystals.

4.5.2 Static Bed Height

The effect of static bed height on the combustion efficiency of rice husk was investigated by varying the static heights of the sand bed (250 – 595 μm sand) from 0.25 – 0.75 D_c . In all experiments, the fluidising velocities and primary air factors were held constant at approximately $3 U_{mf}$ and 1.0, respectively. Rice husk feeding was commenced once the bed had been pre-heated to the temperatures of 600 – 650°C.

a) Temperature Profile and Combustion Characteristics

For comparison purposes, the size of gas bubbles just before eruption at the bed surface and the bubble rise velocity were estimated for different static bed heights from Equation 2-1 and Equation 2-2. The results were shown in Figure 4.1-5 and

could aid in the explanation of why it was more difficult for the rice husk to penetrate the sand bed when the static bed height was increased.

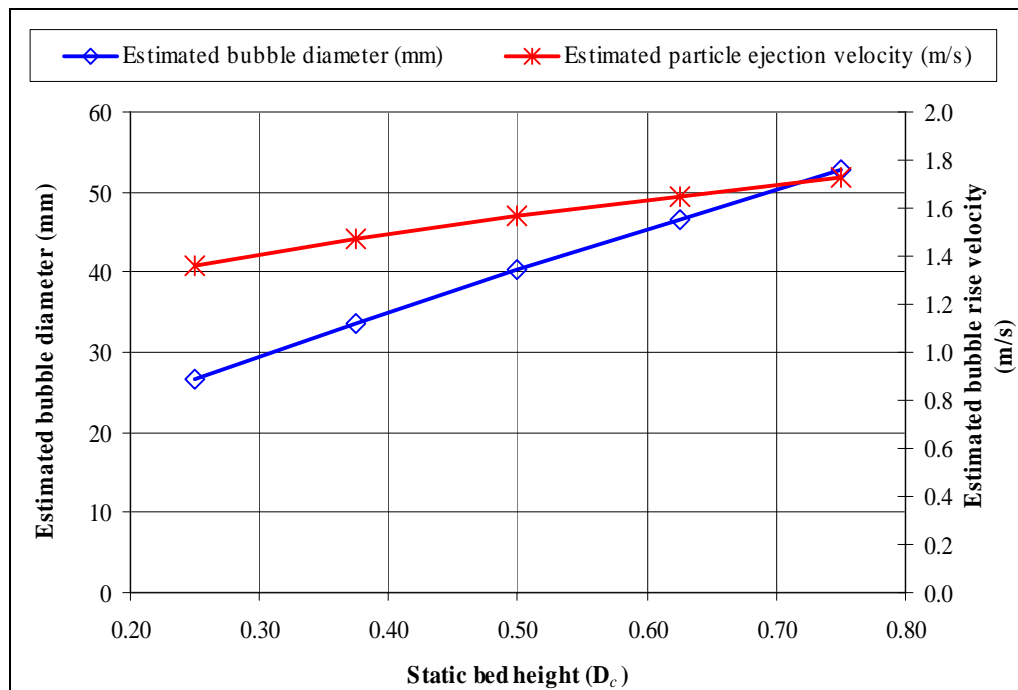


Figure 4.1-5: Estimated bubble size just before eruption at the bed surface and bubble rise velocity at different static bed heights in the 210-mm inner diameter fluidised bed combustor (sand size = 250 – 595 μm , fluidising velocity = 3 U_{mf})

At the static bed height of 0.25 D_c (equivalent to 50mm bed depth), it was observed via the viewing port that the rice husk did not penetrate into the bubbling sand bed at all. Instead, they formed a stagnant layer at the top of the sand bed and due to the interlocking nature of rice husk, the layer increased with time until burning was restricted only to this layer. As a result, the bubbling behaviour in the sand bed was significantly disrupted. In addition, the temperature at this layer reached very high (up to 830°C, as registered by thermocouple T2). Also, hot-spots observed as flaming red areas with the size of 15-mm circles occurred randomly all over the surface of the stagnant rice husk layer, which by then had been reduced to chars due to the devolatilisation process. These hot-spots were actually zones whereby the oxidation of char took place in the absence of mixing. The experiment had to be stopped as the stagnant rice husk char layer and temperature at this layer (T2) kept increasing. The resulting char and ash obtained by purging out the stagnant layer

were found to retain their rigid skeleton-like shape. The residual carbon content in the ash was also very high (6.8 wt%). The real-time temperature profiles (T1 and T6) during this experiment (Figure 4.1-6) was characterised by very unsteady rise and drop in temperatures. The pulsating trend in all the temperature measured (with T1 being the most prominent, with difference as high as 190°C) was due to the intermittent feeding of LPG into the bed in attempts to bring up the bed temperature and to prevent the quenching of flame at the bed once the temperature dropped too low. With the feeding of LPG into the bed, T1 increased steadily, as with T2 – T6. In the absence of LPG feed into the bed, T1 and the temperatures at the rest of the column dropped rapidly. This finding accentuated the importance of the role of the sand bed as a ‘thermal fly-wheel’. In the presence of good bubbling and mixing behaviours, the sand bed stores the heat evolved during the combustion of rice husk and subsequently transfers the heat to the freshly-fed rice husk to initiate the drying and devolatilisation processes. Both drying and devolatilisation are endothermic processes and since rice husk constitutes a significant amount of volatile matters (up to 64 wt% on wet basis as shown in Table 3-1), most of the heat evolved during the oxidation of the evolved volatiles and chars were absorbed for the devolatilisation process of the fresh rice husk feed. The process of drying requires much less heat compared to the devolatilisation as rice husk were relatively dry, with moisture content of approximately 10 wt% only. Hence, when the sand bed became stagnant due to the formation of a thick layer of rice husk at the top of the bed, the role of the sand bed as ‘thermal fly-wheel’ was relinquished. The heat required to devolatilise the fresh feed could not be provided by the stagnant rice husk layer which burning was only sustained by the flame from the intermittent LPG feed. The onset of devolatilisation in an oxidising environment was approximately 230°C (Mansaray and Ghaly, 1998b) while a temperature of at least 500°C is required for the complete oxidation of chars (Di Blasi et al., 1999). However, although the temperature at the stagnant rice husk char layer (ranging from 567 – 830°C and averaged at 710°C) was theoretically high enough for the complete oxidation of chars, the fact that these carbon were encapsulated in the char skeleton and not readily available for conversion resulted in a practically low rate of carbon oxidation. Subsequently, not much heat was evolved while in the meantime, heat was constantly being absorbed to devolatilise the fresh rice husk feed. It was speculated from the observation through the viewing glass that practically all of the fresh rice husk feed were

devolatilised as no rice husk particles were observed to be present amongst the chars at the stagnant layer. Hence, it could be concluded that the combustion process could not take place further as the heat required for the perpetual devolatilisation of the fresh rice husk feed could not be compensated considering the very low rate of char oxidation (which releases the potential energy content in the chars).

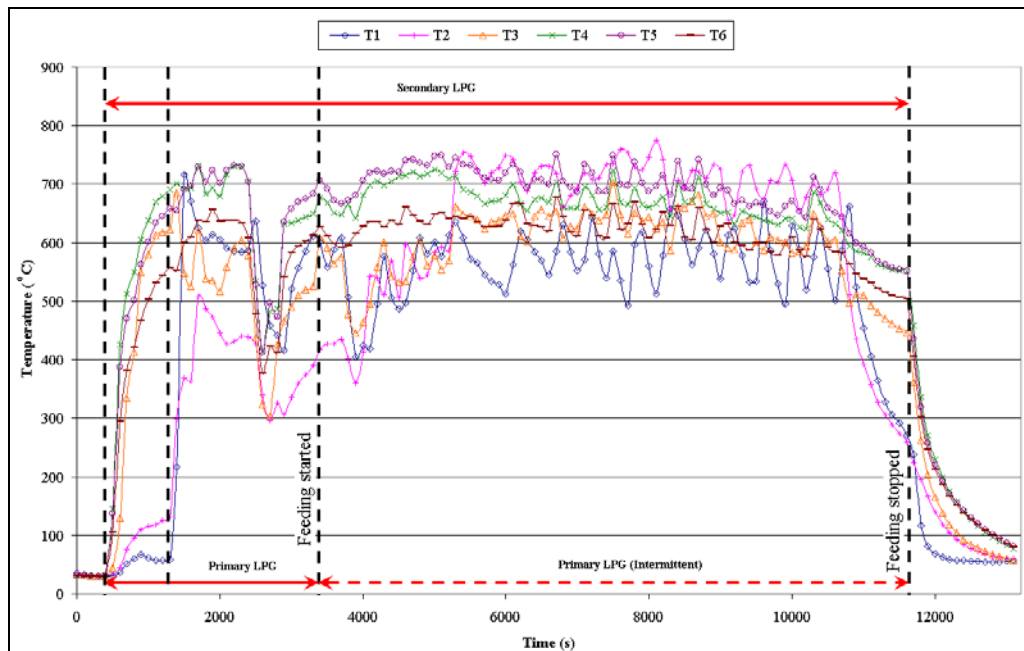


Figure 4.1-6: Real-time temperature profiles during the combustion of rice husk in the 210-mm inner diameter fluidised bed combustor with sand static bed height of $0.25 D_c$ (sand size = $250 - 595 \mu\text{m}$, fluidising velocity $\approx 3 U_{mf}$, primary air factor ≈ 1.0)

When the static bed height was increased to $0.375 D_c$ (equivalent to 80mm bed depth), most of the rice husk were observed to penetrate the bubbling bed. From Figure 4.1-5, the estimated bubble size just before eruption at the bed surface was 34 mm while the estimated particle ejection velocity was 1.5 m/s. The velocity of the pneumatic air which conveyed the rice husk feed into the combustor was 1.2 m/s (entering at ambient temperature of 30°C). This velocity was 20% lower than the estimated particle ejection velocity. Nevertheless, the rice husk was observed to penetrate the bubbling sand bed, due probably to the volume expansion of the pneumatic air to a certain degree based on the high temperature in the combustor, which subsequently increased its velocity. The stagnant rice husk or char layer did

not form and thus temperature at T2 was maintained around 600°C throughout the experiment. The mixing of rice husk with sand in the bed was quite good with constant streams of small bubbles erupting at the bed surface. The resulting ash was also much whiter and finer than those obtained from experiment using a static bed height $0.25 D_c$. The residual carbon in the ash from the former, at 3.4 wt%, was 50% lower than the latter. This could be attributed to the turbulence in the bubbling sand bed at the height of $0.375 D_c$, which broke the char skeletons thus enabling further oxidation of the released carbon to take place and resulting in finer ash particles. In addition, the concept of ‘thermal fly-wheel’ was realised at the static bed height of $0.375 D_c$ as a significant portion of rice husk was observed to be burnt inside the sand bed. The variation in bed temperature (T1), at 120°C in the case of $0.375 D_c$ was relatively lower than that of $0.25 D_c$ (at 190°C). Temperature at the bed surface as registered by T2 was due to the burning of a small portion of rice husk at the top of the bed as well as the combustion of the evolved volatiles gases. The pulsating trend in the temperature profile could still be observed, but not as prominent compared to the case $0.25 D_c$.

Increasing the static bed height to $0.5 D_c$ (equivalent to 105mm bed depth) further improved the combustion process. More rice husk was observed to penetrate deep into the bubbling bed and got burnt. The estimated bubble size just before eruption at the bed surface was 40 mm while the estimated particle ejection velocity was 1.6 m/s (Figure 4.1-5). The velocity of the pneumatic air in this case, at 1.4 m/s (at entering ambient temperature of 30°C), was only 13% lower than the particle ejection velocity. The bed temperature increased to approximately 670°C and remained very stable throughout the experiment with fluctuation of less than 25°C. Temperatures throughout the combustor column were maintained in the range of 550 – 700°C and remained essentially stable (Figure 4.1-7). The particle size of the resulting ash from this experiment was similar to that of $0.375 D_c$, but much whiter due to very low residual carbon content (1.9 wt%).

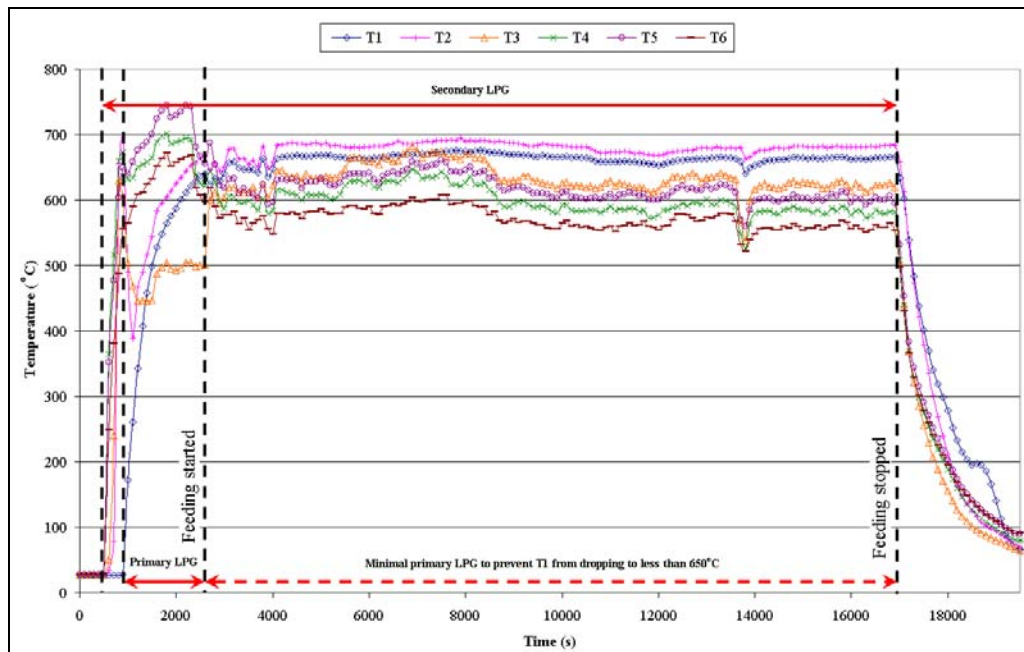


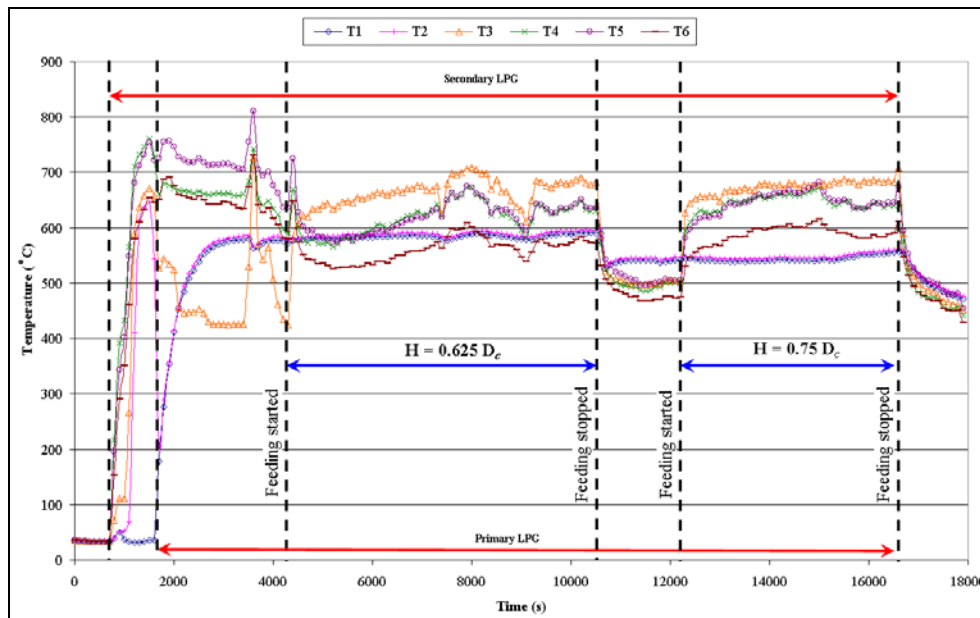
Figure 4.1-7: Real-time temperature profiles during the combustion of rice husk in the 210-mm inner diameter fluidised bed combustor with sand static bed height of $0.5 D_c$ (sand size = $250 - 595 \mu\text{m}$, fluidising velocity $\approx 3 U_{mf}$, primary air factor ≈ 1.0)

Combustion of rice husk in deeper beds ($0.625 D_c$ and $0.75 D_c$) yielded ashes of higher residual carbon contents compared to that of $0.5 D_c$. The residual carbon contents in the ashes from $0.625 D_c$ and $0.75 D_c$ were 2.4 wt% and 4.0 wt%, respectively. Deeper beds were hypothesised to give better ash quality as the residence time of the rice husk in the bed will be higher, provided that the rice husk actually penetrated the bed. However, these findings proved otherwise as it was observed that lesser amount of rice husk actually penetrated the sand bed due to eruption of bigger bubbles in deeper beds. From Figure 4.1-5, the estimated bubble sizes just before eruption at the bed surface was 47 mm and 53 mm for the static bed heights of $0.625 D_c$ and $0.75 D_c$, respectively. The estimated particle ejection velocities for both cases were approximately 1.7 m/s whereas the pneumatic air velocities (entering at ambient temperature of 30°C) were 1.0 m/s and 1.2 m/s for the static bed heights of $0.625 D_c$ and $0.75 D_c$, respectively. Hence, these velocities were 30 – 40% lower than the estimated particle ejection velocities, explaining why it was quite difficult for the rice husk particles to penetrate the bed. Further, the ashes from both experiments were also relatively coarser compared to that from the static bed

height of $0.5 D_c$, indicating a lesser degree of bed penetration. In the case of $0.625 D_c$, the ash consisted of a considerable amount of chars still in the skeleton form whereas for the case of $0.75 D_c$, the ash was mostly black with considerable amount of grey and white ash. Deeper beds enabled the bubbles that formed at the distributor plate to coalesce into bigger bubbles prior to eruption at the bed surface. The upward motion of the sand particles due to the eruption of these big bubbles caused the bed surface to be very turbulent, thus reducing the chances of the freshly-fed rice husk to penetrate the sand bed. During the experiments, vigorous motions of sand was observed at the bed surface with the static bed heights of $0.625 D_c$ and $0.75 D_c$ due the constant splashing of sand particles high into the freeboard region as the big bubbles erupted upon reaching the bed surface. Apart from decreasing the amount of rice husk penetration into the bed, beds deeper than $0.5 D_c$ were much harder to be started-up via pre-heating with LPG (Lim, 2002) as the eruption of bigger bubbles prevented the flame from being retained inside the sand bed as well as resulting in higher heat loss as the sand travelled from the top to the bottom of the deep beds. For example, sand bed at a static height of $0.5 D_c$ only took 36 minutes to be pre-heated to a temperature of 650°C whereas the same sand bed at a static height of $0.625 D_c$ only reached a temperature of 580°C for the same duration and remained essentially at the same temperature even after one hour of bed pre-heating period.

The lower degree of rice husk penetration into the sand bed for static bed heights of $0.625 D_c$ and $0.75 D_c$ resulted in lower bed temperatures (580°C and 540°C , respectively). The temperature profiles for both experiments, on the other hand, remained essentially stable throughout (Figure 4.1-8).

Comparisons on the average temperatures along different heights of the combustor during rice husk combustion at different static bed heights were depicted in Figure 4.1-9.



Note: H – Static bed height

Figure 4.1-8: Real-time temperature profiles during the combustion of rice husk in the 210-mm inner diameter fluidised bed combustor with sand static bed heights of $0.625 D_c$ and $0.75 D_c$ (sand size = $250 - 595 \mu\text{m}$, fluidising velocity $\approx 3 U_{mf}$, primary air factor ≈ 1.0)

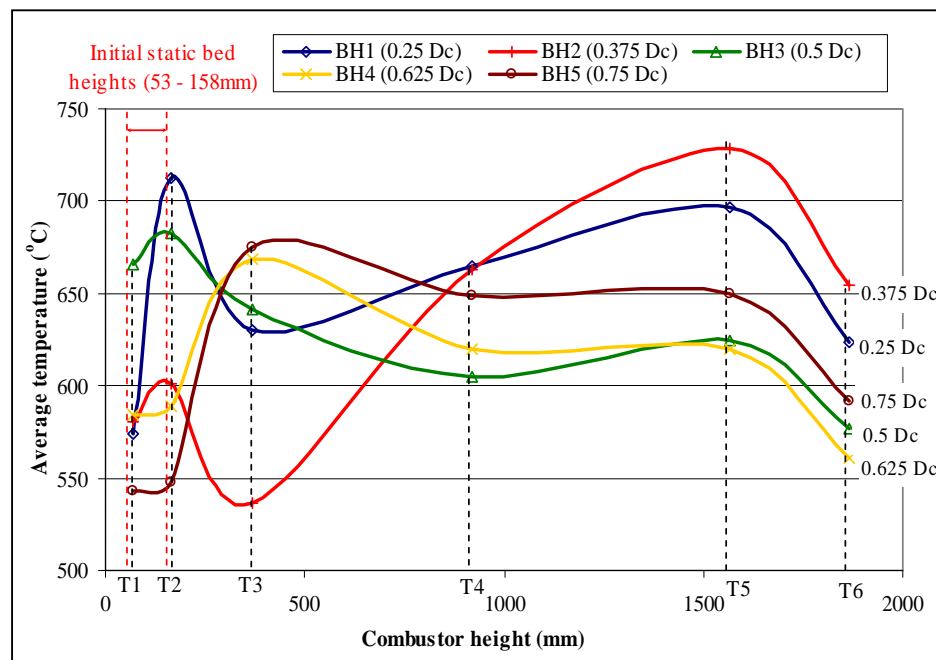


Figure 4.1-9: Temperature profiles during the combustion of rice husk in the 210-mm inner diameter fluidised bed combustor at different static bed heights (sand size = $250 - 595 \mu\text{m}$, fluidising velocity $\approx 3 U_{mf}$, primary air factor ≈ 1.0)

Based on Figure 4.1-9, it was observed that temperature plots for the static bed heights of $0.25 D_c$ and $0.375 D_c$ exhibited a significantly different trend compared to the rest of static bed heights investigated ($0.5 D_c$, $0.625 D_c$ and $0.75 D_c$). Both temperature plots were characterised by two prominent peaks at T2 and T5, with a minimum at T3. The significantly higher peak temperature at T2 for the case of $0.25 D_c$ but lower peak temperature at T5 indicated that combustion of the evolved volatile gases was concentrated near the bed region. This was consistent with the observation of stagnant layer of rice husk at the bed surface which was continuously pyrolysed, thus releasing a high amount of volatile gases into this region. For the case of $0.375 D_c$, the higher peak temperature at T5 indicated that most of the volatile gases were burnt off in this region. This was also consistent with the observation that some of the rice husk did penetrate the bed at this region and thus most of the rice husk were pyrolysed in the bed region. The evolved volatile gases travelled above the freeboard region with the intense burning occurring adjacent to T5. The drop in temperature after T2, which reached a minimum at T3 for both temperature plots of $0.25 D_c$ and $0.375 D_c$ were due to the effect of air cooling by the pneumatic air entering at ambient temperature at a distance equivalent to the location of thermocouple T3.

The average bed temperature (T1) for the static bed height of $0.5 D_c$ was the highest, followed by $0.625 D_c$ and $0.75 D_c$. This decrease in temperature with the increase in static bed height indicated that the degree of rice husk combustion in the bed region decreased as the bed got deeper. This was because deeper beds tended to produce bigger bubbles and the subsequent eruption of these big bubbles at the bed surface formed a very turbulent region which made it difficult for the rice husk to penetrate the bed. The pneumatic air cooling effect was still present at the static bed height of $0.5 D_c$, but was not detected in the temperature plots for deeper beds ($0.625 D_c$ and $0.75 D_c$). This was because most of the rice husk did not penetrate the bed upon feeding but were 'floating' near the bed surface in such cases. Therefore, the pyrolysis and the corresponding burning of the evolved volatiles gases at this region resulted in the rise in temperature at T3. The pneumatic air entering near T3 probably supplied the oxygen-rich air required for the combustion of these volatile gases, whereby the substantial amount of heat thus released overrode the air cooling effect. The higher freeboard temperatures for the static bed height $0.75 D_c$ compared

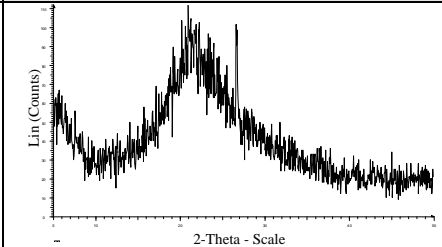
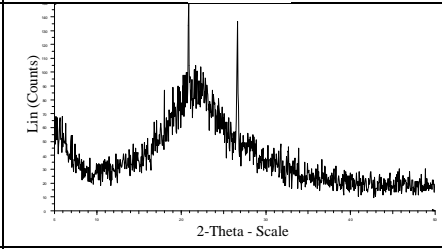
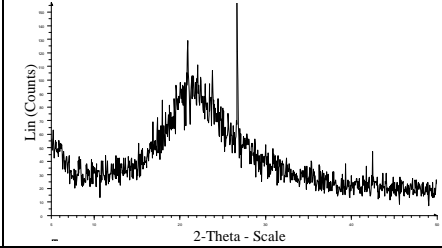
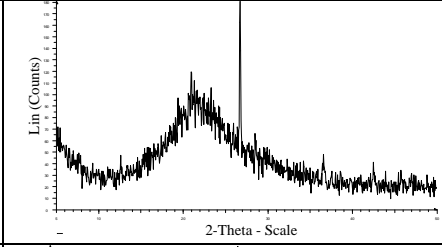
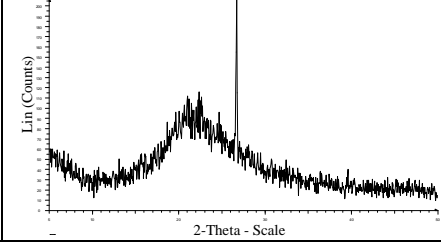
to that of $0.625 D_c$ indicated that most of the combustion process of rice husk took place in the freeboard region in the form of suspension burning, consistent with the observation that most rice husk particles did not penetrate the bed region upon feeding but were entrained into the freeboard region towards the cyclone.

b) Ash Quality

i) Silica Structure

The diffractograms of fly ash samples from the experiments were compared in Table 4.1-19. Due to the absence of cristobalite and tridymite crystals, it could be concluded that all ash samples retained their amorphous structures. However, the presence of quartz crystals (at peak positions of 20.85° and 26.66°) showed that they had been contaminated with carry-over sand particles from the bubbling bed. The degree of contamination increased as the bed height was increased, as could be observed from the higher peaks which indicated higher concentrations of sand in the ash samples. The size of bubbles increased with bed height, and the eruption of these bubbles at the bed surface, together with the higher bed height, tended to throw more sand particles into the freeboard region. The freeboard height of the 210-mm inner diameter fluidised bed was insufficient to disengage these suspended sand particles and return them to the bed region. As a result, they were elutriated together with the fly ash into the cyclone.

Table 4.1-19: Diffractograms of fly ash samples from the combustion of rice husk in the 210-mm inner diameter fluidised bed at different static bed heights (sand size = 250 – 595 μm , fluidising velocity $\approx 3 U_{mf}$, primary air factor ≈ 1.0)

Case Study	Static Bed Height (D_c)	Average Bed Temperature ($^{\circ}\text{C}$)	Diffractogram
BH1	0.25	574	
BH2	0.375	580	
BH3	0.5	666	
BH4	0.625	584	
BH5	0.75	543	

ii) Residual Carbon Content

The average bed temperature and residual carbon content in the rice husk ash (fly ash) were plotted against the static bed height, as shown in Figure 4.1-10. It was

observed that the static bed height of $0.5 D_c$ gave the highest bed temperature and lowest residual carbon content in the fly ash (1.9 wt%).

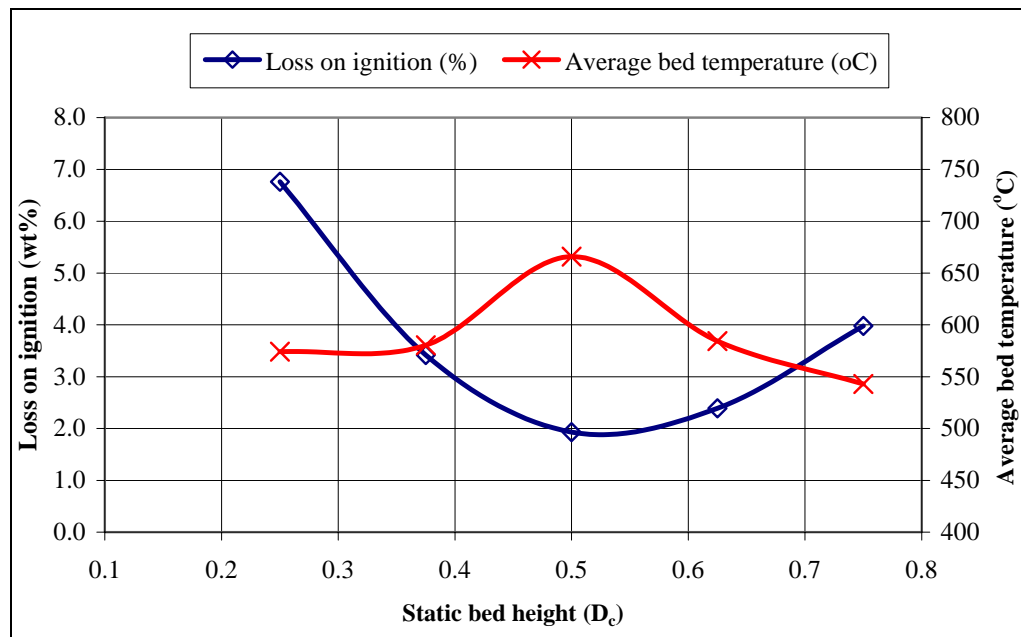


Figure 4.1-10: Effect of static bed height on the bed temperature and residual carbon content in fly ash during combustion of rice husk in the 210-mm inner diameter fluidised bed combustor (sand size = 250 – 595 μm , fluidising velocity $\approx 3 U_{mf}$, primary air factor ≈ 1.0)

The fly ash samples obtained from all five experiments were shown in Table 4.1-20. In the table, the particle sizes of each sample were also compared qualitatively with respect to each other as observed through visual inspection.






The findings on the ash quality and rice husk burning behaviour showed that the static bed height of $0.5 D_c$ was the optimum static bed height for rice husk combustion. These results accentuated the findings by other researchers, which investigated the combustion of rice husk in fluidised bed with static bed heights seldom higher than $1 D_c$, such as at $0.15 - 0.75 D_c$ (Peel and Santos, 1980) and $0.67 D_c$ (Bhattacharya et al., 1984). However, it should be noted that further studies on larger-scale fluidised beds need to be carried out to determine whether the results from the current research is still applicable. This is because it is not confirmed whether the static bed height of $0.5 D_c$ could still provide good mixing and

combustion behaviours for rice husk in such larger fluidised beds, or its equivalent at approximately 105 mm is the overriding factor. With larger fluidised beds, the bed height at $0.5 D_c$ will be much higher, and the bubble formation characteristics might differ. In such cases, there is a possibility that the optimum static bed height at approximately 105 mm from the current study could be sufficient although if expressed in terms of D_c of the larger fluidised beds, it would be less than $0.5 D_c$.

c) **Findings**

Based on the experimental results, it could be concluded that the static bed height of $0.5 D_c$ was the optimum static bed height for the combustion of rice husk in the 210-mm inner diameter fluidised bed combustor. This was because the static bed height of $0.5 D_c$ gave the best ash quality with the lowest residual carbon content (at 1.9 wt%) and the highest average bed temperature (670°C). The latter indicated that most of the rice husk feed was being burnt in the bed and as such, the vigorous motion of the bubbles in the bed was able to break down the char skeletons, thereby releasing the entrapped carbon for further oxidation process and resulting in lower residual carbon content. This phenomenon could be attributed to the bubble characteristics in the bed at this height, which formed medium-sized bubbles compared to the other range of static bed heights investigated. Deeper beds are preferable as theoretically, they offer higher residence time of the husk feed in the bed. However, in actuality, it was very difficult for the rice husk feed to penetrate the sand bed with static height greater than $0.5 D_c$ due to the formation of very big bubbles and the vigorous splashing of sand particles to the freeboard region upon eruption at the bed surface. Also, the particle ejection velocity at the bed surface was relatively lower than those of deeper beds. Beds deeper than $0.5 D_c$ is also much more difficult to be started-up due to the higher amount of heat loss due to bigger bubble eruption as well as the greater length at which the sand particles need to travel from the top to the bottom of the bed. Nevertheless, the results from the current study need to be validated in larger-scale fluidised beds to determine whether the bed height of $0.5 D_c$ is still applicable, or its equivalent at approximately 105 mm is the overriding factor.

Table 4.1-20: Fly ash samples from the combustion of rice husk in the 210-mm inner diameter fluidised bed at different static bed heights (sand size = 250 – 595 μm , fluidising velocity $\approx 3 U_{mf}$, primary air factor ≈ 1.0)

Case Study	Static Bed Height (D_c)	Fly Ash Sample	Qualitative Comparison of Particle Size
BH1	0.25		Retained the original shape of rice husk, presence of intact char skeletons
BH2	0.375		Finer than sample BH1, presence of mostly char fragments as char particles had been broken into smaller fragments, contained very small amount of char skeletons
BH3	0.5		Finer than sample BH2, absence of char skeletons as char particles been broken into smaller fragments
BH4	0.625		Coarser than sample BH3, particle size comparable to sample BH1, presence of intact char skeletons amongst white ash still in the shape of original rice husk
BH5	0.75		Coarser than sample BH4, presence of significant amount of char skeletons

4.6 Effect of Temperature on the Combustion Efficiency of Rice Husk in Fluidised Bed

4.6.1 Bed Temperature

Experiments were conducted in the 80-mm inner diameter fluidised bed by varying the bed temperatures from 650 – 800°C. For each experiment, the bed temperature was maintained at the desired value ($\pm 25^\circ\text{C}$) via manipulation of the LPG combustion rate. For each bed temperature investigated, experiments were conducted using the sand size of 250 – 595 μm . The static bed height was fixed at $0.5 D_c$ or equivalent to 40mm, the fluidising velocity at $4 U_{mf}$ (at corresponding bed temperature) and rice husk was fed at stoichiometric proportion (primary air factor of 1.0). The diffractograms of the resulting ash (fly ash and bottom ash) samples were compared in Table 4.1-21.

The residence time of fly ash in this fluidised bed was observed to be in the range of 30 – 40 seconds only, whereas it was expected to be longer for the bottom ash. However, the bottom ash particles tended to be elutriated together with the fly ash when they were broken into smaller fragments in the bubbling bed. Therefore, they were continuously being replenished with the ash liberated from the combustion of the fresh incoming feed and as such, their residence time in the bed region was expected to be not much higher than that of the fly ash particles.

a) Silica Structure

From Table 4.1-21, all ash samples were still amorphous due to the absence of cristobalite peak at the position of 21.93° (primary peak). This confirmed the hypothesis that the short residence time of ash in the fluidised bed even at high temperatures (up to 800°C) was insufficient for the formation of silica crystals.

Table 4.1-21: Diffractograms of fly and bottom ashes from the combustion of rice husk in the 80-mm inner diameter fluidised bed at different bed temperatures (sand size = 250 – 595 μm , static bed height = 0.5 D_c , fluidising velocity $\approx 4 U_{mf}$, primary air factor ≈ 1.0)

Sample Reference	Bed Temp. ($\pm 25^\circ\text{C}$)	Diffractograms of Fly and Bottom Ashes
1	650	
2	700	
3	750	
4	800	

Note:

For each bed temperature, diffractogram at the top was for fly ash while at the bottom was for bottom ash

However, quartz peaks were present at at positions of 26.66° (primary peak) and 20.85° (secondary peak) in these diffractograms, indicating the contamination of sand in the ash products. The concentration of sand in the fly ash samples were higher compared to the bottom ash samples, as indicated by the height of the quartz peaks. This was due to the short freeboard height of the 80-mm inner diameter fluidised bed combustor (total column height of 1000mm only), which resulted in the elutriation of sand particles together with fly ash into the cyclone. This could be prevented by using a fluidised bed with higher freeboard height to disengage any sand particles thrown into the freeboard region.

b) Residual Carbon Content

The residual carbon contents in the fly and bottom ashes from the experiments were compared in Figure 4.1-11. It was found that increasing the bed temperature led to a higher carbon burnout in both the fly and bottom ashes. For both fly and bottom ashes, the decrease in residual carbon contents was observed to be steep from the bed temperatures of 650°C to 700°C , after which the decrease tended to reach a plateau. This might be attributed to the transition from kinetically-controlled reaction to diffusion-controlled reaction for char oxidation at this temperature band. Reaction that is kinetically-controlled is largely dependent on temperature, whereby lower temperature led to the lower rate of char oxidation in the ash. This finding confirmed the speculation that combustion of rice husk chars is diffusion-limited beyond temperatures of 650°C . Beyond the temperatures of 700°C , the oxidation of char is diffusion-limited and the rate of reaction depends on the turbulence and residence time amongst the reactants. These two parameters in turn depend on the degree of mixing in the bed region, which remained more or less similar in all experiments as the fluidising velocity and static bed height were held constant. Thus, the curve for the residual carbon contents tended to reach a plateau beyond the temperatures of 700°C . Nevertheless, higher temperatures tended to decrease the time required for complete combustion of rice husk (Sen and Ghosh, 1992). Therefore, the use of bed temperatures higher than 700°C is favourable during the operation of the fluidised bed.

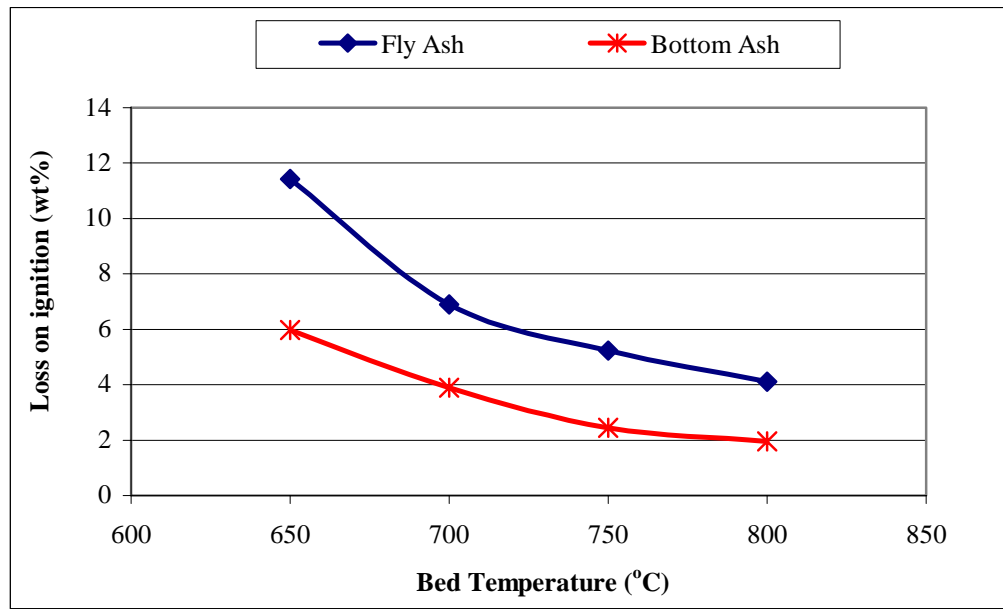


Figure 4.1-11: Residual carbon contents in ash samples from the combustion of rice husk in the 80-mm inner diameter fluidised bed at different bed temperatures (sand size = 250 – 595 μm , fluidising velocity $\approx 4 U_{mf}$, primary air factor ≈ 1.0)

4.6.2 Freeboard Temperature

The effect of freeboard temperature on the combustion efficiency of rice husk was investigated by varying the temperatures in the freeboard region (T4 – T6) of the fluidised bed with the use of auxiliary burners, with Case FT1 (400 – 600°C), Case FT2 (550 – 600°C), Case FT3 (600 – 650°C) and Case FT4 (600 – 700°C). The locations of the auxiliary burners were shown in Figure 4.1-12. In all experiments, the static bed height was maintained at $0.5 D_c$ (250 – 595 μm sand), fluidising velocities at $4 - 5 U_{mf}$ and primary air factors at approximately 1.0. The oxygen level in the freeboard region (measured at the cyclone) was ensured to be above 6 vol%, preferably in the range of 10 – 12 vol%. The amount of excess air required is based on the guideline value of achieving a final flue gas composition of higher than 6% oxygen level (Environment Agency, 1996). If the oxygen level dropped below these

range, the amount of supplementary airflow to the freeboard region was increased accordingly.

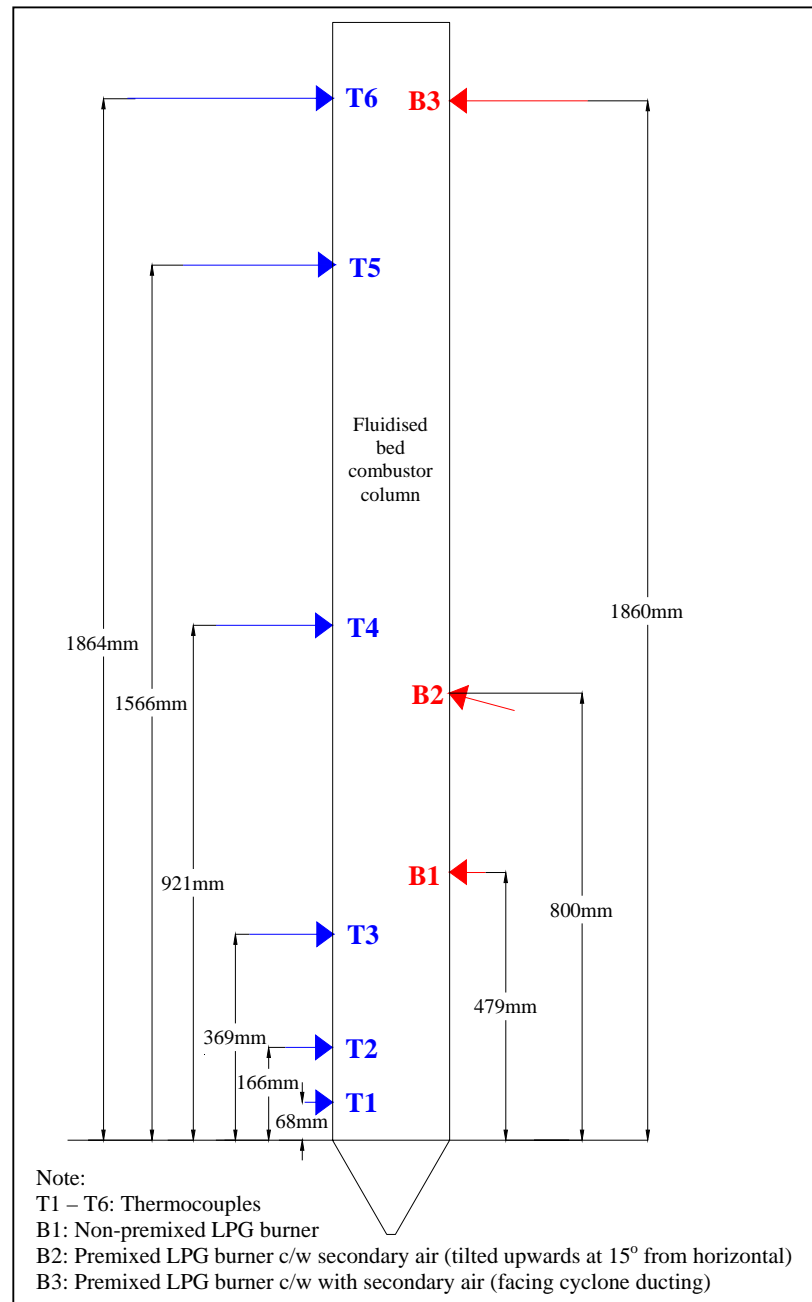
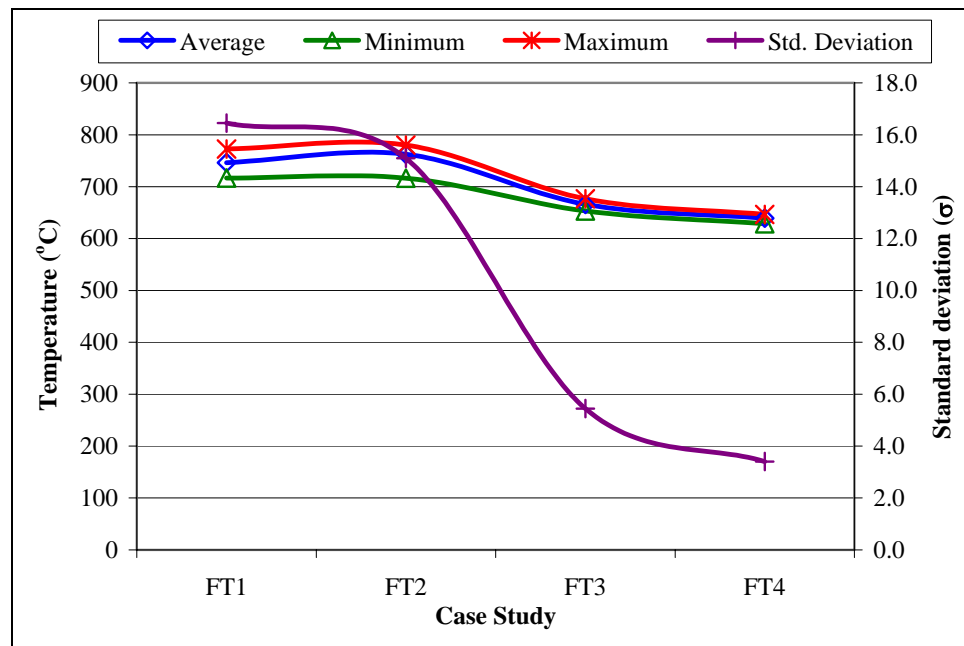


Figure 4.1-12: Exact locations of thermocouples and secondary burners at the 210-mm inner diameter fluidised bed combustor column

a) Temperature Profile and Combustion Characteristics

The real-time temperature profiles during the combustion of rice husk in case studies FT1 – FT4 were included in Appendix E. Meanwhile, results on the statistical

analysis on the bed temperatures in all four experiments were depicted in Figure 4.1-13.



Note:

Variations in freeboard temperatures (T4 – T6) in different case studies:-

FT1: 400 – 600°C, FT2: 550 – 600°C; FT3: 600 – 650°C; FT4: 600 – 700°C

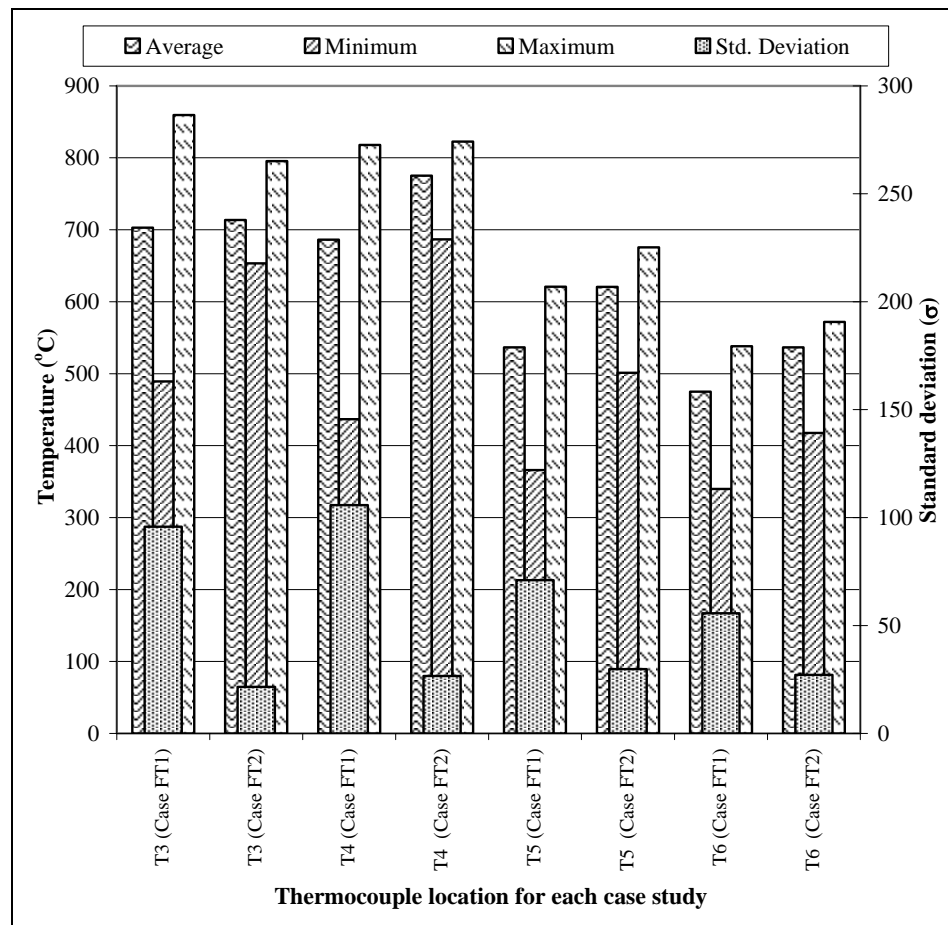
Figure 4.1-13: Statistical analysis on the bed temperatures (T1) during combustion of rice husk in the 210-mm inner diameter fluidised bed at different freeboard temperatures (sand size = 250 – 595 μm, static bed height = 0.5 D_c, fluidising velocity = 4 – 5 U_{mf}, primary air factor ≈ 1.0, oxygen level in cyclone ≥ 6 vol%)

From Figure 4.1-13, it was observed that the fluctuations (as indicated by the value of standard deviation) in bed temperature (T1) was decreased with the presence of more secondary burners. This was due to the heat generated by the secondary burners, which raised the temperature near the feeding region to that sufficient to ignite the rice husk particles. Thermogravimetric analysis of rice husk by Mansaray and Ghaly (1998b) showed that the evolution of volatiles and their subsequent oxidation was observed at approximately 230 – 330°C, whereas the oxidation of char took place in the temperature range of 300 – 500°C. As such, when the freeboard temperatures were in the excess of 500°C (as in Case Studies FT2 to FT4), most of the volatiles in the entering rice husk particles had been evolved, exposing the

remaining char particles which then proceeded to oxidise as they were heading towards the bed region. Hence, the bed temperatures could be maintained steadily. On the contrary, rice husk particles that were not ignited upon feeding (such as in Case Study FT1) will tend to absorb heat from the bed region, thus causing the bed temperature to drop. The bed temperature will increase again when the volatiles had been evolved and the rice husk proceeded to the char oxidation stage.

The presence of more heat generated by the secondary burner also explained why the combustion process in Case FT2 was autogenous as opposed to Case FT1, since the operating parameters for both case studies were similar (except for the presence of a secondary burner (B1) in the former). In the former case, as soon as the rice husk feed entered the combustor, the heat generated by the secondary burner aided in igniting the rice husk particles, including the evolved volatile gases. Thereafter, these burning rice husk particles proceeded towards the bubbling bed region, thus increasing the bed temperature to as much as 40°C compared to the case without the presence of the secondary burner B1. The phenomenon of ignition of rice husk feed and their evolved volatiles by the heat generated by the secondary burner could be further proven by the temperature recorded by thermocouple T3, located 369 mm above the distributor plate. As the feed entry port was located at 365 mm above the distributor plate, the temperature profile of T3 acted as an indicator as to whether the rice husk particles were ignited upon entry into the fluidised bed combustor. In Case FT1, the real time-temperature profile of T3 (Appendix E) displayed great fluctuations (as much as 370°C), indicating the occasional catching of flame by the rice husk upon their entry into the combustor. On the other hand, the temperature profile of T3 for Case FT2 showed minimal fluctuations (less than 30°C) throughout the experiment, which indicated that the rice husk feed was steadily ignited and burned upon entry into the combustor, hence raising the temperature at this region to a steady average of 770°C. The statistical analysis for temperatures at T3 – T6 for both case studies FT1 and FT2 was shown in Figure 4.1-14. In general, it could be concluded that the freeboard temperatures (T3 – T6) in Case FT2 was higher compared to Case FT1 and showed lesser fluctuations (as indicated by the lower values of standard deviation) due primarily to the presence of the secondary burner in Case FT2. As such, the presence of such burner actually improved the combustion

characteristics by maintaining a stable and higher temperature profile in the freeboard region when all other parameters were held constant.



Note:

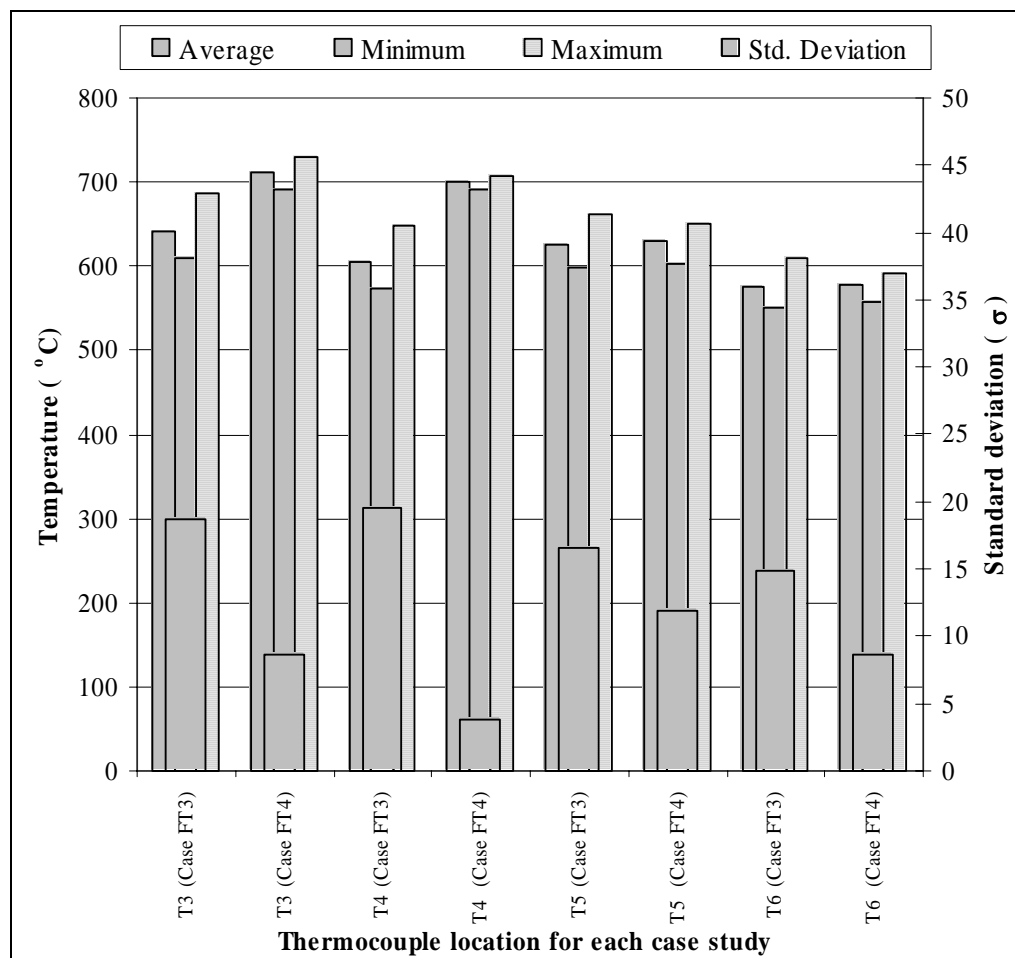
Variations in freeboard temperatures (T4 – T6) in different case studies:-

FT1: 400 – 600°C, FT2: 550 – 600°C

Figure 4.1-14: Statistical analysis on the freeboard temperatures (T3 – T6) during combustion of rice husk in the 210-mm inner diameter fluidised bed – Lower freeboard temperature range (400 – 600°C) (sand size = 250 – 595 μm, static bed height = 0.5 D_c, fluidising velocity = 4 – 5 U_{mf}, primary air factor ≈ 1.0, oxygen level in cyclone ≥ 6 vol%)

Likewise, the statistical analysis for temperatures at T3 – T6 for both case studies FT3 and FT4 was shown in Figure 4.1-15. In general, the analysis reflected the similar findings for both case studies FT1 and FT2, whereby in this case, the

presence of more secondary burners resulted in higher temperature profile with lesser fluctuations.



Note:

Variations in freeboard temperatures (T4 – T6) in different case studies:-

FT3: 600 – 650°C; FT4: 600 – 700°C

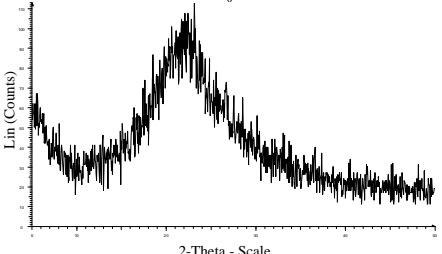
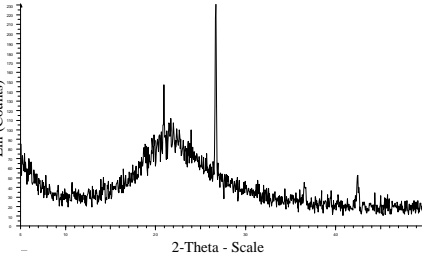
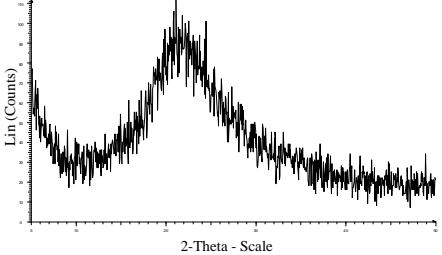
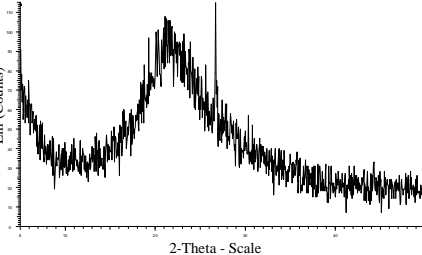
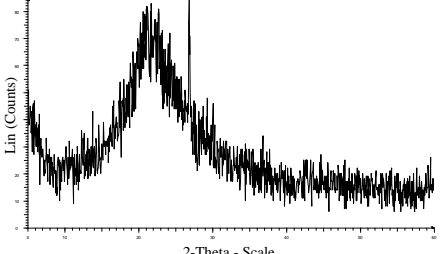
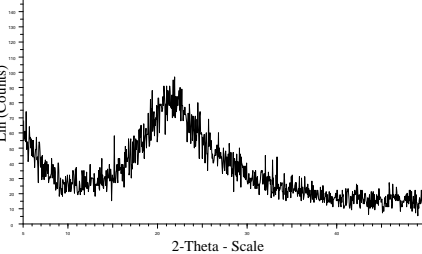
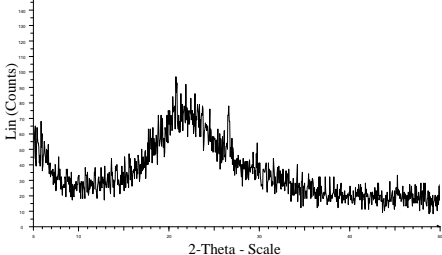
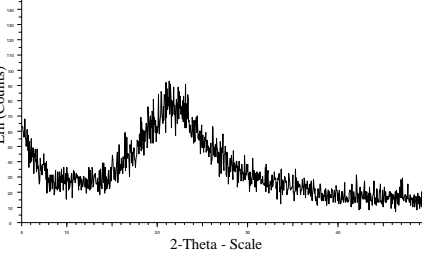
Figure 4.1-15: Statistical analysis on the freeboard temperatures (T3 – T6) during combustion of rice husk in the 210-mm inner diameter fluidised bed – Higher freeboard temperature range (600 – 700°C) (sand size = 250 – 595 μm, static bed height = 0.5 D_c, fluidising velocity = 4 - 5 U_{mf}, primary air factor ≈ 1.0, oxygen level in cyclone ≥ 6 vol%)

Hence, it could be concluded that the presence of secondary burner improved the combustion process by generating sufficient heat to ignite the feed materials, thereby resulting in a steady temperature profile with lesser fluctuations. These effects were enhanced with the presence of more secondary burners.

b) Ash Quality***i) Silica Structure***

Table 4.1-22 showed that all the ash samples retained their amorphous structures despite being exposed to combustion temperatures in the excess of 700°C. This could be attributed to the short exposure time that did not allow for formation of crystals in the ash, as the crystal formation process was reported to be a 'gradual process' (Gorthy and Pudukottah, 1999). The crystal peaks in some of the diffractograms (at $2\theta = 20.85^\circ$ and 26.66°) were due to slight contamination from the bed media (in the form of quartz crystals), whereby trace amounts of silica sand were elutriated into the cyclone together with the ash particles.

Table 4.1-22: Diffractograms of ash samples from the combustion of rice husk in the 210-mm inner diameter fluidised bed combustor at different freeboard temperatures (sand size = 250 – 595 μm , static bed height = 0.5 D_c , fluidising velocity = 4 – 5 U_{mf} , primary air factor ≈ 1.0 , oxygen level in cyclone ≥ 6 vol%)

Case Study	Freeboard Temperature (T4 – T6) ($^{\circ}\text{C}$)	Fly Ash	Bottom Ash
FT1	400 – 600		
FT2	550 – 600		
FT3	600 – 650		
FT4	600 – 700		

ii) Residual Carbon Content

The residual carbon contents in all ash samples from case studies FT1 – FT4 were shown in Figure 4.1-16. For Cases FT1 and FT2, it was observed that the residual carbon contents in the fly ash samples were similar (at approximately 7.0 wt%), as well as for the bottom ash samples (2.0 – 3.4 wt%). This could be attributed to the following reasons:-

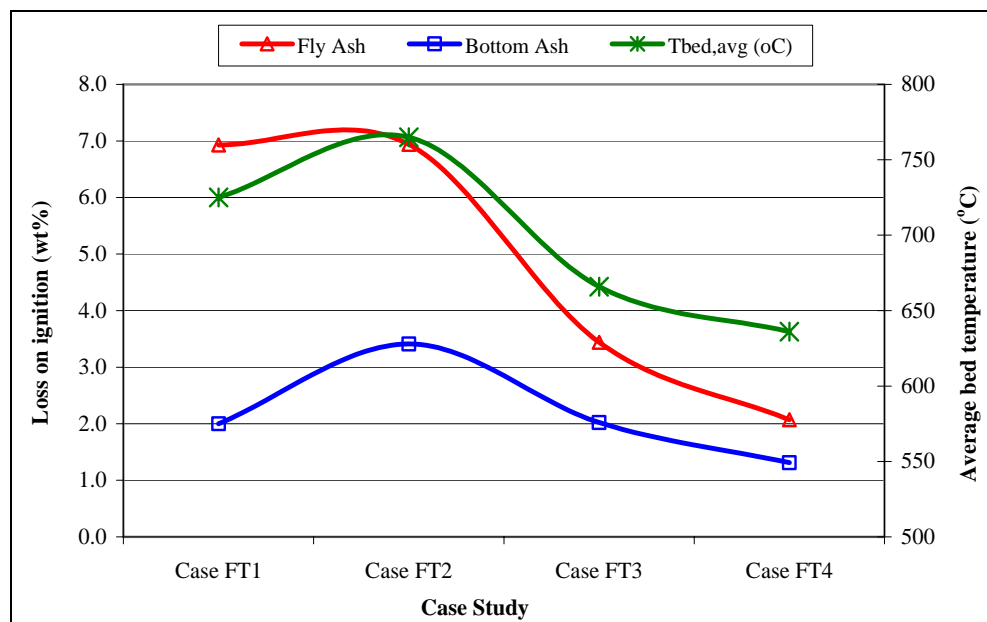
- 1) The bed temperatures (Figure 4.1-13) for both Cases FT1 and FT2 were quite similar, in terms of the average, minimum and maximum values and their standard deviations;
- 2) The freeboard temperatures for both Cases FT1 and FT2 were less than 600°C beyond mid-height of the combustor (as indicated by T5 and T6 in Figure 4.1-14). According to Sen and Ghosh (1992), temperatures beyond 650°C was required to achieve effective oxidation (more than 95% conversion) of fixed carbon in the rice husk at short exposure times (less than 2 minutes);
- 3) The freeboard temperatures at the lower mid-height of the combustor (as indicated by T3 and T4 in Figure 4.1-14) showed great fluctuations for both Cases FT1 and FT2. The standard deviation values for T3 and T4 for both cases ranged from 25 – 100.

According to factor (2) explained above, the rate of carbon oxidation in the freeboard region for both Cases FT1 and FT2 could be rendered negligible. As such, the combustion rate at the bed region was the key factor in determining the final ash quality. As had been described in item (1) above, the combustion rate of rice husk in both Cases FT1 and FT2 were also expected to be similar and thus, the similar ash quality (in terms of residual carbon content) was duly expected.

Meanwhile, for Cases FT3 and FT4, it was observed that the residual carbon contents in the fly ash samples were reduced by 40% from 3.4 wt% to 2.0 wt%. As for the bottom ash, the residual carbon content showed a reduction of 35% from 2.0 wt% to 1.3 wt%. These could be attributed to the following reasons:-

- 1) The freeboard temperatures for both Cases FT3 and FT4 were in the excess of 600°C up to three-quarter height of the combustor (as indicated by T3 – T5 in Figure 4.1-15), indicating there was effective carbon oxidation in the fly ash particles during entrainment into the cyclone;
- 2) The freeboard temperatures for Case FT4 showed much less fluctuations (as indicated by the standard deviation values for T3 – T5 which ranged from 4 – 12 in Figure 4.1-15). In comparison, the standard deviation values for the same parameters ranged from 15 – 20 for Case FT3.

The uniformity in freeboard temperatures contributed to the higher rate of carbon oxidation in the fly ash in Case FT4, thus resulting in better fly ash quality compared to Case FT3.











Note:

Variations in freeboard temperatures (T4 – T6) in different case studies:-
 FT1: 400 – 600°C, FT2: 550 – 600°C; FT3: 600 – 650°C; FT4: 600 – 700°C

Figure 4.1-16: Comparisons of residual carbon contents in ash samples from the combustion of rice husk in the 210-mm inner diameter fluidised bed at different freeboard temperatures (sand size = 250 – 595 μm, static bed height = 0.5 D_c, fluidising velocity = 4 – 5 U_{mf}, primary air factor ≈ 1.0, oxygen level in cyclone ≥ 6 vol%)

All the ash samples from the current experimental study were shown and compared in Table 4.1-23. In general, the quality of ash samples (in terms of residual carbon content, which could be visually compared based on their shades) improved with the inclusion of more secondary burners and thus higher freeboard temperatures. Fly ash sample from Case FT4 (presence of two secondary burners) attained a greyish shade compared to the darker shades of the other three fly ash samples. The comparisons in terms of the shades of these ash samples were included in Table 4.1-23 (in column for remarks).

Table 4.1-23: Ash samples from the combustion of rice husk in the 210-mm inner diameter fluidised bed at different freeboard temperatures (sand size = 250 – 595 μm , static bed height = 0.5 D_c , fluidising velocity = 4 – 5 U_{mf} , primary air factor \approx 1.0, oxygen level in cyclone \geq 6 vol%)

Case Study	Freeboard Temperature ($T_4 - T_6$) ($^{\circ}\text{C}$)	Fly Ash (FA)	Bottom Ash (BA)	Remarks
FT1	(400 – 600 $^{\circ}\text{C}$)			FA: Overall dark shade interspersed with small amount of white ash BA: Overall greyish shade
FT2	(550 – 600 $^{\circ}\text{C}$)			FA: Similar to Case FT1, overall dark shade interspersed with small amount of white ash BA: Overall greyish shade
FT3	(600 – 650 $^{\circ}\text{C}$)			FA: Overall dark shade but with presence of more white ash skeletons compared to Cases FT1 and FT2 BA: Visibly white shade interspersed with very small amount of black char skeletons
FT4	(600 – 700 $^{\circ}\text{C}$)			A: Overall greyish shade BA: Visibly white to greyish shade with absence of black char skeletons

c) Findings

From the current study, it could be concluded that **the presence of secondary burners and thus higher freeboard temperatures improved the combustion efficiency of rice husk in the fluidised bed combustor**. The improvements attained were as follows:-

- 1) More stable and uniform temperature profiles in the combustor due to the generation of sufficient heat from the secondary burners to continually ignite the fresh incoming rice husk particles and the evolved volatile gases;
- 2) Fly ash with lower residual carbon content due to the higher freeboard temperatures (in the excess of 600°C) allowing for the effective oxidation rate of residual carbon in the fly ash particles as they were being entrained towards the cyclone.

4.6.3 Heat Loss

The effect of heat loss on the combustion efficiency of rice husk was investigated by first carrying out combustion in a non-insulated combustor and then in an insulated fluidised bed combustor. In both experiments, the static bed height was held constant at $0.5 D_c$ (250 – 595 μm sand), fluidising velocity at approximately $3 U_{mf}$ and the primary air factor at 1.5. The combustor was pre-heated until T1 and T2 were approximately 650°C prior to commencement of rice husk feeding.

a) Temperature Profile and Combustion Characteristics

The real-time temperature profiles during the combustion of rice husk in the non-insulated and insulated fluidised bed combustors were shown in Figure 4.1-17 and Figure 4.1-18, respectively.

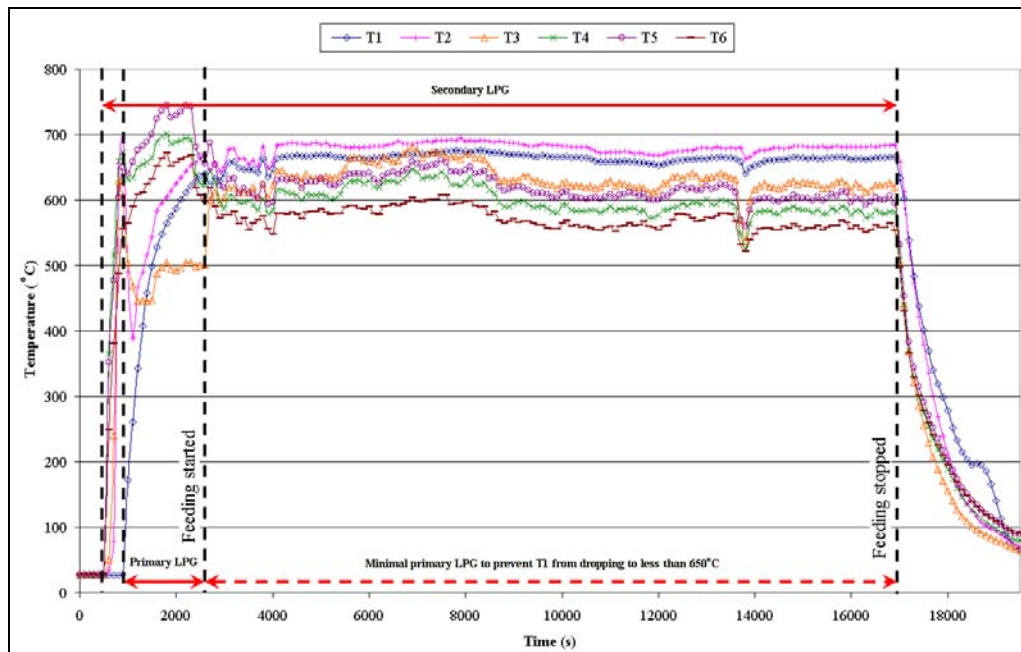


Figure 4.1-17: Real-time temperature profiles during combustion of rice husk in the non-insulated 210-mm inner diameter fluidised bed combustor system (Case Study HL1) (sand size = 250 – 595 μm , static bed height = 0.5 D_c , fluidising velocity $\approx 3 U_{mf}$, primary air factor ≈ 1.5)

From Figure 4.1-17, it was observed that the temperatures in the non-insulated combustor hovered in the range of 600 – 700°C throughout the experiment. The temperatures in the bed region (T1 and T2) were the highest, registering average values of 666°C and 682°C, respectively. As the flue gas flowed higher along the height of the combustor, the temperatures dropped, the reason being the significant amount of heat loss via convection and radiation from the surface of the non-insulated combustor consistent with that observed by Armesto et al. (2002) (Figure 4.1-26). Theoretically, in an adiabatic system, the temperature in the combustor should be higher as the flue gas flows higher up the combustor. This is because hotter gas is less dense and tends to travel upwards. As can be seen from Figure 4.1-19, the average combustor temperatures beyond mid-height of the non-insulated fluidised bed (i.e T4 – T6) were in the range of 580 – 600°C only.

Inserting the values of variables in this experiment into Equation 2-6 through Equation 2-11 yielded a rice husk feeding rate of approximately 140 g/min in order for the combustion process to be autogenous. Further, substituting this value into

Q_p to determine the heat that would have evolved assuming complete reaction to take place, **the degree of heat loss was estimated to be as high as 84%**. However, it should be noted that, in reality, the degree of heat loss will be lower as some of the rice husk might not be burnt into completion. The potential energy in the rice husk will remain unreleased in the form of chars (carbon). The findings on the degree of heat loss in the non-insulated combustor explained the need for using primary and secondary burners throughout the current experiment. This was to compensate the rapid heat loss from the combustor as well as to ensure that the combustion process could be continued. In addition, the high degree of heat loss resulted in a very low cyclone temperature of only 370°C. This relinquished the function of the cyclone as an effective tertiary combustion chamber, as the swirling actions of the flow inside the cyclone was known to induce a very turbulent region which increased the contact time of the unburnt char particles with the oxidising agent (air).

On the other hand, combustion of rice husk in the insulated fluidised bed combustor could be carried out with the occasional auxiliary fuel supplement (primary and secondary burners), as illustrated in Figure 4.1-18. Calculation results showed that to maintain a combustion temperature of 650°C, a feeding rate of only 34 g/min was required. Therefore, the feeding rate of 40 g/min in this experiment was theoretically sufficient to ensure an autogenous combustion process. Nevertheless, as with the previous case, not all of the heat was released due to incomplete combustion, and therefore the occasional use of the primary burner was necessary. During the experiment, the primary burner had to be cut-off intermittently to prevent the bed temperature (T1) from reaching as high as 750°C. The presence of insulation resulted in the temperature above the combustor (T5 and T6) to be elevated to the region of 700 – 750°C, as opposed to only 610 – 660° in the non-insulated combustor. Also, as can be seen from Figure 4.1-18, the combustor temperatures were increasing with the height of the combustor, and clearly supported the theory that with proper conservation of heat inside the combustor (adiabatic system), the highest end of the combustor will register the highest temperature. The temperature in the cyclone was elevated to the region of 510 – 540°C, which although was 38 – 46% higher than the cyclone temperature in the non-insulated combustor, was not high enough for oxidation of chars to be effective. This is because although the

temperature of at least 500°C is required for the complete oxidation of biomass chars (Di Blasi et al., 1999), further weight loss of chars is still observed in the temperature region of 500 – 700°C (Mansaray and Ghaly, 1998b). The residual weight loss become less significant from 600°C onwards, and stopped beyond the temperature of 700°C, as illustrated in the results of thermogravimetric analysis of rice husk by Mansaray and Ghaly (1998b). Therefore, the temperature of at least 600°C in the cyclone is considered necessary for more complete oxidation of residual carbon in the ash. This could be achieved, for example, via installation of a burner adjacent to the cyclone inlet.

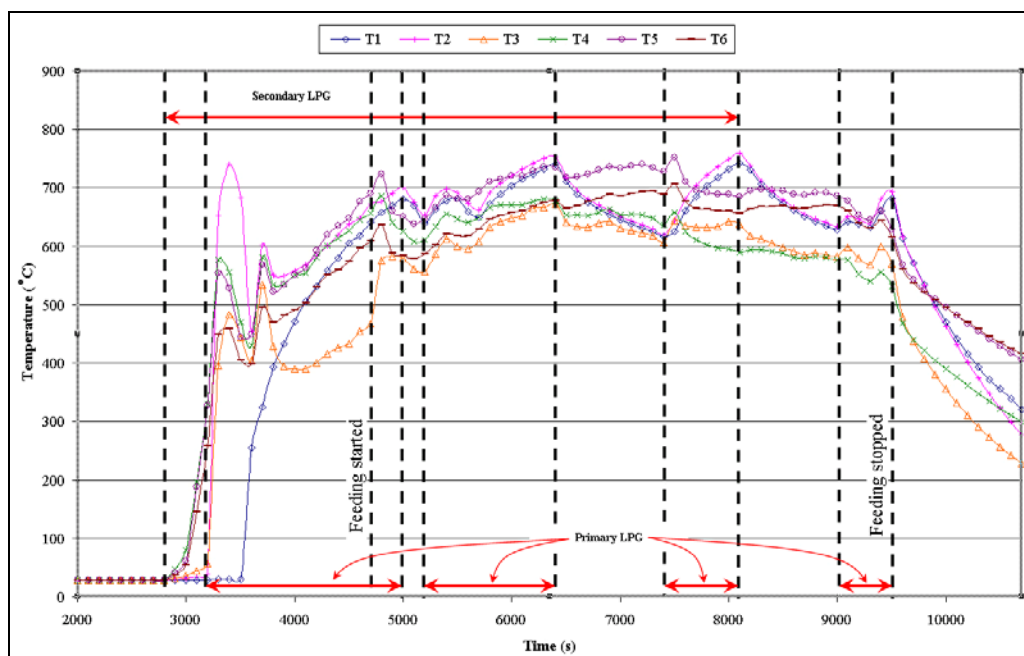


Figure 4.1-18: Real-time temperature profiles during combustion of rice husk in an insulated 210-mm inner diameter fluidised bed combustor system (Case Study HL2) (sand size = 250 – 595 μm , static bed height = 0.5 D_c , fluidising velocity $\approx 3 U_{mf}$, primary air factor ≈ 1.5)

Compared to the combustion of rice husk in the non-insulated combustor and assuming complete combustion to take place, **the heat loss in the insulated combustor was estimated to be only 20%**. Again, the degree of heat loss could be lower due to the fact that not all the rice husk actually burnt to completion. Further, comparisons between the combustion of rice husk in both the non-insulated and insulated combustor (once again assuming complete combustion) **showed that the**

heat loss in the non-insulated combustor was 76% higher than the non-insulated combustor. These findings accentuated the importance of applying proper insulation in a combustor, especially if the combustor is operating at high temperatures because heat loss is more pronounced at higher temperatures due to the higher difference in temperature.

The average temperatures along the height of the combustor during rice husk combustion in the non-insulated and insulated fluidised bed combustors were compared in Figure 4.1-19. In general, the temperature plot for the non-insulated combustor exhibited a decreasing trend as opposed to the increasing trend for the insulated combustor. The decline in temperature for both plots from T2 to T4 was could be attributed to the cooling effect of the pneumatic air entering at ambient temperature near T3. Beyond this zone of air cooling, the temperature resumed to rise steadily for the case of the insulated combustor (T4 – T5) whereas for the non-insulated combustor, there was only a slight increase in temperature. Since both experiments were carried out at exactly the same operating parameters except for the factor of insulation, such difference in temperature could be attributed solely to heat loss to the surroundings. The heat loss was more pronounced in the freeboard region (T4 – T6) compared to the bed region (T1 and T2). As such, it was hypothesised that the combustion rate at the bed region for both cases should remained more or less similar and any difference in the final ash (fly ash) were attributable to char oxidation rate at the freeboard region.

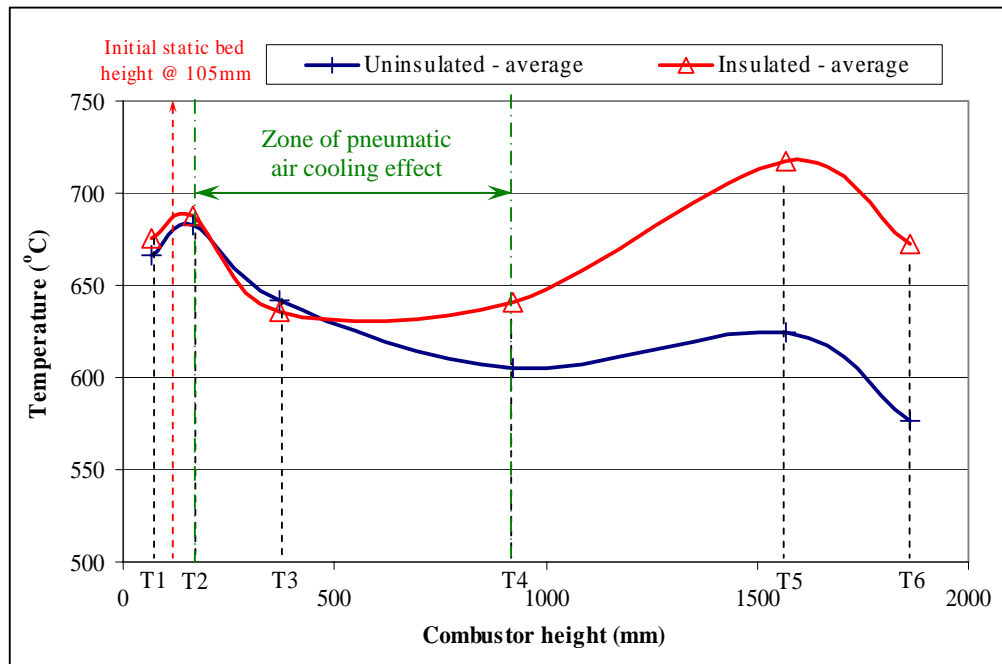


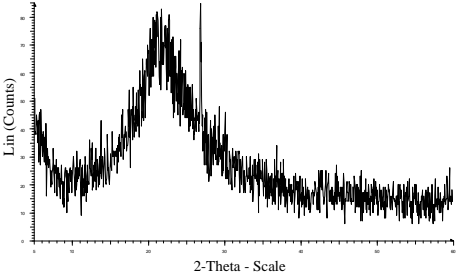
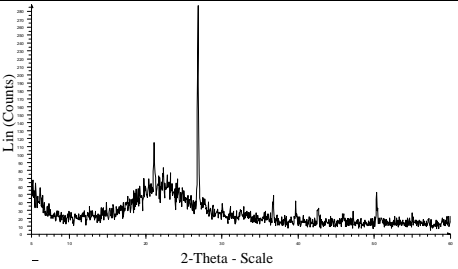
Figure 4.1-19: Average combustor temperatures during combustion of rice husk in the non-insulated and insulated 210-mm inner diameter fluidised bed combustors (sand size = 250 – 595 μm , static bed height = 0.5 D_c , fluidising velocity $\approx 3 U_{mf}$, primary air factor ≈ 1.5)

b) Ash Quality

i) Silica Structure

The fly ash samples from both experiments were found to be still in their amorphous forms, as shown in Table 4.1-24. However, both samples were found to be contaminated with sand (quartz crystals).

Table 4.1-24: Diffractograms of fly ash samples from the combustion of rice husk in the non-insulated and insulated 210-mm inner diameter fluidised bed combustors (sand size = 250 – 595 μm , static bed height = 0.5 D_c , fluidising velocity $\approx 3 U_{mf}$, primary air factor ≈ 1.5)

Case Study	Description	Diffractogram
HL1	Non-insulated fluidised bed	
HL2	Insulated fluidised bed	

ii) Residual Carbon Content

The residual carbon contents in the fly ash samples from the non-insulated and insulated combustors were 1.9 wt% and 1.7 wt%, respectively. The improvement of carbon burnout in the insulated combustor was quite low, showing an improvement of only 12.5% compared to the non-insulated combustor due to the relatively short freeboard height of the 2000-mm tall fluidised bed. It was expected that such decrease will be more significant in taller fluidised beds. However, it was observed that the fly ash sample from the non-insulated combustor contained more unburnt char skeletons compared to the sample from the insulated combustor (Figure 4.1-20). The improvement in carbon burnout in the latter could be attributed to two factors, both related to the char and/or residual carbon oxidation rate in the freeboard region, namely:-

- i) Higher temperature levels at the freeboard region (700 – 750°C) compared to only 610 – 660° in the non-insulated combustor; and

- ii) Higher temperature at the cyclone (up to 540°C) compared to only 370°C in the non-insulated combustor.

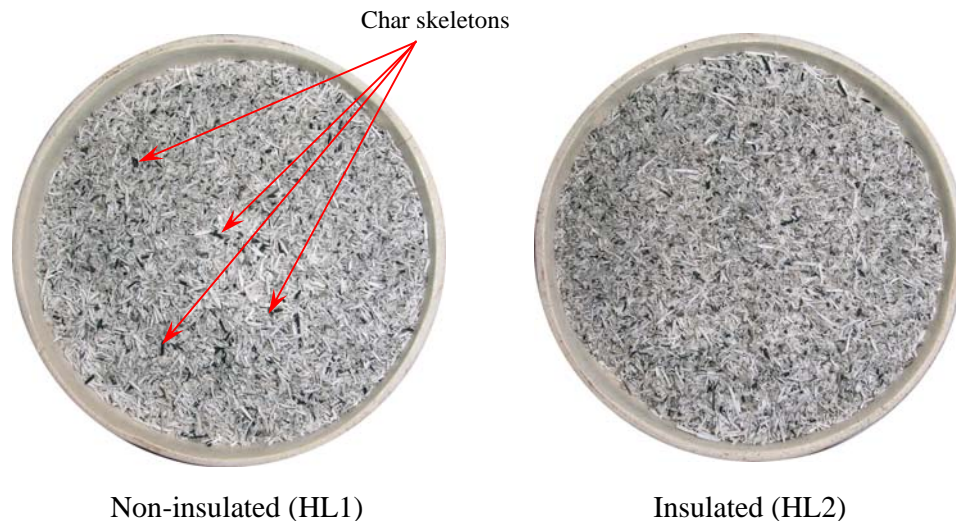


Figure 4.1-20: Fly ash samples from the combustion of rice husk in the non-insulated and insulated 210-mm inner diameter fluidised bed combustors (sand size = 250 – 595 μm , static bed height = 0.5 D_c , fluidising velocity $\approx 3 U_{mf}$, primary air factor ≈ 1.5)

As had been discussed earlier, the oxidation of char will only be complete beyond the temperature of 700°C. Thus, the temperatures in the excess of 700°C in the freeboard region of the insulated combustor increased the chances for the unburnt carbon in the ash to be oxidised more completely as they were travelling towards the cyclone. This phenomenon was reflected in the resulting ash, whereby the amount of char skeletons was less significant (Figure 4.1-20) compared to that from the non-insulated combustor. Exposure of the char skeletons to the temperature range of 610 – 660°C in the freeboard region of the latter might not be sufficient to enable them to be burnt to completion, hence the presence of considerable amount of intact char skeletons in the ash samples. Further, the cyclone temperature in the non-insulated combustor, which at 370°C, was even lower than the minimum temperature required (of 385°C according to Di Blasi et al, 1999) to achieve the maximum combustion rate. With such findings, it could be concluded that the differences in the residual carbon contents in the fly ash samples between the two experiments were due to the higher degree of combustion in the freeboard region of the insulated combustor with

relatively higher freeboard temperatures. The degree of rice husk burning in the bed region could be expected to be approximately the same level as the bed temperatures for both experiments were largely similar (averaging at 666 – 676°C).

c) **Findings**

The presence of insulation materials (calcium silicate boards) minimised the degree of heat loss in the 210-mm inner diameter fluidised bed combustor by as much as 70%. This resulted in an increasing temperature profile along the height of the combustor as opposed to the non-insulated combustor, whereby the highest temperatures were registered near the bed region (T1 and T2). The higher temperature along the freeboard region enabled further oxidation of the carbon content in the ash particles as they were being entrained in the flue gas stream towards the cyclone, thus resulting in an **overall improvement in the carbon oxidation rate in the freeboard region.** Consequently, the residual carbon content in the ash was lower compared to that from the non-insulated combustor. The bulk of weight loss for char occurred in the temperature region between the maximum combustion rate (of 385°C) up to 600°C, after which the weight loss is quite insignificant up to 700°C. Thus, the temperature of above 700°C was considered necessary to ensure complete oxidation of the char fraction to take place. In this study, the temperatures in the upper half of the non-insulated combustor were lower than 600°C, whereas in the insulated combustor, these temperatures averaged from 620 – 700°C. Hence, this study demonstrated the significance of conserving the heat in the combustor during the combustion process by means of insulation materials. The combustion process, in terms of combustion efficiency and carbon conversion efficiency, could therefore be maximised.

4.7 Effect of Washing of Rice Husk on Its Combustion Efficiency in Fluidised Bed

4.7.1 Determination of Pretreatment Method for Rice Husk

In order to investigate the suitable pretreatment method to be applied to rice husk prior to combustion in the fluidised bed combustor, three batches of rice husk samples at 100 g each were subjected to the following pretreatments, all conducted at ambient temperature (30°C):-








- 1) Immediate rinsing with tap water
- 2) Leaching with hydrochloric acid (2 N) followed by rinsing with tap water
- 3) Soaking in tap water for 16 hours

In addition to these three pretreated samples, one batch of raw rice husk was also used as a control sample. The raw rice husk sample and samples from pretreatments (1) and (2) were exposed suddenly to temperatures of 650 – 750°C (representing sudden heating) in a muffle furnace for 3 minutes each and the resulting ashes were shown in Table 4.1-25.

As expected, the ash from the raw rice husk consisted of black char skeletons consistent with findings of Krishnarao et al. (2001) and Jenkins et al. (1996). The sudden heating effect resulted in the melting of the alkali metals (in particular potassium) on the surface of the ash, thus entrapping any unburnt carbon and preventing them from being further oxidised. Ash sample from pretreatment (1) took on an amber hue, indicating that some alkali metals were leached out to a certain extent but were still present in small amounts. Jenkins et al. (1996) also noted that the immediate rinsing effect (spraying with tap water for 1 minute) was less effective in removing alkali metals (potassium and sodium) compared to soaking in tap water at ambient temperature for 24 hours. In their study, they found that soaking in tap water reduced the levels of potassium and sodium in rice straw samples by as much as 82% and 90% (in the resulting ash on a dry basis) compared to only 34% and 15% respectively, for samples sprayed with water for 1 minute. Meanwhile, the ash from acid-leached sample from pretreatment (2) was completely

white, which showed that the acid was very effective in removing the unwanted alkali metals. However, if applied to large batches of samples as required in combustion in fluidised bed, pretreatment (2) may seem infeasible due to the added unit operations (acid leaching and subsequently water rinsing), chemical cost and problem of leachate disposal (considered a form of hazardous waste). From Table 4.1-25, soaking in water (as in pretreatment (3)) was effective in removing the highly-soluble potassium and sodium responsible for the formation of black particles in the ash. The ash samples from pretreatment (3) were comparable with that from pretreatment (2) after being exposed suddenly to temperatures of 650 – 750°C for 2 minutes in a muffle furnace. Hence, for the combustion experiments in the fluidised bed combustor considered in this study, the rice husk samples will be subjected to pretreatment (3), as this pretreatment method proved sufficient in removing the potassium and sodium compounds to the extent of preventing the formation of black char particles.

Table 4.1-25: Ash samples from thermal treatment of raw, water-washed and acid-leached rice husk

Residence time = 3 min			
	Raw rice husk	Water-washed rice husk (Immediate rinsing with tap water)	Acid-leached rice husk (Rinsing with HCl 2 N followed by tap water)
	C = 0.13 wt%	C = 0.09 wt%	C = 0.03 wt%
Residence time = 2 min			
	Water-washed rice husk (Soaked in tap water for 16 hours)		Acid-leached rice husk (Rinsing with HCl 2 N followed by tap water)
	C = 0.04 wt%		C = 0.05 wt%
Residence time = 1 min			
	Water-washed rice husk (Soaked in tap water for 16 hours)		Acid-leached rice husk (Rinsing with HCl 2 N followed by tap water)
	C = 0.06 wt%		C = 0.05 wt%

Note:

- i) Washing of rice husk (with tap water or acid) performed at ambient temperature
- ii) All samples thermally-treated in muffle furnace at temperatures of 650 – 750°C
- iii) C = residual carbon content as determined by thermogravimetric analysis due to very small amount of carbon in samples (<0.5 wt%). Sample was ground into powder form and analysis conducted by (1) moisture removal in nitrogen atmosphere at 110°C until no further mass loss; (2) volatile matters removal in nitrogen atmosphere at 925°C until no further mass loss and (3) carbon removal in oxygen atmosphere at 925°C until no further mass loss.

4.7.2 Effect of Alkali Metals Removal in Rice Husk on Its Combustion Efficiency in Fluidised Bed

The effect of removal of alkali metals in rice husk through water-washing on its combustion efficiency in the fluidised bed was carried out in two stages, first to determine its effect in the dense phase (primary) combustion and secondly to study its effect in the dilute phase (secondary) combustion. The water-washed rice husk was prepared by soaking them overnight (24 hours) in tap water at ambient temperature. Then, they were rinsed and dried to their original moisture content of approximately 10 wt%.

4.7.2.1 Primary Stage Combustion

The experiments were conducted using raw and water-washed rice husk. For each experiment, the static bed height was held constant at $0.5 D_c$ (250 – 595 μm sand), the fluidising velocity at approximately $3 U_{mf}$, primary air factor at 1.2 and feeding was commenced upon pre-heating of the bed to temperatures of 600 – 650°C. The freeboard oxygen levels were maintained at 6 – 12 vol% (measured at the cyclone) throughout the experiment.

a) Temperature Profile and Combustion Characteristics

The bed temperatures (registered by T1 in the data-logging system) during the combustion of raw and water-washed rice husk at approximately 10 wt% moisture content was shown in Table 4.1-26, while the real-time temperature profiles at the combustor during each experiment were enclosed in Appendix F. It was observed that the bed temperature during the combustion of raw rice husk was generally higher than that of the water-washed rice husk. This could be attributed to the effect of water-washing on the rice husk structure. It was observed that the outer layer of the water-washed rice husk took on a darker shade and were less ‘shiny’ compared to that of raw rice husk (Table 4.1-27). The former was also more brittle and was more prone to breakage. It was speculated that prolonged soaking (24 hours) of the

husk in water and the subsequent rinsing step somehow altered the structure of the waxy coating on the outer cell wall to a certain extent, thereby weakening its structure and making it more prone to breakage. As such, upon entry into the fluidised bed combustor via the feeding port, the turbulence in the bed tended to break the water-washed rice husk into smaller fragments and facilitating its entrainment into the freeboard region. Thus, with less penetration of these rice husk particles into the bubbling bed region, the degree of burning in the bed region was also lower, resulting in overall lower bed temperature compared to the case of burning raw rice husk.

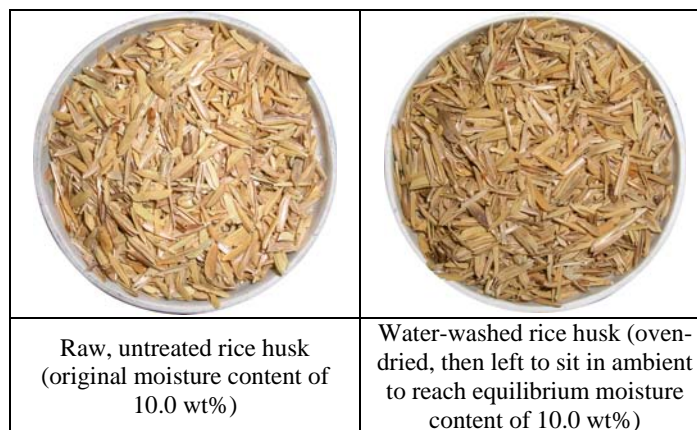
Table 4.1-26: Effect of alkali metals removal from rice husk on the bed temperatures during combustion of rice husk in the 210-mm inner diameter fluidised bed (primary stage combustion) (sand size = 250 – 595 μm , static bed height = 0.5 D_c , fluidising velocity $\approx 3 U_{mf}$, primary air factor ≈ 1.2)

Bed temperature ($^{\circ}\text{C}$)	Raw Rice Husk (Presence of Alkali Metals Compounds)	Water-Washed Rice Husk (Negligible Amount of Alkali Metals Compounds)
Minimum	653.3	585.1
Average	665.9	608.3
Maximum	676.7	634.9

Note:

Moisture contents in both rice husk samples ~ 10 wt%

Table 4.1-27: Physical appearances of the raw and water-washed rice husk samples

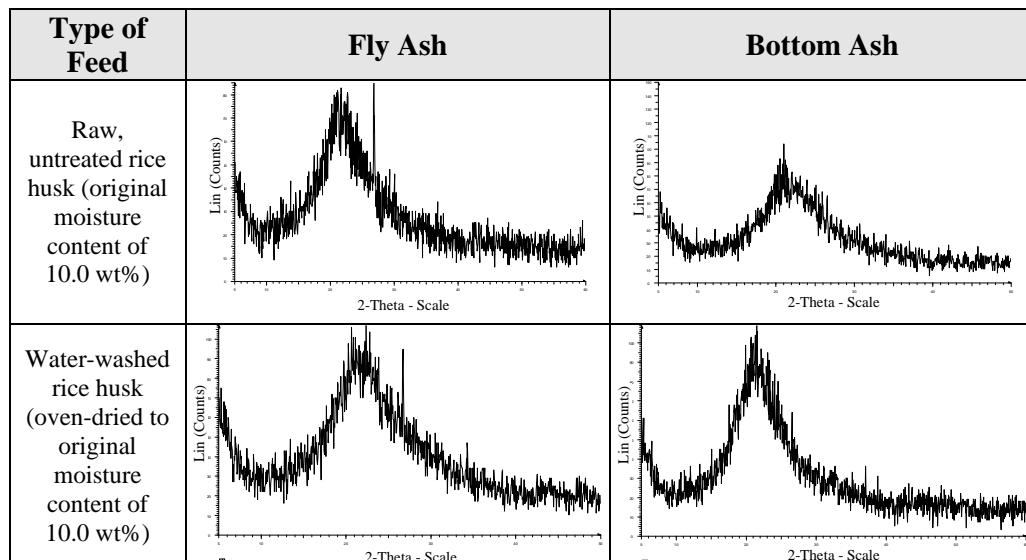


b) Ash Quality

i) Silica Structure

The silica structures of ash samples from both experiments were compared in Table 4.1-28. It was observed that all ash samples retained their amorphous structures. However, the fly ash samples were contaminated with minor amount of quartz crystals from the elutriated sand.

Table 4.1-28: Diffractograms of ash samples from the combustion of raw and water-washed rice husk in the 210-mm inner diameter fluidised bed combustor (effect of alkali metals removal on combustion efficiency in the primary stage) (sand size = 250 – 595 μm , static bed height = 0.5 D_c , fluidising velocity $\approx 3 U_{mf}$, primary air factor ≈ 1.2)







ii) Residual Carbon Content

The residual carbon contents in the ash samples obtained during combustion of raw and water-washed rice husk (both at approximately 10 wt% moisture content) was shown in Table 4.1-29. As expected, the fly ash from water-washed rice husk had twice the residual carbon content (at 3.9 wt%) compared to that from raw rice husk (at 1.9 wt%) due to the lower degree of combustion in the bed region. Water-washing caused the rice husk particles to become more brittle and easily broken into smaller fragments. This caused them to be easily entrained into the freeboard region rather than being burnt inside the bubbling bed region. Since the effective operation of the fluidised bed warrants that approximately 40% of the combustion to take

place in the bed (Chen et al., 1998), such entrainment resulted in the poor oxidation of the carbon in the ash. However, the bottom ash from both rice husk types had similar residual carbon content (at approximately 2.0 wt%) due to their prolonged retainment in the bed region, allowing for sufficient contact time with oxidants and heat for the carbon oxidation process.

Table 4.1-29: Ash samples from the combustion of raw and water-washed rice husk in the 210-mm inner diameter fluidised bed combustor (effect of alkali metals removal on combustion efficiency in the primary stage) (sand size = 250 – 595 μm , static bed height = 0.5 D_c , fluidising velocity $\approx 3 U_{mf}$, primary air factor ≈ 1.2)

Type of Feed	Fly Ash	Bottom Ash
Raw, untreated rice husk (original moisture content of 10.0 wt%)		
	LOI = 1.93 wt%	LOI = 2.02 wt%
Water-washed rice husk (oven-dried to original moisture content of 10.0 wt%)		
	LOI = 3.85 wt%	LOI = 1.87 wt%

Note: LOI = Loss on ignition

Table 4.1-29 also showed the ash samples obtained from both experiments. It should be noted that although the bottom ash from the water-washed rice husk (10 wt% moisture) was white in shade compared to that from the raw rice husk, their residual carbon contents were similar due to the presence of some partially-burnt rice husk fragments in the former, which was also registered as mass loss in the loss on ignition test. Observation on the particle sizes of all fly ash samples also showed that the fly ash from raw rice husk mostly still retained their skeleton-like shape and

were coarser in size. On the other hand, the fly ash sample from the water-washed rice husk were much finer in size, which was attributable to their more brittle nature after soaking in water for a prolonged period of time.

c) Findings

Water-washing (soaking in tap water at ambient temperature for 24 hours) of rice husk was effective in removing the problematic impurities (potassium and sodium) that caused undesirable surface melting on ash particles. At similar moisture contents of approximately 10 wt%, the water-washed rice husk gave poorer combustion characteristics (lower bed temperature and higher residual carbon content) compared to raw rice husk. Water-washing seemed to weaken the structure of the husk, making them more brittle and easily broken into smaller fragments in the bubbling bed region. Entrainment of these small fragments led to lower degree of burning in the bed region.

4.7.2.2 Secondary Stage Combustion

The experiments were conducted using raw and water-washed rice husk. For each experiment, the static bed height was held constant at $0.5 D_c$ (250 – 595 μm sand), the fluidising velocity at approximately $3 U_{mf}$, primary air factor at 1.2 and feeding was commenced upon pre-heating of the bed to temperatures of 600 – 650°C. The freeboard temperatures (T4 – T6) and freeboard oxygen level were maintained above 700°C and 6 – 12 vol% (measured at the cyclone), respectively throughout the experiment.

a) Temperature Profile and Combustion Characteristics

The temperature profiles at the fluidised bed combustor during both experiments were shown in Figure 4.1-21 and Figure 4.1-22, respectively. In general, there were not many differences between both temperature profiles, whereby temperatures at the bed region (T1 and T2) were maintained at approximately 750°C throughout the

feeding period. Meanwhile, the freeboard temperatures ($T_3 - T_6$, $T_{cyclone}$) were in the range of 600 – 900°C throughout the feeding period.

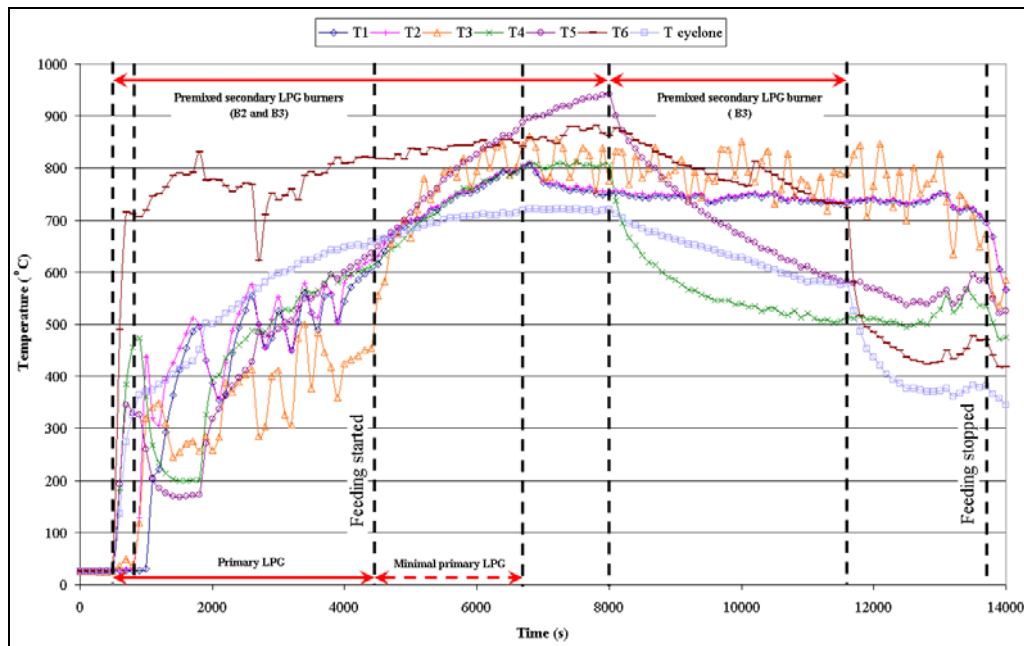


Figure 4.1-21: Real-time temperature profile during combustion of raw rice husk in the 210-mm inner diameter fluidised bed combustor (sand size = 250 – 595 μm , static bed height = $0.5 D_c$, fluidising velocity $\approx 3 U_{mf}$, primary air factor ≈ 1.2 , oxygen level in cyclone = 6 – 12 vol%)

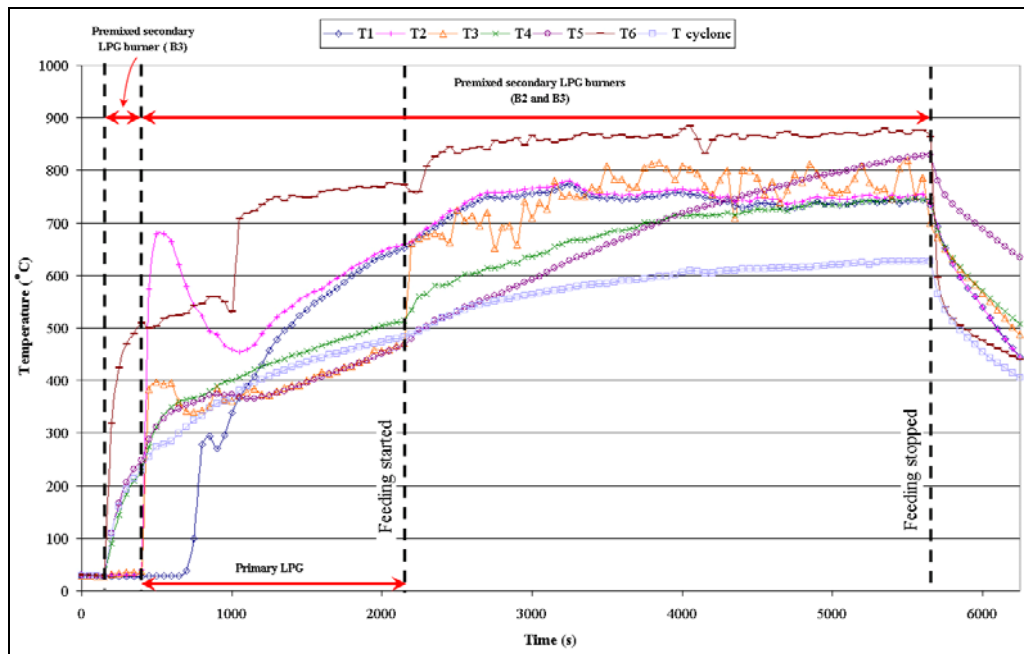


Figure 4.1-22: Real-time temperature profile during combustion of water-washed rice husk in the 210-mm inner diameter fluidised bed combustor (sand size = 250 – 595 μm , static bed height = 0.5 D_c , fluidising velocity $\approx 3 U_{mf}$, primary air factor ≈ 1.2 , freeboard temperatures (T4 – T6) = 700 – 900°C, oxygen level in cyclone = 6 – 12 vol%)

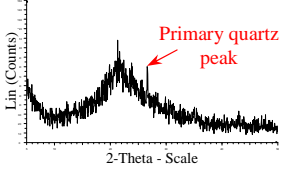
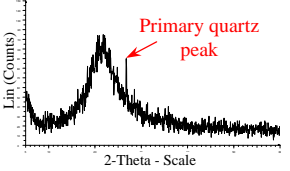
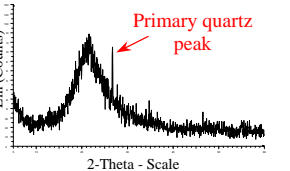
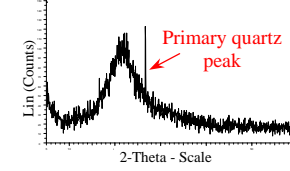
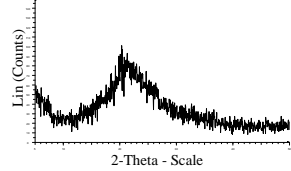
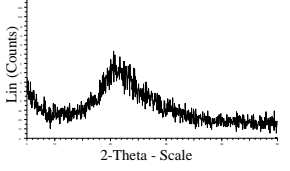
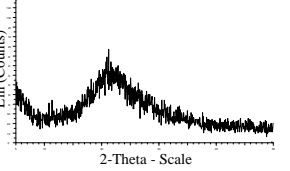
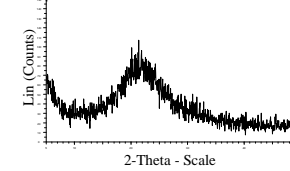
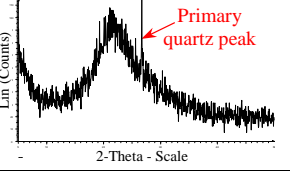
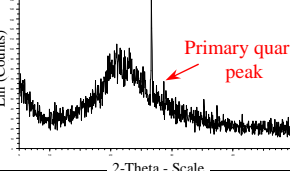
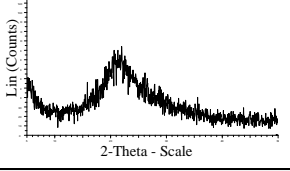
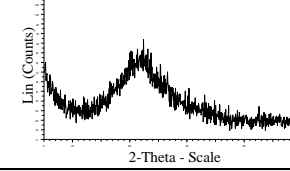
b) Ash Quality

i) Silica Structure

The silica structure of ash samples from both experiments were shown in Table 4.1-30. It was observed that all ash samples retained their amorphous structure. The bottom ash was exposed continuously to the temperature in the range of 700 – 750°C whereas the fly ash were exposed more briefly (estimated to be less than 2 minutes) to temperatures in the freeboard ranging from 700 – 900°C. For the bottom ash, it was expected that these ash were continuously replenished with the ash liberated from the fresh rice husk feed as those retained in the bed were broken into smaller fragments by the vigorous bubbling action of the bed, allowing them to be entrained in the gas stream towards the cyclone to constitute a portion of the fly ash. Previous studies (Section 4.2) had shown that for raw rice husk, exposure to temperature as high as 850°C for 3 minutes was insufficient for the crystallisation of silica in the ash to take place.

At atmospheric pressure, tridymite and cristobalite are crystallised at 867 – 1470°C and 1470 – 1727°C, respectively (Shinohara and Kohyama, 2004). However, due to the impurities found in raw rice husk, the transition from amorphous to crystalline cristobalite and tridymite forms occurs at a much lower temperature. The presence of impurities (such as potassium and sodium compounds) significantly reduced the transition temperature. Further, the formation of cristobalite was reported to be accelerated with the presence of potassium (Nakata et al. 1989). In the water-washed rice husk, the amount of potassium was negligible. Therefore, the operating temperature of such rice husk could be increased without the risk of crystallisation.

Table 4.1-30: Silica structures of ash samples from the combustion of raw and water-washed rice husk in the 210-mm inner diameter fluidised bed (effect of alkali metals removal on combustion efficiency in the secondary stage) (sand size = 250 – 595 μm , static bed height = 0.5 D_c , fluidising velocity $\approx 3 U_{mf}$, primary air factor ≈ 1.2 , oxygen level in cyclone = 6 – 12 vol%)







Ash Sample / Parameter		PRH1 (Raw Rice Husk)			PRH2 (Water-Washed Rice Husk)
Fly Ash	Before sand decontamination stage				
	After sand decontamination stage*				
Sample		PRH1-a	PRH1-b	PRH1-c	PRH2-a
Freeboard Temp. (T4 – T6) (°C)		700 – 900	500 – 700	400 – 550	700 – 900
Bottom Ash	Before sand decontamination stage				
	After sand decontamination stage*				
Sample			PRH1-d		PRH2-b

* Ash samples had been subjected to sand removal stage (as described in Section 4.5.1 (b) (i) prior to XRD analysis)

ii) Residual Carbon Content

The ash samples obtained from both experiments were compared in Table 4.1-31. It could be observed that the removal of alkali metals from rice husk by washing with water prior to combustion in the fluidised bed resulted in much brighter shade for the fly and bottom ashes. The water-washing effect was especially more prominent on the bottom ash, whereby the bottom ash from the water-washed rice husk attained a bright white shade indicating very low residual carbon content. Leaching out of the alkali metals responsible for the formation of surface melt on ash particles enabled the unburnt carbon to be oxidised further as long as they were retained within the hot bubbling bed region. The continuously 'roasting' process resulted in a much higher rate of carbon oxidation compared to the ash from burning raw rice husk. The surface of the ash from raw rice husk consisted of surface melt attributable to the low melting point alkali metals, which entrapped the unburnt carbon and preventing the carbon molecules to be further oxidised even at higher temperatures or sufficiently long residence time in the bed, as they were not in direct contact with the oxidants (air).

Table 4.1-31: Ash samples from the combustion of raw and water-washed rice husk in the 210-mm inner diameter fluidised bed (effect of alkali metals removal on combustion efficiency in the secondary stage) (sand size = 250 – 595 μm , static bed height = 0.5 D_c , fluidising velocity $\approx 3 U_{mf}$, primary air factor ≈ 1.2 , oxygen level in cyclone = 6 – 12 vol%)

Case Study	PRH1 (Raw Rice Husk)			PRH2 (Water-Washed Rice Husk)
Fly Ash				
Sample	PRH1-a	PRH1-b	PRH1-c	PRH2-a
Freeboard Temperatures (T3 – T6) (°C)	700 – 900	500 – 700	400 – 550	700 – 900
Loss on Ignition (wt%)	1.16	2.25	3.13	1.13
Bottom Ash				
Sample	PRH1-d			PRH2-b
Loss on Ignition (wt%)	1.69			0.73

The results from loss on ignition tests on the ash samples were also shown in Table 4.1-31. From Table 4.1-31, it was found that washing the rice husk with water prior to combustion in the fluidised bed significantly reduced the residual carbon content in the bottom ash by more than 50% (from 1.7 wt% in sample PRH1-d to 0.7 wt% in sample PRH2-b). This could be attributed to the absence of alkali metals, in particular potassium, in the water-washed rice husk, which eliminated the detrimental phenomenon of surface melting. As such, any carbon molecules fixated within the char and ash particles could be oxidised continuously as long as they were retained in the hot bubbling sand bed. On the other hand, the formation of surface melt mixture at the surface of the incompletely-oxidised char or ash from raw rice husk prevented further reaction of the carbon molecules irrespective of how long they stayed in the bed or how high the bed temperature was.









The phenomenon of sudden, rapid heating occurred as soon as the rice husk feed entered the fluidised bed combustor. The temperature registered by thermocouple T3 indicated the initial exposure temperature of the rice husk feed upon their first entry into the combustor, due to the location of this thermocouple being in direct vicinity with the feed entry port (T3 and the feed entry port were located at 369 mm and 365 mm above the distributor plate, respectively as shown in Figure 3-14). During the combustion of raw rice husk, T3 was in the range of 700 – 870°C throughout the experiment. Thus, the formation of black particles in the fly ash due to the sudden heating effect as reported by Krishnarao et al. (2001) was duly expected. In their study on the effect of sudden heating of raw and acid-leached rice husk at temperatures ranging from 400 – 700°C, they found that the presence of black particles (carbon) in the raw rice husk increased at higher temperature whereas for the acid-leached rice husk (whereby potassium was absent), the resulting ash was completely white and free from any carbon particles. The effect of sudden heating coupled with the presence of potassium led to the phenomenon of surface melting which entrapped the carbon particles within the ash structure. As such, in the current experimental study, the fly ash obtained from the combustion of raw rice husk showed the presence of significant amount of black particles (sample PRH1-a, Table 4.1-31) compared to that obtained from burning water-washed rice husk (sample PRH2-a, Table 4.1-31). The presence of minor amount of black particles in the latter was expected to be attributed to two factors: (1) insufficient residence time in the

combustor for complete oxidation to occur as some of the low-density rice husk particles (especially broken fragments) were blown out directly from the combustor upon entry into the combustor and (2) incomplete removal of potassium in very little amount of the water-washed rice husk. From Table 4.1-31, it was observed that the residual carbon content in the fly ash samples from burning raw and water-washed rice husk (samples PRH1-a and PRH2-a) were similar, at 1.1 wt%. However, it should be noted that minor discrepancy might arise from the loss on ignition test of the fly ash sample PRH1-a, due primarily to the unavailability of the carbon entrapped in the surface melt mixture to be oxidised completely. As such, the residual carbon content registered was not fully representative of its actual carbon content. The product after loss on ignition test of this fly ash sample was slightly darker in shade as opposed to the bright white ash product of other samples (Table 4.1-32). It also contained some black specks of carbon distributed amongst the final ash product. Thus, it was concluded that the actual carbon content of this sample could probably be higher than the registered value of 1.1 wt%.

Attempts were made to minimise the extent of sudden heating by lowering the temperature at the vicinity of the feed entry (T3) during the combustion of raw rice husk by lowering the freeboard temperatures to 500 – 700°C (switching off secondary LPG burner B2) and subsequently 400 – 550°C (switching off secondary LPG burner B3). The resulting fly ash samples (samples PRH1-b and PRH1-c in Table 4.1-31, respectively) showed increased amount of residual carbon content compared to the case whereby all secondary burners were switched on (sample PRH1-a). This could be attributed to the lower temperature at the freeboard region when one or both burners were switched off, leading to ineffective oxidation temperature for the carbon in the char or ash particles. However, the extent of sudden heating was somewhat lower for samples PRH1-b and could be considered negligible for sample PRH1-c. The product from loss on ignition test for sample PRH1-b were slightly greyish in colour as opposed to the bright white product for sample PRH1-c, indicating that the extent of sudden heating still took place in the former. Sample PRH1-b was obtained when the freeboard temperatures (T4 and T5) were in the range of 500 – 700°C whereas sample PRH1-c were obtained when the freeboard temperatures (T4 – T6) were in the range of 400 – 550°C. Such lower freeboard temperatures in the latter resulted in minimal effect of sudden heating and

thus, the product from loss of ignition were bright white. Nevertheless, elimination of the effect of sudden heating in this case was offset by the ineffective oxidation temperature at such low freeboard temperature range (400 – 550°C, which was slightly higher than the temperature for complete conversion of chars at 517°C, as noted by Di Blasi et al., 1999). As such, the residual carbon content in sample PRH1-c was found to be highest (at 3.1 wt%) amongst fly ash samples from burning of raw rice husk (samples PRH1-a to PRH1-c), although the residual carbon content for samples PRH1-a and PRH1-b did not take into account some of the entrapped carbon that could not be completely oxidised during the loss of ignition test. However, it was expected that although such discrepancy were taken into account, the residual carbon contents of these samples were still relatively lower than sample PRH1-c.

Table 4.1-32: Comparisons of ash samples before and after loss on ignition tests (ash from combustion of raw rice husk in the 210-mm inner diameter fluidised bed at different freeboard temperatures; sand size = 250 – 595 μm , static bed height = 0.5 D_c , fluidising velocity $\approx 3 U_{mf}$, primary air factor ≈ 1.2 , oxygen level in cyclone = 6 – 12 vol%)

Sample	Freeboard Temperatures (T3 – T6) (°C)	Sample (before loss on ignition test [#])	Sample (after loss on ignition test*)
PRH1-a (Fly ash)	700 – 900		 Black carbon specks Slightly greyish ash product
PRH1-b (Fly ash)	500 – 700		 Slightly greyish ash product
PRH1-c (Fly ash)	400 – 550		 Bright white ash product
PRH1-d (Bottom ash)	Not applicable		 Bright white ash product

Note:

[#] Ground into powder form

*Loss on ignition – 900°C for 2 hours or until no weight loss was observed

c) Findings

The advantage of using water-washed rice husk was found to be more prominent with effective secondary stage combustion taking place in the fluidised bed. Rapid heating of the rice husk particles occurred as soon as they entered the hot fluidised bed combustor. This rapid heating process resulted in the surface melting phenomenon by the alkali metals and subsequently the formation of black char particles in the ash of raw rice husk. Removal of the detrimental alkali metals through water-washing eliminated the surface melting phenomenon, thereby resulted in ash with significantly lower residual carbon (from 3.2 wt% to 1.1 wt% in fly ash, and from 1.7 wt% to 0.7 wt% in bottom ash). Once formed, the surface melt permanently encapsulate any unburnt carbon in the char or ash particles, preventing further oxidation to take place even when they are exposed to high temperatures in the freeboard region. As such, when using raw rice husk, very minimal particle combustion in the secondary stage actually takes place. On the other hand, with water-washed rice husk, any unburnt carbon in the ash or char particles could be oxidised effectively, due mostly to the absence of surface melt thereby enabling direct contact of carbon with oxygen and heat. Therefore, good ash quality (amorphous and residual carbon content less than 1.0 wt%) can only be obtained by burning rice husk that are free from alkali metal compounds (such as water-washed rice husk) in the fluidised bed.

4.8 Effect of Air Supply on the Combustion Efficiency of Rice Husk in Fluidised Bed**4.8.1 Primary Air Factor**

The primary air factors investigated ranged from 0.6 (gasification) to 1.5 (excess air combustion). Calculation procedures to determine the amount of stoichiometric air requirement (primary air factor of 1.0) for combustion of rice husk were included in Appendix G. For all experiments, the static bed height was held

constant at $0.5 D_c$ (250 – 595 μm sand), the fluidising velocity at approximately $5 - 6 U_{mf}$ while feeding was commenced once the bed had been pre-heated to 650°C .

a) Temperature Profile and Combustion Characteristics

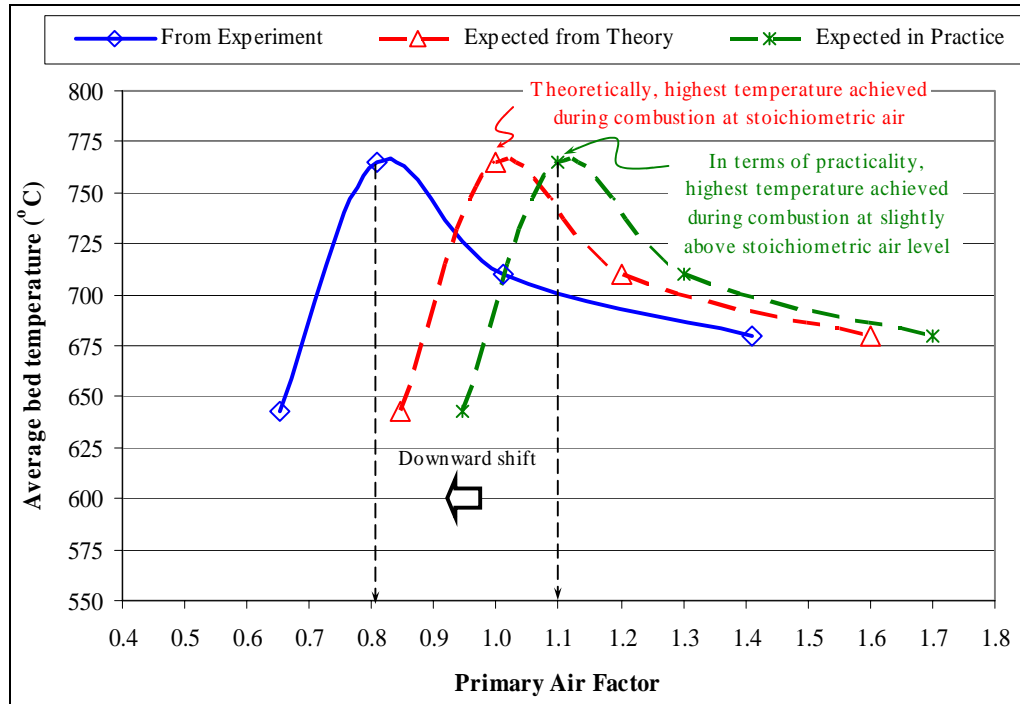
Figure 4.1-23 showed the average bed temperatures obtained during the experiments of burning rice husk in the fluidised bed at primary air factors ranging from 0.65 to 1.4. Also included in Figure 4.1-23 were the expected temperature curves based on theory and actual practice.

Theoretically, the combustion temperature is the highest at air factor of one (stoichiometric air level) as shown in (Figure 3-1). Below the stoichiometric air level, starved-air combustion (gasification) takes place and the potential energy in the feed material could not be released due to insufficient air for oxidation process. Therefore, the combustion temperature is lower as not all of the energy (heat) is released. Beyond air factor above stoichiometric, part of the heat evolved from the combustion process is used to heat up the excess air, therefore resulting in a steady drop in temperature as the air factor is increased.

However, in practice, feeding the air at slightly above stoichiometric level (namely 10 – 20% excess) is necessary in order to provide ‘stoichiometric conditions’ at micro-level in the bed region (Figure 4.1-23) due to the mass transport phenomena, whereby a certain lag time exists at the point of air feed to the primary combustion (bed) region. The slightly excess air is required for replenishing the oxygen that is continuously being depleted in the bed region, thereby increasing its level to near-stoichiometric level.

In this study, the highest bed temperature was recorded at the primary air factor of 0.81, thus combustion air at micro-level in the bed area probably had reached stoichiometric amount (theoretical temperature curve in Figure 4.1-23). Therefore, in actuality, rice husk combustion was being carried out at excess air level when the primary air factor was set at ‘stoichiometric’ (Case PAF3) during experiment. Another possible explanation was that not all of the rice husk feed was completely burnt in the bed region. Thus, if the air factor of 0.8 had probably reached the

slightly above stoichiometric air level (air factors of 1.1 or 1.2), it could be concluded that only 60 – 70% of the rice husk feed actually burnt completely inside the bed. This finding also indirectly justified the need for a sufficient freeboard region in order to complete the remaining 30 – 40% of the combustion process, most likely the oxidation of the chars and to a certain extent, some unburnt rice husk feed that tended to be entrained into the freeboard region due to its low bulk density.



Note: The theoretical and practical temperature curves were predicted taking into account heat losses to the surrounding and due to incomplete reaction in the bed region

Figure 4.1-23: Comparisons of average bed temperatures during combustion of rice husk in the 210-mm inner diameter fluidised bed at different primary air factors (sand size = 250 – 595 μm , static bed height = 0.5 D_c , fluidising velocity = 5 - 6 U_{mf})

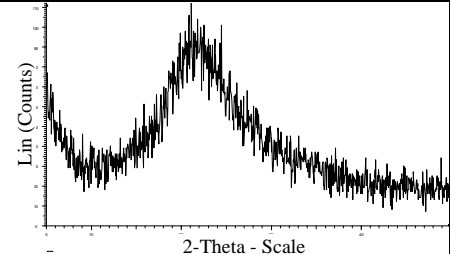
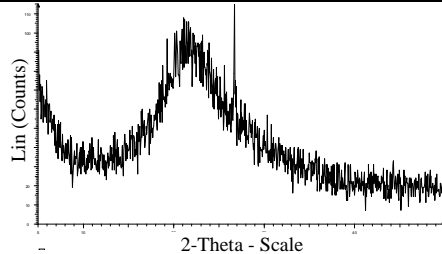
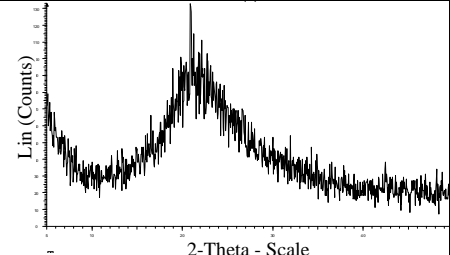
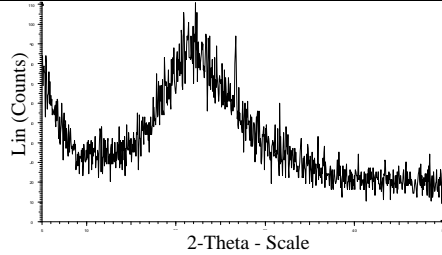
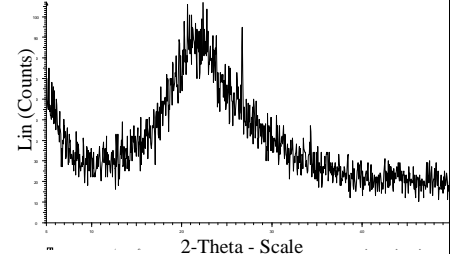
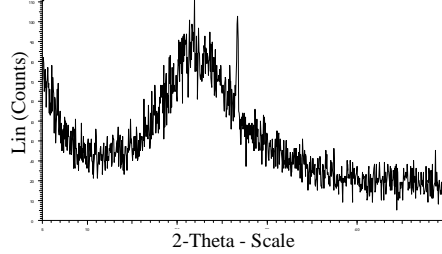
b) Ash Quality

i) Silica Structure

Table 4.133 showed that all the ash samples retained their amorphous structures despite being exposed to combustion temperatures in the excess of 700°C. This could be attributed to the short exposure time that did not allow for formation of crystals in the ash, as the crystal formation process was reported to be a ‘gradual

process' (Gorthy and Pudukottah, 1999). The crystal peaks in some of the diffractograms (at $2\theta = 20.85^\circ$ and 26.66°) were due to slight contamination from the bed media (in the form of quartz crystals), whereby trace amounts of silica sand were elutriated into the cyclone together with the ash particles.

Table 4.133: Diffractograms of fly and bottom ashes from the combustion of rice husk in the 210-mm inner diameter fluidised bed at different primary air factors (sand size = 250 – 595 μm , static bed height = $0.5 D_c$, fluidising velocity = $5 - 6 U_{mf}$)

Case Study	Primary Air Factor	Fly Ash	Bottom Ash
		PAF1	0.65
PAF2	0.81		
PAF3	1.01		
PAF4	1.41		

ii) **Residual Carbon Content**

The residual carbon contents in the ash samples (fly and bottom) obtained from the experiments were compared in Figure 4.1-24. It was observed that beyond the primary air factor of 0.8, the residual carbon content in the fly ash remained more or less similar at 7.0 wt%. As had been discussed earlier, the rate of fixed carbon burning in rice husk remained quite similar beyond the temperature of 650°C. Since the average bed temperature in this set of experiments remained above 680°C except for combustion at primary air factor of 0.65 ($T_{bed,avg} = 643^{\circ}\text{C}$), the effect of carbon oxidation in the ash beyond the primary air factor of 0.8 was rendered negligible. As for the bottom ash, the effect of primary air factor was less significant due to the fact that they were continuously retained in the bed region and thus, was continuously exposed to the necessary amount of oxygen in the air. The residual carbon contents in all four bottom ash samples (from Case PAF1 to PAF4) hovered around 3.0 wt%.

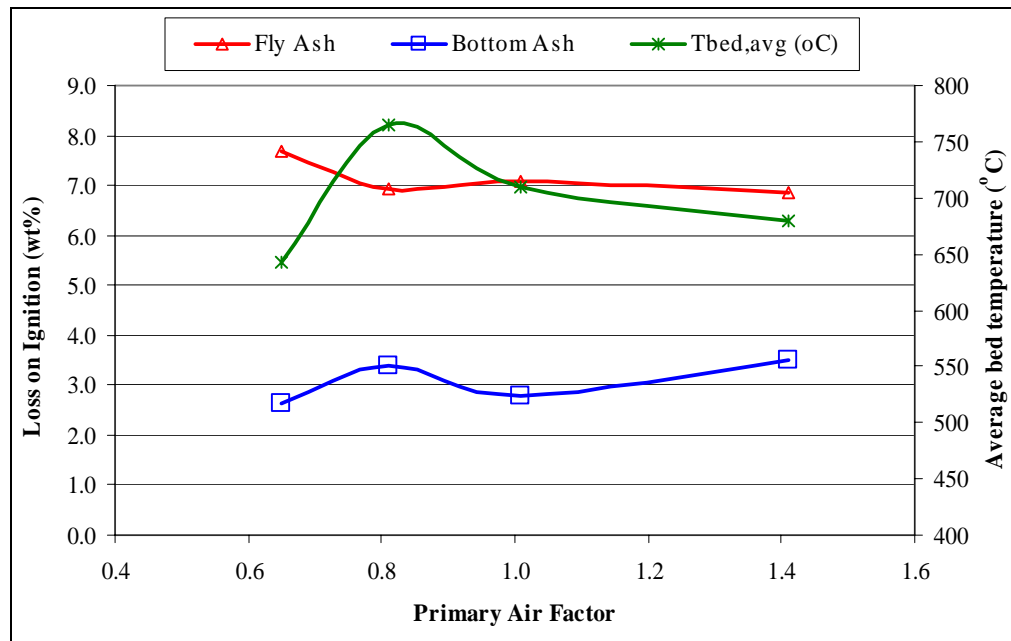


Figure 4.1-24: Residual carbon contents of ash samples from the combustion of rice husk in the 210-mm inner diameter fluidised bed at different primary air factors (sand size = 250 – 595 μm , static bed height = 0.5 D_c , fluidising velocity = 5 – 6 U_{mf})

The ash samples obtained from the current set of experiments were shown in Table 4.1-34. All the fly ash samples attained a dark shade due to the presence of unburnt chars, with the sample obtained at the primary air factor of 0.8 being relatively 'whiter' in shade due to the presence of more white ash skeletons. As for the bottom ash, all samples attained a greyish to slightly whitish shade due to the lower carbon content, which was approximately 2 times lower than that of the fly ash samples.

c) Findings

The primary air factor of 0.8 gave the highest average bed temperature (765°C). In terms of ash quality, the residual carbon content in the fly ash remained similar at primary air factors ranging from 0.8 to 1.4. The effect of primary air factor on the bottom ash was negligible as these ash were retained in the bed region, and thus were exposed continuously to the necessary amount of oxygen. All ash samples remained amorphous in structure.

Table 4.1-34: Ash samples from the combustion of rice husk in the 210-mm inner diameter fluidised bed at different primary air factors (sand size = 250 – 595 μm , static bed height = 0.5 D_c , fluidising velocity = 5 – 6 U_{mf})

Case Study			Fly Ash	Bottom Ash
PAF1	Primary Air Factor	$T_{bed,avg}$ ($^{\circ}\text{C}$)		
PAF1	0.65	643		
PAF2	0.81	765		
PAF3	1.01	710		
PAF4	1.41	680		

4.8.2 Primary-to-Secondary Air Ratio

The effects of primary-to-secondary air ratio on the combustion efficiency of rice husk in the fluidised bed were investigated at the ratios of 6:4 and 7:3. In all experiments, the static bed height was held constant at $0.5 D_c$ (250 – 595 μm sand), the fluidising velocity at approximately $5.7 U_{mf}$, and the primary air factor at 0.65. The primary-to-secondary air ratios were adjusted by varying the flowrate of the secondary air only. The combustor was pre-heated until T1 and T2 were approximately 750 – 800°C prior to commencement of rice husk feeding.

a) Temperature Profile and Combustion Characteristics

The average temperatures at different locations of the fluidised bed combustor during the combustion of rice husk at both primary-to-secondary air ratios investigated were shown in Figure 4.1-25.

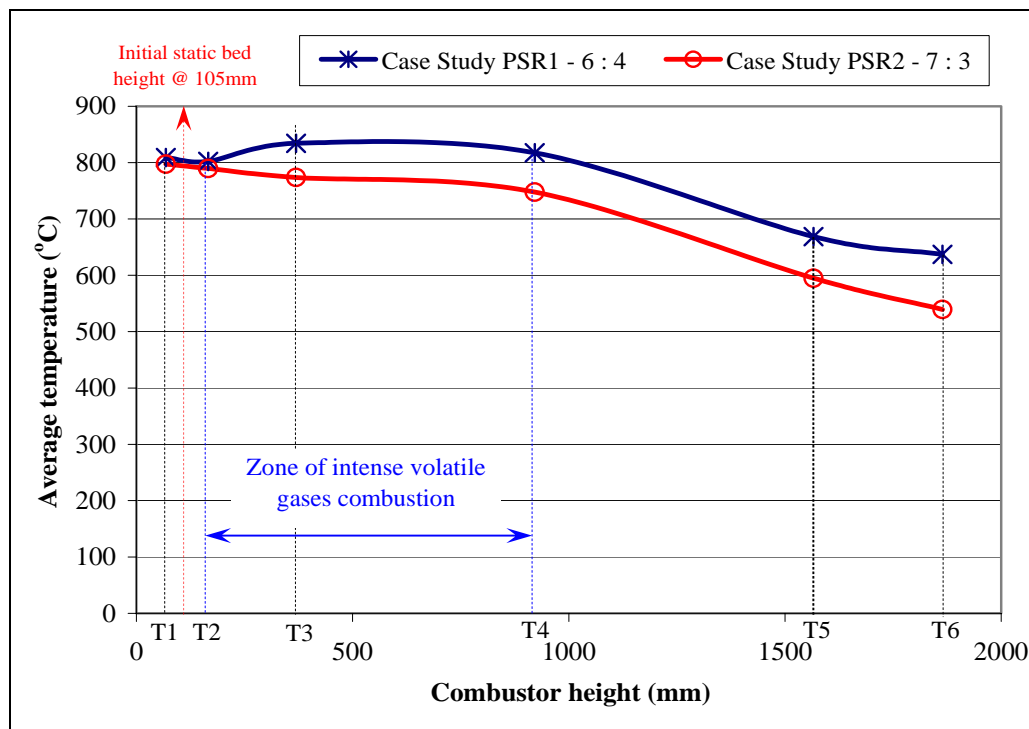


Figure 4.1-25: Average combustor temperatures during combustion of rice husk in the 210-mm inner diameter fluidised bed at different primary-to-secondary air ratios (sand size = 250 – 595 μm , static bed height = $0.5 D_c$, fluidising velocity = $5.7 U_{mf}$, primary air factor = 0.65)

The temperatures in the density phase zone were represented by thermocouples T1 and T2, which were positioned inside and at the surface of the bubbling bed, respectively. Meanwhile, thermocouples T4 to T6 represented the combustion temperatures in the dilute phase zone. It was observed that the peak temperatures as observed by Chen et al. (1998) in their studies (Figure 2-3)) were absent in the current temperature plot. This could be attributed to the absence of insulation material in the current fluidised bed combustor, allowing for heat loss to the surroundings and thus a decreasing temperature profile with the increase in height of the combustor. The temperature profile thus observed was consistent with those of Armesto et al. (2002) which conducted their rice husk combustion studies in a non-insulated combustor (Figure 4.1-26).

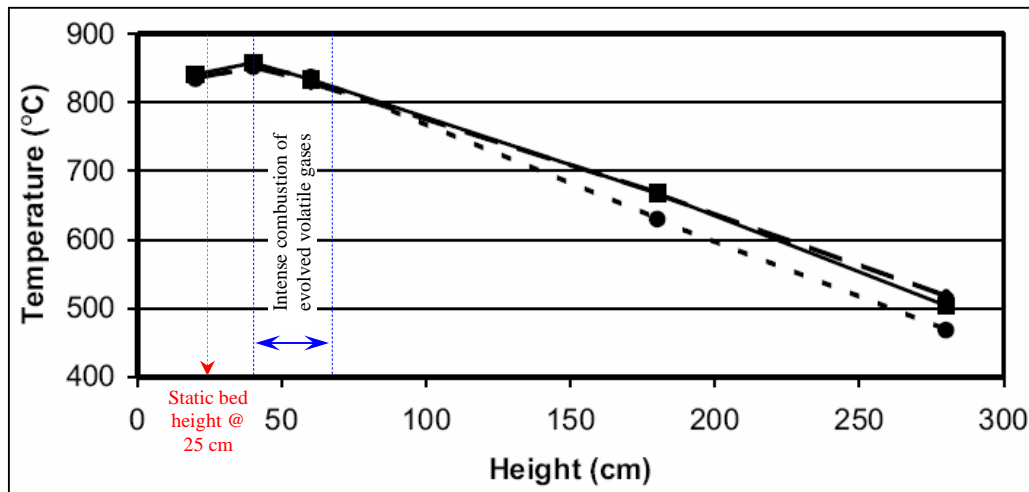


Figure 4.1-26: Temperature profile during the combustion of rice husk in a non-insulated combustor (Armesto et al., 2002)

Nevertheless, consistent with the findings of Chen et al. (1998), it was found that the higher amount of secondary airflow with the case of primary-to-secondary air ratio of 6:4 resulted in the higher freeboard temperature (T3 – T6) compared to using a primary-to-secondary air ratio of 7:3. Also, the combustion was found to be concentrated in the middle of the dilute phase zone as indicated by the higher temperatures at T3 and T4 compared to T5 and T6. The release of volatiles from the bed region resulted in high concentration of volatile gases directly above the bed region, thus the gaseous combustion was concentrated in this region and hence the

higher temperature profile. As the amount of primary air was the same in both cases, the temperatures in the bed region (T1 and T2) were similar at approximately 800°C.

b) Ash Quality

i) Silica Structure

The silica structures of all ash samples from the current experiments were compared in Table 4.1-35. In general, all ash samples retained their amorphous structure except for contamination with sand bed particles in the form of quartz peaks. The higher freeboard gas velocity in the case of using the primary-to-secondary air ratio of 6:4 resulted in significant contamination of quartz in the fly ash, as indicated by the higher crystal peaks.

Table 4.1-35: Ash samples from the combustion of rice husk in the 210-mm inner diameter fluidised bed at different primary-to-secondary air ratios (sand size = 250 – 595 μm , static bed height = 0.5 D_c , fluidising velocity = 5.7 U_{mf} , primary air factor = 0.65)





Case Study	Primary-to-Secondary Air Ratio	Freeboard Gas Velocity (m/s)	Fly Ash	Bottom Ash
PSR1	6 : 4	0.81		
PSR2	7 : 3	0.72		

ii) Unburnt Residues

The total combustibles in the resulting fly and bottom ashes from both experiments were compared in Table 4.1-36. It was observed that using at the primary-to-secondary air ratio of 7:3 gave fly ash with higher burnout (8.5 wt% total

combustibles as opposed to 11.7 wt% when using the primary-to-secondary air ratio of 6:4). This could be attributed to the higher flowrate of secondary air in the latter case, resulting in a higher gas velocity in the freeboard region and subsequently lower residence time of char particles in the freeboard. The freeboard gas velocity in the case of using primary-to-secondary air ratio of 6:4 was 0.81 m/s, which was 12.5% higher than when using the primary-to-secondary air ratio of 7:3 (freeboard gas velocity at 0.72 m/s). The lower residence time of char particles in the freeboard region resulted in insufficient time for oxidation of carbon even though the temperature was sufficiently high (550 – 800°C in both cases). The difference in shade for both fly ash samples were prominent as could be seen from Table 4.1-36, whereby the fly ash at primary-to-secondary air ratio of 6:4 was constituted mainly of black chars while that of primary-to-secondary air ratio of 7:3 was greyish-white. As for the bottom ash, there was not much difference in terms of the carbon burnout and visual appearance for both cases. This finding was duly expected due to the use of exactly the same amount of primary airflow in both cases. As such, the combustion in the density phase zone was similar in both cases, thereby giving ash of similar carbon burnout (with approximately 6.0 wt% total combustibles).

Table 4.1-36: Ash samples from the combustion of rice husk in the 210-mm inner diameter fluidised bed combustor at different primary-to-secondary air ratios (sand size = 250 – 595 μm , static bed height = 0.5 D_c , fluidising velocity = 5.7 U_{mf} , primary air factor = 0.65)

Case Study	Primary-to-Secondary Air Ratio	Freeboard Gas Velocity (m/s)	Fly Ash	Bottom Ash
PSR1	6 : 4	0.81		
Total Combustibles (wt%)			11.7	5.9
PSR2	7 : 3	0.72		
Loss on Ignition (wt%)			8.5	5.7

c) Findings

The presence of higher amount of secondary air in the fluidised bed combustor was favourable to promote higher combustion rate of volatile gases in the dilute phase zone or freeboard region. However, when the amount of primary air was held constant, the use of higher amount of secondary air resulted in higher freeboard gas velocity and subsequently lower residence time of char particles in the freeboard. This gave an overall effect of lower carbon burnout rate in the fly ash particles. In the current study, the **air split of 7:3 (primary air to secondary air) was found to**

give better fly ash quality, consistent with the findings of Chen et al. (1998) which suggested such a ratio for good combustion behaviour of rice husk in the fluidised bed.

4.8.3 Pneumatic Air Feeding Velocity

The effect of pneumatic air feeding velocity on the burnout of rice husk was investigated by varying the feeding velocity of rice husk from 0.4 – 1.4 m/s. The lowest value of terminal velocity of rice husk reported in existing literature was 0.76 m/s (Hao et al., 1995). Therefore, the upper limit of pneumatic air feeding velocity (at 1.4 m/s) used in this study was based on the consideration that the combined air flowrates (both primary air and pneumatic air) will give a final freeboard velocity (inside the 210-mm inner diameter fluidised bed) of less than 0.6 m/s at the corresponding combustion temperature in order to prevent the rice husk elutriation phenomenon. In all experiments, the static bed height was held constant at $0.5 D_c$ (250 – 595 μm sand), the fluidising velocity at approximately $3 U_{mf}$, the primary air factor at approximately 1.5 while the combustor was pre-heated until T1 and T2 were approximately 650°C prior to commencement of rice husk feeding.

a) Temperature Profile and Combustion Characteristics

The real time-temperature profiles observed during this set of experiments were included in Appendix H. Meanwhile, the average temperatures along different heights of the combustor during the combustion of rice husk at different pneumatic air feeding velocities were compared in Figure 4.1-27.

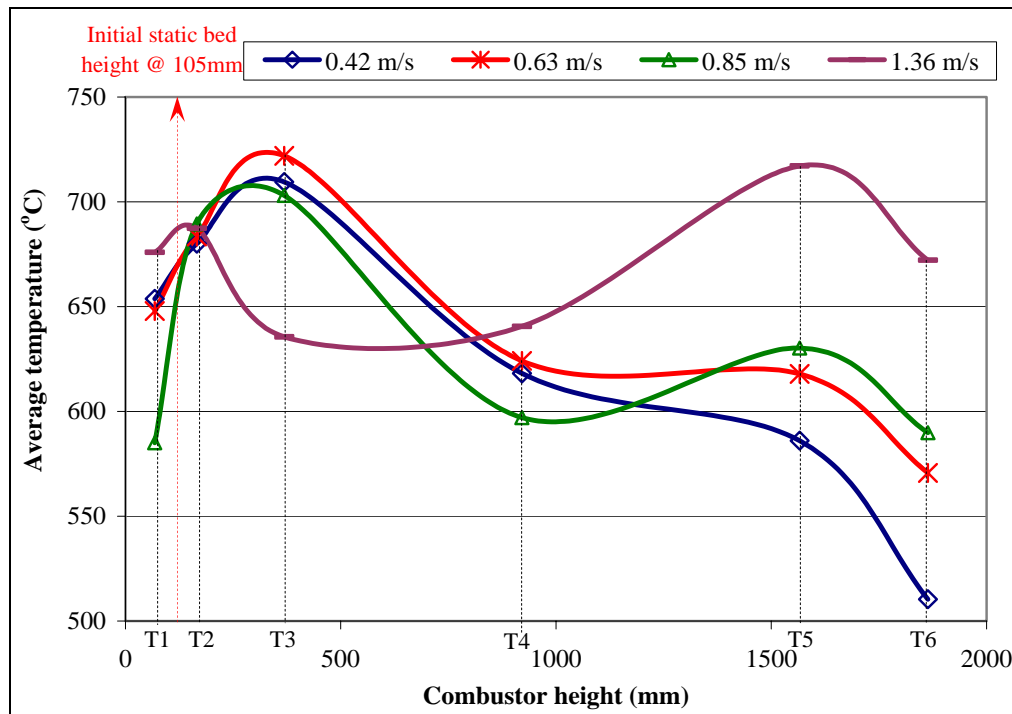


Figure 4.1-27: Temperature profile along the 210-mm inner diameter fluidised bed combustor during combustion of rice husk at different pneumatic air feeding velocities (sand size = 250 – 595 μm , static bed height = 0.5 D_c , fluidising velocity $\approx 3 U_{mf}$, primary air factor ≈ 1.5)

From Figure 4.1-27, it was observed that the temperature plots during combustion of rice husk at pneumatic air feeding velocities of 0.42 m/s and 0.63 m/s exhibited an increasing trend just above the bed region (T2 to T3), reaching a peak at T3. This region coincided with the zone of intense volatile gases combustion, thus giving rise to the high temperatures. Beyond T3, the freeboard temperatures decreased along the height of the combustor as there was a decline in the rate of volatile gases combustion. Such trend in both temperature plots were consistent with the temperature profile of rice husk combustion carried out in an insulated combustor, such as that reported by Chen et al. (1998) (who carried out their experiments in a fire-brick insulated fluidised bed combustor) and as shown in Figure 2-3. At such low pneumatic air velocities, or the equivalent amounts of pneumatic airflow, the cooling effect to the entry region (at T3) was not significant. Further, both temperature plots were also consistent with that observed by Chen et al. (1998) in their experiments (Figure 2-3) whereby higher secondary airflow resulted in higher

temperature profile at the freeboard region (T2 – T6) due to the higher amount of air available for the burning off of evolved volatile gases in the freeboard. In the current experiment, the pneumatic air used to convey the rice husk into the combustor during feeding also functioned as secondary air. As the pneumatic air feeding velocity was increased further to 0.85 m/s, the equivalent amount of airflow resulted in some degree of cooling effect spanning the height from T2 to T4. Beyond the region affected by the cooling effect, there was a steady rise in temperature indicating the burning off of volatile gases. The average bed temperature in this case (T1) was also the lowest, indicating that rice husk combustion in the bed region was not as effective compared to using pneumatic velocities of 0.42 m/s and 0.63 m/s. Such ineffective burning of rice husk in the bed region also resulted in lesser amount of volatiles gases being evolved and thus, an overall lower temperature profile compared to that observed at 0.42 m/s and 0.63 m/s. Increasing the pneumatic air feeding velocity further to 1.36 m/s resulted in the highest average bed temperature, an indication that most of the rice husk could reach the bed region and thus effective burning could take place. Such effective burning of most of the rice husk being fed into the combustor subsequently resulted in higher amount of evolved volatile gases. This was evident in the temperature plot whereby the highest peak temperature (at T5) in the freeboard region was registered by the pneumatic air velocity of 1.36 m/s, which was due to the burning off of such high amount of volatile gases. One prominently unusual feature observed for the temperature plot at pneumatic air velocity of 1.36 m/s was the sharp decline in temperature from T2 to T3. This could be attributed to the more enhanced cooling effect with the use of higher amount of pneumatic airflow in such case. There seemed to be a plateau in the temperature plot from T3 to T4, indicating that the rate of volatile gases combustion in this region remained more or less similar. However, beyond T4, there was a steady increase in temperature, due mostly to the burning of the volatile gases. The presence of the plateau in this temperature plot was unusual considering the trend of the other temperature plots (i.e. at 0.42 m/s, 0.63 m/s or 0.85 m/s). It was hypothesised that the hydrodynamics inside the combustor at this region at the pneumatic air velocity of 1.36 m/s could be significantly different from that of the other three pneumatic air feeding velocities investigated. As such, computational fluid dynamics (CFD) modelling was carried out to investigate the airflow profile inside the combustor at these pneumatic air velocities. As will be discussed in Section 5.2.1, the plateau at

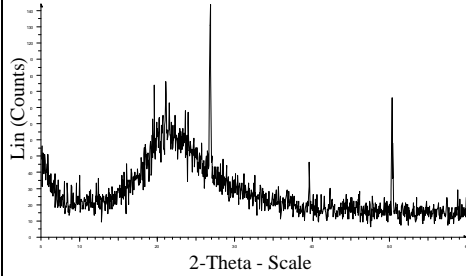
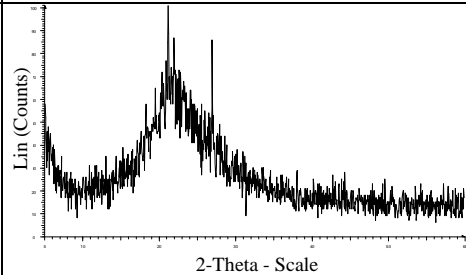
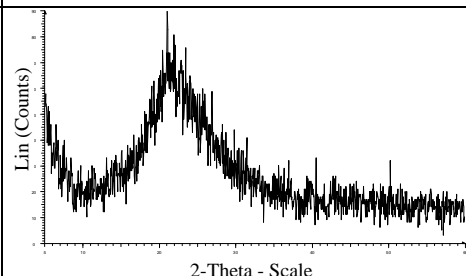
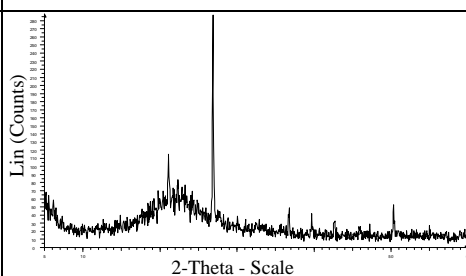
the temperature plot at the velocity of 1.36 m/s was due to the presence of a 'recirculating' zone (Figure 5-8) spanning the distance of approximately 300mm directly above the feeding port (located at the height equivalent to the location of thermocouple T3).

b) Ash Quality

i) Silica Structure

The XRD analysis results on the fly ash samples obtained from all four experiments were compared in Table 4.1-37. It was observed that except for Case PV3, all ash samples were contaminated with sand due to the presence of quartz peaks (2θ scale: primary peak 26.66° , secondary peak 20.85° , tertiary peak 50.16°). Since crystal peaks indicating the crystallisation of silica in the ash, namely cristobalite or tridymite, were absent, it could be concluded that all ash samples still retained their amorphous nature. The presence of sand impurities in the ash samples was due primarily to the short freeboard height of the fluidised bed combustor (total height at 2000mm only), which enabled the elutriation of fine sand particles together with fly ash into the cyclone. It was expected that the degree of sand contamination will be higher with the higher amount of pneumatic airflow due to the higher velocity in the combustor freeboard. However, observation on the diffractograms showed that this was not the case. Case PV2, with pneumatic air velocity 50% higher compared to Case PV1, were contaminated with less sand particles whereas Case PV3 with twice the pneumatic air velocity compared to Case PV1, were not contaminated with any sand particle. Based on these observations, it was hypothesised that the different amount of pneumatic air entering through the inclined feeding port into the combustor did alter its hydrodynamics to the extent of either increasing or decreasing the degree of sand elutriation into the cyclone.

Table 4.1-37: Diffractograms of fly ash samples from the combustion of rice husk in the 210-mm inner diameter fluidised bed at different pneumatic air feeding velocities (sand size = 250 – 595 μm , static bed height = 0.5 D_c , fluidising velocity $\approx 3 U_{mf}$, primary air factor ≈ 1.5)

Case Study	Pneumatic Air Feeding Velocity (m/s)	X-Ray Diffraction Analysis	Remarks
PV1	0.42		Amorphous, contaminated with sand particles
PV2	0.63		Amorphous, contaminated with sand particles but at concentration lower than Case PV1
PV3	0.85		Amorphous, sand-free
PV4	1.36		Amorphous, contaminated with sand particles at the highest concentration

ii) Residual Carbon Content

The burnout of rice husk particles during combustion in the fluidised bed is indicated by the residual carbon content in the resulting ash. The residual carbon contents (from loss on ignition test) in the ash samples from the experimental study

were shown in Figure 4.1-28. It was observed that the operating conditions giving the highest residual carbon content (Case PV3, with pneumatic air feeding velocity of 0.85 m/s) coincided with the lowest average bed temperature. This might indicate that very little amount of rice husk particles actually penetrated the sand bed and be burnt inside the bed, as the latter will contribute to the rise in the average bed temperature due to the heat evolved. Thus, it was hypothesised that the residence time of rice husk inside the combustor in this case was the lowest. On the other hand, the residence time of rice husk was expected to be the highest for Case PV4 (with pneumatic air feeding velocity of 1.36 m/s) as the residual carbon content in the ash was the lowest (at 2.7 wt%) and the average bed temperature was the highest (at approximately 680°C). This further indicated that most of the rice husk were retained in the bed and be burnt there, hence increasing the bed temperature. As with Case PV1 and Case PV2, since there were not much difference in the residual carbon contents and average bed temperatures (at approximately 4.0 wt% and 650°C, respectively), it was hypothesised that the residence times of burning rice husk particles in the fluidised bed remained more or less similar. Further, the total air velocity in the freeboard region of the fluidised bed combustor due to the combined airflows (primary air and pneumatic air) at different pneumatic air feeding velocities were shown in Figure 4.1-29. It was observed that the upper limit of pneumatic air feeding velocity used in this study resulted in a freeboard velocity inside the combustor of less than 0.6 m/s, which was necessary to prevent the onset of elutriation of rice husk particles from the combustor.

From the experimental study, it could be concluded that Case PV4 (with pneumatic air feeding velocity of 1.36 m/s) gave the best burnout among the range of pneumatic air feeding velocities investigated. The average bed temperature during this experiment was the highest, indicating that most of the rice husk particles were being retained and burnt in the hot bubbling bed. Consequently, the highest burnout was achieved as indicated by the lowest residual carbon content in the resulting ash.

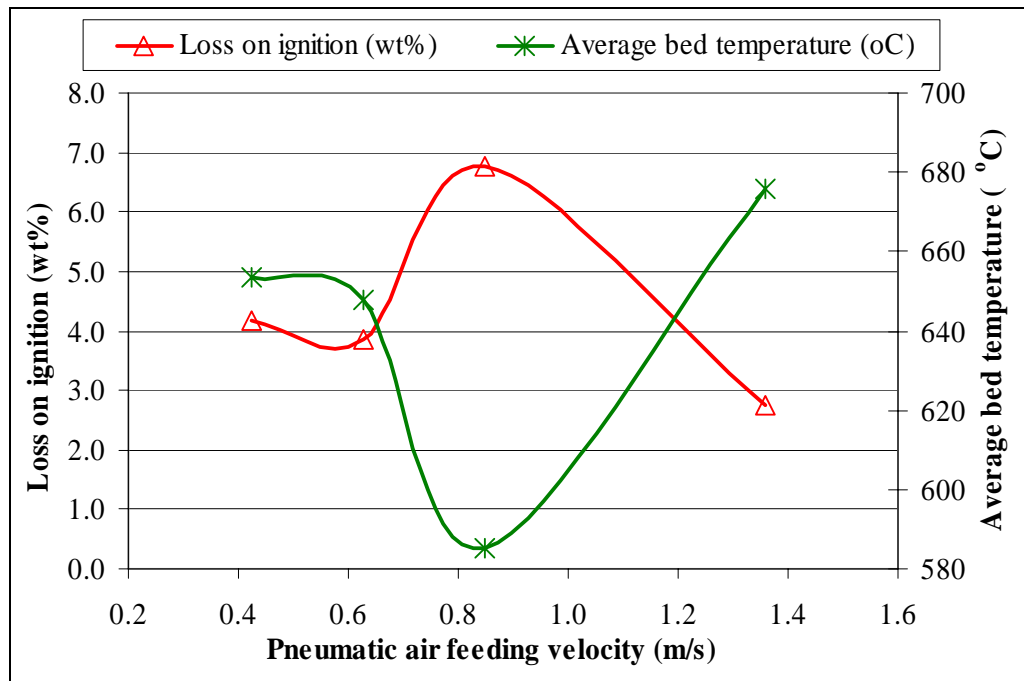


Figure 4.1-28: Average bed temperatures and residual carbon contents in ash samples from the combustion of rice husk in the 210-mm inner diameter fluidised bed at different pneumatic air feeding velocities (sand size = 250 – 595 μm , static bed height = 0.5 D_c , fluidising velocity $\approx 3 U_{mf}$, primary air factor ≈ 1.5)

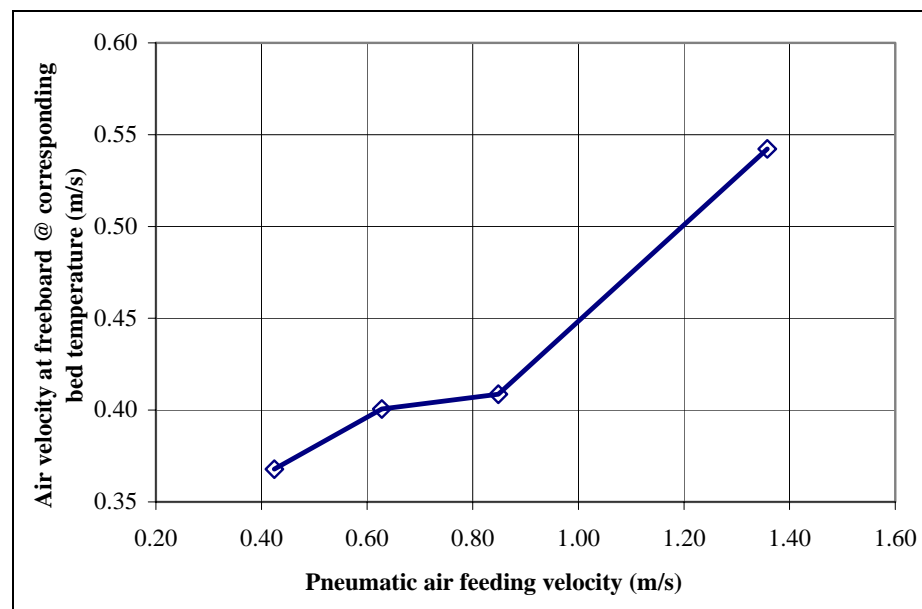
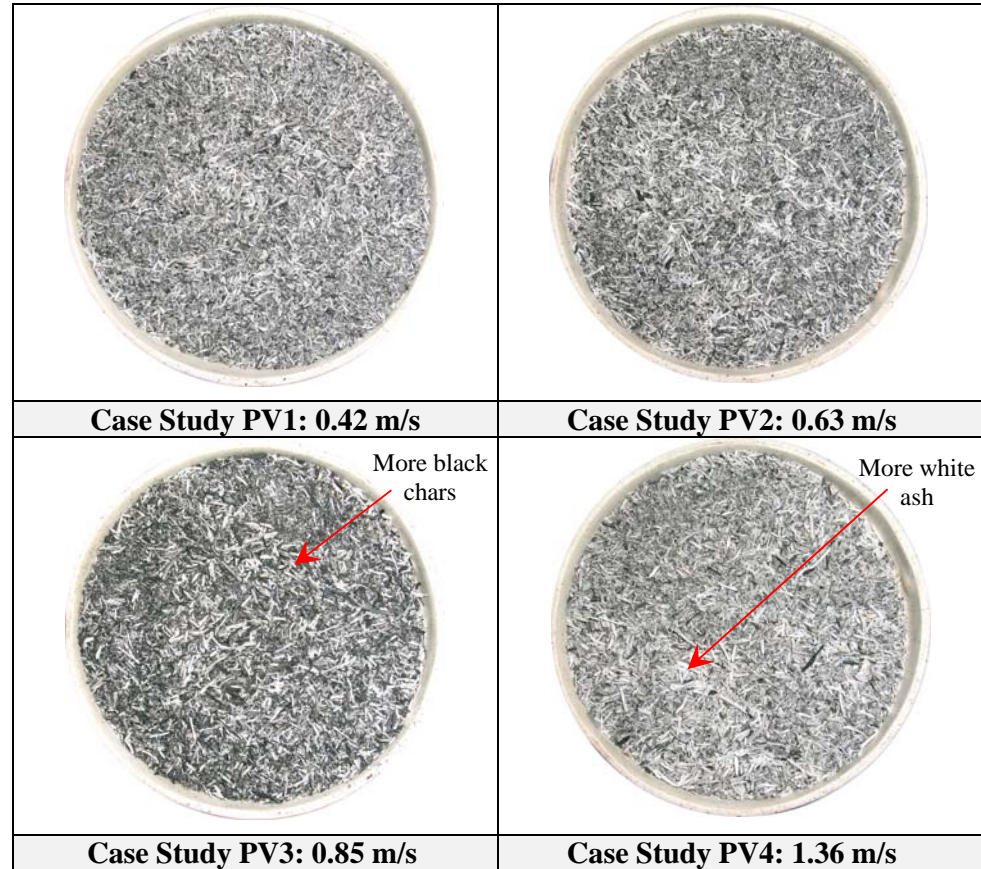


Figure 4.1-29: Total air velocity at the freeboard region of the fluidised bed combustor at different pneumatic air feeding velocities

During the experiments, the residence time of rice husk particles in the combustor could not be determined distinctly. However, it was estimated that the rice husk particles were being retained in the combustor for approximately 25 – 40 seconds (estimated by feeding a small batch of rice husk and determining the period it took for the fly ash to reach the cyclone). In addition, most of the rice husk ash collected in the cyclone still retained their skeleton-like shape (Table 4.1-38), due to the combustion of rice husk occurring according to the shrinking core model. However, it is necessary to investigate whether the bulk of the residence time is spent in the bed or freeboard region, as this will also affect the burnout rate. Higher burnout is expected to be achieved in the bed region due to the turbulence arising from the bubbling bed, which aids in the heat and mass transfer to the rice husk particles. Therefore, in order to relate the burnout of rice husk particles with their residence time in the combustor, these four experiments were modelled in FLUENT using actual experimental data wherever available. The modelling results were expected to offer significant insights as to the behaviours of the burning rice husk particles inside the combustor, which subsequently led to their burnout as reflected in the carbon contents in their ash.

Table 4.1-38: Fly ash samples from the combustion of rice husk in the 210-mm inner diameter fluidised bed at different pneumatic air feeding velocities (sand size = 250 – 595 μm , static bed height = 0.5 D_c , fluidising velocity $\approx 3 U_{mf}$, primary air factor ≈ 1.5)



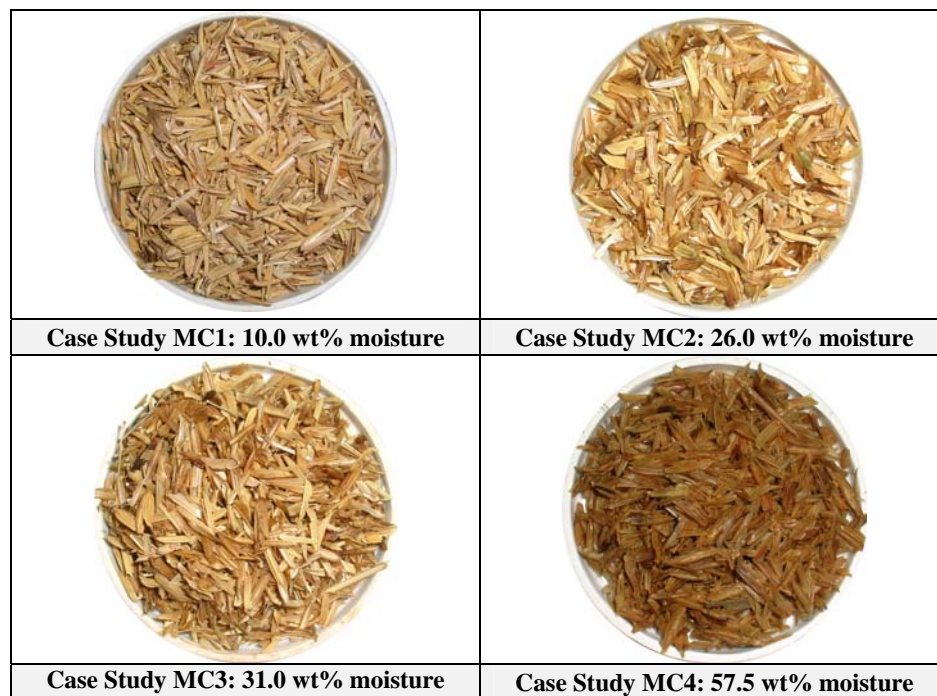
c) Findings

From the experimental study, Case PV4 (with pneumatic air feeding velocity of 1.36 m/s) gave the highest average bed temperature (at 680°C) and the lowest residual carbon content in the ash (2.7 wt%). **The onset for the formation of recirculating zone near the bed surface was observed with the use of pneumatic air feeding velocity at 1.36 m/s, which was beneficial in increasing the residence time of particles (rice husk and ash) inside the fluidised bed combustor.** The recirculating zone tended to ‘trap’ the particles and returned them to the bed region, thus increasing their carbon burnout rates.

4.9 Effect of Moisture Content in Rice Husk on Its Combustion Efficiency in Fluidised Bed

Experiments were conducted by using water-washed rice husk with moisture contents ranging from 10 – 58 wt% (Table 4.1-39). In each experiment, the static bed height was held constant at $0.5 D_c$ (250 – 595 μm sand), the fluidising velocity at approximately $3 U_{mf}$, the primary air factor at 1.2 and the oxygen level in the freeboard region (measured at the cyclone) at 6 – 12 vol%. The bed was pre-heated to 650°C prior to commencement of rice husk feeding.

Table 4.1-39: Rice husk samples used for the combustion of water-washed rice husk at different moisture contents in the 210-mm inner diameter fluidised bed combustor



a) Temperature Profile and Combustion Characteristics

Figure 4.1-30 showed the comparisons of bed temperatures during combustion of water-washed rice husk at different moisture contents in the fluidised bed combustor. Among all four moisture contents investigated, it was observed that the highest bed temperature was achieved when burning water-washed rice husk having moisture content of 26.0 wt%. The presence of the extra moisture (above the

equilibrium value at approximately 10 wt%) in the rice husk increased the bulk density of the rice husk, allowing them to penetrate the bubbling bed better thus allowing for combustion to take place and subsequently increasing the bed temperature. However, increasing the moisture content beyond 31.0 wt% resulted in a drop in bed temperature, due to the absorption of heat from the bed for the vapourisation of the moisture, which is an endothermic process. The standard deviation in the bed temperatures during combustion water-washed rice husk with both moisture contents of 31.0 wt% and 57.5 wt% were also the highest due to the inconsistent rate of feeding into the combustor. These wet rice husk particles tended to agglomerate and drop into the combustor in big clumps, lowering the bed temperature during the moisture vaporisation stage while increasing the bed temperature during the subsequent combustion process. On the contrary, the standard deviation in bed temperature was the lowest when burning water-washed rice husk with moisture content of 26.0 wt% as at this moisture content, the rice husk particles did not form clumps and therefore, consistent feeding rate could be achieved.

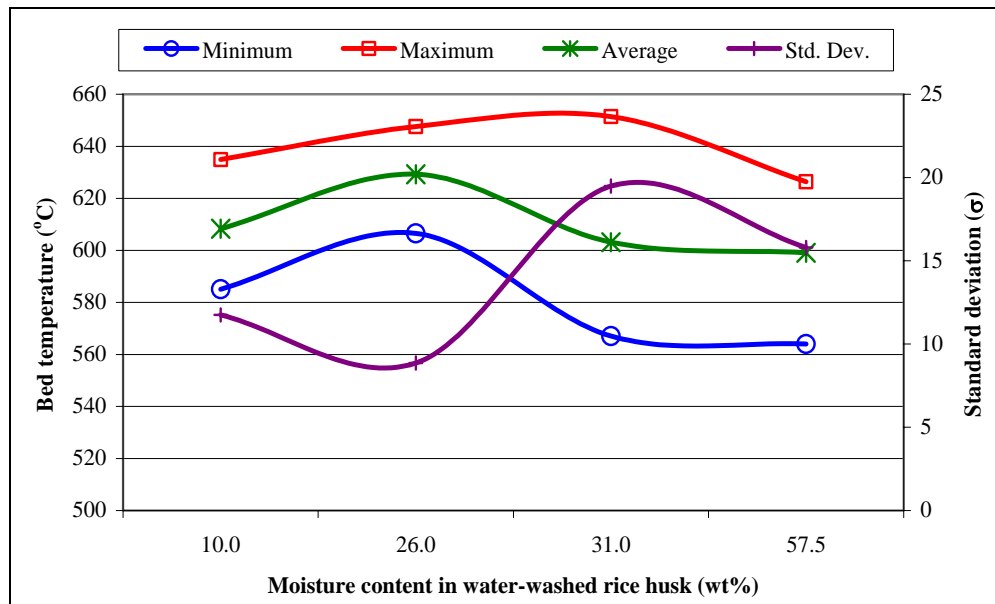


Figure 4.1-30: Comparisons of bed temperatures during the combustion of water-washed rice husk at different moisture contents in the 210-mm inner diameter fluidised bed combustor (sand size = 250 – 595 μm , static bed height = $0.5 D_c$, fluidising velocity $\approx 3 U_{mf}$, primary air factor ≈ 1.2)

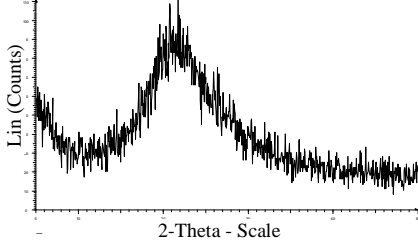
b) Ash Quality

i) Silica Structure

The silica structures of all ash samples from the current experiments were compared in Table 4.1-40. In general, all ash samples retained their amorphous structure except for some minor contamination of sand bed particles in the form of quartz peaks in three fly ash samples (from burning rice husk at moisture contents of 10 – 31 wt%).

Table 4.1-40: Diffractograms of ash samples from the combustion of water-washed rice husk at different moisture contents in the 210-mm inner diameter fluidised bed combustor (sand size = 250 – 595 μm , static bed height = 0.5 D_c , fluidising velocity $\approx 3 U_{mf}$, primary air factor ≈ 1.2)

Case Study	Moisture Content in Water-Washed Rice Husk (wt%)	Fly Ash	Bottom Ash
MC1	10.0		
MC2	26.0		
MC3	31.0		

MC4	57.5		Not available
-----	------	---	---------------

ii) Residual Carbon Content

The comparisons of residual carbon contents in the ash samples obtained while burning water-washed rice husk at different moisture contents were shown in Figure 4.1-31 while the ash samples were shown in Table 4.1-41. Due to the consistent feeding and high degree of penetration into the bed as discussed earlier, combustion of water-washed rice husk with 26.0 wt% moisture resulted in the lowest residual carbon content in both the fly ash (at 2.4 wt%) and bottom ash (0.9 wt%). At the moisture content of 26.0 wt%, the water-washed rice husk could penetrate the bubbling bed better compared to the relatively dry rice husk particles (at moisture content of 10.0 wt%), leading to higher combustion rate in the bed and thus lower residual carbon content in the ash. Beyond the moisture content of 31.0 wt%, the increased amount of moisture in the rice husk significantly lowered the bed temperature to less than 600°C, which was deemed ineffective to achieve good carbon oxidation rate considering their short residence time in the bed.

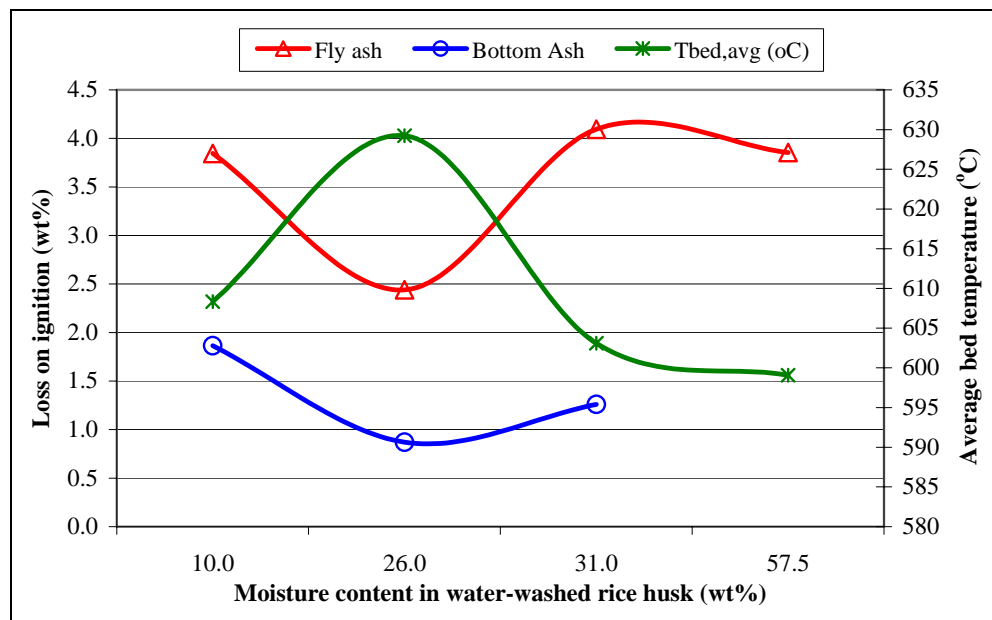








Figure 4.1-31: Comparisons of residual carbon contents of ash samples from the combustion of water-washed rice husk at different moisture contents in the 210-mm inner diameter fluidised bed combustor (sand size = 250 – 595 μm , static bed height = 0.5 D_c , fluidising velocity $\approx 3 U_{mf}$, primary air factor ≈ 1.2)

Hence, it could be concluded that using the water-washed rice husk with moisture content of 26.0 wt% gave the best temperature profile and ash quality compared to water-washed rice husk at other moisture contents.

Table 4.1-41: Ash samples from the combustion of water-washed rice husk at different moisture contents in the 210-mm inner diameter fluidised bed combustor (sand size = 250 – 595 μm , static bed height = 0.5 D_c , fluidising velocity $\approx 3 U_{mf}$, primary air factor ≈ 1.2)

Case Study	Moisture Content in Water-Washed Rice Husk (wt%)	Fly Ash	Bottom Ash
MC1	10.0		
MC2	26.0		
MC3	37.0		

MC4	57.5		Not available
-----	------	--	---------------

c) Findings

Using water-washed rice husk with moisture content of 26.0 wt% gave the best combustion characteristics in terms of the highest bed temperature and the lowest residual carbon content in ash (fly and bottom) amongst the range of moisture contents investigated. This could be attributed to the increased bulk density in rice husk due to the presence of moisture, allowing for better penetration into the bubbling bed region. Beyond the moisture content of 31.0 wt%, the increased amount of moisture in the water-washed rice husk tended to lower the bed temperature significantly (due to more heat absorbed as latent heat of vaporisation) as well as the formation of clumps that led to inconsistent feeding.

4.10 Effect of Feeding Design on the Combustion Efficiency of Rice Husk in Fluidised Bed

4.10.1 Vortex Feeding

The effect of vortex feeding on the combustion of rice husk in the fluidised bed was investigated by first carrying out the combustion process utilising the inclined feeding port (Plate 4.1-13) as a means for feeding rice husk into the combustor. The static bed height was held constant at $0.5 D_c$ (250 – 595 μm sand), the fluidising velocity at approximately $3 U_{mf}$, the primary air factor at 1.2 while the bed was pre-heated to 650°C prior to commencement of rice husk feeding. The same experiment was then repeated in the same combustor by replacing the inclined feeding port with the inclined, tangential feeding port (Plate 4.1-14).

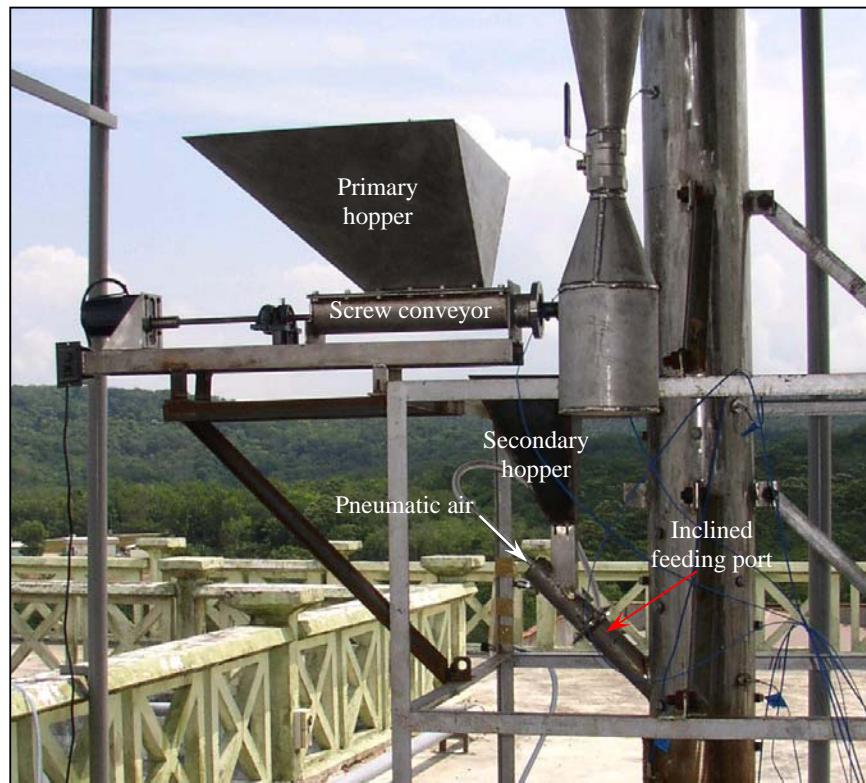


Plate 4.1-13: The inclined feeding port at the 210-mm inner diameter fluidised bed combustor

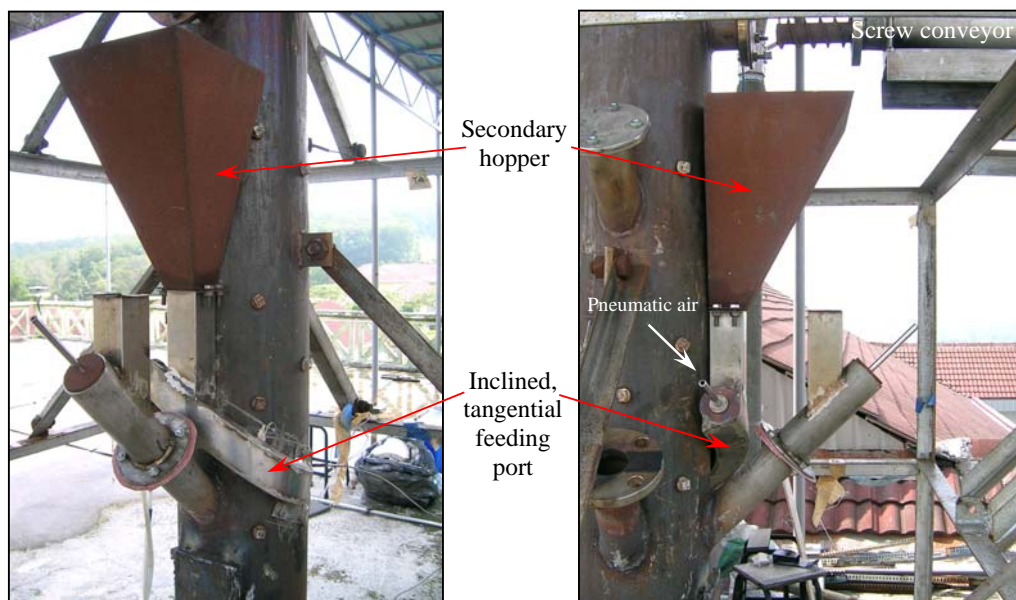


Plate 4.1-14: The inclined, tangential feeding port at the 210-mm inner diameter fluidised bed combustor

a) Temperature Profile and Combustion Characteristics

The real-time temperature profiles during combustion of rice husk in the 210-mm inner diameter fluidised bed combustor utilising the inclined feeding port and the inclined, tangential feeding port were shown in Figure 4.1-32 and Figure 4.1-33, respectively. Meanwhile, the average temperatures along different heights of the combustor during the combustion process (rice husk feeding period) were compared for each type of feeding method in Figure 4.1-34.

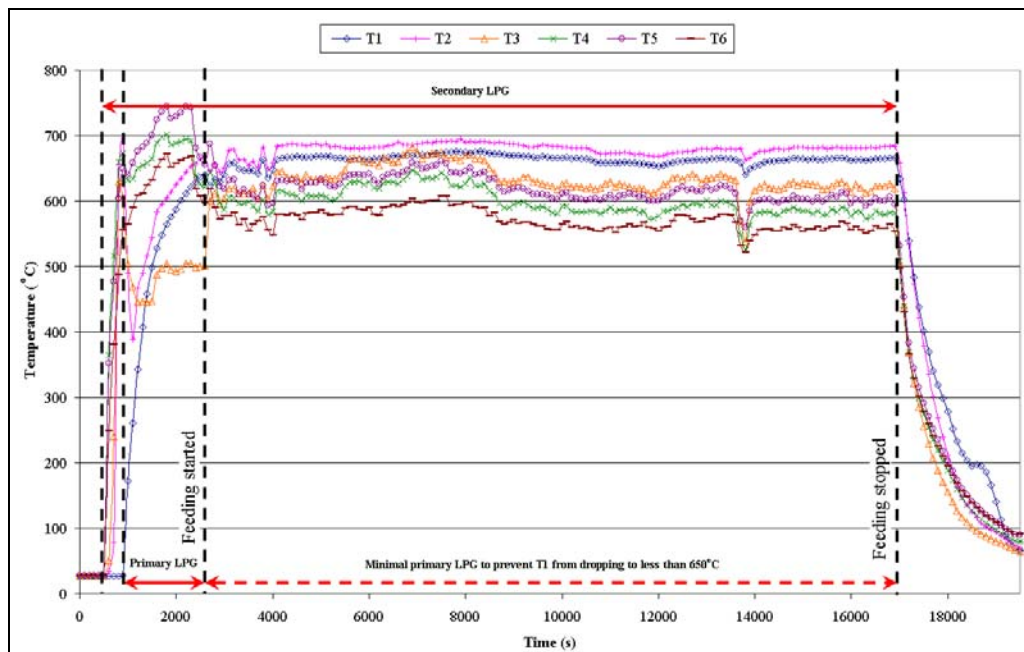


Figure 4.1-32: Real-time temperature profiles during combustion of rice husk in the 210-mm inner diameter fluidised bed combustor with inclined feeding port (Case Study FM1) (sand size = 250 – 595 μm , static bed height = $0.5 D_c$, fluidising velocity $\approx 3 U_{mf}$, primary air factor ≈ 1.2)

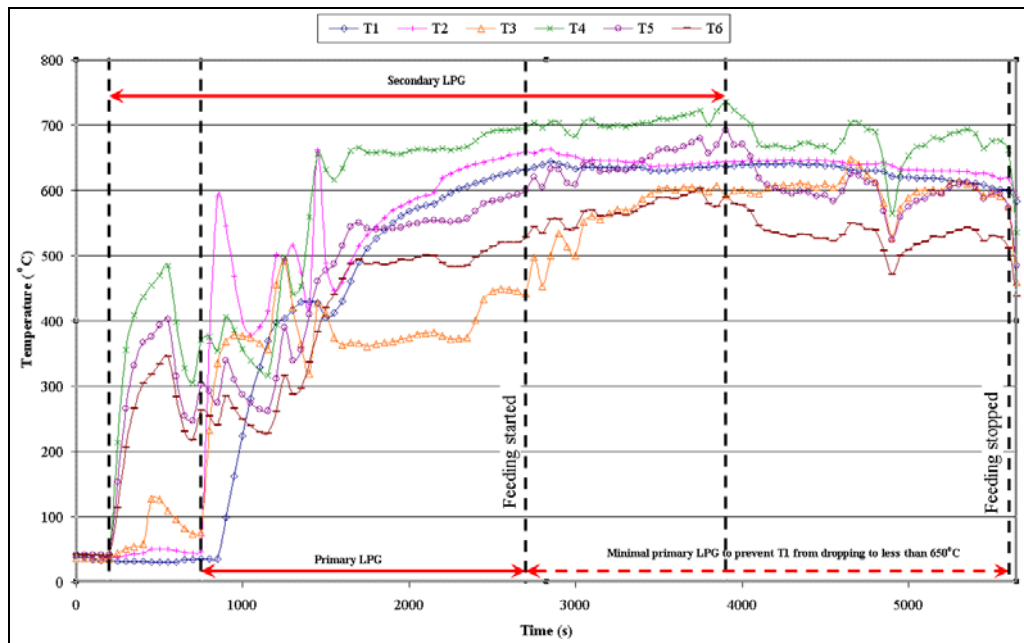


Figure 4.1-33: Real-time temperature profiles during combustion of rice husk in the 210-mm inner diameter fluidised bed combustor with inclined, tangential feeding port (Case Study FM2) (sand size = 250 – 595 μm , static bed height = 0.5 D_c , fluidising velocity $\approx 3 U_{mf}$, primary air factor ≈ 1.2)

Based on Figure 4.1-32 and Figure 4.1-33, it was observed that the real-time temperature profiles for the combustion of rice husk in the fluidised bed combustor with inclined feeding port was steadier with minimal fluctuations compared to that of using the inclined, tangential feeding port. Combustion of rice husk by feeding them through the inclined feeding port was more easily controlled due to the stable temperature profile compared to that of the inclined, tangential feeding port. Although the temperatures at the bed region (as indicated by T1 and T2) were quite steady during the feeding period for the latter case, the freeboard temperatures however showed great fluctuations. In addition, as the experiment progressed, the temperature in the freeboard region reached up to as high as 740°C (T4), which necessitated the need to switch off the secondary burner to prevent the possibility of ash crystallisation due to exposure to temperature above its crystallisation point.

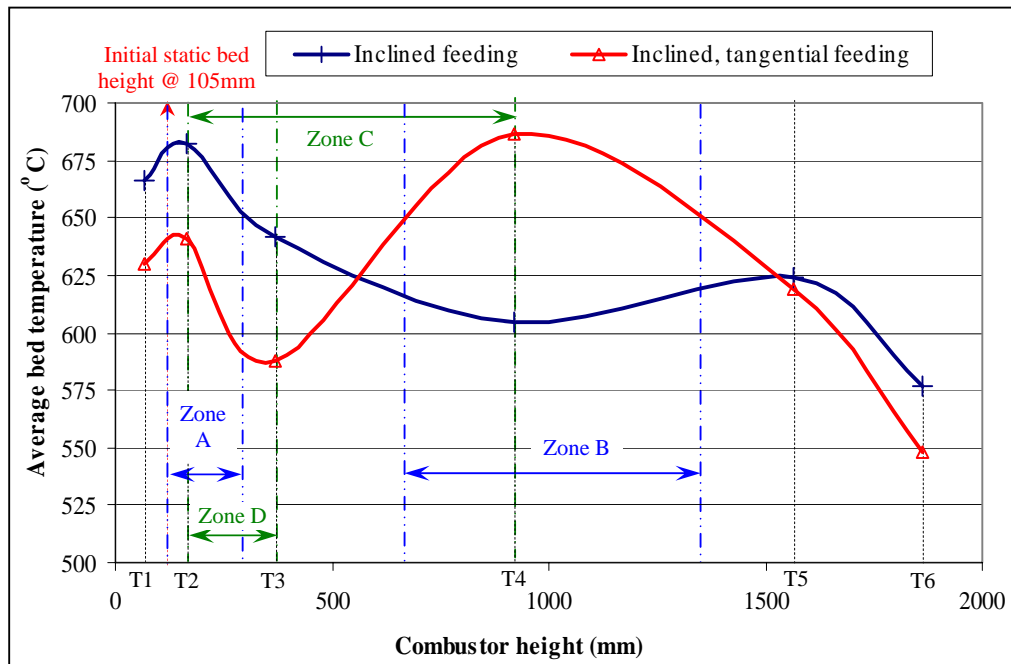


Figure 4.1-34: Average combustor temperatures during combustion of rice husk in the 210-mm inner diameter fluidised bed combustor utilising different feeding methods (sand size = 250 – 595 μm , static bed height = 0.5 D_c , fluidising velocity $\approx 3 U_{mf}$, primary air factor ≈ 1.2)

Based on Figure 4.1-34, it was observed that the region of intense volatile gases combustion was concentrated just above the bed region for the case with inclined feeding due to the peak in the temperature plot (Zone A). This region was shifted higher to the freeboard region (Zone B) for the case with inclined, tangential feeding. The temperature plot during feeding of rice husk via the inclined feeding port exhibited an overall decreasing trend along the combustor height. Such decreasing trend was consistent with combustion of rice husk performed in a non-insulated combustor due inherent significant amount of heat loss to the surroundings (Armesto et al., 2002 as in Figure 4.1-26). However, the temperature plot for inclined feeding in Figure 4.1-34 exhibited a sharp decline spanning one-third the height of the combustor from T2 to T4 (Zone C), which was contributed by the cooling effect of pneumatic air entering together with the rice husk into the inclined feeding port at the height equivalent to the location of thermocouple T3. Beyond Zone C, there was a slight increase in temperature along such plot with a minor peak at T5, indicating the probable burning off of residual volatile gases in this region. As

for the case with the inclined, tangential feeding, the temperature plot exhibited two sharp peaks, one at the region of intense volatile gases combustion (Zone B) as discussed earlier and another at the bed region. The even sharper decline (Zone D) in the temperature plot in this case compared to that of the inclined feeding indicated a more significant air cooling effect. The tangential feeding port induced a swirling flow effect to the entering pneumatic air (at ambient temperature) and such 'recirculating' flow at Zone D probably increased the residence time of the relatively cool pneumatic air in this region, contributing to an overall sharp decrease in temperature. Such 'swirling, recirculating flow region was proven to exist from the results of the computational fluid dynamics (CFD) modelling of this particular experiment, as will be discussed in Section 5.2.2 (Figure 5-14). Beyond Zone D, there was a steady increase in temperature indicating the onset of burning off of the evolved volatile gases, which subsequently led to the peak in Zone B.

Comparisons of average combustor temperatures during both experiments (as shown in Figure 4.1-34) showed that the combustor temperatures during combustion of rice husk utilising the inclined feeding method were generally higher by 30 – 50°C (except for T4 and T5) than that utilising the inclined, tangential feeding method. The exceptionally high temperature difference in the bed region (T1 and T2) between both experiments were due to the accumulation of most of the rice husk ash (estimated to be up to 75% of the total ash amount) in the bed in the case of feeding via the inclined, tangential feeding port. The amount of fly ash collected in the cyclone when feeding using the inclined, tangential feeding method was relatively little compared to that using the inclined feeding port, whereby most of the ash was collected in the cyclone with minimal amount being retained in the bed as bottom ash. Due to such accumulation in the former, the sand bed became thicker as the experiment progressed and thus, part of the heat evolved was also absorbed by the significant amount of ash accumulating in the bed. This resulted in the lower average bed temperature at approximately 630°C compared to approximately 670°C for the case of feeding via the inclined feeding port although feeding for both experiments were initiated at similar bed temperatures (640 – 650°C). The heat absorbed by the accumulated ash in the sand bed could be significant due to the high heat capacity of the ash, as shown in Table 4.1-42, which was estimated to be approximately 70% higher than that of the silica sand used as the bed material.

Further, as it was observed that most of the rice husk particles were penetrating the bubbling sand bed upon entry from the inclined, tangential feeding port, the heat in the bed was also absorbed by these rice husk particles. Such geometrical design of the feeding port imparted a tangential velocity component to the pneumatic air carrying the rice husk into the combustor, resulting in a highly turbulent swirling flow which subsequently caused the rice husk particles to impact the wall, lose their momentum and slide down to the bed. The heating capacity of rice husk was predicted to be even higher than that of silica sand or the silica in the ash (Table 4.1-42). Such phenomena resulted in the overall lower bed temperature when feeding was by means of the inclined, tangential feeding port.

Table 4.1-42: Heat capacities of materials used in the experimental study

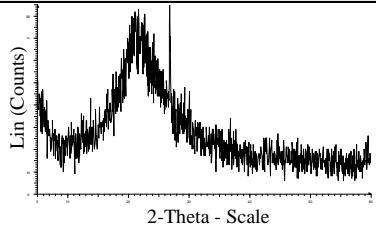
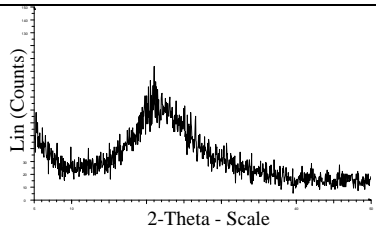
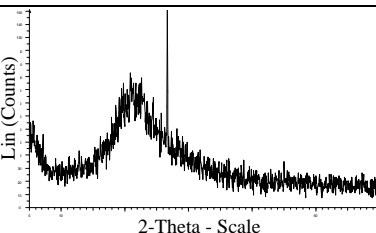
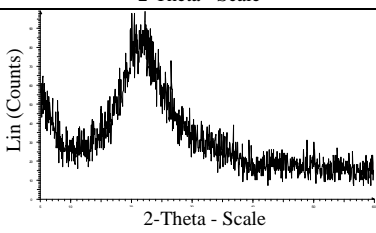
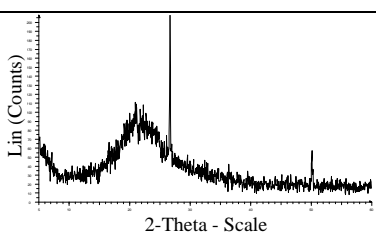
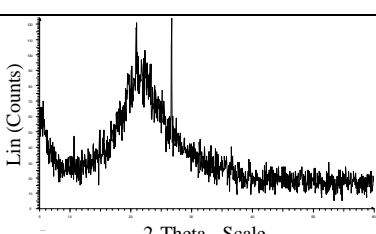
No.	Material	Value [J/(g • °C)]	Reference	Remarks
1	Silica sand	0.799	Perry et al. (1997)	-
2	Rice husk	2.094	Kaupp (1984)	Average value for wood, assumed to be applicable for rice husk as value for rice husk is not available
3	Rice husk ash	1.327	Perry et al. (1997)	Value for silica, assumed be applicable for rice husk ash as >95 wt% of rice husk ash is silica

Hence, based on the temperature profiles and combustion behaviours observed during the combustion of rice husk utilising both feeding methods, it was concluded that feeding via the inclined feeding port was better in terms of temperature control and ash collection. The accumulation of ash as bottom ash in the case of feeding via the inclined, tangential feeding port eliminated the possibility of continuous operation as these bottom ash need to be purged out occasionally to prevent the changes in mixing behaviours and bed hydrodynamics as the bed got thicker with time.

b) Ash Quality***i) Silica Structure***

The silica structures of the ash samples obtained from the combustion of rice husk in the 210-mm inner diameter fluidised bed combustor using different feeding methods were compared in Table 4.1-43. All the ash samples were found to be still in amorphous form, but were contaminated with silica sand particles (in the form of quartz crystals at primary peak position of 26.66° and secondary peak position at 20.85°) with the exception of Sample FM2-a.

Table 4.1-43: Comparisons of silica structures of ash samples from the combustion of rice husk in the 210-mm inner diameter fluidised bed with different feeding methods (sand size = 250 – 595 μm , static bed height = 0.5 D_c , fluidising velocity $\approx 3 U_{mf}$, primary air factor ≈ 1.2)

Feeding Method	Sample	Ash Sample	Remarks
Inclined feeding port (Case Study FM1)	Fly ash (Sample FM1-a)		Amorphous but contaminated with trace amount of silica sand (quartz primary peak at 35 counts per second, cps)
	Bottom ash (Sample FM1-b)		Amorphous and sand-free
Inclined, tangential feeding port (Case Study FM2)	Fly ash (Sample FM2-a)		Amorphous but contaminated more sand particles compared to Sample FM1 (quartz primary peak at 150 cps)
	Bottom ash - first purge (Sample FM2-b)		Amorphous and sand-free
	Bottom ash - second purge (Sample FM2-c)		Amorphous but contaminated with more sand particles compared to Sample FM2-a (quartz primary peak at 205 cps)
	Bottom ash - final purge (Sample FM2-d)		Amorphous but contaminated with more sand particles compared to Sample FM2-c (quartz primary peak at 125 cps and secondary quartz peak at 120 cps)

ii) Residual Carbon Content

The appearance, residual carbon content and particle size of the ash samples from both experiments were compared in Table 4.1-44. It was observed that although the residual carbon contents for the fly ash from both feeding methods (Sample FM1-a and Sample FM2-a) were similar, the fact that the ash particles in the latter were broken in tiny fragments and that these fragments (white ash and black char) were mixed homogeneously, resulted in an overall darker shade of Sample FM2-a compared to Sample FM1-a. In Sample FM1-a, the ash particles were coarser in size compared to Sample FM2-a, and consisted of slightly-broken white ash and char fragments. These relatively bigger fragments could be distinguished in a distinct manner with each other; therefore the ash appeared to be in a lighter shade as the black char were present as specks of black amongst the mostly white ash.






The bottom ash obtained from feeding via the inclined, tangential feeding port was found to be finer and whiter (i.e. lower residual carbon content) as they were purged out in different stages (Table 4.1-44). Ash particles obtained from the last purge (Sample FM2-d) were the finest in size and the whitest, containing residual carbon of only 1.0 wt%. This was because most of the rice husk particles were directed towards the bed upon entering the inclined, tangential feeding port and as such, their degree of penetration and burning in the bed was high. The turbulence in the bed caused by the vigorous bubbling action aided in breaking down the resulting skeleton-like shape of the char/ash into smaller fragments, thereby releasing the entrapped carbon and making them more readily available for further conversion. Also, as the particle density of char ($400 - 560 \text{ kg/m}^3$) (as determined experimentally and as reported by Zevenhoven and Järvinen, 2002; Watari et al., 2003; Bishnoi et al. 2004) were lower than that of white siliceous ash ($1800 - 2100 \text{ kg/m}^3$) (Yalçın and Sevinç, 2001; Nehdi et al., 2003; Feng et al., 2004), most of the white ash tended to accumulate in the bed whereas the relatively lighter char flew out towards the cyclone and be collected as fly ash. In comparison, the bottom ash when feeding through the inclined feeding port (Sample FM1-a) was coarser and contained higher carbon content (at 1.3 wt%).

The shape and size of the ash particles obtained from the combustion of rice husk in fluidised bed combustors varies according to the mixing and combustion

characteristics that take place, and were able to give some insights as to the degree of penetration of rice husk into the sand bed and subsequently, the degree of burning taking place in the bed. The comparisons of the shapes and sizes of rice husk at different stages of processing were shown in Table 4.1-45. Originally, rice husk has a boat-like shape consisting of two interlocking halves. Upon the release of volatiles during the devolatilisation stage, the resulting black char retained the skeleton-like shape, which was brittle and could easily be broken into smaller fragments. The fly ash particles obtained from the combustion of rice husk in the fluidised bed with inclined feeding port were observed to be broken down into smaller fragments, thereby indicating that the rice husk did penetrate and get burnt in the sand bed to a certain degree. Much finer particle size was observed for the bottom ash obtained using the inclined, tangential feeding method. This was due to the constant attrition amongst the sand and ash particles in the bed due to the vigorous bubbling action. These bottom ash particles had been broken in tiny fragments and were comparable to ground ash, which resembled powder form.

Comparisons among the ash samples from both experiments (inclined feeding and inclined, tangential feeding) showed that apart from the difference in particle size, there was no difference in the residual carbon content of the fly ash (at 1.9 wt%). The bottom ash particles from the latter case contained even lower residual carbon content (1.0 – 1.7 wt%) and were much finer in size. However, the drawback was that these bottom ash particles were retained in the sand bed and could not be recovered during the experiment. Unless a method of bleeding off the accumulated bottom ash in the sand bed is developed, this accumulation problem could lead to changes in the bed mixing and combustion characteristics, and could be detrimental to the overall operation of the fluidised bed. Hence, taking into consideration that the continuous operation of the fluidised bed is desired, whereby ash with low residual carbon content could be collected continuously from the cyclone, the experimental settings utilising the inclined feeding port is more preferable. Although the size of the particles collected from this feeding method is coarser, it does not pose a problem as these particles could be easily grounded to the desired size range due to its brittle nature.

Table 4.1-44: Ash samples from the combustion of rice husk in the 210-mm inner diameter fluidised bed with different feeding methods (sand size = 250 – 595 μ m, static bed height = 0.5 D_c , fluidising velocity $\approx 3 U_{mf}$, primary air factor ≈ 1.2)

Feeding Method	Sample	Ash Sample	Residual Carbon Content (wt%)	Qualitative Comparison of Particle Size and Colour
Inclined feeding port (Case Study FM1)	Fly ash (Sample FM1-a)		1.9	Coarse, white ash in the form of broken fragments of rice husk skeleton, broken fragments of char skeletons scattered amongst white ash
	Bottom ash (Sample FM1-b)		1.3	Finer than Sample FM1-a, broken fragments of char skeletons scattered amongst white ash
Inclined, tangential feeding port (Case Study FM2)	Fly ash (Sample FM2-a)		1.9	Finer than Sample FM1-a, complete absence of any skeleton-like shape, white ash and char homogeneously mixed resulting in overall darker shade than Sample FM1
	Bottom ash - first purge (Sample FM2-b)		1.7	Finer and whiter shade compared to Sample FM2-a
	Bottom ash - second purge (Sample FM2-c)		1.1	Finer and whiter in shade than Sample FM2-b

	Bottom ash - final purge (Sample FM2-d)		1.0	Very fine in size (powder-like) and whiter in shade than Sample FM2-c
--	--	---	-----	---

Table 4.1-45: Comparisons of physical appearances of different particles from the combustion of rice husk in fluidised bed combustor

Sample	Ash Sample	Qualitative Comparison of Particle Shape and Structure
Whole rice husk (as received)		Boat-like shape and rigid skeleton-like shape
Rice husk char		Retained skeleton-like shape similar to rice husk, brittle
Sample FM1		Skeleton-like shapes been broken into smaller fragments, brittle
Sample FM2-c		Absence of skeleton-like shape



iii) *Particle Size*

1) Fly Ash

The resulting fly and bottom ashes were subjected to particle screen analysis to determine their size ranges, the results of which were shown in the following histograms. The fly ash from Case FM1: Inclined feeding (Sample FM1-a) consisted mainly of particles in the size range of 75 – 500 μm (94%) with the majority being in the range of 75 – 300 μm (78%) as shown in Figure 4.1-35. The volume-surface mean diameter, D_{vs} of these fly ash particles was 190 μm . Meanwhile, the fly ash from Case FM2: Inclined, tangential feeding (Sample FM2-a) consisted primarily of particles in the size range of less than 300 μm (94%) as shown in Figure 4.1-35, with a volume-surface mean diameter, D_{vs} of 83 μm . An approximately 6% of these particles were in the size range of 300 – 500 μm , with negligible amount in the excess of 500 μm . In general, the particle size of Sample FM1-a was coarser compared to that of Sample FM2-a.

Therefore, in the CFD modelling study (Section 5.2.2), it was expected that in Model FM-A (representing Case FM1: Inclined feeding), burnt rice husk particles in the excess of 1000 μm will be retained in the bed whereas particles of less than 1000 μm will be elutriated into the cyclone. As for Model FM-B (representing Case FM2: Inclined, tangential feeding), it was hypothesised that the burnt rice husk particles in the excess of 500 μm will be retained inside the bed whereas particles of less than 500 μm will be elutriated into the cyclone.

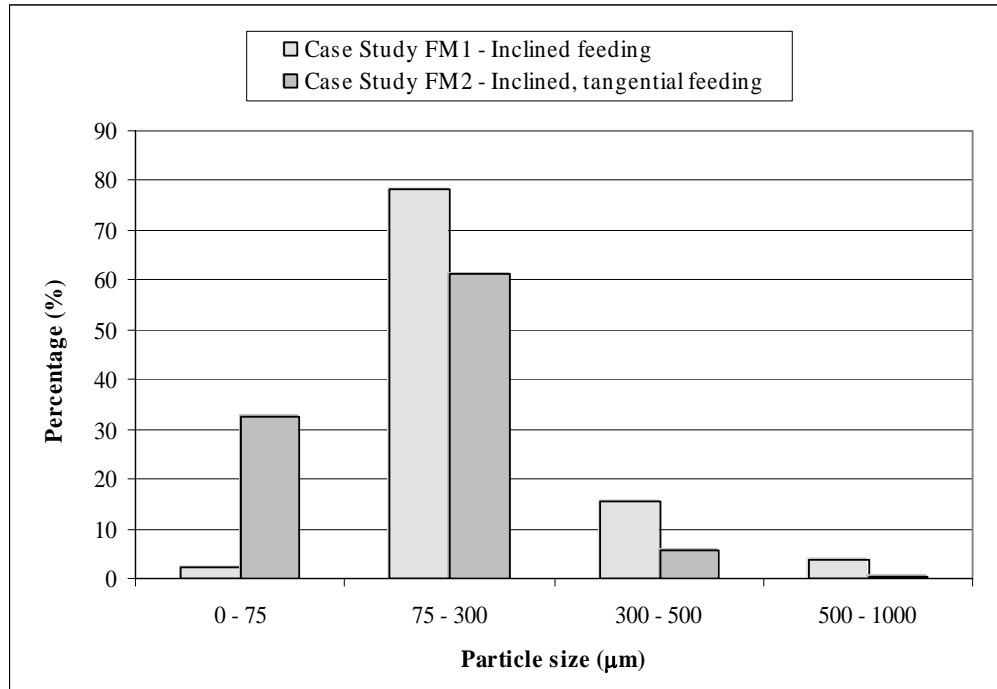


Figure 4.1-35: Histogram of particle size distribution for fly ash from the combustion of rice husk in the 210-mm inner diameter fluidised bed combustor with different feeding methods (sand size = 250 – 595 µm, static bed height = 0.5 D_c , fluidising velocity $\approx 3 U_{mf}$, primary air factor ≈ 1.2)

2) Bottom Ash

Based on Figure 4.1-36, the bottom ash from Case FM1: Inclined feeding (Sample FM1-b) consisted mostly of particles less than 500 µm (91.5%) with a volume-surface mean diameter of 120 µm. Meanwhile, the majority of the bottom ash from Case FM2 (Sample FM2-b) was in the size range of 75 – 500 µm (86.5%). The volume-surface mean diameter of these particles was calculated to be 142 µm. In Case FM2: Inclined, tangential feeding, since it was expected that the burnt rice husk particles in the excess of 500 µm will be retained in the bed, the results on this screen analysis seemed contradictory. Nonetheless, this phenomenon was explicable as once retained in the bed, the vigorous bubbling action of the fluidised bed tended to break down these particles into smaller fragments, thereby resulting in the particle size of the bottom ash being in the range of less than 500 µm. Within Case FM2, compared to the fly ash, the bottom ash consisted more of particles in the range of 300 – 500 µm and less of particles in the range of less than 75 µm. This was because

smaller-sized particles (less than 75 μm) were easily entrained into the gas stream and elutriated out of the combustor as fly ash, resulting in lesser amount being retained as bottom ash in the bed. Coarser particles (300 – 500 μm) were not that easily entrained into the gas stream, therefore most were retained in the bed as bottom ash. Besides, the constant attrition in the bed region tended to break down the larger particles (more than 500 μm) into smaller fragments, thus contributing to the overall amount of the 300 – 500 μm particles.

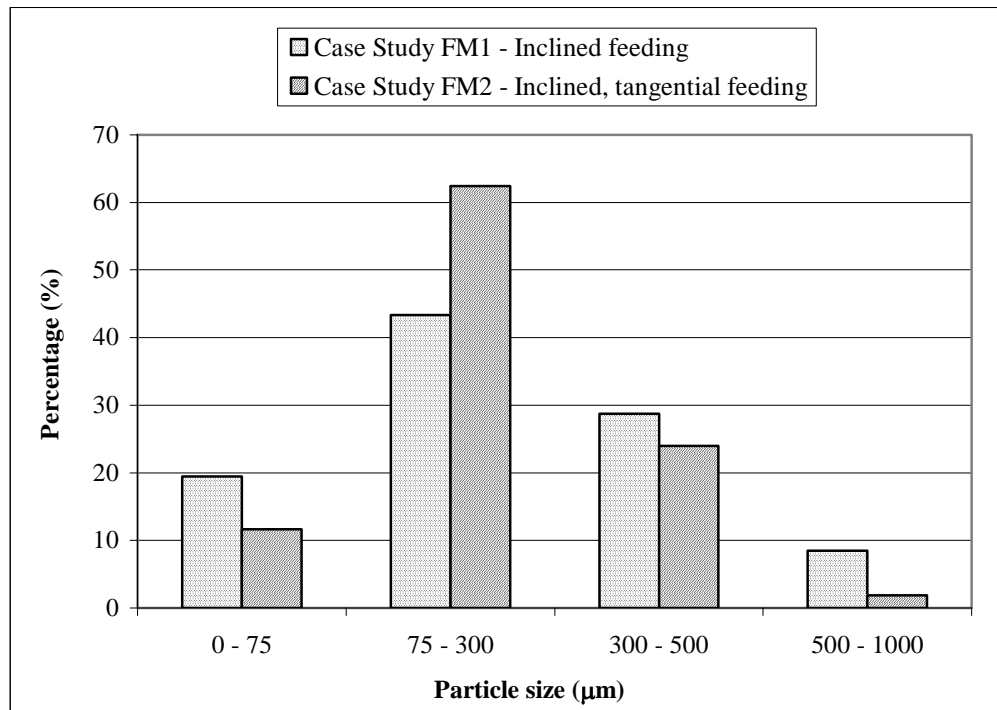


Figure 4.1-36: Histogram of particle size distribution for bottom ash from the combustion of rice husk in the 210-mm inner diameter fluidised bed combustor with different feeding methods (sand size = 250 – 595 μm , static bed height = 0.5 D_c , fluidising velocity $\approx 3 U_{mf}$, primary air factor ≈ 1.2)

Further, comparing between Case FM1 and Case FM2, the bottom ash from Case FM1 was coarser (due to the presence of particles in the size range of 500 – 1000 μm at 8.5%). This might be due to the absence of the swirling turbulent flow adjacent to the bed region in Case FM1, which as in Case FM2 aided in breaking down further the rigid char skeleton of the rice husk, resulting in negligible amount of particles in the excess of 500 μm . When the experiment was stopped, subsequent

purges of the bottom ash from Case FM2 (Samples FM2-c and FM2-d) consisted of fine ash particles, all of which passed the mesh size of 300 μm .

Correlating this to the CFD modelling, it was speculated that the bottom ash in both Model FM-A and Model FM-B as represented by the inert silica particles with size in the excess of 150 μm will be retained in the bed. The hypotheses for the particle trajectories in the CFD model for both Case FM1 and Case FM2 (Model FM-A and Model FM-B) were summarised in Table 4.1-46.

Table 4.1-46: Expected trajectories of particles in the computational fluid dynamics (CFD) model of rice husk combustion in the 210-mm inner diameter fluidised bed combustor with different feeding methods

Type of Particle	Diameter (μm)	Expected Fate of Particle in CFD Model		Remarks
		Model FM-A (Inclined Feeding)	Model FM-B (Inclined, Tangential Feeding)	
Rice husk	25	Will elutriate from fluidised bed (FB) combustor	Will elutriate from fluidised bed (FB) combustor	Final burnout of rice husk particles to represent fly ash in the CFD model
	50			
	75			
	100			
	200			
	300			
	500	Will retain inside bed region		
	750			
	1000			
1600	Will retain inside bed region			
Silica (final ash)	10	Will elutriate from fluidised bed (FB) combustor	Will elutriate from fluidised bed (FB) combustor	To represent bottom ash in the CFD model
	25			
	50			
	75			
	150			
	300	Will retain inside bed region	Will retain inside bed region	
	500			
	750			
	1000			
1600				

The modelling results based on these experimental data were presented in Section 5.2.2.

c) **Findings**

Utilisation of the inclined, tangential port for feeding of rice husk into the fluidised bed combustor resulted in a higher degree of rice husk penetration and burning in the sand bed. This was because the rice husk particles were imparted a tangential velocity component upon entry into the combustor. Subsequently, these particles tended to impact the wall and lost their momentum before sliding down to the sand bed and be ‘engulfed’ into the bed by the eruption of air bubbles above the bed. Due to the constant attrition process taking place in the sand bed, the resulting ash particles were broken down into very small fragments, thereby releasing the entrapped carbon for further conversion. Thus, the residual carbon content in these bottom ash particles was found to be lower than that of the fly ash particle. **However, the drawback of utilising the inclined, tangential feeding method was that the accumulation of ash in the bed was significant and posed the problems of continuity in operation and ash collection.** This was probably due to the presence of turbulent swirling flows adjacent to the bed surface, which tended to continuously ‘trap’ any fly ash particles entrained to the freeboard region and returned them to the bed. It was speculated that increasing the fluidising velocity might be able to allow these ash particles to be entrained to the freeboard region and subsequently be collected as fly ash in the cyclone. On the other hand, utilisation of the inclined feeding port resulted in fly ash with similar residual carbon content (at 1.9 wt%) as that from the inclined, tangential feeding port although the particle size in the latter was much finer due to the higher degree of penetration into the bed region.

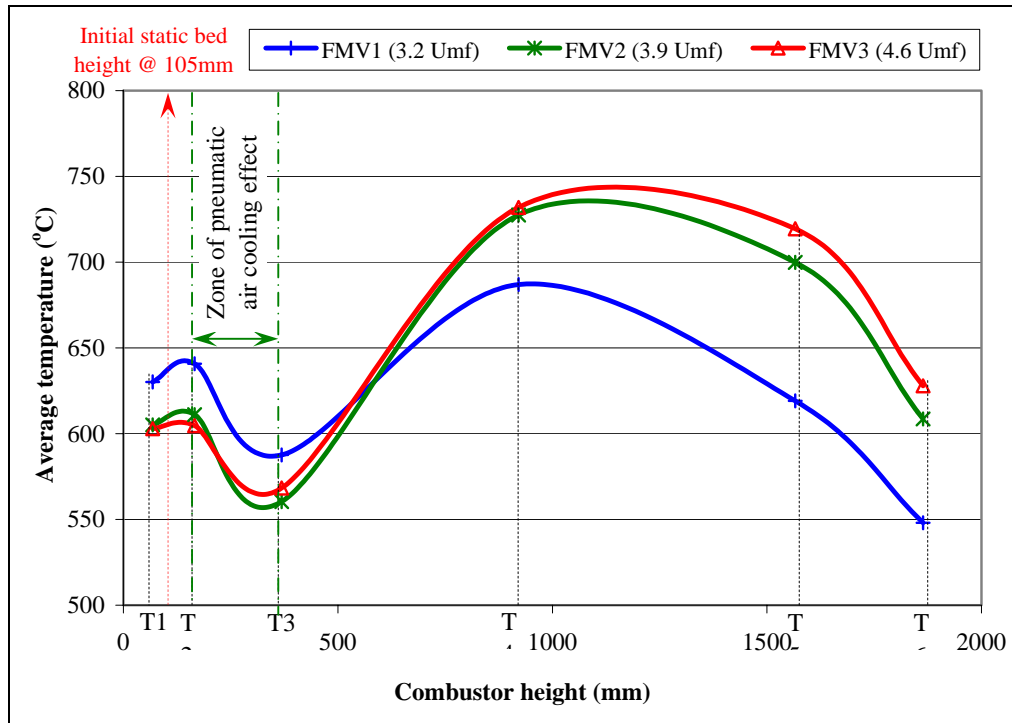
4.10.2 Vortex Feeding with Higher Fluidising Velocity

The experiments were conducted at fluidising velocities of 3 – 5 U_{mf} utilising the inclined, tangential feeding method. In all experiments, the static bed height was

held constant at $0.5 D_c$ ($250 - 595 \mu\text{m}$ sand), the primary air factor at 1.2 and feeding was commenced upon pre-heating the bed to 650°C .

a) Temperature Profile and Combustion Characteristics

The average bed temperatures during the period of rice husk combustion were plotted and compared in Figure 4.1-37.



Note: Average temperature during feeding period

Figure 4.1-37: Average temperatures in the combustor during combustion of rice husk in the 210-mm inner diameter fluidised bed combustor with inclined, tangential feeding port at different fluidising velocities (sand size = $250 - 595 \mu\text{m}$, static bed height = $0.5 D_c$, primary air factor ≈ 1.2)

Based on Figure 4.1-37, it was observed that the region affected by the pneumatic air cooling effect was restricted to approximately 10% of the combustor height (at a zone spanning from T2 to T3) when the inclined, tangential feeding method was employed in place of the inclined feeding method (at the zone spanning from T2 to T4 in Figure 4.1-34, Section 4.10.1). The average bed temperature (T1) decreased with the increase in fluidising velocity, with the highest bed temperature obtained

when operating at $3.2 U_{mf}$. This decrease in bed temperature was expected as the increase in fluidising velocity tended to reduce the amount of rice husk reaching the bed region and thus, the burning of lesser amount of rice husk in the bed region resulted in lower bed temperature. The lower fluidising velocity at $3.2 U_{mf}$ also probably allowed for a relatively higher residence time of evolved volatile gases at the bed surface, thus the higher temperature observed at this region was attributable to the burning of these volatile gases.

Temperatures at the freeboard region, however, exhibited a reversed trend whereby higher temperatures were achieved when operating at higher fluidising velocities. This could be attributed to the higher amount of air available for the burning off of evolved volatile gases in the freeboard region with the use of higher fluidising velocities. Nevertheless, the peak freeboard temperature was observed to occur beyond mid-height of the combustor around T4 for all three fluidising velocities investigated. The increase in fluidising velocity also seemed to shift the zone of intense volatile gases combustion higher to the freeboard height towards T5.

b) Ash Quality

i) *Silica Structure*

The silica structures of all ash samples from the current experiments were compared in Table 4.1-47. In general, all ash samples retained their amorphous structure except for some minor contamination of sand bed particles in the form of quartz peaks in some ash samples.

Table 4.1-47: Diffractograms of ash samples from the combustion of rice husk in the 210-mm inner diameter fluidised bed with inclined, tangential feeding port at different fluidising velocities (sand size = 250 – 595 μm , static bed height = 0.5 D_c , primary air factor ≈ 1.2)



U_{mf} number at corresponding bed temperature (average)		
Case Study FMV1	Case Study FMV2	Case Study FMV3
3.2 U_{mf}	3.9 U_{mf}	4.6 U_{mf}
Fly ash (Sample FMV1-a)	Fly ash – first purge (Sample FMV2-a)	Fly ash – first purge (Sample FMV3-a)
Bottom ash – first purge (Sample FMV1-b)	Fly ash – second purge (Sample FMV2-b)	Fly ash – second purge (Sample FMV3-b)
Bottom ash – second purge (Sample FMV1-c)	Bottom ash – first purge (Sample FMV2-c)	Bottom ash – first purge (Sample FMV3-c)
Bottom ash – third purge (Sample FMV1-d)	Bottom ash – second purge (Sample FMV2-d)	Bottom ash – second purge (Sample FMV3-d)

ii) Residual Carbon Content

During the combustion of rice husk (feeding period), the amount of fly ash collected at the fluidising velocity of 3.2 U_{mf} was very little. Most of the ash were retained in the sand bed and were collected as bottom ash, which amount was approximately

three times higher than that of the fly ash. Increasing the fluidising velocity to $3.9 U_{mf}$ increased the amount of fly ash, with the amount collected at the cyclone being similar to that of the bottom ash. Increasing the fluidising velocity further to $4.6 U_{mf}$ resulted in most of the ash being blown towards the cyclone as fly ash. The amount of fly ash collected was three times higher than that of bottom ash. The appearances of these ash samples were shown in Table 4.1-48 while the residual carbon contents in these ash samples as determined through loss on ignition tests were shown in Figure 4.1-38. The particle size of the fly ash and bottom ash from all three experiments were generally similar, which were characterised by the presence of tiny fragments of char and white ash (as in fly ash) and white ash only (as in bottom ash) as well as the complete absence of any char skeletons. The only exception was the bottom ash collected from the last purge (Sample FMV1-d, FMV2-d and FMV3-d) which were even finer in size and appeared powder-like. The fine size observed from these ash particles was due to their long residence time in the bubbling sand bed, whereby the vigorous bubbling action increased the rate of attrition amongst the ash and sand particles and thereby breaking the original skeleton-like shape of the ash into smaller fragments. This phenomenon was deemed beneficial as the entrapped carbon could be released for further conversion. The overall effect was the higher carbon burnout in these ash particles, as reflected in their lower residual carbon contents. The longer the retention period of the ash particles in the sand bed, the higher the exposure period to the attrition process and thereby the resulting particle size were much finer, resembling a powder form.

Table 4.1-48: Ash samples from the combustion of rice husk in the 210-mm inner diameter fluidised bed with inclined, tangential feeding port at different fluidising velocities (sand size = 250 – 595 μm , static bed height = 0.5 D_c , primary air factor ≈ 1.2)

U_{mf} number at corresponding bed temperature (average)		
Case Study FMV1	Case Study FMV2	Case Study FMV3
3.2 U_{mf}	3.9 U_{mf}	4.6 U_{mf}
		
Fly ash (Sample FMV1-a)	Fly ash – first purge (Sample FMV2-a)	Fly ash – first purge (Sample FMV3-a)
		
Bottom ash – first purge (Sample FMV1-b)	Fly ash – second purge (Sample FMV2-b)	Fly ash – second purge (Sample FMV3-b)
		
Bottom ash – second purge (Sample FMV1-c)	Bottom ash – first purge (Sample FMV2-c)	Bottom ash – first purge (Sample FMV3-c)
		
Bottom ash – third purge (Sample FMV1-d)	Bottom ash – second purge (Sample FMV2-d)	Bottom ash – second purge (Sample FMV3-d)

Note: Ash samples from the fluidising velocity of 3.2 U_{mf} contained mostly bottom ash with small amounts of fly ash

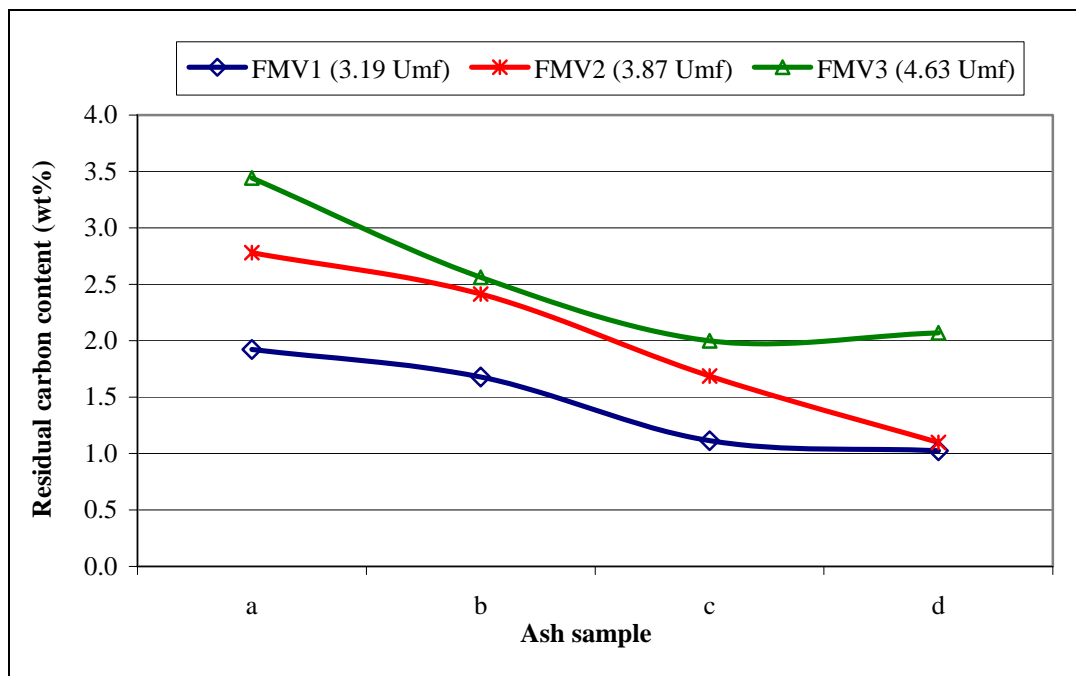


Figure 4.1-38: Comparisons of residual carbon contents in ash samples from the combustion of rice husk in the 210-mm inner diameter fluidised bed combustor with inclined tangential feeding port at different fluidising velocities (sand size = 250 – 595 μm , static bed height = 0.5 D_c , primary air factor ≈ 1.2)

From Figure 4.1-38, it was observed that operating at lower fluidising velocities resulted in lower residual carbon contents in both the fly and bottom ashes. The lowest residual carbon content was obtained from the final purge of bottom ash at fluidising velocity of 3.2 U_{mf} (Sample FMV1-d), which at 1.0 wt% was half compared to that obtained from the final purge of bottom ash at fluidising velocity of 4.6 U_{mf} (2.1 wt%). The residual carbon content in the fly ash was found to increase by approximately 45% from 1.9 wt% to 2.8 wt% when the fluidising velocity was increased from 3.2 U_{mf} to 3.9 U_{mf} . Operating at fluidising velocity of 4.6 U_{mf} resulted in a residual carbon content of 3.4 wt% in the fly ash. This trend in residual carbon contents in the fly ash were expected due to the lower residence time in the freeboard region as the fluidising velocity was increased. The lower residence time decreased the exposure time of the ash particles to high temperatures, which was necessary for the oxidation of carbon. The bottom ash generally contain less amount of carbon compared to the fly ash as they were retained longer in the bed, whereby the oxidation of carbon could continue to take place. However, similar to the

trend with the fly ash, the higher the fluidising velocity, the higher the residual carbon content in the bottom ash. This was also due to the factor of residence time, as the higher fluidising velocity tended to blow the air (and gaseous components) more rapidly to the freeboard region towards the cyclone. This also explained why more fly ash particles were collected in the cyclone as the fluidising velocity was increased. Based on this results, it was recommended that the fluidising velocity be maintained at a level sufficient for good mixing in the bed while enabling the longer retention of ash in the bed, namely at approximately $3 U_{mf}$.

iii) Particle Size

1) Fly Ash

The particle size distributions of the fly ash samples (first purge of fly ash, i.e. samples FMV1-a, FMV2-a and FMV3-a) were as shown in Figure 4.1-39. It was observed that the increase in fluidising velocities resulted in lower fraction of fine particles (less than $75 \mu\text{m}$). The percentage of fly ash at this size range was reduced from 32.6% when operating at $3.2 U_{mf}$ to 24.2% ($3.9 U_{mf}$) and 21.9 ($4.6 U_{mf}$). This was expected as the lower fluidising velocity enabled the ash particles to stay at the bed region at a relatively longer period of time, thus increasing their chances of being broken down into much smaller fragments due to the turbulent bubbling bed. The percentage of fly ash particles in the size range of $75 - 300 \mu\text{m}$ remained similar at approximately 60% for all three fluidising velocities, whereas operating beyond the fluidising velocity of $3.9 U_{mf}$ resulted in similar amount of ash particles in the size range of $300 - 50 \mu\text{m}$ (at approximately 17%).

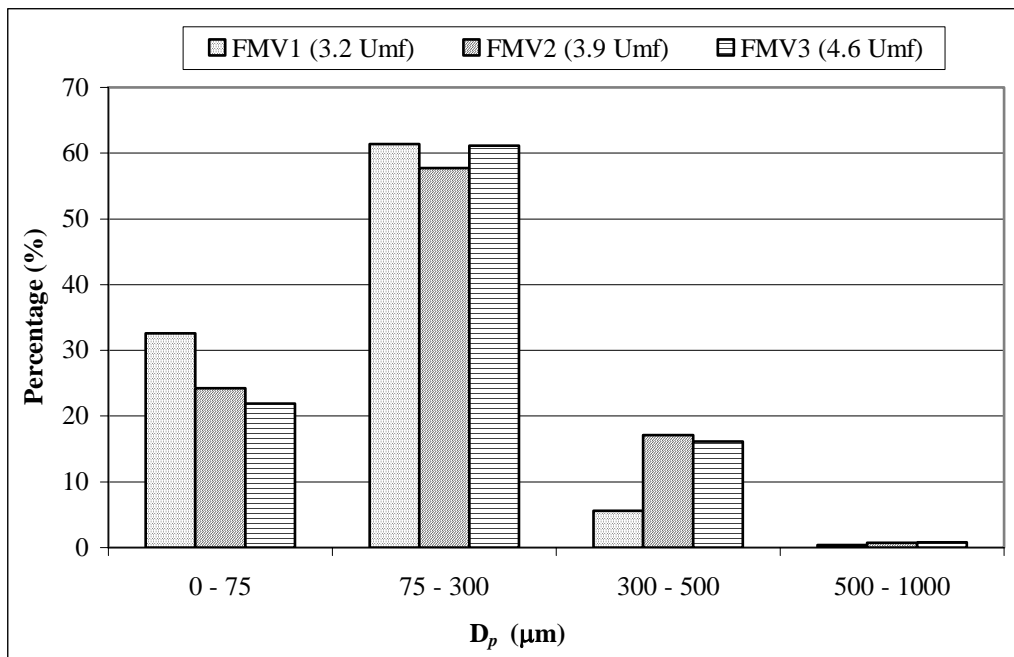


Figure 4.1-39: Particle size distribution of fly ash samples from the combustion of rice husk in the 210-mm inner diameter fluidised bed combustor with inclined, tangential feeding at different fluidising velocities (sand size = 250 – 595 μm , static bed height = 0.5 D_c , primary air factor \approx 1.2)

2) Bottom Ash

The particle size distributions of the bottom ash samples (first purge of bottom ash, i.e. samples FMV1-b, FMV2-c and FMV3-c) were as shown in Figure 4.1-40. It was observed that there was no prominent trend in the particle size distribution as opposed to that of the fly ash samples. This observation was also expected as these ash samples were retained for a considerable period of time in the turbulent bubbling bed as opposed to the brief exposure period of the fly ash, and thus were all exposed to the similar breaking force from the turbulent bubbling bed. However, it was observed that the percentage of finer particles (less than 75 μm) was lower than that of the fly ash, at less than 20% for all three bottom ash samples compared to 20 – 30% for the fly ash samples because finer particles had lower terminal velocities and thus were much more easily elutriated as fly ash. The bottom ash samples were instead constituted mainly of larger particles (75 – 500 μm), which at 80 – 88% were quite high compared to that of fly ash (at 66 – 77% only).

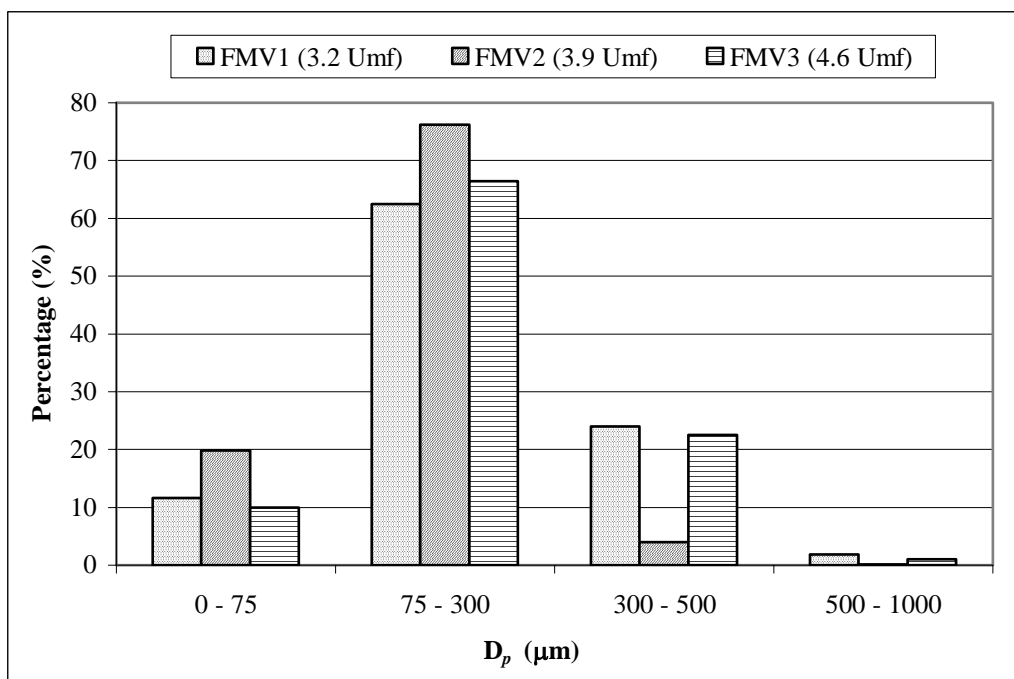


Figure 4.1-40: Particle size distribution of bottom ash samples from the combustion of rice husk in the 210-mm inner diameter fluidised bed combustor with inclined, tangential feeding at different fluidising velocities (sand size = 250 – 595 μm , static bed height = 0.5 D_c , primary air factor \approx 1.2)

c) Findings

Fluidising velocity in the region of 3 U_{mf} was found to give the lowest carbon content in both the fly and bottom ashes when inclined, tangential feeding method was employed. This was consistent with the case whereby the inclined feeding method was employed, where the fluidising velocity of approximately 3 U_{mf} was also found to be optimum to obtain ash with the lowest carbon content, as discussed in Section 4.5.1. These results showed that the optimum fluidising velocity during combustion of rice husk in the fluidised bed was not affected by the feeding method (overbed feeding only). The validity of these results, however, needed to be further investigated if underbed feeding methods were to be employed.

With inclined, tangential feeding, the operation of the fluidised bed was not continuous when operated at fluidising velocity in the range of $3 U_{mf}$ due to significant accumulation of the ash in the bed region, as discussed in Section 4.10.1. This accumulation problem tended to lower the bed temperature as well as disrupting the bed mixing behaviour due to the increase in bed height. Increasing the fluidising velocity could reduce the rate of ash accumulation in the bed, whereby the higher fluidising velocity enabled the ash particles to be elutriated towards the freeboard region as fly ash. However, this increase in fluidising velocity also reduced the residence time of ash particles in the bed region, resulting in ash (especially fly ash) with higher carbon content. It was forecasted that the swirling gas stream induced by the pneumatic air feed (as proven in the computational fluid dynamic or CFD modelling results in Section 5.2.2) created a 'vortex' near the bed surface which perpetually trapped and returned the ash particles into the bed region, thus resulting in ash accumulation in the bed. Therefore, it was concluded that the inclined, tangential feeding method was not feasible for continuous operation of the 210-mm inner diameter fluidised bed combustor. Further, it was recommended that the swirling effect of the gas stream in the combustor, which was beneficial in increasing the residence time of particles or gas in the freeboard region, be induced at a higher level so as to eliminate the detrimental 'vortex flow' near the bed surface.

4.11 Summary of Findings

The major findings in this chapter were summarised as follows:-

a) Basic Combustion Characteristics of Rice Husk

The combustion times of rice husk (raw or water-washed) in a muffle furnace at the temperature range of 650 – 750°C was 20 – 30 seconds (single particle combustion) and 39 – 52 seconds (group particle combustion). The removal of alkali metals compounds (potassium oxide and sodium oxide) by washing the rice husk with water prior to thermal

treatment eliminated the formation of black char particles in the final ash product. Combustion of rice husk in the fluidised bed proceeded according to the single particle model, with combustion times of 29 – 34 seconds at temperatures of 650 – 750°C.

b) Effect of Temperature and Residence Time on the Formation of Silica Crystals in Rice Husk Ash

Silica in rice husk ash from thermal treatment of rice husk at the temperatures of up to 900°C and 3 minutes was still amorphous. Completely white ash could not be obtained from rice husk unless the alkali metals compounds (potassium oxide and sodium oxide) were removed prior to thermal treatment.

c) Effects of Fluidisation Parameters on the Mixing of Rice Husk in Fluidised Bed

i) Sand Size

The sand size of 250 – 595 μm gave good mixing of rice husk within the bed region.

ii) Fluidising Velocity

The fluidising velocity of 3 – 6 U_{mf} gave good mixing of rice husk within the bed without resulting in significant elutriation of rice husk.

iii) Static Bed Height

The static bed height of 0.5 D_c gave good mixing of rice husk within the bed region.

d) Effects of Fluidisation Parameters on the Mixing of Rice Husk in Fluidised Bed during Combustion Process

i) Sand Size

The suitable sand size for good mixing and combustion behaviours of rice husk in the fluidised bed was 250 – 595 μm .

ii) Fluidising Velocity

The fluidising velocities to achieve good mixing and combustion behaviours of rice husk in the fluidised bed was in the range of 3 – 6 U_{mf} . The short freeboard height of 80-mm inner diameter fluidised bed was insufficient to disengage any sand particles thrown to the freeboard region, resulting in contamination of sand (quartz crystals) in the fly ash.

e) Effects of Mixing Parameters on the Combustion Efficiency of Rice Husk in Fluidised Bed

i) Fluidising Velocity

The optimum fluidising velocity for high combustion efficiency of rice husk in the fluidised bed was approximately 3 U_{mf} (at corresponding bed temperature).

ii) Static Bed Height

The optimum static bed height for high combustion efficiency of rice husk in the 210-mm inner diameter fluidised bed was 0.5 D_c .

f) Effect of Temperature on the Combustion Efficiency of Rice Husk in Fluidised Bed

i) Bed Temperature

Amorphous ash could be obtained from rice husk combustion in fluidised bed with bed temperatures of up to 800°C. The significant increase in carbon conversion efficiency occurred at the temperature region of 650 – 700°C.

ii) Freeboard Temperature

The freeboard temperatures in the fluidised bed should be maintained consistently at high temperatures (600 – 700°C) to achieve high carbon conversion in the fly ash while maintaining their amorphous structures.

iii) Heat Loss

The presence of insulation materials at the fluidised bed combustor increased the carbon oxidation rate in the freeboard region due to the higher gas temperatures as it flowed upwards.

g) Effect of Washing of Rice Husk on Its Combustion Efficiency in Fluidised Bed

Removal of alkali metals compounds in rice husk by water-washing did not improve the combustion efficiency of rice husk in the bed region (primary stage combustion). However, removal of alkali metals from rice husk was found to improve its combustion efficiency in the freeboard region (secondary stage combustion).

h) Effect of Air Supply on the Combustion Efficiency of Rice Husk in Fluidised Bed

i) Primary Air Factor

The carbon conversion efficiency during combustion of rice husk in the fluidised bed remained essentially constant at primary air factors of 0.8 to 1.4.

ii) Primary-to-Secondary Air Ratio

The air split of 7:3 (primary air to secondary air) was found to give better fly ash quality.

iii) Pneumatic Air Feeding Velocity

The pneumatic air feeding velocity of 1.4 m/s gave the highest carbon conversion efficiency of rice husk in the 210-mm inner diameter fluidised bed.

i) Effect of Moisture Content in Rice Husk on Its Combustion Efficiency in Fluidised Bed

Water-washed rice husk with moisture content of 26.0 wt% gave the highest combustion efficiency in the fluidised bed.

j) Effect of Feeding Design on the Combustion Efficiency of Rice Husk in Fluidised Bed

i) Vortex Feeding

The presence of vortex flow adjacent to the surface of the bubbling bed prevented the fly ash to be entrained to the cyclone, thus resulting in significant accumulation of ash in the

bed region. At similar fluidising velocities, the inclined feeding method was found to be more suitable for the continuous operation of the 210-mm inner diameter fluidised bed.

ii) Vortex Feeding with Higher Fluidising Velocity

The inclined, tangential feeding method was found to be unsuitable for the continuous operation of the 210-mm inner diameter fluidised combustor unless the vortex flow is induced higher away from the bubbling bed surface.

CHAPTER 5

RESULTS AND DISCUSSIONS ON IMPROVEMENT IN DESIGN AND OPERATION OF THE FLUIDISED BED THROUGH CFD MODELLING

5.1 Increase in Fluidised Bed Freeboard Height

a) Effect on Elutriation of Sand Particles

The trajectories of the five different sizes of sand particles were shown in Figure 5-1 to Figure 5-5. It was observed that the 25 μm and 50 μm sand particles were disengaged at the height of approximately 4000mm, and therefore a freeboard height of at least 4500mm was required to prevent their elutriation. Meanwhile, the 75 μm sand particles was disengaged at the height of approximately 3000mm. Larger particles (100 μm and 125 μm) were disengaged below the height of 3000mm. These observations were consistent with the screen analysis of the elutriated sand particles, whereby sand particles of as large as 125 μm were still being elutriated from the 2000-mm tall fluidised bed combustor as they required a transport disengaging height of at least 3000mm. Hence, a fluidised bed with a height of 5000mm should be sufficient to disengage all the sand particles to prevent the the phenomenon of sand elutriation. The contamination of quartz crystals (sand) in the fly ash could therefore be prevented.

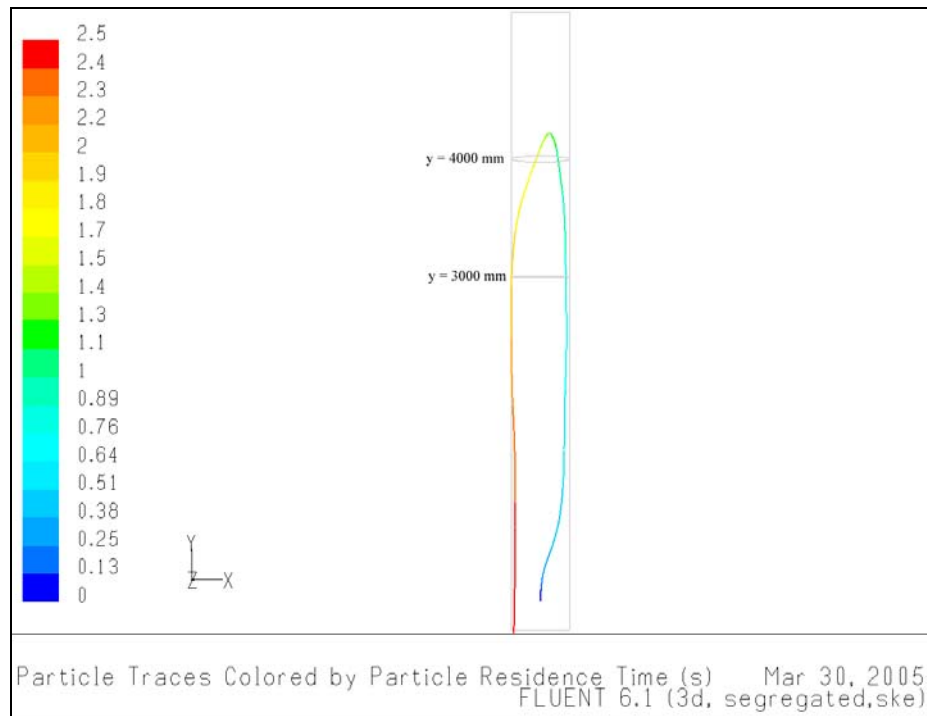


Figure 5-1: Trajectory of the 25 μm sand particle in the fluidised bed combustor model ($\text{\O}500\text{mm} \times 5250\text{mm}$)

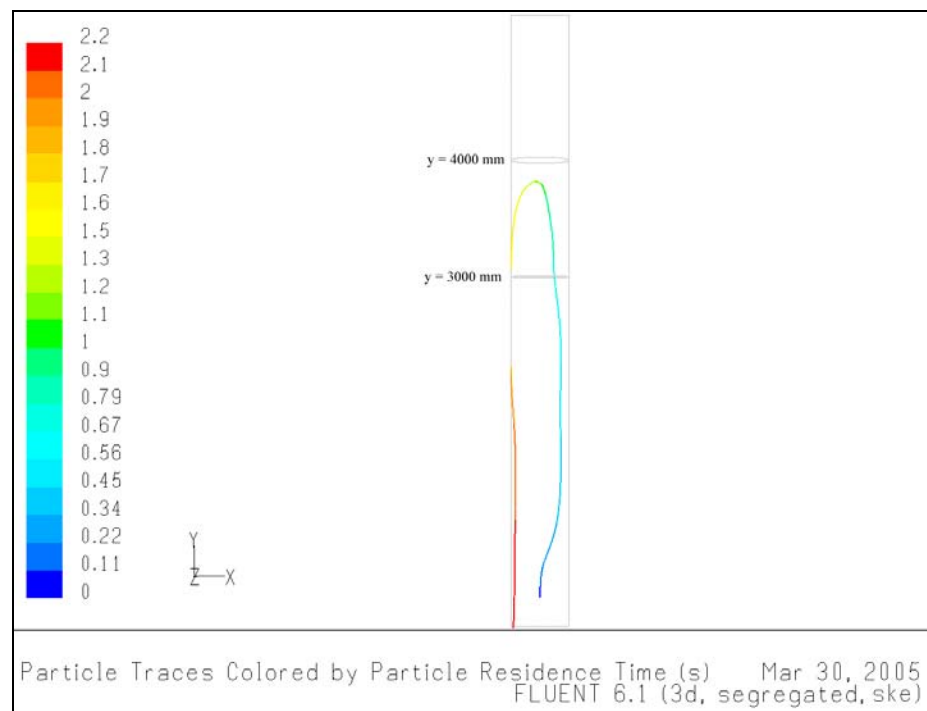


Figure 5-2: Trajectory of the 50 μm sand particle in the fluidised bed combustor model ($\text{\O}500\text{mm} \times 5250\text{mm}$)

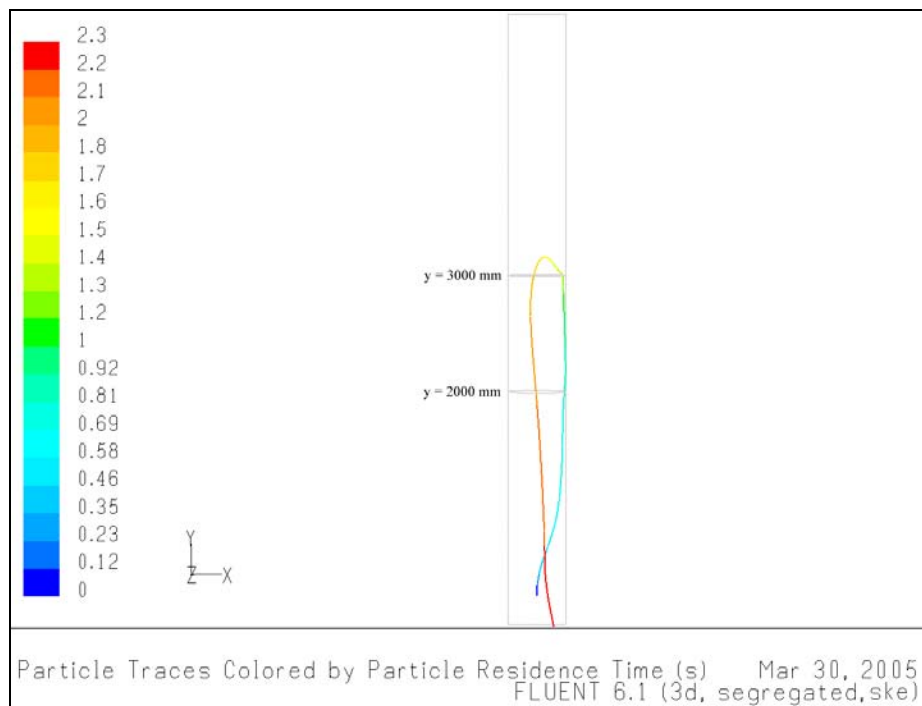


Figure 5-3: Trajectory of the 75 μm sand particle in the fluidised bed combustor model ($\text{\O}500\text{mm} \times 5250\text{mm}$)

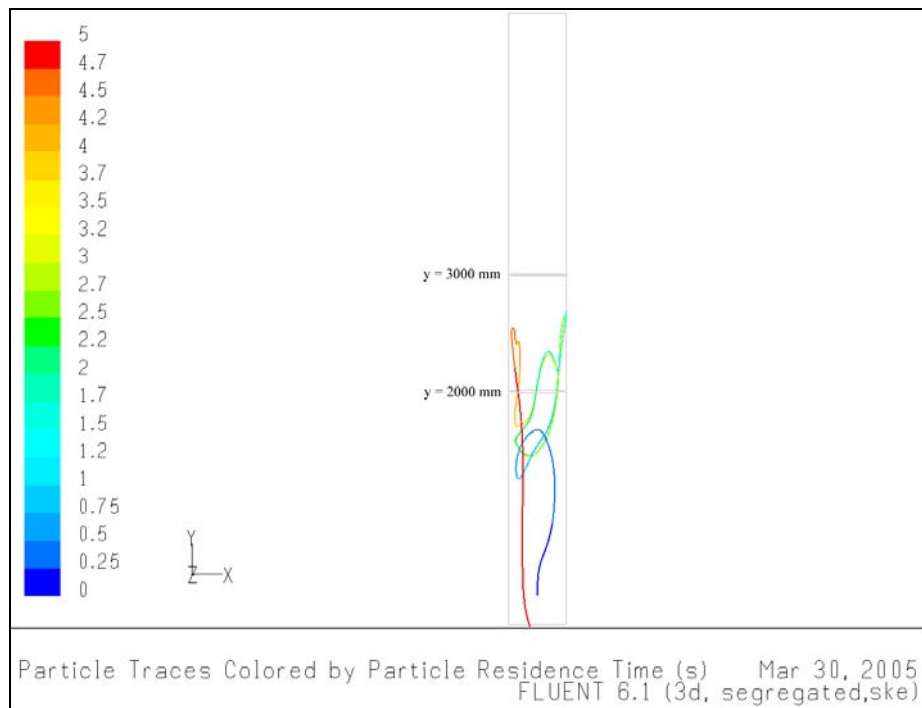


Figure 5-4: Trajectory of the 100 μm sand particle in the fluidised bed combustor model ($\text{\O}500\text{mm} \times 5250\text{mm}$)

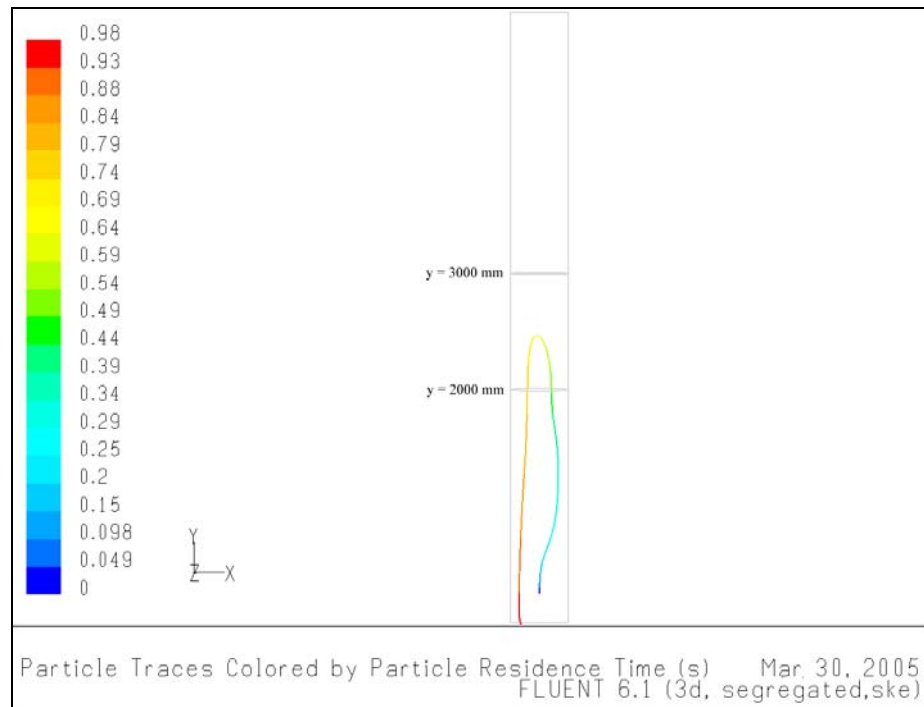


Figure 5-5: Trajectory of the 125 μm sand particle in the fluidised bed combustor model ($\text{Ø}500\text{mm} \times 5250\text{mm}$)

b) Effect on Combustion Efficiency of Rice Husk in the Freeboard Region

The trajectories and mass loss history of the five different sizes of rice husk particles inside the fluidised bed combustor model were compared in Table 5-1 while their residence times in the freeboard region were compared in Figure 5-6. The mass loss history were expressed in terms of fractional conversions of reactants in rice husk, namely the volatile matters and fixed carbon since the mass of particle in the model were expressed in dry basis. The conversion curve were characterised by a slight but gradual release of volatiles followed by an instantaneous and complete release of volatiles from the particles (sudden increase in conversion from 0.35 to 0.86). This was followed by the gradual oxidation of fixed carbon in the remaining char until the combustion process was completed (conversion = 1.0). This conversion curve was observed to be consistent with the mass loss curve from thermogravimetric analysis of rice husk in an air atmosphere (Mansaray and Ghaly, 1998b), except that the drastic decrease in mass in the latter was not as steep due to the gradual heating nature of thermogravimetric analysis.

Table 5-1: Trajectories and mass loss history of burning rice husk particles with different sizes in the fluidised bed combustor model (Ø500mm × 5250mm)

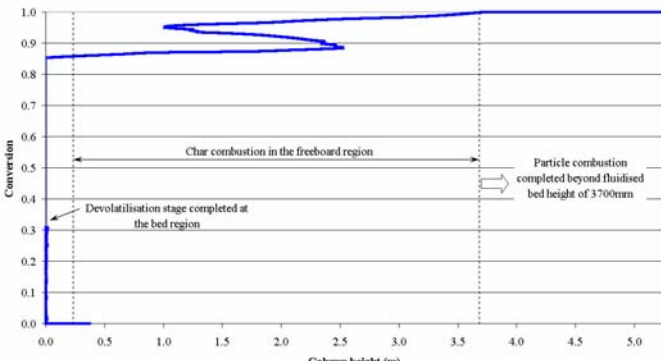
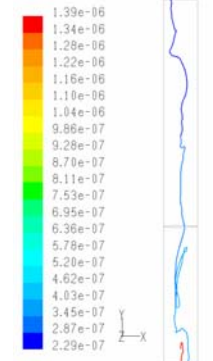
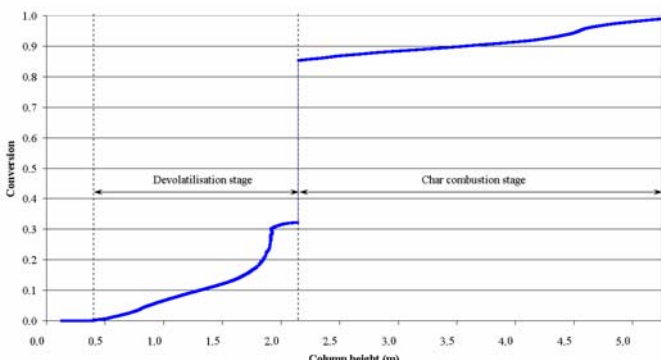
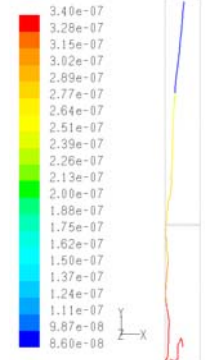
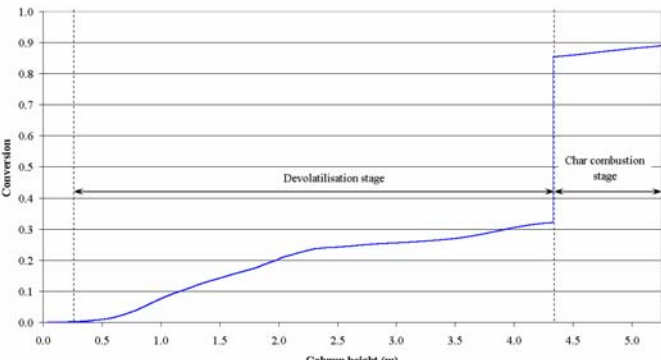
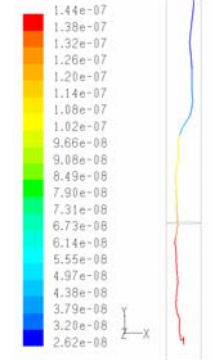
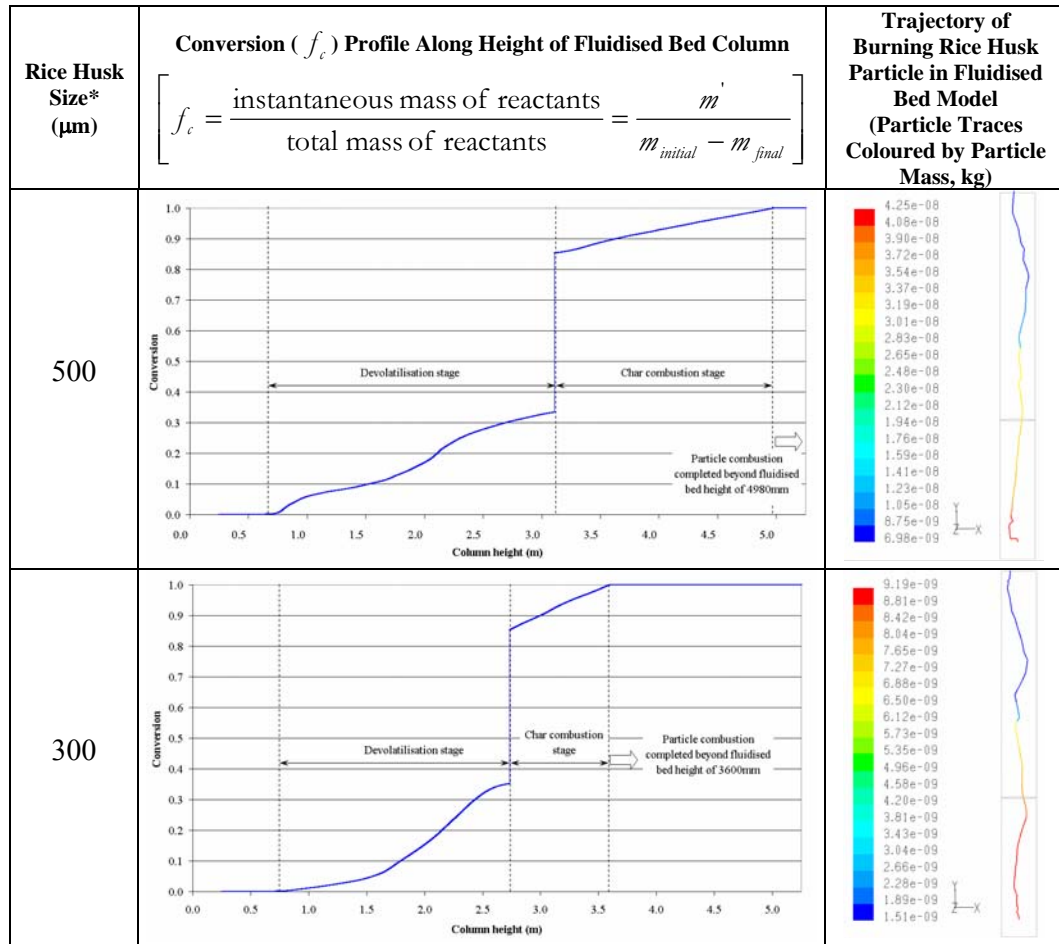
Rice Husk Size* (µm)	<p style="text-align: center;">Conversion (f_c) Profile Along Height of Fluidised Bed Column</p> $f_c = \frac{\text{instantaneous mass of reactants}}{\text{total mass of reactants}} = \frac{m'}{m_{initial} - m_{final}}$	<p style="text-align: center;">Trajectory of Burning Rice Husk Particle in Fluidised Bed Model (Particle Traces Coloured by Particle Mass, kg)</p>
1600 (whole husk)		
1000		
750		

Table 5-1 (continued...): Trajectories and mass loss history of burning rice husk particles with different sizes in the fluidised bed combustor model (Ø500mm × 5250mm)



Note: * Volume-surface mean diameter (D_{vs})

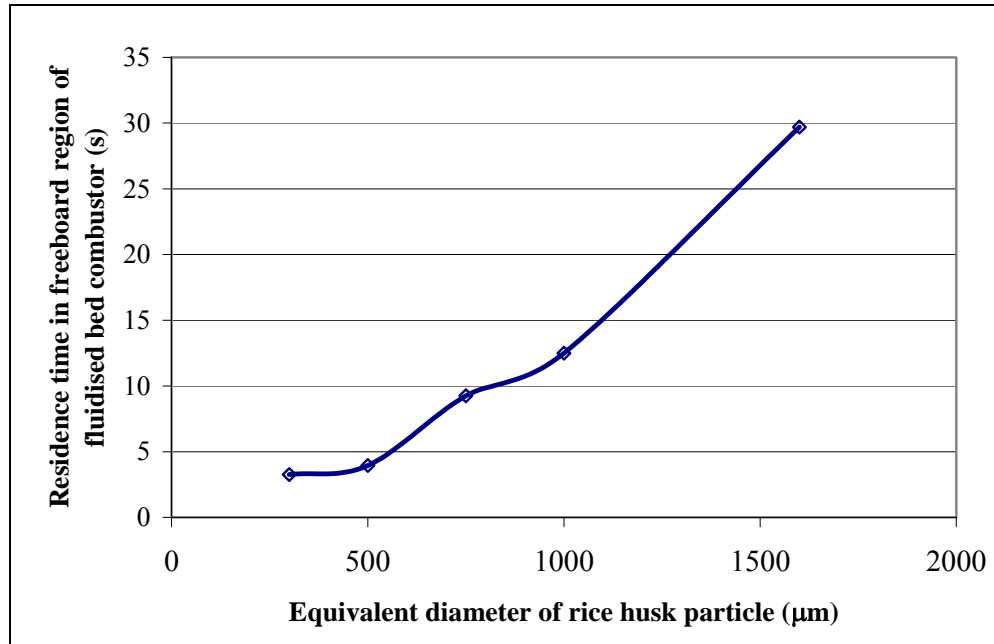


Figure 5-6: Residence time of burning rice husk particles with different sizes in the fluidised bed model ($\text{Ø}500\text{mm} \times 5250\text{mm}$)

Except for rice husk particles with sizes of 1000 µm and 750 µm, the combustion process to liberate carbon-free ash was completed inside the fluidised bed for all the particle sizes. The whole husk particle tended to be returned to the bed region upon ejection to the freeboard region due its higher mass. From thereon, the devolatilisation process took place until the release of volatiles was completed and the relatively lighter char skeleton was blown towards the freeboard region. The char oxidation process in the freeboard region was observed to take place up to the combustor height of 3700mm. In addition, due to its relatively bigger particle size, the char skeleton from the whole husk tended to be recirculated at the combustor height of 1000 – 2500mm, thus increasing its residence time inside the combustor to 30 seconds. This time period was found experimentally to be sufficient for the complete combustion of whole husk particles. Meanwhile, the conversions for the 1000-µm and 750-µm rice husk fragments were 99% and 89%, respectively. Since the mass of these rice husk fragments were lower than the whole husk particle, they tended to be blown more easily towards the freeboard region. The devolatilisation stage for both particles proceeded up to the combustor height of 2150mm and 4350mm, respectively. This resulted in the insufficient time to complete the char oxidation stage, especially for the 750-µm rice husk fragment. On the other hand,

combustion of the smaller rice husk fragments (500 μm and 300 μm) was completed although they were also blown up to the freeboard region more easily due mostly to their high-surface area per unit volume. This increased the rate of heat and mass transfer to the particles, thus reducing their reaction time. The combustion process for both rice husk fragments were completed beyond the combustor height of 4980mm and 3600mm, respectively. This showed that the fluidised bed height of at least 5000mm was required to obtain complete combustion of even the smaller fragments of rice husk particles. This modelling study was based on the worst-case scenario of operating at very high freeboard gas velocity of 1.0 m/s. Thus, it was expected that the combustion of all rice husk particles with different sizes could be completed inside a fluidised bed with column height of 5000mm.

5.2 Improvement of Feeding Conditions

5.2.1 Pneumatic Air Feeding Velocity

a) Effect on Carbon Conversion Efficiency of Rice Husk

The residence time distribution of burning rice husk particles at different pneumatic air feeding velocities were summarised in Figure 5-7. The corresponding histograms to depict the shape of the distribution of residence times of these rice husk particles were given in Table 5-2. As hypothesised, Model IV (which corresponded to Case PV4 in the experimental study, pneumatic air feeding velocity of 1.36 m/s), gave the highest mean residence time, at 52 seconds. Since this period of time was more than double the minimum time required for the complete combustion of rice husk particles (25 – 30 seconds), high burnout of rice husk could be achieved and therefore, the residual carbon content in this case was the lowest.

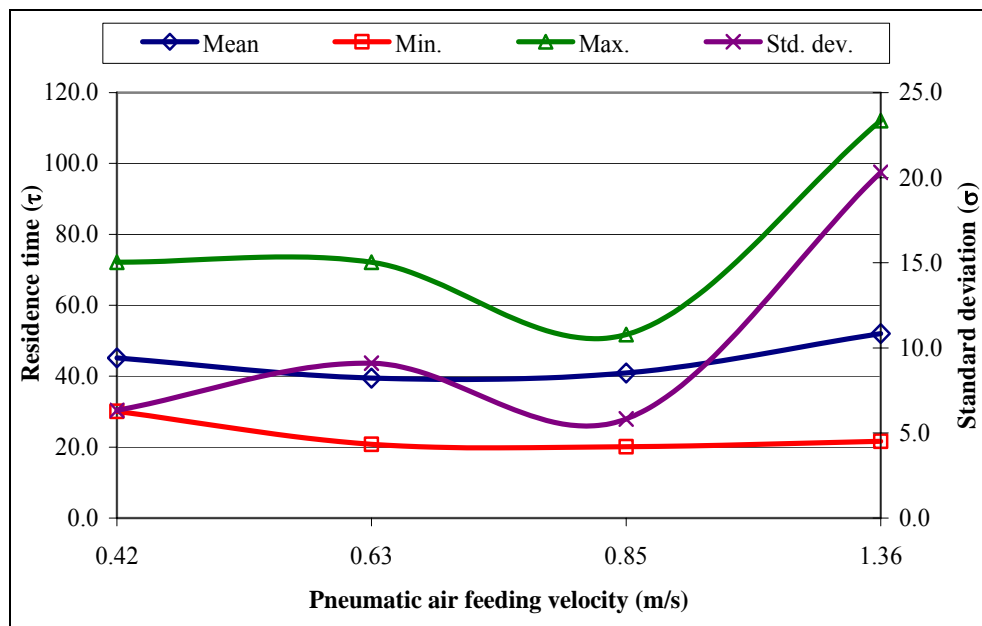
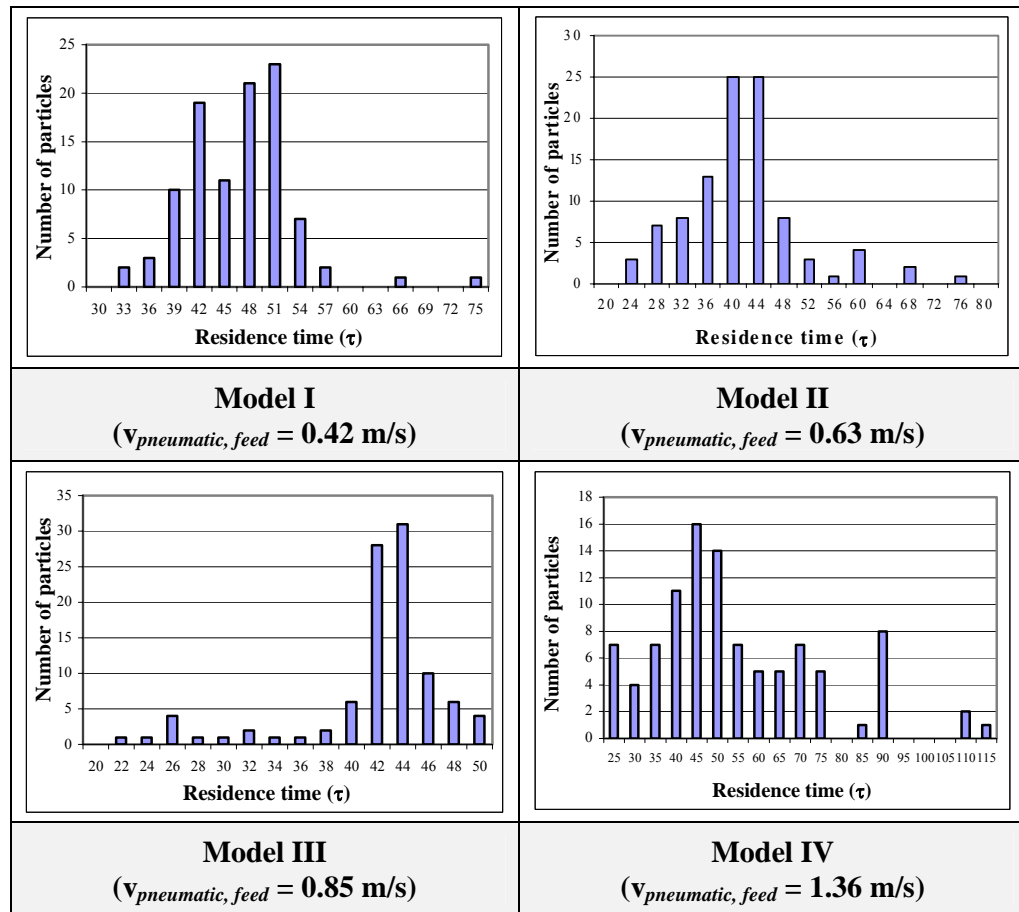


Figure 5-7: Statistical analysis on the residence time distribution from computational fluid dynamics (CFD) modelling of burning rice husk particles in the 210-mm inner diameter fluidised bed combustor at different pneumatic air feeding velocities

Table 5-2: Histograms for residence time distribution from computational fluid dynamics (CFD) modelling of burning rice husk particles in the 210-mm inner diameter fluidised bed combustor



As could be observed from the trajectories of rice husk particles inside the combustor (Table 5-3), as soon as they entered the combustor, the rice husk particles tended to stay at the bed region or be recirculated inside the freeboard of the combustor. The residence time of rice husk in this case could reach as high as 115 seconds, approximately 4 times higher than the minimum required period for complete combustion. The observed trajectories of rice husk particles were mostly due to the pneumatic airflow which created a ‘recirculating’ zone (Table 5-3, Model IV (iii)) near the feeding port (Figure 5-8), which was beneficial as it aided in ‘trapping’ and returning the rice husk particles into the bed region, as well as increasing their residence time in the freeboard region. In addition, most of the rice husk particles were retained in the bed region for more than 40 seconds before being entrained to the freeboard region (Table 5-3, Model IV (ii) and (iii)).

Table 5-3: Trajectories and residence times of burning rice husk particles in the 210-mm inner diameter fluidised bed combustor from CFD modelling

Model	Corresponding Exp. Case Study	pneumatic Air Feeding Velocity (m/s)	Trajectories of Burning Rice Husk Particle from Stochastic Tracking in the FLUENT CFD Model								
I	PV1	0.42	<p>35 33.3 31.6 29.8 28 26.3 24.5 22.9 21 19.3 17.5 15.8 14 12.3 10.5 8.7 7 5.25 3.5 1.75 0</p> <p>RH comb. in 210mm FB (8.5 Dc, 3.3 Umf, Rh, Dp = 1.6mm, sphericity) Particle Traces Colored by Particle Residence Time (s) * bubble eruption @ bed surface FLUENT 6.1 (3d, segregated)</p>	<p>38.5 36.6 34.7 32.7 30.8 28.9 27 25.1 23.1 21.2 19.3 17.3 15.4 13.6 11.6 9.83 7.7 5.78 3.85 1.93 0</p> <p>RH comb. in 210mm FB (8.5 Dc, 3.3 Umf, Rh, Dp = 1.6mm, sphericity) Particle Traces Colored by Particle Residence Time (s) * bubble eruption @ bed surface FLUENT 6.1 (3d, segregated)</p>	<p>56 53.2 50.4 47.6 44.8 42 39.2 36.4 33.6 30.8 28 25.2 22.4 19.6 16.8 14 11.2 8.4 5.6 2.8 0</p> <p>RH comb. in 210mm FB (8.5 Dc, 3.3 Umf, Rh, Dp = 1.6mm, sphericity) Particle Traces Colored by Particle Residence Time (s) * bubble eruption @ bed surface FLUENT 6.1 (3d, segregated)</p>	(i)	(ii)	(iii)			
			II	PV2	0.63	<p>22.4 21.3 19.2 18.1 17.3 16.8 15.7 14.6 13.5 12.3 11.2 10.1 8.97 7.85 6.73 5.61 4.49 3.36 2.24 1.12 0</p> <p>RH comb. in 210mm FB (8.5 Dc, 3.3 Umf, Rh, Dp = 1.6 mm, sphericity) Particle Traces Colored by Particle Residence Time (s) * bubble eruption @ bed surface FLUENT 6.1 (3d, segregated)</p>	<p>36.9 34.9 33 31.1 29.1 27.2 25.2 23.3 21.4 19.4 17.5 15.5 13.6 11.6 9.71 7.77 5.82 3.88 1.94 0</p> <p>RH comb. in 210mm FB (8.5 Dc, 3.3 Umf, Rh, Dp = 1.6 mm, sphericity) Particle Traces Colored by Particle Residence Time (s) * bubble eruption @ bed surface FLUENT 6.1 (3d, segregated)</p>	<p>59 55.1 52.2 49.3 46.4 43.5 40.6 37.7 34.8 31.9 29 26.1 23.2 20.3 17.4 14.5 11.6 8.7 5.8 2.9 0</p> <p>RH comb. in 210mm FB (8.5 Dc, 3.3 Umf, Rh, Dp = 1.6 mm, sphericity) Particle Traces Colored by Particle Residence Time (s) * bubble eruption @ bed surface FLUENT 6.1 (3d, segregated)</p>	(i)	(ii)	(iii)
						III	PV3	0.85	<p>23.9 22.6 21.4 19.2 19 17.8 16.6 15.5 14.3 13.1 11.9 10.7 9.51 8.32 7.13 5.94 4.75 3.57 2.38 1.19 0</p> <p>RH comb. in 210mm FB (8.5 Dc, 3.8 Umf, Rh, Dp = 1.6 mm, sphericity) Particle Traces Colored by Particle Residence Time (s) * bubble eruption @ bed surface FLUENT 6.1 (3d, segregated)</p>	<p>36.9 34.9 32.9 31 29.1 27.1 25.2 23.3 21.3 19.4 17.4 15.5 13.6 11.6 9.89 7.75 5.81 3.88 1.94 0</p> <p>RH comb. in 210mm FB (8.5 Dc, 3.8 Umf, Rh, Dp = 1.6 mm, sphericity) Particle Traces Colored by Particle Residence Time (s) * bubble eruption @ bed surface FLUENT 6.1 (3d, segregated)</p>	<p>49 43.7 41.4 39.1 36.8 34.5 32.2 29.9 27.6 25.3 23 20.7 18.4 16.1 13.8 11.5 9.2 6.9 4.6 2.3 0</p> <p>RH comb. in 210mm FB (8.5 Dc, 3.8 Umf, Rh, Dp = 1.6 mm, sphericity) Particle Traces Colored by Particle Residence Time (s) * bubble eruption @ bed surface FLUENT 6.1 (3d, segregated)</p>
IV	1.36	<p>26 24.7 22.1 20.8 19.5 18.2 16.9 15.6 14.3 13 11.7 10.4 9.03 7.78 6.49 5.19 3.89 2.6 1.3 0</p> <p>RH comb. in 210mm FB (8.5 Dc, 3.4 Umf, Rh, Dp = 1.6mm, sphericity) Particle Traces Colored by Particle Residence Time (s) * bubble eruption @ bed surface FLUENT 6.1 (3d, segregated)</p>							<p>44.6 42.4 40.2 37.9 35.7 33.5 31.2 29 26.8 24.5 22.3 20.1 17.9 15.6 13.4 11.2 9.03 6.89 4.66 2.23 0</p> <p>RH comb. in 210mm FB (8.5 Dc, 3.4 Umf, Rh, Dp = 1.6mm, sphericity) Particle Traces Colored by Particle Residence Time (s) * bubble eruption @ bed surface FLUENT 6.1 (3d, segregated)</p>	<p>67.3 62.9 58.5 54.2 49.8 45.4 41.1 36.7 32.4 28 23.6 19.3 14.9 10.5 6.2 1.9 0</p> <p>RH comb. in 210mm FB (8.5 Dc, 3.4 Umf, Rh, Dp = 1.6mm, sphericity) Particle Traces Colored by Particle Residence Time (s) * bubble eruption @ bed surface FLUENT 6.1 (3d, segregated)</p>	(i)

Note:
Three different trajectories depicted for each model due to the stochastic tracking approach, which predicted the particle path based on the fluctuating, instantaneous fluid velocity in the combustor

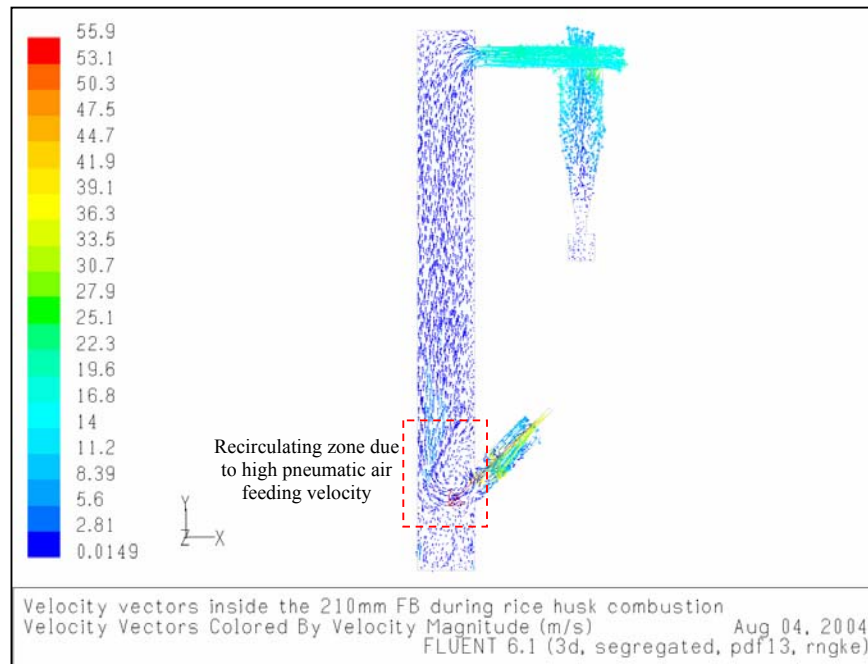
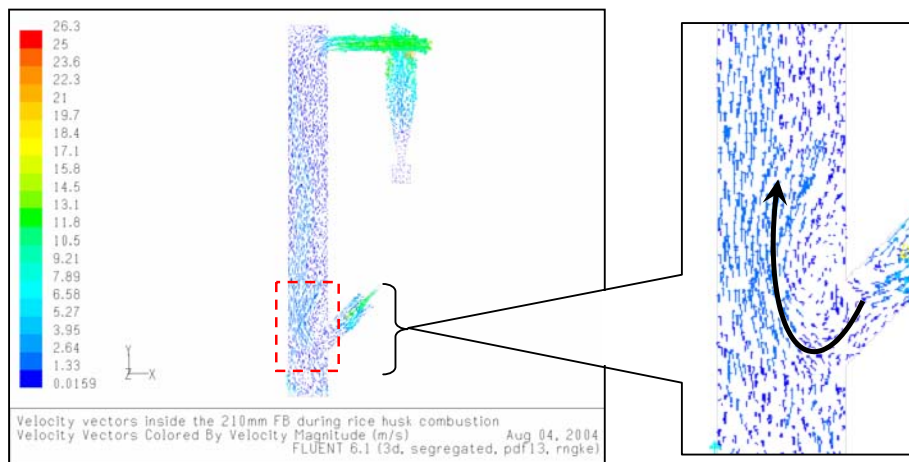
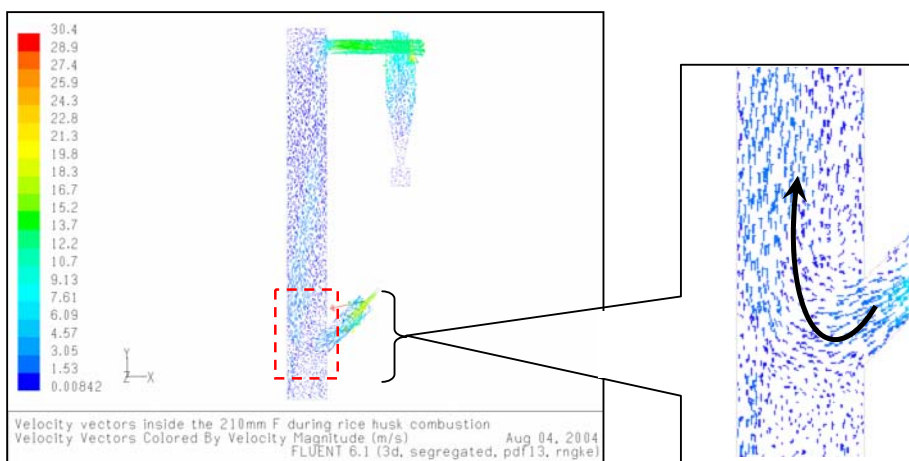


Figure 5-8: Recirculating zone near the feeding port of the combustor in Model IV (pneumatic air feeding velocity = 1.36 m/s)

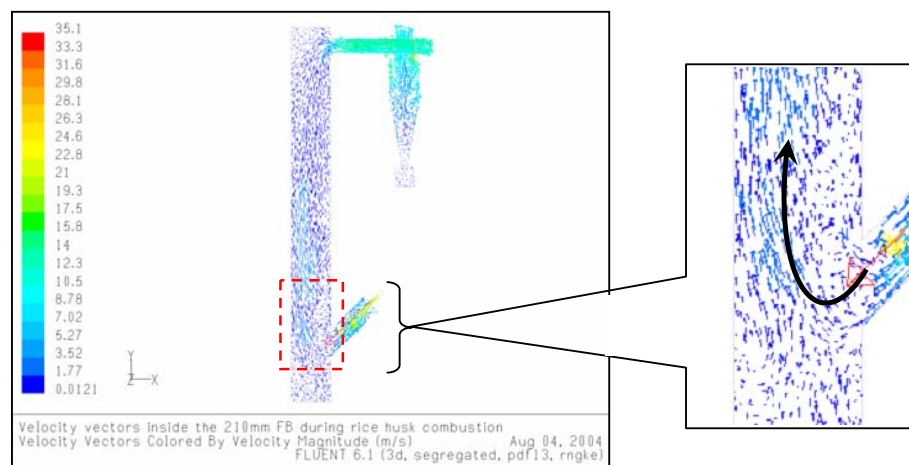
From Figure 5-7, it was found that the mean residence time for Models I, II and III were similar at approximately 40 seconds. However, the maximum residence time of rice husk recorded for Model III was the lowest amongst the three models, at only 52 seconds compared to 72 seconds for both Models I and II. Thus, the lowest burnout of rice husk particles as observed in the experimental study was duly expected. The rice husk particles spend less than 20 seconds in the bed region, as observed in Table 5-2 (Model III (i) – (iii)). The short period of time that the rice husk particles spent in the bed region was insufficient for complete burnout to take place. In comparison, the rice husk particles in both Models I and II were retained in the bed region for a relatively longer period of time (25 – 35 seconds), thereby allowing for more complete burnout to take place. Further, compared with Model IV, the ‘recirculating’ zone (Figure 5-8) was non-existent in all three Models I – III (Figure 5-9).



Model I (pneumatic air feeding velocity = 0.42 m/s)



Model II (pneumatic air feeding velocity = 0.63 m/s)



Model III (pneumatic air feeding velocity = 0.85 m/s)

Figure 5-9: Absence of recirculating zones inside the fluidised bed combustor in Models I, II and III (pneumatic air feeding velocities of 0.42 – 0.85 m/s)

b) Comparisons of Experimental and Modelling Results

Analyses on the experimental results (burnout of rice husk as indicated by the residual carbon content in the ash) and the modelling results (residence time distribution and trajectories of rice husk particles) showed a high level of agreement. Through the modelling results, it could be explained that the highest burnout was obtained in Case PV4 (pneumatic air feeding velocity of 1.36 m/s) due to the highest value of residence time (mean and maximum) of the rice husk particles in the combustor (Model IV). Further, the modelling results were able to offer an explanation as to the reason the residence time distribution in this case was the highest amongst the four models, in the form of occurrence of a 'recirculating' zone near the feeding port (Figure 5-8) due to the high pneumatic air feeding velocity. This phenomenon could not be observed experimentally as the hydrodynamics occurring inside the combustor was 'opaque' to the observer. This recirculating zone was observed to be absent in the other three models (I, II and III) (Figure 5-9). In Models I and II (pneumatic air feeding velocities of 0.42 and 0.63 m/s), the velocity vectors inside the combustor were quite similar, whereby most of the pneumatic air was rushing upwards to the freeboard region, entraining the burning rice husk and ash particles along with the airflow (Figure 5-9, Model I and II). This similarity in combustion characteristics were reflected in the similar temperature profile and carbon content in the ash during the experimental study (Figure 4-28).

When the pneumatic air feeding velocity was increased further to 0.85 m/s (Model III), the high velocity near the feeding port resulted in excessive entrainment of the freshly-fed rice husk particles, resulting in the lowest residence time and subsequently the highest carbon content in the ash (at 6.8 wt%). In this case, the bulk of the residence time as well as the burning process were spent in the freeboard region, with the char particles still undergoing the oxidation process as they are being entrained to the freeboard region towards the cyclone (Figure 5-10). In comparison, most of the char portion had been burnt off in Model IV, with very minimal burning taking place in the freeboard region as the bulk of the char burning had taken place in the bed region (Figure 5-11).

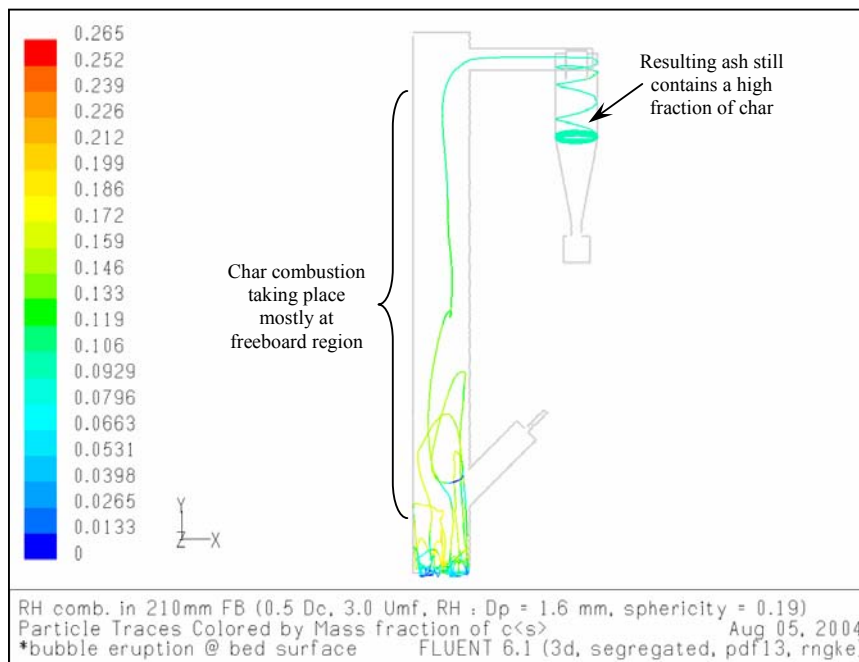


Figure 5-10: Char fraction of a burning rice husk particle in Model III
 (pneumatic air feeding velocity = 0.85 m/s)

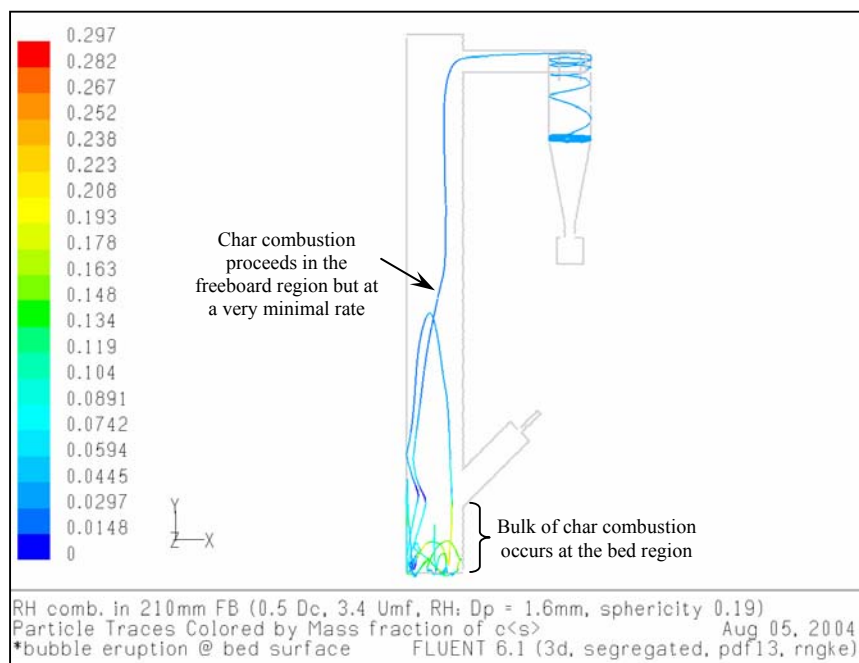


Figure 5-11: Char fraction of a burning rice husk particle in Model IV
 (pneumatic air feeding velocity = 1.36 m/s)

5.2.2 Vortex Feeding

a) Effect on Gas Flow Profile

The gas flow profile in the fluidised bed combustor during both case studies were shown in Figure 5-12 and Figure 5-13 (Model FM-A representing Case FM1: Inclined feeding method), and Figure 5-14 (Model FM-B representing Case FM2: Inclined, tangential feeding method). In Model FM-A, there was a tendency for occurrence of recirculating flow regions adjacent to the feed entry. The velocity vectors (Figure 5-13) showed the presence of two prominent recirculating regions in Model FM-A, one immediately adjacent to the feed entry and another directly above it. In Model FM-B, it was observed from the modelling results that there existed a high degree of swirling flow at the flow entry region due to the tangential entry route. Owing to this swirling flow region, the residence time of gas in the fluidised bed combustor was twice higher (at 4.2 seconds) compared to that without the swirling flow region as in Model FM-A.

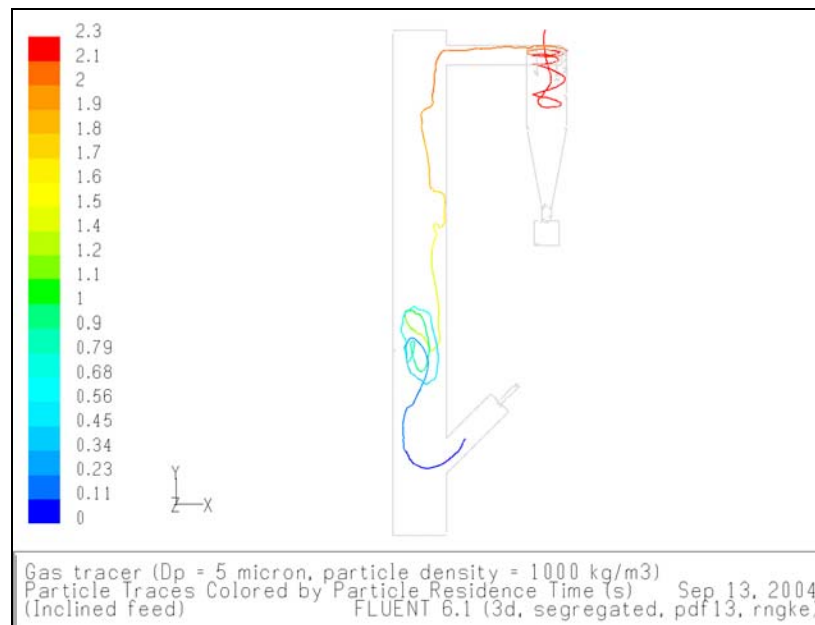


Figure 5-12: Gas flow profile as indicated by trajectory of tracer particle in the 210-mm inner diameter fluidised bed with inclined feeding port (Model FM-A)

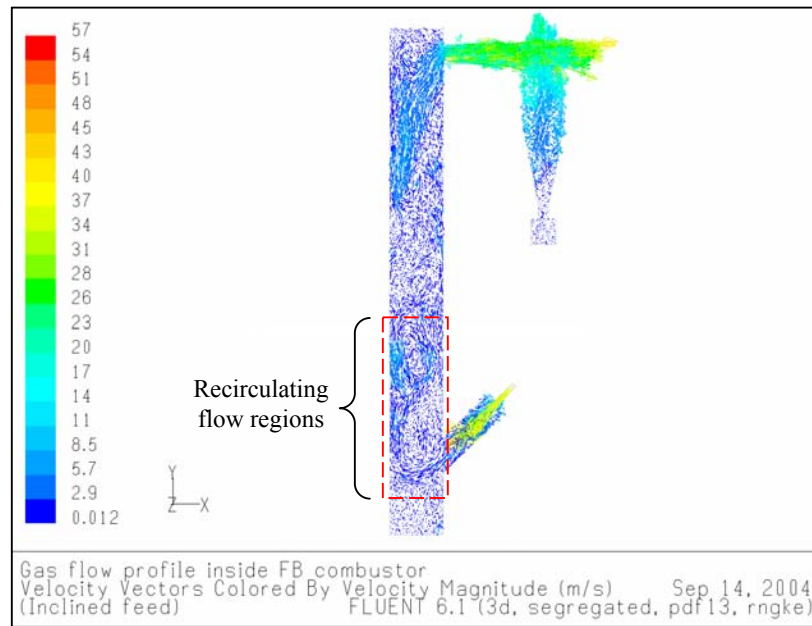


Figure 5-13: Gas flow profile inside in fluidised bed combustor with inclined feeding port (Model FM-A)

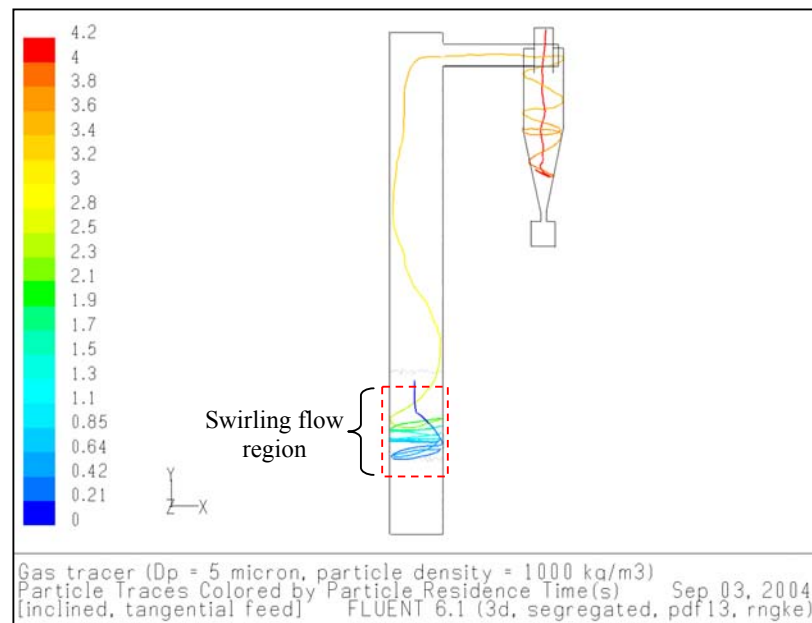


Figure 5-14: Gas flow profile as indicated by trajectory of tracer particle in the 210-mm inner diameter fluidised bed with inclined, tangential feeding port (Model FM-B)

b) Effect on Carbon Conversion Efficiency of Rice Husk

The fate of the particles during the combustion of rice husk utilising the different feeding methods as represented by Model FM-A (inclined feeding) and Model FM-B (inclined, tangential feeding) were tabulated in Table 5-4 and Table 5-5, respectively. The residence time of particle was defined as the period it took for the particle to be blown out from the combustor into the cyclone (i.e. the point where the particle exited the top of the fluidised bed column).

Table 5-4: Computational fluid dynamics (CFD) modelling results on the trajectories and residence times of particles during the combustion of rice husk in the 210-mm inner diameter fluidised bed combustor with inclined feeding port (Model FM-A)

Type of Particle Injection	Particle Representation in CFD Model	Diameter (μm)	Hypothesis on Particle Trajectory	Results from CFD Model		Remarks
				Particle Trajectory	Residence Time inside Fluidised Bed Combustor	
Rice husk (reacting particle)	Fly ash (burnt out rice husk skeleton)	25	Will elutriate from fluidised bed (FB) combustor	Elutriated from cyclone	0.5	Particles less than 750 μm will be elutriated from the FB combustor
		50		Elutriated from cyclone	0.7	
		75		Elutriated from cyclone	1.1	
		100		Elutriated from FB	2.8	
		200		Elutriated from FB	5	
		300		Elutriated from FB	6	
		500		Elutriated from FB	9	
		750		Elutriated from FB	22	
		1000	Will retain inside bed region	Retained inside FB	∞	
		1600		Retained inside FB	∞	
Silica / final ash (inert particle)	Bottom ash (similar shape as rice husk, particle density set at a constant 2000 kg/m^3 , injection at bed surface with bubble eruption velocity)	10	Will elutriate from fluidised bed (FB) combustor	Elutriated from cyclone	1.6	Particles less than 150 μm will be elutriated from the FB combustor
		25		Elutriated from FB	1.6	
		50		Elutriated from FB	1.9	
		75		Elutriated from FB	2.3	
		150		Elutriated from FB	3.8	
		300	Will retain inside bed region	Retained inside FB	∞	
		500		Retained inside FB	∞	
		750		Retained inside FB	∞	
		1000		Retained inside FB	∞	
		1600		Retained inside FB	∞	

Table 5-5: Computational fluid dynamics (CFD) modelling results on the trajectories and residence times of particles during the combustion of rice husk in the 210-mm inner diameter fluidised bed combustor with inclined, tangential feeding port (Model FM-B)

Type of Particle Injection	Particle Representation in CFD Model	Diameter (μm)	Hypothesis on Particle Trajectory	Results from CFD Model		Remarks
				Particle Trajectory	Residence Time inside Fluidised Bed Combustor	
Rice husk (reacting particle)	Fly ash (burnt out rice husk skeleton)	25	Will elutriate from fluidised bed (FB) combustor	Elutriated from cyclone	2.5	Particles less than 750 μm will be elutriated from the FB combustor
		50		Elutriated from cyclone	3.1	
		75		Elutriated from FB	3.6	
		100		Elutriated from FB	3.5	
		200		Elutriated from FB	14	
		300	Elutriated from FB	24		
		500	Will retain inside bed region	Retained in <i>swirling flow region</i> * for 20 seconds, finally elutriated from FB	28	
		750		Retained in <i>swirling flow region</i> * for 70 seconds, finally elutriated from FB	80	
		1000		Retained inside bed region indefinitely	∞	
		1600		Retained inside bed region indefinitely	∞	
Silica / final ash (inert particle)	Bottom ash (similar shape as rice husk, particle density set at a constant 2000 kg/m^3 , injection at bed surface with bubble eruption velocity)	10	Will elutriate from fluidised bed (FB) combustor	Elutriated from cyclone	1.1	Particles less than 150 μm will be elutriated from the FB combustor
		25		Elutriated from FB	1.3	
		50		Elutriated from FB	1.2	
		75		Elutriated from FB	1.3	
		150		Elutriated from FB	28	
		300	Will retain inside bed region	Retained inside bed region indefinitely	∞	
		500		Retained inside bed region indefinitely	∞	
		750		Retained inside bed region indefinitely	∞	
		1000		Retained inside bed region indefinitely	∞	
		1600		Retained inside bed region indefinitely	∞	

Note:-

* *Swirling flow region* = region between the surface of bed to the height of tangential feed inlet or $105 \leq y \leq 650$ mm in CFD model, bed region = $0 \leq y \leq 105$ mm

i) Particle Trajectory and Residence Time Distribution

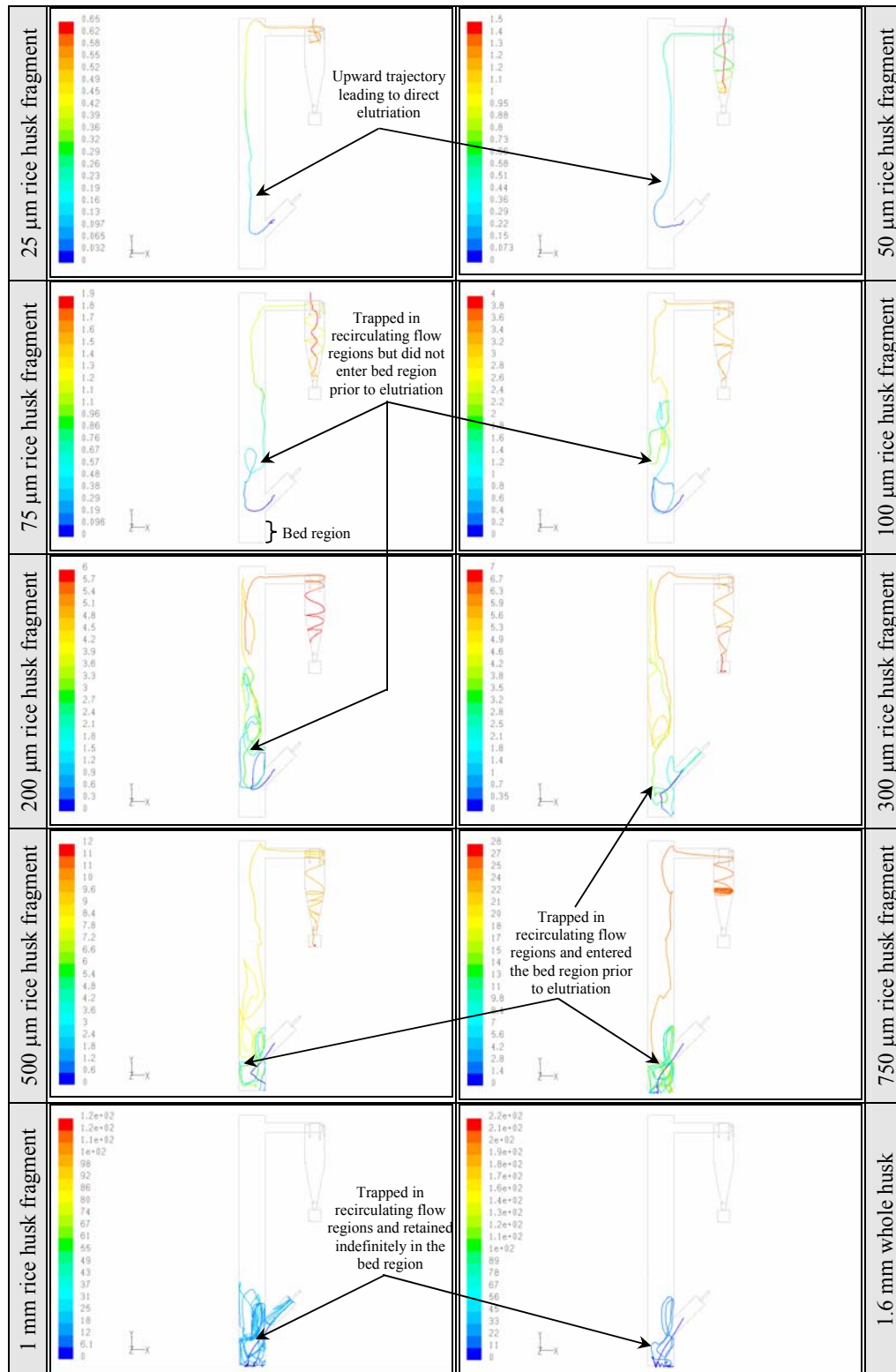
From Table 5-4, it was found that the hypotheses on the particle trajectories based on the particle screen analysis (fly ash from Case FM1: Inclined feeding method) matched the modelling results for Model FM-A for all 10 particle streams. The burnt rice husk particles of less than 1mm were observed to be entrained into the gas stream and be blown out of the combustor, as shown in Table 5-6. Table 5-6 also showed that bigger rice husk fragments (75 – 750 μm) tended to be ‘trapped’ in the recirculating flow regions in the fluidised bed combustor (Figure 5-13) prior to elutriation, thereby increasing their residence times. For instance, the residence time of the 750 μm burning rice husk fragment was approximately 2 times higher than that of the 500 μm fragment. When the fragments were in the excess of 1mm, they tended to be retained at the bed region.

Similarly, in Model FM-B (inclined, tangential feeding method), the burnt rice husk fragments in the excess of 1mm were also retained in the bed region. Also, hypotheses based on the particle screen analysis (fly ash from Case FM2) matched the modelling results for Model FM-B for all 10 particle streams. However, there were two clear differences. First, all of the rice husk fragments including those in the range of 25 – 200 μm entered the bed region, as shown in Table 5-7. Secondly, in Model FM-B, the residence times of the burning rice husk fragments were much higher due to the presence of the swirling flow region which tended to recirculate the particles before they were finally blown out into the cyclone (Table 5-7). The tangential velocity component in the rice husk particles tended to cause them to impact the combustor wall and lose their momentum, after which they slid down towards the bed region. This was especially more prominent for particles in the excess of 200 μm ; for instance the residence time increased by 4 times to 14 seconds for the 200 μm fragment compared to only 3.5 seconds for the 100 μm fragment. After sliding down the wall, the turbulent action in the bubbling bed region proceeded to break these particles into smaller fragments. Hence, this explained the reason why the fly ash particles when feeding via the inclined, tangential feed inlet (Case FM2) was much finer in size compared to that obtained from feeding via the inclined feeding port (Case FM1). As can be seen from Table 5-7, it was increasingly more difficult for the bigger particles (200 – 750 μm) to be entrained

into the gas stream as they tended to get trapped in the swirling flows region. For rice husk fragment of size 750 μm , modelling results from Model FM-B showed that their residence time could be as high as 80 seconds, nearly 3 times higher than that of the 500 μm particles. The phenomenon of ash particles being trapped in the swirling flows region could be prevented, for example, by lowering the tangential feed velocity of the entering rice husk particles. Table 5-8 showed that the swirling flows were less intense and the bigger fly ash particles (200 – 750 μm) were more easily blown towards the cyclone when the tangential feeding velocity was reduced by half from 1.1 m/s to 0.55 m/s. This velocity reduction also enabled 1-mm fragments of ash particles to be entrained towards the cyclone instead of being retained in the bed region (Table 5-8).

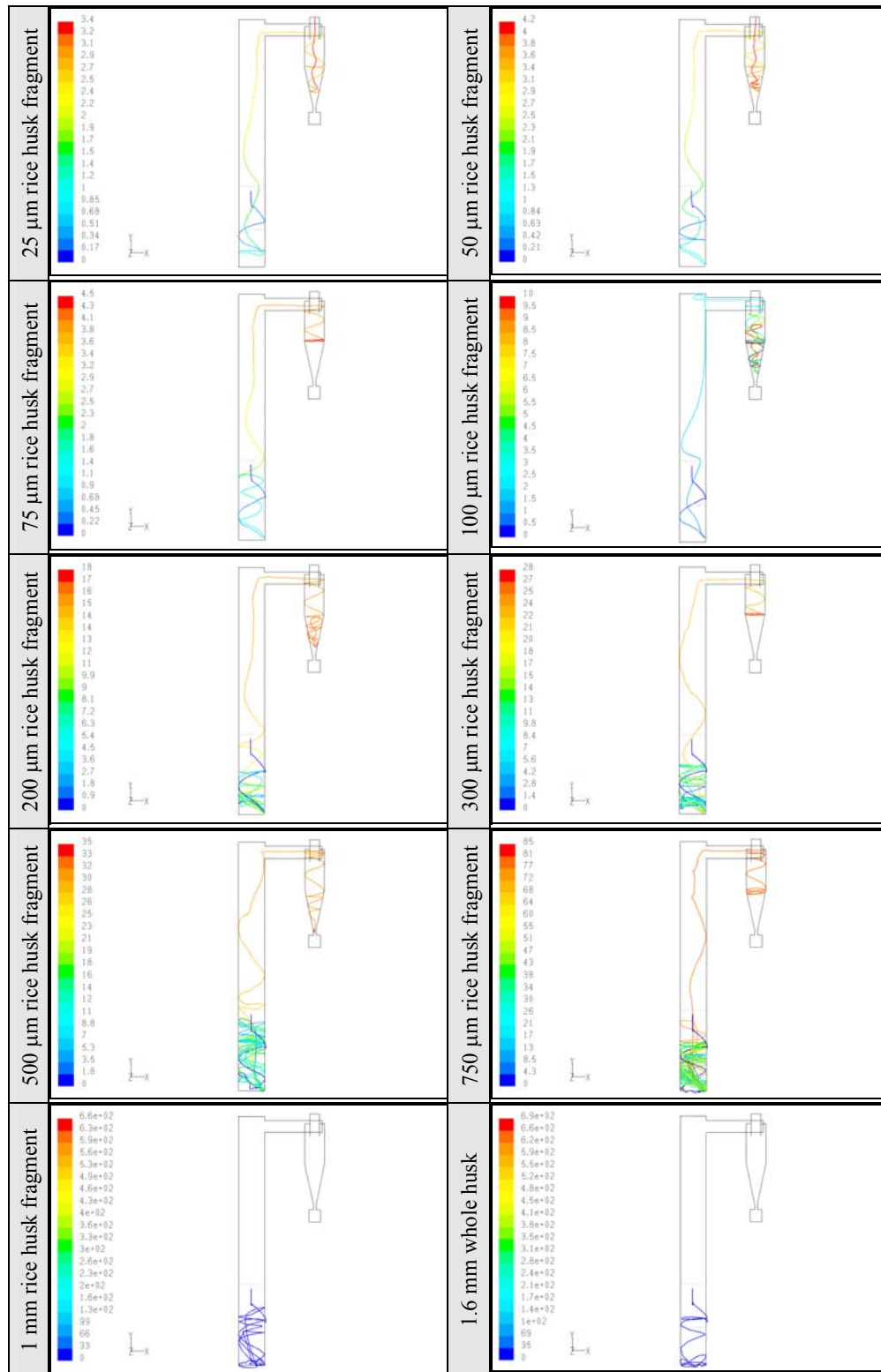
The residence times of fly ash particles in both Model FM-A and Model FM-B were compared in Figure 5-15. It was observed that the difference in residence times were more prominent when the rice husk particle were more than 200 μm . The presence of the swirling flows due to the inclined, tangential feed entry could increase the residence time of rice husk particles for as high as 4 times (for 750 μm fragment) compared to that without the swirling flow component (inclined feed entry).

Table 5-6: Trajectories and residence times of fly ash particles in Model FM-A (inclined feeding method)



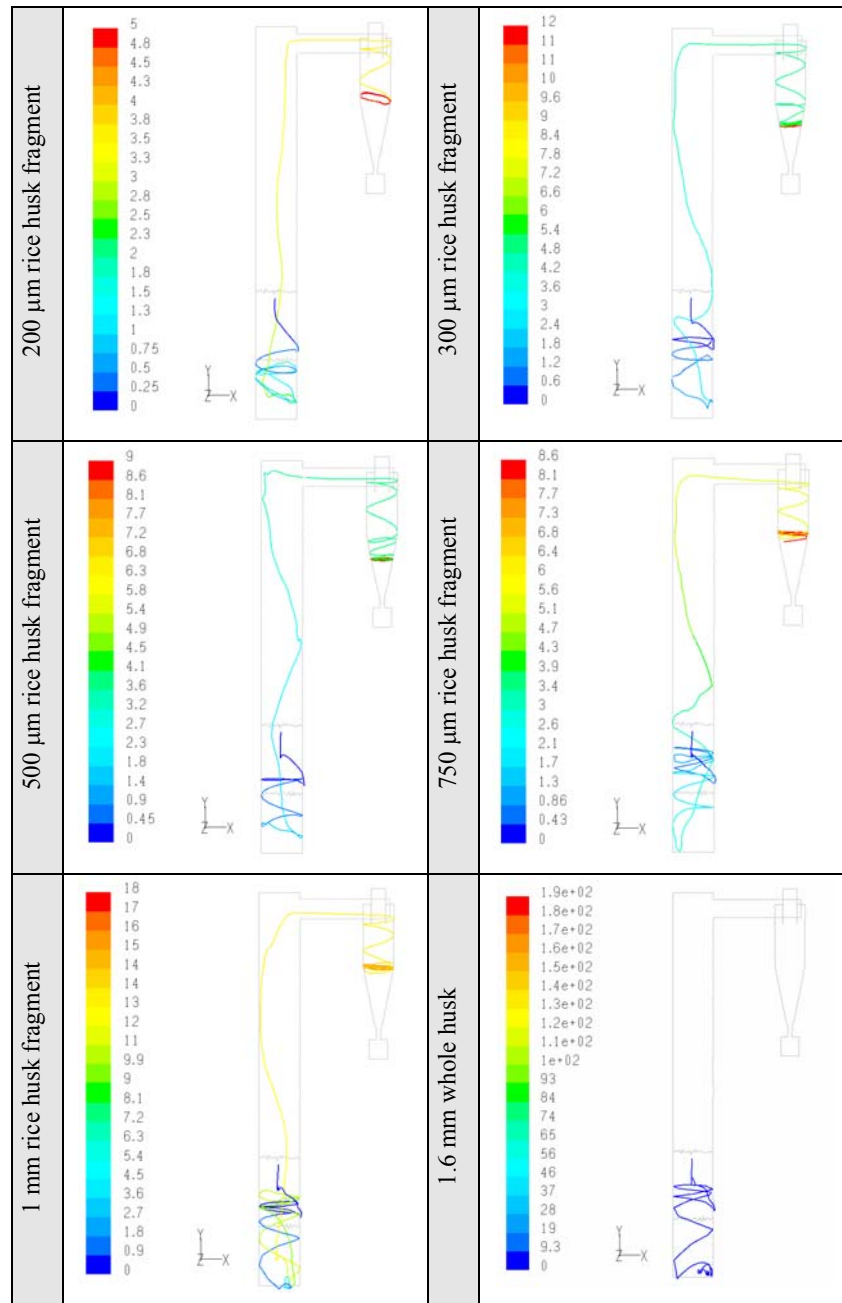
Note:
Particle traces coloured by particle residence time (s)

Table 5-7: Trajectories and residence times of fly ash particles in Model FM-B (inclined, tangential feeding method)



Note:
Particle traces coloured by particle residence time (s)

Table 5-8: Trajectories of fly ash particles in Model FM-B (inclined, tangential feeding) when the tangential feeding velocity was reduced by half (from 1.1 m/s to 0.55 m/s)



Note:

Particle traces coloured by particle residence time (s)

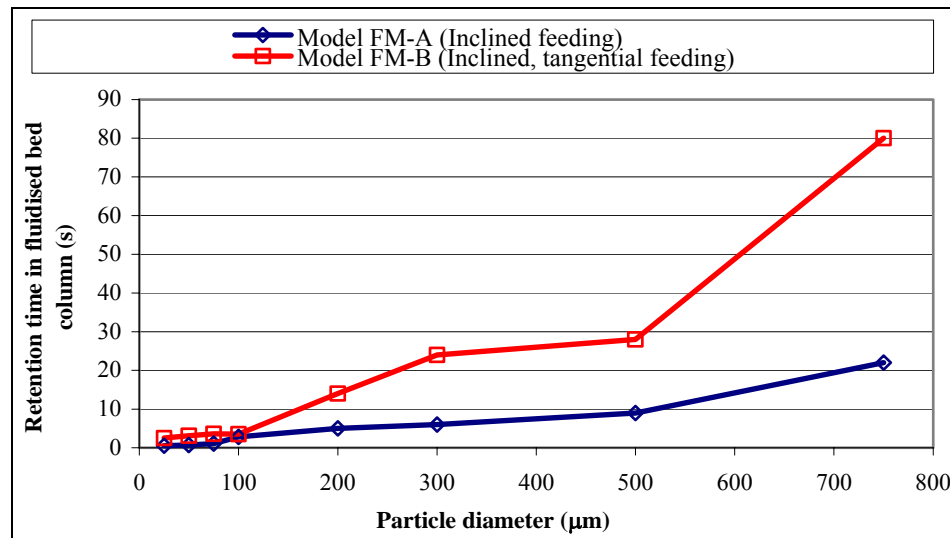
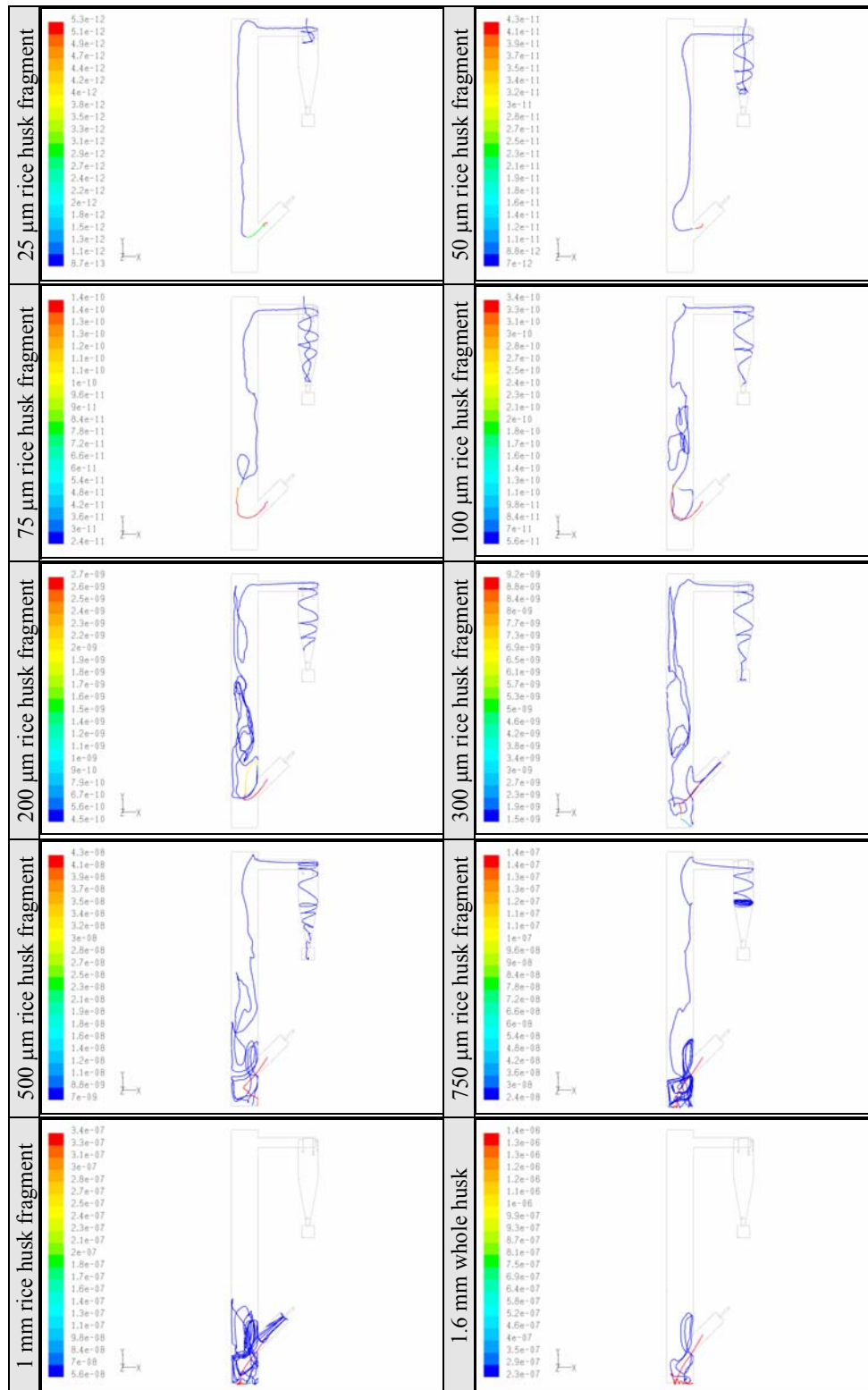


Figure 5-15: Comparisons of residence time of fly ash of different sizes in Model FM-A (inclined feeding) and Model FM-B (inclined, tangential feeding)

ii) Mass Loss History of Rice Husk Particles

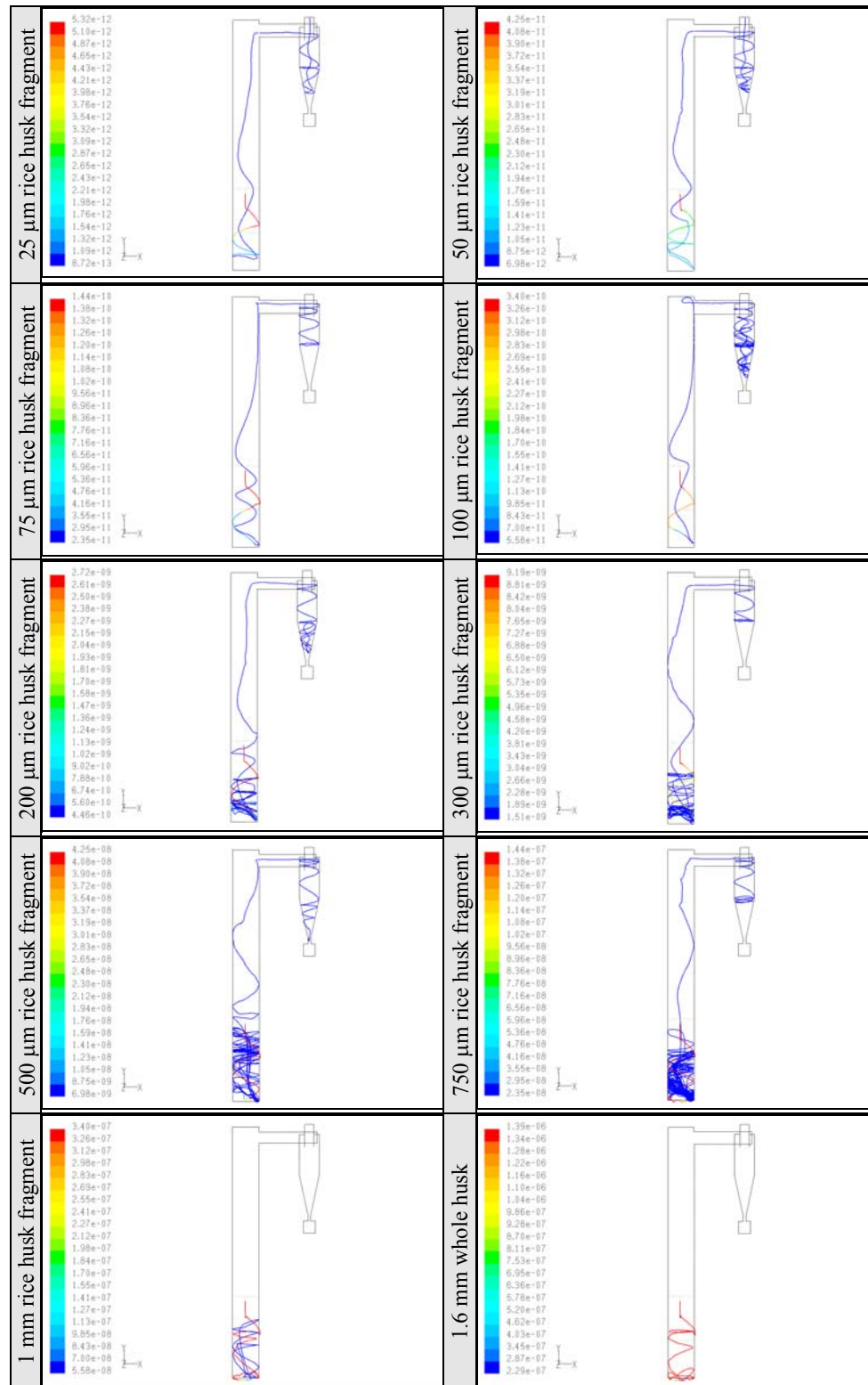
In Model FM-A (inclined feeding method), burning of rice husk fragments with sizes less than 200 µm tended to occur at the freeboard region without entering the bed region (Table 5-9). Their mass losses due to the evolution of volatiles and char burning proceeded as they were blown upwards towards the cyclone. As for rice husk fragments in the range of 300 – 1000 µm including the whole husk particle (1.6mm in size), their mass losses only occur once they reached the bed region. Once burning was completed, the resulting ash at sizes of 300 – 750 µm were recirculated for a period of time in the bed and feed entry regions prior to elutriation into the cyclone. Ash particles with sizes in the excess of 1000 µm (1mm) could not be entrained into the freeboard region but were retained in the bed and feed entry regions instead. Meanwhile, in Model FM-B (inclined, tangential feeding method) (Table 5-10), the pneumatic/secondary air entering through the tangential feed inlet resulted in highly turbulent, swirling flows at the lower portion of the fluidised bed combustor (one-third the height of entire combustor, including the bed region at the height of 105mm). This phenomenon aided in increasing the retention of rice husk particles near the bed region. Thus, most of the rice husk particles were burnt completely in this region prior to entrainment into the freeboard region. Further, these burnt out particles were subsequently elutriated (particle sizes less than 750 µm) into the cyclone.

Table 5-9: Mass loss history of burning rice husk particles in Model FM-A (inclined feeding method)



Note:
Particle traces coloured by particle mass (kg)

**Table 5-10: Mass loss history of burning rice husk particles in Model FM-B
(inclined, tangential feeding method)**

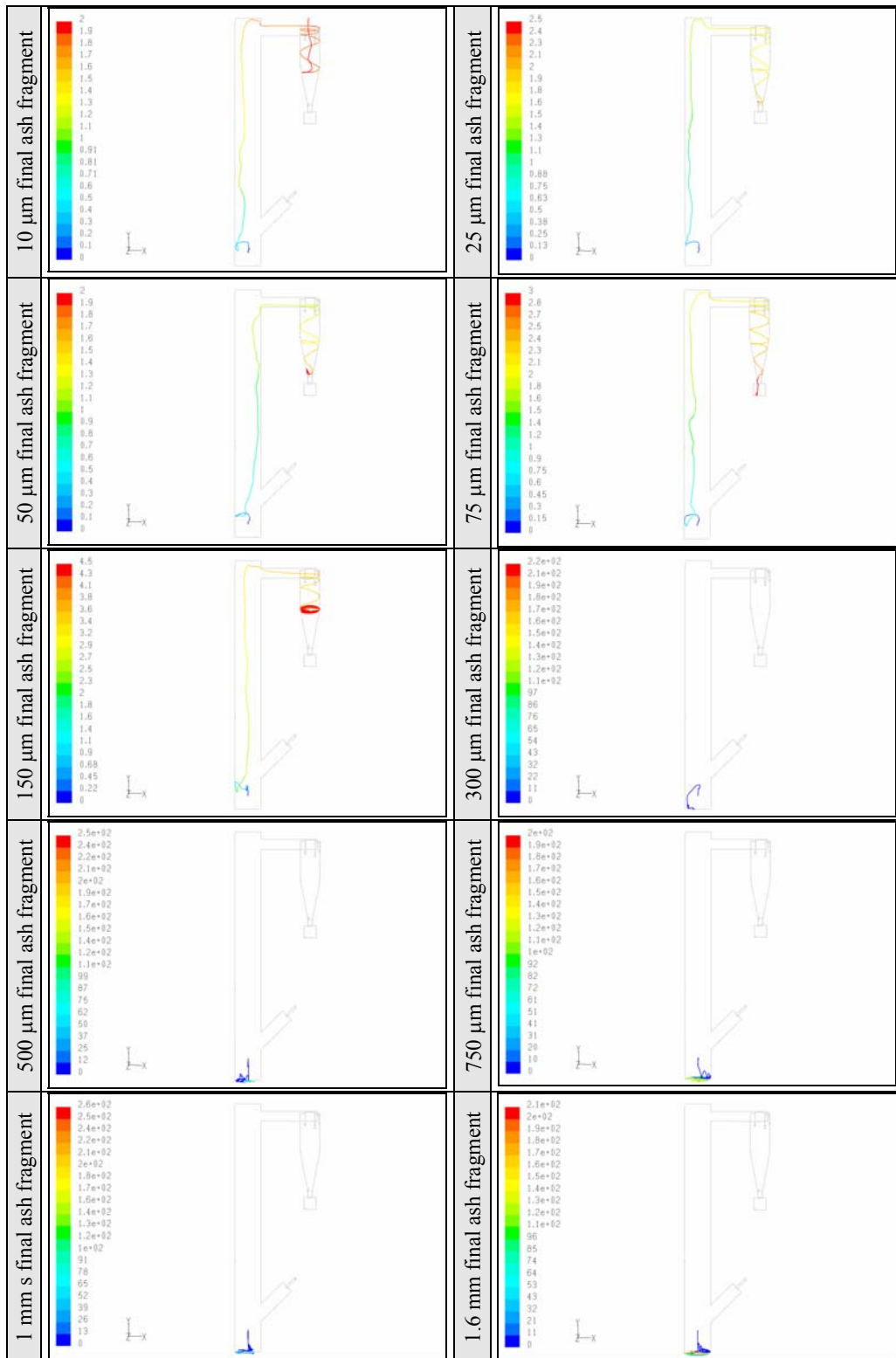


Note:
Particle traces coloured by particle mass (kg)

c) Effect on the Accumulation of Ash in the Bed Region

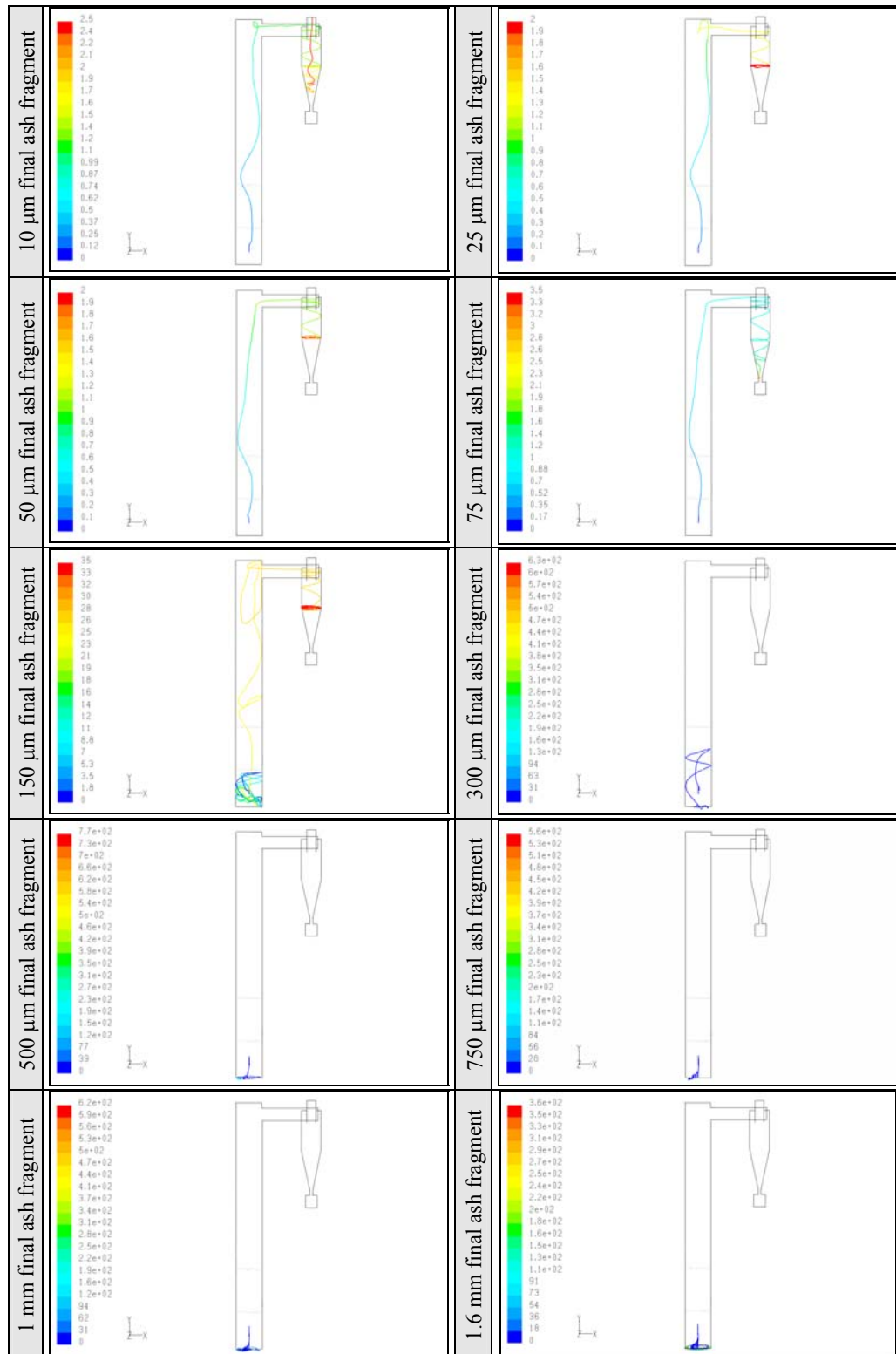
From the observations of particle trajectories in both Table 5-11 and Table 5-12, it could be concluded that the hypotheses made based on the particles screen analysis on the bottom ash samples (Case FM1: Inclined feeding method and Case FM2: Inclined, tangential feeding method) were true. Both models showed that bottom ash with sizes more than 150 μm were retained in the bed region. The significant differences were the residence time and trajectories of the elutriated particles. In Model FM-A (inclined feeding method), the trajectories of the elutriated bottom ash particles were mostly in the form of upward vertical path as they were blown towards the cyclone. In Model FM-B (inclined, tangential feeding method), this form of upward vertical path was also observed for particles of sizes less than 75 μm , which was as expected. Since they were injected in the midpoint of the bed cross section, they were easily caught up in the centre, upward 'vortex' of the swirling flow region. Bigger particles, such as that of the 150 μm , tended to be caught in the swirling flow region for sometime, thereby increasing their residence times by approximately 7 times (to 28 seconds) compared to the same particle size in Model FM-A. Further, in Model FM-A, the high downward-flowing pneumatic air velocity from the inclined feed inlet (up to 4 m/s at the boundary with the fluidised bed combustor) tended to push the particles down towards the bed. Thus, smaller particles such as that with sizes of less than 75 μm tended to be pushed downwards before they were ejected upwards by the bubble eruption at the bed surface, hence resulting in slightly higher residence times compared to similar particles (also less than 75 μm only) in Model FM-B.

Table 5-11: Trajectories and residence times of bottom ash particles in Model FM-A (inclined feeding method)



Note:
Particle traces coloured by particle residence time (s)

Table 5-12: Trajectories and residence times of bottom ash particles in Model FM-B (inclined, tangential feeding method)



Note:
Particle traces coloured by particle residence time (s)

d) Comparisons of Experimental and Modelling Results

Analyses on both the modelling and experimental results showed that the modelling results were able to offer some explanations on the temperature profile and ash quality observed during experiments.

i) Temperature Profile

CFD modelling on rice husk particle combustion in the fluidised bed combustor with inclined feeding (Model FM-A) showed that the bulk of weight loss due to devolatilisation and char oxidation for rice husk particles especially those in the excess of 500 μm (Table 5-9), occurred at the lower portion of the combustor (spanning a height up to one-third of the combustor to approximately 600mm from the distributor plate). This was found to be consistent with the temperature profile (Figure 4-34) whereby the temperature in this region was in the excess of 600°C. Beyond this region, the combustor temperature remained less than 625°C, which indicated that the carbon oxidation rate was quite low. As the exposure period of the fly ash to the temperatures in the freeboard was very brief (estimated to be less than 2 minutes), a temperature in the region of 700°C was necessary to achieve complete conversion of fixed carbon in the fly ash, as reported by Sen and Ghosh (1992). As such, any fly ash particles entrained to the freeboard beyond the height of 600mm was expected not to undergo significant rate of char oxidation.

On the other hand, for Model FM-B (inclined, tangential feeding method), the bulk of weight loss for rice husk particles (size in the excess of 300 μm) also took place in the same region as that of model FM-A, i.e. at a height up to 600mm from the distributor plate (Table 5-10). However, the temperature profile in Figure 4-34 showed that the bulk of weight loss for the rice husk particles took place mainly in and near the bed region, as indicated by temperature above 600°C at a combustor height of up to 180 mm (Zone A in Figure 4-34). The discrepancy thus demonstrated by the model could be attributed to the fact that the CFD model was unable to simulate the ‘breaking’ effect on the rice husk particles due to the turbulence in the swirling flow region. This ‘breaking’ effect was expected to result in small fragments of rice husk and or char/ash which were more difficult to penetrate the bubbling bed. These broken fragments may instead be elutriated to the freeboard

region while still undergoing considerable rate of char oxidation due to the relatively high temperature (650 – 680°C, Zone B in Figure 4-34) compared to the case of using the inclined feeding method (Case Study FM1). The good penetration rate of the broken rice husk and or char/ash fragments into the bed region as well as the subsequent retention or accumulation of the ash in the bed region, explained why the bed temperature for Case Study FM2 was lower than that of Case Study FM1. This was because some of the heat in the bed was also absorbed by these accumulated ash particles having relatively higher heat capacity (at 1.3 J/(g • °C), Table 4-42) compared to that of the bed material (silica sand, at 0.8 J/(g • °C)). The significant accumulation of ash particles in the bed when feeding was by the tangential method was proven experimentally, whereby the amount of bottom ash was three times higher than that of the fly ash.

ii) Ash Quality

In terms of residual carbon content in the ash samples, it was found that fly ash samples from both experiments (Sample FM1-a and FM2-a) contained similar amount of residual carbon, at 1.9 wt%. The only difference was the fly ash particles from the inclined, tangential feeding (Sample FM2-a) were finer in size, constituted by 94% of particles with sizes less than 300 µm (Figure 4-35). This was in comparison with the fly ash sample from the inclined feeding method (Sample FM1-a), which was constituted of mainly of particles in the size range of 75 – 500 µm (at approximately 94%, also according to Figure 4-35). There was also approximately 4% of the particles in Sample FM1-a which was in the size range of 500 – 1000 µm. Correlating these observations with the modelling results, it could be explained that the presence of finer fly ash particles with the inclined, tangential feeding was due to the presence of swirling flows above the bed region (Figure 5-14). This swirling flow thus formed caused the rice husk particles to impact the wall upon feeding, and then slid down the wall to the bubbling bed region. Thereafter, the turbulent bubbling action of the bed tended to break them into smaller fragments. After the ash portion was liberated from these rice husk fragments due to combustion in the bed region, some of these ash particles were elutriated to the freeboard region and got trapped at the ‘vortex’ of the swirling flows, as could be seen from Table 5-7, whereby fly ash particles with sizes more than 300 µm were caught up for a

considerable period of time before being blown towards the cyclone. It was speculated that these brittle ash particles were broken down by the turbulence in the swirling flows, and hence, giving an overall finer size of fly ash. When the ash particles were broken down into the size range of less than 300 μm , they were more easily blown towards to them, as could be seen in Table 5-7, thus explaining why Sample FM2-a consisted mostly of particles less than 300 μm .

As for the bottom ash, it was found that sample from the inclined, tangential feed method (Sample FM2-b) was generally coarser than that obtained from the inclined feeding method (Sample FM1-b). The CFD modelling results showed that the particles of Sample FM2-b, especially those in the range of 150 – 300 μm (Table 5-12), were caught up in the swirling flow region directly above the bubbling bed region whenever they were ejected to the freeboard region. The swirling flow imparted tangential velocity components to these particles, after which they tended to be returned to the bed region and be broken down into smaller fragments, thus giving an overall finer size of bottom ash, in particular later purges of the samples (Sample FM2-c and FM2-d, which were powder-like).

5.3 Summary of Findings

The major findings in this chapter were summarised as follows:-

a) Increase in Fluidised Bed Freeboard Height

i) Effect on Elutriation of Sand Particles

The height of the fluidised bed column should be at least 5000mm to prevent the elutriation of sand particles into the cyclone.

ii) Increase in Fluidised Bed Freeboard Height – Effect on Combustion Efficiency of Rice Husk in the Freeboard Region

The height of the fluidised bed column should be at least 5000mm for complete combustion of rice husk to produce carbon-free ash.

b) Improvement of Feeding Conditions***i) Effect of Pneumatic Air Feeding Velocity***

From the modelling study, it could be explained that the highest bed temperature and lowest residual carbon content in the ash in Case PV4 (pneumatic air feeding velocity of 1.36 m/s) were due to the presence of a recirculating zone near the feeding port just above the bed surface. This phenomenon aided in increasing the residence time of the rice husk particles in the combustor by ‘trapping’ and returning them to the bed region. The modelling study complemented the experimental study very well in that it offered some explanations as to the phenomena occurring inside the combustor, which otherwise were difficult if not impossible to be investigated experimentally.

ii) Effect of Vortex Feeding

From the modelling study, it could be explained that the lower average bed temperature in the case of the inclined, tangential feeding was due to the significant accumulation of ash in the bed region. This phenomenon was due to the presence of the swirling flow region directly above the bubbling bed, which constantly imparted tangential velocity components to ash particles ejected to the freeboard region from the bed due to bubble eruption. The presence of these tangential velocity components caused the ash particles to impact the wall and slid down again to the bed region, whereby they were broken down into smaller fragments. This cycle was repeated until the ash particles were fine enough to pass through the vortex flow and be blown towards the cyclone. This was proven experimentally whereby the amount of bottom ash was three times higher than that of the fly ash. The modelling study complemented the experimental study very well in that it offered significant graphical depiction of the hydrodynamics in the combustor, especially in the case of the inclined, tangential feeding method, which led to the phenomenon of ash accumulation in the bed region.

The presence of swirling flow components directly above the bubbling bed region was found to interrupt with the continuous operation of the fluidised bed, due to the significant accumulation of ash in the bed region. To overcome this problem, it was recommended that these swirling flow regions be induced at a higher freeboard height. This could be carried out by using the inclined feeding method but with the

addition of a tangential secondary air inlet, probably at mid-height of the combustor (i.e. 1000mm from the distributor). As such, the residence time of the ash particles in the freeboard region could be increased while at the same time, the ash accumulation problem could be eliminated. To achieve effective realisation of this recommendation, it was further recommended that the following parameters be investigated through CFD modelling prior to experimental studies:-

- Optimum location of tangential inlet for secondary airflow
- Optimum entering angle of the tangential inlet for secondary airflow
- Optimum flowrates of the pneumatic air and secondary air

CHAPTER 6

DESIGN, FABRICATION, INSTALLATION AND COMMISSIONING OF PILOT PLANT

6.1 Introduction

The previous investigation of rice husk combustion in a muffle furnace, lab-scale fluidized bed reactor and bench-scale fluidized bed combustor showed the following outcome:

- a) Rice husk required about 20 – 30 seconds (for single particle) and about 39 – 52 seconds (for group) in the temperature range of 650 - 750°C to burn to completion in order to obtain amorphous, carbon-free siliceous ash. The method of removing impurities from raw rice husk in particular potassium and sodium oxide helped in obtaining completely white rice husk ash in amorphous form.
- b) Exposure of rice husk at high temperature of 900°C and residence time of 3 minutes retained the amorphous state of siliceous ash. This finding was significant to the operation of Fluidised Bed Combustor (FBC), as the combustor could be operated confidently at the range of 700 - 900°C in order to achieve high carbon burnout without damaging the rice husk ash due to short retention time in fluidised bed. However, the residence time in

bench-scale fluidised bed combustor was less than minutes which resulted in incomplete burnout of carbon in rice husk. In addition, the combustor temperature was also not enough to obtain total carbon burnout.

- c) Optimum operating parameters such as sand size, fluidizing velocity, static bed height to achieve good mixing behavior and efficient combustion of rice husk in a fluidised bed were investigated. It was found that sand size of 295 – 595 μm was deemed optimum keeping the terminal velocity of sand, rice husk and rice husk ash in consideration with objective of achieving good mixing behavior. However, the rice husk ash was contaminated with sand as showed from XRD analysis due to short freeboard height of the combustor. Fluidizing velocity of $3.3 U_{mf}$ was optimum resulting in high degree of mixing and stable rice husk combustion compared to higher U_{mf} . Experimental and computational results showed that static bed height of $0.5 D_c$ was optimum in giving slow rising bubbles that distribute the rice husk uniformly in the bed region. Among this the optimum fluidizing condition (fluidising velocity and static bed height) achieved high combustion efficiency in a fluidised bed combustor.
- d) Bed temperature and freeboard temperature in a bench-scale fluidised bed combustor was in the range of 650 to 800°C which produced amorphous rice husk ash with 2.0 wt% carbon in fly ash and around 1.0 wt% in bottom ash.
- e) The ash samples from bench-scale fluidised bed combustor were not completely carbon-free due to short freeboard height of 2 m. this problem was expected to be solved by increasing the freeboard height of the fluidised bed. The optimum freeboard height to prevent sand contamination as well as to achieve complete carbon burnout in the rice husk ash was found to be at least 5 m from computational results.

Therefore, the optimum set of operating parameters for production of amorphous siliceous ash obtained from experiments conducted in a 210 mm fluidised bed combustor could be applied to scale up fluidised bed design of 5 m tall and 0.5 m in diameter pilot-scale fluidised bed combustor.

A pilot scale fluidized bed combustor was fabricated based on the conclusion and recommendations from the experimental works and Computational Fluid Dynamics (CFD) modelling as discussed above. The combustor was of 500 mm inner diameter and 5000 mm in height which was installed by February 2006. The commissioning of this pilot-scale fluidised bed combustor was carried out from March 2006 until July 2006. During commissioning stage, several problems were encountered such as insufficient air supply, inadequate piping system and rice husk feeding. In order to overcome the problem, modifications were recommended so as to run the combustor at an efficient condition. After completion of commissioning the combustor and fixing the problems investigated, the experiments were carried out from the month August 2006 to December 2006 on the pilot scale fluidized bed combustor.

6.2 Pilot-Scale Fluidised Bed Combustor Set-Up

The general assembly of whole pilot-scale fluidised bed combustor consists of combustor, blower (air supply), exhaust fan at top of the combustor (easing of flue gas), burner, temperature data acquisition system to measure the continuous temperature along the combustor and flue gas analyzer. The details of these equipments are as discussed in the following Sections.

6.2.1 Fluidised Bed Combustor

The combustor consists of a cylindrical column made of stainless steel with an internal diameter of 500 mm and height of 5000 mm. the combustor is facilitated with a viewing port located at a height of 1.22 m from the distributor plate and inclined at an angle of 45°. The thermocouples were positioned along the height of the combustor. The port for burner was provided at particular distance of the combustor. The schematic diagram of the pilot scale set-up is as shown in Figure 6-1.

6.2.2 Cyclone

The cyclone performed dual functions, firstly removing the fly ash from the flue gas and lastly as combustion chamber to burnout remaining carbon from rice husk ash if enough combustion condition are favored.

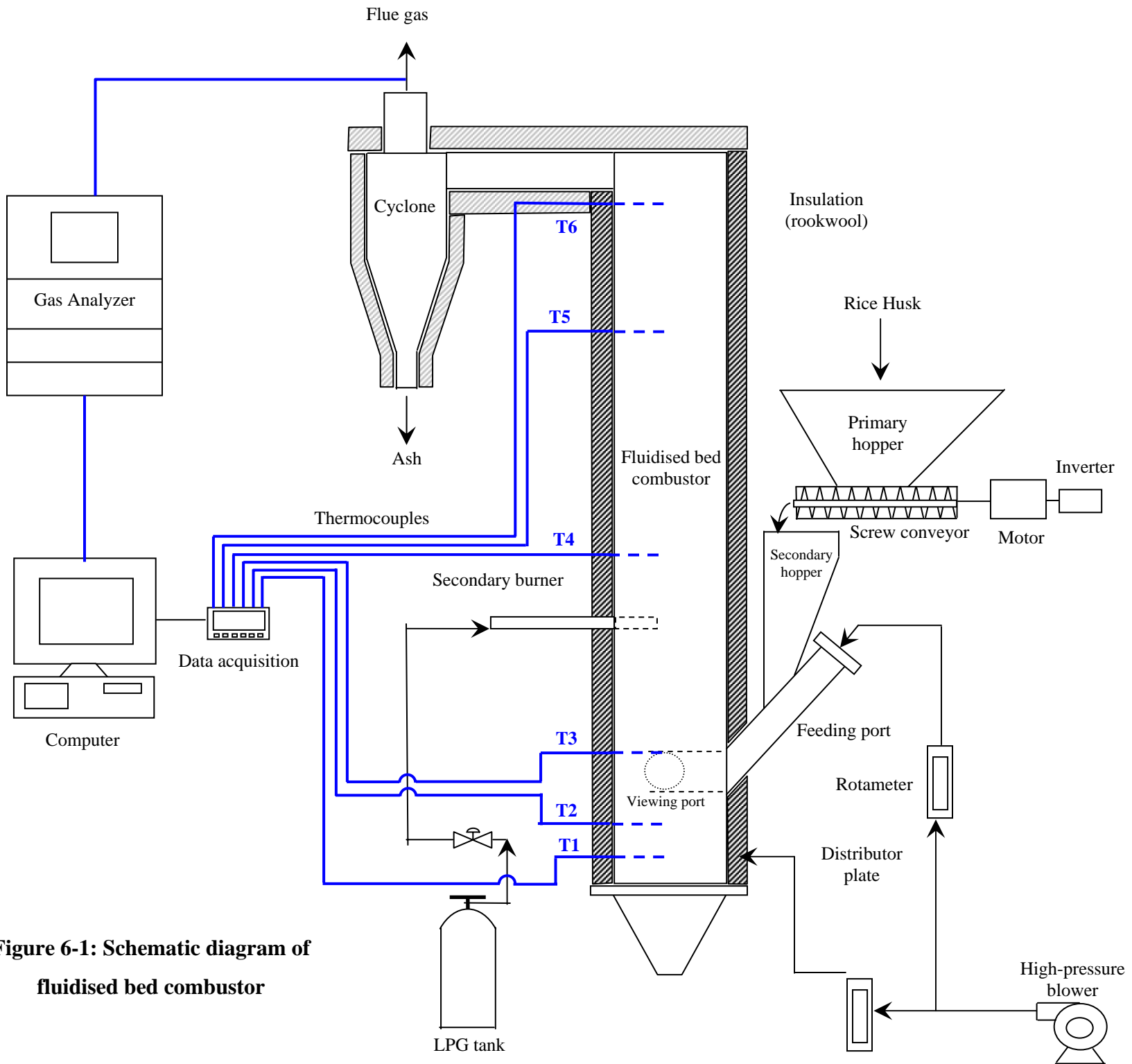


Figure 6-1: Schematic diagram of fluidised bed combustor

6.2.3 Fluidising and Pneumatic Air Feeding System

Fluidizing air was supplied through high-pressure blower having capacity of conveying 35,000 L/min of air from the main pipe of 8 inch diameter. The digital images of blower set-up are shown in Figure 6-2. The system was fitted with relief valve in order to avoid any back pressure which can damage the blower from over heating. The fluidizing air and pneumatic air was metered with 200 to 1400 Liter Per Minute (LPM) rotameter obtained from Dwyer Inc., USA, company and has accuracy of $\pm 3\%$ for full scale reading. The secondary air was positioned at different distance of the combustor as stated in Figure 6- 4.

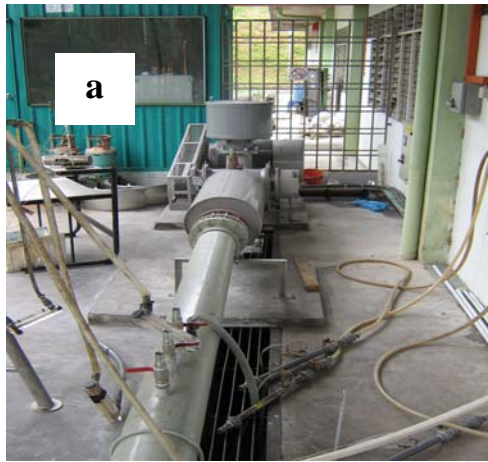
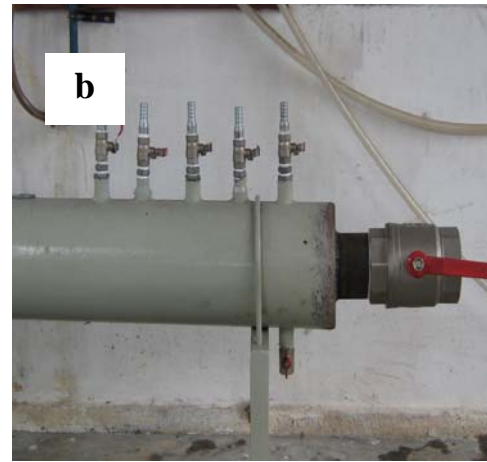


Figure 6-2: a) Blower set-up



b) Pipe fittings for fluidizing air inlet into combustor

6.2.4 Combustor Start-Up

The procedure of combustor start-up for each experimental run is outlined as follows:

- i. A quantity of silica sand as bed material of optimum size (295 – 595 μm sieved from company) was charged into the combustor to a desired static bed height of about 0.5 Dc.
- ii. A very minimal amount of fluidizing air was passed through the bed via stand pipe distributor plate. This fluidizing velocity was not enough to fluidize the bed and the bed still maintained in the fixed region. It was just to provide oxidant to the burning palm shell used to heat-up the bed to a desired temperature.
- iii. Palm shell soaked in kerosene or diesel was spread on the bed in the combustor. This was ignited and was left to heat the bed with the fluidizing velocity stated in point ii.
- iv. Once the heat was transferred to bed region, gradually the fluidizing velocity was increased to homogenously heat up the whole bed.
- v. The rice husk feeding was initiated once the bed temperature (T1) reached about 750° C.
- vi. The ash was collected from cyclone and stored in plastic bags.

6.2.5 Rice Husk Feeding System

Feeding of rice husk was by means of a combination of screw feeder and pneumatic air, which allows the smooth feeding into the combustor (see Figure 6-3). The rice husk was conveyed from primary hopper to secondary hopper, thereon combined with pneumatic air was pushed into the combustor via the feeding port, sloped at 45° and located at a distance of 1.22 m above the distributor plate. The pneumatic air also served as secondary air for combustion of rice husk whose direction was towards the bed region.

The rice husk feeding rate was controlled by the speed of the motor which was connected to primary hopper via belt and pulley system. The calibration of feeding rate was done by allowing the rice husk to flow into an empty bag for a period of five minutes. This bag was then weighted to obtain the desired feeding rate and the nobe of the motor was fixed at that particular position.

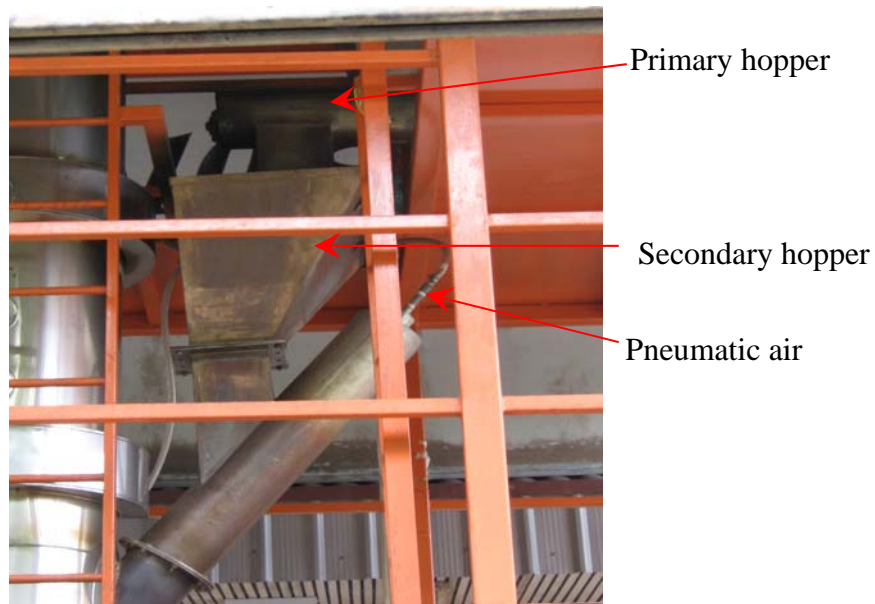


Figure 6-3: Feeding system of pilot-scale fluidised bed combustor

6.2.6 Temperature Measurement

Fifteen (15) type-K thermocouple was placed at different heights of the combustor to measure the temperature at bed, freeboard and cyclone region. The arrangement of thermocouple and its distance from distributor plate is shown in Figure 6-4. Thermocouple T1 indicated the bed temperature, T2 the bed surface temperature, T3 to T13 the freeboard temperature, T14 the connector temperature joining freeboard to cyclone, T15 and T16 cyclone temperature. These thermocouples were attached to data

acquisition system known as PICO technology, UK through which a continuous temperature measurement was achieved.

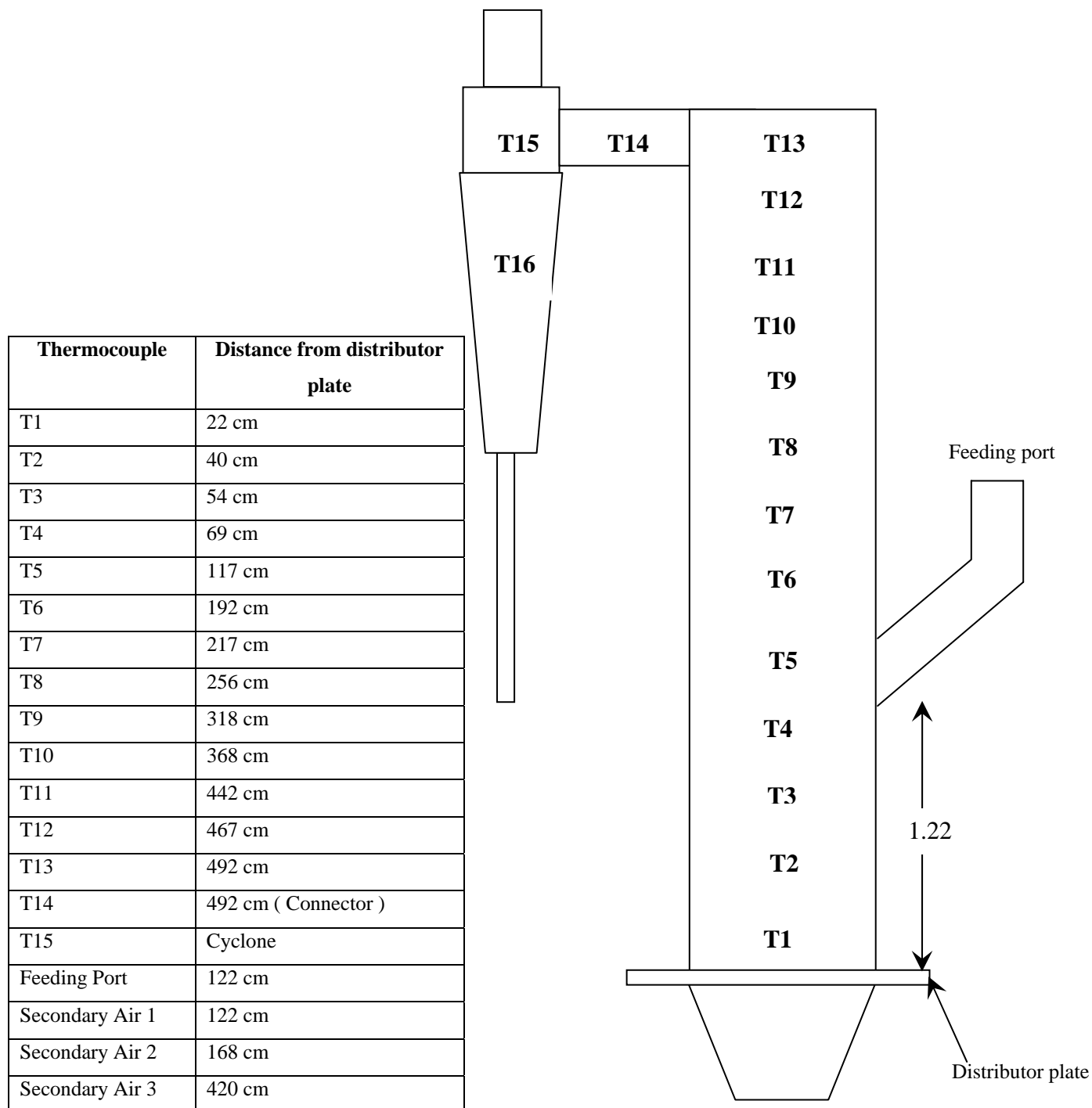


Figure 6-4: Schematic diagram of thermocouple position in a pilot-scale fluidised bed combustor

6.2.7 Flue Gas Sampling and Analysis

The sample probe was used to analyze the flue gas exiting form cyclone as shown in Figure 6-1. The MRU gas analyzer model (as shown in Figure 6-5) from Germany was facilitated with installed sampling, cleaning and drying of flue gas. Number of gas concentration can be measured using this analyzer. However, for present study CO, CO₂, NO_x, NO, SO_x and SO₂ were measured for rice husk firing in a pilot-scale fluidizes bed combustor. The measurements of these gases were shown on-line and continuously recorded using personnel computer.



Figure 6-5: Flue gas analyzer, MRU

During the continuous gas sampling for analytical measurement, an additional dust filtration made of glass wool was inserted inside the sampling probe at the sampling spot to trap the particulate and tar. The moisture in the sample gas was absorbed by silica gel desiccant before entering the gas analyzer unit. In order to avoid condensation inside the external piping system, the sample gas temperature was kept constant above the dew point of the exhaust gas by means of the heated gas sampling line of about 150⁰C.

Inside the analyzer unit, the sample gas was supplied to a gas cooler system (ECP – 1000) where it was lowered to 5°C to minimize damages on sensors. The developed condensate was then deviated by means of a hose pump. The cooled gas was then directed to an internal filtration system comprised of two fine dust filters. The flow rate of the sample gas was regulated and maintained at approximately 30 to 40 l/hr and finally passed to sensors for gas detection and analyzing.

6.2.7.1 Measuring Principle

The oxygen content of the sample was measured with two electrodes electro chemical sensors. The sensor comprised of an anode, electrolyte an air cathode as shown in Figure 6-6. Oxygen cells are current generators and the current is proportional to the rate of oxygen consumption. At the cathode, oxygen is reduced to hydroxyl ions and then oxidizes the metal anode. This process produces electrical current and can be measured by connection a resistor across the output terminals to produce a voltage signal.

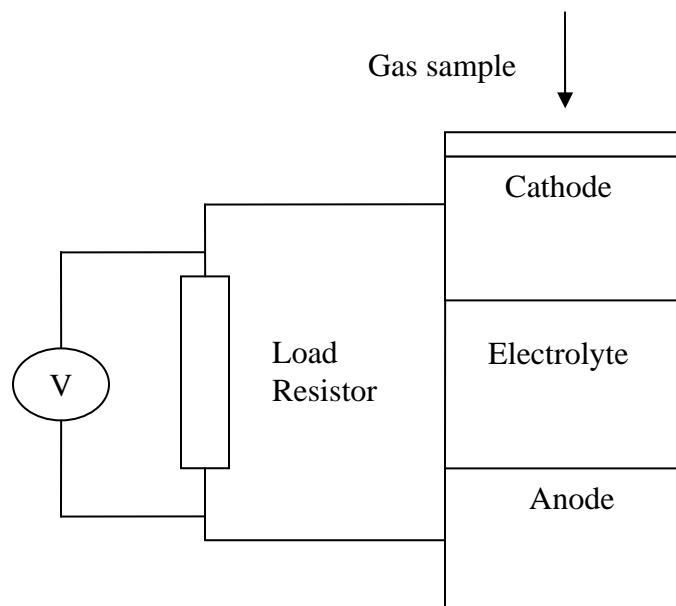


Figure 6-6: Oxygen measurement principle

The SWG 300⁻¹ gas analyzer has the capability to measure toxic gases like carbon monoxide CO, nitrogen oxide NO, nitrogen dioxide NO₂, sulphur dioxide SO₂, hydrogen sulphide H₂S by means of three electrodes sensors. The sample gas reaches the electrodes and reacts on the electrode surface, producing electrical current which is then converted to voltage signal.

6.7.2.2 Technical Specifications and Measuring Ranges

General specification of SWG 300⁻¹ gas analyzer and measuring ranges of selected gases as given by the manufacturer is shown in Table 6-1 and Table 6-2 below:

Table 6-1: General specification of SWG 300⁻¹ gas analyzer

Operating temperature	5 ⁰ C to 40 ⁰ C
Recommended storage temperature	-20 ⁰ C to 50 ⁰ C
Power supply	230 V AC 50 Hz
Internal main fuse	10 A
Sample gas conditioning	Integrated gas cooler with dew point = 5 ⁰ C Particle filtering < 1μ
Output signals	8 x analog output, 4-20 mA RS485 digital data transmission (inclusive PC software MRU 32-bit Data Logger

Table 6-2: Measuring ranges and accuracy as given by the manufacturer

Gas	Ranges	Accuracy
O ₂	0-25 Vol%	± 0.2 Vol%
CO ₂	0-20 Vol%	± 0.1 Vol%
CO	0-35200 ppm	± 1700 ppm
NO	0-494 ppm	± 15 ppm
NO ₂	0-49.5 ppm	± 5 ppm
SO ₂	0-505 ppm	± 25 ppm

6.3 Results and Discussions

The as installed pilot-scale fluidized bed combustor was commissioned and the problems arising was solved step by step. This took about 5 to 6 months to complete the commissioning and necessary modifications were done accordingly which made the fluidised bed combustor to run without further hindrances.

6.3.1 Bed Pre-Heating and Starting of Combustor

This was briefly discussed in the Section 6.2.4; however a detailed explanation will be discussed in this Section. Bed pre-heating was the primary step in starting up the combustor. This can be achieved by various methods. Nevertheless, the bed pre-heating was done by the combustion of a palm shell waste arising from palm oil mills. The freeboard temperatures increased rapidly to about 700° C after the ignition of palm shell on the bed surface. However, it took a long time to reach the bed temperature (T1) which was preferred at about 700° C. Figure 6-7 illustrates the bed starting temperature profiles before commencing of rice husk feeding. It took approximately 2 hours to reach the bed temperature of 700° C. After initial charging of palm shell the bed temperature started to

drop since the heat transferred gradually into the bed region. Hence, at interval it was necessary to feed the palm shells in order to maintain the combustor temperature and particular to bring the bed temperature (T1) to a desired value. The upper surface of the bed turned red in color due to the burning of palm shell which could be observed through the viewing port.

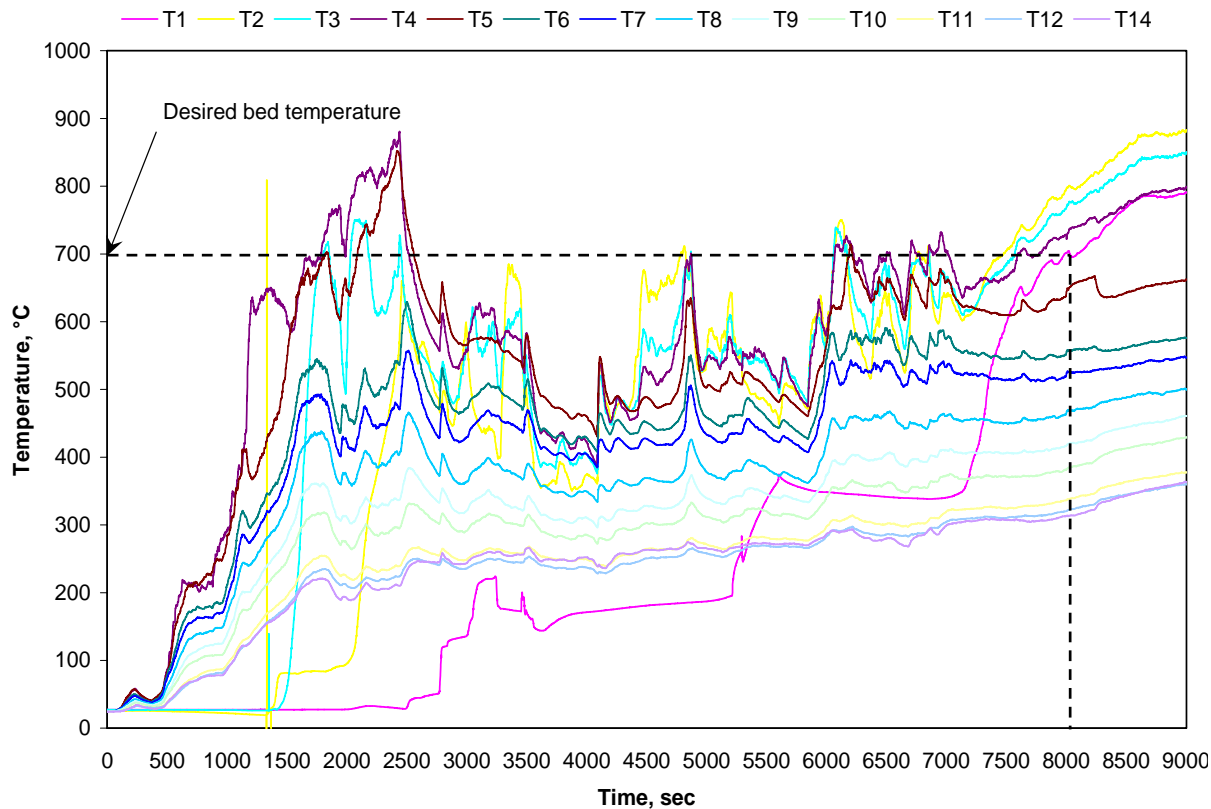


Figure 6-7: Temperature profile during bed pre-heating

Initially the bed temperature (T1) remained fairly constant at room temperature, which was due to lack of heat being transferred to the bed region even though the bed surface temperature (T2) was as high as 700 °C. The fluidizing velocity was increased gradually along the time with the indication of increasing bed temperature (T1). Experiences showed that care should be taken to avoid a sudden increase in fluidising velocity which quenched the burning process of palm shell by penetrating it into the cold

bed and this resulted in re-starting the bed heating procedure. This might cause a significant delay in combustor start-up. Initially the large difference between T1 and T2 shows the poor mixing of bed medium as well as low heat transfer rate. However, the difference reduces as fluidizing velocity was increased indicating good mixing behavior and high rate of heat transfer from splash zone into the bed region. This can be revealed in Fig. 6 that the temperature profile of T1 and T2 was almost parallel after operating time of about 2 hours. At this point, the whole bed started to turn into bright orange. The fluidizing velocity was maintained constant at this stage and the bed was left at this condition.

Overall bed pre-heating using palm shell was good, but certain difficulties arised. It was difficult to control the bed temperature in the desired range (700 - 900°C) due to continuous burning of palm shell. There was a danger of temperature exceeding 1000 °C due to run-away reaction that could melt the bed and damage the reactor. The bed temperature cannot be controlled by increasing the primary fluidizing velocity. Indeed, the increment in fluidising velocity caused the bed temperature to increase. The reason might be the oxidation of palm shell char particles after completion of volatile combustion. This phase shows the similarity with that of coal combustion since the palm shell is hard in physical nature and might tend to burn like coal char.

In the present study the combustion of palm shell in the bed can be explained by two steps. The release of volatile compound liberating high energy with rapid increase of temperature (T3 to T10) as can be seen in Figure 6-7 in the time range of 700 to 2500 seconds. This shows that significant amount of volatiles was being burnt in the region above the bed. Another reason might be the burning of kerosene or diesel used to ignite the palm shell. These fuels contain high volatile matters with high calorific value. Later on, the palm shell started to burn which might lower the temperature due to release of water content and endothermic reactions of devolatisation of the volatile matters. Once the char started to burn, the bed temperature increased. The higher bed temperature compared to freeboard indicated char particle burning inside the bed region.

6.3.2 Effect of Fluidizing Velocity on Rice Husk Combustion

Rice husk combustion at different fluidizing velocity (4 to 7 U_{mf}) was carried out to investigate the stable combustion, the combustion zone and optimum range of fluidizing velocity to operate the pilot-scale fluidized bed combustor. Rice husk feeding was started as soon as bed temperature (T1) reached desired temperature of 700 °C. It should be noted that the palm shell feeding was terminated as soon as desired bed temperature was reached. The real time temperature profile at fluidizing velocity of 4 to 7 U_{mf} is illustrated in Figure 6-8.

When the feeding of rice husk was started, the bed temperature dropped to a certain level and then increased for a short time after which it dropped significantly throughout the experiment of 4 to 6 U_{mf} (Figure 6-8a). However, the freeboard temperature particularly T5 to T8 showed abrupt increase reaching value of 1000° C. Compared to this the highest bed temperature recorded for 4 to 6 U_{mf} was 850° C. Nevertheless, the bed temperature for 4 U_{mf} fluctuated in the range of 700 to 850° C while it was almost stable during 5 U_{mf} and dropped drastically at 6 U_{mf} . The reason was that the major rice husk combustion specifically volatile release (where sufficient amount of energy gets liberated) took place near the feeding port i.e. in freeboard region. Hence, T5 and T6 situated just near the feeding port recorded abrupt increase in temperature profile. There was little possibility for the burnt rice husk (char) to fall in the bed and sustain the bed temperature. This might be due to high fluidizing velocities. Whereas, the freeboard temperature was fluctuating in a range of 600 to 900° C. Once the bed temperature dropped below 500° C, the combustion could no longer be sustained and experiment has to be stopped.

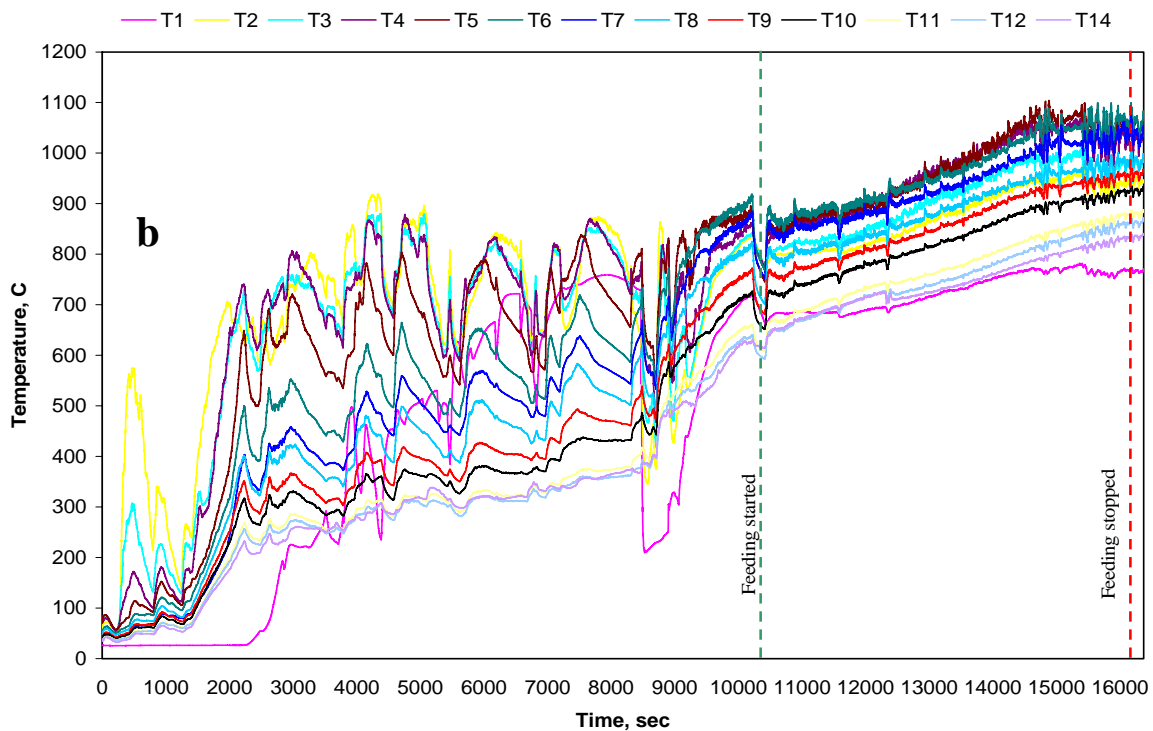
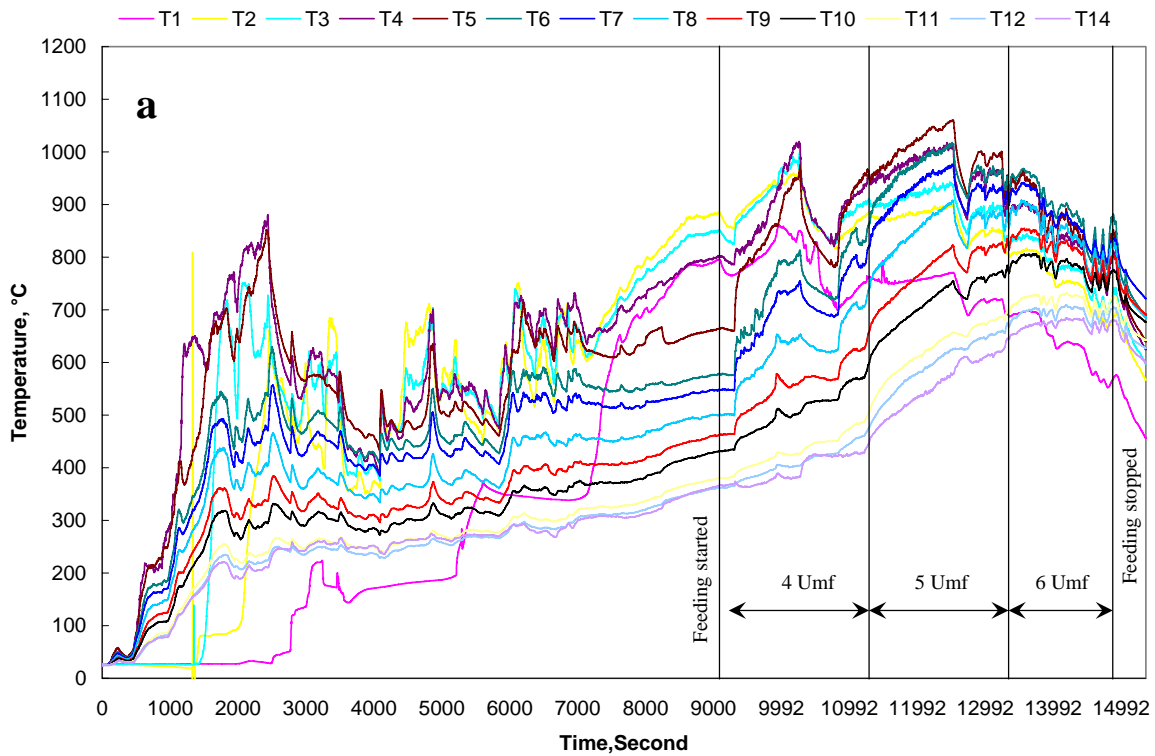


Figure 6-8: Real time temperature profile of rice husk combustion at a) 4, 5 and 6 U_{mf} and b) 7 U_{mf} fluidizing velocity

For $7 U_{mf}$ case (Figure 6-8b), during the combustion of palm shell for bed pre-heating the bed temperature was higher than the freeboard region. However, during combustion of rice husk, the bed temperature was lowered than the flue gas temperature and freeboard temperature. These shows that major fraction of rice husk combustion took place in the freeboard region which should be avoided. This could also be explained by the difference in temperature between the bed region (T_1) and bed surface temperature (T_2) which was approximately 100°C in case of 4 to 6 U_{mf} and 150°C in case of 7 U_{mf} .

Even though the combustor temperatures were good enough for rice husk combustion, the high fluidizing velocity has the possibility to carry away the hot flue gas and rice husk char towards the cyclone region with lower residence time. This brings incomplete combustion and unstable combustion behavior problem in the Fluidised Bed Combustor. It can be solved by tuning the fluidizing velocity with secondary air so that major combustion takes place in the bed region rather than in freeboard region.

6.4 Conclusions

The pilot-scale fluidized bed combustor was successfully fabricated and installed at Faculty of Chemical and Natural Resources Engineering, UTM, Skudai. The set-up was commissioned and facility was confirmed to run smoothly during the further experimental work. The facility has advantage of handling wide range of feed materials including coal. Presently, rice husk as feed material was combusted in pilot-scale fluidized bed combustor. Overall, there was no serious problem in treating rice husk in newly installed fluidized bed combustor. The desired temperature and expected product was almost obtained. However, more experimental work was needed to optimize the operating conditions of pilot-scale FBC for more efficient results.

CHAPTER 7

CONCLUSIONS AND RECOMMENDATIONS

7.1 Conclusions

In this research, amorphous silica with very low residual carbon content (approximately 1.0 wt% residual carbon) was successfully being produced from the combustion of rice husk in the fluidised bed ($\text{Ø}210\text{mm} \times 2000\text{mm}$). Although the operating parameters for the combustion process had been optimised, amorphous silica that was free from sand contaminants and residual carbon still could not be obtained. This was due to the setback in the design of the current experimental fluidised bed rig, namely its relatively short freeboard height. This setback led to the contamination of sand in the fly ash as the ejected sand particles could not be disengaged and be returned to the bed region. In addition, amorphous silica that was carbon-free could not be obtained due to the insufficient freeboard height to allow for the complete oxidation of residual carbon in the fly ash as they were being entrained towards the cyclone. Nevertheless, this setback was expected to be overcome by increasing the freeboard height of the fluidised bed and the optimum freeboard height had been determined through computational fluid dynamics (CFD) modelling. Another improvement in design of the fluidised bed that was expected to increase the combustion efficiency of rice husk were the application of vortex feeding that tended to increase the residence time of rice husk/char/ash in the fluidised bed. With the experimental and modeling results obtained, the pilot scale fluidized bed combustion system ($\text{Ø}500\text{mm} \times 5000\text{mm}$) has been successfully designed, fabricated, installed and commissioned for the production of amorphous

silica from rice husk. However, due to time and budget constraints of this research, detailed combustion study has not been fully investigated for the production of amorphous products.

The experimental and modelling results obtained from this research were summarised as follows:-

a) Minimum residence time required for complete combustion of rice husk particles to liberate carbon-free, siliceous ash

Rice husk requires a residence time of at least 20 – 30 seconds (single particle combustion) and 39 – 52 seconds (group particle combustion) at the temperature range of 650 – 750°C to burn to completion in order to liberate amorphous, carbon-free siliceous ash. There was no difference in combustion times for the raw or water-washed rice husk. However, rice husk ash that was completely white could not be obtained from burning raw rice husk unless the alkali metals compounds (potassium oxide and sodium oxide) were removed (e.g. by washing with water) prior to thermal treatment. These low-melting point alkali metals compounds in raw rice husk were responsible for the formation of melt mixtures on the surface of the ash particles upon sudden exposure to high temperatures. These surface melt mixtures tended to encapsulate any unburnt carbon molecules within the ash and prevented their subsequent oxidation as they were not in direct contact with oxygen. This led to the formation of black char particles amongst the ash, which could not be removed even after heating for a prolonged period of time. The combustion of rice husk in a fluidised bed followed the single particle combustion model, with combustion times of 29 – 34 seconds. The bubbling action in the bed aided in dispersing the rice husk particles uniformly within the bed, whereas the high heat and mass transfer rates eliminated the ‘barriers’ due to overlapping associated with burning a group of particles.

b) Upper limits of temperature-residence time combinations during combustion of rice husk to maintain amorphous structure in the resulting ash

The silica in rice husk ash remained amorphous when rice husk was subjected to thermal-treatment up to temperatures of 900°C and residence time of up to 3 minutes. The brief exposure time of 3 minutes even at such high temperatures was not sufficient for the crystallisation of silica to take place as crystallisation is a gradual process. The rapid reaction time in the fluidised bed means that the rice husk particles are exposed to high temperatures at a very short period of time (estimated to be less than 2 minutes). Thus, the fluidised bed could be operated up to 800 – 900°C to achieve higher carbon conversion efficiency while preserving the amorphous structure of silica in the ash.

c) Optimum sand size, fluidising velocity and static bed height to achieve good mixing behaviour in fluidised bed for combustion of rice husk

The optimum fluidising parameters to achieve good mixing behaviour of rice husk in the fluidised bed were:-

i) $Sand\ size = 250 - 595\ \mu m$

The use of this sand size (minimum fluidising velocity, $U_{mf} = 0.09\ m/s$ and surface mean diameter, $D_{vs} = 342\ \mu m$) enabled a considerable amount of rice husk to be mixed within the bed region. The bubbles that formed within the bed were smaller compared to a bed of 595 – 841 μm sand, and as such the eruption of these medium-sized bubbles did not cause the bed surface to become very turbulent, which could in turn could made it difficult for the rice husk particles to enter the bed. Operating at the fluidising velocities of 3 – 7 U_{mf} to attain good mixing behaviour in the bed resulted in a superficial velocity of 0.27 – 0.63 m/s, which was less than the terminal velocity of rice husk (0.8 – 1.1 m/s). Thus, the elutriation of rice husk particles could be prevented.

ii) *Fluidising velocity* = $3 - 6 U_{mf}$

A fluidising velocity of at least $3 U_{mf}$ was required to break the interlocking layer of rice husk that formed at the bed surface to give uniform distribution of rice husk within the bed region. Increasing the fluidising velocity from $3 U_{mf}$ up to $6 U_{mf}$ resulted in higher degree of mixing as the bed became more turbulent, but this was offset by elutriation of more broken fragments of rice husk. At $7 - 8 U_{mf}$, the bed was bubbling vigorously and the turbulent upward splashing of sand particles at the bed surface made it difficult for the rice husk to enter the bed region. In addition, most of the rice husk particles were suspended in the freeboard region at these high fluidising velocities with small broken fragments being blown out of the fluidised bed.

iii) *Static bed height* = $0.5 D_c$

The static bed height of $0.5 D_c$ resulted in the formation of a steady stream of small, slowly rising bubbles that provide the agitation force to distribute the rice husk uniformly within the bed region. Below $0.5 D_c$, the bed was too thin to allow for complete formation of gas bubbles, thereby leading to the formation of rice husk clumps within the bed due to poor mixing. Beyond $0.5 D_c$, the bed was too thick and this allowed for the formation of bigger gas bubbles as they coalesced when rising to the bed surface. The eruption of the bigger gas bubbles caused the bed surface to be very turbulent and prevented the rice husk from entering the bed region. This reduced the amount of rice husk that could be mixed within the bed.

d) The optimum fluidising velocity and static bed height to achieve high combustion efficiency of rice husk in fluidised bed

The optimum fluidising parameters to achieve high combustion efficiency of rice husk in fluidised bed were:-

i) *Fluidising velocity* = $3 U_{mf}$

The fluidising velocity of approximately $3 U_{mf}$ gave the lowest residual carbon content of fly ash (at 2.9 wt%) while preserving the amorphous structure of silica. The considerable amount of rice husk that entered and be burnt within the bed region enabled the bed temperature to be maintained

steadily at approximately 650°C throughout the experiment. Below the fluidising velocity of $3 U_{mf}$, the rice husk tended to form a stagnant layer at the bed surface and burning could not be sustained as the heat from the bed was continuously being absorbed for the devolatilisation (endothermic process) of rice husk at this layer. Increasing the fluidising velocity of $3 U_{mf}$ resulted in lower residence time of ash in both the bed and freeboard regions, thus giving fly ash with higher residual carbon content.

ii) *Static bed height = 0.5 D_c.*

The static bed height of $0.5 D_c$ gave the lowest residual carbon content of fly ash (at 1.9 wt%) while preserving the amorphous structure of silica. Amongst the range of static bed heights investigated ($0.25 - 0.75 D_c$), the highest average bed temperature (at 670°C) was observed at this bed height due to the higher amount of rice husk that entered and be burnt within the bed region. The higher degree of rice husk penetration into the bed also resulted in finer-sized fly ash with the absence of skeleton-like char or ash as they were being broken down by the bubbling action of the bed. This further increased the oxidation rate of the char/ash as the entrapped carbon molecules were exposed more readily to the heat and oxidants available in the bed. Below $0.5 D_c$, mixing of rice husk within the bed was poor with the rice husk forming a layer at the bed surface. This led to the formation of char/ash with higher residual carbon contents that still retained their rigid skeleton-like shape. Beyond $0.5 D_c$, the turbulent upward splashing of sand due to bubble eruption at the bed surface prevented the rice husk from entering the bed. This led to a lower amount of rice husk being mixed and burnt in the bed region, thus resulting in a lower bed temperature. As most of the rice husk particles were being burnt in suspension form at the freeboard region, the resulting char/ash had higher residual carbon contents and retained their skeleton-like shape.

e) **Optimum temperature, air supply, type of rice husk feed, moisture content of rice husk and feeding design to achieve high combustion efficiency of rice husk in fluidised bed**

The optimum combustion parameters and design to achieve high combustion efficiency of rice husk in the fluidised were as follows:-

i) *Bed temperature = 650 – 800°C*

The bed temperature of 800°C gave the lowest residual carbon contents of fly and bottom ashes (at 4.0 wt% and 2.0 wt%, respectively) while preserving the amorphous structure of silica. The residence time of rice husk in the fluidised bed (Ø80mm × 1000mm) was estimated to be 30 – 40 seconds only. Therefore, this brief exposure time was insufficient for the crystallisation of silica in the ash to take place. Increasing the bed temperature from 650 – 700°C led to a steep decrease in residual carbon content in the ash whereas beyond the bed temperature of 700°C, the decrease in residual carbon contents tended to reach a plateau. This was most likely due to the transition from the kinetically-controlled reaction to diffusion-controlled reaction at the temperature band of 650 – 700°C.

ii) *Freeboard temperature = 650 – 800°C*

The freeboard temperatures of 650 – 800°C gave the lowest residual carbon contents of fly and bottom ashes (at 2.1 wt% and 1.3 wt%, respectively) while preserving the amorphous structure of silica. These high freeboard temperatures enabled the effective oxidation of the fly ash particles as they were being blown towards the cyclone. The presence of secondary burners to elevate the freeboard temperatures also generated sufficient heat to continuously ignite the fresh rice husk feed, thereby resulting in a more steady temperature profile along the combustor with lesser fluctuations.

iii) *Heat loss = to be prevented by presence of insulation at combustor and cyclone*

The presence of insulation reduced the amount of heat loss at the fluidised bed (Ø210mm × 2000mm) by up to 70%. This resulted in an increasing

temperature profile along the combustor height as the hot gases rised upwards. This was in contrast with the decreasing temperature profile along the combustor height due to substantial heat loss to the surroundings in the absence of insulation. The higher freeboard temperatures in the insulated fluidised bed enabled the effective oxidation of unburnt carbon molecules within the elutriated ash, leading to a 12.5% decrease in residual carbon content (to 1.7 wt%). The decrease was quite low due to the short residence time of fly ash at the freeboard region in the fluidised bed with relatively short freeboard height. The silica in the fly ash remained amorphous.

iv) Type of rice husk = water-washed rice husk that is free from alkali metals compounds (potassium oxide and sodium oxide)

The removal of alkali metals compounds (impurities) in rice husk improved their combustion efficiency in the freeboard region (secondary stage combustion). Upon feeding into the hot fluidised bed, raw rice husk underwent rapid heating and the low-melting point alkali metals tended to form a melt mixture on the surface of the resulting char/ash. This melt mixture entrapped any unburnt carbon molecules within the char/ash particles and prevented their subsequent oxidation even at higher temperatures or residence times. With the removal of these detrimental alkali metals compounds, the phenomenon of surface heating could be eliminated and the char/ash particles could be oxidised more effectively when they were elutriated into the freeboard region. The fly ash from the combustion of water-washed rice husk contained residual carbon content of 1.1 wt% while the bottom ash contained lower residual carbon content (at 0.8 wt%) due to their longer contact time with heat and oxidants in the bed region. Both the fly and bottom ashes retained their amorphous silica structure.

v) Primary air factor = 0.8

The primary air factor of 0.8 gave the highest average bed temperature (at 765°C) amongst the primary air factors investigated (at 0.65 – 1.4). This was because the air factor at the bed region had reached the stoichiometric level due to the local accumulation of unused oxygen since not all the rice husk were burnt completely. The residual carbon contents in the amorphous fly

and bottom ashes were 6.9 wt% and 3.4 wt%. Beyond the primary air factor of 0.8, there was a drop in bed temperature as part of the heat was absorbed to increase the temperature of the excess air. However, the residual carbon contents of the fly and bottom ashes remained more or less similar to that of the primary air factor of 0.8. However, at higher excess air level, for example at the primary air level of 1.4, the lower bed temperature resulted in bottom ash with higher residual carbon content due to the corresponding drop in bed temperature.

vi) Primary-to-secondary air ratio = 7:3

With the use of the same primary air level, the increase in secondary air level (which entry point was positioned near the bed region) resulted in higher freeboard gas velocity and subsequently lower residence time of rice husk in the fluidised bed. The primary-to-secondary air ratio of 7:3 gave a lower freeboard gas velocity (0.72 m/s) compared to the ratio of 6:4 (freeboard gas velocity of 0.81 m/s). Therefore, its fly ash contained unburnt components that were approximately 27% lower compared to that from the primary-to-secondary air ratio of 6:4.

vii) Pneumatic air feeding velocity = 1.4 m/s

The pneumatic air feeding velocity of 1.4 m/s gave the highest average bed temperature (680°C) and amorphous fly ash with the lowest residual carbon content (2.7 wt%). The onset for the formation of recirculating zone near the bed surface was observed with the use of pneumatic air feeding velocity at 1.4 m/s, which was beneficial in increasing the residence time of particles (rice husk and ash) inside the fluidised bed. This recirculating zone was not observed when operating at a pneumatic air feeding velocity of 0.4 – 0.9 m/s.

viii) Moisture content in water-washed rice husk = 26.0 wt%

The moisture content of 26.0 wt% in water-washed rice husk gave the highest average bed temperature (630°C) amongst the range of moisture contents investigated (10 – 58 wt%). Its amorphous fly and bottom ashes also had the lowest residual carbon contents, at 2.4 wt% and 0.9 wt%, respectively. Below the moisture content of 26.0 wt%, the lower bulk density

of the rice husk prevented them from penetrating the bed, thus resulting in lower bed temperatures and correspondingly, poorer ash quality. Beyond the moisture content of 26.0 wt%, the rice husk tended to form agglomerates giving rise to feeding problems. They also dropped into the bed in huge clumps and lowered the bed temperature significantly due to huge amount of heat absorbed for the drying process. The subsequent drop in bed temperature also resulted in poorer ash quality.

ix) Feeding design = inclined feeding near bed surface

When the feed entry was located near the bed surface, it was preferable to use the inclined feeding method as opposed to vortex feeding. This was because the formation of swirling flows adjacent to the bed surface tended to trap and returned the ash particles into the bed, thus resulting in significant accumulation of ash in the bed region. Although the degree of ash penetration in the bed could be increased (thus giving ash with finer size), the combustion process could not be sustained after one hour due to the drop in bed temperature and changes in bed mixing behaviour with the increase in bed height in the presence of plenty of fine ash. In terms of ash quality, the fly ash from both the inclined feeding and vortex feeding remained amorphous with similar residual carbon contents (at 1.9 wt%). However, the fly ash from the former was not as fine and consisted of broken fragments of ash skeletons. The fly ash was continuously being collected at the cyclone with the inclined feeding method and accumulation of ash in the bed region was minimal. Therefore, the inclined feeding method was more suitable for the continuous operation to produce amorphous silica from fluidised bed.

f) Optimum ash quality (silica structure, carbon content and particle size) that could be produced from combustion of rice husk in fluidised bed

The optimum ash qualities that could be produced from combustion of rice husk in the fluidised bed ($\varnothing 210\text{mm} \times 2000\text{mm}$) were as follows:-

i) *Silica structure = amorphous but contaminated with quartz crystals from elutriated sand particles*

All fly and bottom ash samples from this research were found to be amorphous. However, most of them were contaminated with elutriated sand registered as quartz crystals in their diffractograms. The short freeboard height of the 2000-mm tall fluidised bed was not sufficient to disengage any sand particles ejected to the freeboard region by bubble eruption at the bed surface. It was expected that this contamination problem could be solved by increasing the freeboard height of the fluidised bed.

ii) *Residual carbon content = 1.1 wt% (fly ash), 0.8 wt% (bottom ash)*

The ash samples were not completely carbon-free due also the the short freeboard height of the 2000-mm fluidised bed combustor, which did not allow for sufficient residence time for complete carbon oxidation in the freeboard region. It was also expected that this problem could be solved by increasing the freeboard height of the fluidised bed.

iii) *Particle size = size range of 75 – 300 μm with volume-surface mean diameter of 190 μm*

The fly and bottom ash samples consisted mostly of broken fragments of skeleton-like shapes with their sizes largely governed by their degree of penetration into the bed region. Ash particles that were retained longer in the bed region, for example tended to be ground to finer sizes by the bubbling action in the bed region. The ash particles were very brittle and tended to break easily.

g) Optimum fluidised bed freeboard height and feeding conditions (feeding velocity and presence of vortex flow) to prevent sand contamination and to improve carbon burnout in the ash (as determined from the CFD modelling study)

The optimum freeboard height to prevent sand contamination and to achieve complete carbon burnout in the rice husk ash was found to be at least 5000mm. Sand particles with sizes of 25 – 50 μm (which were ejected to the

freeboard region from bubble eruption at the bed surface) were found to be disengaged at the height of 4000mm. Bigger particles (75 – 125 μm) could be disengaged at a lower height of approximately 3000mm. Meanwhile, the combustion of rice husk particles could be completed inside the 5000-mm tall fluidised bed even though they were blown towards the freeboard region at very high freeboard velocity (at 1.0 m/s). Therefore, the use of a 5000-mm tall fluidised bed could prevent the contamination of sand in the fly ash while achieving complete combustion of rice husk to produce carbon-free ash.

As for the feeding conditions, a pneumatic air feeding velocity of 1.36 m/s was found to result in the highest average bed temperature and amorphous ash with the lowest residual carbon content in comparison to the other feeding velocities investigated. This was due to the presence of a recirculating zone near the feeding port just above the bed surface which aided in increasing the residence time of the rice husk particles in the combustor by ‘trapping’ and returning them to the bed region. The induction of swirling airflow in the freeboard region by means of tangential air feeding was found to be beneficial in increasing residence time of rice husk particles inside the combustor. However, this swirling flow is preferably induced at a distance further away from the surface of the bubbling bed as it tends to trap the entrained ash particles in its vortex and returns them to the bed region again. This phenomenon subsequently resulted in the significant accumulation of ash in the bed region thus interfering with the continuous operation of the fluidised bed.

7.2 Recommendations for Future Study

A number of problems had been identified in this research and the recommendations to solve these problems in future studies were as follows:-

a) Removal of sand contaminants from the ash samples

Preliminary studies had shown that the sand contaminants in the ash samples could be removed completely by bubbling in an atmospheric fluidised bed. The ash

samples were ground and fluidised at velocities above the terminal velocity of the ground ash but below the terminal velocity of the sand contaminants. Further studies need to be carried out to determine the optimum size to which the ash sample should be ground into and the optimum fluidising velocities to enable complete removal of sand contaminants while maximising the recovery of the ash sample.

b) Roasting of ash samples

The residual carbon content in the ash samples could be removed by further roasting, for example in a muffle furnace. Further studies need to be carried out to determine the optimum combinations of roasting time and temperature to remove the residual carbon completely while maintaining the amorphous structure of silica in the ash.

c) Removal of alkali metals compounds in raw rice husk

It was found that the removal of alkali metals compounds such as potassium oxide and sodium oxide from raw rice husk are imperative towards achieving complete carbon burnout in the ash. Further studies need to be carried out to determine the optimum soaking time in water for the removal of these alkali metal compounds. Apart from soaking in water, other techniques such as water-spraying should be investigated to determine the optimum technique for simple and efficient removal of these alkali metal compounds. The leachate from the washing process contains high concentrations of potassium oxides and sodium oxides, which have the potential to be used as fertiliser liquid after being concentrated.

d) Induction of swirling flow at the freeboard region

The presence of swirling flows at the freeboard region of the fluidised bed was found to be beneficial in increasing the residence time of rice husk/char/ash in the fluidised bed (both bed and freeboard regions), thus resulting in higher carbon conversion efficiency. As such, further studies need to be carried out to determine the optimum height at which these swirling flows should be induced to maximise the residence time of particles in the freeboard region. Due to time and budget constraints, the effect of the swirling flow in the pilot scale fluidised bed combustion system has not been studied.

APPENDICES

Appendix A

Estimation of Bubble Eruption Velocity

Ejection of particles from the bubbling fluidised bed into the freeboard region is the result of bubble eruption at the bed surface. It was reported by Rozainee (1998) that the initial velocity of ejected particles is independent of the size and density of the particles, being largely dependant on the size and rise velocity of the bubble (Caram et al., 1984). It was further reported that if the ejected particles were from bubble wakes, the particle ejection velocity could be as high as 2.5 times the bubble rise velocity ($V_m = 2.5 U_b$) (Pemberton and Davidson, 1986).

The bubble rise velocity could be estimated based on the following equation by Davidson and Harrison (1963):-

$$U_b = U - U_{mf} + 0.71 \sqrt{gd_b} \quad (\text{A1})$$

where

U_b	=	bubble velocity
U	=	fluidising velocity
U_{mf}	=	minimum fluidising velocity
g	=	gravitational acceleration
d_b	=	bubble diameter

All parameters for Equation A1 were evaluated at the bed surface of the fluidised bed. In estimating the bubble velocity, the bubble diameter was assumed to be 20 mm, a value obtained by Rozainee (1998) from his visual observation of the bubbling bed in a Perspex rotating fluidised bed. Consistent with the prediction of particle ejection velocity by Pemberton and Davidson (1986), the maximum ejected particles velocities at each operating condition was evaluated. The eruption of bubbles was assumed to have ejected the particles in the y-direction only. Therefore, the axial velocity of the ejected particles was assumed to be zero.

Appendix B

Determination of Particle Sphericity (ϕ_s)

B.1 Theoretical Equations

Quantification of a non-spherical particle is given by the sphericity (ϕ_s), defined as:-

$$\phi_s = \frac{\text{surface area of a sphere of the same volume as the particle}}{\text{surface area of the particle}} \quad (\text{B1})$$

Difficulties in measuring the sphericity of irregular particles have led to recommendations by Kunii and Levenspiel (1991) and Howard (1989) that the sphericity be measured from a minimum fluidising velocity experiment. By measuring the bulk density ρ_b of a loosely packed bed of particles and particle density ρ_p , the voidage at minimum fluidisation (ε_{mf}) can be determined using Equation B2. Subsequent calculation of the Archimedes Number (Ar , Equation B3) and Reynolds Number (Re_{mf} , Equation B4) are possible, and along with U_{mf} , fluid viscosity μ_f and density ρ_f , and the mean particle diameter d_m , they are then substituted into Equation B5. The sphericity ϕ_s can then be solved.

$$\varepsilon = 1 - \frac{\rho_b}{\rho_p} \quad (\text{B2})$$

$$Ar = \frac{\rho_f (\rho_p - \rho_f) g d_m^3}{\mu_f^2} \quad (\text{B3})$$

$$Re_{mf} = \frac{\rho_f U_{mf} d_m}{\mu_f} \quad (\text{B4})$$

$$Ar = 150 \frac{(1 - \varepsilon_{mf})}{\phi_s^2 \varepsilon_{mf}^3} Re_{mf} + 1.75 \frac{(1 - \varepsilon)}{\phi_s \varepsilon_{mf}^3} Re_{mf}^2 \quad (\text{B5})$$

B2. Sample Calculations of Sphericity for Rice Husk

The fluidisation properties of rice husk as shown **Error! Reference source not found.** are as follows:-

- i) $\rho_b = 100 \text{ kg/m}^3$
- ii) $\rho_p = 650 \text{ kg/m}^3$
- iii) $d_m = 1.6 \text{ mm}$
- iv) $U_{mf} = 0.5 \text{ m/s}$ (average of values from literature, theoretical calculations and experiment)

Air (fluid) properties at ambient conditions (30°C):-

- i) $\rho_f = 1.16 \text{ kg/m}^3$
- ii) $\mu_f = 1.8 \times 10^{-5} \text{ kg/(m} \bullet \text{ s)}$

Substitution of values of ρ_b and ρ_p into Equation B2 gives $\varepsilon = 0.85$

Substitution of values of ρ_f , ρ_p , d_m and μ_f into Equation B3 gives $Ar = 93611.1$

Substitution of ρ_f , U_{mf} , d_m and μ_f into Equation B4 gives $Re_{mf} = 51.8$

Thus, solving for ϕ_s in Equation B5 gives a value of 0.19.

Appendix C

Properties of Rice Husk for its Definition as the Burning Fuel Particle in CFD Modelling (Input Data to Preprocessor PrePDF)

Table C1: Proximate contents of rice husk

Proximate Content	Wt% (wet basis)	Wt% (dry basis)	Wt% (dry-ash-free basis)
Moisture	10.10	-	-
Volatiles	64.10	71.30	85.24
Char [C(s)]	11.10	12.35	14.76
Ash	14.70	16.35	-
GCV (MJ/kg)	13.30	14.79	17.68

Table C2: Ultimate analysis of rice husk

Ultimate Content	Wt% (dry basis)	Wt% (dry-ash-free basis)
C	37.80	45.19
H	5.00	5.98
O	40.25	48.12
N	0.60	0.71
Ash	16.35	-

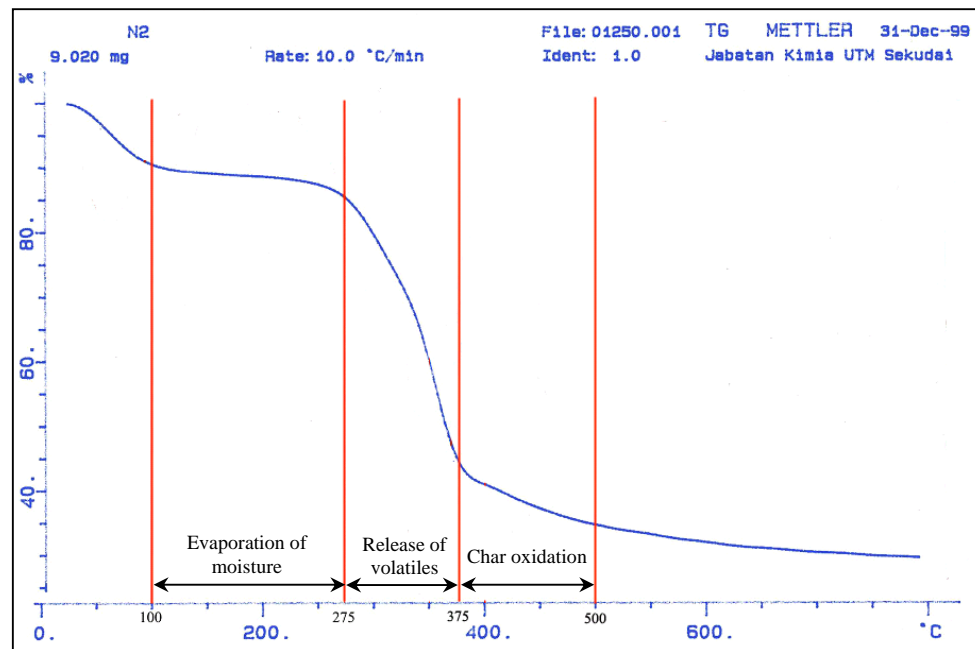


Figure C1: Thermogravimetric analysis of rice husk in a reducing environment (N₂) (heating rate 10.0°C/min)

Appendix D

Chart for Determining Sphericity (ϕ_s) of Particles and Theoretical Equations for Estimating Minimum Fluidising Velocity (U_{mf}) and Terminal Velocity (U_t)

D.1 Sphericity (ϕ_s) of Particles

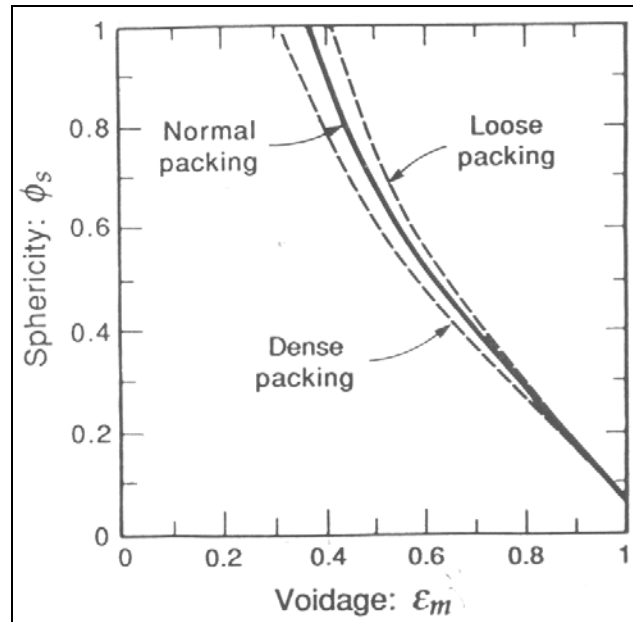


Figure D.1: Voidage of a randomly packed bed of uniformly sized particles increases as particles become less spherical (Brown, 1950)

D.2 Minimum Fluidising Velocity (U_{mf}) by Wen and Yu (1966)

$$Re_{mf} = (33.7^2 + 0.0408 Ar)^{1/2} - 33.7 \quad (D1)$$

where Archimedes Number, Ar:-

$$Ar = \frac{\rho_f (\rho_p - \rho_f) g d_p^3}{\mu_f^2} \quad (D2)$$

and the Reynolds Number at incipient fluidisation is defined as:-

$$\text{Re}_{mf} = \frac{\rho_f U_{mf} d_p}{\mu_f} \quad (\text{D3})$$

D.3 Terminal Velocity (U_t) by Haider and Levenspiel (1989)

The terminal velocity of non-spherical particles could be determined from the following dimensionless expressions from Haider and Levenspiel (1989) and as cited by Kunii and Levenspiel (1991):-

$$d_p^* = d_p \left[\frac{\rho_g (\rho_p - \rho_g) g}{\mu^2} \right]^{1/3} \quad (\text{D4})$$

$$u^* = u \left[\frac{\rho_g^2}{\mu (\rho_p - \rho_g) g} \right]^{1/3} \quad (\text{C5})$$

Determination of u_t using these expressions required the reference of Figure C.2, which is the graphical representation of the expression for C_D developed by Haider and Levenspiel (1989).

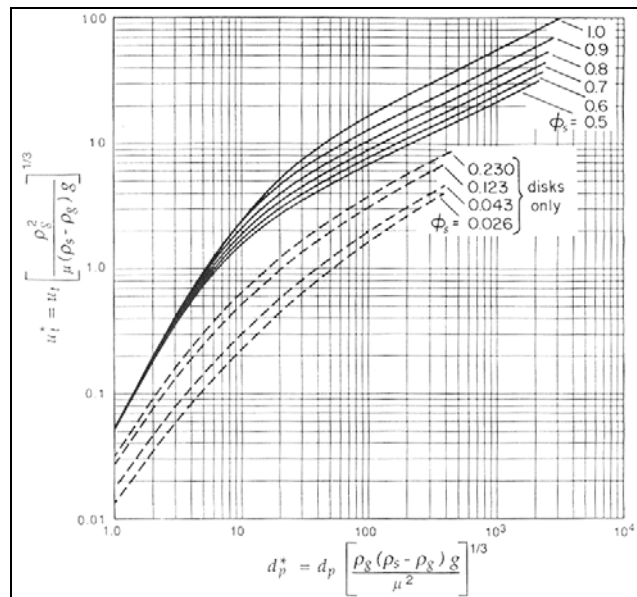


Figure D.2: Chart for determining the terminal velocity of particles falling through fluids (Haider and Levenspiel, 1989)

Appendix E

Real-Time Temperature Profiles during Combustion of Rice Husk in the 210-mm Inner Diameter Fluidised Bed at Different Freeboard Temperatures

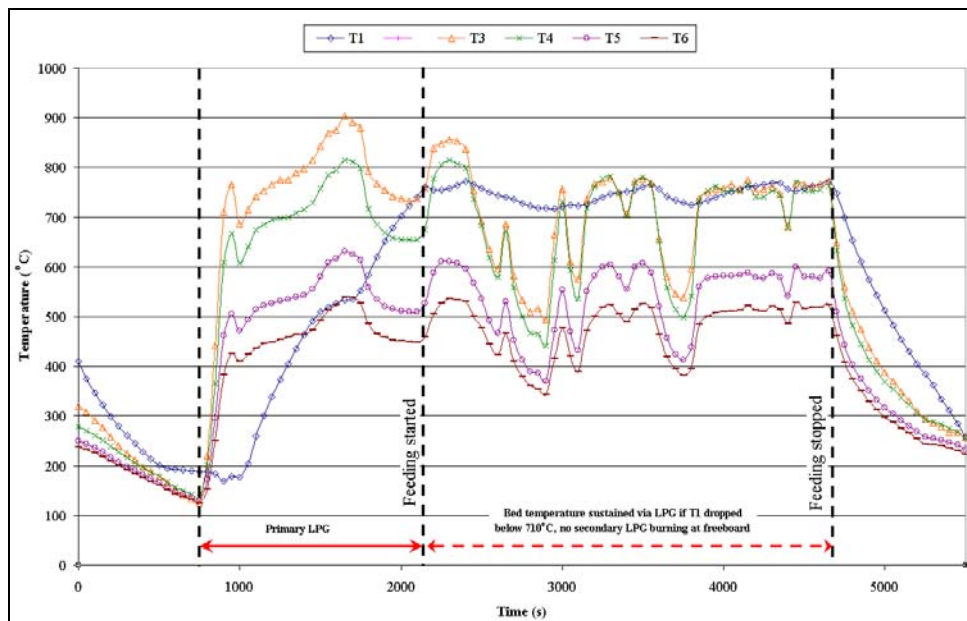


Figure E.1: Real-time temperature profiles during combustion of rice husk in Case FT1 (absence of secondary burner; $T_4 - T_6 = 400 - 600^{\circ}\text{C}$)

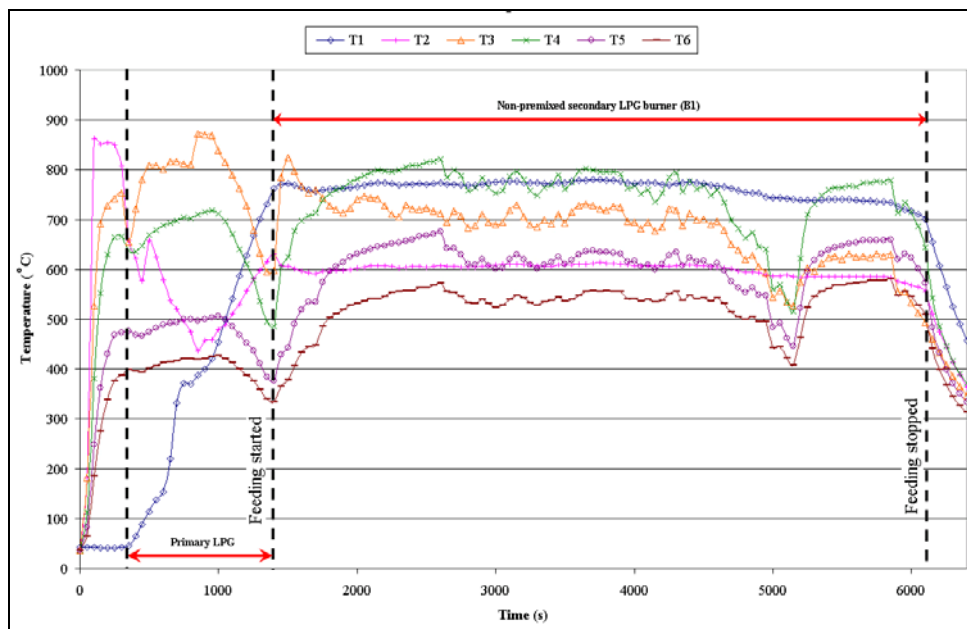


Figure E.2: Real-time temperature profiles during combustion of rice husk in Case FT2 (presence of a non-premixed LPG burner at 479mm above distributor plate; $T_4 - T_6 = 550 - 600^{\circ}\text{C}$)

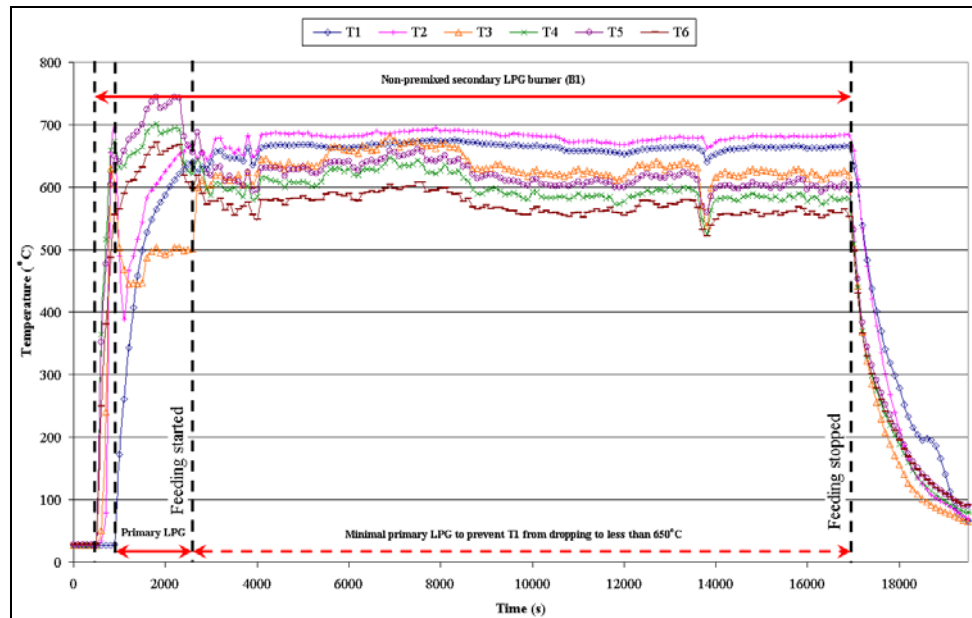


Figure E.3: Real-time temperature profiles during combustion of rice husk in Case FT3 (presence of a non-premixed LPG burner at 479mm above distributor plate; $T_4 - T_6 = 600 - 650^{\circ}\text{C}$)

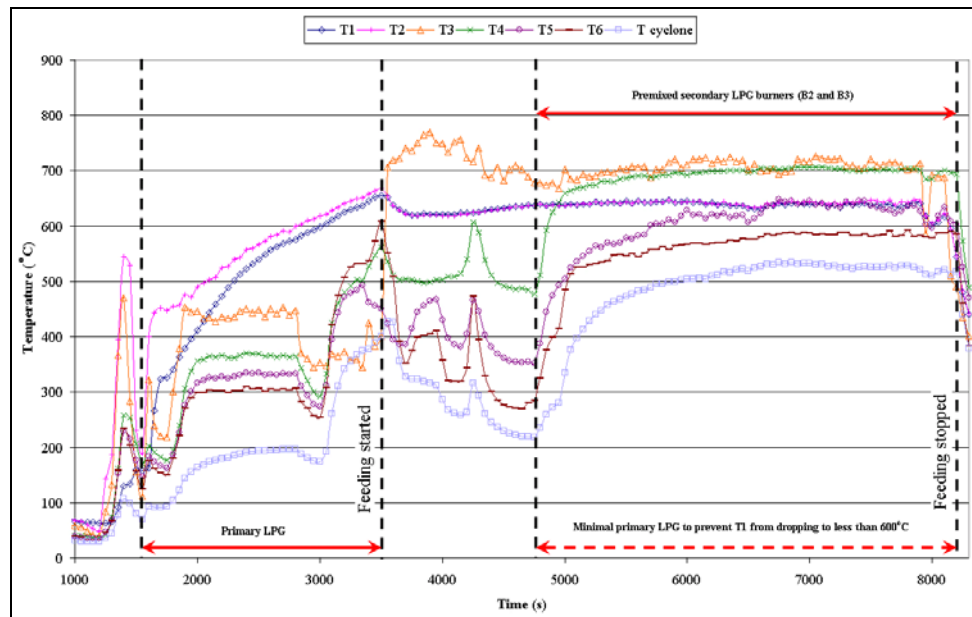


Figure E.4: Real-time temperature profiles during combustion of rice husk in Case FT4 (presence of two premixed LPG burners at 800mm and 1860mm above the distributor plate, respectively; $T_4 - T_6 = 600 - 700^{\circ}\text{C}$)

Appendix F

Real-Time Temperature Profiles during Combustion of Raw and water-Washed Rice Husk in the 210-mm Inner Diameter Fluidised Bed

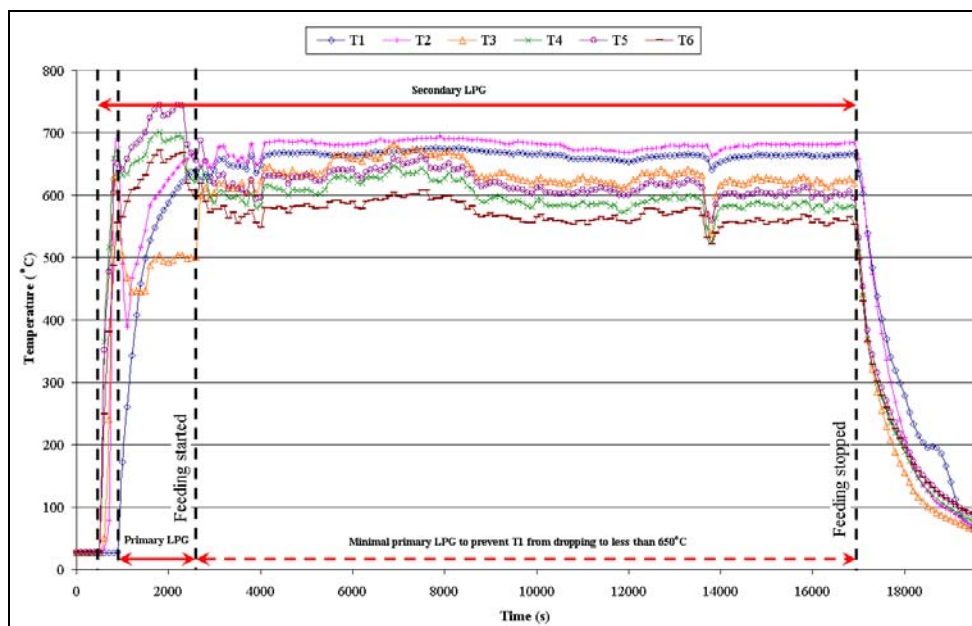


Figure F.1: Real-time temperature profiles during combustion of raw rice husk at moisture content of 10 wt%

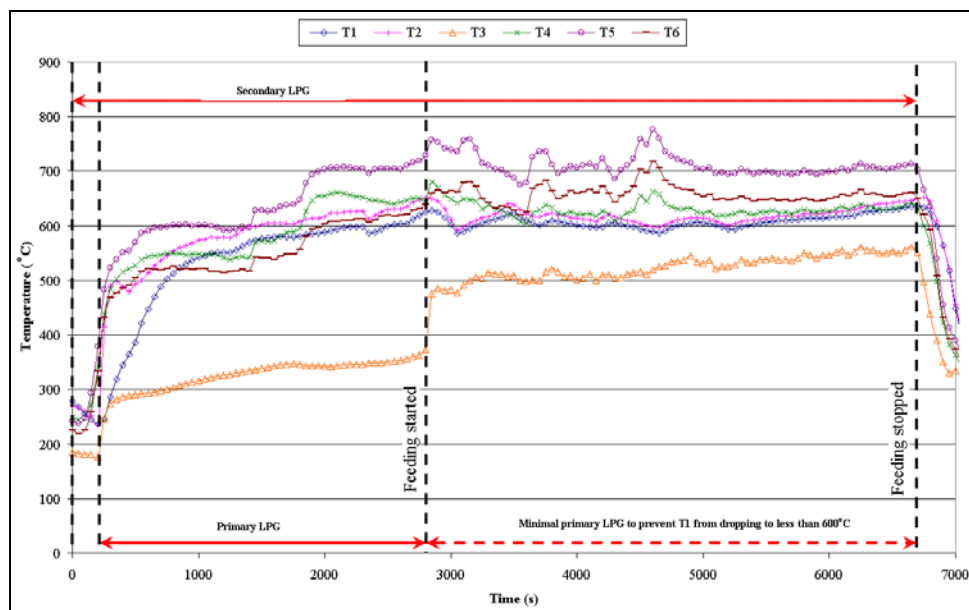


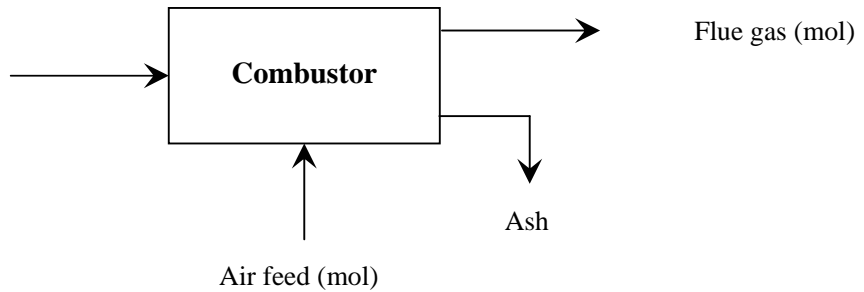
Figure F.2: Real-time temperature profiles during combustion of water-washed rice husk at moisture content of 10 wt%

Appendix G

Mass Balance to Determine the Amount of Stoichiometric Air for Combustion of Rice Husk

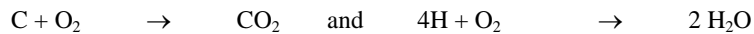
Rice husk feed on wet basis: 100g

H₂O = 10.10 g
 Ash = 14.70 g
 C = 33.98 g
 H = 4.50 g
 O = 36.18 g
 N = 0.54 g



C	=	33.98 g	≡	2.83 mol
H	=	4.50 g	≡	4.50 mol
O	=	36.18 g	≡	2.26 mol

Assuming complete combustion, carbon and oxygen in the feed will be oxidised in the following manner:-



∴ 1 mol C ≡ 1 mol O₂
 1 mol H ≡ 0.25 mol O₂

Stoichiometric oxygen requirement:-

2.83 mol C	≡	2.83 mol O ₂
4.50 mol H	≡	1.13 mol O ₂
2.26 mol O	≡ (-)	1.13 mol O ₂

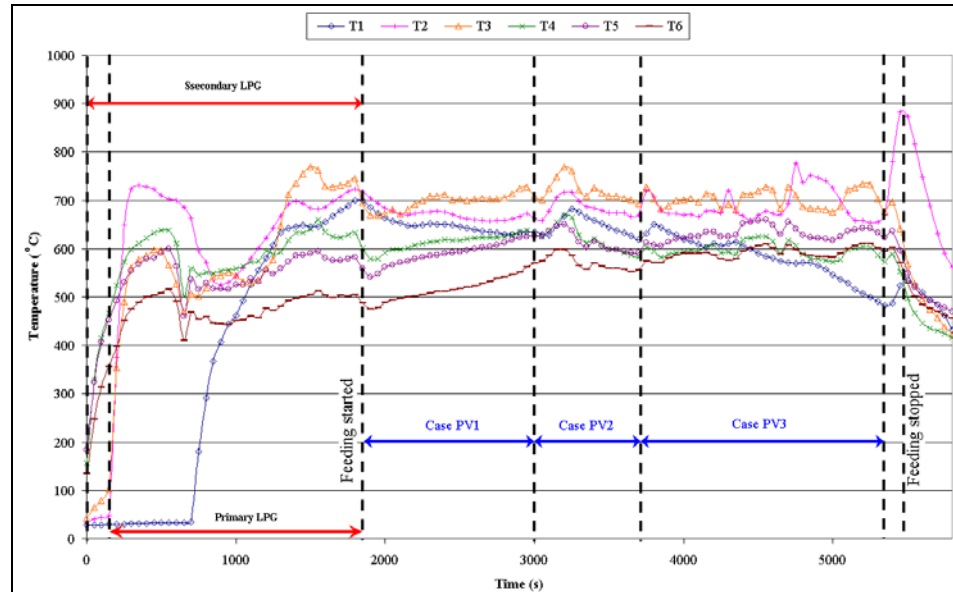
Amount of oxygen required = 2.83 mol

Stoichiometric air requirement = $\frac{1 \text{ mol air}}{0.21 \text{ mol O}_2} \times 2.83 \text{ mol O}_2$
 = 13.48 mol

Air feed at ambient (30°C) = $13.48 \text{ mol} \times \frac{22.414 \text{ L}}{\text{mol}} \times \frac{303 \text{ K}}{273 \text{ K}}$
 = $\frac{335.3 \text{ L}}{100 \text{ g feed}}$ or $\frac{3.353 \text{ m}^3}{\text{kg feed}}$

Appendix H

Real-Time Temperature Profiles during Combustion of Rice Husk at Different Pneumatic Air Feeding Velocities



Note: Case studies based on different pneumatic air feeding velocities: PV1 – 0.42 m/s, PV2 – 0.63 m/s, PV3 – 0.85 m/s

Figure H.1: Real-time temperature profiles during combustion of rice husk at pneumatic air feeding velocities of 0.42 – 0.85 m/s (Case Studies PV1 – Case PV3)

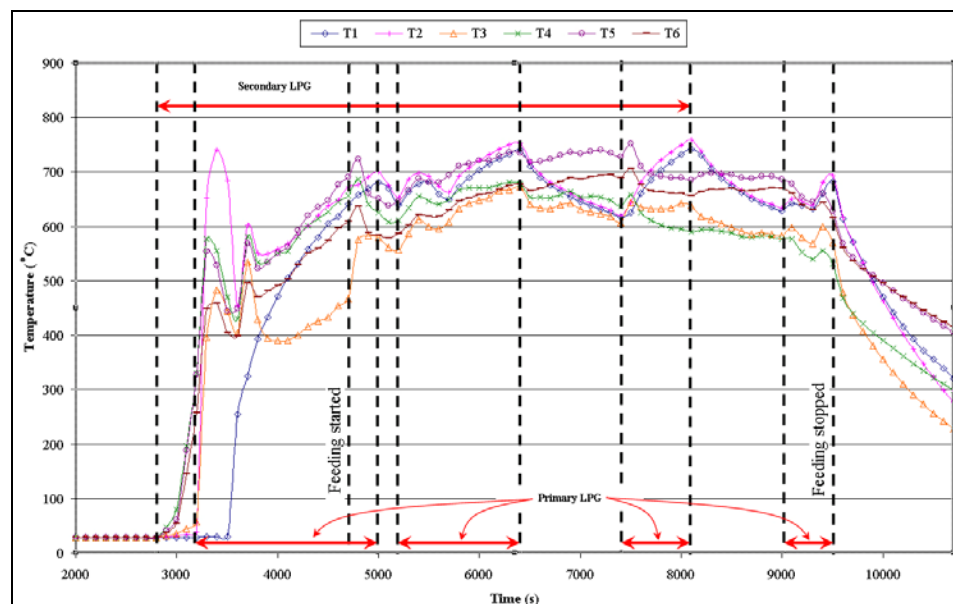


Figure H.2: Real-time temperature profiles during combustion of rice husk at pneumatic air feeding velocity of 1.36 m/s (Case Study PV4)

Appendix I

LIST OF PUBLICATIONS

I.1 Technical Papers (Local and International)

1. M. Rozainee, S. P. Ngo and K. G. Tan. (2004). *Production of Amorphous Silica from Rice Husk in Fluidised Bed*. Proceedings for the Ninth Asian Conference on Fluidized Bed and Three-Phase Reactors. 21 – 24 November, 2004. Taiwan, Taipei: The Chinese Institute of Chemical Engineers. 163 – 168.
2. M. Rozainee and S. P. Ngo. (2004). *Computational Fluid Dynamics Modelling on the Combustion of Rice Husk in a Fluidised Bed Combustor*. Presented at the Symposium on Science and Mathematics 2004 (SSM 2004) organised by Universiti Teknologi Malaysia on 4 – 5 December 2004.
3. M. Rozainee and S. P. Ngo. *Effect of Static Bed Height on the Combustion of Rice Husk in a Fluidised Bed Combustor*. Refereed paper accepted for oral presentation (paper no. FBC2005-78005) at the 18th International Conference on Fluidized Bed Combustion organised by the American Society of Mechanical Engineers (ASME) on 22 – 25 May 2005 in Canada.
4. M. Rozainee; A. A. Salema; S. P. Ngo. And Z. Zairinfarid. *Rice Husk Particle Movement Analysis in a Newly-Designed Columnar-Conical Fluidised Bed*. Accepted for Brunei International Conference on Engineering and Technology (BICET 2005) to be organised by Institut Teknologi Brunei on 15 – 18 August 2005.

I.2 Patent Pending

Malaysian Patent (Application No. PI 2005 0020) titled “*Process for Production of High Purity, Amorphous, Carbon Free Silica*” filed to Intellectual Property Corporation of Malaysia (Perbadanan Harta Intelek Malaysia) on 4th January 2005.

I.3 Commercialisation Activity

Application for a business plan titled “*Development of Rice Husk Industry in Malaysia*” submitted for Cradle Investment Programme (CIP) under Malaysia Venture Capital Management Sdn. Bhd. (MAVCAP) on 5th July 2005.

REFERENCES

- Ajiwe, V. I. E.; Okeke, C. E. and Akigwe, F. C. (2000). *A Preliminary Study of Manufacture of Cement from Rice Husk Ash*. *Bioresource Technology*. 73: 37-39.
- Amick, J. A.; Milewski, J. V. and Wright, F. J. (1980). *Method for Producing Solar-Cell Grade Silicon from Rice Hulls*. U. S. Patent No. 4,214, 920.
- Amick, J.A. (1982). *Purification of Rice Hulls as a Source of Solar-Grade Silicon for Solar Cells*. *J. Electrochem. Soc.* 129: 864-866.
- Armesto, L.; Bahillo, A.; Veijonen, K.; Cabanillas, A. and Otero, J. (2002). *Combustion Behaviour of Rice Husk in a Bubbling Fluidised Bed*. *Biomass and Bioenergy*. 23: 171-179.
- Ashish Bhat; Ram Bheemarasetti, J. V. and Rajeswara Rao, T. (2001). *Kinetics of Rice Husk Char Gasification*. *Energy Conversion and Management*. 42: 2061-2069.
- Bartha, P. and Huppertz, E. A. (1974). *The Structure of Silica in Rice Husks and Their Crystallization*. *Proc. Rice By-Products Conference Valencia, Spain*. 89.
- Beagle, E. C. (1974). *Basic and Applied Research Needs for Optimizing Utilization of Rice Husk*. In *Proc. of the Rice Husk By-Products Utilization, Int. Conf. Valencia*. pp 1-43.
- Beagle, E. C. (1978). *Rice Husk, Conversion to Energy*. *FAO Agricultural Bulletin* 31, Chap. 3. Rome.
- Bhattacharya, S. C. and Shah, N. (1987). *Spouted Bed Combustion of Paddy Husk*. *Energy Research*. 11: 429-432.
- Bhattacharya, S. C. and Wu, W. (1989). *Fluidized Bed Combustion of Rice Husk for Disposal and Energy Recovery*. *Energy from Biomass and Wastes*. XII: 591-601.
- Bhattacharya, S. C.; Shah, N. and Alikhani, Z. (1984). *Some Aspects of Fluidized Bed Combustion of Paddy Husk*. *Applied Energy*. 16(4): 307-316.
- Bingyan, X and Zhongnan, L. (1987). *A Study of Fluidized Bed Gasification Rice Hulls*. *Advances in Solar Energy Technology, Biennial Congress, Hamburg, Germany*. pp 2312-2316.

- Bishnoi, N. R.; Bajaj, M.; Sharma, N. and Gupta, A. (2004). *Adsorption of Cr(VI) on Activated Rice Husk Carbon and Activated Alumina*. *Bioresource Technology*. 91: 305-307.
- Black and Veatch (Thailand). (2000). *Thailand Biomass-Based Power Generation and Cogeneration within Small Rural Industries*. National Energy Policy Office (NEPO). Chapter 5, pp 5-4.
- Boateng, A. A.; Walawender, W. P.; Fan, L. P. And Chee, C. S. (1992). *Fluidized-Bed Steam Gasification of Rice Hull*. *Bioresource Technology*. 40: 235-239.
- Bogue, R. H. (1989). *Cement in the World Book Encyclopedia*. A Scoh Fetzer Company. Chicago, London, Sydney, Toronto. 3: 344-345.
- Bogush, G. H.; Tracy, M. A.; and Zukoski, C. F. (1988). *Preparation of Monodisperse Silica Particles: Control of Size and Mass Fraction*. *Journal of Non-Crystalline Solids*. 104(1): 95-106.
- Botterill, J. S. M.; Teoman, Y. and Yuriger, K. R. (1982). *The Effect of Operating Temperature on the Velocity of Minimum Fluidisation Bed Voidage and General Behaviour*. *Powder Technology*. 31: 101-110.
- Briens, C. L.; Bergougnou, M. A. And Baron, T. (1988). *Prediction of Entrainment from Gas-Solid Fluidized Beds*. *Powder Technology*. 54: 86-196.
- Bronzeoak Ltd. (2003). *Rice Husk Ash Market Study*. Doc. Ref. No. ETSU U/00/00061/REP, DTI/Pub URN 03/668.
- Brown, G. G. (1950). *Unit Operations*. New York: Wiley.
- Caram, H. S.; Efes, Z. and Levy, E. K. (1984). *Gas and Particle Motion Induced by a Bubble Eruption at the Surface of a Gas Fluidized Bed*. *AIChE Symposium Series*. 80 (234): 103-106.
- Chakraverty, A. and Kaleemullah, S. (1991). *Conversion of Rice Husk into Amorphous Silica and Combustible Gas*. *Energy Convers. Mgmt.* 32(6): 565-570.
- Chakraverty, A.; Mishra, P. and Banerjee, H. D. (1985). *Investigation of Thermal Decomposition of Rice Husk*. *Thermochim. Acta*. 94: 267-275.
- Chakraverty, A.; Mishra, P. and Banerjee, H.D. (1988). *Investigation of Combustion of Raw and Acid-Leached Rice Husk for Production of Pure Amorphous White Silica*. *J. Mater. Sci*. 23: 21-24.

- Chandrasekhar, S.; Satyanarayana, K. G.; Pramada, P. N.; Raghavan, P. and Gupta, T. N. (2003). *Review Processing, Properties and Application of Reactive Silica from Rice Husk – An Overview*. Journal of Materials Science. 38: 3159-3168.
- Chemical Market Reporter (18th January 1999). *Sodium Silicates*.
- Chemlink Pty Ltd. (1997). *Silicon and Silicon Chemicals*. Publications No. ACN 007 034 022.
- Chen, G. Y.; Fang, M. X.; Luo, Z. Y.; Yu, C. J.; Li, X. T.; Ni, M. J. and Cen, K. F. (1998). *The Study of Combustion Characteristics of Rice Husk-Fired Fluidized Bed Boiler*. Journal of Combustion Science and Technology. 4(2): 193-198. In Mandarin language.
- Chouhan, R. K.; Kujur, B.; Amritphale, S. S. and Chandra, N. (2000). *Effect of Temperature of Ashing of Rice Husk on the Compressive Strength of Lime-Rice Husk Silica Mortar*. Sil. Ind. 65(5-6): 67-71.
- Conradt, R.; Pimkhaokham, P. and Leela-Adisorn, U. (1992). *Nanostructured Silica from Rice Husk*. Journal of Non-Crystalline Solids. 145: 75-79.
- Das, P.; Ganesh, A. and Wangikar, P. (2004). *Influence of Pretreatment for Deashing of Sugarcane Bagasse on Pyrolysis Products*. Biomass and Bioenergy. 27: 445-457.
- Davidson, J. F. and Harrison, D. (1963). *Fluidised Particles*. Cambridge University Press, New York.
- De Souza, M. F.; Batista, P. D. S. and Liborio, J. B. L. (2004). *Oxides Extracted from Vegetal Matter and Process Therefor*. U. S. Patent Application Publication No. US 2004/0175321 A1, Sept. 9, 2004.
- Della, V. P.; Kühn, I. and Hotza, D. (2002). *Rice Husk Ash as an Alternate Source for Active Silica Production*. Material Letters. 57: 818-821.
- Department of Statistics Malaysia (2004). *Key Statistics*. Website: <http://www.statistics.gov.my/English/keystats.htm> (accessed on 20th June 2005)
- Di Blasi, C.; Buonanno, F. and Branca, C. (1999). *Reactivities of Some Biomass Chars in Air*. Carbon. 37(8): 1227-1238.
- Dielt, J.; Helmreich, D. and Sirtl, E. (1981). *Crystal: Growth, Properties and Applications 5, Silicon*. Springer-Verlag, Berlin, Heidelberg.

- Dutta, S. and Wen, C. Y. (1977). *Reactivity of Coal and Char and Ash 2. In Oxygen-Nitrogen Atmosphere*. Ind. Eng. Chem. Process Des. Dev. 16(1): 31-37.
- Environment Agency (1996). *Integrated Pollution Control (IPC) Guidance Note, Series 2 (S2): Waste Disposal and Recycling Sector, S2 5.01: Waste Incineration*. London: IPC S2 5.01
- Fang, M.; Yang, L.; Chen, G.; Shi, Z; Luo, Z. and Cen. K. (2004). *Experimental Study on Rice Husk Combustion in a Circulating Fluidised Bed*. Fuel Processing Technology. 85: 1273-1282.
- Feng, Qingge; Yamamichi, H.; Shiya, M. and Sugita, S. (2004). *Study on the Pozzolanic Properties of Rice Husk Ash by Hydrochloric Acid Pre-treatment*. Cement and Concrete Research. 34(3): 521-526.
- Flanigan, V. J.; Xu, B. Y. and Huang, E. (1987). *Fluidized Bed Gasification of Rice Hulls*. The Tenth Annual Energy-Sources Technology Conference and Exhibition, Dallas, Texas. pp 19-34.
- FLUENT 6 User's Guide. (2002). Fluent Incorporated, Centerra Resource Park, 10 Cavendish Court, Lebanon NH 03766.
- Geldart, D. (1973). *Type of gas fluidization*. Powder Technology. 7:285-292.
- Ghosh, T. B.; Nandi, K. C.; Acharya, H. N. and Mukherjee, D. (1991). *XPS Studies of Magnesium Silicide Obtained from Rice Husk*. Material Letters. 11(1-2): 6-9.
- Gorthy, P. and Pudukottah, M. G. (1999). *Production of Silicon Carbide from Rice Husks*. Journal of the American Ceramic Society. 82(6): 1393-1400.
- Haider, A. and Levenspiel, O. (1989). *Drag Coefficient and Terminal Velocity of Spherical and Nonspherical Particles*. Powder Technology. 58: 63-70.
- Hamad, M. A. (1981 – 1982). *Combustion of rice hulls in a static bed*. Energy in Agriculture. 1: 311-315.
- Hamad, M. A. and Khattab, I. A. (1981). *Effect of the Combustion Process on the Structure of Rice Hull Silica*. Thermochemica Acta. 48: 343-349.
- Hanafi, S.; Abo-El-Enein, S. A.; Ibrahim, D. M. and El-Hemaly, S. A. (1980). *Surface Properties of Silicas Produced by Thermal Treatment of Rice Husk Ash*. Thermochemica Acta. 37: 137-143.

- Hanjalic, K. (1994). *Advanced Turbulence Closure Models, a View of Current Status and Future Prospects*. International Journal of Heat and Fluid Flow. 15 (3): 178-203.
- Hanna, S. B.; Farag, L. M. and Mansour, N. A. L. (1984). *Pyrolysis and Combustion of Treated and Untreated Rice Hulls*. Thermochemica Acta. 81: 77-86.
- Hao Liu, Zhijie Lin, Dechang Liu and Weiheng Wu. (1995). *Combustion Characteristics of Rice Husk in Fluidised Beds*. Proceedings of the 13th International Conference on Fluidised Bed Combustion. 1: 615-618.
- Hartiniati, A.; Soemardjo, A. and Youvial, M. (1989). *Performance of a Pilot-Scale Fluidized Bed Gasifier Fuelled by Rice Husk*. Proc. Int. Conf. Pyrolysis and Gasification. pp 257-263.
- Henrich, E.; Bürkle, S.; Meza-Renken, Z. I. And Rumpel, S. (1999). *Combustion and Gasification Kinetics of Pyrolysis Chars from Waste and Biomass*. Journal of Analytical and Applied Pyrolysis. 49: 221 – 241.
- Hiler, E. A. (1982). *On-site Energy Production from Agricultural Residues*. Cent. Energy Miner. Resour., Texas A and M Univ., TX Report: TENRAC/EDF-074, Order No. DE83900814.
- Ho, T. C.; Paul, K. and Hopper, J. R. (1988). *Kinetic Study of Biological Sludge Incineration in a Fluidized Bed*. AIChE Symposium Series 84(262): 126-133.
- Houston, D. F. (1972). *Rice: Chemistry and Technology*. American Society of Cereal Chemists, St. Paul, Minnesota. Chapter 12, pp 301.
- Howard, J. R. (1989). *Fluidized Bed Technology*. New York: Adam Hilger.
- Huang, S.; Jing, S.; Wang, J. F.; Wang, Z. W and Jin, Y. (2001). *Silica White obtained from Rice Husk in a Fluidized Bed*. Powder Technology. 117: 232-238.
- Hunt, L.H.; Dismukes, J.P.; Amick, J.A.; Schee, A. and Larsen, K. (1984). *Rice Hulls as a Raw Material for Producing Silicon*. J. Electrochem. Soc. Vol. 131(7): 1683-1686.
- Ibrahim, D. M. and Helmy, M. (1981). *Crystallite Growth of Rice Husk Ash Silica*. Thermochemica Acta. 45: 79-85.
- Ibrahim, D. M.; El-Hemaly, S. A.; Abo-Enein, S. A.; Hanafi, S. and Helmy, M. (1980). *Thermal Treatment of Rice Husk Ash: Effect of Time of Firing on Pore Structure and Crystallite Size*. Thermochemica Acta. 37: 347-351.

- Islam, M. N. and Ani, F. N. (2000). *Techno-Economics of Rice Husk Pyrolysis, Conversion with Catalytic Treatment to Produce Liquid Fuel*. *Bioresource Technology*. 73: 67-75.
- James, J. and Rao, M. S. (1986). *Silica from Rice Husk through Thermal Decomposition*. *Thermochimica Acta*. 97: 329-336.
- Jauberthie, R.; Rendell, F.; Tamba, S. and Cisse, I. (2000). *Origin of the Pozzolanitic Effect of Rice Husks*. *Construction and Building Materials*. 14: 419-423.
- Jenkins, B. M. (1989). *Physical Properties of Biomass*. In *Biomass Handbook*, ed. O. Kitani and C. W. Hall. Gordon & Breach, New York. pp 860-891.
- Jenkins, B. M.; Bakker, R. R. and Wei, J. B. (1996). *On the Properties of Washed Straw*. *Biomass and Bioenergy*. 10(4): 177-200.
- Jenkins, B. M.; Baxter, L. L.; Miles Jr., T. R. and Miles, T. R. (1998). *Combustion Properties of Biomass*. *Fuel Processing Technology*. 54: 17-46.
- Jones, J. M.; Pourkashanian, M.; Williams, A. and Hainsworth, D. (2000). *A Comprehensive Biomass Combustion Model*. *Renewable Energy*. 19: 229-234.
- Kalopathy, U.; Proctor, A. and Shultz, J. (2000). *A Simple Method for Production of Pure Silica from Rice Hull Ash*. *Bioresource Technology*. 73: 257-264.
- Kalopathy, U.; Proctor, A. and Shultz, J. (2002). *An Improved Method for Production of Silica from Rice Hull Ash*. *Bioresource Technology*. 82: 285-289.
- Kamath, S. R. and Proctor, A. (1998). *Silica Gel from Rice Hull Ash: Preparation and Characterisation*. *Cereal Chem*. 75: 484-493.
- Kapur, P. C. (1985). *Production of Reactive Bio-Silica from the Combustion of Rice Husk in a Tube-in-Basket (TiB) Burner*. *Powder Technology*. 44: 63-67.
- Kaupp, A. (1984). *Gasification of Rice Husks: Theory and Practices*. Eschborn: Deutsches Zentrum fuer Entwicklungs Technologien (GATE).
- Kaupp, A. and Goss, J. R. (1981 – 1982). *Technical and Economical Problems in the Gasification of Rice Husks. Physical and Chemical Properties*. *Energy in Agriculture*. 1: 201-234.
- Krishnarao, R. V. and Subrahmanyam, J. (1995). *Formation of SiC from Rice Husk Silica-Carbon Black Mixture: Effect of Rapid Heating*. *Ceramics International*. 22:489-492.

- Krishnarao, R. V.; Subrahmanyam, J. and Jagadish Kumar, T. (2001). *Studies on the Formation of Black Particles in Rice Husk Silica Ash*. Journal of the European Ceramic Society. 21: 99-104.
- Kulasekaran, S.; Linjewile T. M.; Agarwal, P. K. and Biggs, M. J. (1998). *Combustion of a Porous Char Particle in an Incipiently Fluidized Bed*. Fuel. 77(14): 1549-1560.
- Kunii, D. and Levenspiel, O. (1991). *Fluidization Engineering*. 2nd Ed. Boston: Butterworth-Heinemann.
- Leung, D. Y. C.; Xu, B. Y. and Wu, C. Z. (2001). *The Development of Biomass Gasification Technology towards Market Penetration in China*. Int. J. Global Energy Issues. 15(1/2): 132-140.
- Lide, D. R. (2001). *CRC Handbook of Chemistry and Physics*. 82nd Edition. Boca Raton: CRC Press.
- Lim, S. Y. (2002). *Combustion Efficiency of Palm Wastes in Spouting and Bubbling Fluidised Beds*. Universiti Teknologi Malaysia: Master Thesis.
- Lin, K. S.; Paul Wang, H.; Lin, C. J. and Ching I-Juch. (1998). *A Process Development for Gasification of Rice Husk*. Fuel Processing Technology. 55: 185-192.
- Liou, Tzong-Horng. (2004). *Preparation and Characterization of Nano-Structured Silica from Rice Husk*. Materials Science and Engineering A364: 313-323.
- Luan, T. C. and Chou, T. C. (1990). *Recovery of Silica from the Gasification of Rice Husks/Coal in the Presence of a Pilot Flame in a Modified Fluidized Bed*. Ind. Eng. Chem. Res. 29: 1922-1927.
- Madhiyanon, T.; Piriyaunroj, N. and Soponnarit, S. (2004). *A Novel Vortex-Fluidized Bed Combustor with Two Combustion Chambers for Rice-Husk Fuel*. (In Thai language). Songklanakarin J. Sci. Technology. 26(6): 875-893.
- Mahin, B. (1986). *Rice Husk Energy Systems*. Bioenergy Systems Report, Office of Energy-U.S. Agency for International Development.
- Mansaray, K. G. and Ghaly, A. E. (1997). *Physical and Thermochemical Properties of Rice Husk*. Energy Sources. 19: 989-1004.
- Mansaray, K. G. and Ghaly, A. E. (1998a). *Agglomeration Characteristics of Silica Sand-Rice Husk Ash Mixtures at Elevated Temperatures*. Energy Sources. 20: 631-652.

- Mansaray, K. G. and Ghaly, A. E. (1998b). *Thermogravimetric Analysis of Rice Husk in an Air Atmosphere*. Energy Sources. 20: 653-663.
- Mansaray, K. G., Ghaly, A. E.; Al-Taweel, A. M.; Hamdullahpur, F. and Ugursal, I. (1999). *Air Gasification of Rice Husk in a Dual Distributor Type Fluidized Bed Gasifier*. Biomass and Bioenergy. 17: 315-332.
- Martin, J. I. (1938). *The desilification of rice husk and a study of the products obtained*. Louisiana State University, USA: Master Thesis.
- McDonald, R. H. (1991). *Silica in Nova Scotia*. Information Circular ME 14, Second Edition, Nova Scotia Department of Natural Resources, Mineral Resources Branch, Government of Nova Scotia.
- Miles, T. R. Jr. and Miles, T. R. (1995). *Alkali Deposits Found in Biomass Power Plants – A Preliminary Investigation on Their Extent and Nature*. Summary report for the National Renewable Energy Laboratory (NREL), Subcontract TZ-2-11226-1, Golden, CO.
- MineSet Partners LLC. (2004). *Specialty Silicas: Global Strategic Analysis 2002 – 2004*. Regional Business Report, New Jersey, USA, March 2004.
- Mishra, P.; Chakraverty, A. and Banerjee, H.D. (1985). *Production and Purification of Silicon by Calcium Reduction of Rice-Husk White Ash*. J. Mater. Sci. 20: 4387-4391.
- Mori, S. and Wen, C. Y. (1975). *Estimation of Bubble Diameter in Gaseous Fluidized Beds*. AIChE J. 21(1): 109-115.
- Morris, G.P.; Norman, N. A. and Gleick, P. H. (1991). *Greenhouse-Gas Emission from Biomass Energy Use: Comparison with other Energy Technologies*. Energy from Biomass and Wastes XIV, Institute of Gas Technology, Chicago.
- Morsi, S. A. and Alexander, A. J. (1972). *An Investigation of Particle Trajectories in Two-Phase Flow Systems*. J. Fluid Mech. 55(2): 193-208.
- Mukunda, H. S.; Shrinivasa, U.; Paul, P. J.; Dasappa, S. and Rajan, N. K. S. (1996). *Stand Alone Small Power Level Systems*. Presented at the 7th Annual Conference of India Nuclear Society on India's Energy Needs and Options, BARC, Mumbai, April 1996.

- Nakata, Y.; Suzuki, M.; Okutani, T.; Kikuchi, M. and Akiyama, T. (1989). *Preparation and Properties of SiO₂ from Rice Hulls*. J. Ceram. Soc. Jpn. 97: 842-852.
- Nasserzadeh, V.; Swithenbank, J.; Schofield, C.; Scott and D. W.; Loader. (1994). *Effects of High Speed Jets and Internal Baffles on the Gas Residence Times in large Municipal Incinerators*. Environmental Progress. 13(2): 124-133.
- Nasserzadeh, V.; Swithenbank, J.; Schofield, C.; Scott, D. W.; Loader, A.; Leonard, A.; Russell, R. and Winn, D. (1993). *Three-Dimensional Modelling of the Coventry MSW Incinerator Using Computational Fluid Dynamics and Experimental Data*. Trans IChemE. 71(B): 269-279.
- Natarajan, E.; Nordin, A and Rao, A. N. (1998a). *Overview of Combustion and Gasification of Rice Husk in Fluidized Bed Reactors*. Biomass and Bioenergy. 14(5/6): 533-546.
- Natarajan, E.; Öhman, M.; Gabra, M.; Nordin, A.; Liliedahl, T. and Rao, A. N. (1998b). *Experimental Determination of Bed Agglomeration Tendencies of Some Common Agricultural Residues in Fluidized Bed Combustion and Gasification*. Biomass and Bioenergy. 15(2): 163-169.
- National Energy Balance Malaysia Year 1998 Report. Ministry of Energy, Communications and Multimedia, Malaysia. pg 1. Website: <http://ns2.ptm.org.my/medishomepage/PDFReport/energy%balance1998.pdf> (accessed on 29th March 2003)
- National Energy Balance Malaysia Year 2000 Report. Ministry of Energy, Communications and Multimedia, Malaysia. pg 3. Website: <http://ns2.ptm.org.my/medishomepage/PDFReport/NEB2000.pdf> (accessed on 26th March 2003)
- National Energy Balance Malaysia Year 2001 Report. Ministry of Energy, Communications and Multimedia, Malaysia. pg 1. Website: <http://ns2.ptm.org.my/medishomepage/PDFReport/NEB2001.pdf> (accessed on 26th March 2003)
- National Institute for Occupational Safety and Health, NIOSH (1998). *Silica, Crystalline, by XRD Method 7500*. 3: 2.

- Nehdi, M.; Duquette, J. and El Damatty, A. (2003). *Performance of Rice Husk Ash Produced Using a New Technology as a Mineral Admixture in Concrete*. Cement and Concrete Research. 33: 1203-1210.
- New Straits Times Press (29th June 2002). *Poor Response to Recycling Campaign*.
- Ngo, S. P. (2002). *Design and Three-Dimensional Computational Fluid Dynamics of the Horizontal Rotating Fluidised Bed Combustor*. Universiti Teknologi Malaysia: Master Thesis.
- Niessen, W. R. (1995). *Combustion and Incineration Processes: Applications in Environmental Engineering*. 2nd Edition. New York: Marcel Dekker, Inc.
- Patel, M.; Karera, A. and Prasanna, P. (1987). *Effect of Thermal and Chemical Treatment on Carbon and Silica Contents in Rice Husk*. Journal of Materials Science. 22: 2457-2464.
- Peel, R. B. and Santos, F. J. (1980). *Fluidized Bed Combustion of Vegetable Fuels*. In Proc. of Int. Conf. On Fluidized Bed Combustion: Systems and Applications. pp IIB.2.1-IIB.2.9.
- Pemberton, S. T. and Davidson, J. F. (1986). *Elutriation from fluidized beds – 1. Particle ejection from the dense phase into the freeboard*. Chemical Engineering Science. 41: 243-251.
- Permchart, W. and Koupryanov. (2004). *Emission Performance and Combustion Efficiency of a Conical Fluidized-Bed Combustor Firing Various Biomass Fuels*. Bioresource Technology. 92: 83-91.
- Perry, R. H.; Green, D. W. and Maloney, J. O. (Eds.) (1997). *Perry's Chemical Engineer's Handbook*. 7th Edition. New York: McGraw-Hill.
- Pitt, N. (1976 and 1994). *Process for the Preparation of Siliceous Ashes*. United States Patent No. 3,959,007.
- Pongsak, P. (1992). *Preparation of Silica from Rice Husk by Fluidised Bed Method*. Chulalongkorn University (Dept. of Chemical Technology): Master Thesis.
- Preto, F.; Anthony, E.J.; Desai, D. L. and Friedrich, F. D. (1987). *Combustion Trials of Rice Husk in a Pilot-Scale Fluidized Bed*. Proceeding of the 9th International Conference on Fluidized Bed Combustion. 2: 1123-1127.

- Rao, T. R. and Bheemarasetti, J. V. R. (2001). *Minimum Fluidization Velocities of Mixtures of Biomass and Sands*. Energy. 26: 633-644.
- Real, C.; Alcala, M. and Criado, J.M. (1996). *Preparation of Silica from Rice Husks*. J. Am. Ceram. Soc. 79(8): 2012-2016.
- Rieber, R. S.; Mallow, W. A. and Conner, J. R. (2003). *Production of Soluble Silicates from Biogenic Silica*. United States Patent No. 6,524,523.
- Rozainee (1998). *Incineration of Sludge Waste in a Novel Rotating Fluidized Bed*. University of Sheffield: PhD Thesis.
- Sadasivan, S.; Rasmussen, D. H.; Chen, F. P. and Kannabiran, R. K. (1998). *Preparation and Characterization of Ultrafine Silica*. Colloids and Surfaces A: Physicochemical and Engineering Aspects. 132(1): 45-52.
- San José M.J.; Olazar M.; Aguayo A.T. and Bilbao J., (1996a). *Influence of conical section geometry on the hydrodynamics of shallow spouted bed*. Chemical Engineering Journal. 62: 113-120.
- Sanchez, C. G. and Lora, E. S. (1994). *Biomass Fluidized Bed Gasification Research in the State University of Campinas*. Energy for Sustainable Development. 1(4): 31-33.
- Schiefelbein, G. F. (1989). *Biomass Thermal Gasification Research*. Recent results from the United States DOE's research program. Biomass. 19(1-2): 145-159.
- Sen, R. and Ghosh, D. N. (1992). *Fluidization and Combustion Characteristics of Rice Husk*. Indian Chemical Engineer. 34(4): 206-211.
- Seville, J. P. K.; Silomon-Pflug, H. and Knight, P. C. (1998). *Modelling of Sintering in High Temperature Gas Fluidisation*. Powder Technology. 97(2): 160-169.
- Sharma, A. and Rao, T. R. (1999). *Kinetics of Pyrolysis of Rice Husk*. Bioresource Technology. 67: 53-59.
- Shinohara, Y. and Kohyama, N. (2004). *Quantitative Analysis of Tridymite and Cristobalite Crystallised in Rice Husk Ash by Heating*. Industrial Health Vol. 42: 277-285.
- Singh, R.; Maheshwari, R. C. and Ojba, T. P. (1980). *Efficient Use of Agricultural Wastes in Energy Production*. Journal of Agricultural Mechanisation in Asia, Africa and Latin America. 11: 31-37.

- Sloan, D. G.; Smith, P. J. and Smoot, L. D. (1986). *Modelling of Swirl in Turbulent Flow Systems*. Progress in Energy and Combustion Science. 12(3): 163-250.
- Sridhar, G.; Sridhar, H. V.; Dasappa, S.; Paul, P. J.; Rajan, N. K. S.; Shrinivasa, U. and Mukunda, H. S. (1996). *Technology for gasifying pulverised bio-fuels including agricultural residues*. Energy for Sustainable Development. 3(2): July 1996.
- Srinivasan, R. and Moagia, H. C. (1980). *Numerical Computation of Swirling Recirculating Flow*. NASA CR. No. 165197.
- Stephens, D. K.; Wellen, C. W.; Smith, J. B. and Kubiak, K. F. (2003). *Precipitated silicas, silica gels with and free of deposited carbon from caustic biomass ash solutions and processes*. United States Patent No. 6,638,354.
- Sturgess, G. J. and Syed, S. A. (1985). *Calculation of Confined Swirling Flows*. AIAA Paper. No. 85-0060.
- Sugita, S. (1994). *Method of Producing Active Rice Husk Ash*. United States Patent No. 5,329,867.
- Sumran, M. and Kongkachuichay, P. (2003). *Synthesis of Silica from Rice Husk by One-Step Combustion, Fluidised Bed Combustion and Alkaline Extraction*. KKU Engineering Journal. 30(2): 165-172.
- Swasdisevi, T.; Soponronnarit, S.; Thepent, V.; Shujinda, A. and Srisawat, B. (2000). *Quality Assurance in Agricultural Produce*. Edited by Johnson, G. I.; To. L. V.; Duy Duc, Nguyen and Webb, M. C. ACIAR Proceedings. 100: 277-285.
- Tanner, P. A.; Yan, B.; Zhang, H. (2000). *Preparation and Luminescence Properties of Sol-Gel Hybrid Material Incorporated with Europium Complex*. Journal of Materials Science. 35: 4325-4327.
- The Hindu Newspaper (19th January 2003). *Potential Seen for Rice Husk Ash-Based Power Plants*. Online Edition of India's National Newspaper: <http://www.hinduonnet.com/thehindu/2003/01/19/stories/2003011901441300.htm> (accessed on 17th May 2004)
- The Star, 7th September 2003. *Rice Husk Turned into Nanomaterial*.
- Tobiś, J. (2000). *Influence of Bed Geometry on Its Frictional Resistance Under Turbulent Flow Conditions*. Chemical Engineering Science. 55: 5359-5366.

- Tomozawa, M.; Kim, D. L. and Lou, V. (2001). *Preparation of High Purity, Low Water Content Fused Silica Glass*. Journal of Non-Crystalline Solids. 296(1-2): 102-106.
- Torftech Application Description (August 2002). *Energy and Amorphous Silica Production from Rice Husk*.
- Torftech News, 24th November 2003. *Torftech Announces the Successful Testing of a Commercial Torbed Rice Hull Combustor in India*.
- Tutsek, A. and Bartha, P. (1977). *Method of Producing Low-Carbon White Husk Ash*. United States Patent No. 4,049,464.
- van den Aarsen, F. G.; Beenackers, A. A. C. M. and van Swaij, W. P. M. (1982). *Performance of a Rice Husk Fluidized Bed Pilot Plant Gasifier*. In Producer Gas 1982: First Int. Conf., Sri Lanka. pp 381-391.
- Vempati, R. K. (2002). *Composition and Method of Forming Low-Carbon, Amorphous Siliceous Ash from Siliceous Waste Material*. United States Patent No. 6,444,186.
- Watari, T.; Tsubira, H.; Torikai, T.; Yada, M. and Furuta, S. (2003). *Preparation of Porous Carbon/Silica Composites from Rice Husk Powder*. Journal of Ceramic Processing Research. 4(4): 177-180.
- Wen, C. Y. and Yu, Y. H. (1966). *A Generalized Method for Predicting the Minimum Fluidising Velocity*. AIChE Journal. 12: 610-612.
- Williams, P. T. and Nugranad, N. (2000). *Comparisons of Products from the Pyrolysis and Catalytic Pyrolysis of Rice Husks*. Energy. 25: 493-513.
- Wong, W. Y.; Lu, Y.; Nasserzadeh, V. S.; Swithenbank, J.; Shaw, T. and Madden, M. (2000). *Experimental investigation into the incineration of wool scouring sludges in a novel rotating fluidised bed*. Journal of Hazardous Materials. 73(2): 143-160.
- Wu, G.; Wang, J.; Shen, J.; Tang, T.; Zhang, Q.; Zhou, B.; Deng, Z.; Bin, F.; and Zhang, F. (2000). *Properties of Sol–Gel Derived Scratch-Resistant Nano-Porous Silica Films by a Mixed Atmosphere Treatment*. Journal of Non-Crystalline Solids. 275(3): 169-174.
- Xia, J. L.; Yadigaroglu, G.; Liu, Y. S.; Schmidli, J. and Smith, B. L. (1998). *Numerical and Experimental Study of Swirling Flow in a Model Combustor*. Int. J. Heat Mass Transfer. 41(11): 1485-1497.

- Xu, B. Y.; Huang, W. C.; Flanigan, V. J. and Sitton, O. C. (1985). *Design and Operation of a 6 Inch Fluidized Bed Gasifier for Rice Hulls*. Symposium on Energy from Biomass and Waste **IX**. Organised by IGT, Chicago, U. S. A. pp 595-613.
- Yalçın, N. and Sevinç, V. (2001). *Studies on Silica Obtained from Rice Husk*. *Ceramics International*. 27: 219-224.
- Yin, X. L.; Wu, C. Z.; Zheng, S. P. and Chen, Y. (2002). *Design and Operation of a CFB Gasifier and Power Generation System for Rice Husk*. *Biomass and Bioenergy*. 23: 181-187.
- Zenz, F. A. and Weil, N. A. (1958). *A Theoretical-Empirical Approach to the Mechanism of Particle Entrainment from Fluidised Beds*. *AIChE Journal*. 4:472.
- Zevenhoven, R. and Järvinen, M. (2002). *CFB Combustion, Particle Slip Velocity and Particle/Turbulence Interactions*. Proceedings of the 7th International Conference on Circulating Fluidized Beds (CFB7), Niagara Falls, Ontario, Canada. Grace, J. R.; Zhu, J. X. and de Lasa, H. I. (Eds.) pp 475-482.